TRIUMF

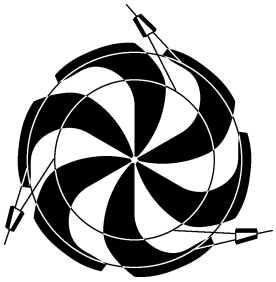

ANNUAL REPORT
SCIENTIFIC ACTIVITIES
2000

ISSN 1492-417X

CANADA'S NATIONAL LABORATORY
FOR PARTICLE AND NUCLEAR PHYSICS

OPERATED AS A JOINT VENTURE

MEMBERS:

THE UNIVERSITY OF ALBERTA
THE UNIVERSITY OF BRITISH COLUMBIA
CARLETON UNIVERSITY
SIMON FRASER UNIVERSITY
THE UNIVERSITY OF VICTORIA

ASSOCIATE MEMBERS:

THE UNIVERSITY OF MANITOBA
L'UNIVERSITÉ DE MONTRÉAL
QUEEN'S UNIVERSITY
THE UNIVERSITY OF REGINA
THE UNIVERSITY OF TORONTO

UNDER A CONTRIBUTION FROM THE
NATIONAL RESEARCH COUNCIL OF CANADA

OCTOBER 2001

TRIUMF

ISSN 1492-417X

ANNUAL REPORT
SCIENTIFIC ACTIVITIES
2000

Postal Address:

TRIUMF
Publications Office
4004 Wesbrook Mall
Vancouver, BC V6T 2A3
Canada

http://www.triumf.ca/annrep

BEAM LINES AND EXPERIMENTAL FACILITIES

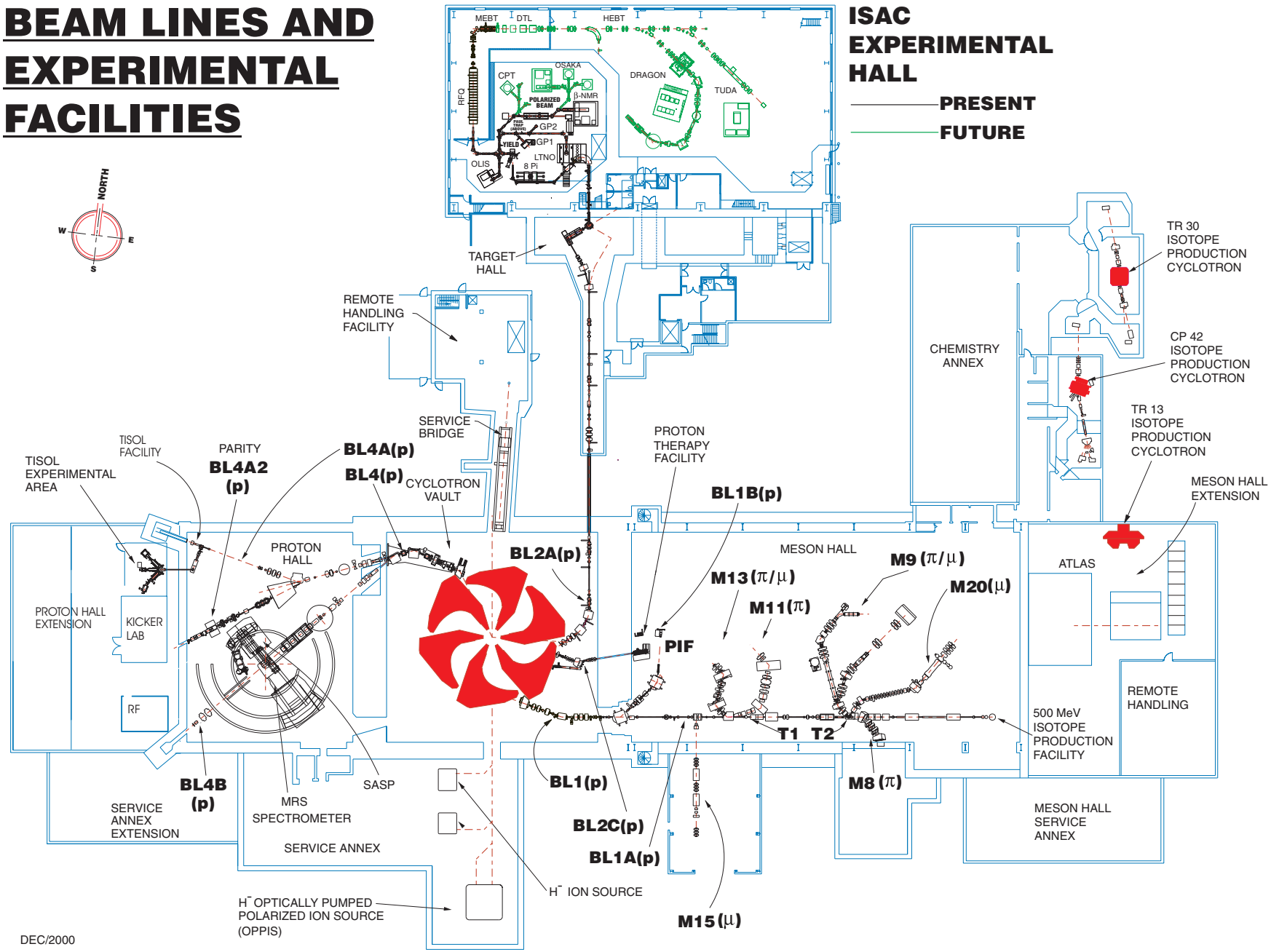

The contributions on individual experiments in this report are outlines intended to demonstrate the extent of scientific activity at TRIUMF during the past year. The outlines are not publications and often contain preliminary results not intended, or not yet ready, for publication. Material from these reports should not be reproduced or quoted without permission from the authors.

FOREWORD

I am delighted to report that the year 2000 was one of exceptional achievement for TRIUMF.

This was clearly reflected in the announcement by the federal government that our funding for 2000–2005 would be $200 million, a remarkable 20% increase over our previous level of funding. This represented a strong vote of confidence in TRIUMF by the federal government and recognised the successful construction and commissioning of ISAC-I, our success in the continuing provision of Canada's contribution to the LHC at CERN and our strong commitment to providing infrastructure support to subatomic physics across Canada.

I had the privilege of visiting CERN in the summer of 2000 and seeing first-hand the nature of our LHC contribution and can report on the very high regard in which TRIUMF is held by CERN.

With the announcement of our renewed funding, the Joint Venture Agreement was revised and updated to allow the admission of Carleton University as a full member of TRIUMF. Carleton became the first full member to join TRIUMF in over 25 years and TRIUMF will be strengthened considerably by their presence. It was also necessary for the full member universities to sign a new Contribution Agreement with the National Research Council formalising the laboratory's responsibilities under the new funding envelope. The Board is grateful to the universities for their support and cooperation in acting expeditiously, both on the Joint Venture and the Contribution Agreement.

During 2000, the search for a new Director to replace Alan Astbury in September of 2001 was concluded and the Board was very pleased to appoint Dr. Alan Shotter of the University of Edinburgh as the incoming Director. The Board certainly looks forward to working closely with Alan Shotter in the coming years.

In closing, I would like to recognise on behalf of the Board the commitment and the quality of the contribution of all of the TRIUMF staff, of the Division Heads and of the Director, Alan Astbury, and the outstanding record of achievement of the last six years. In particular, Alan Astbury has brought to TRIUMF a leadership and a vision that has raised the laboratory to true national stature and when he steps down in September 2001 he will leave the enviable legacy of a laboratory which is achieving at the highest levels and which has remarkable promise for the future. We, and indeed Canadian science, owe him a debt of gratitude.

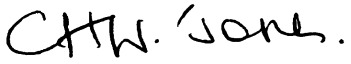

C.H.W. Jones
Chair, Board of Management

TRIUMF was established in 1968 as a laboratory operated by the University of Alberta, the University of British Columbia, Simon Fraser University and the University of Victoria under a contribution agreement from the National Research Council of Canada. The initial consortium has been expanded to include Carleton University as a full member, and the University of Manitoba, the Université de Montréal, Queen's University, the University of Regina and the University of Toronto as associate members. The facility is operated for all Canadian as well as foreign users.

The experimental program is based on a cyclotron which is capable of producing four simultaneous beams of protons, two of which are individually variable in energy from 180–520 MeV, the third from 472–510 MeV, and the fourth between 70 and 110 MeV. The potential for high beam currents – 100 μA at 500 MeV to 300 μA at 400 MeV – qualified this machine as a "meson factory". The third high intensity beam line feeds the new isotope production facility, ISAC, which started operation in 1998 and qualifies as a second generation radioactive beam facility.

Fields of research include basic science, such as particle physics, nuclear physics, nuclear astrophysics, and condensed matter research, as well as life sciences based primarily on isotope research. There is also a biomedical research facility which uses protons for treatment of ocular melanomae. TRIUMF is providing the Canadian contribution to the Large Hadron Collider at CERN and TRIUMF resources are also available to support the Canadian subatomic program at other laboratories.

The ground for the main facility, located on the UBC campus, was broken in 1970. Assembly of the cyclotron started in 1971. The machine produced its first full-energy beam in 1974 and its full current in 1977.

The laboratory employs approximately 325 staff at the main site in Vancouver and 19 based at the participating universities. The number of university scientists, graduate students and support staff associated with the present scientific program is about 625.

CONTENTS

INTRODUCTION 1

SCIENCE DIVISION 3

Introduction and Overview 3
Particle Physics 5
(Expt. 497) Measurement of the flavour conserving hadronic weak interaction 5
(Expt. 614) Precision measurement of the Michel parameters from muon decay 10
(Expt. 761) Measurement of parity violation in pp scattering at 221 MeV 14
(ATLAS) The ATLAS experiment at the LHC 18
(BaBar) The BaBar experiment at the Stanford Linear Accelerator Center 20
(BNL 787/949) Measurement of $K^+ \to \pi^+ \nu\bar{\nu}$ and other rare decays 22
(BNL KOPIO) Measurement of $K_L^0 \to \pi^0 \nu\bar{\nu}$ and other rare decays 23
(HERMES) The HERMES experiment 26
(KEK 246) Search for T-violation in $K_{\mu 3}$ decay 29
(TJNAF 00-006) Measurement of the flavour singlet form factors of the proton ($G\emptyset$) 30
Nuclear and Atomic Physics 35
(Expt. 704) Charge symmetry breaking in $np \to d\pi^0$ close to threshold 35
(Expt. 715) Weak interaction symmetries in β^+ decay of optically trapped $^{37,\,38m}$K 39
(Expt. 741) Beta-delayed proton decay of ^{17}Ne to α-emitting states in ^{16}O 43
(Expt. 778) $\pi^{\pm} p$ differential cross sections in the region of Coulomb-nuclear interference 46
(Expt. 801) Studies of multi-phonon states via β-decay 47
(Expt. 812) Proposed study of the ^{8}Li$(\alpha, n)^{11}$B reaction 48
(Expt. 823) Pure Fermi decay in medium mass nuclei 49
(Expt. 826) Studies of ultra-thin magnetic films with implanted isotopes 51
(Expt. 838/864) Double radiative decay of pionic atoms 52
(Expt. 863) Ground state magnetic moments of $^{75,\,77,\,79}$Ga (LTNO) 53
(Expt. 869) Pion charge exchange at low energies 53
(Expt. 875) Muon scattering in low Z materials for muon cooling studies 54
(Expt. 880) Ortho-para effect of muon catalyzed fusion in solid deuterium 57
Chemistry and Solid-State Physics 59
(Expt. 684) μSR spin relaxation studies of small molecules in the gas phase 59
(Expt. 749) Muonium-substituted free radicals 59
(Expt. 768) Generalized FFLO state and anomaly of flux line lattice state in novel superconductors 60
(Expt. 774) Muon charge state dynamics in LPE GaAs 61
(Expt. 776) Rare-earth materials with disordered spin structures 62
(Expt. 777) Vortex state of s-wave superconductors investigated by muon spin rotation 62
(Expt. 782) Non-fermi-liquid behaviour and other novel phenomena in heavy-fermion alloys 64
(Expt. 783) Paramagnetic frequency shifts in unconventional superconductors 66
(Expt. 784) μSR studies of spin-singlet states in oxides 67
(Expt. 791) Electronic structure and dynamics of charged muonium centres in semiconductors 68
(Expt. 804) Muonium in gallium nitride 69
(Expt. 814) μSR studies of unconventional superconductivity in Sr_2RuO_4 71
(Expt. 834) μSR study of transverse spin freezing in bond-frustrated magnets 73
(Expt. 835) μSR studies on magnetic properties of layered superconductors HfNCl and ZrNCl 74
(Expt. 842) Muonium-substituted free radicals in sub- and supercritical water 75
(Expt. 846) Complex order parameter symmetry in $YBa_2Cu_3O_{7-\delta}$ at low T and high magnetic field 76
(Expt. 847) Electron-doped high-T_c superconductors 77
(Expt. 849) Static magnetism in stage-4 $La_2CuO_{4.12}$ and $La_{1.88}Sr_{0.12}CuO_4$ 78
(Expt. 852) Magnetic phases in geometrically frustrated rare earth pyrochlores 79
(Expt. 860) Mass and charge transport in disordered media: orientational glasses 84
(Expt. 876) Disordered magnetism near magnetic instabilities in f-electron materials 87
(Expt. 882) μSR studies of unconventional superconductivity in an organic superconductor $(TMTSF)_2ClO_4$ 89

Life Sciences 91
Introduction 91
(Expt. LS0) PET facilities 91
(Expt. LS2) Synthesis of radiohalogenated carbohydrates for use as imaging agents in PET and SPECT 92
(Expt. LS3) Synthesis of radiopharmaceuticals for positron emission tomography 93
(Expt. LS4) Targets for PET radioisotope production 94
(Expt. LS8) Radiotracers for the physical and biosciences 94
(Expt. LS10) Aptamer imaging agents 96
(Expt. LS29) Production and distribution of FDG for clinical studies 97
(Expt. LS32) ^{18}F-H_2O to the University of Alberta 97
(Expt. LS33) Evaluation and improvement of a dual head coincidence camera 97
(Expt. LS35) Development of ^{18}F labelled nitroimidazole PET imaging agents for tissue hypoxia 97
(Expt. LS37) ^{125}Xe implantation as a source for ^{125}I brachytherapy 98
(Expt. LS38) Dopaminergic tracers kinetic modelling with minimally invasive scanning procedures 98
(Expt. LS39) PET (profiling) for pulp and paper 100
(Expt. LS42) Configuration modelling and image reconstruction studies on a depth encoding research tomograph 100
Theoretical Program 101
Introduction 101
Nuclear Structure and Reactions, Nuclear Astrophysics 101
Few-Body and Medium Energy Processes 103
Effective Field Theories and Chiral Perturbation Theory 106
Hadronic Structure and QCD 108
The Standard Model and Beyond 110
Miscellaneous 111
Experimental Facilities 112
Proton Irradiation Facility 112
Proton Therapy Facility 112
μSR User Facility 112
Beam Lines 114
Cryogenic Targets 114
Computing Services 114
Data Acquisition Systems 117
Detector Facility 119
GEANT4 119
Scientific Services 120
Sudbury Neutrino Observatory 122
Expt. 715 Off-Line; Precision Optical Pumping 123
β-Detected Nuclear Magnetic Resonance at ISAC 124
Nuclear Astrophysics with DRAGON at ISAC 127
8π Spectrometer 130
Low Temperature Nuclear Orientation 130
Experiments 870, 874, 879, 900 “TUDA” 131

CYCLOTRON OPERATIONS DIVISION 133

Introduction 133
Beam Production 133
Winter Shutdown 138
Beam Schedule 97 138
Fall Shutdown 139
Beam Schedule 98 139
High-Current Beam Development 140
Radio Frequency Systems 140

RF Operations 140
RF Support 140
Radio Frequency Controls 141
Cyclotron Probes and Diagnostics 141
ISAC Diagnostics 141
Probes MRO 141
Monitor MRO 141
Probes and Diagnostics: Developments and Upgrades 142
Vacuum and Engineering Physics 143
Vacuum 143
Engineering Physics 143
ISIS and POLISIS 143
Primary Beam Lines 143
2C 144
Controls 145
CCS Facilities 145
Other Systems 146
Miscellaneous 146
Operational Services 146
Remote Handling 146
Magnet Power Supplies 147
Electrical Engineering Services 147
Electrical Systems 147
Power Delivery 148
Mechanical Systems 149

ISAC PROJECT 150

Introduction 150
ISAC Operations 150
ISAC Beam Statistics for Beam Schedules 97 and 98 151
Conventional Facilities and Infrastructures 153
Building Services 153
Electrical Services 153
Mechanical Services 153
Safety and Radiation Control 154
Licensing 154
Access Control and Radiation Monitoring 154
Commissioning 154
Remote Handling Group 154
ISAC Target Modules 154
Target Hall 154
Beam Lines Servicing 154
Hot Cell Facility 154
Remote Crane Handling System 155
Ion Sources for ISAC 155
Electron Cyclotron Resonance (ECR) Source 155
Off-Line Ion Source (OLIS) 155
Charge State Booster (CSB) 155
ISAC Targets 155
ISAC Polarizer 156
Engineering 157
RF Systems 158
RFQ 158
MEBT 158

DTL 159
HEBT 160
RF Controls 162
ISAC Accelerator Commissioning 162
Test #2 162
Test #3 163
Test #4 166
ISAC Controls 166
Hardware 166
Software 167
Commissioning and Operation 167
ISAC Diagnostics 168
ISAC-II Accelerator Studies 169
Multi-Charge Acceleration 169
Hardware Studies 173
ISAC Planning 174
Target Areas and Hot Cells 174
MEBT 174
DTL Systems 174
HEBT 174
Low Energy Experiments 175
High Energy Experiments 175
DRAGON 175
ISAC-II 175
Contract Administration 175
Personnel Resources 175

ACCELERATOR TECHNOLOGY DIVISION 178

Introduction 178
Beam Dynamics 178
CERN Neutrino Factory Proton Driver 178
Micro-Bunching at Brookhaven AGS 179
Space-Charge Compensation with Electron Lenses at the Fermilab Booster 179
Magnets 180
ISAC 180
Experiment 614 – TWIST 180
Kickers 180
Magnet Measurements 181
Mechanical Engineering 181
ISAC 181
Engineering – Other 183
ATLAS – University of Victoria 184
Planning 185
ISAC 185
CERN 186
Shutdown Activities 186
TWIST (Expt. 614) 186
Design Office 186
Machine Shop 186
Building Program 187
Electronics Services 187
Overview 187
Technical Support 187
Experimental and Target Support 187

Electronics Shop ... 187
Electronics Repair Shop ... 188
High Level Software Support ... 188
PC Support – Hardware ... 188
PC Support – Systems ... 188
Communications Support ... 188
Electronics Development ... 188
ISAC Support ... 188
CERN ... 189
Miscellaneous ... 189

CERN COLLABORATION ... 190

Introduction ... 190
Beam Dynamics ... 190
Second Harmonic in the PS Booster ... 190
Injection and Collimation in the PSB ... 191
Beam Stability ... 191
Beam Optics and Collimation ... 192
Controls and Instrumentation ... 192
Fast Blade Scanner ... 192
Fast Wire Scanner ... 193
LHC Orbit System Components ... 193
Power Supplies ... 194
Booster Transfer Line Power Supplies ... 194
Magnet Development ... 195
Kicker Magnets ... 195

TECHNOLOGY TRANSFER DIVISION ... 198

Introduction ... 198
Technology Transfer ... 198
Applied Technology Group ... 198
500 MeV Isotope Production Facility ... 198
CP42 Facility ... 198
TR30 Facility ... 198
ATG Development Projects ... 198
Radioisotope Processing (MDS Nordion) ... 198

ADMINISTRATION DIVISION ... 201

Introduction ... 201
Human Resources and Administration ... 201
Operational Safety ... 201
AECB/CNSC Licensing ... 201
Training ... 201
Occupational Health and Safety ... 202
Interlocks and Monitoring ... 202
Personnel Dosimetry ... 202
Administration Computing ... 202
Data Processing ... 202
Word Processing ... 203
Telephones ... 203

CONFERENCES, WORKSHOPS AND MEETINGS 204

ORGANIZATION 207

APPENDICES

A. Publications 210
B. Seminars 228
C. Users Groups 230
D. Experiment Proposals 232
E. Life Sciences Project Proposals 244

INTRODUCTION

The millennium year 2000 proved to be appropriately a banner year for TRIUMF. In February, with its "Budget 2000", the federal government announced a funding package of $200M for TRIUMF, to cover the five years 2000–2005. This amount represents a 20% increase over the level which had prevailed for the previous quinquennium. The staff of the laboratory are to be congratulated, since the new figure signifies a solid vote of confidence from the federal government for a facility which has truly become Canada's National Laboratory for Particle and Nuclear Physics. However a word of caution is in order. A 20% increase is always very welcome, but TRIUMF has very ambitious plans, particularly for capital expenditure, and some priority decisions will be required, between ISAC-II – an upgrade of ISAC-I to an energy of 6.5 MeV/u – and a continuation of the contribution on behalf of Canada to the Large Hadron Collider (LHC) at the high level anticipated by CERN. One thing is clear, the main Canadian responsibilities to LHC can be discharged, but no new opportunities can be explored.

The proposal for ISAC-II has now become a reality. Its realization will open up the experimental program with ISAC to nuclear physics with ions of 6.5 MeV/u, an energy comfortably above the Coulomb barrier. The immediate issue became the acquisition from the BC provincial government of the money required for the civil construction associated with ISAC-II. An application was made to the BC Knowledge Development Fund, and December brought the news of an award of $8.7M. TRIUMF now has all the pieces in hand to move forward to the realization of one of the best centres in the world for science with exotic radioactive ion beams. This is a dramatic turnaround from the possibilities which confronted the laboratory in the dark days of February 1994 after the refusal of the KAON proposal.

The program of science using ISAC-I at low energies begins to take shape. The electron-neutrino correlation in the β-decay of ^{38m}K is being studied in the TRIUMF neutral atom trap (TRINAT) as a means of revealing a possible level of a heretofore undetected scalar coupling in the weak interaction. This low energy study will be complementary to the high energy particle searches for S=0 leptoquarks in the DØ experiment at Fermilab and at HERA. The historic series of measurements on superallowed Fermi β-decay transitions can be extended to include ^{74}Rb, which proves to be an excellent nucleus in which to test theoretical models. The ISAC results have so far yielded the best estimate of the half-life and branching ratio of ^{74}Rb, two vital ingredients for the determination of the transition rate. In July polarization was achieved in a ^{8}Li beam, and with the target sample placed at high voltage a "soft landing" was achieved also. The β-decay of the ^{8}Li yields a unique probe in condensed matter physics, especially in the study of surface phenomena. Several other experiments are beginning to come online, and the richness of the science with low energy ion beams becomes very evident.

TWIST is the flagship experiment of the subatomic program based on the 500 MeV cyclotron. The decay parameters of the muon are being revisited in a precision test of the theory of the weak interaction. The targeted accuracy is roughly a part in ten thousand, which represents a gain of a factor of ten over previous results. This is a very difficult task, and will in essence represent a tour de force in the understanding of systematic errors. The experiment moved on to the floor late in the year and ambitiously projects a run with all equipment installed within one year.

TRIUMF continues to provide contributions to the LHC in CERN on behalf of Canada. The new funding level permits the provision of the equipment for which TRIUMF had previously assumed technical responsibility. The initial phase of the project, which was dedicated to the upgrading of the CERN PS complex, has been successfully completed, and the PS has operated with a beam of appropriate brightness for injection into the LHC. TRIUMF had a major role in this upgrade. Now the responsibilities move into the LHC itself, where they concentrate on two main components – the injection kicker magnets and warm quadrupoles. The provision of power supplies and pulse forming networks for the injection kickers are well in hand. The warm quadrupoles which will carry the counter rotating proton beams through the LHC cleaning insertions have not yet been realized. The prototype, produced in 1998, indicated that in order to achieve the desired quality of magnetic field, the mechanical tolerances would have to be tightened by about a factor of five to $\sim$100 μm in the placement of laminations. This requirement makes these quadrupoles the most mechanically precise warm magnets in the project. The company selected for the series production of the magnets is ALSTOM of Montreal. They appear to have the capability to deliver the product, but the successful series production has yet to be established.

A large international community uses the TRIUMF muon beams for experimental work in chemistry and condensed matter using the technique known as μSR. This year they have been joined by a group from the Rutherford Appleton Laboratory in a project known as MuScat. In the world of high energy physics, some very

forward looking proposals aim to employ stored muons as an intense source of neutrinos in complexes which are becoming known as "neutrino factories". In order to make these proposals practical, muons must be produced, trapped, and their phase space cooled before rapid acceleration to the stored energy. An old measurement has cast doubt on the validity of the theory of large angle multiple scattering of muons at low energies. MuScat will provide a practical answer by measuring the scattering process in the laboratory, yielding an important piece of input into the design of a neutrino factory.

TRIUMF is providing infrastructure support to a number of experiments within the Canadian program in subatomic physics in concert with the NSERC Grant Selection Committee. The production in TRIUMF of modules for the ATLAS HEC calorimeter proceeds smoothly and is keeping to its timescales. The laboratory also has significant involvement in the feedthrough project at the University of Victoria, where signal feedthroughs are now in production for the ATLAS HEC calorimeter. At Brookhaven, experiment E787 has been upgraded significantly and has emerged as E949, which will endeavour to collect $\sim$10 decays of $K^+ \to \pi^+ \nu\bar{\nu}$; a very ambitious project working with a branching ratio of $\sim 10^{-10}$. TRIUMF has provided apparatus for the $G\emptyset$ experiment at TJNAF, HERMES at HERA, and SNO. Additionally, a small group in TRIUMF provides ongoing collaborative effort in the global GEANT 4 project.

The PET component of the Life Sciences program achieved an outstanding success in obtaining the funds for a new state-of-the-art PET camera which will be installed at the Neurodegenerative Disorders Centre at the UBC Hospital. The money came from three sources: the Canadian Foundation for Innovation, the Canadian Institutes of Health Research, and the BC provincial government. In addition the TRIUMF/UBC PET group assured renewed funding for a five year term, putting the group on a very solid financial footing.

The Year 2000 ended on a very high note. On December 21, one day before the laboratory closed for Christmas, the ISAC team accelerated alpha particles to 1.5 MeV/u. The milestone had been promised some two years earlier and was gratifyingly passed, albeit in the "nick of time". The outstanding success of accelerated beam means that TRIUMF can anticipate commencing an experimental program in nuclear astrophysics during the year 2001. This will be an exciting period and should place TRIUMF on the world map with a number of unique measurements.

A. Astbury,
Director

SCIENCE DIVISION

INTRODUCTION AND OVERVIEW

The previous millennium ended on an excellent note for the Science Division with several notable achievements, as reported in this Annual Report. Just before closing year 2000, the full accelerator complex of ISAC delivered its first (stable) beam. This is the culmination of a four-year effort to develop a radioactive beam facility at TRIUMF which should trigger the data-taking phase of the nuclear astrophysics program next year.

On the way to that, ISAC has produced its first publication in Physics Review Letters from an experiment in the low energy area which measured the lifetime of the short lived ^{74}Rb isotope. Several beams were developed and provided to experiments in the low energy area. Experiment 715 completed its data-taking on the beta-neutrino correlation in the decay of ^{38m}K using the TRINAT facility. With an improved control of the systematic effects, a preliminary test of the standard model was obtained at the 0.5% precision level. Polarization of a ^{8}Li beam was observed and a soft landing test was realized at the beginning of July demonstrating that all the tools are in place to start a condensed matter program with light polarized ions. There is still some more commissioning to go through before routine high polarization operation can be achieved, but all the signs are encouraging and new proposals are being developed. The low temperature nuclear orientation fridge (LTNO) operated several times at temperatures well below 10 mK. Polarization was achieved for implanted ^{79}Rb ions; however, the test NMRON experiment was not successful and there may be good physics reasons for the non-observation of the resonance at the previously predicted location. The tape transport system used for the studies of ^{74}Rb was also used by the Yale group to search for multi-phonon excitations of deformed nuclei in the Er region.

There is also very good progress reported on the preparation for the nuclear astrophysics program, which is the ultimate objective for ISAC-I. The TUDA facility was completed and is ready to accept accelerated beam, while the DRAGON recoil spectrometer was entering its commissioning phase.

The visibility of ISAC has improved considerably and the large number of new proposals being submitted to our Experiments Evaluation Committee is a good measure of the attractiveness of our new facility. This in turn is placing great pressure on our ability to respond to users' requests so, late in the year, it was decided to change our priority to emphasize versatility and reliability rather than pushing on high intensity right away. The new east target station for ISAC has become a high priority item for 2001.

In the base program, our major effort is to install the spectrometer for the TWIST experiment (Expt. 614) which is aimed at a precision measurement of the Michel parameters describing the decay of polarized muons. The magnet, including the superconducting coil and its return yoke, made it to the M13 beam line by Christmas and the production and testing of the 52 high precision drift chambers is well under way. The first half of the tracking system should see beam in the spring of 2001.

Several experiments are in the final stages of analysis. The parity experiment produced its first preliminary result on the asymmetry in polarized proton scattering from protons at 221 MeV. The current precision is at the 3×10^{-8} level and shows a small positive effect. The analysis of the full data set is still in progress. The charge symmetry experiment (Expt. 704) is also in the final stages of the analysis and one can expect a result soon in the new year. A detailed study of the SASP spectrometer acceptance has been necessary and its dependence on the source size is such that one has to rely on the elastic scattering data to validate its simulation. CHAOS completed its data-taking for Expt. 778, the Coulomb nuclear interference experiment in low energy elastic pion scattering, which ran in both M13 and M11. The RMC spectrometer was also active with data-taking on the two-photon radiative capture reactions which could access the pion Compton scattering amplitudes. A collaboration from the UK and TRIUMF took data on the multiple scattering of low energy muons from light targets. This was a preliminary study to assess the feasibility of performing such a test on hydrogen targets, to validate the studies on cooling of muon beams in future muon colliders.

The condensed matter program was also very active, occupying two or three beam lines for most of the seven months of high intensity running. The main themes remain superconductivity and exotic superconductors, magnetism, behaviour of impurities in semiconductors, with a small program in chemistry on free radicals, supercritical water and gas phase reaction rates.

The life sciences program is also in good health and received a major grant from the Canadian Foundation for Innovation to purchase a new state-of-the-art PET tomograph. The demand for isotopes and for radiopharmaceuticals is increasing, as is the acceptance of PET as a clinical tool, placing a heavy load on our production facilities and crew. More efficient produc-

tion of ^{18}F is being tested to alleviate such problems. Several high purity ^{7}Be targets were also produced and delivered to the University of Washington for the measurement of $^{7}\mathrm{Be}(p,\gamma)^{8}\mathrm{B}$. Preliminary data are available for energies around the resonance at 640 keV. A new phase to push the study towards much lower energies is starting.

A unique program runs at the UBC Botany Department based on the availability of ^{13}N from TRIUMF. This has been recognized internationally as a golden opportunity to study the dynamics of nitrogen uptake in plants. Several major publications resulted from this program this year and the prospects of extending the research to potassium uptake studies with ^{42}K isotopes produced at ISAC are very good.

Our Theory group, built around four staff members, is very active on many fronts thanks to a young group of eight research associates who rotate on a two-year cycle, allowing for wide coverage of theoretical questions. Linkages with the experimental program are sought-after in the hiring of these research associates. Currently the Theory group provides support for the radiative pion capture program, the $^{7}\mathrm{Be}(p,\gamma)$ experiment, and the weak decay studies.

A significant part of TRIUMF's activities is the support of experiments abroad for the benefit of Canadian researchers. The most visible effort at present is the construction of the Canadian contribution to the ATLAS detector at CERN. The hadronic end-cap calorimeter modules are being shipped regularly to CERN and this will continue for the next year-and-a-half. In Victoria, the project to provide the feedthrough connectors for the liquid argon vessel is well under way. TRIUMF's infrastructure is used to support an experiment at the Brookhaven AGS accelerator searching for rare decays of kaons, and to build components of a parity experiment in electron-proton scattering at the Thomas Jefferson National Accelerator Facility.

When you add the support from the service groups, you realize how effective the TRIUMF team can be at delivering science at an international level. This team spirit is key to being able to compete and the laboratory has now built a very strong, cohesive approach to science with the resulting focus and timely delivery which we can be proud of.

PARTICLE PHYSICS

Experiment 497
Measurement of the flavour conserving hadronic weak interaction

(J. Birchall, S.A. Page, W.T.H. van Oers, Manitoba)

The parity violation experiment [Page *et al.*, Expt. 497 (1987)] completed data-taking at 221 MeV in 1999. During the past year, Jason Bland has been working intensively on data analysis for his M.Sc. thesis (Manitoba). At the time of writing, the 1999 data set has been completely analyzed, and a reanalysis of the 1998 and 1997 data is under way to ensure that all data sets are treated in a common framework in preparation for a final publication.

The experiment is to determine the parity-violating longitudinal analyzing power in *pp* elastic scattering, $A_z = (\sigma^+ - \sigma^-)/(\sigma^+ + \sigma^-)$, where σ^+ and σ^- are the scattering cross sections for positive and negative helicity. The aim of the experiment is to measure A_z with a precision of $\pm 0.3 \times 10^{-7}$. The measurements are performed in transmission geometry, with beam energy and detector geometries selected to ensure that only parity mixing in the $^3P_2 - ^1D_2$ partial wave amplitude contributes to the measured parity violating asymmetry [Simonius, Can. J. Phys. **66**, 548 (1988)]. This amplitude has never been studied experimentally, and the possibility is unique to the energy regime accessible with the TRIUMF cyclotron. In the context of the weak meson exchange model [Desplanques *et al.*, Ann. Phys. (N.Y.) **124**, 449 (1980)], our measurement of A_z will provide a direct determination of the weak ρ-nucleon coupling constant $h_\rho^{pp} = (h_\rho^0 + h_\rho^1 + h_\rho^2/\sqrt{6})$. Recent experimental and theoretical developments confirm the importance of achieving high quality results from the TRIUMF experiment; a measurement of A_z at 13.6 MeV ($-0.93 \pm 0.20 \pm 0.05 \times 10^{-7}$) has reached the high level of accuracy reported earlier by the SIN group at 45 MeV [Eversheim *et al.*, Phys. Lett. **B256**, 11 (1991); private communication (1994); Kistryn *et al.*, Phys. Rev. Lett. **58**, 1616 (1987)].

A major effort to minimize and understand systematic error contributions is required to successfully perform an experiment to this level of precision. The first significant data set for Expt. 497 was acquired in February, 1997, with a statistical error of $\pm 0.5 \times 10^{-7}$ and most systematic errors at or below the 10^{-7} level. That result represented a major milestone for the experiment, the culmination of many years of effort to reduce both the helicity correlated beam modulations Δx_i and the sensitivities $\frac{\partial A_z}{\partial x_i}$. Data-taking continued with 3 more month-long runs during 1998 and 1999.

Beam line and instrumentation

In addition to the measuring apparatus, the TRIUMF optically pumped polarized ion source (OPPIS), cyclotron, and transport beam lines are critical components of the experimental set-up (see Fig. 1).

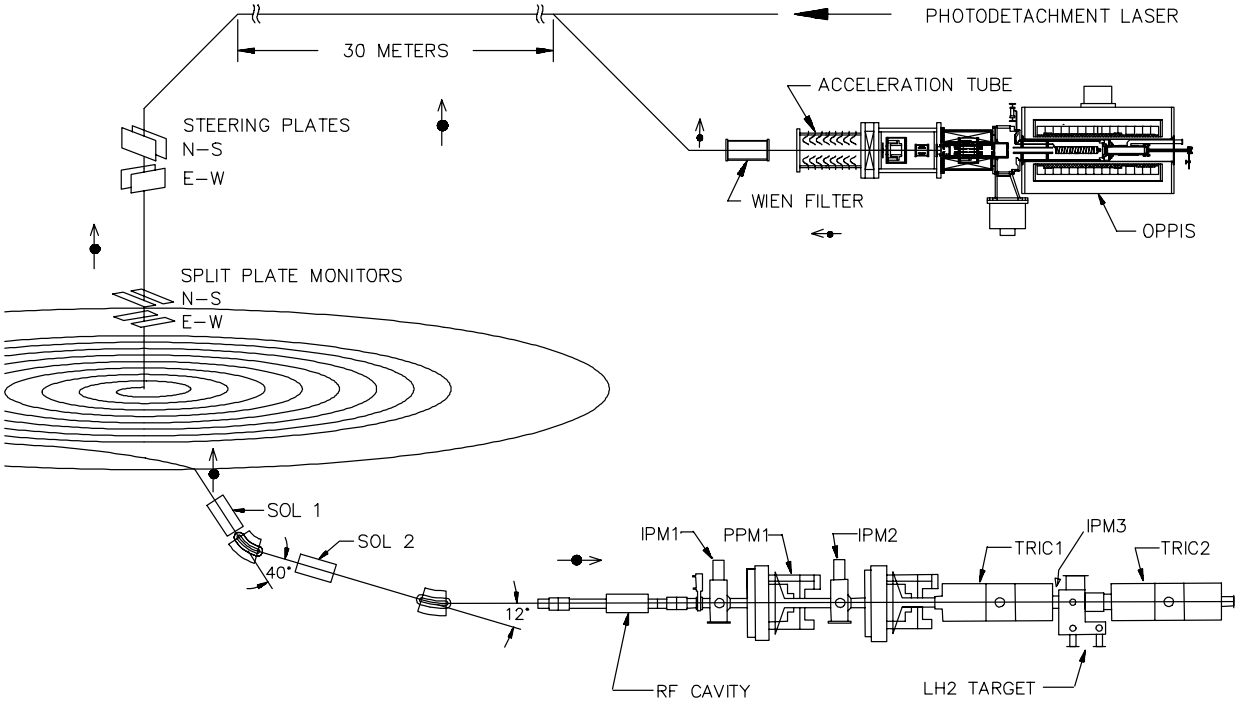

Fig. 1. General layout of TRIUMF parity experiment. (OPPIS: optically pumped polarized ion source; SOL: spin precession solenoid; IPM: intensity profile monitor; PPM: polarization profile monitor; TRIC: transverse field ionization chamber.)

A 5 μA transversely polarized beam is transported to the cyclotron through an approximately 50 m long injection beam line. The ion source Wien filter is tuned to produce vertical polarization at the entrance to the cyclotron. A 200 nA beam at 75–80% vertical polarization is extracted at 221 MeV. Spin precession through a pair of solenoid and dipole magnets results in delivery of a longitudinally polarized beam to the 40 cm long liquid hydrogen target, which scatters 4% of the beam. Note that there are two complementary states of the spin transport, so-called "positive helicity" and "negative helicity" beam line tunes, which transport spin up in the cyclotron into either + or − helicity at the parity apparatus. Half the data are acquired in each of these two beam line tune states, and consistency of the results in the two cases allows limits to be placed on systematic errors associated with the ion source alone, e.g. beam energy modulation, as discussed further below.

The custom-built parity instrumentation occupies approximately 8 m of beam line downstream between the last dipole magnet and the beam dump in the TRIUMF proton hall (beam line 4A/2). Transverse field parallel plate ion chambers TRIC1 and TRIC2 measure the beam current incident on and transmitted through the target. The parity violation signal is derived from the helicity-correlated analogue signal difference between the beam currents measured by the two TRICs. Upstream of the target are two polarization profile monitors (PPMs) to measure the distributions of transverse polarization $P_y(x)$ and $P_x(y)$ across the beam. Two intensity profile monitors (IPMs) measure the intensity distribution of beam current in x and y and are coupled to a pair of servo magnets which lock the beam path on the optimum axis through the equipment.

Major data sets

The full parity data set now consists of four major (1 month) data runs taken in February, 1997, in December, 1997–January, 1998, July–August, 1998, and May–June, 1999. These runs have a raw statistical error of approximately $\pm 0.4 \times 10^{-7}$ each. Systematic error corrections limit the precision of the overall result in all cases. A major effort has been under way to analyze the recent data sets, and preliminary results are summarized below. All but the May–June, 1999 data set have been extensively discussed in previous progress reports; a detailed analysis of the 1999 data set has been the focus of attention for the past year and is summarized in Table I.

The longitudinal analyzing power A_z is deduced from each 8-state data cycle by forming the helicity-correlated digitized TRIC difference signal, multiplied by a scale factor appropriate to the electronic and gas gains etc., and divided by the average incident beam current measured by TRIC1. Random beam and cyclotron instabilities are responsible for a large part of the width of this distribution (the normal "counting statistics" contribution is negligible), which is minimized by aligning the beam along the symmetry or "neutral axis" of the apparatus and ensuring that the two TRICs are as identical as possible in their response to the beam. Helicity-correlated changes in beam properties other than longitudinal polarization give rise to systematic errors which shift the mean of the A_z distribution away from zero; these errors are studied in a series of calibration measurements in which small spin-state-correlated modulations of beam current, energy, position, angle, and transverse polarization are purposely introduced. Interspersed data acquired in the frequent spin-off cycles provide an important zero asymmetry check of the apparatus and electronics.

Table I. Summary of the major parity data sets. χ^2/df is given for the corrected data. Each set consists of 8–10 subsets taken with alternating beam line helicity tunes. References are: 1. Hamian, Ph.D. (1998); 2. TRIUMF Annual Report (1999); 3. TRIUMF Annual Report (1999); 4. J. Bland, private communication.

Data Set	Raw A_z (10^{-7})	Corrected A_z (10^{-7})	χ^2/df
Feb. 1997[1]	1.1 ± 0.5	0.33 ± 0.65	0.5
Dec. 1997[2]	1.8 ± 0.4	0.8 ± 1.8	0.8
July 1998[3]	1.6 ± 0.3	0.9 ± 0.5	1.1
June 1999[4]	1.4 ± 0.4	1.1 ± 0.6	1.4

The dominant correction to all data sets is due to the **intrinsic** moments of transverse polarization $\langle xP_y \rangle$ and $\langle yP_x \rangle$ resulting from a non-uniform distribution of transverse polarization within the beam envelope, as distinct from the corresponding **extrinsic** polarization moments $\langle x \rangle \langle P_y \rangle$ and $\langle y \rangle \langle P_x \rangle$ which arise when a beam with finite transverse polarization is displaced from the polarization neutral axis.

The uncertainties quoted in Table I for the 4 major data sets represent a quadrature sum of statistical and systematic contributions. These are indicated separately in Table II. The statistical error includes the uncertainty in the systematic error correction ΔA_z due to the spread of the helicity correlated beam property measurements, but is dominated by the spread of the raw A_z values. The systematic error, since it is due almost entirely to the uncertainty in the intrinsic first moment sensitivities as determined from the regression analysis of the parity data, is in fact statistics dominated.

Table II. Statistical and systematic error contributions to the major parity data sets (in units of (10^{-7})). The first error is derived from the standard deviation of the corrected A_z distribution ("statistical") and the second is the contribution from the uncertainties in the sensitivity coefficients ("systematic") with first moment sensitivities derived from a regression analysis as described in the text.

Data Set	Stat.	Sys.	Corrected
Feb. 1997	0.6	0.3	0.33 ± 0.65
Dec. 1997	0.4	1.8	0.8 ± 1.8
July 1998	0.3	0.3	0.9 ± 0.5
June 1999	0.5	0.2	1.1 ± 0.6

May–June, 1999 data

Nominally, Expt. 497 ran for five weeks from 19 May, 1999 to 23 June, 1999. Unfortunately, a large number of technical failures occurred which limited the quality and quantity of the polarized data that could be acquired. The most serious problem was a failure of the ion source microwave generator, which was repaired but did not function reliably at full power for the remainder of the run, and this caused problems for the beam stability. The ion source problems were followed by a major rf spark which destroyed some high voltage components that had to be fabricated on site by the RF group, losing 5 days of beam time. Unfortunately the rf was very unstable following this repair, and this too had a major effect on the beam quality for the subsequent data-taking – the statistical variation in the asymmetry signal was erratic and on the average 20% noisier than during previous data runs. In addition, the TRIC analogue subtractor unit was subject to abnormally large time drifts of the optimum dc level for common mode signal rejection, which resulted in significant corrections for helicity correlated intensity modulation and special analysis techniques had to be applied to analyze the data, as outlined below.

Time cuts and raw data reduction

In previous data runs, the noise in the TRIC asymmetry signals was roughly constant and large bodies of data could be treated as arising from the same statistical distribution. During the May–June, 1999 run, the noise in the asymmetry signals varied by up to a factor of 2 depending upon the ion source and cyclotron conditions. A conservative approach was used to exclude anomalously noisy bursts of TRIC data from the analysis, based on determining the width of the asymmetry distribution over 50-event bundles. This resulted in a rejection of 7% of the raw data set. Subsequently, the asymmetry data were calculated as a weighted average over 1000-event bundles with the error calculated from the standard deviation of each bundle. The raw data were further reduced by placing standard cuts on the position of the beam at IPMs 1 and 2 relative to the polarization neutral axis as determined from the calibration data, as well as cuts on the average beam current, size, and the size of the intrinsic polarization moments from the PPMs, which determined the largest systematic error correction. A 20% reduction in the amount of raw data resulted from the reduction process, and the χ^2/df of the raw asymmetry data improved from 22 to 5.7, prior to correcting for systematic effects.

External calibration data

As in previous data runs, considerable beam time was devoted to calibration measurements to determine the sensitivities of the apparatus to helicity correlated position, size and polarization distributions. The latter have been extensively discussed in earlier reports; here, we illustrate the quality of the position and size modulation calibration data. Note that the size modulation data are noisier, since they are obtained with the beam position feedback loops disabled (the fast dipole steering magnets are rewired as quadrupoles and are driven in phase with the spin sequence in this case).

The false analyzing power arising from helicity correlated beam position can be written in the form

$$\begin{aligned}
\Delta A_z &= \left(\frac{\Delta x_1 + \Delta x_2}{2}\right)(a_x x_1 + b_x x_2 + c_x) \\
&+ \left(\frac{\Delta x_1 - \Delta x_2}{2}\right)(d_x x_1 + e_x x_2 + f_x) \\
&+ \left(\frac{\Delta y_1 + \Delta y_2}{2}\right)(a_y y_1 + b_y y_2 + c_y) \\
&+ \left(\frac{\Delta y_1 - \Delta y_2}{2}\right)(d_y y_1 + e_y y_2 + f_y)\,. \quad (1)
\end{aligned}$$

30 calibration runs were taken to find the position modulation sensitivities ($a_x.b_x...$). Figure 2 shows two graphs of the results of the POSMOD analysis. The left graph displays measured A_z as a function of the predicted effect of position modulation as determined from the POSMOD parameter values. The right graph displays the residual from a straight line. Sensitivities were determined by MINUIT (which minimizes χ^2_ν); errors in the fitted parameters are at the $\pm 2\%$ level.

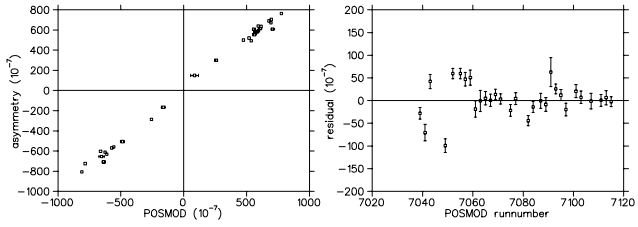

Fig. 2. (left) Measured A_z as a function of A_z predicted from position modulation, and (right) the fit residuals as a function of POSMOD run number.

The false analyzing power due to beam breathing can be expressed as:

$$\begin{aligned}\Delta A_z &= \alpha_x \sigma_{x_1} \Delta\sigma_{x_1} + \beta_x \sigma_{x_2} \Delta\sigma_{x_2} \\ &+ \alpha_y \sigma_{y_1} \Delta\sigma_{y_1} + \beta_y \sigma_{y_2} \Delta\sigma_{y_2}\,. \qquad (2)\end{aligned}$$

22 calibration runs were taken to determine the sensitivity of the parity apparatus to helicity correlated beam size modulation. The measured asymmetries were corrected for position modulation before the fit was carried out. Figure 3 shows the measured A_z values plotted against the A_z predicted from the position modulation fits. Errors in the fitted parameters of equation 2 are at the $\pm 5\%$ level.

Three sets of polarization neutral axis scans were taken to determine the sensitivities of the parity apparatus to components of transverse polarization. The neutral axis data were analyzed using a MINUIT fitting procedure to fit to equation 3, where ΔA_z is the TRIC signal asymmetry for transversely polarized beam, P_x and P_y are fractions of unity, and the positions $< y_1 >$ etc. are measured in mm at the locations of the two PPMs respectively:

$$\begin{aligned}\Delta A_z &= \langle P_x \rangle (a_1 \langle y_1 \rangle + a_2 \langle y_2 \rangle + a_3) \\ &+ \langle P_y \rangle (b_1 \langle x_1 \rangle + b_2 \langle x_2 \rangle + b_3)\,. \qquad (3)\end{aligned}$$

Fitted coefficients are in agreement with those found in previous major data sets, with error bars smaller than $\pm 1\%$.

Intrinsic first moment sensitivities

As remarked previously, the largest systematic error corrections to the parity data are those due to intrinsic first moments of polarization. The correction coefficients are most precisely determined by a regression analysis applied to the asymmetry data, as opposed to using the coefficients obtained by external calibration measurements. For the regression analysis, the input data are combined into 1000-event bundles in order to reduce the influence of the relatively large statistical uncertainties on the individual intrinsic first moment measurements from the PPMs. The bundled data are semi-corrected for all externally calibrated helicity-correlated effects, and are then analyzed to determine the intrinsic first moment sensitivities. Three different approaches were used to evaluate the intrinsic first moment sensitivities from the data. Results are in agreement in all cases with the external sensitivity scans, but with smaller error bars. The optimal sensitivities are determined to $\pm 40\%$ for $< yP_x >$ and $\pm 20\%$ for $< xP_y >$.

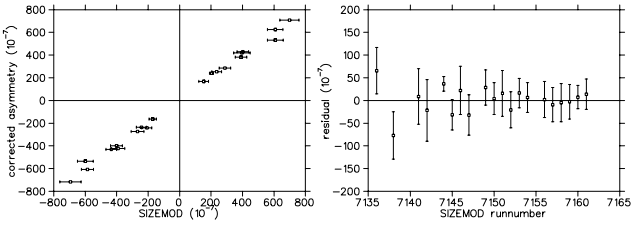

Fig. 3. (left) Corrected A_z as a function of A_z predicted from size modulation, and (right) the fit residuals as a function of SIZEMOD run number.

Helicity correlated current modulation

As noted previously, the ECR microwave tube in the ion source was not functioning properly at full power during the 1999 data run. This had the effect of introducing greater instabilities in the beam intensity than are normally experienced, and helicity-correlated current modulation was larger than usual (typically several $\times 10^{-5}$ and occasionally at the 10^{-4} level). Furthermore, the optimum dc level of the TRIC analogue subtraction unit exhibited unusually large drifts and had to be adjusted frequently during the run. These factors led to larger than usual corrections for helicity correlated current modulation, and a careful study of the sensitivities and corrections was carried out for this effect. The CIM laser which copropagates with the low energy H^- beam in the injection line provides a continuous on-line calibration of the sensitivity to current modulation. A software cut on the correction for helicity correlated current modulation was set to exclude all 2-event pairs with false effects greater than 5×10^{-7} from the data. The residual correction for $\Delta I/I$ is shown as a function of set number (alternate sets represent 2–3 days of data in different beam line helicity tunes, as noted earlier), illustrated in Fig. 4.

Reduced data set

After carrying out the analysis steps described above, a final set of cuts was applied to the data based on the absolute size of the correction to A_z on an event pair basis (recall that a minimum of 2 successive

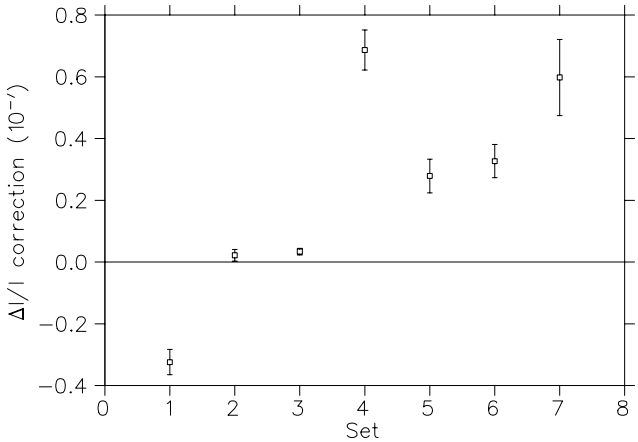

Fig. 4. $\Delta I/I$ correction as a function of set for the May, 1999 run.

$+--+-++-$ spin sequences or "events" are required to determine the polarization components and hence the corrections ΔA_z). Events were excluded with corrections more than 3 standard deviations larger than the run-averaged correction distribution. This resulted in a small reduction of the statistical uncertainty of the corrected result. Data histograms are shown in Fig. 5.

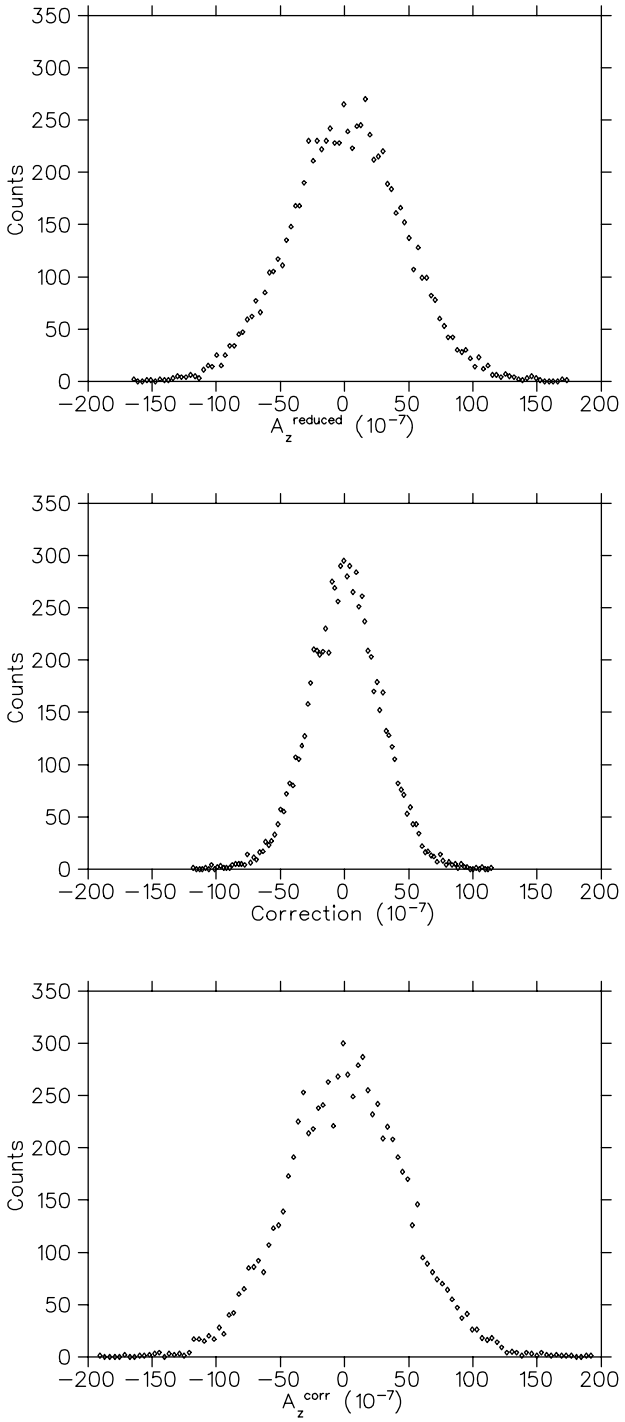

Fig. 5. (top) Histograms of $A_z^{\rm reduced}$, (centre) the correction and (bottom) $A_z^{\rm corr}$. Each event is a 100×2 ev bundle.

The final set of corrected A_z data for the 1999 run is shown in Table III.

Table III. Summary of final corrected data sets for the May, 1999 run. The values labelled "+" and "–" at the bottom of the table represent data for the two beam line helicity tunes respectively. Data are in very good agreement for the "+" and "–" cases.

Set	$A_z^{\rm corr}(10^{-7})$	2-events
1	$-1.17 \pm 1.27 \pm 0.46$	113,657
2	$1.36 \pm 1.03 \pm 0.27$	220,530
3	$3.72 \pm 1.26 \pm 0.34$	138,566
4	$1.30 \pm 1.23 \pm 0.16$	147,282
5	$1.13 \pm 1.72 \pm 0.20$	69,625
6	$-0.48 \pm 1.46 \pm 0.33$	95,045
7	$2.45 \pm 2.82 \pm 0.58$	24,402
Average (χ^2_ν)	$1.13 \pm 0.51 \pm 0.95$ (1.38)	809,107
+	$1.38 \pm 0.76 \pm 0.83$	346,250
−	$0.92 \pm 0.70 \pm 0.46$	462,857

Energy modulation

I4 $\delta A_z/\delta E$ calibration runs (where δE is intrinsic helicity-correlated energy modulation of the beam produced at the ion source) were conducted at interleaved periods of data-taking during the May, 1999 run. In each case, 1000 meV of artificially induced helicity-correlated energy modulation was applied to either of the spin "up" or spin "down" states. Roughly half of the data were taken in each beam line helicity tune. The EMOD calibration data were first corrected for position modulation, size modulation and intensity modulation, with $\Delta I/I$ sensitivities determined from regression analysis of the spin-on EMOD calibration run data, and then used to determine values of $\delta A_z/\delta E$. The positive helicity calibration results agree very well with each other, but unfortunately the negative helicity results are in poor agreement, necessitating an increase to our estimate of the largest possible sensitivity.

In addition to the energy modulation calibration runs, a number of measurements of the intrinsic laser-induced energy modulation in the polarized beam were taken during the acquisition of the parity data. Figure 6 illustrates the results of the intrinsic energy modulation measurements. An average $\delta E^{\rm eff}$ was calculated to be -15 ± 5 meV, where the uncertainty has been artificially enhanced by a factor of 2.5, and this was used to estimate the contribution of energy modulation to the parity data as shown in Table IV.

Table IV. Final summary of corrected helicity sets for the May, 1999 run divided into positive (346,250 event pairs) and negative (462,857 event pairs) beam line helicity. Numbers are in units of 10^{-7}.

Hel.	$A_z^{\rm reduced}$	$\Delta A_z^{\rm EMOD}$	$A_z^{\rm corr}$
+	3.63 ± 0.75	0.20 ± 0.08	$1.13 \pm 0.76 \pm 0.52$
−	0.13 ± 0.65	-0.09 ± 0.07	$1.01 \pm 0.70 \pm 0.34$

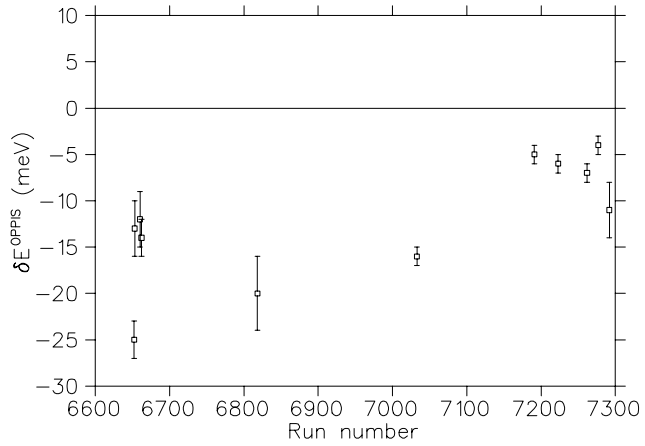

Fig. 6. The measured intrinsic energy modulation at OPPIS during the May, 1999 run.

Final result: May, 1999 data

The final result of the May, 1999 data set is $A_z^{\rm corr} = (1.1 \pm 0.5 \pm 0.2) \times 10^{-7}$. The first error bar is based on the statistical spread of the corrected A_z, while the second error bar is a quadrature sum of the systematic uncertainties for each of the measured helicity-correlated effects, including upper limits on the energy modulation correction uncertainty. The helicity correlated beam properties and individual corrections to A_z are listed in Table V.

Table V. Summary of the A_z corrections and beam properties for the May, 1999 run.

Property	Average value	$10^7 \Delta A_z$
$A_z^{\rm reduced}(10^{-7})$	1.63 ± 0.49	n/a
$y * P_x(\mu m)$	0.0 ± 0.0	-0.005 ± 0.001
$x * P_y(\mu m)$	-0.1 ± 0.0	0.069 ± 0.001
$\langle yP_x \rangle(\mu m)$	2.0 ± 0.8	0.10 ± 0.03
$\langle xP_y \rangle(\mu m)$	6.3 ± 0.9	0.64 ± 0.12
$\Delta I/I(\%)$	0.0011 ± 0.0001	0.15 ± 0.14
$\Delta\sigma_x(\mu m)$	-0.1 ± 0.1	-0.49 ± 0.03
$\Delta\sigma_y(\mu m)$	0.0 ± 0.1	0.23 ± 0.02
$\Delta x(\mu m)$	0.0 ± 0.0	0.014 ± 0.000
$\Delta y(\mu m)$	0.0 ± 0.0	-0.004 ± 0.000
Total	n/a	0.71 ± 0.21
$A_z^{\rm corr}(10^{-7})$	1.1 ± 0.5(stat)	n/a

Adding the statistical and systematic error bars in quadrature, the longitudinal analyzing power found from this analysis of the May, 1999 parity data run is $A_z = (1.1 \pm 0.6) \times 10^{-7}$, as reported in Table I.

Summary and outlook

Major progress on data analysis has been made during the past year. The last data set, taken in May-June, 1999, has now been analyzed and, by early 2001, a reanalysis of the earlier data sets making use of the same procedure should be completed. A preliminary result,

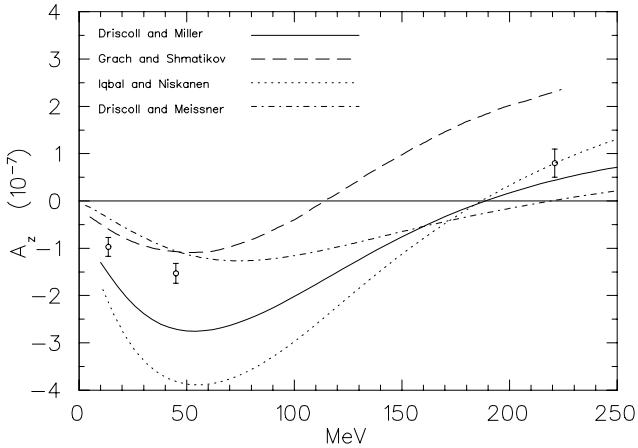

Fig. 7. Theoretical predictions for A_z in pp scattering, calculated by Driscoll and Miller [Phys. Rev. **C39**, 1951 (1989), *ibid.*, **C40**, 2159 (1989)] using DDH predictions for the weak meson-nucleon coupling constants; also shown are quark model calculations by Grach and Shmatikov [Phys. Lett. **B316**, 467 (1993)], meson exchange calculations by Iqbal and Niskanen [Phys. Rev. **C42**, 1872, (1990)], and a calculation by Driscoll and Meissner [Phys. Rev. **C41**, 1303 (1990)]. The highest precision existing experimental data are also shown [Eversheim *et al., op. cit.*; private communication (1994); Kistryn *et al., op. cit.*].

based on the 1997, 1998 and 1999 data sets, excluding December, 1997, is shown in Fig. 7, together with recent theoretical predictions. The existing preliminary result is $A_z = (0.8 \pm 0.3) \times 10^{-7}$. Also shown are the highest precision existing experimental data in this energy range. The TRIUMF data point supports the meson exchange prediction at the level of this first result. The final result from Expt. 497 will serve to determine uniquely for the first time an experimental constraint on the weak meson nucleon coupling constant h_ρ^{pp}.

Experiment 614
Precision measurement of the Michel parameters from muon decay
(D.R. Gill, TRIUMF; N. Rodning, Alberta)

The standard model is at present under increased scrutiny. The elevated interest is spurred primarily by the recent Kamiokande result (among others) that contradicts the usual SM input, massless neutrinos. Historically the electroweak sector of the standard model has been provided with very important input from studies of the muon's properties, its decay perhaps being the paramount characteristic. A new round of μ decay experiments, each with goals that will provide information significantly improved over their historical counterparts, are under way or about to get under way at TRIUMF, PSI and BNL. (Note reverse alphabetical order to remove bias). These new data may add support for or may produce further challenges to the standard model. Except for the presently operating g-2

experiment at BNL and the TWIST (Expt. 614) experiment that is being assembled in M13 at TRIUMF, all of these new endeavours are at PSI. This is due primarily to the considerable advantage in μ flux that PSI possesses.

The final assembly of the TWIST spectrometer, shown schematically in Fig. 8, began in 2000. This spectrometer, composed of a 2 T superconducting solenoid (originally employed for whole-body medical MRI), a set of 44 precision planar drift chambers and 12 proportional chambers, will be used to measure with high precision the differential spectrum $d^2\Gamma/dXd(cos\theta)$ of positrons from the decay $\mu^+ \rightarrow e^+\nu_e\overline{\nu}_\mu$ for polarized muons. Here, X is the positron energy ($X = 1$ corresponds to the maximum positron energy, $E_{\rm max} = 52.83$ MeV), θ is the angle between the muon spin direction and the positron momentum. The "surface" muon beam with a momentum of 29.8 MeV/c from the M13 beam line at TRIUMF will be used as the muon source. The muons will be stopped and decay at the centre, on axis, of the highly symmetrical detector system. This allows the simultaneous measurement of nearly the entire spectrum, allowing the extraction of the Michel parameters from data obtained under consistent conditions.

TWIST milestones of 2000

During 2000, TWIST began assembly of the experimental apparatus in earnest. At year's end more than half of the required drift chamber planes and almost half of the required proportional counter planes were strung. The array of drift chambers inside the spectrometer consists of 14 pairs of planes and 2 sets of 8 planes each. The former are referred to as UV modules since they measure UV (XY rotated by 45°).

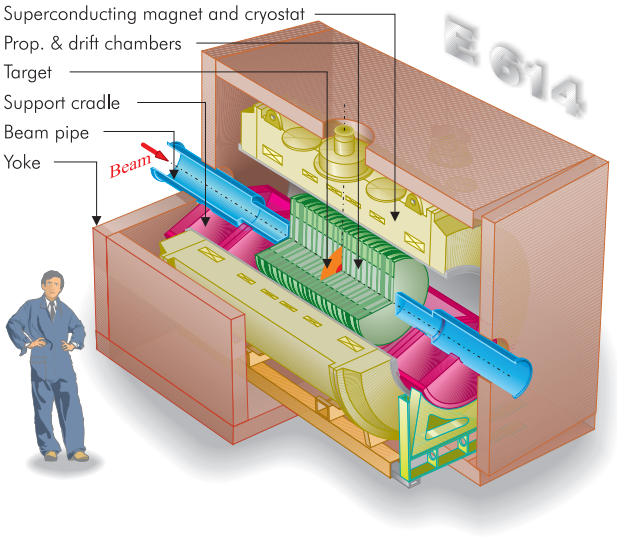

Fig. 8. The TWIST spectrometer.

Each of the 8 plane groups, also employed to measure UV, are referred to as a dense stack. The UV modules and the dense stacks are enclosed in individual gas boxes and in the final configuration will be in a helium gas envelope, 7 UV modules and a dense stack on each side of the muon stopping target. Many parts for these detectors, as well as parts for the TWIST electronics, are being made at the remote sites of the TWIST member institutions.

The accuracy of the TWIST results will be directly related to the quality of the detector. To this end special materials and special techniques are being employed in the assembly of the chambers. As well, a quality control (QC) regime is being followed as the chamber planes come off the production line. As part of the QC, the positions of the wires are measured at each end and in the centre and the tension of each wire is being determined. The high quality of the procedures being employed for the positioning and tensioning of the wires is indicated in Figs. 9–11. Figure 9 shows the typical accuracy with which the wires in a drift chamber plane are positioned, in this case at the centre of plane number 035DC. Figure 10 shows the σ of the wires across the centre of the planes as determined for 25 planes, thus the statement that Fig. 9 presents typical results. Very similar results are found for measurements of the positions at both ends of the wires, the pad end and the readout end. Figure 11 shows the results of the QC measurement of the tension of the wires for 38 drift chamber planes which have 80 wires per plane.

The experimental requirement that the drift chambers be configured into UV modules and dense stacks makes for straightforward testing of each module as it comes off the production line. In the fall, three UV modules were assembled and stacked vertically "on the bench" for testing employing cosmic rays. The results

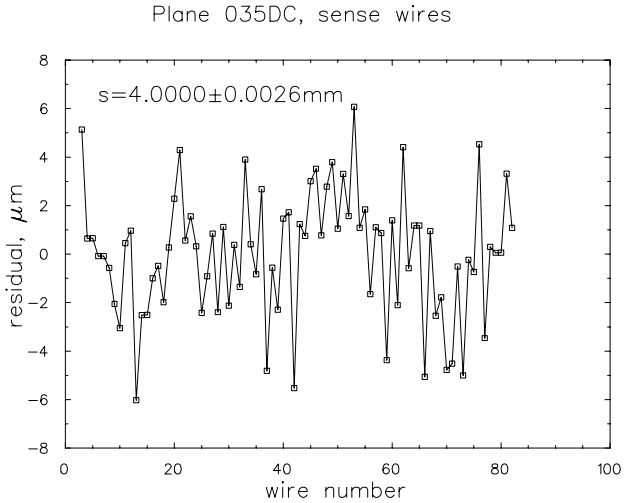

Fig. 9. A scan of wire positions across the centre of a plane. The σ of ≈3 μm is typical.

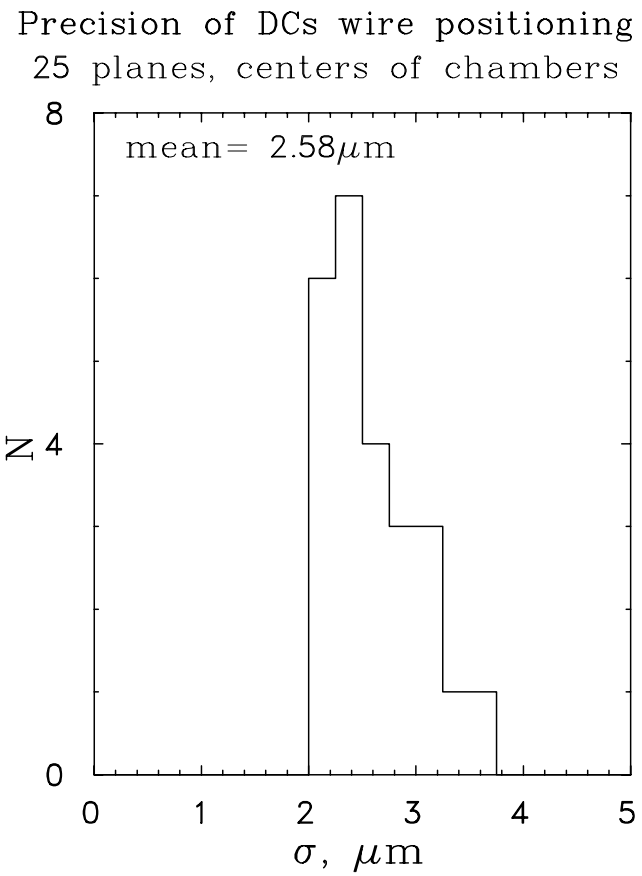

Fig. 10. The σ of wire positions for 25 planes.

of these tests indicate that the drift chambers, their electronics and the data acquisition system are performing as required. A test of the first assembled dense stack is planned for January, 2001.

The production of the required electronics, preamps and postamps, and the cabling is keeping pace with the detector production.

The steel for the magnet yoke was delivered to TRIUMF in the spring. The machining of this steel was contracted in early summer to a local firm and was completed, after several delays, and delivered to TRIUMF on December 8. TRIUMF personnel supervised the assembly of the yoke at the fabricator and it was reassembled in M13 at TRIUMF before Christmas with the solenoid in place. The commissioning and field mapping of the magnet is scheduled for early 2001.

The precision of the results of the TWIST experimental program will depend partly on the control and measurement of the M13 beam line parameters such as position, size and divergence (or emittance), momentum spread, etc. These properties of the M13 surface beam also depend on the position and profile of the proton beam when it strikes the BL1A T1 production target.

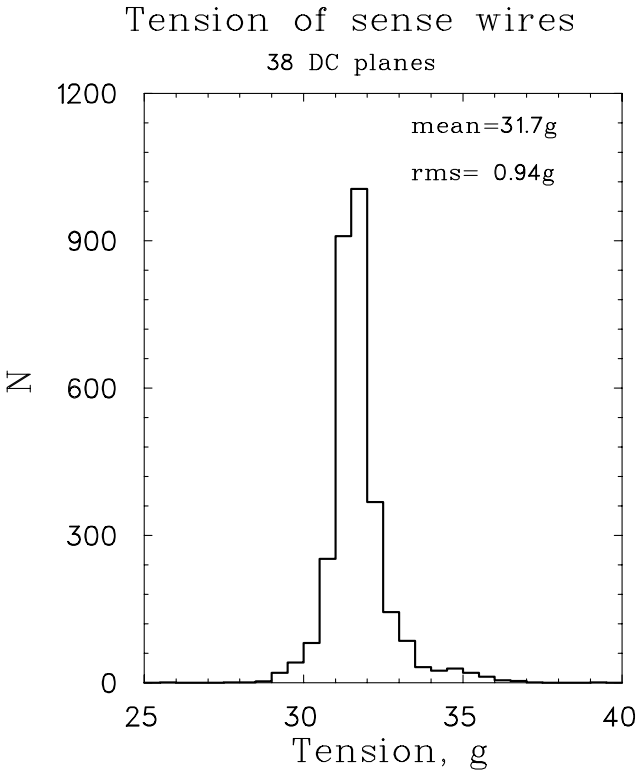

Fig. 11. The wire tensions for 38 DC planes.

The position of the proton beam at T1 is determined using the T1 protect monitor. Studies early in 2000 showed that the sensitivity of the existing protect monitor to the horizontal position of the proton beam was not adequate for TWIST. A new protect monitor was therefore manufactured and installed for the fall running period. This new monitor has 5 mm separation between the top and bottom plates and 4 mm separation between the left and right plates. The latter have been moved in from the 5 mm separation of the original version. The protect monitor was calibrated by scanning a low intensity beam across each plate and recording the signal output. The results are dependent on the polarity of M11. Data were logged on a second by second basis and showed that the proton beam position can remain stable within $\approx$0.1 mm. These results were achieved for a beam of sufficient width that the plates were sensing the beam halo on both sides. However, for a narrow beam, for example one with a base width of 2.3 mm, it is possible for the beam to wander almost 1 mm before any halo is intercepted by the plates separated by 4 mm. This level of sensitivity may be adequate for TWIST but proton beams narrower than this could be problematic.

The stability and control of the magnetic elements of the M13 channel were monitored during a shutdown period. These studies showed the present system for monitoring the quadrupole magnets to be far from ad-

equate for the stringent requirements of TWIST. Monitoring of quadrupole currents by a TWIST-specific system, using new current transformers, should be in place by the first running period of 2001.

Much effort has been spent by different individuals and groups to determine M13 beam parameters since installation over twenty years ago, but with the stringent TWIST requirements an opportunity to repeat and extend these measurements was taken prior to installation of the TWIST solenoid, during high intensity beam time in the fall. Many of the studies described below were made with a Be target at T1, but a limited set of data was taken with a TWIST preferred graphite target. As part of these studies a μSR apparatus was installed to examine the muon polarization vs. momentum and vs. TOF of the particles down the channel. Preliminary analysis of these measurements, assuming the surface muons are perfectly polarized, gives a polarization for the cloud muons of –0.30 ± 0.02 (where the errors of both measurements have been added in quadrature). It is interesting to note that the cloud and surface muon components of the beam have opposite polarizations.

The μSR apparatus was removed and a set of wire chambers and scintillators was installed. Measurements were then made regarding the effects of different production targets, production target alignment, and beam alignment. As well, tuning studies were performed. In particular, a set of TWIST-specific beam element settings was studied to determine if the beam profiles and emittances would be as predicted. In order to minimize the influence of multiple scattering on tuning and alignment studies, these were made with 120 MeV/c pions. With all the M13 quadrupoles turned off, scans of rates vs. position of the second slit in the central leg of M13 (F2HS) for different positions of first slit (F1HS) were used to check relative slit alignment. One of the set of maximum values was chosen such that the sum of the absolute distances of the slits from the nominal zero position was a minimum; these distances were ±0.7 mm, i.e., nearly zero, evidence that target, dipoles and final focus are in reasonable mechanical alignment. However, when the quadrupoles were turned on, steering effects were encountered. In some cases the steering was so large that operation of the quadrupoles at their nominal values removed the beam from the active area of the XY chambers at the end of the channel. The results indicated strong horizontal steering effects from Q6 and Q7, with smaller effects in other cases. When all quads are set to nominal values, B2 requires adjustment in order to centre the beam on the first chamber at the end of the channel. The required B2 setting is 0.9% higher than that with the quadrupoles off.

The surface muon beam edge was employed to tune M13 Q2 for a horizontal dispersed focus at F1HS. This was accomplished by a scan of the F1HS position (with narrow width) for various values of Q2, the best setting being indicated by the steepest gradient in the rate as the slit is moved to higher momentum, beyond the momentum of surface muons. A contour plot is shown in Fig. 12, and the optimum value for Q2 is clearly visible.

The surface muon edge was then scanned to provide a calibration of the momentum and momentum bite of the channel. The results of several such scans, made to compare production target effects, are presented in Table VI. A scan of the positron rate near 52.83 MeV/c (the maximum for a surface positron from muon decay at rest in the production target) provides a second momentum calibration, although not as precise.

Table VI. Momentum calibration and momentum bite from momentum scans for the beryllium and graphite targets.

Beryllium target		
B1 field at edge(G)	879.6±0.4	
Momentum bite	2.1%	
Graphite target	**1st scan**	**2nd scan**
B1 field at edge(G)	878.7±0.4	878.1±0.4
Momentum bite	1.6%	1.7%

Several proposals for modifications to the beam line and its control and operation follow from the results of these studies. Some of the required improvements, such as the new current transformers for the quadrupole power supplies, are already under way. The study results have also led to suggestions for further beam studies which will be carried out in future beam periods.

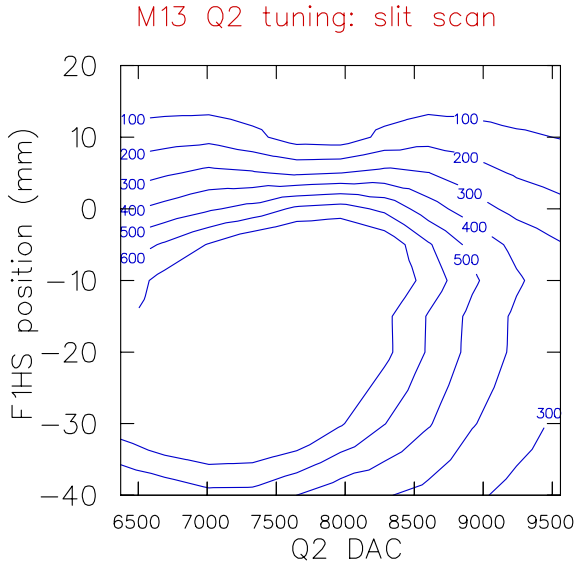

Fig. 12. Muon rate contours for a grid of settings of F1HS position and Q2 DAC. The close contour lines indicate a steep gradient at the surface muon edge, a requirement for a dispersed focus at F1.

Experiment 761
Measurement of parity violation in *pp* scattering at 221 MeV
(J. Birchall, W.T.H. van Oers, Manitoba)

Experiment 761 is a second generation parity violation experiment which aims to do a much better job of suppressing the dominant sources of systematic error – transverse polarization and current modulation – which were found in the previous experiment, Expt. 497. To this end, very high precision current mode detectors have been added to the scanning polarimeters and high resolution direct digitization of the main ion chamber signals has been adopted. Engineering runs in July/August and December were very successful and demonstrated that greatly reduced systematic uncertainty should be possible.

At the time of writing, analysis of the Expt. 497 data indicates that the parity-violating analyzing power, A_z, in the scattering of protons from hydrogen will be determined to a precision of 0.3×10^{-7}. 221 MeV is chosen because, at this energy, the ${}^1S_0 - {}^3P_0$ component of A_z averages to zero over the angular acceptance of the parity equipment, leaving the ${}^3P_2 - {}^1D_2$ part as the dominant contribution (see Fig. 13). This part is proportional to the weak rho meson nucleon coupling h_ρ^{pp*} alone, unlike the low energy results which are sensitive roughly equally to both h_ρ^{pp} and $h_\omega^{pp\dagger}$ –

$$\begin{aligned} A_z(45\text{ MeV}) &= 0.15h_\rho^{pp} + 0.11h_\omega^{pp}, \\ A_z(221\text{ MeV}) &= -0.030h_\rho^{pp}. \end{aligned}$$

It is evident that, while it is important to measure at 221 MeV to isolate h_ρ^{pp}, a given uncertainty in A_z translates into 4 to 5 times as much uncertainty in the coupling constants as does the same A_z uncertainty at low energy; measurement at 221 MeV demands high accuracy. Although Expt. 497 has met its goal in measuring A_z, the even higher precision promised by Expt. 761 is very desirable.

At a workshop on parity violation held at ECT, the European Centre for Theoretical Studies in Nuclear Physics and Related Areas, in Trento, Italy, June 5–16, consideration was given to what are the most important calculations and experiments that should be performed in the next few years. A very strong recommendation was made to "Proceed vigorously to improve the statistical and systematic errors of the TRIUMF 221 MeV measurement to arrive at a fractional error comparable to that of the low energy results." And further, "The 221 MeV experiment *must* be completed with a most significant determination of the ${}^3P_2 - {}^1D_2$ transition, which is closely related to the value of the weak rho-nucleon coupling constant."

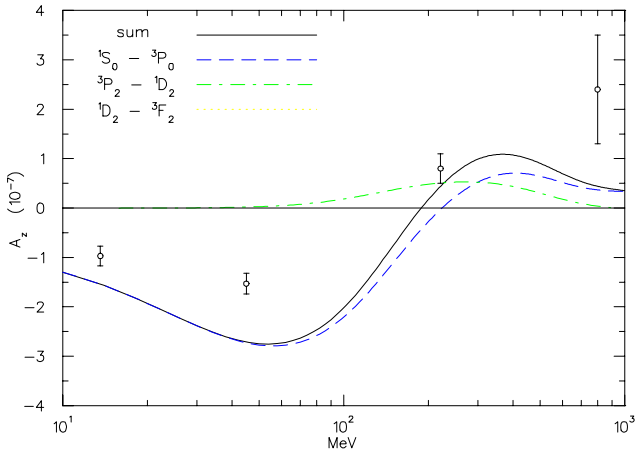

Fig. 13. ${}^1S_0 - {}^3P_0$, ${}^3P_2 - {}^1D_2$ and ${}^1D_2 - {}^3F_2$ contributions to A_z. The calculations are by Driscoll and Miller. The TRIUMF result at 221 MeV is preliminary, based on the February, 1997, July, 1998 and June, 1999 Expt. 497 data sets. The two low energy results are from Bonn and PSI. The 800 MeV result is from LANL.

Measurement of the strangeness-conserving weak meson-nucleon coupling constants is also of interest to those investigating parity violation in electron scattering (e.g. SAMPLE, $G\emptyset$ experiments). The coupling constants are needed to calculate radiative corrections. If Expt. 761 is successful in reaching its goal, the dominant remaining uncertainty will be due to f_π.

Improvement of the measurement of A_z at 221 MeV

Polarization profile monitors

A key to an improved measurement of A_z at 221 MeV is better determination of polarization moments which are the main cause of uncertainties in systematic error corrections to A_z. This has been accomplished by using current mode polarimeters. Instead of detecting individual protons scattered from hydrogen in the polarization profile monitor (PPM) scanning CH_2 blades (counting mode operation, count-rate limited), the scattered flux of protons is measured via the integrated light output produced in large solid angle scintillators viewed by vacuum photodiodes (current mode operation). Data taken elsewhere indicated that the analyzing power for proton scattering from carbon at 225 MeV should be in excess of 0.6, even without screening out inelastic events. By adding absorbers to range out inelastic events, Expt. 761 has achieved an effective analyzing power of 0.8 for the current mode PPMs. Counting mode operation of the PPMs has been retained so that results can be compared.

Figure 14 shows the clean signals obtained from the new current mode detectors. Shown are outputs

* $h_\rho^{pp} = h_\rho^0 + h_\rho^1 + h_\rho^2/\sqrt{6}$
† $h_\omega^{pp} = h_\omega^0 + h_\omega^1$

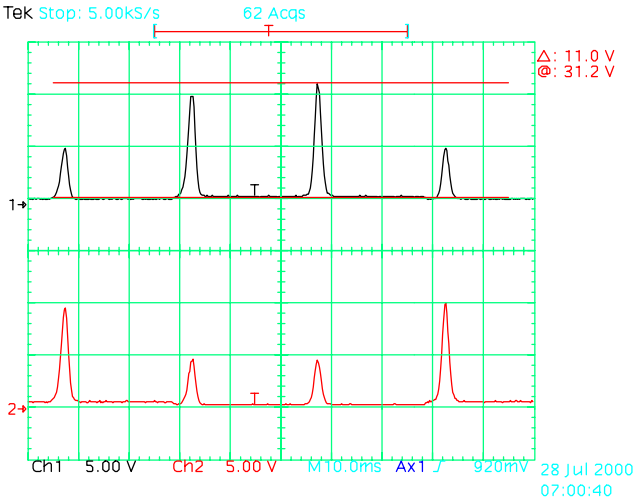

Fig. 14. Clean signals obtained from the new current mode detectors. Shown are outputs of the left and right scintillators (upper and lower traces) as the four blades of PPM1 make a single pass through the beam. The beam polarization is down, up, up and down for the four peaks in each trace. The left/right and spin up/spin down asymmetries are clearly visible.

of the left and right scintillators (upper and lower traces) as the four blades of PPM1 make a single pass through the beam. The beam polarization is down, up, up and down for the four peaks in each trace. The left/right and spin up/spin down asymmetries are clearly seen. The PPM counting time was extended in the DAQ so that background could be measured both before and after a PPM blade passed through the beam. This allows background subtraction to be performed and beam halo to be assessed much better than before. A small spin-dependence of the background is evident, which disappears when the beam is either unpolarized or polarized longitudinally at the parity apparatus. A possible effect due to the parity-allowed analyzing power, A_y, when beam scatters in the cyclotron stripping foil is not seen. The current mode detectors also work well at the PPM2 location where background might be expected to be higher.

Figure 15 shows the polarization distribution across the beam spot at PPM2 for a vertically polarized beam measured during the summer run. The upper figure shows P_y as a function of x across the beam spot in steps of 0.6 mm. The left and right detector results (short dashed lines) are from single scintillators for spin up and down normalized by beam current. The solid curve, marked "ratio", combines left, right, spin up and down results in a ratio

$$r = \sqrt{\frac{L^+R^-}{R^+L^-}},\ P_yA_y = \frac{r-1}{r+1}$$

which is inherently less subject to systematic errors. This method has been adopted as the standard for the

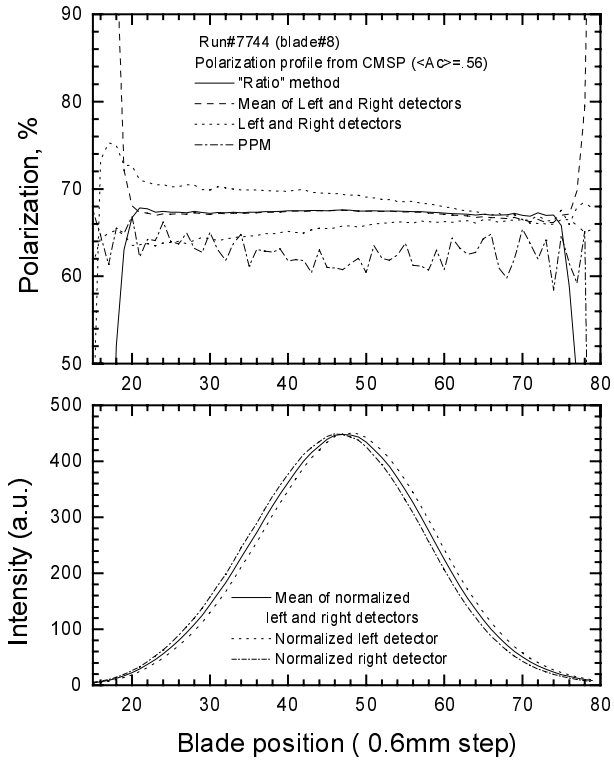

Fig. 15. The distribution of beam polarization (upper curves) and beam intensity (lower curves) across the beam spot as measured by the current-mode polarimeter at the location of PPM2.

new PPMs. Results from the counting-mode PPM are shown for comparison, marked "PPM". The statistical spread is much larger. The lower figure shows the distribution of beam current across the beam spot, as given by the left and right current-mode scintillators. The left-right mean is used to calculate first moments of transverse polarization.

Figure 16 shows a comparison of intrinsic first moments $\langle xP_y \rangle$ measured simultaneously by counting ("old") and current mode ("new") polarimeters. The uncertainties of the current mode results are too small to plot. A given precision in transverse polarization and first moment was achieved in about two orders of magnitude less time than with the counting mode PPM. In other words, what took an hour, now takes a minute or less. This will be invaluable from two points of view. First, correlations of first moments with a false parity signal will be much cleaner and corrections more precise. Correction for polarization moments was the major source of systematic error in Expt. 497. The current-mode PPMs will suppress that error. Second, it is possible to explore in a much more systematic way ion source, cyclotron and beam line parameters that minimize polarization moments. Finding the source or the sources of polarization moments has been impractical so far, because many hours of running were

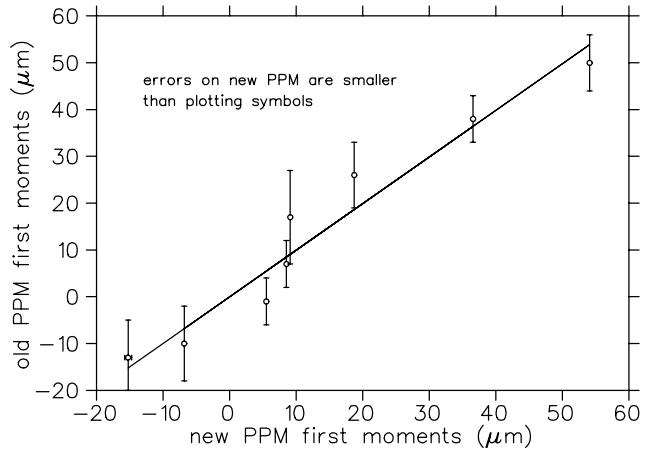

Fig. 16. Intrinsic first moments of polarization $\langle xP_y \rangle$ measured simultaneously with counting ("old") and current mode ("new") polarimeters. The two devices agree within statistics, but the new one has greatly improved precision.

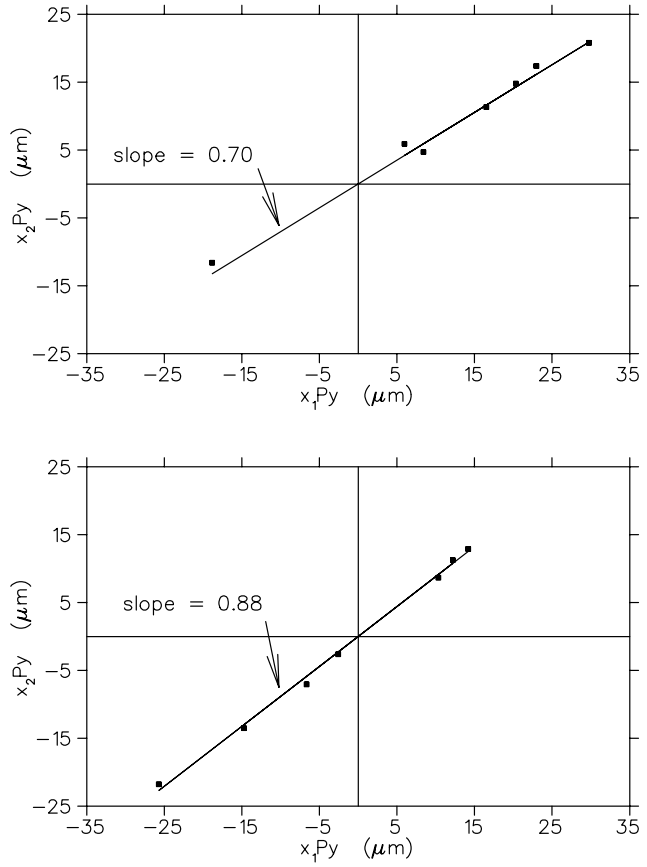

Fig. 17. First moments of transverse polarization at PPM1 and PPM2 for a wide range of cyclotron tunes (rf, main magnet, foil, ...). The difference between the top and bottom plots is the setting of the beam line magnets. It is seen that for a given beam line tune, the first moments can vary widely, but the *ratio*, $\langle xP_y \rangle_2 / \langle xP_y \rangle_1$, is essentially constant. By adjusting the beam line tune to give the "magic moment ratio", the systematic error introduced by first moments can be eliminated.

required to gain sufficient statistical precision. By use of the current mode polarimeters, we were able to very quickly study the effect of cyclotron and beam line tunes. Figure 17 shows some results from the December run. The important conclusion is that, at least to a very good approximation, the ratio of first moments at PPM1 and PPM2 is set by the beam line magnets. As cyclotron parameters change, the first moments can vary widely, but their ratio at PPM1 and PPM2 stays the same. Since the new PPMs are so fast, we can then adjust the first moment ratio to give the "magic ratio" which reduces our systematic error from first moments to zero.

Digitization of ion chamber signals

A second major improvement was in the digital subtraction of ion chamber (TRIC) signals using a new TRIUMF-designed VME digital signal averager. The previous analogue subtraction was retained for comparison. Digital subtraction has the strong advantage that it can be optimized off-line, so that the effects of current modulation can be minimized, which is the second most important source of systematic error.

Direct digitization of TRIC signals was considered for Expt. 497, but ADCs of sufficient linearity and resolution were not available at the time. Data was processed in Expt. 497 as follows. A hardware subtraction of TRIC signals was performed, the result amplified by a factor of 1000 and digitized. As the energy of the beam is 27 MeV lower at TRIC2 than at TRIC1, the TRIC2 gas pressure was lowered relative to TRIC1 to equalize ion chamber currents. A hardware gain was applied to the TRIC1 signal to minimize common-mode noise in the difference signal $1000 \times (I_2 - gI_1)$ which was digitized, where g is the hardware gain. The difference, which should be proportional to A_z, nevertheless contains a common mode (current modulation) component due to gain mismatch and nonlinearity of the ion chambers. If the current signal from TRIC2 is $I_2^{\pm} = \alpha I_1^{\pm}(1 - S(1 \pm P_z A_z))$, with $I_1^{\pm} = I_1 \pm \delta I_1$, then we can define an "analogue asymmetry",

$$\begin{aligned} \epsilon_a &= \frac{(I_2^+ - gI_1^+) - (I_2^- - gI_1^-)}{2I_1} \\ &= -S\alpha P_z A_z + \left(\alpha T - g + I_1 T \frac{d\alpha}{dI_1} \right) \frac{\delta I_1}{I_1}, \end{aligned}$$

where S is the nuclear scattering probability in the LH_2 target ($S = 0.04$) and $T = 1 - S$. α is a function of TRIC1 and TRIC2 gas gains, is nominally equal to $1/T$ and is adjusted with TRIC2 gas pressure. The hardware gain g is set by zeroing the false parity signal when the beam current is modulated by the photodetachment laser. Because of the nonlinearity term, g

must be reset if the beam current changes. Constant adjustments of g were needed during Expt. 497, partly because of electronic drifts. Note that some information is lost by digitizing the signal difference. It cannot be recovered in the data analysis so that an optimum correction cannot be applied.

When I_1 and I_2 are digitized individually, many problems disappear. The following "digital asymmetry" was formed in tests for Expt. 761:

$$\epsilon_d = \frac{I_2^+/I_1^+ - I_2^-/I_1^-}{I_2^+/I_1^+ + I_2^-/I_1^-} = -\frac{S}{T}P_z A_z + \frac{1}{\alpha}\frac{d\alpha}{dI_1}\delta I_1.$$

The gain terms are gone; only the TRIC nonlinearity term remains. A correction must now be applied for current modulation. It can be from current modulation data taken concurrently with parity data; it can be deduced from the parity data itself by applying a correction that minimizes the spread of the parity signal. In both cases, the correction is applied to the data itself, in contrast to the analogue method where the correction is applied in advance via the hardware gain, g, which may not be optimum. The digital system was first tested during the summer runs. It produced results as good as or better than the analogue system. During the December run, coherent intensity modulation data were taken and the ability to reject the intensity modulation is being analyzed.

Upgrades to data acquisition system

The parity data acquisition system was brought up to TRIUMF's currently supported standard for the summer test run. The previous system was a CAMAC/J-11 system controlled by a VAX station. Data were farmed out to two VAX stations and one ULTRIX machine for on-line analysis and data storage. The new system is shown in Fig. 18. The CAMAC

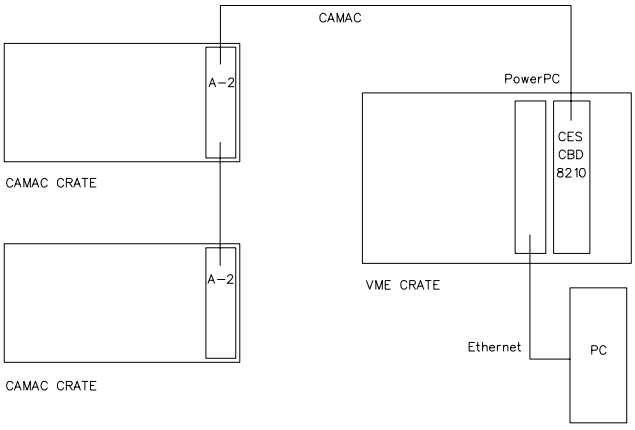

Fig. 18. Data acquisition system for Expt. 761. Existing CAMAC modules are retained. New VME modules digitize the ion chamber signals.

crates are read at a high enough rate that the J-11 in-crate processors have been eliminated, their functions having been taken over by the Power PC. The three machines in the old system are replaced by one dual processor Pentium III running Linux. Most of the data acquisition and on-line analysis routines were ported to Linux in time for the test run. Further progress made during the run was impressive. Porting of software is now essentially complete, although some debugging remains, and it will be used in the 2001 running periods.

Status of optically pumped ion source

Several upgrades will be necessary to meet the demands of Expt. 761 running. Greatly increased current will be required so that sufficient beam current will be available to run ISAC at the same time as Expt. 761. To this end, TRIUMF plans to install a new Na ionizer cell which will greatly improve the beam emittance and permit much more beam to be transported to the injection line. With the greatly reduced sensitivity of Expt. 761 to transverse polarization, helicity correlated modulations of other beam properties will become much more important. This will require careful tuning of the source with all lasers and diagnostic equipment operational. Control of energy modulation will be particularly important. One TRIUMF proposal which promises to reduce all unwanted modulations is to replace the tilting etalon with a less disruptive method of shifting the frequency of the optical pumping lasers. Other planned upgrades are a new photodetachment laser for intensity modulation control measurements, and a new, more dependable power supply for the microwave generator.

Summary

The optimum energy to determine h_ρ^{pp} and h_ω^{pp} when combined with the low energy data is 221 MeV, to cancel the $^1S_0 - {}^3P_0$ component of A_z and to add to the data accumulated in Expt. 497. Significant improvements have been made to the parity apparatus that will allow corrections for polarization moments to be made an order of magnitude more precisely than in Expt. 497. A systematic search for sources of polarization moments is now feasible. The high resolution digitization of ion chamber signals will remove a second major source of systematic error. The collaboration is ready to start data-taking. We anticipate a short run in the summer of 2001 and a longer run in the fall.

The ATLAS experiment at the LHC
(C. Oram, TRIUMF)

As described in detail in the 1996 Annual Report, ATLAS is building a general purpose *pp* detector which is designed to exploit the full discovery potential of the Large Hadron Collider (LHC) at CERN. The TRIUMF group is responsible for the engineering of the hadronic endcap (HEC) calorimeter, and the feedthroughs for the endcap cryostat. For the HEC, this year has seen the continuation of module production and the final stages of the design of the wheel assembly equipment, while for the feedthrough project, at the University of Victoria, the project has started production, although some problems have been encountered with the batch to batch variation of low inclusion steel. This year the TRIUMF HEC group has had two visitors from China as part of its close collaboration with a Chinese group. This group is a three university cluster of Nanjing University, USTC Hefei, and Shangdong University.

Physics goals

The present theoretical understanding of elementary particles is in the context of the standard model. The standard model is a remarkably successful model, providing predictions which have been consistently confirmed by experiment for over two decades. Its agreement with experimental results, to enormous accuracy in some cases, makes it the most accurately verified model in science. Of the many elementary particles contained in the standard model, only the Higgs remains to be discovered. The central goal of ATLAS is the search for the Higgs particle.

There are good theoretical reasons to believe that the discovery of the Higgs will at least contain hints at, and more likely direct evidence of, what lies beyond the standard model. If the Higgs is composite, its existence requires as yet unknown ultra-strong forces. If it is elementary, it would be the only spinless particle to be discovered so far. There is a theoretical "naturalness" problem for the masses of spinless particles. In the standard model, which is a highly nonlinear dynamical system, the elementary particles tend to take on the heaviest of all possible mass scales which in such a model are at inaccessible energies and inconsistent with other requirements of the model. All other particles discovered thus far have natural mechanisms, such as gauge and chiral symmetries, for protecting their masses so that they can lie in the observable range. For the Higgs particle, there is no such symmetry in the present model. The only theoretical scenarios which leave the Higgs particle light enough to observe are hypothetical ones, either technicolour or supersymmetry, both radical departures from the present structure of the standard model. If Higgs is seen at LHC, one of these scenarios should be seen at the same time.

Particle theory has progressed enormously over the last few decades with many appealing scenarios for physics beyond the standard model. The most likely of these is supersymmetry and the boldest of these is superstring theory. These theories are intimately related and are both radical ideas which promise a new conceptual framework for understanding elementary particles. Though far from being complete theories so far, there are superstring models which resemble the standard model in their low energy limit. These models have a great appeal as they contain a unification of fundamental forces which includes gravity. They have already had substantial impact on gravitational physics where, for example, in addition to the long sought reconciliation of gravity with quantum mechanics, they have been used to derive a fundamental understanding of black hole thermodynamics. Superstring theory is still in its infancy, but progress has been dramatic and the promise of great things to come has captured the imagination of a substantial fraction of the world's theoretical particle physicists.

The present theoretical view is that the conventional grand unification of the strong, weak and electromagnetic forces can only work in the supersymmetric extension of the standard model. In that model, the grand unified energy scale is only two decades below the Planck scale, the ultimate energy where spacetime itself has quantum fluctuations. It is not out of the realm of imagination that, at energy scales where supersymmetry would be observed, evidence for an ultimate theory of everything, at least everything that can exist once spacetime is formed, is within human grasp.

Experiments at LHC, where the ATLAS detector will take data, will probe the energy region where the Higgs particle, possibly supersymmetry, or other structures will be visible. This will be the first experimental probe of an energy region where fundamentally new physics is expected to occur in many years. There is every reason to believe that the results will be among the most dramatic ever.

Basic ATLAS design considerations

The most prominent issue for the LHC is the quest for the origin of the spontaneous symmetry-breaking mechanism in the electroweak sector of the standard model (SM). This is related to one of the most fundamental questions of physics: What is the origin of the different particle masses? New direct experimental insight is required to answer this question.

One of the possible manifestations of the spontaneous symmetry-breaking mechanism could be the existence of a SM Higgs boson (H), or of a family of Higgs particles ($H^{\pm}$, h, H and A) when considering the minimal supersymmetric extension of the standard model

(MSSM). The Higgs search is therefore used as a first benchmark for the detector optimization. For the SM Higgs, the detector has to be sensitive to the following processes ($\ell = e$ or μ) in order to cover the full mass range above the discovery limit set by the final LEP operation in the fall of 2000:

$H \to b\bar{b}$ from WH, ZH and $t\bar{t}H$ using a $\ell^{\pm}$ and b-tagging,
mass range $80 < m_H < 100$ GeV;

$H \to \gamma\gamma$
mass range $90 < m_H < 150$ GeV;

$H \to WW^* \to \ell^{\pm}\nu\ell^{\pm}\nu$
mass range $150 < m_H < 200$ GeV;

$H \to ZZ^* \to 4\ell^{\pm}$
mass range 130 GeV $< m_H < 2m_Z$;

$H \to ZZ \to 4\ell^{\pm}, 2l^{\pm} + 2\nu$
mass range $m_H > 2m_Z$;

$H \to WW, ZZ \to l^{\pm}\nu + 2$ jets, $2\ell^{\pm} + 2$ jets
from WW, ZZ fusion using tagging of forward jets for m_H up to about 1 TeV.

Here the inclusion in the above list of the decay of the Higgs to WW^* has significantly improved the sensitivity to the Higgs in the energy region around twice the mass of the Z. The sensitivity of ATLAS to the standard model Higgs is displayed in Fig. 19. The sensitivity improvement can be seen by comparing with the same figure in the 1999 TRIUMF Annual Report.

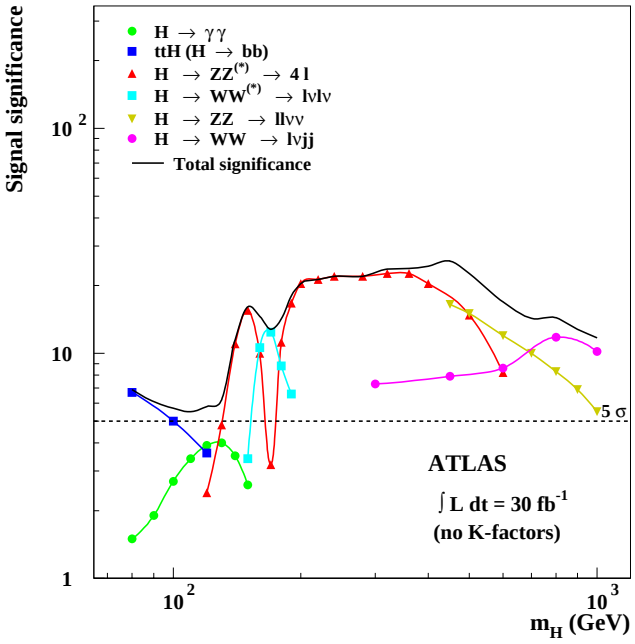

Fig. 19. Expected significance in ATLAS of the standard model Higgs boson signal, as a function of the Higgs mass, for an integrated luminosity of 10^5 pb^{-1} for several decay channels.

In addition to signatures similar to these, the MSSM Higgs searches also require sensitivity to processes such as:

$$\begin{aligned} A \to \tau^+\tau^- \quad &\to e\mu + \nu\text{'s} \\ &\to \ell^{\pm} + \text{hadrons} + \nu\text{'s}; \\ H^{\pm} \quad \to \tau^{\pm}\nu \quad &\text{from } t\bar{t} \to H^{\pm}W^{\mp}b\bar{b} \text{ and using} \\ &\ell^{\pm} \text{ tag and } b\text{-tagging} \\ \to 2 \text{ jets}&. \end{aligned}$$

The observable cross sections for most of these processes are small over a large part of the mass range to be explored at the LHC. Hence it is important to operate at high luminosity, and to maximize the detectable rates above backgrounds by high-resolution measurements of electrons, photons, and muons.

Canada's participation in ATLAS

The Canadian group consists of 35 grant eligible physicists from TRIUMF, University of Alberta, Carleton University, UBC, University of Toronto, University of Victoria, and York University. We are strongly involved in three construction projects centred around detecting hadrons in the endcap region: the hadronic endcap project, the hadronic portion of the forward calorimeter project, and the pipeline electronics for calorimetry. In addition we are committed as part of our common project contribution to providing the feedthroughs for the two endcap cryostats. TRIUMF is directly involved in all these projects, and in the trigger and physics simulations.

The hadronic endcap project

The hadronic endcap calorimeter (HEC) is a liquid argon sampling calorimeter with copper absorbers [ATLAS Collab., ATLAS Liquid Argon Technical Design Report, December 15 (1996)]. A concise overview of this design was provided in the 1996 TRIUMF Annual Report. An artist's impression of a module can be seen in Fig. 20.

Hadronic endcap module production

This year the major scheduled milestone was the series module production of half of one wheel, and by year end production was nearly at the two-thirds mark. We are well advanced on catching up on our production schedule which was delayed by the EST board production design problem discussed in last year's Annual Report. The new design of the boards successfully passed the test beam studies in the spring. Production has been in full swing since.

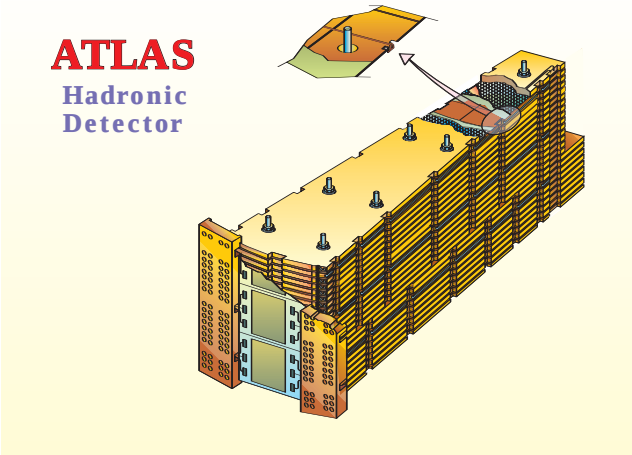

Fig. 20. Artist's impression of a hadronic endcap module.

Test beam measurements of the hadronic endcap modules

Two test beam periods on the CERN H6 beam line this year have tested the performance of the series production modules of the calorimeter. The H6 beam line provides beams from 20 to 180 GeV. Analysis of the data is on-going, and provisional results agree with the anticipated values. The resolution is the same as in previous years but the coherent noise has been reduced since the 1999 test beams. A NIM paper is in preparation. The layout of the beam line and associated systems is described in detail in the 1999 TRIUMF Annual Report.

Preparations for wheel assembly at CERN

32 modules of the HEC form a wheel. There are two wheels at each end of ATLAS, so we must construct 128 modules into four wheels. The equipment to undertake this is a Canadian responsibility. These four wheels and the two wheels of the EM calorimeter, which go in the same calorimeter, are assembled in the horizontal orientation. Hence each wheel, which weighs about 90 tonnes, must be taken from its assembly table, rotated to the vertical and moved to the cryostat. This translation and rotation of equipment is a Canadian responsibility. The engineering is being undertaken by a collaboration between Alberta and TRIUMF personnel. The project has this year entered the detailed design stage. In the spring of 2001 a production readiness review, for the stacking table and rotation/translation equipment, will be undertaken at CERN to establish that the design meets all requirements so that the project can enter the production stage.

The BaBar experiment at the Stanford Linear Accelerator Center

(C. Hearty, UBC)

Introduction

BaBar is an experiment to study the electroweak sector of particle physics using B mesons produced at the high-luminosity e^+e^- collider PEP-II. The highest-profile measurements to be performed are of the violation of the CP symmetry, which relates matter to antimatter. But BaBar will also measure sufficient parameters of the CKM matrix to determine by itself whether or not the standard model provides a consistent description of weak interactions. The high luminosity provided by PEP-II will make accessible a wide range of rare B decays, which can be sensitive to new physics both in rate and in kinematic distributions.

The first data run for BaBar started in October, 1999 and ended in September, 2000. The run – particularly the performance of PEP-II – was a tremendous success. PEP-II achieved a peak luminosity of 3.3 $\times$ 10^{33} cm^{-2}s^{-1}, 10% above design, and a total integrated value of 23.3 fb^{-1}. Backgrounds, which had been considered a potentially serious problem prior to the run, were found to be acceptable.

TRIUMF's role in BaBar was the construction of the drift chamber, one of six major detector systems. The chamber performed reliably during the run, with good tracking performance close to design value (Fig. 21). It is felt, however, that improvements to the alignment, both internal and to the other tracking system, could provide even better performance. For example, the mass resolution for reconstructing J/ψ mesons

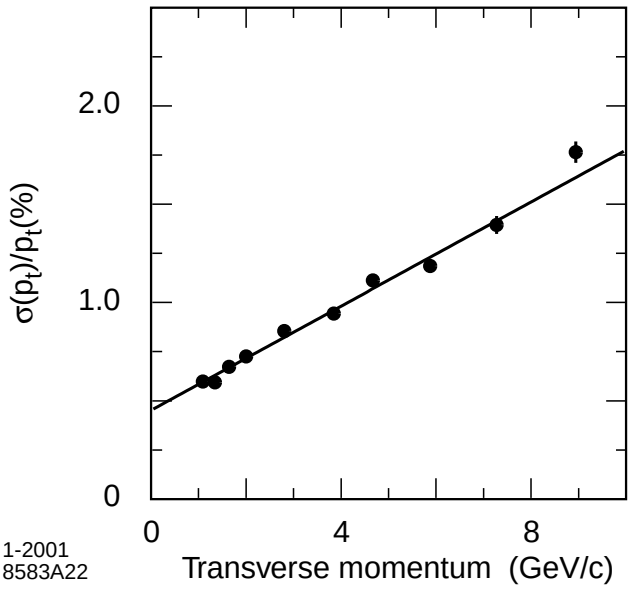

Fig. 21. Momentum resolution of the BaBar drift chamber measured using cosmic rays. $\sigma_{p_t}/p_t = 0.13\% \cdot p_t + 0.45\%$.

is currently 11.4 ± 0.3 MeV/c^2; simulations predict that resolution below 10 MeV/c^2 is possible. Another avenue being pursued is to improve the resolution when the chamber is operated at a lower voltage, 1900 V instead of 1960 V. Although not critical at the moment, a lower operating voltage would extend the eventual lifetime of the device. Canadian group members are active in both of these tracking improvements.

Measurement of sin 2β

CP violation in the B sector is characterized by the CKM parameter $\sin 2\beta$. A non-zero value would indicate a difference in the decay rates of B^0 and $\overline{B}^0$ mesons. Based on measurements of B mixing, CP violation in K mesons, and B semi-leptonic decay rates, the expectation in the standard model is $\sin 2\beta \approx 0.70$.

The centre of mass energy of PEP-II is selected to be the mass of the $\Upsilon(4S)$ meson which decays 100% to $B\overline{B}$. Its production is approximately 25% of the total hadronic cross section. The events useful in the asymmetry analysis require a B^0 to decay to a CP eigenstate, such as $J/\psi K_S$. In order to understand what type of B decayed (i.e., B^0 or $\overline{B}^0$), the other B (called the "tag") must be partially reconstructed in a way that allows its nature to be determined. For example, the sign of the electric charge of a kaon or a high-momentum lepton is correlated with the nature of the mother B.

The correlation between the nature of the tag and signal B mesons is statistical only. Although there is one B^0 and one $\overline{B}^0$ at the instant when the first of the two decays, the remaining meson can "mix" – transform into the other type of B through higher-order box diagrams. Errors in identifying the nature of the tag meson can also dilute the relationship. The probability of error is obtained by applying the reconstruction procedure to events in which the signal B decays into fully-reconstructed final states that are not a CP eigenstate, and therefore do not have any asymmetry due to CP violation.

Of the 23 million $\Upsilon(4S)$ events produced, approximately 360 tagged signal events are measured in the final states $J/\psi K_S$ ($K_S \to \pi^+\pi^-, \pi^0\pi^0$), $\psi(2S)K_S$ ($K_S \to \pi^+\pi^-$), and $J/\psi K_L$. The asymmetry between the number of events in which the tag meson is a B^0 and the number in which it is a $\overline{B}^0$ is measured as a function of the time between the tag and signal decays to derive a value for $\sin 2\beta$. Figure 22 shows this asymmetry separately for signal events with a K_S and K_L in the final state, since these have opposite CP eigenvalues.

The result is $\sin 2\beta = 0.34 \pm 0.20(\text{stat}) \pm 0.05(\text{syst.})$. The dominant component of the systematic error is uncertainty in the parameterization of the resolution function in the time difference. (The value of the resolution is derived in the fit to the asymmetry.)

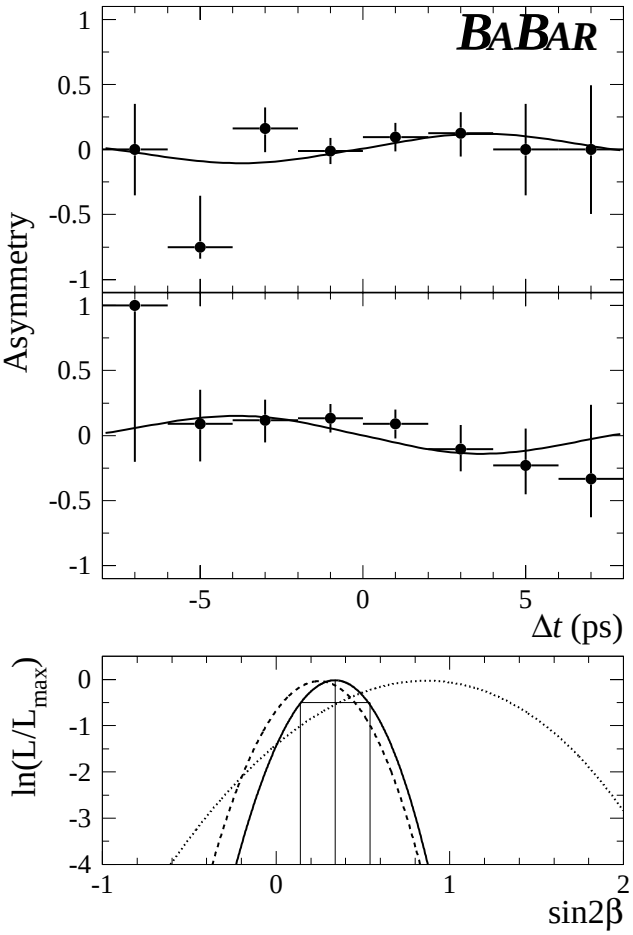

Fig. 22. The asymmetry in the number of B^0 and $\overline{B}^0$ tags as a function of Δt for (top) the $J/\psi K_S$ and $\psi(2S)K_S$ modes and (middle) the $J/\psi K_L$ mode. Bottom: variation of the log likelihood of the fit as a function of $\sin 2\beta$ for the full data set (solid line) and the subsets in (top) and (middle).

The value of $\sin 2\beta$ is somewhat low with respect to the standard model expectation and is equally consistent with no CP violation at all. The data run in 2001 is expected to more than double the integrated luminosity and help clarify the situation.

Activities of the local group

The members of BaBar local to TRIUMF have been responsible for two major analysis activities. The first is in the development of the basic event selection code used to select the events used in the CP violation analysis. More generally, this code is used to calculate the number of $\Upsilon(4S)$ events in the data set. The method starts by counting the number of events selected by the criteria and the number of muon pairs in the on-resonance data set. The same criteria are then applied

to data recorded at energies slightly below the threshold for producing an $\Upsilon(4S)$. (Approximately 13% of BaBar data are recorded at this lower energy.)

The difference in the ratio of hadronic events to muon pairs at the two energies is due to $\Upsilon(4S)$ decays. The number of such events is then corrected for the efficiency of the selection to obtain the number of produced $\Upsilon(4S)$ mesons. The key features of the analysis are that the selection criteria be efficient for desired events, so that the efficiency can be calculated with low uncertainty; and that they strongly suppress beam-gas and cosmic ray events, the rate of which does not scale with the number of recorded muon pairs.

The second analysis is of "charmonium" mesons – $c\bar{c}$ states – produced in the decay of B mesons and in direct production in e^+e^- annihilation. The former has been previously observed, but BaBar will achieve significant improvements in the inclusive B branching fractions to J/ψ, $\psi(2S)$ and χ_{c1} mesons, and will make measurements of the momentum and polarization distributions of the decays.

The direct production of J/ψ mesons in e^+e^- annihilation has not previously been published. The mesons are distinguished from the far more copious production in B decays by using only those with momentum greater than is possible from a B decay, or by using the data set recorded below the $\Upsilon(4S)$ threshold (Fig. 23). The rate and angular distribution of J/ψ mesons strongly differentiate between two different approaches to QCD calculations, the "colour singlet" model and non-relativistic QCD. The latter is felt by many theorists to be a rigorous perturbative approach, while others feel it is either irrelevant at our energy or wrong. Our results strongly favour NRQCD.

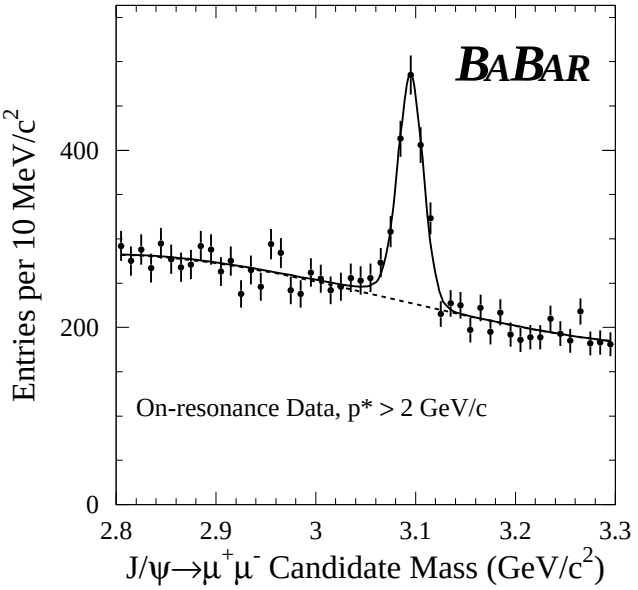

Fig. 23. Mass distribution of J/ψ candidates with momentum higher than is possible in B decays.

Our analysis also rules out the direct production of J/ψ mesons in $\Upsilon(4S)$ decay, a process that is currently listed by the particle data group with a branching fraction of $(0.22 \pm 0.07)\%$.

Outlook

The performance of the PEP-II collider has led to plans for running at luminosities above design values. Current models call for the total integrated luminosity by the end of 2004 – the fifth year of running – to be approximately 15 times the size of the first year data set. This luminosity will enable a number of precision CP violation measurements and make a wide range of rare decays accessible.

This dramatic increase in luminosity will require a substantial increase in computing power. The BaBar group, as one of several TRIUMF-based efforts, is collaborating in a consortium that is submitting a large CFI request. If successful, this would lead to a CPU farm of approximately 1000 CPUs at TRIUMF, with associated storage and networking. The facility would be used by BaBar for the production of Monte Carlo events, an area in which the BaBar collaboration is currently under-powered.

BNL 787/949
Measurement of $K^+ \to \pi^+\nu\bar{\nu}$ and other rare decays

(D. Bryman, UBC)

The ultra-rare kaon decays $K^+ \to \pi^+\nu\bar{\nu}$ and $K_L^0 \to \pi^0\nu\bar{\nu}$ offer unique access to the details of higher order phenomena associated with quark mixing and the origin of charge-parity (CP) non-invariance. Experiment 787 at the BNL AGS has presented evidence for the $K^+ \to \pi^+\nu\bar{\nu}$ decay [Adler *et al.*, Phys. Rev. Lett. **84**, 3768 (2000); Phys. Rev. Lett. **79**, 2204 (1997)] based on the observation of a single clean event. The branching ratio indicated by this observation, $1.5^{+3.4}_{-1.2} \times 10^{-10}$, is consistent with the standard model (SM) expectation. After the 1998 data set analysis is completed, the BNL 787 sensitivity for $K^+ \to \pi^+\nu\bar{\nu}$ should extend well below the most probable SM level to less than 7×10^{-11}.

Together with the proposed measurement of $K_L^0 \to \pi^0\nu\bar{\nu}$ [see BNL KOPIO, this Annual Report], a complete picture of standard model CP violation in the K system will emerge. Theoretically, these decays provide the cleanest route to the CKM parameters ρ and η. Such measurements are complementary to those to be obtained from the B system and any discrepancy in the values found would be a strong indicator of new physics.

$K^+ \to \pi^+\nu\bar{\nu}$ is a flavour-changing neutral current process, arising at the one loop level in the SM. The

presence of the top quark in the loops makes this decay very sensitive to the magnitude of the elusive CKM coupling V_{td} [Buchalla and Buras, Nucl. Phys. **B400**, 225 (1993); *ibid.*, **B412**, 106 (1994); Marciano and Parsa, Phys. Rev. **D53**, R1 (1996)]. This sensitivity arises out of the hard GIM suppression which singles out the heavy t quark, the relatively small QCD corrections which have been calculated to next-to-leading-logarithmic order, and the fact that the hadronic matrix element is measured to a few per cent via an isospin transformation from $K \to \pi e \nu$ (K_{e3}) decay. Long-distance contributions are negligible so the effects of SM short-distance (vertex) physics can be clearly discerned, as well as the effects of possible non-SM physics. Overall, the branching ratio can be calculated theoretically to 5% uncertainty, most of which is due to a charm quark contribution. Using current data in the SM, the branching ratio is expected to be $\mathrm{B}(K^+ \to \pi^+ \nu\bar{\nu}) = (0.6\text{–}1.5)\times 10^{-10}$.

Most postulated new physics beyond the SM has implications for $B(K^+ \to \pi^+ \nu\bar{\nu})$ [Leurer, Phys. Rev. Lett. **71**, 1324 (1993); Davidson *et al.*, Z. Phys. **C61**, 613 (1994); Buras *et al.*, Nucl. Phys. **B520**, 3 (1998); Cho, hep-ph/9804327, KEK-TH-568 (1998); Goto *et al.*, hep-ph/9804294, KEK-TH-567 (1998); Grossman and Nir, Phys. Lett. **B398**, 163 (1997); Couture and König, Z. Phys. **C69**, 167 (1996)]. Attention has recently focused on the possible effects of a fourth generation [Hattori *et al.*, hep-ph/9804412, TOKUSHIMA-98-01 (1998)], leptoquarks, and of various forms of supersymmetry (SUSY). In the latter case, it is interesting to note that the effects of SUSY upon the K and B system generally turn out to be discernibly different.

In mid-2001, a new measurement, BNL Expt. 949, will commence. The AGS will be operated during the next several years in conjunction with the Relativistic Heavy Ion Collider (RHIC) which requires injection roughly twice per day leaving about 22 h available for AGS slow extracted beam. BNL 949 will be the primary user during the 2001–2003 period. Two years of data-taking are expected to yield a single event sensitivity of $(8\text{–}14)\times 10^{-12}$, roughly an order of magnitude below the SM prediction. In order to reach this sensitivity modest upgrades of the BNL 787 detector system are being implemented. With the completion of BNL 949, the possibility of an inconsistency with the SM prediction will be fully explored or the important top-down quark mixing parameter will be determined to a precision 15–30% if the SM expectation is confirmed.

The detection of $K^+ \to \pi^+ \nu\bar{\nu}$ (a single incident K^+ followed by the decay to a single π^+ of momentum $P < 227$ MeV/c and no other observable products) requires suppression of all backgrounds to well below the sensitivity for the signal, preferably to the level of 10^{-11}. The two most significant backgrounds are the two-body decays $K^+ \to \mu^+ \nu$ and $K^+ \to \pi^+ \pi^0$. The other significant background comes from either a π^+ in the beam scattering into the detector or from K^+ charge exchange (CEX). Careful measurement and rejection of these backgrounds which can occur at levels 10^9 to 10^{10} greater than the signal is vital.

The AGS LESB3 beam line transports 3×10^6 K^+ per 3 s spill at 700 MeV/c with a K/π ratio of 4:1 for 10^{13} protons on the production target. The K^+ are stopped in a scintillating fibre target in the centre of the detector. The fully hermetic detector is located in a 1 T solenoidal magnetic field. The central drift chamber which measures the momentum of decay products is a low-mass cylindrical chamber built at TRIUMF. The energy, range, and decay sequence of charged particles are measured in the range stack array of scintillators with two embedded layers of straw tube detectors. The range stack is instrumented with 500 MHz flash-ADC transient digitizers to measure the $\pi \to \mu \to e$ decay chain. To enhance background characterization, other elements among the beam detectors and photon veto systems are digitized by ∼1000 channels of 500 MHz GaAs CCDs built at TRIUMF.

The photon veto system covering 4π sr consists of a barrel assembly outside the range stack, two endcap assemblies whose main components are arrays of pure-CsI crystals, and additional systems on the beam axis both upstream and downstream of the target.

The enhancements to the BNL 787 detector for BNL 949 include new or upgraded systems in the beam instrumentation, range stack, photon veto and data acquisition. A new beam hodoscope and active degrader will improve beam tracking and photon vetoing in the beam direction. Several layers of the range stack have been replaced with brighter scintillators, and new, brighter trigger counters with better geometry have been installed. Additional radiation lengths have been added to the photon veto barrel, and other photon veto systems have been augmented or upgraded also. A new fibre-optic LED flasher system has been added to monitor range-stack and photon-veto PMTs and to assist with improving energy callibration. Many refinements to the data acquisition hardware and software have been implemented primarily to accommodate higher rates.

BNL KOPIO

Measurement of $K_L^0 \to \pi^0 \nu\bar{\nu}$ and other rare decays

(D. Bryman, UBC)

Since the discovery of CP violation in K decay in 1964, its complete understanding has been one of the most important outstanding problems in elementary

particle physics. CP violation has profound implications for our picture of the relationships among the quarks and, perhaps, the leptons, as well as the origin of matter in the universe. With the advent of the standard model (SM), the primary question has revolved around establishing whether the observed CP violation was due to the complex phase in the CKM quark-mixing matrix, i.e. the existence of direct CP violation. Among all possible measurements relating to CP violation, four "golden" processes which stand out as theoretically unambiguous will allow complete elucidation of CP violation in the SM. Two are B experiments: asymmetries in $B \to \psi K_S$ decays and the ratio of B_s to B_d mixing (x_s/x_d). The other two are the branching ratios of the charged and neutral $K \to \pi\nu\overline{\nu}$ decays.

The single most incisive measurement in the study of direct CP violation will come from a measurement of the branching ratio for $K_L^0 \to \pi^0\nu\bar{\nu}$. This decay mode is unique in that it is completely dominated by direct CP violation. Within the SM $B(K_L^0 \to \pi^0\nu\bar{\nu})$ measures the area of the CKM unitarity triangles, the physical parameter that characterizes all CP violation phenomena, or the height of the triangle shown in Fig. 24. Measurements of both $B(K_L^0 \to \pi^0\nu\bar{\nu})$ and $B(K_L^+ \to \pi^+\nu\bar{\nu})$ (Expts. 787/949 at BNL [Adler *et al.*, Phys. Rev. Lett. **84**, 3768 (2000); *ibid.*, **79**, 2204 (1997)]) will allow the triangle to be reconstructed from K decay information alone.

Since theoretical uncertainties are extremely small, measurement of $B(K_L^0 \to \pi^0\nu\bar{\nu})$ will provide the standard against which all other measures of CP violation will be compared, and even small deviations from the expectation derived from SM predictions or from other measurements will unambiguously signal the presence of new physics. Using current estimates of SM parameters, $B(K_L^0 \to \pi^0\nu\bar{\nu})$ is expected to lie in the range $(3.1 \pm 1.3) \times 10^{-11}$ [Buras and Fleischer, in *Heavy Flavours II*, Buras and Linder, eds. (World Scientific, 1997), p.65; Buchalla and Buras, Nucl. Phys. **B400**, 225 (1993); *ibid.*, **B412**, 106 (1994); Marciano and Parsa, Phys. Rev. **D53**, R1 (1996)].

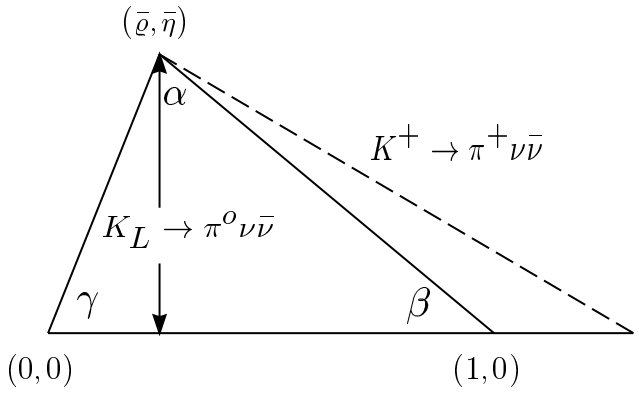

Fig. 24. The unitarity triangle.

The experiment is challenging. The decay $K_L^0 \to \pi^0\nu\bar{\nu}$ is a kinematically poorly constrained three-body decay where only a π^0 is observed, and there are competing decays also with π^0s but with branching ratios that are millions of times larger. With a 10^{-11} branching ratio, a prodigious number of kaons are required in order to achieve the desired sensitivity. The detection technique must ensure that the observed π^0 is the only observable particle from the K_L^0 decay, and provide maximum redundancy for identifying all possible backgrounds. The KOPIO experiment has been designed with these issues in mind.

The international KOPIO collaboration currently includes about a dozen institutions from Canada, the U.S.A., Japan, Russia and Switzerland. The experiment is scheduled to begin operation in 2005–6.

Measurement technique

The complete experimental signature for the $K_L^0 \to \pi^0\nu\bar{\nu}$ decay mode consists of exactly two photons with the invariant mass of a π^0, and nothing else. The experimental challenge arises from the 34% probability that a K_L^0 will emit at least one π^0 in comparison with the expected decay probability for $K_L^0 \to \pi^0\nu\bar{\nu}$ which is ten orders of magnitude smaller. Compounding the difficulty, interactions between neutrons and kaons in the neutral beam with residual gas in the decay volume can also result in emission of single π^0s, as can the decays of hyperons which might occur in the decay region.

The most important means to determine that nothing other than one π^0 was emitted in the decay is to use hermetic high sensitivity photon vetoing to eliminate any extra particles. On its own, this strategy would require an extremely high (perhaps unachievable) photon detection efficiency, and another complementary handle is needed. That handle is provided by detailed measurement of the decay kinematics in the K_L^0 centre of mass. The K_L^0 momentum is measured from time of flight (TOF) which can be obtained at the AGS in an appropriately time structured beam, and a full reconstruction of each observed photon is made through measurements of position, angle and energy. From knowledge of the decaying K_L^0 momentum, the π^0 can be transformed to the K_L^0 centre-of-mass frame and kinematic constraints can be imposed on an event-by-event basis. This technique facilitates rejection of bogus kaon decays and suppression of all other potential backgrounds.

Along with the challenge of obtaining sufficient detection sensitivity, one of the main issues in measuring

an ultra-rare process is the control of systematic uncertainties in estimating tiny levels of backgrounds. The only reliable recourse is to use data to systematically study the backgrounds. This is feasible when there is enough experimental information for each event that the signal can be securely characterized, and the backgrounds confidently determined and rejected at a level well below the experiment's sensitivity.

The beam and detectors for KOPIO are based on previously established measurement techniques and new aspects have been studied in beam measurements and with prototypes and simulations. Figure 25 shows a simplified representation of the beam and detector concept. The 24 GeV primary proton beam strikes the kaon production target in 200 ps wide pulses at 25 MHz, giving a microbunch separation of 40 ns. A 500 μsr solid angle neutral beam is extracted at $\sim$40° to produce a "soft" K_L spectrum in the range from about 0.4 GeV/c to 1.3 GeV/c. The vertical acceptance of the beam (0.005 r) is much smaller than the horizontal acceptance (0.1 r) in order to severely limit beam halos and to obtain another constraint on the decay vertex position. Downstream of the final beam collimator is a 4 m long decay region which is surrounded by the main detector. Approximately 16% of the kaons decay yielding a decay rate of about 14 MHz. The beam region is evacuated to a level of 10^{-7} torr to suppress neutron-induced π^0 production in the residual gas. The decay region is surrounded by an efficient Pb/scintillator photon veto detector ("barrel veto"). In order to simplify triggering and off-line analysis, only events with the signature of a single kaon decay producing two photons occurring within the period between microbunches are accepted.

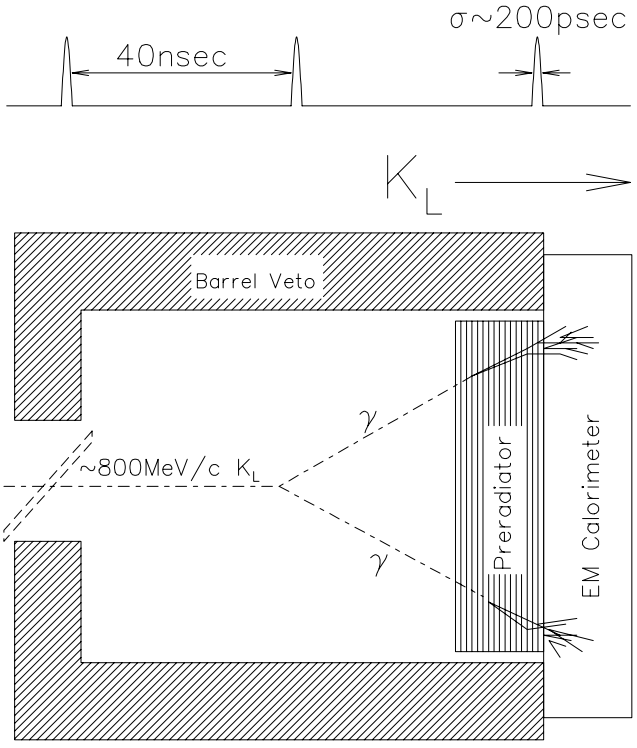

Fig. 25. Elements of the KOPIO concept: a pulsed primary beam produces low energy kaons whose time of flight reveals their momentum when the π^0 from $K_L^0 \to \pi^0\nu\bar{\nu}$ decay is reconstructed.

Photons from $K_L^0 \to \pi^0\nu\bar{\nu}$ decay are observed in a two-stage endcap detector comprised of a fine-grained preradiator followed by an 18-radiation-length (X_0) electromagnetic calorimeter. The preradiator obtains the times, positions and angles of the interacting photons from π^0 decay by determining the initial trajectories of the first e^+e^- pairs. The preradiator consists of 64 0.034 X_0 thick layers, each with plastic scintillator, converter and dual coordinate drift chamber, for a total effective thickness of 2 X_0.

The calorimeter behind the preradiator consists of "shashlik" modules, roughly 10 cm by 10 cm in cross section and 18 X_0 in depth. A shashlik module consists of a stack of square tiles with alternating layers of Pb and plastic scintillator read out by penetrating wavelength shifter (WLS) fibres. The preradiator-calorimeter combination is expected to have an energy resolution of $\sigma_E/E \simeq 0.033/\sqrt{E}$.

Suppression of most backgrounds is provided by the hermetic high efficiency charged-particle and photon detector barrel veto. This system includes scintillators inside the vacuum chamber, decay-volume photon veto detectors and veto detectors downstream of the main decay volume. The barrel veto detectors are constructed of Pb/scintillator sandwiches providing about 18 X_0 for photon conversion and detection. The downstream section of the veto system is needed to reject events where photons or charged particles escape the decay volume through the beam hole. It consists of a sweeping magnet with a horizontal field, scintillators to detect charged particles deflected out of the beam, and photon veto modules. A special group of Čerenkov radiators – the "catcher" – vetoes particles that remain in the beam phase space. This system takes advantage of the low energy nature of our environment to provide the requisite veto efficiency while being blind to the neutrons and K^0s in the beam.

TRIUMF's role

The main contribution of the Canadian group is proposed to be the KOPIO preradiator detector. Each preradiator layer consists of a flat square-cell drift chamber based on an extruded Al comb backplane, and an extruded scintillator read out using WLS fibres. The preradiator position measurements are obtained from cathode strips in the drift chambers running perpendicular to the wires. Prototype chambers are under

construction and a preliminary design has already been used to successfully establish the functionality for photon pointing in beam tests at the BNL LEGS by KOPIO collaborators at Yale University. A scheme for the analogue electronics for the cathode strips has been developed using on-board front-end amplifiers, ADCs and programmable logic devices. The timing electronics is based on front-end chips which include the preamp and a programmable discriminator followed by an ASIC developed for PHENIX and ATLAS muon chambers with a tapped delay line for the drift time measurement. The entire preradiator will consist of 64 layers with a total of approximately 80,000 wires with timing readout, 80,000 strips with analogue readout, and 840 phototubes for the scintillator layers.

The HERMES experiment

(C.A. Miller, M.C. Vetterli, TRIUMF; M.G. Vincter, Alberta)

More than a decade ago, the HERMES experiment was conceived as a comprehensive and concise investigation of the spin structure of the nucleon. It was designed with unique capabilities to produce data that were not possible with previous measurements at SLAC, CERN, and Fermilab. Most prominently, it combines pure nuclear-polarized atomic gas targets in a high-energy stored polarized electron beam, with a large acceptance spectrometer to detect hadrons associated with the scattered electron. Since the commissioning in 1995, the collaboration has collected and analyzed millions of deep-inelastic scattering (DIS) events using longitudinally polarized electrons and positrons incident on longitudinally polarized internal gas targets of ^{1}H, ^{2}H, and ^{3}He. Much thicker unpolarized gas targets have also been used to study certain single-spin asymmetries for the first time, as well as novel QCD effects in the nuclear environment. These data together with large sets of photoproduction events have yielded several results that were unexpected and are provoking new work, both theoretical and experimental.

Productivity of 2000 running

January–September, 2000 was a golden year for both the HERA accelerator and for HERMES. The performance and reliability of the accelerator was outstanding. Both the integrated luminosity and the beam polarization were high. Furthermore, there were no serious beam losses in the region of the HERMES target cell, resulting in continuous use of one high-quality small-aperture cell throughout the year, with high deuteron polarization and low molecular recombination. The effective polarized target thickness was almost a factor of two larger than in previous years.

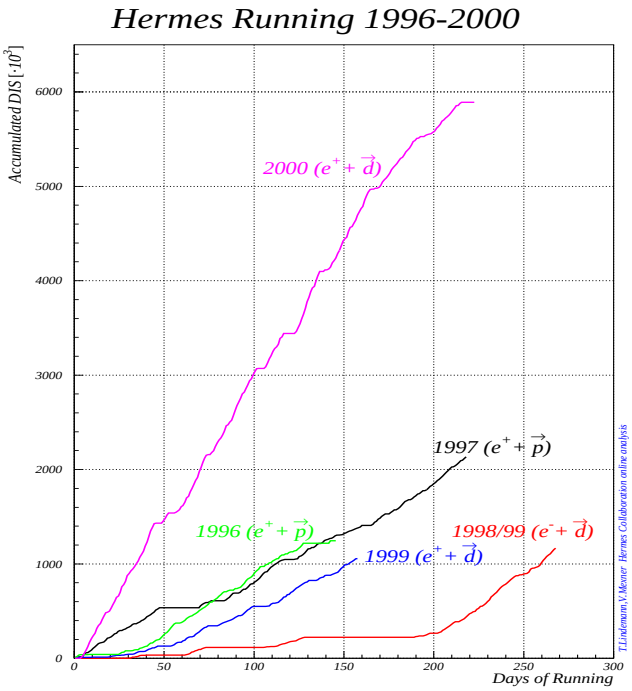

Fig. 26. Comparison of the productivity of the various running years in terms of million DIS events with polarized targets.

Figure 26 compares the accumulated number of DIS events with that of previous years.

In 2000, a new HERA operating mode was instituted for the benefit of HERMES, at negligible cost to the collider experiments. For the last hour of each beam fill, unpolarized target gas is injected at a rate limited only by either the HERMES dead time or backgrounds in the front tracking detectors. Beam lifetimes as low as 1 hour are possible, corresponding to luminosities in the range $3 \times 10^{33}\,\mathrm{cm}^{-2}\mathrm{s}^{-1}$. Such data with unpolarized targets but polarized beam are useful for several aspects of the spin physics program, especially the new study of hard exclusive processes.

Research results

The HERMES physics program has evolved to cover a broad range of topics. Here we offer a few highlights of the past year.

Polarized quark distributions

The modern generation of DIS experiments has done much to unravel the polarizations of the three flavours of valence and sea quarks, especially the controversial strange sea. However, a key limitation of inclusive DIS measurements is that they are sensitive only to linear combinations of quark flavours weighted by the *squares* of their charges, and hence can't distinguish quarks from anti-quarks. A technique that can distinguish the polarizations of anti-quarks is semi-inclusive DIS, where the flavour of the struck quark

is statistically "tagged" by a hadron h detected in coincidence with the scattered lepton. This technique has been applied by both SMC and HERMES, with only limited success up to now mainly because of the limitations of the published semi-inclusive data on the neutron. However, this situation is changing radically as analysis proceeds on the 1999/2000 HERMES data set on the deuteron, which complements the large 1996/97 proton data set. An impression of this impact is given by the preliminary result of an analysis including only data recorded up to the end of 1999, and without yet making use of the new RICH detector to distinguish kaons from pions. Figure 27 shows preliminary polarized quark distributions extracted from these combined inclusive and semi-inclusive DIS data. When all the data in hand are analyzed, it is expected that the statistical error bars will become negligible for all but those for the strange sea, which are expected to be smaller than those shown in Fig. 27 for $\Delta\bar{u}$.

Hard exclusive processes

As recently as 5 years ago, one aspect of the nucleon spin puzzle threatened to remain clouded in mystery. No practical experimental access to the *orbital* angular momenta of partons had been identified. However, a seminal paper by X. Ji led to an explosion of theoretical activity, and the recent appearance of intriguing

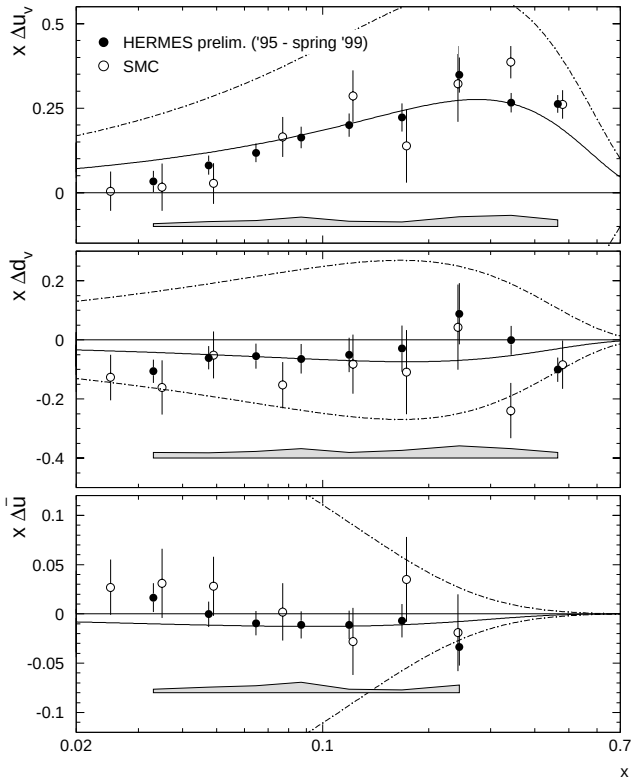

Fig. 27. Polarized quark distributions from 1995–1999 HERMES data.

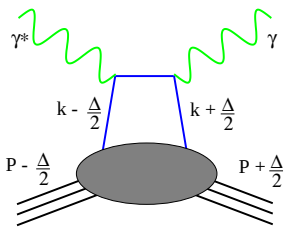

On the lightcone:
$x \equiv k^+/P^+$ (Bjørken x)
$\xi \equiv -\Delta^+/2P^+$
$t \equiv \Delta^2$ (Mandelstam t)
$\Delta \neq 0 \Rightarrow$ **correlations**

Fig. 28. Feynman ("handbag") diagram for DVCS.

new data. This paper demonstrated that the so-called generalized or "skewed" parton distributions (SPDs) embody information about parton orbital angular momentum, and that information about this could be extracted from exclusive processes such as deeply virtual Compton scattering (DVCS), illustrated in Fig. 28.

There are four SPDs, two of which appear in inclusive DIS – the unpolarized function $H(x,\xi,t)$ and the polarized one $\tilde{H}(x,\xi,t)$. In the forward limit, they reduce to familiar distributions:

$$\begin{aligned} q(x) &= H^q(x,\xi=0,t=0), \quad \text{and} \\ \Delta q(x) &= \tilde{H}^q(x,\xi=0,t=0). \end{aligned}$$

Two analogous functions are associated with target helicity flip and appear experimentally only at finite t: $E(x,\xi,t)$ and $\tilde{E}(x,\xi,t)$. Although they are all functions of three variables, their behaviour is strongly constrained by symmetry principles – e.g. their first x-moments are independent of ξ and are connected with elastic form factors.

Of primary interest to us is the "Ji sum rule" that relates their second moments to *total* (including *orbital*) quark angular momentum:

$$\begin{aligned} J^q &= \frac{1}{2}\Delta\Sigma + L^q \\ &= \frac{1}{2}\int_{-1}^{1} x\, dx\, \left[H^q(x,\xi,t=0) + E^q(x,\xi,t=0)\right]. \end{aligned}$$

It is the second term involving E^q to which experimental access is difficult. It must be measured at finite t and extrapolated to the forward limit. Another apparent obstacle is a large background contribution from the indistinguishable Bethe-Heitler process – radiative "elastic" lepton-proton scattering. However, this can be turned to advantage. Interference between the two processes provides direct experimental access to the DVCS amplitudes by giving rise to large asymmetries in the azimuthal distribution of the detected photons about the direction of the incident virtual photon. These asymmetries are associated with, e.g., the beam lepton charge, and also in some cases with its polarization. Furthermore, each of several different moments of these azimuthal asymmetries is associated with a particular linear combination of DVCS amplitudes in the interference cross section.

HERMES kinematics are ideal for observing the DVCS/Bethe-Heitler interference. Figure 29 shows the first measurement of lepton beam spin asymmetries in the azimuthal distribution of photons, in leptoproduction from an (unpolarized) hydrogen target. In the vicinity of $M_X = M_p$, the observed $\sin\phi$ moment of the asymmetry is large, as predicted. Several other observables can be expected to emerge soon from HERMES data, for both DVCS and exclusive production of various mesons. A recoil detector to identify truly exclusive final states is under development. This field is still in its infancy, and a large program will be needed to understand and disentangle the SPDs. Transverse target polarization is expected to be particularly fruitful. Each measurement constrains only a moment of one or more functions, along a trajectory in the 3-dimensional kinematic space. Exclusive meson production by longitudinal photons can provide independent constraints. HERMES is in a good position to lead the present exploratory phase.

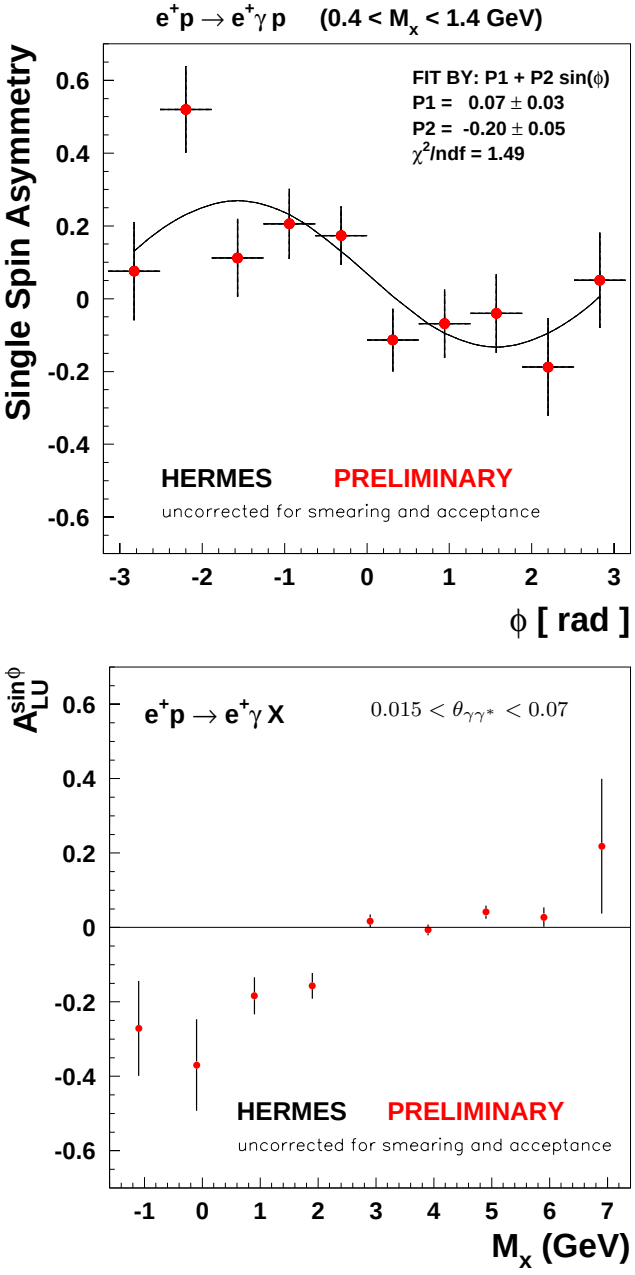

Fig. 29. Lepton beam spin asymmetries in the azimuthal distribution of photons produced semi-exclusively from an unpolarized hydrogen target.

Hadron formation times

In deep-inelastic scattering (DIS), an incident lepton interacts with a target via the exchange of a gauge boson between the lepton and a parton (a quark or an anti-quark). The struck parton is subjected to a sequence of hard parton- and soft hadron-production processes, resulting in the formation of hadrons. By carrying out DIS experiments on nuclear targets, it is possible to study the hadronization process during the time period immediately after the quark has been struck by the virtual photon. In the simplest scenario the nucleus, which has the size of a few fm, acts as an ensemble of targets with which the struck quark or the produced hadron may interact. If an interaction occurs, the number of leading hadrons produced per DIS event and per nucleon is reduced compared to that for a free nucleon. The reduction of hadron multiplicity depends on the distance traversed by the struck quark before the hadron is formed, the (unknown) quark-nucleon cross section and the (known) hadron-nucleon cross section. Hence, measurements of the multiplicity of hadrons produced on nuclei can provide information on the space-time structure of the hadronization process.

The differential multiplicity of charged hadrons and identified charged pions from nitrogen relative to that from deuterium has been measured as a function of the virtual photon energy ν and the fraction z of this energy transferred to the hadron. The results are much more precise than previous such data. There are observed substantial reductions of the multiplicity ratio R_M^h at small ν and at large z, both of which are well described by a gluon-bremsstrahlung model of hadronization, as shown in Fig. 30. The effect at large z is observed here for the first time, and is inconsistent with simple phenomenological models. A significant difference of the ν-dependence of R_M^h is found between positive and negative hadrons. This is interpreted in terms of a difference between the formation times of protons and pions, using a phenomenological model to describe the ν- and z-dependence of R_M^h.

Outlook

The HERMES collaboration intends to continue recording data in the years 2001–2006, i.e., after the

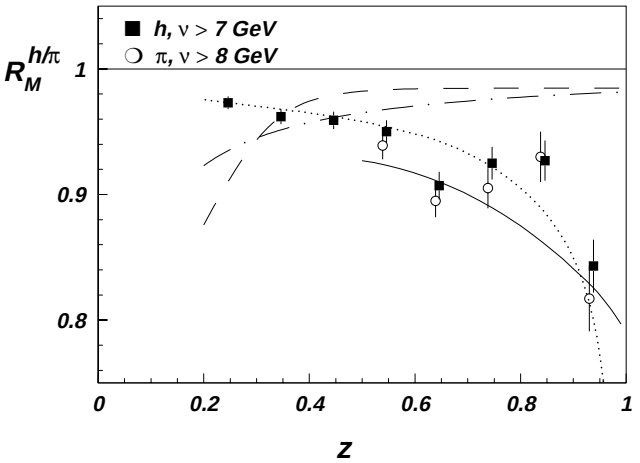

Fig. 30. The multiplicity ratio as a function of z for all charged pions (open circles) and all charged hadrons including pions (closed squares). The full curve represents a gluon-bremsstrahlung model calculation for pions. The dotted, dashed and dot-dashed curves represent phenomenological formation-time calculations, the latter with an *ad hoc* z-dependence.

HERA luminosity upgrade, as many important (and often unique) measurements can be made concerning the (spin) structure of the nucleon and related areas. The most prominent measurements foreseen include: (1) the transverse polarization of quarks, (2) the longitudinal polarization of gluons, (3) the longitudinal polarization of strange quarks, and (4) constraints on generalized or skewed parton distributions that can eventually shed light on the *orbital* angular momenta of partons. In some cases, the new measurements will enhance the precision of results already obtained at HERMES in the past years.

HERA is in a long shutdown from October, 2000 to summer, 2001 for the collider luminosity upgrade. During this time, HERMES is installing a transversely-polarized proton target with the purpose of making the first measurement of transversity, the only remaining unmeasured one of the three most fundamental (leading twist) flavour-sets of parton distribution functions. Furthermore, a wheel-shaped array of silicon counters is being installed just downstream of the target such that the acceptance for Λ^0 hyperons and J/ψ mesons (in conjunction with new wide-angle scintillators behind the magnet) will be increased by a factor of four. It is now planned to spend the next two years of running for the measurement of transversity, together with certain critical observables in exclusive processes.

HERMES collaborators include: H. Coombes, L. De Nardo, P. Green, L.G. Greeniaus, P. Kitching, G. Kotik, B. Seitz, M.G. Vincter (Univ. of Alberta); L. Felawka, M. Hartig, C.A. Miller, R. Openshaw, J. Stewart, M.C. Vetterli, S. Yen (TRIUMF); J. Wendland (Simon Fraser Univ.).

KEK Expt. 246 (Japan-Russia-Canada-Korea-U.S.A. Collaboration)
Search for T-violation in $K_{\mu 3}$ decay
(M.D. Hasinoff, UBC.; J.A. Macdonald, B. Shin, TRIUMF)

Measurement of the muon transverse polarization, P_T, in the decays $K^+ \to \pi^0\mu^+\nu$ ($K_{\mu 3}$) and $K^+ \to \mu^+\nu\gamma$ ($K_{\mu 2\gamma}$) can provide important insight to new physics beyond the standard model (SM). In $K_{\mu 3}$ decay, P_T is a T-odd observable $\mathbf{s}_\mu \cdot (\mathbf{p}_\pi \times \mathbf{p}_\mu)$ determined by the π^0 momentum $\mathbf{p}_\pi$ and the muon momentum $\mathbf{p}_\mu$ and spin $\mathbf{s}_\mu$. In $K_{\mu 2\gamma}$ decay, P_T is proportional to $\mathbf{s}_\mu \cdot (\mathbf{q} \times \mathbf{p}_\mu)$, where $\mathbf{q}$ is the photon momentum. These observables are predicted to be very small in the SM [Golovich and Valencia, Phys. Rev. **D40**, 112 (1989)], so they can be interesting probes of non-SM CP-violation mechanisms [Garisto and Kane, Phys. Rev. **D44**, 2038 (1991); Fabbrichesi and Vissani, Phys. Rev. **D55**, 5334 (1997); Wu and Ng, Phys. Lett. **B392**, 93 (1997); Bélanger and Geng, Phys. Rev. **D44**, 2789 (1991); Kobayashi *et al.*, Prog. Theor. Phys. **95**, 361 (1995)] where P_T could be as large as 10^{-3} in either $K_{\mu 3}$ or $K_{\mu 2\gamma}$.

Whether CP or T is violated or not, a non-vanishing P_T in both decays can be induced by electromagnetic final-state interactions (FSI). The value of P_T due to the FSI is expected to be about 4×10^{-6} for $K_{\mu 3}$ decay, i.e., much smaller than the expected non-SM effects. However, for $K_{\mu 2\gamma}$ decay, the FSI can induce a P_T up to 10^{-3} [Efrosinin and Kudenko, Yad. Fiz. **62**, 1054 (1999)] depending on the values of the axial vector form factor F_A and the vector form factor F_V. Moreover, P_T varies significantly over the Dalitz plot, reaching a maximum value of $10^{-3}-10^{-2}$ at large muon energies, i.e., in the region of high sensitivity to T-violating parameters.

In 1999, after the analysis of data taken in 1996 and 1997, we reported a value for P_T in $K_{\mu 3}$ of $-0.0042 \pm 0.0049(stat) \pm 0.0009(\text{syst})$ and $\text{Im}(\xi) = -0.013 \pm 0.016(\text{stat}) \pm 0.003(\text{syst})$ [Abe *et al.*, Phys. Rev. Lett. **83**, 4253 (1999)]. During 2000 we obtained the final data set and we have now completed the analysis of the 1998 data. The results continue to be consistent with zero transverse muon polarization. The statistical error of P_T for the combined 1996-98 result is expected to be about 3×10^{-3} (1σ level) which corresponds to $\delta\text{Im}(\xi) \sim 1.1 \times 10^{-2}$. The final KEK Expt. 246 sensitivity to P_T in $K_{\mu 3}$ is expected to be $\sim 2 \times 10^{-3}$ corresponding to $\delta\text{Im}(\xi)$ of about 7×10^{-3}. The systematic error will be one third the statistical error. Since statistics mainly determine the sensitivity, the detector still has a capability to improve the sensitivity at least by a factor of 3–4 using a more intense kaon beam.

Including our final run in 2000, we expect to accumulate $(2-3)\times 10^5$ "good" $K_{\mu 2\gamma}$ events. The final sensitivity to T-odd muon polarization in $K_{\mu 2\gamma}$ decay is expected to be at the level of about 1.5×10^{-2}.

In addition to the polarimeter experiments, the KEK Expt. 246 apparatus has been used to study other physics of K decays. In 2000, results were published based on the decays $K^+\to\pi^+\pi^0\pi^0$ ($K^+_{\pi 3}$) [Shin *et al.*, Eur. Phys. J. **C12**, 627 (2000)] and $K^+\to\pi^0 e^+\nu_\mu$ (K_{e3}) [Shimizu *et al.*, Phys. Lett. **B495**, 33 (2000)].

The matrix element of $K^+_{\pi 3}$ can be expanded [Weinberg, Phys. Rev. Lett. **4**, 87 (1960)] to lowest order in s_i as:

$$|M|^2 \sim 1 + gY + hY^2 + jX + kX^2....$$

where $Y=(s_3-s_0)/m^2_{\pi^+}$, $X=(s_1-s_2)/m^2_{\pi^+}$ with $s_i=(M_K-M_i)^2-2M_kT_i$ and $s_0=(M_K^2+2M^2_{\pi^0}+M^2_{\pi^+})/3$, $g=0.594\pm 0.0219$ and $h=0.035\pm 0.015$. In the present experiment both π^0s can be reconstructed; hence the values j and k can be determined for the first time. j should be zero if CP invariance holds. If CP violation is present, it should be about –3.3 times the value observed in $K^+\to\pi^+\pi^+\pi^-$. The coefficients h and k provide information on whether the final state contains more than one state of isospin, and thus provide a test of the $\Delta I=1/2$ rule, which states that $\Delta I=1/2$ transitions are dominant in kaon decays. The confirmation of this rule stems from the ratio of branching ratios, $\frac{\Gamma(\pi^0\pi^0\pi^+)}{\Gamma(\pi^+\pi^+\pi^-)}$, which proves $\Delta I=5/2$ and $\Delta I=7/2$ are absent but nothing about the presence of $\Delta I=3/2$ terms, which may arise from a $\Delta I=1/2$ strangeness-nonconserving current. In this experiment we have determined the following values: $g=0.518\pm 0.039$ and $k=0.043\pm 0.020$. Hence the quadratic term in (s_2-s_1) is small but nonzero, and the new world average value for g becomes $g=0.587\pm 0.019$, in excellent agreement with the value $g=0.582\pm 0.021$ for the CP symmetry partner $K^-\to\pi^-\pi^0\pi^0$. Furthermore, the $\Delta I=1/2$ rule seems to be violated since the prediction for g_{+00} is 0.43 using $g_{++-}=-0.2154\pm 0.004$ and $g_{--+}=-0.217\pm 0.010$.

This kinematically complete experiment also allows a nearly model independent determination of both the isoscalar and isotensor $\pi-\pi$ scattering lengths free from the usual problems caused by the final state hadronic and Coulomb interactions. Our measured values lead to a value for the Weinberg parameter in nearly perfect agreement with the value $W=0.56$ currently predicted by the Goldberger-Treiman relation.

The semi-leptonic K_{e3} decay proceeds via W exchange in the SM with pure $V-A$ coupling. However, a previous in-flight K^+-decay experiment [Akimenko *et al.*, Phys. Lett. **B259**, 225 (1991)] reported anomalous scalar and tensor couplings, as did a KTeV result [Tesarek, hep-ex/9903069 (1999)] from neutral K_{e3}. The existence of these exotic couplings is in distinct disagreement with the SM and requires an acurate experimental check.

Using the KEK Expt. 246 apparatus with its high degree of control over systematic effects, we were able to obtain clean samples of K^+_{e3} decays using the torroidal spectrometer at two values of the magnetic field to analyze e^+'s, and the CsI(Tl) array to measure the π^0's. Selection criteria on time of flight, two-photon invariant mass and e^+ – π^0 opening angle were the main strategies used to reject the major backgrounds to less than 0.3% of the total 4×10^4 K^+_{e3} events.

The Dalitz plot of the selected events was then fit to the theoretical Dalitz plot derived using the general Lorentz invariant form of the matrix element, with the potential scalar, f_S, and tensor, f_T, coupling strengths and the q-dependence, λ_+, of the vector coupling as parameters. When the pure $V-A$ form is assumed, λ_+ is the only free parameter. It was found that the value of λ_+ was consistent with the world average, with or without the inclusion of exotic couplings, and that the values of f_S and f_T were consistent with pure $V-A$ coupling, in contrast to the previous experiments.

TJNAF Experiment E00-006
Measurement of the flavour singlet form factors of the proton ($G\emptyset$)
(W.T.H. van Oers, Manitoba)

The structure of the nucleon at low energies in terms of the quark and gluon degrees of freedom is not well understood. The $G\emptyset$ experiment is to measure two proton ground state matrix elements which are sensitive to point-like strange quarks and hence to the quark-antiquark sea in the proton. The matrix elements of interest are the elastic scattering vector weak neutral current charge and magnetic form factors, G^Z_E and G^Z_M, respectively. These can be extracted from a set of parity-violating electron-proton scattering measurements. If one assumes a relationship between the proton and neutron structure in that the proton and neutron differ only by the interchange of up and down quarks, i.e., isospin symmetry, the strange quark (as well as the up and down quark) contribution to the charge and magnetic form factors of the nucleon can be determined. This would result from taking appropriate linear combinations of the weak neutral form factors and their electromagnetic counterparts.

Determinations of both the charge and magnetic strange quark form factors are of fundamental interest, as these would constitute the first direct evidence of the quark sea in low energy observables. It is the objective of the $G\emptyset$ experiment to determine these contributions to the proton form factors at the few percent level. Observations at high energy suggest that the

strange quarks carry about half as much momentum as the up and down quarks in the sea. It is important to determine both the role of the quark sea and the relevance of strange quarks at low energy where there are voids in understanding the theory of the strong interaction (quantum chromodynamics, QCD). Even if the strange quark contributions do not amount to the level of sensitivity of the experiment, upper limit determinations at this level are as valuable as non-zero results. The matrix elements, G_E^Z and G_M^Z, are also relevant to discussions of the Ellis-Jaffe sum rule and the pion-nucleon sigma term; there is uncertainty in both of these about the strange quark contributions. The $G\emptyset$ experiment will allow the determination of the strange contributions to the proton charge and magnetic form factors in a much more straightforward manner than is possible with regard to the corresponding observables in the above two deduced relations.

In the $G\emptyset$ experiment, parity-violating longitudinal analyzing powers will be measured in electron-proton scattering in the range $0.1 \leq Q^2 \leq 1.0\,\mathrm{GeV}^2$ at both forward and backward angles. The longitudinal analyzing power is defined as

$$A_z = (1/P)\frac{[\sigma^+(\theta) - \sigma^-(\theta)]}{[\sigma^+(\theta) + \sigma^-(\theta)]}$$

where P is the polarization of the incident electron beam and the $+$ and $-$ signs indicate the helicity state. Making pairs of measurements at forward and backward angles will allow the separation of G_E^Z and G_M^Z. Predicted longitudinal analyzing powers range from about (–3 to 35) $\times\ 10^{-6}$; it is planned to measure the longitudinal analyzing powers with statistical uncertainties of $\Delta A/A = 5\%$ and systematic uncertainties related to helicity correlated effects of $\Delta A \leq 2.5 \times 10^{-7}$. In the first phase of the experiment longitudinal analyzing powers will be measured concurrently at seven values of the momentum transfer in the range $0.1 \leq Q^2 \leq 1.0\ \mathrm{GeV}^2$. It now appears highly probable that by the time of data-taking for the $G\emptyset$ experiment (starting in 2002) higher beam polarizations ($\sim$70%) will also be available at the reduced beam pulse frequency of 31 MHz, decreasing considerably the original estimate of 700 hours for the first phase of the experiment. However, it must be realized that the length of the experiment is in part governed by making rather elaborate control measurements to determine the corrections that have to be made to the measured asymmetries and to assess systematic errors. In the second phase of the experiment each subsequent backward angle analyzing power measurement would require from one half to one month of running time. The results of the SAMPLE experiment at the MIT-Bates Laboratory have shown the importance of measuring the axial form factor corrections, since these appear to be quite different from the theoretical predictions. Therefore, companion measurements of quasi-elastic scattering from deuterium will also be made at the backward angles (to be proposed at a future Program Advisory Committee meeting). With these measurements, the effective axial current of the nucleon will also be determined. This current includes effects from the effective axial coupling of the photon to the nucleon or anapole moment, which are relevant also in other processes, e.g., parity violating Moller scattering and atomic parity violation.

The $G\emptyset$ collaboration

The $G\emptyset$ experiment will be carried out in Hall C at TJNAF by a collaboration of scientists from Canada, France, Georgia, and the United States, with funding provided through NSERC (Canada), IN2P3 (France), and DOE/NSF (US).

Canadian contributions

The Canadian members of the $G\emptyset$ collaboration, based at the universities of Manitoba and Northern British Columbia, and TRIUMF, have been asked to: (i) develop and produce specialized photomultiplier tube bases for the main detector arrays; (ii) prototype and produce the cryostat exit detector arrays for the backward angle measurements; (iii) prototype and produce the Aerogel Čerenkov arrays for background rejection in the backward angle measurements; (iv) coordinate the implementation of TJNAF built specialized beam monitors and control apparatus, and TRIUMF built parity-type electronics to read out these monitors on the Hall C beam line; (v) design, build, and test an automated magnetic field measuring apparatus complete with its own data acquisition system; and (vi) devise a set of measurements to determine the neutron background to which the $G\emptyset$ detector system will be subjected. Much progress has been made in the designing and building of the various subsystems listed above.

The $G\emptyset$ main detector array

The heart of the $G\emptyset$ detection system is a spectrometer which consists of an eight-sector toroidal magnet, with an array of scintillation detectors located at the focal surface of each sector (see Fig. 31). Since data will not be acquired in event-by-event mode in this experiment, and the scintillator arrays are the only detectors to measure the scattered particles in the forward angle mode, the performance of these focal-plane detectors (FPD) is of critical importance. The timing and pulse shape characteristics of this system must be fine-tuned at the hardware level as it will not be possible to reconstruct individual events. Furthermore, the rates associated with many of the FPD elements

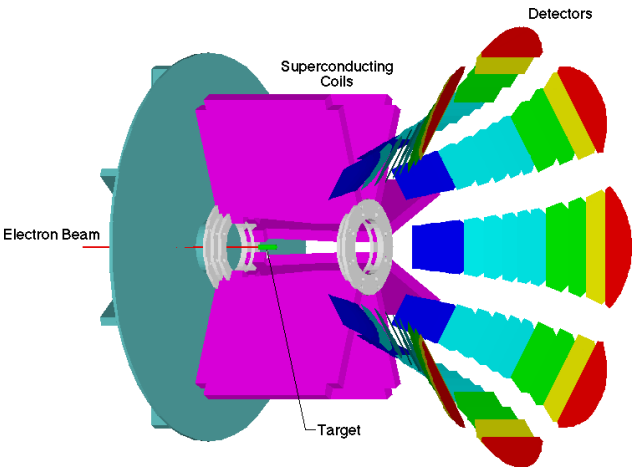

Fig. 31. View of the $G\emptyset$ superconducting toroidal spectrometer with one sector and the housing removed.

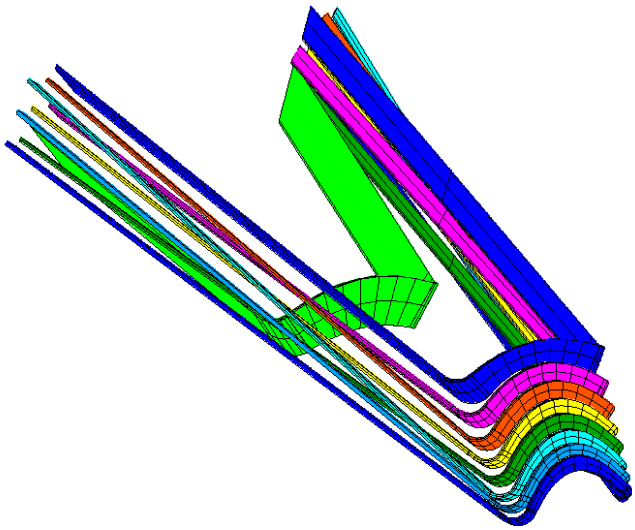

Fig. 32. Geometry of the cryostat exit detector (CED) array for a single octant.

will be quite high (1 MHz) and the photon yield(s) will have a large dynamic range. As such, very special demands will be made on the photomultiplier tubes (PMT) and especially on their associated divider/base circuit. Much progress has been made in the design, development, and building of the $G\emptyset$ bases at TRIUMF. Several iterations of prototype high-rates bases were constructed and tested in late 1997 and early 1998. In the summer of 1998, 12 final prototype bases were constructed and delivered to TJNAF for tests with the first set of prototype FPDs, and fabrication of the production bases began. With the help of summer students (funded partly through the TRIUMF Summer Students program and partly through the $G\emptyset$ NSERC grant), the fabrication of the electrical components for all of the production bases was completed in late summer, 1998. The design of the mechanical housing for the PMT-base subsystem depended on the final design of the FPD support structure and, after much effort resolving subsystem integration issues, the final design for the PMT-base housing assembly was completed in late 1998. The fabrication and assembly of the mechanical housings and integration of the electrical components was completed over the summer of 1999 (again with the help of summer students at TRIUMF). Final testing of the completed bases was carried out in late fall, 1999, and shipment of all the bases (300 units) to TJNAF occurred at the end of calendar year 1999. The remaining task for this subsystem, integration with the FPD arrays and the DAQ electronics, is presently being carried out at TJNAF as assembly of the FPD system proceeds.

The cryostat exit detector array

For the backward angle measurements during the second phase of the $G\emptyset$ experiment, simulation results have shown that the addition of a second array of scintillation detectors, located near the spectrometer-cryostat exit windows, will be required in order to separate the elastic and inelastic electrons. The geometry of these cryostat exit detector (CED) arrays has been studied in detail (see Fig. 32), and a reference design was completed in the spring of 1999. Due to the resident expertise at TRIUMF in producing high quality scintillation detectors and lightguides, the Canadian subgroup has been asked to play the main role in the prototyping and production of the CEDs. A set of prototypes was built at TRIUMF and delivered to Louisiana Tech University for further studies in early summer, 1999. Results from these studies indicate that the reference design and the prototype detectors will meet the specification requirements for the CED arrays. Upon finalizing the CED design in the summer, production of a set of final blank prototype detectors was completed at TRIUMF and delivery made to Louisiana Tech University for assembly tests with the CED support structure. Construction of the CEDs started at TRIUMF in late 2000 and will continue on into 2001. The CEDs will also make use of the same photomultiplier tubes and specialized TRIUMF/$G\emptyset$ bases as the FPDs.

Aerogel Čerenkov array

Recent Monte Carlo simulation results have shown that backgrounds due to negative pions will be problematic for the second phase backward angle measurements. Present efforts of the $G\emptyset$ Simulation subgroup (which includes members of the Canadian subgroup) include studying and characterizing this π^- background and providing options regarding the design of a set of veto detectors. The $G\emptyset$ Canadian subgroup has been asked to undertake the prototyping and construction of this crucial set of veto detectors, which will

be made up of arrays of Aerogel Čerenkov counters. A conceptual design is shown in Fig. 33.

Beam position and current monitors

Five sets of XYQ monitors will be required in order to measure the beam current and trajectory at several critical locations. A beam current sensitivity of $\pm\, 4 \times 10^{-5}$ measured in a 33 ms integration-time sample will be required to monitor and correct for possible helicity correlated intensity modulations. For the beam position monitors (BPM), a spatial resolution of better than 25 μm at an integration time of 33 ms will be required. The beam current and position monitors were tested during an engineering run in July, 1997 at TJNAF. The run was organized by members of the $G\emptyset$ Canadian subgroup and personnel from TJNAF (Hall C), with much of the parity-type electronics provided by the Canadian subgroup. Helicity correlated properties of the TJNAF polarized electron beam and noise characteristics of some of the beam monitors were successfully measured. Analysis of the data indicates that the beam current and position monitors will meet the specification requirements listed above. Further test beam time is planned for the future. To read out the analogue signals from the beam current and position monitors, and to provide feedback control signals, specialized parity-type electronics is required for the $G\emptyset$ experiment. Much of this electronics, such as precision analogue subtractors/dividers and precision voltage-to-frequency converters, has already been designed and used by members of the Canadian subgroup in their parity experiments at TRIUMF. Modifications, driven by $G\emptyset$ requirements, were made to some of these modules and they were operated successfully at the July, 1997 engineering run at TJNAF, as mentioned above. Since that time, several voltage-to-frequency converters of the TRIUMF/parity variety have been requested by TJNAF for the $G\emptyset$ experiment. Construction of these 32-channel precision V-to-Fs was completed at TRIUMF and delivery made to TJNAF in early 1998. With the successful implementation of these first sets of converters, a second set of V-to-F modules was requested by TJNAF in summer, 1999. This second set of V-to-F modules was again constructed at TRIUMF and delivered to TJNAF in fall, 1999. At present, a third set of V-to-F modules has been requested by TJNAF and is presently under construction at TRIUMF. It is anticipated that several more sets of V-to-F modules, as well as other specialized parity-type electronics modules, will be required by the $G\emptyset$ collaboration over the next few years as the experiment moves into the commissioning and data-taking phase.

Fig. 33. Conceptual layout of the Aerogel Čerenkov veto detector for a single octant.

Magnetic field measuring apparatus

An automated field measuring apparatus will be used to provide a magnetic verification of the $G\emptyset$ superconducting toroid by determining the locations of a pre-specified set of magnetic reference points. These reference points correspond to the zero-crossing locations of specific field components at selected points of symmetry around the toroidal magnet. This measurement will be carried out by scanning a predefined set of contour lines, and determining where specific field components reverse signs. The system must be capable

of providing a position determination of ± 0.2 mm and a field determination of ± 0.2 G. Over the past year, considerable effort has gone into the design and construction of this magnetic field measuring apparatus or magnetic verification device at TRIUMF and the University of Manitoba (see Fig. 34). The device consists of a programmable gantry – capable of full 3D motion anywhere within a 4 m × 4 m × 2 m volume – with a set of high precision Hall probes, temperature, inclination, and photo sensors mounted at the end of a probe boom on the gantry. Procurement of parts commenced in early 2000, and assembly and testing began in late spring at TRIUMF. The magnetic verification device was completed in mid-summer and transported to the University of Illinois for final tests and commissioning. This task was carried out by members of the $G\emptyset$ Canadian subgroup and TRIUMF personnel at the University of Illinois during the fall, and will be followed by a first set of measurements on the $G\emptyset$ spectrometer in early 2001. Although this magnetic verification device is being designed, tested, and built by the Canadian subgroup at TRIUMF and the University of Manitoba, it should be noted that funding for all hardware components of this subsystem has been provided via NSF funding for $G\emptyset$ through the University of Illinois. Infrastructure support, however, has been provided by TRIUMF and the University of Manitoba.

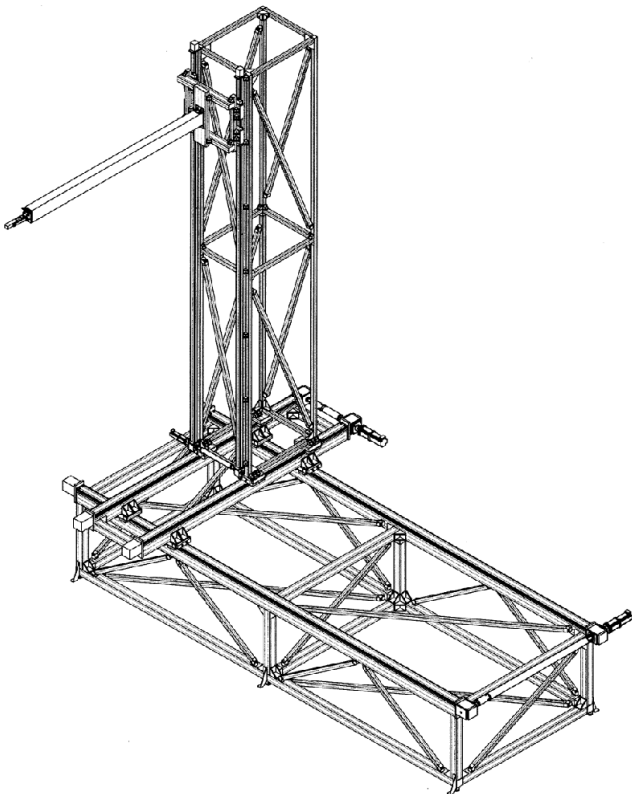

Fig. 34. Drawing of the magnetic verification device, which consists of a programmable gantry (capable of full 3D motion anywhere within a 4 m × 4 m × 2 m volume) with a set of high precision Hall probes, temperature, inclination, and photo sensors mounted at the end of a probe boom on the gantry.

Neutron background studies

A set of measurements is being devised to determine the neutron background and energy spectrum in the vicinity of the $G\emptyset$ detector system. This effort is being coordinated by the Canadian subgroup with help from members of the TRIUMF Safety group (L. Moritz and others) and personnel from TJNAF. The present set of proposed measurements makes use of a Multisphere (Bonner sphere) detector system, which is capable of determining the neutron energy spectrum at specific locations. The Multisphere detector consists of a ^{6}LiI(Eu) scintillation counter system, used in conjunction with a set of moderating polyethylene spheres. Neutron rates/yields are measured via the neutron capture reaction $^6\mathrm{Li}(n,\alpha)t$ in the scintillator, under different moderating sphere configurations. The underlying neutron energy spectrum can then be unfolded from the set of yield measurements. Test beam time in Hall C was made available in December, 1999, and a first set of neutron background measurements using the Multisphere detector(s) was carried out. Data from this test run have been analyzed and preliminary results have been disseminated. Further test beam time is planned for the future. Presently, one Multisphere detector system exists at TRIUMF and was made available for this measurement. Current plans are to build 2 more ^{6}LiI(Eu) scintillation counters to enable the studies to be completed in a timely manner.

Canadian subgroup of the $G\emptyset$ collaboration: J. Birchall, W.R. Falk, E. Gamroth, A. Horning, C. Hynes, L. Lee, S.A. Page, W.D. Ramsay, A. Rauf, G. Rutledge, W.T.H. van Oers (Manitoba); E. Korkmaz, T. Porcelli (Northern British Columbia); C.A. Davis (TRIUMF).

Experiment 704
Charge symmetry breaking in $np \rightarrow d\pi^0$ close to threshold
(A.K. Opper, Ohio; E. Korkmaz, UNBC)

Experiment 704 expects to have a high precision measurement of charge symmetry breaking in the strong interaction completed by mid-2001. The observable of interest is the forward-backward asymmetry (A_{fb}) in $np \rightarrow d\pi^0$, which must be zero in the centre of mass if charge symmetry is conserved and has a predicted value that ranges between $(-35 \rightarrow +70) \times 10^{-4}$ [Niskanen, Few-Body Systems **26**, 241 (1999); van Kolck *et al.*, Phys. Lett. **B493**, 65 (2000)] depending on the strengths of the various contributions (see Fig. 35). The forward-backward asymmetry is defined as $A_{fb}(\theta) \equiv \frac{\sigma(\theta)-\sigma(\pi-\theta)}{\sigma(\theta)+\sigma(\pi-\theta)}$ with the relevant contributions being the neutron-proton mass difference (δ), exchange of an isospin mixed $\eta-\pi$ meson, and the effect of the d u quark mass difference on pion nucleon scattering.

The experiment was carried out with a 279.5 MeV neutron beam, a liquid hydrogen target, and the SASP spectrometer positioned at 0°. With these kinematics and the large acceptance of SASP the full deuteron distribution was detected in one setting of the spectrometer, thereby eliminating many systematic uncertainties. Measurements of np elastic scattering with incident neutron beams that fill the same target space and produce protons that span the momentum distribution of the $np \rightarrow d\pi^0$ reaction provide a stringent test of the acceptance description of the spectrometer. A measurement of the $pp \rightarrow d\pi^+$ distribution accompanied the primary measurement as a test of the analysis and simulation codes, since the deuteron distribution from $pp \rightarrow d\pi^+$ must be symmetric in the centre of mass. With over seven (ten) million $np \rightarrow d\pi^0$ ($pp \rightarrow d\pi^+$) events and six million np elastic events, the statistical uncertainty of this measurement is 5×10^{-4}. The anticipated systematic uncertainty is 10×10^{-4}.

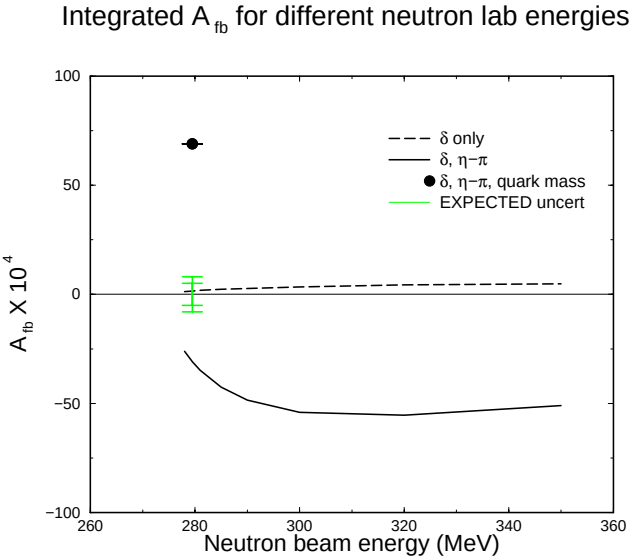

Fig. 35. Calculated contributions to A_{fb} and *anticipated* uncertainties.

Data analysis

Experiment 704 production data are analyzed in four successive passes: (1) detector calibration, (2) beam direction determination in the SASP-centric front end wire chamber coordinate system, (3) final extraction of the deuteron kinematic locus, and (4) efficiency determination. Analysis of all $np \rightarrow d\pi^0$ data had been completed by the end of 1999 and the $pp \rightarrow d\pi^+$ data analysis was completed a few months later.

Analysis efforts at the beginning of 2000 focused on developing and using code to determine the proton contamination and detection efficiencies for pions and protons in the $pp \rightarrow d\pi^+$ data as these are required in the simulation of this reaction. Thorough examination of these data uncovered anomalous wire hits which could not be correlated with problems in the FASTBUS readout system. Eventually an inconsistency between the readout code and the analysis code was discovered that led to the unusual hit patterns. The analysis code has since been modified to check for consistency between it and the readout code and make corrections if necessary. The first pass of the data to calibrate the detectors only uses events with a single cluster of wires in each of the front end wire chamber (FEC) planes. Consequently, events in which the additional hits led to multi-clusters in the wire planes were not used to calibrate the detectors and the effect of the code inconsistency was a small reduction in the statistical determination of the calibrations. A similar situation exists in the second pass of the analysis which determines the incident beam angle to within ± 0.10 mrad and showed a difference between 0.10 and 0.20 mrad when the new code was used. Although the effect of this on A_{fb} was later shown to be small, all $np \rightarrow d\pi^0$ data were reanalyzed through the second pass and a combined third-fourth pass.

In addition to extracting the kinematic locus and detector efficiencies, the last pass of analysis also produced a filtered data set of 8 words/event (four target variables and four focal plane variables) for all good locus events. The filtered data set of ∼200 Mb can be re-sorted and analyzed in one hour on a Linux box. The

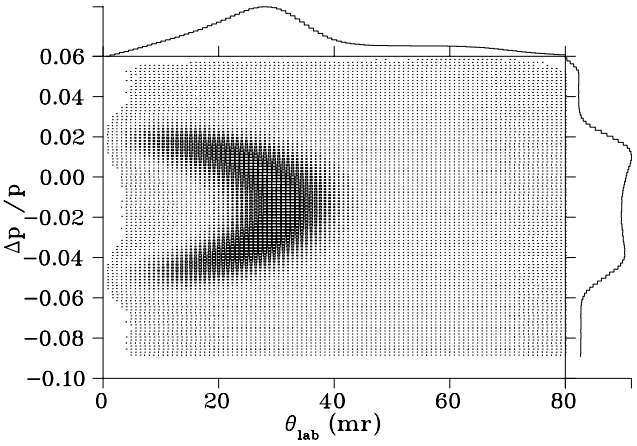

Fig. 36. Kinematic locus of all $np \to d\pi^0$ data.

reanalysis of the $np \to d\pi^0$ data took approximately two months and was finished at the end of September. The kinematic locus for these data is seen in Fig. 36. Three cycles of $pp \to d\pi^+$ data (November, 1997; July, 1997; August, 2000) have been reanalyzed and were used in the development of a $pp \to d\pi^+$ simulation. The reanalysis of the remaining $pp \to d\pi^+$ data is ongoing.

GEANT simulation of Expt. 704

At the beginning of the year a full review of the GEANT description of the experimental equipment was undertaken to verify consistency between it and reality. This description includes modelling of the beam, definition of all volumes and surfaces from the target to the focal plane detectors, as well as the orientation of magnetic fields with respect to the equipment. With the exception of a few constraining surfaces which are discussed below, the model of the equipment is in agreement with the best known blueprints, "as-built drawings", and recent measurements. This was a major job taking almost four months to complete.

Systematic effect of uncertainty in incident beam direction

As discussed above, the incident beam direction can be determined to within ±0.10 mrad. The systematic effect of this on A_{fb} was expected to be small and with the GEANT simulation of the experiment in good agreement with reality an investigation was carried out to quantify this effect. Nine GEANT runs were generated filling a 3 × 3 parameter space of angle offset vs. A_1/A_0. The inputs to the GEANT run at the centre of this 3 × 3 space were nominal (incident angle = 3.5 mrad, A_1/A_0 = 0.00%); the step size in the incident angle was ±1.0 mrad and that of A_1/A_0 was ±1.00%. Each run had 2.8 million events in it. These runs were compared to a statistically independent nominal run and the resulting χ^2 space analyzed. The error matrix from this indicated that the correlated uncertainty in A_1/A_0 due to an uncertainty in the incident angle is ±0.06%/mrad. Thus, the systematic effect on A_{fb} due to the uncertainty in the incident beam angle is $\pm 0.6 \times 10^{-4}$.

Minimization of a three dimensional space

As a test of the simulation and the χ^2 minimization procedure, a 3 × 3 × 3 parameter space was generated, the 27 runs compared to the data of a single $np \to d\pi^0$ cycle, and a χ^2 minimum found. The parameters of this test were the incident beam energy, momentum of the central ray of SASP, and target thickness. The nominal values for the simulation were taken from the data: the beam energy was extracted from the maximum lab scattering angle and found to be 279.755 MeV, a target thickness of 20.44 mm was determined from the centroid of H0 calibration data and target temperature of that cycle, and the magnetic fields of SASP were set to a central momentum of 711.425 MeV/c. Step sizes in the simulation were ±0.5 MeV in beam energy, ±2.0 mm in target thickness, and ±2% in central momentum. The three dimensional minimization found a strong correlation in (target thickness, p_0) space and a consequently larger $\sigma(p_0)$. This was tested by manually zeroing the χ^2 (target thickness, p_0) partial derivatives. While the values of the parameters listed in Table VII are in good agreement and the χ^2/dof is very close to one, obvious disagreements between the data and simulation can be seen in Fig. 37. The source of this disagreement is thought to be an incorrect description of the SASP acceptance, which is described below.

Table VII. Results of a 3-D minimization and data.

	3D minimization	Data
LH_2 (mm)	19.23 ± 0.12	20.44 ± 0.66
E_{beam} (MeV)	279.806 ± 0.005	279.755 ± 0.020
p_0 (MeV/c)	713.405 ± 0.054	711.425 ± 0.035
χ^2/dof	1.116	

Input from other mechanisms

This experiment requires a knowledge of the energy dependence of deuteron reaction losses in the range of 100 to 150 MeV, with an accuracy of order 0.1%, for input to the GEANT simulation. The GEANT subroutine GHEISHA treats deuterons as "heavy fragments" and is improper in that (1) the total cross sections are purely geometric "black disk" with no energy dependence, (2) no inelastic scattering occurs for kinetic energies above 100 MeV, and (3) below 100 MeV the relative cross sections for various reaction channels seem to be chosen purely on the basis of reaction Q-values and

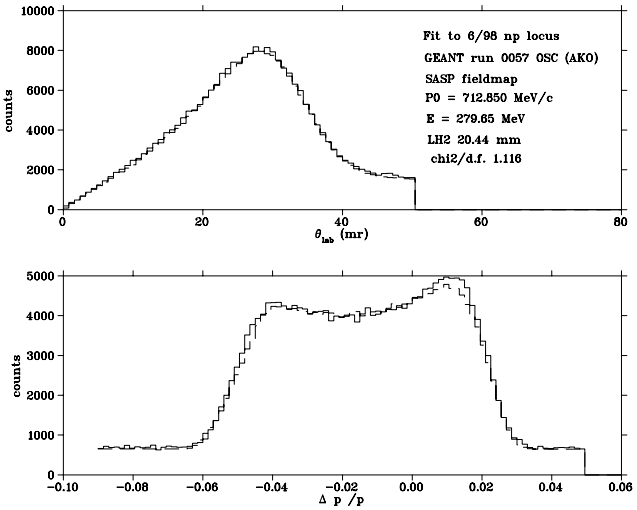

Fig. 37. Projections of the kinematic locus of one $np \to d\pi^0$ cycle and a GEANT simulation using target thickness, beam energy, and p_0 values that minimize χ^2.

the energy/angle distributions based solely on phase space.

Data on total reaction cross sections of deuterons on various nuclei, of elastic scattering of deuterons by ^{1}H, ^{12}C and ^{16}O, as well as a model (due to Glauber) for deuteron breakup cross sections have been incorporated into lookup tables which the GEANT simulation uses. The simulation gives good agreement with measured reaction rates and the energy dependence of those rates. An analysis with a simple Monte Carlo indicates that an uncertainty of 50% in the momentum dependence of these rates will produce a systematic effect of $\pm 14 \times 10^{-4}$ on A_{fb}. The collaboration is searching the literature for more precise deuteron cross section measurements so we can meet our precision goal of $\pm 10 \times 10^{-4}$.

Model of SASP acceptance

The acceptance of SASP is a complicated function of the position and angle at which the deuteron is produced and its momentum (X_i, θ_i, Y_i, ϕ_i, and δ). Describing this acceptance properly requires an accurate model of the magnetic fields in SASP because (1) deuterons can collide with interior surfaces of SASP and be lost from the locus and (2) the reconstructed momentum variable, which is a function of the focal plane variables X_f and θ_f, may be distorted in a momentum dependent way by an inaccurate model. The SASP dipole has a non-uniform gap and magnetic saturation causes the field to sag at the high-field (small gap) region, relative to ideal. Experiment 704 took data with the spectrometer powered to a field that lies between that of the comprehensive field maps. We now have four descriptions of the SASP dipole: (1) a model based on RAYTRACE, (2) the 875 A map scaled to 907 A, (3) the 950 A map scaled to 907 A, and (4) a linear combination of the two maps that correspond to 907 A. The map-based models were developed in the latter part of 2000.

Robust tests of the simulation must involve comparison of the model and data for observables that are independent of A_{fb}. To that end, two sets of acceptance calibration data were taken, namely (1) the measurements of the SASP dispersion, taken with high resolution ^{208}Pb(p,p') (small beamspot on target), and (2) measurements of (n,p) elastic scattering (large secondary beam on target). The measurements of np elastic scattering were done with fixed magnet settings and three different incident beam energies to produce protons with δ = –4, 0, +4% and thereby span the momentum distribution of the $np \to d\pi^0$ deuterons.

The ^{208}Pb(p,p') calibration data were taken with constant fields on the SASP magnets and different beam energies so as to also span the momentum range of interest. Extracting the dependence of the projectile momentum on its detected position in the focal plane detectors (X_F) from these data led to a third order function of X_F:

$$\delta = \left(\frac{X_F}{P_1}\right)\left[1 + \frac{X_F}{P_2}\left(1 + \frac{X_F}{P_3}\right)\right],$$

where P_i are the coefficients of the fit. We see a discrepancy of ∼17% between the P_2 extracted from this calibration data and that extracted from a simulation using the scaled 875 A map. The other coefficients from the simulation are in good agreement with those from data or have no effect on A_{fb}. We believe the description of the SASP magnetic fields will not improve greatly and there will still be a discrepancy between the value it gives for P_1 and that of the data. Consequently we will treat the simulation as a "different spectrometer" but be consistent in the analysis techniques used. Thus, we will use the techniques developed to determine the functional form of $\delta = \delta(X_F)$ from the ^{208}Pb(p,p') data in a simulation with the best model of the SASP magnetic fields to determine a similar function for analysis of simulated data.

Investigation of the dependence of the focal plane proton peak centroids and widths (from the np elastic scattering data) on the position or scattering angle at the target reveals good agreement between data and simulation if analysis is restricted to a small acceptance volume. However, some discrepancies do exist if the full acceptance employed in the analysis is used. These discrepancies could result from a mismatch in the SASP optical parameters. Reducing any differences between the measured and GEANT np elastic matrix elements may increase the range of acceptance that we can safely use.

Comparisons of matrix elements from np elastic data and those from simulations with models (1) and (2) above, for all three momentum values, show better overall agreement with model (2). The matrix elements from the RAYTRACE model show discrepancies with data that range from a few to 20%, whereas those from the 875 A map range from 0 to 8%. The increased agreement with the field map is especially pronounced for the $< X_f|X_i >$ matrix element which must be described well if we are to use most of the large spatial extent of the target. The precision of the matrix element description is at the 5% level. GEANT simulations that used $< X_f|X_i >$ correlations differing by 6% yielded A_{fb} values that differed by 1.4×10^{-4}.

To investigate the momentum dependent effects, projections of Y_i and ϕ_i have been made for slices in X_i and θ_i and ratios of these distributions made for data vs. GEANT and for the –4% vs. +4% momentum sets. The basic features of these ratios are understood in terms of the focusing action of the SASP entrance quads, Q1 and Q2. For "onside" rays, those in which Y_i and ϕ_i have the same sign, the –4% rays are defocused more strongly by Q1 than are the +4% rays and they tend to be lost at the exit of Q1. For "offside" rays, those which have opposite signs for Y_i and ϕ_i, the differential losses occur at the exit of Q2, where it is the +4% rays which tend to be lost more due to less defocusing in Q2. These features appear in both data and GEANT but GEANT does not accurately represent the shoulder region where the acceptance in ϕ_i begins to fall. The inner surfaces of the quads are complex and modelled consistently with the most reliable blueprints. It is unlikely that the model of these magnetic elements will improve in a reasonable amount of time. Consequently, we have determined cuts which exclude those portions of the acceptance that cannot be adequately modelled. These cuts are on target position and angle and define regions of uniform acceptance. Much effort was directed at developing a method to find the flat acceptance range in an automated and unbiased manner. Fits were done for three ranges in θ_i and only a weak dependence on θ_i was found. The application of these acceptance defining cuts from np elastic data on the $np \to d\pi^0$ data are found in Table VIII; a similar procedure remains to be done on the GEANT simulations.

Table VIII. Effect of tabular cuts on $np \to d\pi^0$ data.

Cut	Total events in locus $\times 10^6$	Deuterons in locus $\times 10^6$	Fraction
X_i, Y_i	14.19	7.78	100.0%
$+ \theta_i$	11.38	7.34	94.3
$+ \phi_i$	9.49	6.34	90.07

Other activities

Near threshold the maximum deuteron scattering angle in the lab is strongly dependent on the beam energy. Relative beam energies have been extracted from the maximum deuteron scattering angle for all cycles. In these data, the uncertainty in that angle is $\pm$ 0.1 mrad which leads to an uncertainty in the average beam energy of $\pm$ 20 keV. Target thicknesses for all cycles have been extracted from centroids of H0 running and np elastic scattering. The thicknesses have been corrected for target temperature variations.

The last pass of the analysis produces efficiency profiles for the detectors; these exist for all $np \to d\pi^0$ data. Typically the VDC planes are ∼99% efficient. These efficiency distributions vary across the VDC planes and lead to false values of A_{fb} that range from -0.000530 ± 0.000085 to $+0.000280$ with a comparable uncertainty. While these instrumental asymmetries are small, they are significant on the anticipated scale of the observable and must be included in the simulation. Code to use these efficiency profiles has been added to the simulation.

To reduce the possibility of psychological bias in matching simulation to data, a "black box" subroutine has been added to the simulation. This routine adds a (hidden) offset to the A_1/A_0 asymmetry parameter used to set up the $np \to d\pi^0$ generator in the simulation. A member of the collaboration not involved in simulation development selected the offsets from a predetermined range, compiled the subroutine on all simulation farms, mailed the source code to two people outside the collaboration, and deleted the source code.

Final steps

As described below, A_{fb} can be determined from the $np \to d\pi^0$ and np elastic scattering data. The $pp \to d\pi^+$ data might possibly be used to constrain the deuteron reaction losses. However, these data may be too difficult to model accurately, due to the momentum correlated charged particle backgrounds. These and other uncertainties may make the reaction loss information obtained from $pp \to d\pi^+$ of limited precision and, therefore, limited usefulness. With the human resources for this experiment being very limited we have decided to use the $np \to d\pi^0$ and np elastic scattering data to determine A_{fb} and return to the $pp \to d\pi^+$ data and simulation at a later date.

Determine acceptance

The np elastic scattering data provide the best means to determine the acceptance in that the incident beam of this reaction fills the target parameter space in a way that is similar to that of the $np \to d\pi^0$ reaction. Consequently the simulation must agree with these

data. Improvements to the description of the SASP magnetic fields are (1) determine $\delta = \delta(X_F)$ for the simulation and (2) remove aberrative effects from the simulation using the same techniques that are used for the data. We will then finalize the cuts that define uniform acceptance in the np elastic scattering data and in the magnetic field based simulation, and apply these to the $np \to d\pi^0$ data. A robust test of the acceptance will be simulation vs. data comparisons of A_1/A_0 extracted from target subspaces, e.g. A_1/A_0 from $X_i > 0$ and from $X_i < 0$. If the difference between simulated and measured values of A_1/A_0 is larger than can be expected from statistics, the tightness and ranges of the acceptance cuts will have to be changed so as to bring the simulation into agreement with the data.

Determine systematic sensitivities

Simulation vs. simulation comparisons will be carried out to determine how strongly the experimental parameters are correlated with A_1/A_0. For each parameter this will involve simulating kinematic locus scatter plots for a 3×3 grid of the experimental parameter vs. A_1/A_0, calculating the χ^2 of those nine plots when compared to a plot simulated with nominal values, and fitting the χ^2 space. The correlation of A_1/A_0 with the experimental parameter will be obtained from the error matrix based on the curvature of the χ^2 space. Combining this correlation with the uncertainty in the parameter gives the systematic sensitivity of A_1/A_0. Note that the uncertainty in the parameter comes from a separate determination and not from the χ^2 minimization. We are currently going through this procedure for ten different parameters; the results for the sensitivity to the incident beam direction are discussed above.

Determine correlated parameters

The effects of some of the parameters are correlated and they will have to be treated differently. This step will also involve simulation vs. simulation tests, however this time the χ^2 minimization and correlation studies will be done in parameter$_i$ vs. parameter$_j$ space, where i and j indicate correlated parameters. If necessary, three parameters may have to be fit simultaneously.

Obtain A_1/A_0

At this point all the inputs to the simulation will be fixed except for p_0, the average nominal beam energy, and A_1/A_0. If there are other parameters which cannot be constrained by an independent determination, they will have to be added to the fit. Note that for each parameter added to the fit, a dimension is added to the χ^2 space and the number of "grid" points increases dramatically. The whole data set will then be simulated with appropriate weightings of target thickness, relative beam energy, and efficiency profiles for each cycle. A_1/A_0 will be determined by minimizing χ^2 over this multidimensional parameter space. Correcting this value of A_1/A_0 for the offset from the "black box" subroutine will yield A_{fb}.

Experiment 715
Weak interaction symmetries in β^+ decay of optically trapped ^{37,38m}K

(J.A. Behr, TRIUMF; K.P. Jackson, TRIUMF/SFU)

Summary

The β^+-ν correlation measurement in the $0^+ \to 0^+$ Fermi decay of ^{38m}K has collected data this August and October with statistical error on the angular correlation coefficient a of $\approx 0.3\%$. The electric field apparatus was completely redesigned and rebuilt, and a successful external review was held. Our intention now is to publish our preliminary number based on the ISAC April, 1999 data as soon as possible. The final answer will be published when the analysis is complete. As the new geometry is cleaner, we hope to extend the analysis to as low a β energy as possible. This will enable simultaneous extraction of limits on a and the Fierz interference term bm/E from a single experiment; something which only we can do.

The spin-polarized program has made considerable progress. Vector polarization of $P = < M_I > \approx 90\%$ in stable ^{41}K was demonstrated in the off-line lab with a simple atomic probe, in a simplified version of what is eventually planned. The apparatus was moved to the on-line lab. Four shifts were spent in a test run to evaluate nuclear detection hardware, using the present chamber geometry to explore limitations to assist design of the next apparatus. Approximately 60% nuclear polarization of ^{37}K was achieved. The goal was to attempt a first time-reversal violating D coefficient test; although this was not possible, much was learned about potential systematic effects.

Scalar search in ^{38m}K β^+-ν correlation

Present status of other experiments and theory

In addition to the published work in the β-delayed p emission of ^{32}Ar [Adelberger *et al.*, Phys. Rev. Lett. **83**, 1299 (1999)], which achieved $\tilde{a}_{\rm Fermi} = \frac{a}{1+b\frac{m_e}{E}} = 0.9989 \pm 0.0052 \pm 0.0039$, there are two other experiments approaching publication and several other proposals. A Dubna/Orsay/Louvain collaboration has an experiment on the γ-ray Doppler shift of ^{18}Ne and a published preliminary result with an error on a of 0.10 [Egorov *et al.*, Nucl. Phys. **A621**, 745 (1997)], and is close to publishing a result with a statistical error of 0.01 on a. A Dubna/Louvain/PSI experiment using a forbidden transition in μ capture on ^{16}O says they will

publish a number soon with a statistical error of 0.01 on C_S (the above experiments are primarily sensitive to C_S^2), but with unknown and possibly large theoretical error.

In addition to the possibilites cited in the past of constraining the couplings and masses of elementary exchange bosons like a charged Higgs [Herczeg, in *Precision Tests of the Standard Electroweak Model*, P. Langacker, ed., p.786 (1994)], additional phenomenological motivation exists for constraining the parameters C_S and C'_S. The Los Alamos Theory group can explain a possible excess of events at the tritium β decay endpoint by an admixture of ν_e with a 5 eV ν and in addition a non-standard model interaction, either a right-handed vector interaction or a scalar interaction – in particular, constraints on scalars coupling to right-handed neutrinos are required [Stephenson *et al.*, Phys. Rev. **D61**, 093013 (2000)]. If the above limit of Adelberger *et al.* can be improved by a factor of three, that would rule out the scalar interaction explanation [Goldman, private communication].

To interpret the eventual result on C_S and C'_S in terms of exchange bosons, which couple to the quarks and leptons, a scalar form factor for the nucleon $g_S = <p|\bar{u}d|n>$ is needed. A compilation and evaluation of previous models gives values between 0.25 and 1.0 [Herczeg, *op. cit.*]. This quantity is related to form factors recently evaluated in lattice gauge theory [Liu *et al.*, Phys. Rev. **D59**, 112001 (1999)] by an isospin rotation, and the result is $|g_S| = 0.63 \pm 0.09$. The calculational method gives quantities such as g_A in agreement with experiment to ≈10% [Woloshyn, private communication], and is therefore more than adequate for this purpose.

Experiment details

Isotope production and trapping

The ISAC production target is now pressed $CaZrO_3$ disks. The target was tested with as much as 2.5 μA proton beam. 1.5×10^7/s ^{38m}K was delivered reliably for 4 weeks of running at 1.5 μA of proton beam. 6×10^6/s ^{37}K was delivered for the 4 shift spin-polarized run.

No Dryfilm degradation was observed during these runs. 15 keV energy ion source operation proved to be difficult and unreproducible, presumably due to transmission problems through the separator. Diffusion of ^{37}K was measured at 30 keV and compared to 15 keV; the percentage released was at most only 20% worse at 30 keV, so 30 keV was used.

E field

An error discovered in the electrostatic field calculation geometry resolved most of the E field error, reducing the discrepancy between measured and calculated field from 4% to < 1%. Nevertheless, we upgraded the apparatus to: 1) shield all ceramics and HV connections with conductors; 2) simplify the geometry to make the field more uniform to allow simpler ion trajectory reconstruction; 3) use lower-Z glassy carbon electrodes to reduce backscattering and minimize eddy currents when switching B fields quickly for polarized experiments; 4) use high-Z passive collimation to reduce straggled β^+s and β^+s from wall backgrounds. A top view of the new apparatus is shown in Fig. 38.

Assuming the trap position is given by the TOF of the neutral recoils (see below), the E field can be measured by the TOF of: the fastest recoils; photoionized atoms at rest; and a population of events where a β^+ hits the MCP, directing the recoils away from the MCP. The three measurements of the E field agree to within 5 V/cm out of 810 V/cm. The field is thus more uniform than the field used in April, 1999. The discrepancy with the 800 V/cm calculated field remains to be understood, but using this measured determination of the field lowers the estimated error in a from the electric field to <0.2%.

Absolute trap position from Ar^0: Ar^- ?

The measured value of the E field is strongly correlated with the trap position. The trap position is given most precisely by the TOF of the fastest neutrals. A 0.4 mm systematic error in trap position would explain the E field discrepancy. The presence of long-lived Ar^- species would affect this leading edge. There is a known 250 ns lifetime Ar^- metastable. To explore this, data were also taken at 400 V/cm field. A precise determination was made of the neutral recoil TOF spectra, with the trap in identical positions. The presence of long-lived Ar^- species would be indicated by a difference from unity of the ratio of the TOF spectra. The

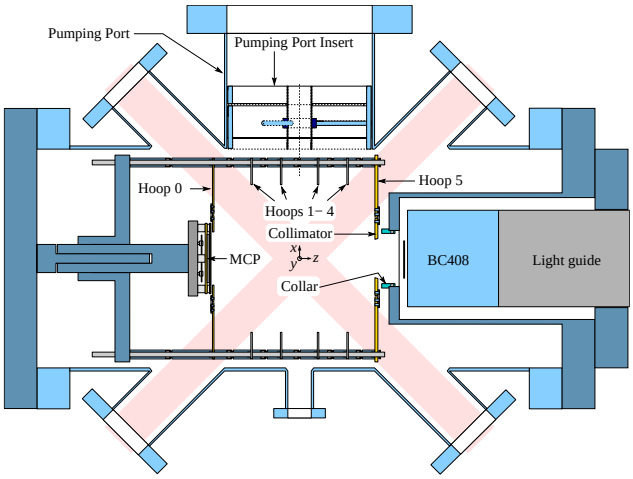

Fig. 38. Top view of new $\vec{E}$ field apparatus.

potential error in trap position was measured to be negligibly small.

Beta telescope

The β^+ telescope is a 0.46 mm thick double-sided Si strip detector with 24 × 24 1 mm wide strips for position sensitivity, backed by a 6.5 cm diameter × 5.5 cm long BC408 plastic scintillator with energy resolution 9.2% at 1.6 MeV. Calibration and characterization of this complex device were completed in the M.Sc. thesis of Dan Melconian, June, 2000.

MCP efficiency has been measured

We have measured the efficiency of the MCP as a function of energy in two ways. Probability of photoionization of ^{41}K was measured, with results limited by systematic power fluctuations of the N_2 laser borrowed from the detector facility. This measurement implies the dependence is very similar to Ar at these energies. ^{38m}K data were taken at electric fields of 765 and 735 V/cm. The resulting recoil energies span the range of interest for the 800 V/cm field where most of the data were taken, and the MCP efficiency is constant to a level that limits the error in a to $< 0.2\%$.

Photoionization of radioactives also allows the size and position of the trap to be determined in the other 2 dimensions (in addition to the TOF axis), which is otherwise not possible to disentangle in the two CCD cameras.

Radiative corrections

We plan to get these from Glück in Budapest, who did similar calculations for ^{32}Ar and has expressed keen interest in the past, now that our analysis is sufficiently advanced that we know what to ask for. The correction to a was 0.3% in ^{32}Ar. It is not needed for the preliminary publication, but must be included in the Monte Carlo for the final analysis. (Glück supplied a table to Adelberger *et al.*)

Ar^0 TOF spectra and MCP efficiency for neutral recoils

We measured the ^{37}K β-ν correlation with better balanced MOT polarized beams, to try to achieve zero polarization. The goal was to test the MCP efficiency as a function of recoil energy for the Ar^0. The ^{37}Ar ion data were consistent with the standard model, while the neutral data were badly inconsistent; suggesting an efficiency for neutrals dropping 25% per 100 eV. This is too large a correction to make in the ^{38m}K data, so we will not use the Ar^0 data for the ^{38m}K β-ν experiment.

Error budget

The systematic errors are shown in Table IX.

Table IX. Systematic errors for ^{38m}K as of December. $\vec{E}$ field error assumes trap position known from Ar^0 TOF (see text). Backgrounds from walls and β^+ backscattering are negligible.

Error	Dec/99	Dec/00
$\vec{E}$ field	0.5-2.0%	<0.2%
$E_{\beta+}$ detector:		
Tail/total	0.2%	0.2%
511 summing/total	0.2%	0.2%
Calibration nonlinearity	<0.5%	<0.25%
MCP Eff[E_{Ar+}]	<0.6%	< 0.2%
Sum systematics	<0.8%	<0.5%
Statistics	≈0.8%	≈ 0.3%

Fits to TOF spectra of Ar ion recoils

The fit to the Ar ion TOF spectra from April, 1999 data is shown in Fig. 39. This produces a preliminary result $\tilde{a} = 0.992 \pm 0.008$ (stat) $\pm$ 0.005 (syst).

Experimental plans for spin-polarized observables

Physics motivation

We have listed in detail in the past the physics justification for the right-handed current experiments. We summarize here the physics justification for direct time-reversal violating measurements. These can be done without complete knowledge of the polarization.

The parity-even coefficient D of the vector product $\vec{J}_N \cdot (\vec{p}_\beta \times \vec{p}_\nu)$ is the time-reversal odd correlation most naturally measured with our β^+-recoil coincidence techniques. A recent calculation of D in the standard model predicts it to be at the 10^{-12} level [Herczeg and Khriplovich, Phys. Rev. **D56**, 80 (1997)]. The best experiments to date have set limits at $<6 \times 10^{-4}$ [Hallin *et al.*, Phys. Rev. Lett. **52**, 337 (1984)]. Thus any violation at experimentally foreseeable levels would be from new physics beyond the standard model.

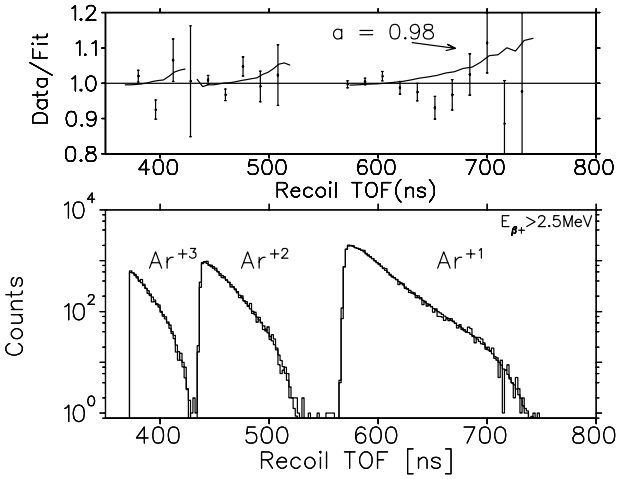

Fig. 39. Preliminary Monte Carlo fit to recoil ^{38}Ar +1,+2,+3 TOF spectra, $E_{\beta+} > 2.5$ MeV.

Some possible contributions to D, such as leptoquarks, are *not* constrained by electric dipole moment experiments, while other contributions (from left-right symmetric models and exotic fermion models) are indirectly constrained by EDM experiments, although in a model-dependent fashion [Herczeg, in *Symmetries and Fundamental Interactions in Nuclei*, Haxton and Henley, eds. (World Scientific, Singapore, 1995), p.111]. Final state effects that mimic time reversal are smaller in ^{37}K than in ^{19}Ne by $\approx 2\times$, on average $\approx 1.0 \times 10^{-4}$, and they have an almost linear dependence on E_{β^+} which can be measured and tested [Holstein, Phys. Rev. **C5**, 1529 (1972)].

Off-line lab polarization progress

Polarization of $\geq 92\%$ of ^{41}K was achieved in the off-line lab. Details are summarized in the Experimental Facilities section of this Annual Report.

First ^{37}K polarization tests

A similar scheme was implemented in the on-line lab, with optical pumping light perpendicular to the detector axis. In the present chamber geometry, the optical pumping beam could not be retroreflected, and this limited the ^{41}K polarization (this can be easily remedied by adding ports). Otherwise, this would be a possible geometry for a D coefficient measurement.

The atoms are polarized along the X direction; β^+s go along the fixed Z direction; charged recoils can be measured going to + or – Y. The position dependence is measured in the MCP, and would shift as the polarization is flipped if there were a finite D coefficient. The polarization can be monitored along the X direction by looking at the recoil asymmetry, both in singles and in coincidence with the β^+; in both cases there is a large, calculable asymmetry.

This geometry provides a complete set of monitors for systematic errors. For example, the recoil singles – which will show no time-reversal violating effect – can be used to monitor unwanted residual polarization along the Y axis. It may be possible to find a true polarization axis about which the recoil singles have no asymmetry, and look for a D coefficient with the recoil coincidences about that axis.

The polarization was also monitored with β^+s in the double-sided silicon strip detector, as even though it is close to 90° it still has finite analyzing power and excellent statistics. In addition, we have demonstrated for ^{38m}K that the MCP has double hits which are β^+'s followed by Ar recoils; that may eventually allow a critical check on D, as false D's will have the same sign for β telescope recoil coincidences as for MCP double hits, while the effect of a true D coefficient will have opposite sign because the β^+ is in opposite directions.

Raw data are shown in Fig. 40, showing asymmetries in the X and Y directions. A clear, large asymmetry in the X direction is generated in each case; unfortunately, a much smaller but still finite unwanted Y asymmetry also exists. The recoils, together with the β^+ singles, indicate that between 50 and 70% nuclear polarization was achieved. We will attempt to find the polarization axis as outlined above, but it is clear that purer polarizations will be needed for real experiments.

Circularly polarized FORT

There are a variety of neutral atom traps that may provide better polarization in the future. In particular, a spin-polarized far-off resonance dipole force trap under development (by Weiman) traps atoms in one magnetic substate. In principle, this trapping technique has little dependence on the quality of circularly polarized light [Cho, J. Korean Phys. Soc. **30**, 373 (1997)], and is free of depolarizing quadrupole B fields. Recent progress has been made in loading this trap efficiently [Corwin *et al.*, Phys. Rev. Lett. **83**, 1311 (1999)]. Our intention is to begin development of this technology in spring, 2001, using an existing Ar ion laser and standing-wave Ti::Sapph.

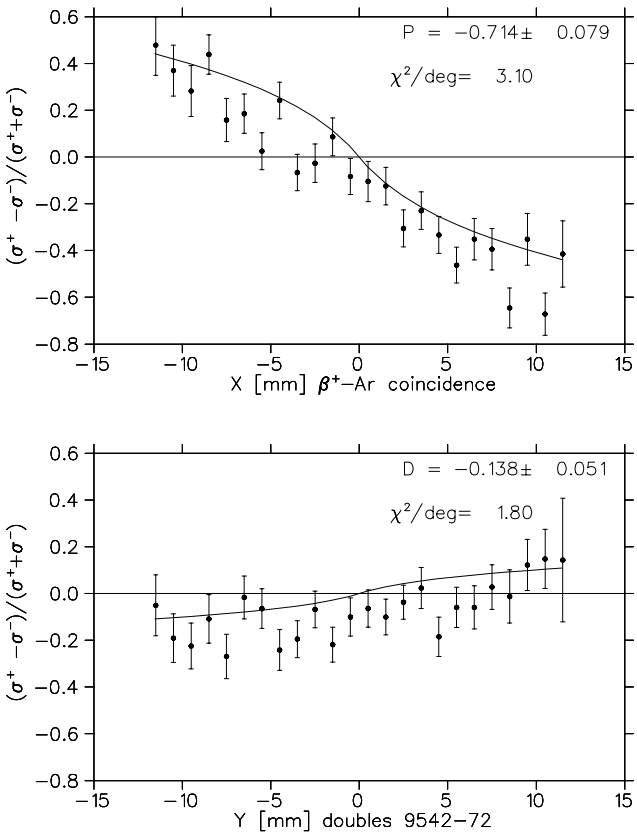

Fig. 40. Asymmetry in MCP position for β^+-Ar coincidence.

Experiment 741
Beta-delayed proton decay of ^{17}Ne to α-emitting states in ^{16}O
(J.D. King, Toronto)

The goal of this experiment is to obtain an α-particle spectrum from the break-up of ^{16}O following the β-delayed proton decay of ^{17}Ne, and to use this spectrum to reduce the uncertainty in the ^{12}C$(\alpha,\gamma)^{16}$O reaction rate, which is of prime importance in determining the ratio of ^{16}O to ^{12}C at the end of helium burning in stars. In Expt. 589 we measured the α-particle spectrum from the break-up of ^{16}O following the β decay of ^{16}N. Through simultaneous R- and K-matrix fits to this spectrum, to the ^{12}C$(\alpha,\gamma)^{16}$O data sets, and to ^{12}C(α,α) scattering data, we were able to reduce considerably the uncertainty in the $E1$ component of the astrophysical S-factor for the ^{12}C$(\alpha,\gamma)^{16}$O reaction, which is determined primarily by the tail of the sub-threshold 1^- state at 7.117 MeV. Since the 2^+ state at 6.917 MeV is not populated in the decay of ^{16}N, the effect of the tail of this sub-threshold state on the $E2$ component was not determined, and a very large uncertainty in this component, which could be as large as the $E1$, still exists. However, 2^+ states in ^{16}O are populated in the β-delayed proton decay of ^{17}Ne and the feasibility of using this decay is being explored in this experiment.

In last year's Annual Report we described the preliminary analysis of data from the runs of November and December, 1998, in which a high-quality time-of-flight (TOF) proton spectrum was obtained, and of the data from a run in April, 1999, in which a high-quality alpha spectrum was obtained using the ratio-cut technique. These spectra have now been fitted using Breit-Wigner line shapes for the excited states of ^{17}F, and complete decay schemes for β- and β-delayed-particle decay of ^{17}Ne have been obtained. Also, using R-matrix techniques, the spectra from β-delayed $p\alpha$ and αp decay through the isobaric analogue state (IAS) in ^{17}F at 11.193 MeV have been fitted and branching ratios for this decay mode have been extracted. Finally, an experimental arrangement which would allow an independent determination of the S-factor for the $E1$ component of the ^{12}C$(\alpha,\gamma)^{16}$O reaction is outlined.

Branching ratios

Branching ratios (BRs) for the decay of several excited states in ^{17}F via proton emission to the 6.130, 6.917 and 7.117 MeV states in ^{16}O have been obtained via proton-gamma coincidence measurements [King *et al.*, Nucl. Phys. **A621**, 169c (1997)]. However, those BRs were incomplete as they did not include proton decay to the 0^+ state at 6.049 MeV or to the ground state. Also they did not include BRs for α decay. In the 1999 Annual Report, we displayed complete proton and α-decay spectra and indicated that detailed analysis of the spectra using Breit-Wigner fitting techniques was in progress. These fits have now been completed (see Fig. 41) and a complete set of proton and α BRs for the decay of excited states in ^{17}F has been obtained. The fit functions in Fig. 41 include 58 proton transitions and 13 α transitions. The decay is complex, as illustrated in Fig. 42, and space does not permit the display of particle-decay BRs here.

Beta-decay BRs were deduced from these results and are shown in Table X, where the present results are compared with the two previous studies. In general, BRs to excited states in ^{17}F that are able to decay to excited states in ^{16}O are much higher than previously reported, since the present study has been sensitive to decay modes missed in the previous work. The BRs of states that can decay only to the ground state of ^{16}O are, accordingly, much lower.

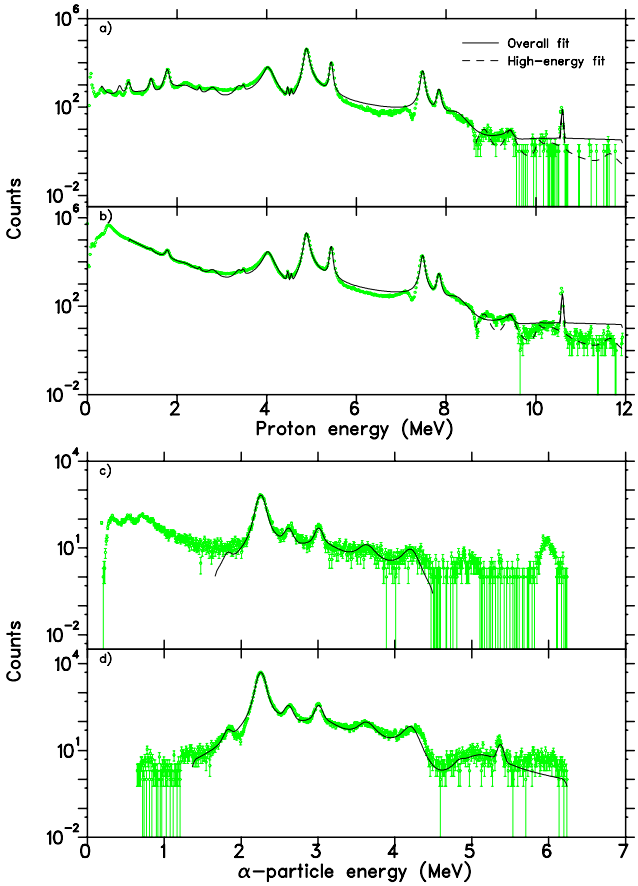

Fig. 41. Results of the simultaneous fits to a) proton TOF, b) ungated particle, c) α-particle TOF and d) α-particle, ratio-cut spectra.

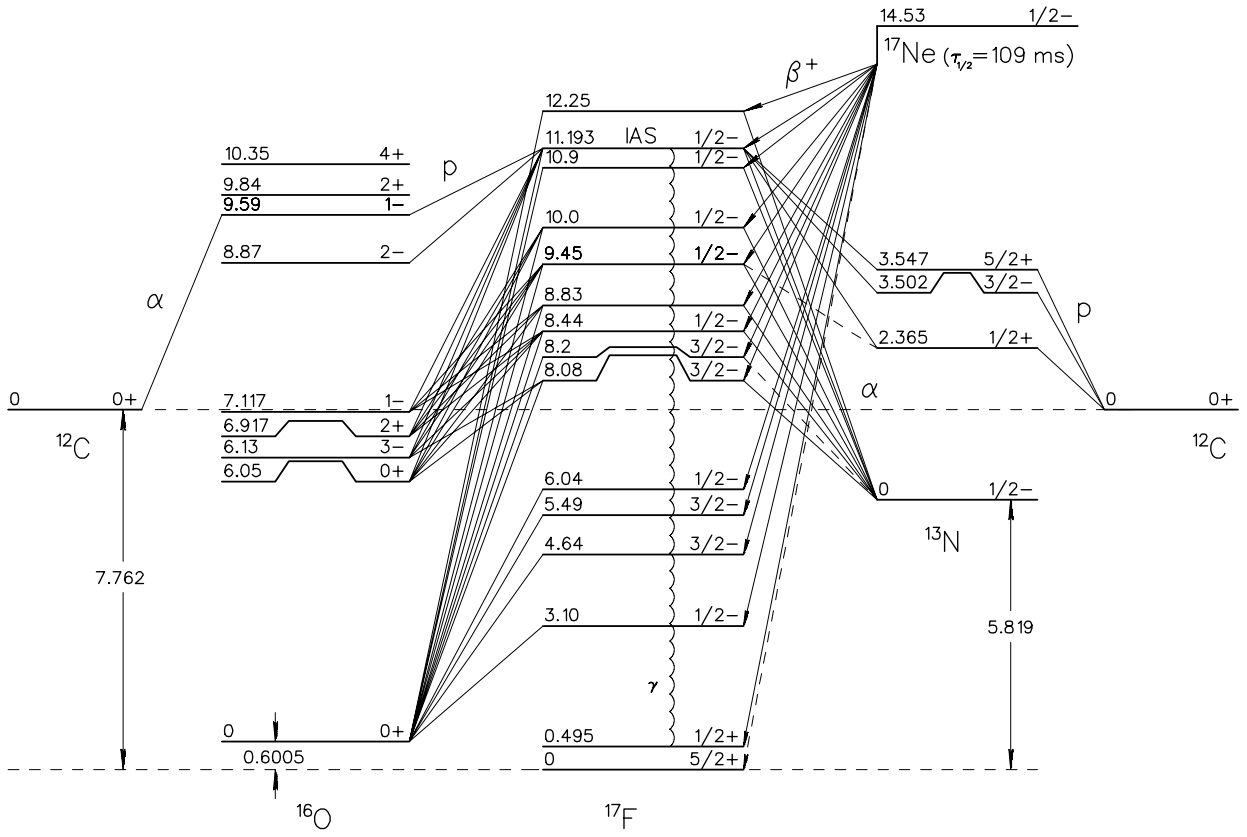

Fig. 42. Decay scheme for the β-delayed particle decay of ^{17}Ne.

Table X. Branching ratios for the beta decay of ^{17}Ne.

Final state	Branching ratios (%)		
(^{17}F)	Ref. [1][a]	Ref. [2][b]	This work
12.25	—	0.001 ± 0.0006	0.0019 ± 0.0004
IAS	$0.71^{+10}_{-0.05}$	0.64 ± 0.14	0.763 ± 0.034
10.91	—	0.016 ± 0.006	1.791 ± 0.031
10.66	—	0.007 ± 0.004	2.159 ± 0.041
10.029	—	0.7 ± 0.3	1.354 ± 0.016
9.45	0.54 ± 0.05[c]	0.6 ± 0.2	2.502 ± 0.034
8.825	1.9 ± 0.06	—	7.344 ± 0.081
8.436	6.51 ± 0.26	4 ± 0.9	7.682 ± 0.079
8.2	—	1.7 ± 0.3	3.61 ± 0.17
8.075	6.83 ± 0.11	7.3 ± 0.9	5.789 ± 0.043
6.037	10.6 ± 0.2	7.8 ± 0.2	6.823 ± 0.032
5.488	54 ± 0.7	59.16 ± 0.4	45.02 ± 0.19
4.64	16.2 ± 0.7	16.54 ± 0.14	12.873 ± 0.076
3.104	0.48 ± 0.07	$0.10^{+0.03}_{-0.01}$	0.1406 ± 0.0051
0.495	1.1 ± 0.5[d]	0.76 ± 0.13[e]	1.61 ± 0.16[f]
0	0.53 ± 0.16[d]		$< 0.55 \pm 0.18$[g]

[a]Hardy *et al.*, Phys. Rev. **C3**, 700 (1971).

[b]Borge *et al.*, Nucl. Phys. **A490**, 287 (1988).

[c]From the assignment of an observed proton group at 2.825 MeV in Ref. [1] to the 9.45 MeV state in ^{17}F.

[d]Calculated by comparison with the mirror decay of ^{17}N [1].

[e]Calculated in Ref. [2].

[f]From Borge *et al.*, Phys. Lett. **B317**, 25 (1993) and Ozawa *et al.*, J. Phys. G: Nucl. Phys. **24**, 143 (1998).

[g]From Millener, Phys. Rev. **C55**, R1633 (1997).

***R*-matrix fits**

In the 1998 and 1999 Annual Reports, we presented α-particle spectra from the β-delayed $p\alpha$ and αp decay of ^{17}Ne through the IAS of ^{17}F. An R-matrix analysis of the spectrum (shown in Fig. 43) has been carried out and branching ratios for this exotic decay have been obtained.

The single-channel, single-level R-matrix formula

$$N_\lambda(E) = \frac{P_i \Gamma_f}{(E_\lambda - E + \Delta_\lambda)^2 + (\Gamma_f/2)^2}$$

was used [Chow, Ph.D. thesis (unpublished, 2000)] to obtain the energy spectrum of the intermediate states for the three observed 3-particle decay channels of the IAS shown in Fig. 43. In this equation P_i is the penetrability of the feeding channel, Γ_f is the width of the exit channel obtained from

$$\Gamma_f = 2 P_f \gamma_\lambda^2,$$

where P_f is the penetrability of the decay channel and γ_λ^2 is the reduced width belonging to the state λ, and λ labels the three intermediate states ^{16}O(9.59), ^{16}N(2.37), and ^{16}N(3.50/3.55). The quantity Δ_λ is the level shift defined by

$$\Delta_\lambda = -[S(E) - b]\gamma_\lambda^2,$$

where $S(E)$ is the shift factor and b is the boundary condition.

This R-matrix expression was used in an algorithm to generate the particle spectra for the three decay channels which were then fitted to the experimental α spectrum as shown in Fig. 43. The fit resulted in the BRs shown in the figure for the decay of the IAS to these three states relative to the BR for the decay of the IAS to the 7.117 MeV state in ^{16}O which is set to 100.

Spectrum showing interference between 1^- states

The discovery of a decay of the IAS to the 9.59 MeV state in ^{16}O [Chow *et al.*, Phys. Rev. C**57**, R475 (1998)] suggested to us that, by using the β-delayed proton decay of ^{17}Ne in an experiment similar in principle to the case of ^{16}N decay [Azuma *et al.*, Phys. Rev. C**50**, 1194 (1994)] we might obtain an additional constraint on the $E1$ component of the ^{12}C$(\alpha,\gamma)^{16}$O reaction. Instead of being populated by a β decay as in the case of ^{16}N, the ^{16}O states are populated by a proton decay in the case of ^{17}Ne. The difference in the feeding channel makes the case of ^{17}Ne more complicated, and the experiment much more challenging, due to the involvement of 3-body kinematics.

The interference between the IAS$\rightarrow^{16}$O(9.59)+p and the IAS$\rightarrow^{16}$O(7.117)+p channels has been studied by means of a single-channel, two-level R-matrix calculation. The algorithm used for calculation of laboratory particle spectra is the same as that used for the BR calculation except that a single-channel, *2-level* R-matrix formula must be used to calculate the α energy spectrum from the decay of the ^{16}O states. The

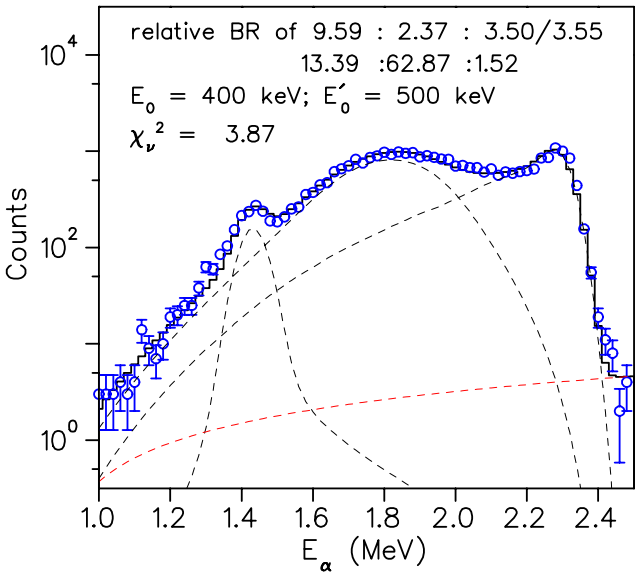

Fig. 43. R-matrix fit to the α spectrum resulting from β-delayed particle decay of ^{17}Ne through the IAS.

expression is

$$N(E,\theta') = \left| \sum_{\ell=0,2} \frac{P_{p\ell}^{\frac{1}{2}} \sum_\lambda \frac{C'_{\lambda\ell}(\theta')\gamma_\lambda}{E_\lambda - E} P_\alpha^{\frac{1}{2}}}{1-(S_\alpha - b_\alpha + iP_\alpha)\sum_\lambda \frac{\gamma_\lambda^2}{E_\lambda - E}} \right|^2,$$

where

$$C'^2_{\lambda\ell}(\theta') = \mathcal{W}_{\lambda\ell}(\theta') C^2_{\lambda\ell}.$$

The $C_{\lambda\ell}$ are proton-feeding amplitudes and the $\mathcal{W}_{\lambda\ell}(\theta')$ are functions describing the angular correlation between the emitted protons and α particles; θ' is the angle between the α and recoil nucleus in the lab frame (and (180-θ') is the angle between the proton and α). $P_{p\ell}$ and P_α are the proton and α penetrabilities, respectively. The reduced α widths obtained in the ^{16}N experiment are used and the proton feeding parameters have been normalized such that

$$\int_0^{2\pi} (C'^2_{12} + C'^2_{20}) \sin\theta' \, d\theta' =$$

$$\int_0^{2\pi} [\mathcal{W}_{12}(\theta') C^2_{12} + \mathcal{W}_{20}(\theta') C^2_{20}] \sin\theta' \, d\theta' = 1.$$

Note that C_{10} and C_{22} are assumed to be negligibly small, i.e., a particular feeding channel only populates a single level ($\ell_p = 2$ to the 7.117 MeV state and $\ell_p = 0$ to the 9.59 MeV state).

Proposed experiment

A detailed study of possible configurations of a 3-detector system using one PIPS and two DSSD detectors was carried out using these R-matrix expressions in the algorithm mentioned above. The angles between detectors and the solid angles subtended by the detectors were varied in small incremental steps. The optimum configuration is shown in Fig. 44. Also shown in this figure are additional detectors positioned so that the entire array of 8 elements provides 6 combinations of 3 elements in the same optimum geometry. An experiment designed to accumulate an α spectrum following β-delayed proton decay of the IAS would employ two such arrays, one rotated at 20° about an axis in the beam plane through the collector foil and the second rotated through 20° in the opposite sense.

Two spectra that could be obtained with such a detector array are shown in Fig. 45. The dashed curve is the α spectrum due to decay only through the 9.59 MeV state. The effect of the tail of the 7.117 MeV state on the spectrum is shown by the simulated data points. The number of counts in each energy bin from this R-matrix Monte Carlo calculation has been randomized with a Gaussian distribution to simulate statistical fluctuations. The error bars represent a 1σ

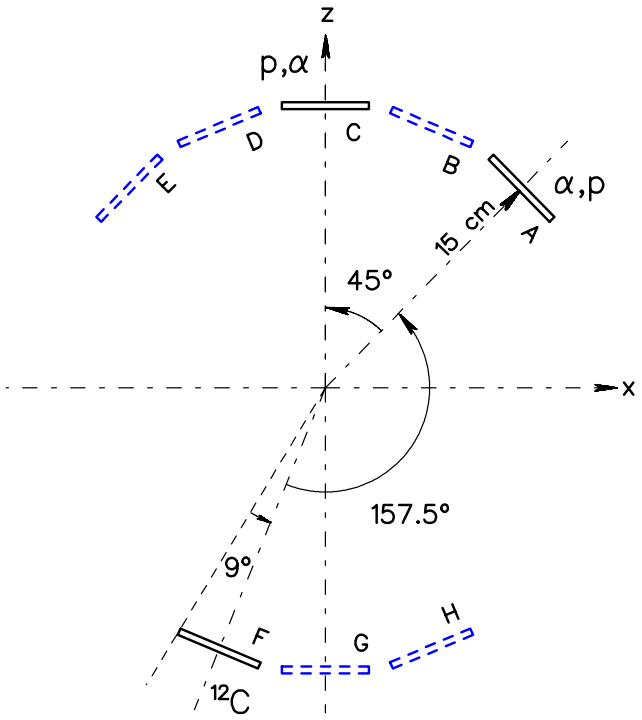

Fig. 44. Proposed detector configuration for detection of interference effects in the α spectrum following proton decay of the IAS.

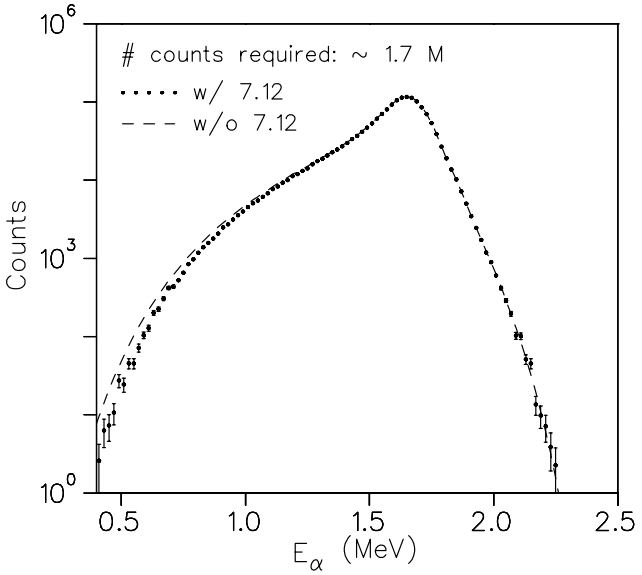

Fig. 45. Alpha spectrum expected from the detector configuration of Fig. 44 showing the effect of interference between the 7.117 and 9.59 MeV states in ^{16}O.

uncertainty and the spectra have been convoluted with an experimental energy resolution of 40 keV. The total number of counts in the spectrum is about 1.7 million.

The maximum separation between the dashed curve and randomized data points of Fig. 45 is 8σ at about 900 keV with the separation falling to about 4σ at 500 keV and 1400 keV. The triple coincidence efficiency calculated for 3 detectors in the optimum geometry is 1.2×10^{-5}. For a ^{17}Ne yield from ISAC of 10^8 s^{-1}, the triple coincidence count rate would be 0.2 s^{-1}. The entire proposed system, with 12 sets in the same geometry, would detect about 2.4 counts s^{-1}. With the estimated ISAC ^{17}Ne yield, the required number of counts could be obtained in 9 days. Yields of ^{17}Ne of more than 10^5 s^{-1} were obtained at TISOL and the extrapolated ISAC yield seems reasonable.

Experiment 778
$\pi^{\pm}p$ differential cross sections in the region of Coulomb-nuclear interference
(K.J. Raywood, TRIUMF; E.L. Mathie, Regina)

The data-taking phase for Expt. 778 was completed during the high-intensity beam periods of 2000. The analysis phase is now under way, with the aim of providing a systematic set of differential cross sections for $\pi^{\pm}p$ elastic scattering at low energy and forward scattering angles. This is the region of Coulomb-nuclear interference (CNI) where Coulomb scattering interferes destructively (constructively) with π^+p (π^-p) hadronic scattering amplitudes. This experiment is part of the CHAOS physics program whose goal is to test predictions and measure parameters of chiral perturbation theory. To this end, measurements have been made in the $\pi^{\pm}p$ sector of pion-induced pion production (Expt. 624) and elastic scattering analyzing powers (Expt. 560).

The data from this experiment will be used to determine, to a precision of a few per cent, the real part of the isospin-even scattering amplitude, D^+, at t = 0. This information is missing in the current partial wave analyses. Its inclusion will greatly improve the determination of the πN scattering amplitudes. As a result, it will improve the determination of the πN coupling constant, the πN scattering lengths and the πN Σ term; all observables of crucial importance. The Σ term, in particular, is a fundamental quantity. It is a direct measure of chiral symmetry breaking and can be obtained experimentally from the isospin-even S- and P-wave scattering lengths: $a^+_{0^+}$ and $a^+_{1^+}$.

The TRIUMF Cryogenic Targets group designed and constructed a planar cryogenic LH_2 target for this experiment. It was used with the same 12.5 mm thick cell that was used in the fall of 1999. Liquid hydrogen was maintained in the cell for periods of two to three weeks during foreground measurements. Following that, the target cell was emptied and background data were taken. The whole cycle was repeated at each energy and the target performed flawlessly throughout both high-intensity periods of 2000.

The CHAOS group was the first at TRIUMF to

use the MIDAS data acquisition system. Early in 2000, several enhancements and bug fixes were made to the software by the primary author (Stefan Ritt, PSI) and Pierre Amaudruz of TRIUMF. The result was a very stable and flexible system that continues to improve and is now used by most TRIUMF experiments.

Throughout its history, the CHAOS programmable second-level trigger has been plagued by failures of some of its component commercially built modules. This problem arose again early in the first high-intensity period of the year. The decision was made to replace the functionality of the hardware with equivalent software running in the front-end processor. This was possible because of the significant increase in speed of the front-end processor compared with the one in use when the second-level trigger was first implemented. A third-level trigger was also designed and implemented for this experiment. It was based on fast ADC information from the π/μ range stack and a rejection of almost 50% was achieved. These improvements enabled Expt. 778 to run at a high data rate with a good live-time.

The CNI experiment received beam during both high-intensity periods of 2000. CHAOS was used to measure the angle and momentum of particles scattered from the liquid hydrogen target. The π/μ range stack was positioned to accept particles scattered at small angles. Its purpose was to distinguish true scatters from the large number of in-flight $\pi \rightarrow \mu$ decays. In the analysis, the information from the stack is fed to an appropriately trained neural network in order to identify pions and muons. At each beam energy, a measurement consisted of three parts at both polarities: foreground, background and neural network training (described in previous Annual Reports). Most of the data were collected in M13, but CHAOS was moved to M11 for the fall running period. The 39 MeV data set will be used as a consistency check as a full measurement was performed on both beam lines at that energy.

A summary of the amount of data collected at each energy and polarity is given in Table XI. The quantity N_π is the live-time fraction of the total number of beam pions incident upon the target for the given configuration. It is tabulated for both foreground (fg) and background (bg) measurements. The quantity $\Delta Y(\theta_{s\text{-}p})$ is the statistical uncertainty of the yield in a 1° angular bin centred at the scattering angle of the minimum in the $\pi^+ p$ cross section. The minimum is caused by the destructive interference between S-waves and P-waves and occurs at a laboratory angle of about 25° for 45 MeV and moves to larger angles at lower energies. Thus, the aim of achieving a 2% statistical uncertainty per 1° bin at the critical minimum in the cross section has been met at most energies.

Table XI. Summary of the data collected at each experimental configuration. The 57 MeV data were collected using beam line M11 and the 39 MeV data were collected using both M13 and M11. The remainder of the data were collected using M13. The 45 MeV values shown here include data taken at two target angles.

T_π (MeV)	Polarity	$N_\pi/10^{10}$ fg	bg	$\Delta Y(\theta_{s\text{-}p})$ (% /1° bin)
15	+	5.1	1.9	< 2
15	−	3.5	1.2	2.0
20	+	3.5	2.6	1.8
20	−	1.6	1.1	2.0
26	+	2.4	1.4	2.6
26	−	2.1	1.2	2.2
32	+	3.9	2.0	2.0
32	−	2.4	1.2	1.5
39 M13	+	5.4	3.6	2.0
39 M13	−	3.1	2.7	1.5
39 M11	+	2.2	1.9	3.1
39 M11	−	1.6	1.5	2.0
45	+	1.8	1.1	3.4
45	−	1.4	0.9	2.2
57	+	6.7	2.4	2.3
57	−	2.2	0.8	1.5

Though not shown in the table, data were also collected at 67 MeV but only at one polarity (π^+) and only at scattering angles larger than those accepted by the $\pi\mu$ stack. This measurement will provide a check on the target thickness as data were taken with two target angles. The energy was chosen in the hope that these data might also resolve a long-standing conflict in the global πN database.

Experiment 801
Studies of multi-phonon states via β-decay
(R.F. Casten, Yale)

The atomic nucleus is a many-body system of strongly-interacting fermions and as such provides a fundamental "laboratory" for the study of collective excitations arising in a quantum mechanical many-body system. One of the most important issues is the relationship between single particle and collective degrees of freedom in such a system, which can be sensitively studied by investigating the properties of multi-phonon excitations of nuclear vibrational modes. Pauli exclusion effects severely restrict the freedom of individual nucleons to participate in multi-phonon collective vibrations, and it was long thought that multi-phonon excitations with unfragmented collectivity could not exist. In recent years, however, intact multi-phonon excitations have been found experimentally, and the very existence of these states provides a critical empirical test of models of nuclear structure.

Vibrational states arising from four-phonon or even five-phonon quadrupole excitations have been identified in spherical nuclei, but in deformed nuclei only a few solid candidates for states with even two phonons have been established, in ^{166,168}Er and ^{232}Th. There are a variety of challenges to the identification of multiple-phonon excitations, since these lie at energies approaching the pairing gap, above which a dense profusion of states of single-particle nature mask and admix with the collective states. A key question is thus whether the scarcity of observed multi-phonon states is due to genuine nonexistence of these states or simply to a lack of sufficiently sensitive data for their identification.

There is a straightforward signature of a two-phonon quadrupole excitation, namely that it is connected by a collective E2 transition matrix element to the one-phonon excitation of the same mode and by noncollective matrix elements to other lower states. In γ-ray intensity spectroscopy experiments, the accessible observables are ratios of matrix elements. A state with significant amplitude for a two-phonon γ vibration ($K^\pi = 0^+$ or 4^+) has a branching ratio

$$\frac{\langle K^\pi = 0^+_{2\gamma}/4^+_{2\gamma}||E2||K^\pi = 2^+_\gamma\rangle}{\langle K^\pi = 0^+_{2\gamma}/4^+_{2\gamma}||E2||K^\pi = 0^+_{\rm g.s.}\rangle} \gg 1$$

and a two-phonon β excitation ($K^\pi = 0^+$) has

$$\frac{\langle K^\pi = 0^+_{2\beta}||E2||K^\pi = 0^+_\beta\rangle}{\langle K^\pi = 0^+_{2\beta}||E2||K^\pi = 0^+_{\rm g.s.}\rangle} \gg 1.$$

The aim of Expt. 801 is to extend the search for multi-phonon excitations in deformed nuclei to the neighbours of ^{166,168}Er, by performing γ-ray spectroscopy of states populated in β-decay. The use of a compact configuration of large-volume Ge detectors, for efficent γ-γ coincidence spectroscopy, coupled with the high intensity and high isotopic purity beams available at ISAC, provides much higher sensitivity than was available in the previous generation of experiments.

In June, an experiment to study ^{162}Er was carried out at the ISAC GPS tape collector. The nuclei were produced through the decay ^{162}Yb$\rightarrow^{162}$Tm$\rightarrow^{162}$Er, which populates several low-lying excited $K^\pi = 0^+$ bands. Beam nuclei from the ISAC separator were implanted into the GPS tape, and the tape was advanced to place a fresh source in front of the detectors at one hour intervals. Two 80%-efficiency coaxial Ge detectors were positioned 12 cm from the source location, oriented obliquely with respect to each other and separated by lead shielding to suppress background coincidence events due to β^+ annihilation photon pairs and Compton cross-scattering (Fig. 46). Data were

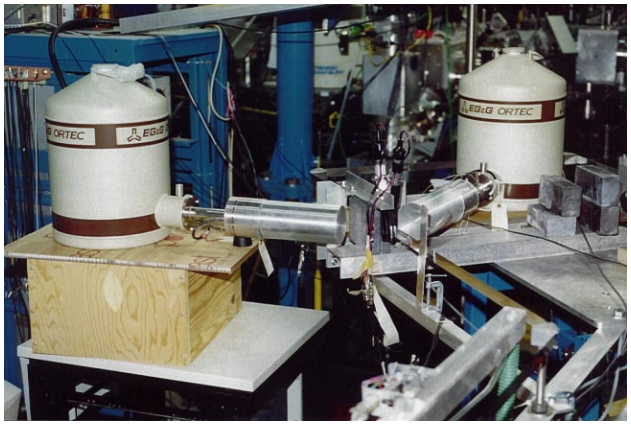

Fig. 46. Experimental set-up for Expt. 801 at the ISAC GPS tape collector system, with a compact configuration of two large-volume Ge detectors for γ-γ spectroscopy.

acquired in event mode for off-line analysis. Both singles data (1.5×10^8 events) and coincidence data (6×10^7 events) were recorded.

Preliminary analysis provides the following branching ratios (and limits) for the two lowest excited $K^\pi = 0^+$ bands, with bandheads at $E(0^+_2) = 1087$ keV and $E(0^+_3) = 1420$ keV:

$$\begin{aligned}
\frac{\langle K^\pi = 0^+_3||E2||K^\pi = 0^+_2\rangle}{\langle K^\pi = 0^+_3||E2||K^\pi = 0^+_{\rm g.s.}\rangle} &< 4 \\
\frac{\langle K^\pi = 0^+_3||E2||K^\pi = 2^+_\gamma\rangle}{\langle K^\pi = 0^+_3||E2||K^\pi = 0^+_{\rm g.s.}\rangle} &= 3.5(2) \\
\frac{\langle K^\pi = 0^+_2||E2||K^\pi = 2^+_\gamma\rangle}{\langle K^\pi = 0^+_2||E2||K^\pi = 0^+_{\rm g.s.}\rangle} &< 3.
\end{aligned}$$

The level scheme is under revision on the basis of the coincidence data. The literature indicates a $J^\pi = 1, 2^+$ level at 1412 keV, nominally the second excited $K^\pi = 2^+$ bandhead, based upon the proposed placements of several transitions. However, coincidence analysis shows these placements to be incorrect, and there is thus no evidence for existence of the level. Continued analysis is under way.

This work was supported by the US DOE under grants DE-FG02-91ER-40609 and DE-FG02-88ER-40417.

Experiment 812
Proposed study of the ^{8}Li$(\alpha, n)^{11}$B reaction
(R.N. Boyd, Ohio State)

The ^{8}Li$(\alpha, n)^{11}$B reaction is being studied with an eye toward both big bang nucleosynthesis and the stellar r-process. In big bang nucleosynthesis, this reaction becomes important if there are density inhomogeneities during that epoch. If that is the case, the ^{8}Li abundance can become large for some tens of seconds, during which time a large abundance of ^{11}B can be made.

While other reactions ultimately lower the primordial abundance of ^{11}B, during the time it is large it can undergo reactions to synthesize nuclei heavier than ^{12}C, which would produce potential big bang signatures.

At the beginning of the r-process, nuclear statistical equilibrium assembles all the nuclei heavier than ^{12}C in accordance with its prescription. However, the conditions that produce NSE are not thought to bring the nuclei lighter than ^{12}C into NSE. ^{12}C is the seed from which the nuclei formed in NSE are created, and which subsequently serve as the r-process seeds. One of the ways to circumvent the mass 5 and 8 gaps is via the ^{8}Li$(\alpha, n)^{11}$B reaction.

This reaction has been measured several times previously, but always by putting a ^{8}Li beam directly into a heavy ion counter filled with ^{4}He gas and using the tracks to determine which of the ^{8}Li ions interacted with ^{4}He nuclei to produce ^{11}B. This is probably a fairly reliable technique at energies above 2 MeV, but becomes difficult to use at lower energies, especially those below 1 MeV that are of interest to big bang nucleosynthesis and the r-process.

Thus we hope to use the ^{8}Li beam at TRIUMF to study this reaction, but to use quite a different technique to measure the cross section. We would use neutron time-of-flight measurements, which should completely circumvent the detection difficulties of the previous experiments. A 1 m^2 neutron wall from RIKEN will be brought to TRIUMF for the experiment. A special ^{4}He gas cell will be built to produce the interactions. Prior to the experiment, a ^{13}C beam will be used to produce the neutrons that will be used to calibrate the neutron wall detectors.

Experiment 823
Pure Fermi decay in medium mass nuclei
(G.C. Ball, TRIUMF)

Precise measurements of the intensities for superallowed Fermi $0^+ \rightarrow 0^+$ β decays have provided a demanding test of the CVC hypothesis at the level of 3×10^{-4} and also led to a result in disagreement with unitarity (at the 98% confidence level) for the CKM matrix [Towner and Hardy, Proc. WEIN '98 (World Scientific, Singapore, 1999) p.318]. Since this would have profound implications for the minimal standard model it is essential to address possible "trivial" explanations for this apparent non-unitarity, such as uncertainties in the theoretical isospin symmetry-breaking correction. Uncertainties in the calculated Coulomb corrections can be studied by extending the precision β-decay measurements to heavier (A $\geq$ 62, $T_z = 0$) odd-odd nuclei where these corrections are predicted to be much larger [Ormand and Brown, Phys. Rev. **C52**, 2455 (1995)]. The primary goal of the Expt. 823 experimental program is to measure the half-lives and branching ratios for the superallowed β-decay of these radioactive nuclei produced at ISAC.

Precision measurement of the lifetime of ^{74}Rb

A precision measurement of the lifetime of ^{74}Rb was carried out at ISAC in 1999. Details of this experiment and preliminary results were reported previously [see 1999 Annual Report]. A proton beam of 10 μA was used to bombard a Nb foil target to produce $\sim$4000 ^{74}Rb ions s^{-1}. A total of 38 runs, each consisting of $\sim 4 \times 10^5$ events, were carried out. The statistical error in the half-life of ^{74}Rb obtained by fitting each decay curve was $\sim$0.14 ms. No evidence of any systematic error was observed, as illustrated by the fit to the full data set shown in Fig. 47 which gives a normalized $\chi^2 = 1.06$. The weighted average of all measurements was 64.768 $\pm$ 0.026 ms; the error quoted is statistical only. A complete analysis of the systematic errors together with an independent analysis of the same data set with different prescreening criteria led to a value of 64.761 $\pm$ 0.031 ms, which includes a systematic error of 0.015 ms added in quadrature. This is the first precision measurement of any of the key decay properties for an odd-odd $N = Z$ nucleus with A $>$ 54. A paper describing this measurement has been accepted for publication in Phys. Rev. Lett.

Search for β-delayed γ emission in the decay of ^{74}Rb

An experiment to search for allowed transitions in the β-decay of ^{74}Rb to excited $(0,1)^+$ states in ^{74}Kr was carried out using a technique similar to that used

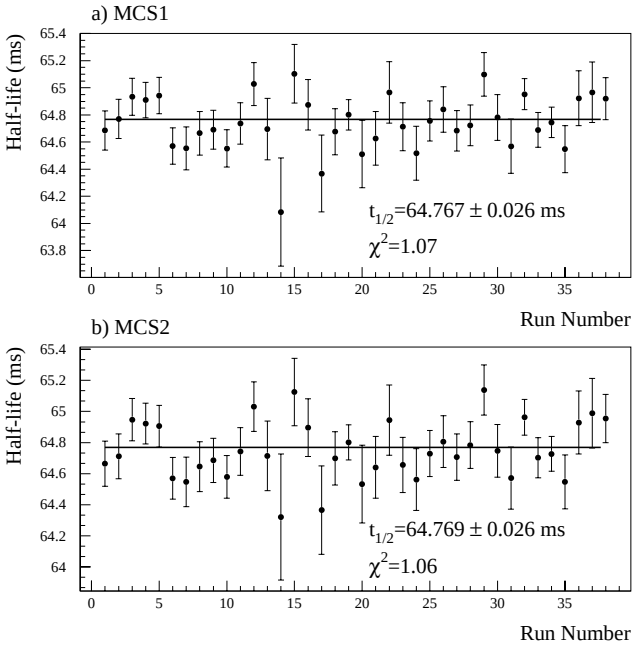

Fig. 47. Half-life results for ^{74}Rb obtained simultaneously with two independent multi-channel scalar modules.

in previous measurements [Hagberg *et al.*, Nucl. Phys. **A571**, 555 (1994)]. The fast tape transport system described previously [1999 Annual Report] was used to collect and move the ^{74}Rb samples out of the vacuum chamber and position them between two thin plastic scintillator paddles each backed by large (∼80%) HPGe detectors mounted colinearly. The cycle time was reduced from that used in the lifetime measurements by shortening the counting time to 0.5 s. The background in the HPGe detectors resulting from positrons was reduced substantially (see Fig. 48) by accepting only those β-γ coincidence events in which a positron was detected in the scintillator paddle located on the opposite side of the tape to the HPGe detector. The β-γ coincidence events were time stamped and recorded event by event. The signals from each paddle were also multiscaled to obtain the β singles rate. A total of ∼15 M positrons were detected, resulting in ∼1 M β-γ coincidence events. The efficiencies of the HPGe detectors were measured using standard sources. In addition, the β-γ coincidence efficiencies were determined by measuring the β-decay of $^{38}K_{gs}$ which has a strong branch (99.8%) to the first excited state of ^{38}Ar that subsequently decays by the emission of a 2.168 MeV γ-ray. Finally, high statistics ^{74}Ga decay data were

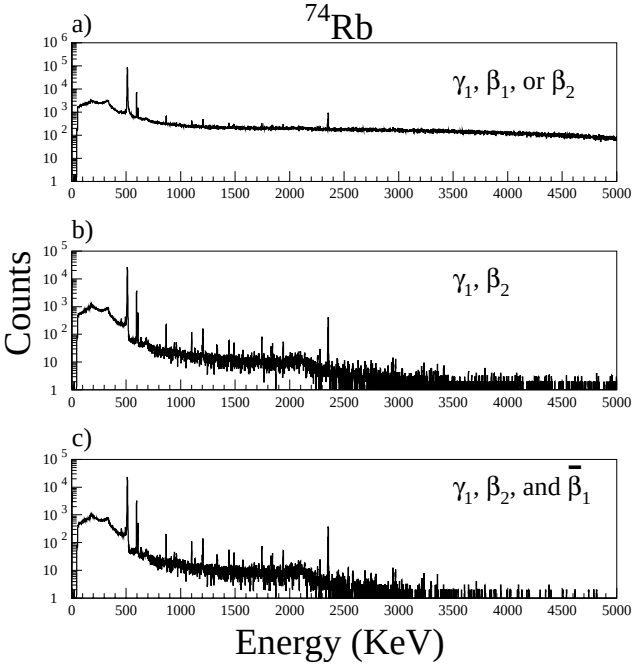

Fig. 48. γ-ray spectra obtained in the β-decay of ^{74}Rb: a) in coincidence with positrons detected in either scintillator paddle, b) in coincidence with positrons detected in the paddle located on the opposite side of the tape from the HPGe detector and c) same as in b) with the additional condition that no positron signal was observed in the scintillator paddle positioned directly in front of the HPGe detector.

obtained to better determine the isobaric contaminant background in the ^{74}Rb γ-ray spectra.

The analysis of these data is in progress. Weak Gamow-Teller/Fermi decays to one or more high-lying levels in ^{74}Kr were observed by their depopulation through the known first excited 2^+ level at 456 keV. Preliminary results indicate that the superallowed branch is the dominant transition (>99%), similar to those observed previously for odd-odd $T_z = 0$ superallowed decays. The limits that can be set for possible high-energy (∼2–5 MeV) γ-rays resulting from the β decay of ^{74}Rb to higher-lying levels in ^{74}Kr are $\lesssim$0.1%.

Search for the non-analogue transition in the β decay of ^{74}Rb to the 0_2^+ state in ^{74}Kr

The determination of the transition strengths for non-analogue $0^+ \rightarrow 0^+$ decays provides a critical test of the model predictions for the isospin mixing component of the Coulomb correction for superallowed β decays. Recently, in-beam experiments [Chandler *et al.*, Phys. Rev. **C56**, R2924 (1997); Becker *et al.*, Eur. Phys. J. **A4**, 103 (1999)] have revealed the existence of a low-lying, isomeric 0_2^+ level in ^{74}Kr at 508 keV which decays primarily by an electric monopole transition to the ground state of ^{74}Kr. A preliminary experiment to search for the β decay of ^{74}Rb to this excited 0_2^+ level was carried out in May-June at a new target station, GP2, provided by TRIUMF. Most of the experimental hardware was provided by new Expt. 823 collaborators from LSU. In this measurement the ^{74}Rb atoms were implanted into a 6 mm wide mylar tape of a moving tape-transport system that operated in vacuum. The collection point was viewed by two large plastic scintillation counters (one thin ΔE counter and one thick E counter) to detect positrons, three LN_2-cooled Si(Li) diodes for the detection of conversion electrons and an (∼80%) HPGe detector for γ-rays. Both Si(Li)-plastic and Ge-plastic coincidence data were recorded. The tape was moved every 5 s to reduce the background from the decay of ^{74}Kr and ^{74}Ga. The β singles events were scaled and recorded for each 5 s counting cycle. A weak transition was observed in the Si(Li) spectra at 495 keV corresponding to the decay of the 508 keV level in ^{74}Kr. From an analysis of these data it should be possible to measure the lifetime for the decay of this level. The efficiencies of the Si(Li) detectors were determined using a ^{207}Bi source. Unfortunately, from these data, it will not be possible to obtain a precise measurement of the transition strength for this decay branch since a small (<5%) fraction of the radioactive beam was not deposited on the tape, resulting in a build up of long-lived ^{74}Ga/^{74}Kr activity which made it more difficult to determine the β singles rate coming from the decay of ^{74}Rb. A new 13 mm wide tape transport system is being designed to eliminate this

problem. In addition, in a test run it has been demonstrated that if the mass separator is operated in the high resolution mode, most of the contaminant ^{74}Ga can be eliminated. This results in a factor of two loss in ^{74}Rb beam intensity; however, if the proton beam current on the Nb target is increased from 10 to 20 μA then it has been shown that the yield of ^{74}Rb increases by a factor of four.

The coincident γ-ray spectra obtained in this experiment contained a much higher ^{74}Ga background component than those measured with the in-air tape-transport system. However, by setting a high energy gate on the coincident β energy spectrum observed with the thick plastic scintillation detector, it was possible to observe the decay of the 456 keV level in ^{74}Kr. These γ-ray spectra would also be greatly improved if we could eliminate the ^{74}Ga isobaric contaminant. Furthermore, since a large fraction (>80%) of the available radioactive atoms decay in front of the detectors it should be possible to reduce the lower limits on possible high-energy (>2 MeV) γ-rays resulting from the β-decay of ^{74}Rb to higher-lying levels in ^{74}Kr.

High-precision lifetime measurement for ^{38m}K

A measurement of the half-life of ^{38m}K, one of the nine well-known superallowed β-emitters, provides an important test of the experimental apparatus. As reported previously [1999 Annual Report], a high-precision lifetime measurement for ^{38m}K is complicated by the long-lived isobaric contaminant ^{38}K$_{gs}$ which is produced at ~100 times the yield of ^{38m}K. A preliminary measurement of the half-life of ^{38m}K was carried out in May, 1999. A more complete data set was obtained in August, 2000. To optimize the ratio for ^{38m}K:^{38}K$_{gs}$, samples were collected for only ~0.3 s and the proton beam on the ISAC target was pulsed with a duty cycle of ~5–10%. As a result it was possible to increase the ratio for ^{38m}K:^{38}K$_{gs}$ to ~60–80:1. A total of 31 runs, each consisting of ~4 M events, were obtained. The statistical error in the half-life of ^{38m}K obtained by fitting each decay curve was ~0.6 ms. The weighted average of all measurements gave a preliminary value of 924.4 ± 0.1 ms (see Fig. 49). The errors quoted are statistical only and estimates of the systematic errors are in progress. The present result is in excellent agreement with the most precise value, 924.3 ± 0.3 ms, measured previously [Koslowsky *et al.*, Nucl. Phys. **A405**, 29, (1983)].

Outlook

During the coming year the objectives are: 1) to complete the analysis of the precision lifetime measurements of ^{37}K and ^{38m}K and submit a paper for publication, 2) to complete the analysis of the precision branching ratio measurement for the decay of ^{74}Rb,

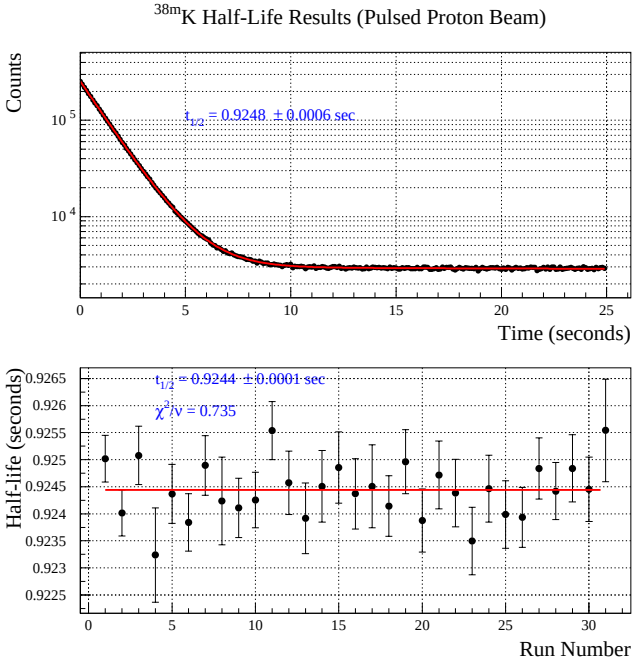

Fig. 49. β-decay half-life for ^{38m}K obtained with the pulsed proton beam on the ISAC production target. The upper plot shows the fit to the data from one run. Below are shown the results from all runs and the (preliminary) mean values obtained.

3) to repeat the measurement of the branching ratio for the decay of ^{74}Rb to the first excited 0^+ state in ^{74}Kr which decay by an E0 transition to the ground state, and 4) to measure the transition strength of the non-analogue $0^+ \rightarrow 0^+$ branch in ^{38m}K.

Experiment 826
Studies of ultra-thin magnetic films with implanted isotopes
(B. Turrell, UBC)

The intention was to implant ^{91}Rb first into iron. This decays to ^{91m}Y and the hyperfine field of Y in Fe is accurately known. An NMRON run would then have been a good diagnostic test for the dilution refrigerator (DR) and the NMR-rf system.

We then planned to top-load a single crystal of terbium, obtained from Dr. W.D. Brewer, Free University of Berlin, implant ^{91}Rb and again study the Y hyperfine field. The surface of the terbium crystal was polished down to 1 μm. Soldering terbium to copper is not easy, but a good join was made using indium as solder and *no* flux. In this procedure the terbium surface must be continually cleaned.

Unfortunately, neither of these experiments were carried out because the DR had developed a leak so that very low temperatures could not be attained.

The beam operators did produce a ^{91}Rb beam. Analysis of the 2564 keV γ-ray in ^{91}Sr from the decay of ^{91}Rb showed an equilibrium count rate of 1.33

counts per second. Taking into account approximate values for the solid angle correction and the efficiency of the detector, we roughly estimate a yield for the ^{91}Rb ion beam into the sample of 5×10^4 per second. This would have been sufficient to perform a nuclear orientation experiment. An NMRON experiment searching for the Y resonance in Tb would have been difficult, but not impossible, because of the relatively low count rate. The sweep in frequency would have been constrained to 4 MHz per hour so that 12 hours running would have only covered about 50 MHz. However, a lower limit on the resonant frequency could have been obtained from the γ-ray anisotropy.

Experiments 838/864
Double radiative decay of pionic atoms
(T. Gorringe, P. Żołnierczuk, Kentucky)

Physics program with the RMC spectrometer

The RMC spectrometer is a large solid angle photon-pair spectrometer. It comprises a cylindrical Pb converter for γ-ray conversion, cylindrical drift and wire chambers for $e^+ - e^-$ tracking, and an axial magnetic field for momentum analysis. Fast triggering on photon events is accomplished through the hit patterns in concentric layers of plastic scintillators. For details see Wright *et al.*, Nucl. Instrum. Methods **A320**, 249 (1992).

During the past year our research program has involved the investigation of double radiative decay of pionic hydrogen (Expt. 838), double radiative decay of pionic deuterium (Expt. 864), and pion charge exchange at low energies (Expt. 869). Production runs on double radiative decay were conducted in April and commissioning runs for pion charge exchange were conducted in July and November.

Experiment 838: Double radiative decay of the π^-H atom

The rare decay of pionic atoms by two-photon emission, $\pi^- A \rightarrow \gamma\gamma X$, was first considered by Ericson and Wilkin in Phys. Lett. **57B**, 345 (1975). They predicted the decay was dominated by annihilation of the stopped, real π^- on a soft, virtual π^+ (i.e. $\pi\pi \rightarrow \gamma\gamma$). As discussed by Ericson and Wilkin and others, the $\pi\pi \rightarrow \gamma\gamma$ mechanism may provide sensitivity to both the electromagnetic properties of the charged pion and the pion field in the nuclear medium. Unfortunately the predicted branching ratio for double radiative decay is only 5×10^{-5}.

The goals of Expt. 838 were the first observation of the double radiative decay of the π^-H atom, the mapping-out of the photon angle and energy spectra, and the verification of the $\pi\pi \rightarrow \gamma\gamma$ mechanism. The major experimental difficulties are the very small branching ratio for double radiative decay and the very large two-photon background from pion charge exchange. Data were collected with a stopping π^- beam and a liquid hydrogen target in December, 1998 and May, 1999 and yielded ∼1000 events from the double radiative decay of the pionic hydrogen atom. A typical event is shown in Fig. 50 and the two-photon opening angle distribution is shown in Fig. 51 (top). Our preliminary value for the branching ratio is $\mathrm{BR}_{[\pi^- p \rightarrow \gamma\gamma n]} = 3.8 \times 10^{-5}$. These results support the theoretical prediction for the dominance of the $\pi\pi \rightarrow \gamma\gamma$ mechanism.

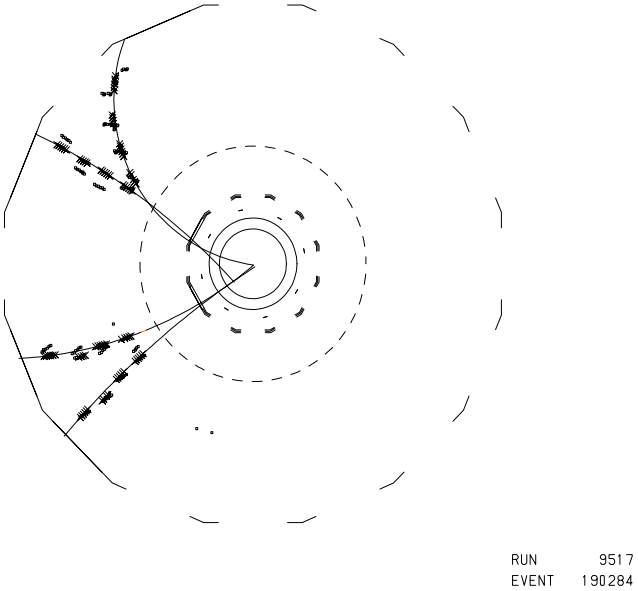

Fig. 50. A typical double radiative decay event from pionic hydrogen. It shows the two $e^+ - e^-$ pairs from photon conversion in the lead converter and characteristic pattern of trigger scintillator hits.

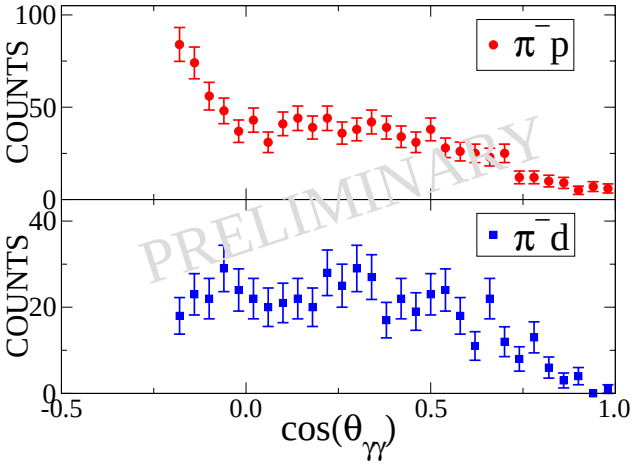

Fig. 51. The two-photon opening angle spectra for pionic hydrogen (top) and deuterium (bottom).

Experiment 864: Double radiative decay of the π^-D atom

Recently a group at JINR have made claims for the existence of a super-narrow NN-decoupled dibaryon – the $d_1^*(1920)$ [Khrykin *et al.*, πN Newslett. **13**, 250 (1997)]. Their claims are based on the energy spectra of double bremsstrahlung events from proton-proton collisions. Subsequently, an assessment by Gerasimov has concluded that if the $d_1^*(1920)$ is observed in double bremsstrahlung from $p-p$ collisions, then the $d_1^*(1920)$ should be observed in double radiative decay of π^-D atoms.

The goals of Expt. 864 were twofold. Firstly, we aimed to employ the double radiative decay of pionic deuterium as a sensitive probe for the possible existence of the $d_1^*(1920)$ dibaryon. Secondly, together with our π^-H data and earlier π^-C data, we aimed at obtaining a first study of the A-dependence of the double radiative decay. Data were collected with a stopping π^- beam and a liquid deuterium target in April and yielded ∼500 events from the double radiative decay of the pionic deuterium atom. Our preliminary result for the branching ratio is $\mathrm{BR}_{[\pi^-\mathrm{D}\to\gamma\gamma nn]} = 1.6\times10^{-5}$ and the two-photon opening angle distribution is shown in Fig. 51 (bottom). Our data show no evidence for production of the $d_1^*(1920)$ dibaryon.

Experiment 863
Ground state magnetic moments of ^{75,77,79}Ga (LTNO)
(P. Mantica, MSU)

The focus of Expt. 863 is to study the evolution of the single-particle structure of medium-mass nuclides having $Z \geq 28$ toward the $N = 50$ shell closure. A well-known shape transition from spherical to moderate deformation ($\beta_2 \sim 0.2$) occurs in the neutron-rich $_{31}$Ga and $_{32}$Ge isotopes between $N = 40-42$. Since the ground state magnetic dipole moment can serve as a sensitive probe of the nuclear ground state wavefunction, the experimental determination of the magnetic moments of the heavy, odd-A Ga isotopes can address the extent to which quadrupole deformation persists toward $N = 50$.

The ground state magnetic moments will be measured using the LTNO facility coupled to the low-energy channel at ISAC. The Ga isotopes of interest will be implanted into an iron foil maintained at ≈ 10 mK at the centre of the ^{3}He/^{4}He dilution refrigerator. Nuclear magnetic resonance on oriented nuclei (NMR/ON) will be used to observe the destruction of the nuclear orientation and extract the ground state magnetic moment. Since Ga isotopes experience only a small hyperfine field in iron, the normal method of extracting orientation parameters from γ-ray angular distributions will prove difficult. We have proposed, therefore, to measure the destruction of the angular distribution of β particles emitted by the implanted Ga isotopes. The β anisotropies are expected to show a larger effect due to reliance on the B_1 orientation parameter.

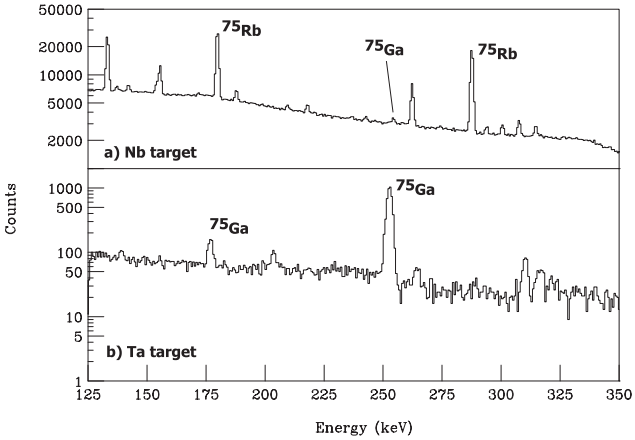

Fig. 52. γ-ray spectra at $A = 75$ for a) Nb and b) Ta ISAC production targets.

Production of ^{75}Ga

Although the β-ray angular distributions are expected to be large for the heavy, odd-A Ga isotopes, the main disadvantage in such a measurement is the continuous nature of the β-ray spectrum and difficulties with contamination from unwanted sources. For example, production of neutron-rich ^{75}Ga from a surface ionization source may also result in significant production of neutron-deficient ^{75}Rb. Since ^{75}Rb and ^{75}Ga have similar decay half-lives and β endpoint energies, it would be difficult to differentiate the β decays of these species.

Production tests for ^{75}Ga have been performed at ISAC using production targets of Nb and Ta. Representative γ-ray spectra are shown in Fig. 52. Using the Nb target, the most significant yield at $A = 75$ is ^{75}Rb. However, employing the more neutron-rich Ta production target strongly favours the production of ^{75}Ga over ^{75}Rb. The observed ^{75}Ga/^{75}Rb ratio is adequate to complete the proposed β-NMR/ON measurements on ^{75}Ga. Favourable ^{77}Ga/^{77}Rb and ^{79}Ga/^{79}Rb ratios have also been measured using the Ta production target at ISAC.

Experiment 869
Pion charge exchange at low energies
(T. Gorringe, P. Żołnierczuk, Kentucky; M. Hasinoff, UBC)

Isospin symmetry is central in understanding the structure and interactions of mesons and baryons. However, the symmetry is approximate; it being violated by the Coulomb interaction and the u,d-quark

mass difference. The πN system represents a fundamental arena for testing our understanding of isospin symmetry breaking. Interestingly, recent analyses of πN elastic scattering and charge exchange data have suggested an unexpectedly large isospin violating effect. The key data in these analyses are the charge exchange data at $T_\pi \sim 50$ MeV and forward angles where destructive interference of s-/p-waves yields high sensitivity to possible effects of symmetry breaking.

The goal of Expt. 869 is a precision measurement of the pion charge exchange differential cross section at low energies and forward angles. The program requires a modification of the RMC detector to operate as a π^0 spectrometer. Such modifications include a new photon converter package, a new beam counter package, and a new trigger system. A new photon converter package is required to enable the determination of the π^0 momentum with the necessary accuracy. A new beam counter package is required to permit variable target positions, high accuracy π^- counting, and minimal π^- energy loss. The various modifications were successfully commissioned in two runs in July and November. Production running of Expt. 869 is scheduled for May, 2001.

Experiment 875
Muon scattering in low Z materials for muon cooling studies
(R. Edgecock, RAL; K. Nagamine, RIKEN)

Muon cooling

A vital requirement of the accelerator complex used to supply muons to a future neutrino factory or muon collider is the ability to cool the muons. In the case of the neutrino factory, the aim is a factor of 10 reduction in the normalized emittance in each transverse plane, while for a muon collider the requirement is a 10^6 reduction in the 6-dimensional phase space. Due to the muon lifetime, such cooling needs to be fast and the currently preferred technique is ionization cooling [MUCOOL Collab., Fermilab Proposal P904 (1998)]. In the case of the transverse cooling required for a neutrino factory, this involves passing the muons through an absorber in which they lose both longitudinal and transverse momentum. The lost longitudinal momentum is then restored using rf cavities following the absorber.

As well as a cooling effect coming from the ionization energy loss, there is heating coming from multiple scattering and the final cooling achieved is a balance between these. Theory suggests this balance is most favourable for elements with low atomic number, in particular, liquid hydrogen. However, an extensive literature search has failed to find any measurements of the muon scattering distribution in light elements [Fernow, MUCOOL Note 123 (2000)]. The most relevant data found comes from the scattering of 2.7 MeV/c electrons on Al, Be and Li [Kulchitsky and Latyshev, Phys. Rev. **61**, 254 (1942); Andrievsky *et al.*, J. Phys. (USSR) **6**, 279 (1942)]. These data show a clear trend: as Z decreases, the agreement with Moliere theory [Moliere, Z. Naturforschg. **3a**, 78 (1948); Scott, Rev. Mod. Phys. **35**, 231 (1963)] gets worse. If this trend continues to hydrogen, there will be two effects:

1. The level of cooling achieved would be less than expected.
2. Due to the increased scattering in the tails, the fraction of muons scattered out of the cooling channel could be much bigger than expected.

Due to the importance of this to ionization cooling, the MuScat experiment has been created to measure the scattering of muons of various momenta in a number of low atomic number materials, in particular liquid hydrogen. As well as checking these observations, MuScat will compare a range of muon scattering models with the data.

A four week test period was allocated to the MuScat experiment in the M11 beam line in June and July. The following sections will describe the experiment and show what was learnt about it during the run. The plans for a further run in 2001 will also be outlined.

The MuScat experiment

As the aim of the experiment is to make a precise measurement of the multiple scattering of muons, the amount of material that the muons must pass through has to be kept to a minimum. For this reason, it is not possible to do any tracking before the target and a collimation system must be employed to reduce the beam dimensions so that the incoming particle position is known accurately enough. In addition, the measurement of the position of the scattered muon relies on the first tracking detector as all subsequent detectors will be affected by scattering in the first. Any additional detectors can only be used to aid in noise rejection and for checking systematics. To minimize scattering in air, as much of the experiment as possible must be mounted in vacuum. Finally, to eliminate particles other than muons, a good time-of-flight system is required.

The detector designed to satisfy these requirements and used in the M11 beam is shown in Fig. 53. The most upstream parts are a veto shield and veto scintillator to eliminate beam halo. These are followed by the first trigger counter, which also acts as the TOF start. This is built from two fingers of scintillator, each 1 mm thick, 28 mm long and 3 mm high. These overlap by 20 mm in length and 3 mm in height. The timing resolution is about 250 ps. The TOF stop comes from the

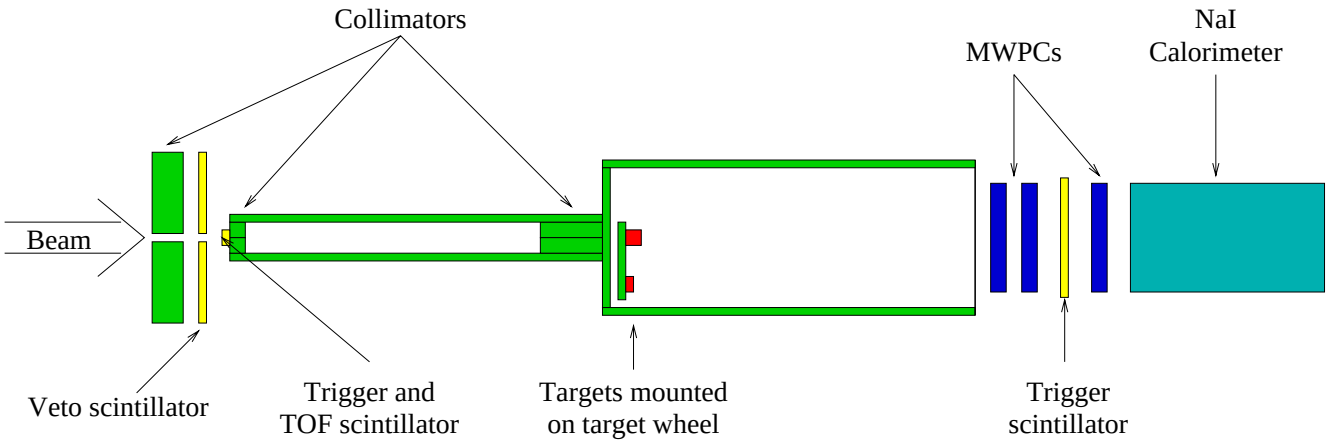

Fig. 53. Schematic longitudinal layout of the MuScat experiment.

following rf bucket of the cyclotron. This is almost a square-wave of length 1.9 ns, the smearing of the edges corresponding to a resolution of about 500 ps.

This trigger scintillator is followed by a 1 m long vacuum tube containing the collimation system. This consists of a 40 mm thick lead block at the front and a 160 mm thick lead block at the back, plus 4 intermediate blocks each 10 mm thick, which are not shown in the figure. The first block has a slit 20 mm long by 2 mm high cut in it, while the slot in the second block is tapered to prevent large angle scatters off the internal face. With this arrangement, the scattering distribution is measured vertically, in the narrow direction of the slot. The second dimension is longer to increase the particle intensity.

The vacuum tube is connected to the main vacuum vessel, which contains the targets. These are:

- Liquid hydrogen, 100 mm and 150 mm thick
- Lithium, 10 mm and 2.5 mm thick
- Beryllium, 2 mm and 0.5 mm thick
- Carbon, 2.5 mm thick
- Aluminum, 1 mm thick
- CH_2, 2 mm thick
- Iron, 0.15 mm and 2 mm thick

The "thick" iron sample is used simply to blow the beam up to give a better coverage of the detectors and improve the measurement of the efficiency. The liquid hydrogen targets were not used during the 2000 run, but are being designed for the second run in 2001. In addition, the possibility of including a LiH target, which is the best candidate absorber for ionization cooling after hydrogen, is being investigated.

The solid targets are mounted on a target wheel that can be controlled from outside the vacuum so it is unnecessary to break this each time a target is changed. The wheel has 10 slots, the last of which has no target mounted and is used to measure the intrinsic properties of the beam. These are monitored on a regular basis.

The tracking detectors used are delay-line chambers. These are multi-wire proportional chambers with two 2 cathode planes and 1 anode plane. Each chamber gives 2-dimensional readout, but with better resolution from the cathode plane perpendicular to the anode plane, ∼0.6 mm compared to 1–2 mm. Rather than each wire being read out, the number of electronics channels required is reduced by recording only two signals from each plane. These are time values, giving the position along the delay-line from which the signal originated. As shown in Fig. 53, three of these chambers are used, each 300 mm by 300 mm in size. The most important of these is the first, which is oriented such that the dimension with the better resolution is vertical. It is approximately 1 m from the target wheel. Between the second and third chambers is the second trigger scintillator.

The final part of the detector is MINA, a NaI calorimeter of 360 mm diameter and 360 mm depth [Waltham *et al.*, Nucl. Inst. Meth. **A256**, 91 (1987)]. It has a measured energy resolution (fwhm) of 5.2% at 90 MeV with an energy dependence of $E^{-0.55}$. It is used for both a muon energy measurement and additional pion/muon separation.

Performance

As already mentioned, a period of 4 weeks was allocated to the experiment in the M11 beam line, including 1 week of setting up. Three beam momenta were used: 130, 150 and 180 MeV/c. However, of these, 180 MeV/c is the most interesting and all the results shown will come from data at this momentum.

Delay-line chambers

During the first 8–10 days of data-taking, a steady and spatially non-uniform drop in the efficiency of two

of the delay-line chambers was noted. Examination of one chamber showed that this was due to wrinkling of the cathode plane and it was thought that this resulted from too high a concentration of the methylal vapour in the argon-isobutane gas mixture. Ultimately, the two most upstream chambers were replaced and the temperature of the methylal bath was reduced to lower the vapour pressure. The measured efficiency of the most upstream chamber (PC2) from a subset of the runs taken after the change is shown in Fig. 54, as a function of vertical and horizontal position. This still indicates a non-uniform efficiency and it has been concluded that these data cannot be used for precise measurements of the muon scattering distribution. Nevertheless, they are proving very useful for checking how the detector works and there have been significant modifications as a result. These studies and the changes implied for the next running period are discussed in the following sections.

In light of the problems with the delay-line chambers, it has been decided to build new tracking chambers for the next run. They will be constructed from crossed planes of scintillating fibres. These will provide a high and uniform efficiency, an improved position resolution of about 200 μm, and a time resolution of 150 ps. In addition, it will be possible to mount the chambers inside the vacuum and eliminate any material between the target and the first detector. A new vacuum vessel is being designed for this purpose.

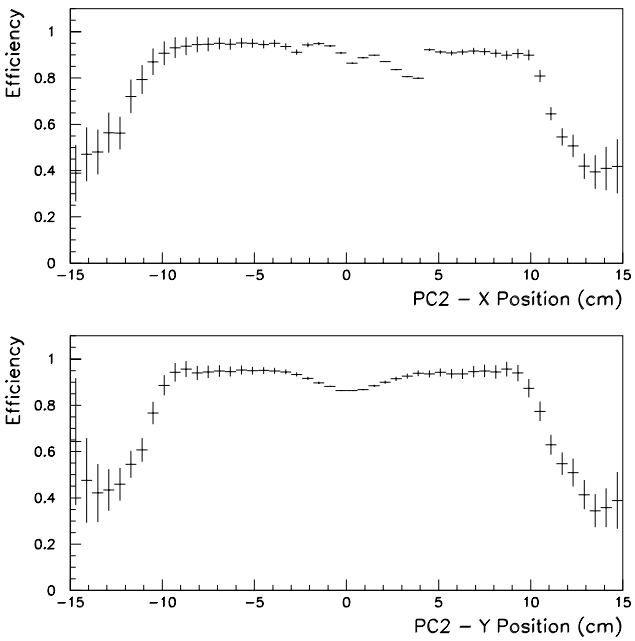

Fig. 54. Efficiency of the most forward delay-line chamber as a function of X (horizontal position) and Y (vertical position).

Event rate

This was important to measure as the fineness of the collimation system could potentially have reduced the muon event rate to an impractical level. The measured rates of events to disk are listed in Table XII. Note that at higher momentum, these are strongly affected by deadtime. The total trigger rate is dominated by pions, so the muon rate is estimated using the muon fraction in the beam determined from the time-of-flight plot (see Fig. 55). As 10^6 muons are required per measurement, it typically takes 10 hours for each of these in M11.

Table XII. Measured event rates and the fraction of muons in the beam at the three beam momenta used in 2000.

p (MeV/c)	Total rate (Hz)	μ/total	μ rate (Hz)
130	210	0.10	21
150	270	0.09	24
180	550	0.06	33

Time-of-flight resolution

Figure 55 shows the difference in time between the arrival of a particle in the TOF scintillator and the next rf beam pulse, in TDC counts, at 180 MeV/c. Note that as the difference is taken with respect to the next beam pulse, the particle velocity increases along the x axis. The time separation between the pions and muons is 4.9 ns and between muons and electrons is 7.5 ns.

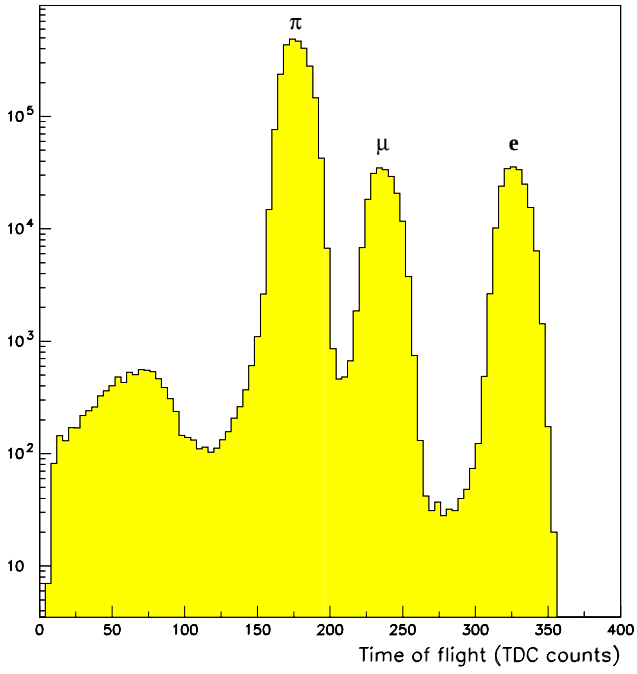

Fig. 55. Measured time of flight at 180 MeV/c using the MuScat detector in the M11 beam at TRIUMF. The π, μ and e peaks are indicated. The broad peak at low velocity comes from protons.

There is a clear separation between the muons and the other particles, allowing a muon signal to be extracted with a negligible background.

Collimation system

Selecting muons using the TOF distribution shown in Fig. 55, the vertical projection of the distribution of these muons in the most upstream delay-line chamber with a 9.5 mm Li target and no target are compared in Fig. 56. To extract the scattering distribution from these, a rigorous unfolding procedure using the maximum entropy technique [see Maximum Entropy and Bayesian Methods, Skilling, ed. (Kluwer Academic, 1989)] is being developed and will be used to determine whether or not the tails in the no target case are being reduced sufficiently by the collimation system. However, simpler techniques are already indicating that this may not be the case. As a result, simulation studies are under way to determine where the tails originate and how they can be further reduced using both additional collimators and veto scintillators.

Conclusion

The MuScat experiment has been designed and built to make a precise measurement of the scattering distribution of muons of momentum in the range 150–180 MeV/c in a number of materials of low atomic number. The performance of the experiment was tested in a run in the M11 beam in the summer. Although largely successful, much has been learnt from this and a number of alterations will be made for a second run in 2001. The main change will be a new set of tracking detectors to replace the delay-line chambers used in 2000.

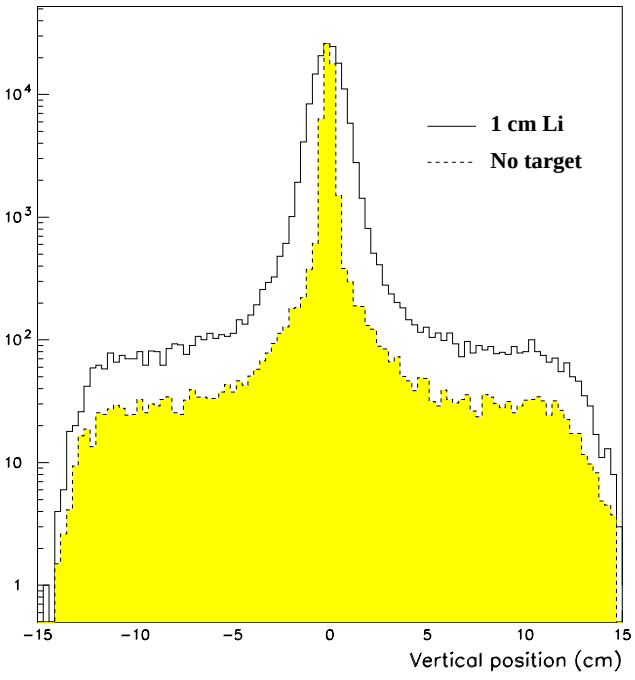

Fig. 56. Vertical projection of the muon distribution in the first delay-line chamber with no target (shown shaded) and with 10 mm of Li. The muons are selected using time of flight.

Experiment 880
Ortho-para effect of muon catalyzed fusion in solid deuterium

(K. Ishida, K. Nagamine, RIKEN/KEK)

The experiment was aimed at measuring the dependence of the rate of muon catalyzed fusion in the D_2 system (dd-μCF) on the ortho-para state of deuterium molecules. In the dd-μCF process, the resonant formation of $dd\mu$, $d\mu + D_2 \rightarrow [(dd\mu)dee]$ is one of the most important processes determining the overall efficiency of producing fusion neutrons. Since this process requires an energy matching between the initial state and the final state, the rate is very sensitive to the states of $d\mu$ (hyperfine states $F = 3/2$ or $1/2$, kinetic energy, etc.) and D_2 (vibrational and rotational molecular states, kinetic energy, etc.). Although the system had been experimentally investigated by changing various parameters such as the temperature and the density, full understanding was not yet achieved. In order to obtain further understanding of this process, we started to investigate the effect of another parameter, namely the ortho-para state of the D_2 molecule.

Especially, the measurement would be used to solve the puzzling "solid-state" effect in dd-μCF. It had been expected by theoretical calculations that the $dd\mu$ molecular formation rate decreases rapidly by decreasing the deuterium target temperature below 20 K, but it was actually found by measurements that the rate stays nearly constant in the solid even down to 3 K. In some of the proposed explanations the para deuterium contributes an essential role, so an experiment with a controlled ortho-para ratio would be a critical test on the contribution of para D_2.

The measurement was performed at the M9B channel in June. The set-up consisted of a 3.5 K solid deuterium target system with cryostat, a deuterium gas handling system with an ortho-para converter and an ortho-para analyzer, and the detection system for incoming muons, muonic X-rays, fusion protons and $\mu \rightarrow e$ decay electrons.

To control the ortho-para ratio of the deuterium gas, we passed the normal deuterium gas (67% ortho and 33% para) through an ortho-para conversion chamber which contained a catalyst (Cr_2O_2 + Al_2O_2 powder) maintained at low temperature (typically 12.5 K). This produced an ortho-rich deuterium (99.7% ortho and 0.3% para). The deuterium gas was then solidified on a thin silver foil maintained at 3.5 K

to make a solid D_2 target of 40 mm in diameter and 0.3 mm in thickness. The measurement was carried out for three different target conditions, namely for 67%-ortho "normal" D_2, for 99.7%-"ortho" D_2, and for silver substrate foil only. The target was irradiated by the negative muon beam and the muonic X-rays as well as protons from *dd*-fusion were detected. The muonic X-rays gave us the number of stopped muons in deuterium as well as being used to determine the upper limit of the impurity level in the deuterium target. For the *dd*-fusion proton detection we used silicon surface barrier (SSB) detectors in pairs, so that the "ΔE vs. E" particle identification method was applied. This enabled us to clearly separate fusion protons from other particles such as muons and deuterons. The fusion proton emission time spectrum after muon stopping was analyzed to extract various parameters such as the effective $dd\mu$ formation rate from the $d\mu(F{=}3/2)$ state, $\tilde{\lambda}_{\frac{3}{2}}$, and the hyperfine transition rate from the $d\mu(F{=}3/2)$ to $d\mu(F{=}1/2)$ state, $\tilde{\lambda}_{\frac{3}{2}\frac{1}{2}}$.

In Table XIII we present a preliminary result of the analysis about these rates for normal D_2 and ortho D_2.

1. The effective $dd\mu$ formation rate as well as hyperfine transition rate is decreased by decreasing the para concentration.
2. Even so, we still see a fast $dd\mu$ formation rate in the ortho D_2 in which the para-D_2 concentration is very small. This result strongly rejects some of the models proposed to explain the "solid-state" effect, such as those assuming that $d\mu$ is heated by collision with para-D_2.
3. The relative effect of the ortho-para conversion seen in the hyperfine transition rate is roughly half of that in the effective $dd\mu$ formation rate. From this, the hyperfine transition via back-decay from the $dd\mu$-molecule was estimated to contribute nearly half of the total hyperfine transition rate (the other half is the direct spin exchange process which is not dependent on the D_2 molecular state). A detailed analysis is in progress.

Table XIII. Obtained values (preliminary) of the effective $dd\mu$ formation rate $\tilde{\lambda}_{\frac{3}{2}}$ and the hyperfine transition rate $\tilde{\lambda}_{\frac{3}{2}\frac{1}{2}}$ in normal D_2 and ortho D_2, and the relative effect due to ortho-para conversion.

	Normal D_2	Ortho D_2	Effect
$\tilde{\lambda}_{\frac{3}{2}}$	2.299(69)	1.611(40)	–30(4)%
$\tilde{\lambda}_{\frac{3}{2}\frac{1}{2}}$	40.3(14)	34.4(9)	–15(4)%

CHEMISTRY AND SOLID-STATE PHYSICS

Experiment 684
μSR spin relaxation studies of small molecules in the gas phase
(J. Pan, D. Fleming, UBC-TRIUMF)

This experiment studies the muon spin relaxation in some simple gas-phase systems with the primary goal of measuring the chemical reaction rates. Due to the loss of beam time as a result of the cyclotron and the M9 beam line problems, only two days of experiment with reduced beam current were carried out for the study of Mu + CO with N_2 as moderator at room temperature in the longitudinal field (LF).

The motive of this year's experiment is to complete the study of the Mu + CO reaction over a wide range of pressures from 2 to 500 bar in the longitudinal field in order to gain better understanding of the spin rotation relaxation process in μSR experiments in general and in Mu + CO reactions in particular. A better understanding of the collisional relaxation process is in turn helpful for the interpretation of data in terms of the chemical kinetics of the reaction. Particularly, the relaxation rate constants of the Mu + CO reaction measured in transverse field have indicated that the collisional relaxation rate is essentially pressure independent over the pressure range of 2–500 bar.

Unfortunately, the little beam we actually had was not sufficient to investigate the reaction in the LF. We were only able to take about 20 runs, while about 10 runs are required to have a complete field dependence survey for each gas mixture and at least 5–6 gas mixtures are required to cover the relevant pressure range. Needless to say, the data obtained were not sufficient to reach any conclusions.

Experiment 749
Muonium-substituted free radicals
(P.W. Percival, SFU)

Addition of muonium (Mu) to an unsaturated molecule such as an alkene or arene results in a free radical incorporating the muon in place of a proton. According to modern terminology such a radical is termed a muoniated radical, to emphasize the formal replacement of a hydrogen atom by muonium in what is otherwise a recognized chemical structure (cf. a deuterated molecule, which contains D instead of H). In terms of electronic structure there is no difference between the H and Mu analogues (at least, to the level of the Born-Oppenheimer approximation). Isotope effects do exist, of course; they are related to intramolecular motion involving Mu. Thus, increased zero-point vibration in C–Mu bonds, for example, can influence the conformations of organic free radicals and the rates of chemical reactions. In other respects, however, the muoniated radical behaves like its H analogue and the muon can be viewed as a passive spin probe, which allows us to explore chemical and physical properties of the radical that may not otherwise be amenable to experiment.

In Expt. 749 and its predecessors we have applied the muon spin probe to investigate topical and/or fundamental questions in free radical chemistry. One of these is the electronic structure of fullerenyl radicals, specifically the unpaired spin distribution in H (or Mu) adducts of fullerenes. We were able to map unpaired spin densities by determining ^{13}C hyperfine constants by means of muon level-crossing resonance (μLCR) [Percival *et al.*, Chem. Phys. Lett. **245**, 90 (1995)].

Another goal of Expt. 749 has been to understand the factors that influence radical addition to curved polyaromatic hydrocarbons (PAHs), of which fullerenes can be considered "ideal" examples, having closed surfaces constructed from carbon atoms alone. In the case of C_{60}, addition of an H atom or other small radical results in a single radical product, since all carbons are identical. In contrast, the ellipsoidal C_{70} molecule has five chemically inequivalent sets of carbon atoms. In principle, therefore, five distinct radicals could be formed.

Several years ago we investigated C_{70} by using TF-μSR to detect muonium adducts, i.e. isomeric C_{70}Mu radicals, but we were only able to distinguish four isomeric radicals [Addison-Jones *et al.*, Hyp. Int. **86**, 817 (1994)]. They have markedly different abundances, which suggests varying reactivity of the different carbon sites in C_{70}. Since the fifth (missing) radical corresponds to addition of Mu (H) to the "equator" of C_{70}, where the curvature of the carbon network is least, we also investigated the Mu adducts of the flat polyaromatic hydrocarbon pyrene [Percival *et al.*, Can. J. Chem. **77**, 326 (1999)], and a curved variant, 1,8-dioxa[8](2,7)pyrenophane [1999 TRIUMF Annual Report].

During 2000 we extended studies to another PAH, triphenylene, and its partially hydrogenated derivative (Fig. 57). TF-μSR and μLCR spectra of triphenylene

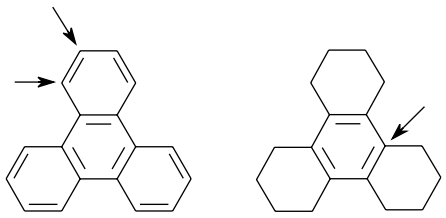

Fig. 57. The chemical structures of triphenylene (left) and dodecahydrotriphenylene (right). TF-μSR and μLCR studies show that Mu adds to these molecules at the positions indicated by the arrows.

revealed the formation of two muoniated radicals, and comparison of the muon and proton hyperfine constants with quantum calculations confirmed our expectation that Mu adds to carbons 1 and 2 (and symmetrical positions in the other benzene rings). These sites are blocked in dodecahydrotriphenylene. Nevertheless, we detected clear signals of a muoniated radical, which can only correspond to addition at the central benzene ring. This is significant because it confirms our view that failure to detect Mu addition at trigonal carbons in other PAHs (including the "equatorial" site in C_{70}) is *not* due to the unreactivity of such sites, but rather to the competition from more reactive sites on the perimeter of the molecules (or more curved areas of C_{70}).

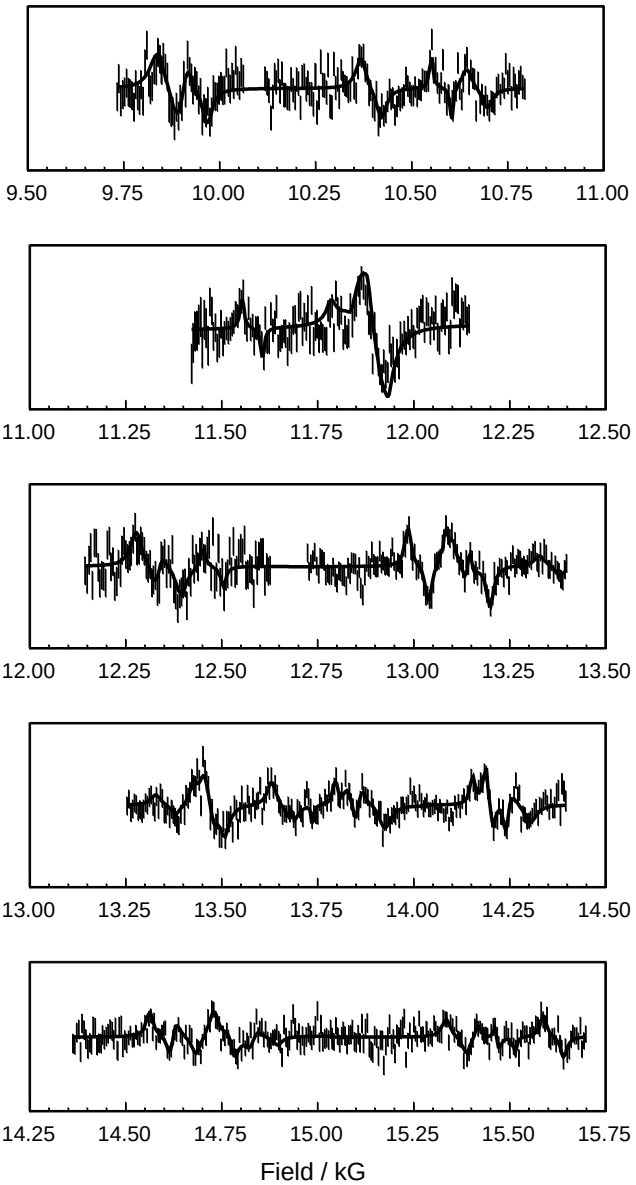

Fig. 58. Segments of the muon level-crossing spectrum obtained from a dilute solution of $^{13}C_{70}$.

Finally, to complete Expt. 749, we returned to an earlier goal, mapping the unpaired spin distribution of the available C_{70}Mu radicals by detecting and assigning the μLCR resonances due to ^{13}C hyperfine constants in $^{13}C_{70}$. This is much more difficult than the earlier study of $^{13}C_{60}$ because of the multiple radical products and the consequent spread of signal intensity and potential overlap of resonances from different isomers. The magnitude of the problem can be gauged from Fig. 58, which shows a compilation of spectra with fitted resonances. Detailed analysis and assignment of signals is under way.

Experiment 768
Generalized FFLO state and anomaly of flux line lattice state in novel superconductors
(R. Kadono, KEK-IMSS; J. Akimitsu, Aoyama Gakuin)

The origin of large hysteresis in the isothermal dc magnetization near the upper critical field H_{c2} (or so-called "peak effect") observed in $CeRu_2$ has been an issue of considerable attention because of the possibility of an associated novel mixed state. Although the peak effect is rather commonly observed in clean type II superconductors and is usually explained by the increase of net pinning force due to the softening of the flux line lattice (FLL) and associated optimization of the vortex configuration along with randomly distributed pinning centres, the one observed in $CeRu_2$ turned out to exhibit an additional feature of field and temperature hysteresis at the onset of the irreversible region. This hysteresis has been interpreted as a manifestation of the first-order phase transition to a further inhomogeneous novel mixed state predicted by Fulde-Ferrel-Larkin-Ovchinnikov (FFLO).

The FFLO state has been predicted to occur in clean type II superconductors (i.e., electronic mean free path l is much longer than the superconducting coherence length ξ_0) with large Pauli paramagnetic spin susceptibility χ_s of the conduction electrons and a large Ginzburg-Landau parameter κ. The system satisfying the latter two conditions can reach the Clogston-Chandrasekhar (CC) limit where the spin polarization (Zeeman) energy $\chi_s H^2/2$ is comparable with the superconducting condensation energy $H_c^2/8\pi$ at fields H near H_{c2}. The recent model including the effect of orbital current predicts that the system near the CC limit falls into a new inhomogeneous state (generalized FFLO state or GFFLO state) at a field H_i below H_{c2} where the order parameter is spatially modulated with periodic planar nodes aligned perpendicular to the vortices. In order to obtain experimental clues to distinguish the origin of FLL softening, the microscopic property of magnetic vortices in the mixed state of a

high-quality $CeRu_2$ crystal has been studied by muon spin rotation (μSR). We note that the sample quality has been much improved from that measured in the earlier μSR experiment, as indicated by the increase of the residual resistivity ratio from 30 to 91.

We have found that the spatial distribution of magnetic induction $\mathbf{B}(\mathbf{r})$ probed by muons is perfectly described by the London model for the triangular vortex lattice with appropriate modifications to incorporate the high-field cutoff around the vortex core and the effect of long-range defects in the vortex lattice structure at lower fields. As shown in Fig. 59, the vortex core radius is proportional to $H^{(\beta-1)/2}$ with $\beta \simeq 0.53$, which is in good agreement with the recently observed nonlinear field dependence of the electronic specific heat coefficient $\gamma \propto H^{\beta}$. In particular, the anomalous increase of magnetic penetration depth in accordance with the peak effect in dc magnetization ($\geq H^* \simeq 3$ T at 2.0 K) has been confirmed (see Fig. 59); this cannot be explained by the conventional pair-breaking effect due to magnetic field. In addition, the spontaneous enhancement of flux pinning, which is also associated with the peak effect, has been demonstrated microscopically. These results strongly suggest the onset of collective pinning induced by a new vortex state having an anomalously enhanced quasiparticle density of states for $H \geq H^*$.

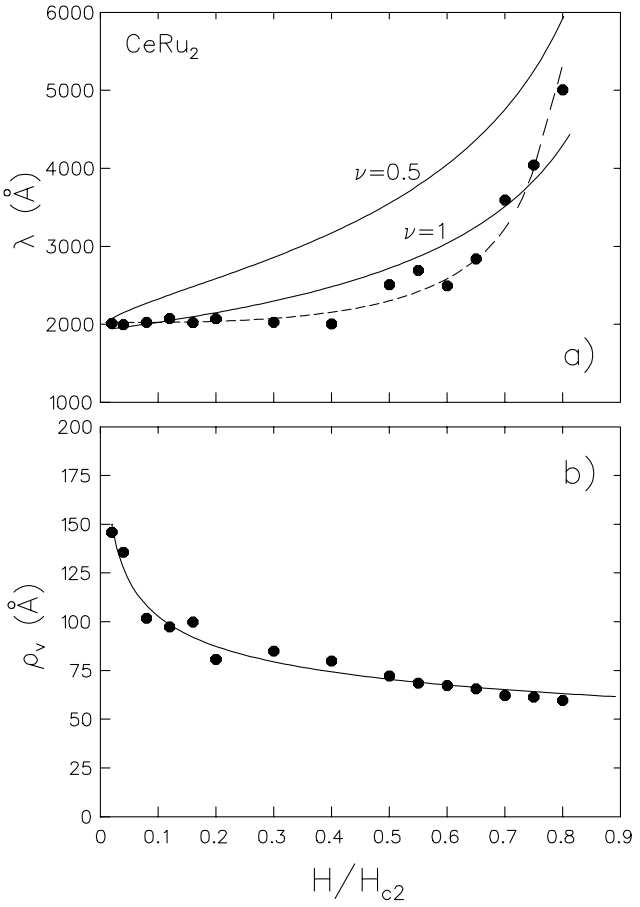

Fig. 59. a) Magnetic penetration depth λ and b) vortex core radius ρ_v vs. field in $CeRu_2$ at 2 K. While λ was obtained by fitting data with the modified London model, ρ_v was determined as a peak of supercurrent density $j(r)$ around the vortex with $j(r)$ calculated directly from $\mathbf{B}(\mathbf{r})$ using Maxwell's relation. Solid curves in a) are calculated by a model (see the forthcoming publication), while the dashed line is a guide for the eye. Fitting the result by a power law is shown in b) as a solid curve.

Experiment 774
Muon charge state dynamics in LPE GaAs
(B. Hitti, S.R. Kreitzman, TRIUMF)

We report on the significant progress achieved to date in understanding the temperature dependence of the various muon states and their dynamics in the technologically important compound semiconductor GaAs. New data were gathered on our high purity LPE samples and their semi-insulating substrate. The new information is used to help unravel the behaviour of muons in the simpler LPE system from that of the less well characterized substrate material. Our results confirm that, at the low dopant concentration where the basic dynamical processes are best revealed, the use of structurally defect free LPE material is essential to study intrinsic processes.

In our previous beam periods the temperature dependence of the final state diamagnetic fraction was measured at 2 kG in a number of samples between 10 and 650 K [see Fig. 75, TRIUMF Annual Report Scientific Activities 1999]. These data clearly identify two regimes where the diamagnetic amplitude as a function of temperature was dramatically different in the LPE and substrate samples. In the low temperature regime (10–100 K), substrate data seemed to display a simple behaviour but lacked the well known double step corresponding to the Mu^0_{BC} ionization. Modelling an electron recapture process, we noticed that the step is not eliminated but significantly suppressed. To clarify this issue we acquired detailed data (Fig. 60) on the substrate at low temperature which clearly shows that a small step is indeed present. At higher temperatures (400–550 K) the LPE behaviour seemed to be infected by features from the substrate. We therefore suspected that about 25% of the low energy muons were penetrating the 200 μm LPE layer and stopping in the substrate. To test this hypothesis the LPE diamagnetic amplitude was re-measured with a 37.5 μm thick Cu degrader to ensure that the muons encountered only LPE material. Under these conditions the suspect high temperature structure indeed vanished (Fig. 61), confirming said hypothesis.

In addition to the radio frequency μSR data described above, transverse field data were obtained on

the diamagnetic and two paramagnetic states of muonium in both the LPE and substrate material. These data confirm the general picture obtained by the radio frequency technique. The model involves the ionization of Mu^0_{BC} at about 100 K, the ionization on Mu^0_T just above room temperature, followed by charge exchange with free electrons from the conduction band above 500 K.

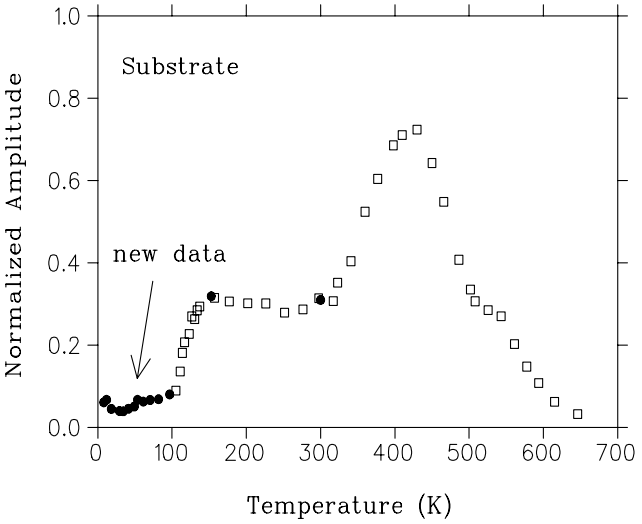

Fig. 60. The diamagnetic amplitude measured in the substrate. Open squares show the previous data and the filled circles show the new data; the small step at 50 K is clearly present.

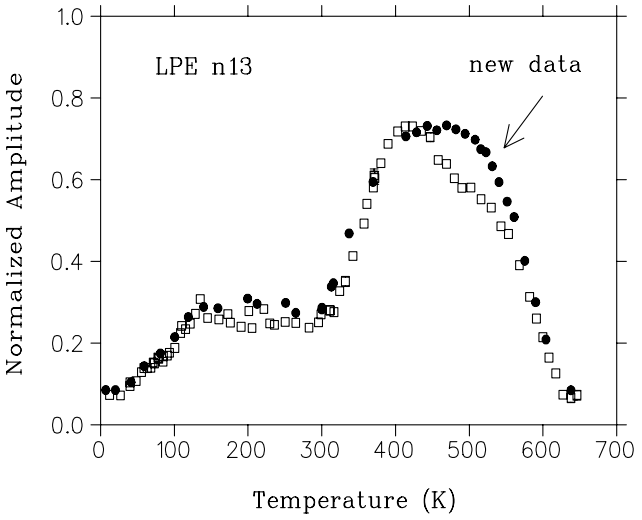

Fig. 61. The diamagnetic amplitude measured in the LPE n13 sample. Open squares show the previous data and the filled circles show the new data. The structure seen previously between 400 K and 550 K is not present in the more recent data.

Experiment 776
Rare-earth materials with disordered spin structures
(D.R. Noakes, Virginia State)

This experiment is a muon spin relaxation (μSR) study of RE-Mg-Zn (RE = rare earth) quasicrystals and PrP_x induced moment "spin glasses", motivated by the common features in the results of Expt. 665 (Al-Mn-Si quasicrystals) and Expt. 640 (low-carrier-density Kondo-lattice CeNiSn and related materials). Study of the rare earth quasicrystals was completed, as described in the 1998 Annual Report. A paper describing the surprising observation of strong-collision-dynamic Lorentzian Kubo-Toyabe relaxation in PrP_x, as discussed in the 1998 and 1999 Annual Reports and presented at the 1999 International Conference on μSR, has appeared in the proceedings of the conference in Physica B. A paper on Monte Carlo simulations of the singlet-ground crystalline electric field level fluctuation model for the observed μSR in PrP_x, described in the 1999 Annual Report, is now in preparation.

Experiment 777
Vortex state of *s*-wave superconductors investigated by muon spin rotation
(A. Price, R. Miller, UBC/TRIUMF)

In Expt. 777, we continued our investigation of the vortex state of conventional superconductors with the three-dimensional superconductors V_3Si and $LuNi_2B_2C$. V_3Si, a cubic superconductor with T_c = 17 K, and $LuNi_2B_2C$, with T_c = 16.6 K, have been extensively investigated with small angle neutron spectroscopy, STM and other methods. Both superconductors show changing vortex lattice geometries as the applied field is increased.

$LuNi_2B_2C$

Transverse field data taken on the M20 beam line on $LuNi_2B_2C$ were analyzed with a field distribution that takes into account non-local effects. Non-local effects in a superconductor arise when the small coherence length London limit no longer applies. This can occur at nodes in the gap in unconventional superconductors or due to strong gap anisotropy, as is the case in $LuNi_2B_2C$. Our analysis confirms the presence of a square vortex lattice at applied fields larger than 2 kOe, as reported by SANS and STM.

Our μSR data indicate that the penetration depth measured by μSR varies considerably with applied magnetic field. This effect has been seen previously in $NbSe_2$ (see previous Expt. 777 Annual Reports), although the magnitude of the field dependence in $LuNi_2B_2C$ is about five times larger (see Fig. 62 top).

The core radius, defined as the distance between

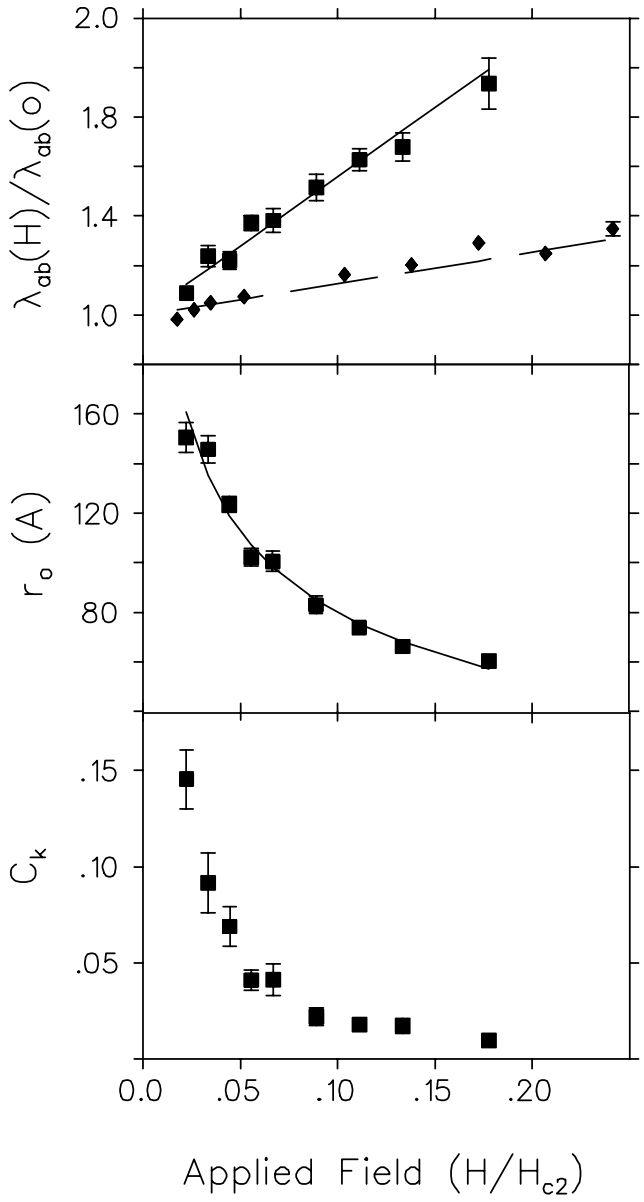

Fig. 62. Magnetic field dependence in $LuNi_2B_2C$ at $T = 2.2$ K of: top) the effective penetration depth, λ_{ab} (squares), and in $NbSe_2$ (diamonds) at $T = 2.4$ K; middle) the vortex core radius in $LuNi_2B_2C$; bottom) fitting parameter c_k.

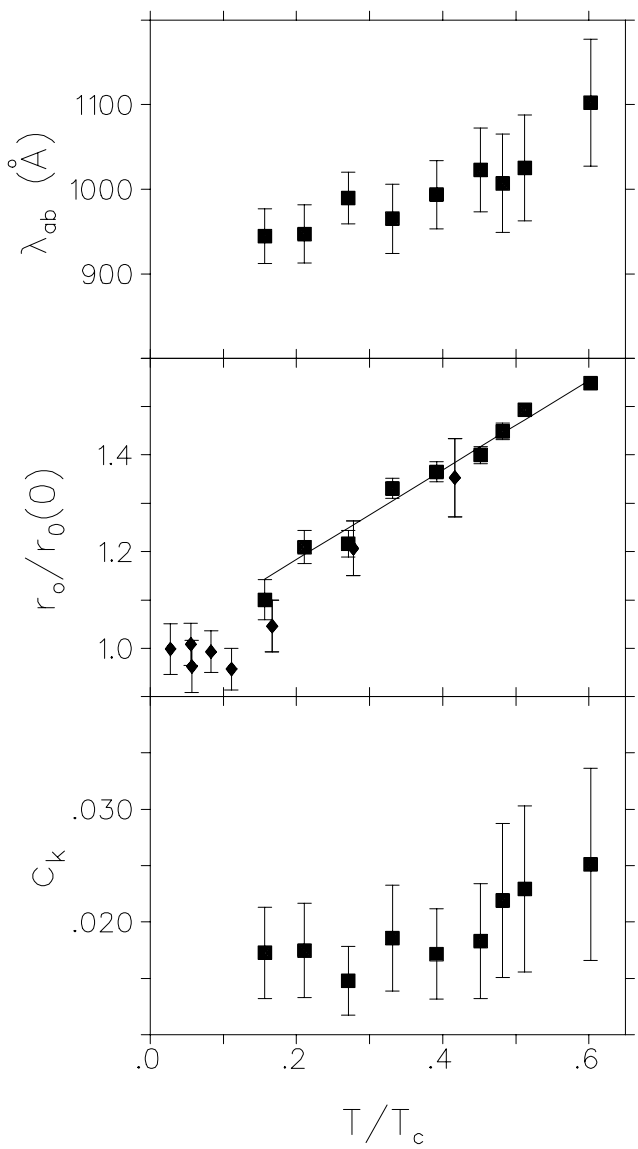

Fig. 63. Temperature dependence in $LuNi_2B_2C$ at $H = 12$ kOe of: top) the effective penetration depth, λ_{ab} (squares); middle) the vortex core radius in $LuNi_2B_2C$ (squares) and in $NbSe_2$ (diamonds) at $H = 5$ kOe; and bottom) fitting parameter c_k.

the vortex core centre and the maximum in the supercurrent, also varies strongly with applied magnetic field. This observation of a magnetic field dependent core radius is the first in a $3D$ superconductor. Previously, μSR measurements reported similar field dependence in $2D$ $NbSe_2$, $YBCO_{6.6}$ and $YBCO_{6.95}$ (see Fig. 62 middle).

Previous Expt. 777 measurements of the vortex core electronic properties of $NbSe_2$ showed that bound quasiparticle states in the vortex core cause the vortex core radius to decrease with decreasing temperature [Miller *et al.*, Phys. Rev. Lett. **85**, 1540 (2000)]. This effect was predicted by Kramer and Pesch in 1974. In $LuNi_2B_2C$, we find a similar effect, shown in Fig. 63. Furthermore, the slope of the core radius as a function of temperature is nearly the same as in $NbSe_2$, indicating the likely presence of bound quasiparticle states in $LuNi_2B_2C$.

V_3Si

Initial μSR measurements of the magnetic field distribution in cubic V_3Si have been made on the M20 beam line, using the MULTI spectrometer. Analyzed with the conventional Ginzburg-Landau field distribution (without non-local effects), the measurements fit relatively well to a hexagonal vortex lattice.

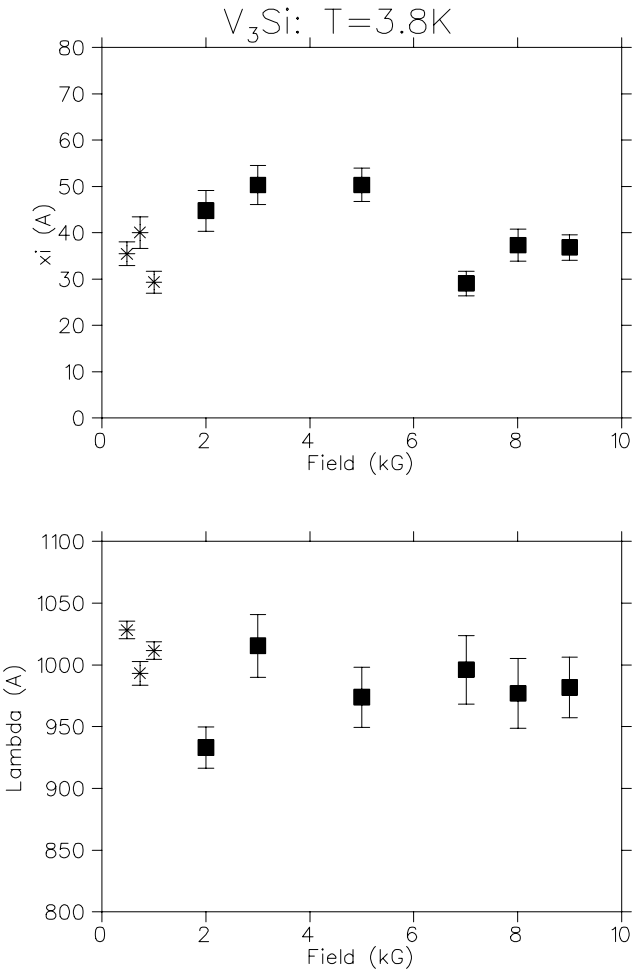

Fig. 64. Magnetic field dependence in V_3Si at $T = 3.8$ K of: top) the effective coherence length, ξ; and bottom) the effective penetration depth, λ_{ab}.

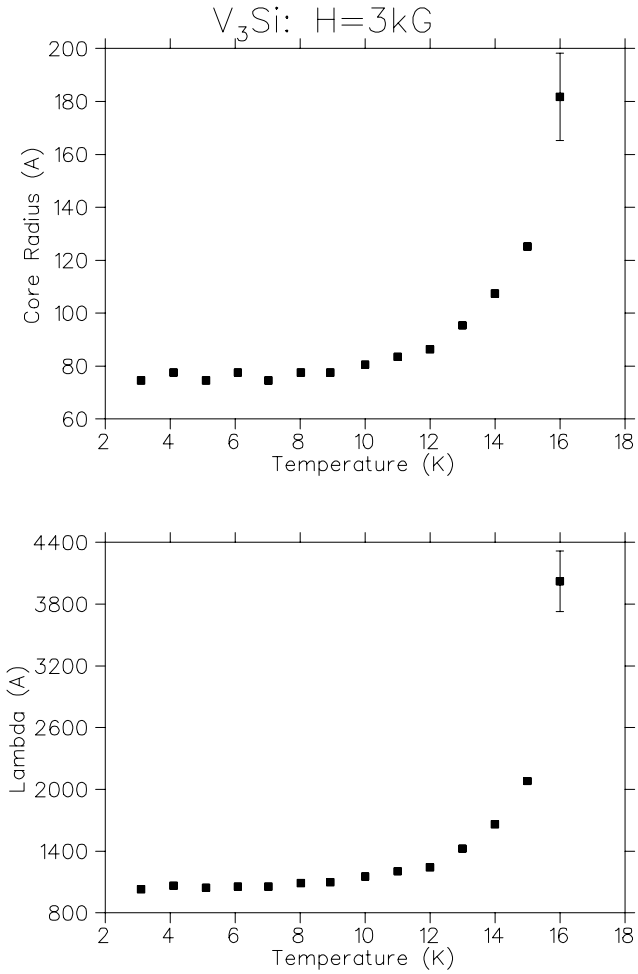

Fig. 65. Temperature dependence in V_3Si at $H = 3$ kOe of: top) the core radius; and bottom) the effective penetration depth, λ_{ab}.

Figure 64 shows the field dependence of the effective coherence length, closely related to the core radius, and of the effective penetration depth. Surprisingly, over this applied field range, neither quantity is dependent on magnetic field, contrary to our earlier measurements. More measurements are planned with a different sample of V_3Si and over an extended magnetic field range.

Finally, Fig. 65 indicates that unlike $NbSe_2$ and $LuNi_2B_2C$, the core radius in V_3Si is not temperature dependent at low temperature and that there is no Kramer-Pesch effect in V_3Si in this temperature range.

Future plans

Because of the surprising absence of either a field dependent core radius or a Kramer-Pesch effect, we plan to repeat the experiment on a different sample of V_3Si. We also plan to investigate the role of Ta doping on the field dependence of the core radius in $NbSe_2$.

Experiment 782
Non-fermi-liquid behaviour and other novel phenomena in heavy-fermion alloys
(D.E. MacLaughlin, California, Riverside)

We have carried out μSR experiments on f-electron heavy-fermion alloys in which deviations from "normal" fermi-liquid heavy-fermion behaviour have been discovered. Thermodynamic and transport measurements indicate that the fermi-liquid description appropriate to a conventional spin-singlet Kondo system does not apply to certain heavy-fermion alloys [i.e. articles in Proc. Conf. on Non-Fermi Liquid Behavior in Metals, Coleman *et al.* eds., J. Phys. Cond. Matter **8** (1996)]. Perhaps the most striking non-fermi-liquid (NFL) low-temperature anomalies are a linear temperature dependence of the resistivity and a logarithmic divergence of the Sommerfeld electronic specific heat coefficient. Both of these properties indicate a serious breakdown of the fermi-liquid picture, and both characterize many NFL heavy-fermion systems discovered

to date.

Evidence has emerged from our μSR and NMR experiments [Bernal *et al.*, Phys. Rev. Lett. **75**, 2023 (1995); Bernal *et al.*, Phys. Rev. **B54**, 13000 (1996); MacLaughlin *et al.*, J. Phys. Cond. Matter **8**, 9855 (1996)] that in some cases this NFL behaviour is due to random disorder in the material. In the simplest disorder-driven picture [MacLaughlin *et al., op. cit.*] this disorder produces an inhomogeneous distribution of Kondo temperatures T_K in the random alloy. Such "Kondo disorder" gives rise to NFL behaviour if a significant fraction of the f spins possess values of T_K lower than the temperature of measurement, in which case these spins are *ipso facto* not in their fermi-liquid ground states. This in turn implies a broad distribution of the heavy-fermion spin polarization, direct signatures of which are correspondingly broad μSR and NMR lines at low temperatures.

Our results have stimulated a considerable amount of theoretical work on disorder-driven mechanisms for NFL behaviour. The Kondo disorder model was put on a firm theoretical footing by Miranda, Dobrosavljević, and Kotliar [J. Phys. Cond. Matter **8**, 9871 (1996)] who found that the effect of structural disorder was enhanced by electron correlation effects. A recent extension of the model by Castro Neto, Castilla, and Jones [Phys. Rev. Lett. **81**, 3531 (1998); Castro Neto and Jones, Phys. Rev. **B62**, 14975 (2000)] takes RKKY interactions between uncompensated spins into account, and predicts NFL behaviour in the form of Griffiths singularities [Phys. Rev. Lett. **23**, 17 (1969)] due to the susceptibilities of RKKY-coupled clusters. Chattopadhyay and Jarrell [Phys. Rev. **B56**, R2920 (1997)] have treated the spin dynamics in the Kondo disorder model, computing the self energy $\Sigma(\omega)$ for distributions of Kondo temperatures including that of Bernal *et al.* [*op. cit.*]. The corresponding low-temperature optical conductivity shows a low-frequency pseudogap, a negative optical mass enhancement, and a linear-in-frequency transport scattering rate, consistent with experimental results in $Y_{1-x}U_xPd_3$ and $UCu_{5-x}Pd_x$.

During the year we carried out μSR studies of two NFL systems at TRIUMF: single-crystal $Ce(Ru_{0.5}Rh_{0.5})_2Si_2$, and $UCu_{5-x}Pt_x$. In the latter we find no evidence for disorder-driven NFL behaviour; this is surprising, given that the isostructural NFL system $UCu_{5-x}Pd_x$ exhibits strong disorder [Bernal *et al., op. cit.*]. In contrast, μSR Knight shifts and linewidths in $Ce(Ru_{0.5}Rh_{0.5})_2Si_2$ are consistent with disorder-driven NFL behaviour, as was also concluded from previous studies [Graf *et al.*, Phys. Rev. Lett. **78**, 3769 (1997); Liu *et al.*, Phys. Rev. **B61**, 432 (2000)]. Our investigations of these and other NFL materials are continuing.

$Ce(Ru_{0.5}Rh_{0.5})_2Si_2$

This NFL alloy had previously been identified as possessing a disorder-driven NFL mechanism from thermodynamic measurements [Graf *et al., op. cit.*] and a ^{29}Si NMR study [Liu *et al., op. cit.*]. But these NMR experiments were carried out in powder samples. The possibility has been raised [Taniguchi *et al.*, J. Phys. Soc. Jpn. **68**, 2026 (1999)] that disorder introduced in the powdering process, or possibly in the original fabrication of the sample, was responsible for the NMR results, and that the mechanism for NFL behaviour in this system is not driven by disorder. We therefore obtained an extremely well-characterized single-crystal sample of $Ce(Ru_{0.5}Rh_{0.5})_2Si_2$ from the group of Y. Myako at Osaka University. NMR on single crystals is difficult due to the small skin depth for radio frequency signals, but no such problem exists for μSR. Furthermore, the NMR experiment used field-aligned epoxy-potted samples, which would not be suitable for μSR because a large fraction of the muons would stop in the epoxy. The single crystal $Ce(Ru_{0.5}Rh_{0.5})_2Si_2$ sample was therefore ideal for a μSR study.

The primary signature of disorder-driven NFL behaviour in TF-μSR is a linewidth which grows faster with decreasing temperature than the bulk susceptibility (or, equivalently, the positive-muon (μ^+) Knight shift). A convenient way to see this behaviour, motivated by the standard Clogston-Jaccarino plot in NMR, is to plot the dimensionless ratio $\delta K(T)/K(T)$ versus the bulk susceptibility $\chi(T)$, with temperature T an implicit parameter. Here $\delta K(T)$ is the rms spread in Knight shifts responsible for the linewidth, and $K(T)$ is the average Knight shift. In a simple heuristic model of disorder-driven NFL behaviour [MacLaughlin, J. Phys. Soc. Jpn. **69**, 33 (2000)] $K(T) \propto \chi(T)$ whereas $\delta K(T) \propto \chi^2(T)$, so that $\delta K(T)/K(T) \propto \chi(T)$.

Preliminary results from our data for $Ce(Ru_{0.5}Rh_{0.5})_2Si_2$, taken with applied field parallel to the c axis of the tetragonal lattice, are shown in Fig. 66. The data bear a striking resemblance to the NMR results [Liu *et al., op. cit.*]; both exhibit a marked increase with increasing susceptibility (decreasing temperature). This strongly indicates that the previously-observed disorder was not an artifact of the particular sample used in the NMR study.

Analysis of our results is not complete, but the data qualitatively confirm that strong disorder in the magnetic susceptibility is present, thus giving evidence for intrinsic structural disorder as a major factor in the NFL properties of $Ce(Ru_{0.5}Rh_{0.5})_2Si_2$. A paper on these results is in preparation.

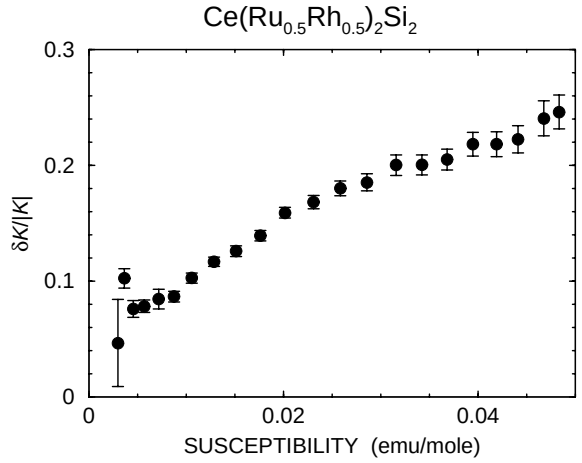

Fig. 66. Dependence of fractional width $\delta K/K$ of μ^+ Knight shift distribution on bulk susceptibility χ, with temperature an implicit parameter, in $Ce(Ru_{0.5}Rh_{0.5})_2Si_2$.

NFL behaviour in $UCu_{5-x}Pt_x$: return to a fermi-liquid?

The alloy system $UCu_{5-x}Pt_x$ is isostructural to $UCu_{5-x}Pd_x$ for $x \lesssim 2.5$ and, like $UCu_{5-x}Pd_x$, exhibits NFL behaviour near $x = 1$ [Chau and Maple, J. Phys. Cond. Matter **8**, 9939 (1996)]. A marked difference between the two systems is found for $x \gtrsim 1.5$, however: $UCu_{5-x}Pd_x$ has a spin-glass phase for $x \gtrsim 2$, whereas $UCu_{5-x}Pt_x$ exhibits fermi-liquid behaviour and no magnetic order [Chau, Ph.D. dissertation, Univ. of California, San Diego (1997)]. This curious behaviour raises questions concerning the role of disorder in the NFL properties of $UCu_{5-x}Pt_x$. Is chemical disorder relevant in this alloy series? Is the loss of NFL behaviour for $x > 1$ related to a QCP at $x = 1$, or is the effect of disorder reduced for some reason?

We have begun TF-μSR studies of this system at TRIUMF. Very preliminary results over the temperature range 2–300 K show considerable differences between μSR spectra of $UCu_{5-x}Pt_x$ and $UCu_{5-x}Pd_x$.

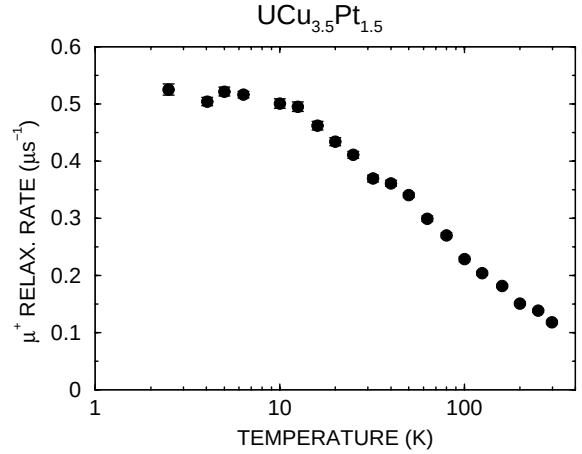

Fig. 67. Temperature dependence of μ^+ Gaussian relaxation rate $\sigma(T)$ in $UCu_{3.5}Pt_{1.5}$. Applied field $H = 10$ kOe.

Figure 67 shows the temperature dependence of the Gaussian width $\sigma(T)$ of the μSR line in $UCu_{3.5}Pt_{1.5}$. Very generally $\sigma(T)/2\pi$ is the rms width of the μ^+ resonance line. At low temperatures $\sigma(T)$ is a factor of six smaller than in $UCu_{5-x}Pd_x$ [Bernal *et al., op. cit.*], which indicates clearly that disorder is not a dominant factor in these alloys.

Experiment 783
Paramagnetic frequency shifts in unconventional superconductors
(R.H. Heffner, LANL; J.E. Sonier, SFU)

$U_{0.965}Th_{0.035}Be_{13}$

In December, 1999 we carried out μ^+ Knight shift measurements in the heavy-fermion superconductor $U_{0.965}Th_{0.035}Be_{13}$ using the dilution refrigerator on the M15 beam line (see Fig. 68). This compound has two superconducting transitions, $T_{c1} = 0.47(5)$ K and $T_{c2} = 0.35(2)$ K, as indicated by heat capacity measurements. There were two key findings in this study:

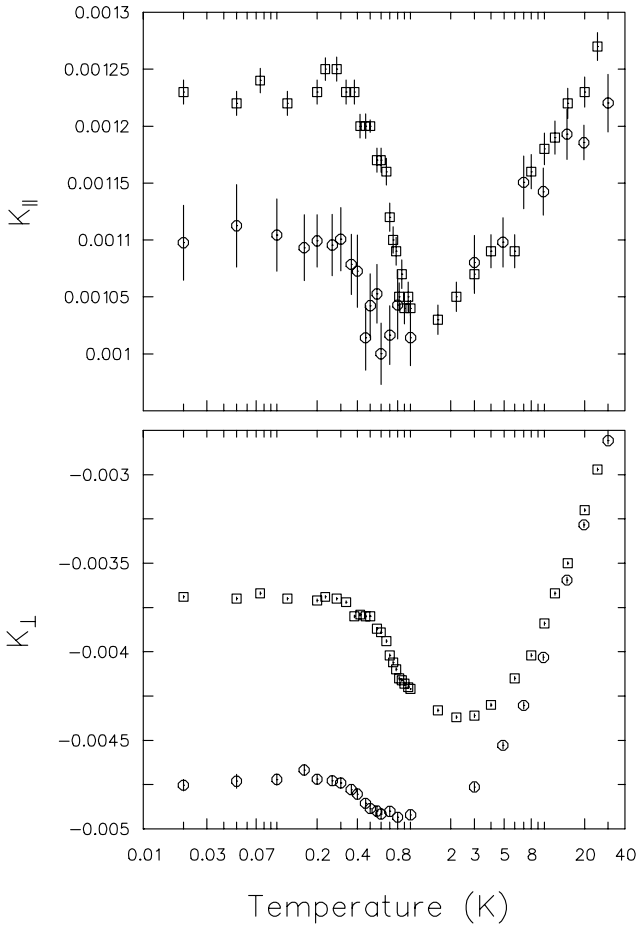

Fig. 68. Temperature dependence of the μ^+ Knight shift K in UBe_{13} (squares) and $U_{0.965}Th_{0.035}Be_{13}$ (circles) measured in an applied magnetic field $H = 10$ kOe. The subscripts $\parallel$ and $\perp$ correspond to two different muon sites.

- In the normal state we observed an anisotropic temperature dependent transferred hyperfine coupling between the μ^+-spin and the U $5f$ electrons.
- An abrupt reduction of χ_s was observed below T_{c1}, whereas χ_s did not change with temperature below T_{c2}.

The first finding is highly unusual, since the contact hyperfine interaction A_c generally involves the s orbitals around the μ^+. The observed anisotropy suggests an admixture of the f and s states, although no definite conclusion has yet been made to explain this result.

The temperature dependence of χ_s shows a sharp drop in χ_s below T_{c1}, indicating that the first superconducting phase consists of Cooper pairs possessing a substate of opposite spin projection (i.e. $S_z = 0$). This state could be of either even or odd parity. There is a clear change in the T-dependence of χ_s below T_{c2}, indicating a change in the superconducting order parameter. The T-independent behaviour is consistent with the development of a multi-component order parameter.

UBe_{13}

In October we performed similar μ^+ Knight shift measurements in pure UBe_{13} crystals. Unlike the Th-doped compound described above, only one superconducting transition at $T_c = 0.87(3)$ K is observed in heat capacity measurements. However, very little is known about this superconducting phase. A preliminary analysis of the Knight shift measurements (Fig. 68) shows that the superconducting phase of UBe_{13} is similar to the first superconducting phase observed in $U_{0.965}Th_{0.035}Be_{13}$; i.e., χ_s decreases as the temperature is reduced. However, unlike the Th-doped compound, the decrease of χ_s continues to $T = 0$ K. The ratio χ_s/χ_n at $T = 0$ K appears to be the same as what would be observed in $U_{0.965}Th_{0.035}Be_{13}$ if the second superconducting phase did not form.

We also observed the onset of an anisotropic transferred hyperfine coupling in the normal state of UBe_{13}. This indicates that the Th impurities are not responsible for this yet unexplained feature.

Present status of Expt. 783

The above observations suggest the possible existence of a multi-component order parameter in $U_{1-x}Th_xBe_{13}$. However, the information gathered so far is not sufficient to decisively identify the superconducting order parameter in either the Th-doped or the pure compound. Thus, we plan to carry out additional Knight shift measurements in 2001 to further address this important issue.

Experiment 784
μSR studies of spin-singlet states in oxides
(A. Fukaya, Y.J. Uemura, Columbia)

In low dimensional Heisenberg antiferromagnetic systems, quantum effects play an important role in macroscopic properties. The ground state may not be a long range Néel ordered state but a singlet state, as observed in Haldane-gap and spin-ladder systems. To study the ground state and spin dynamics of low dimensional quantum spin systems, we have performed comprehensive muon spin relaxation (μSR) studies. We have measured μSR for various oxides: charge ordered system NaV_2O_5, two dimensional (2D) plaquette spin system CaV_4O_9, two-leg ladder system $Sr(Cu,Zn)_2O_3$, and others, and have obtained interesting results. In this report we describe the result of μSR measurements of the 2D quantum system $SrCu_2(BO_3)_2$.

2D quantum systems are quite interesting from the viewpoints of both magnetism and superconductivity. $SrCu_2(BO_3)_2$ is one of only a few 2D compounds with a singlet ground state. Theoretical and experimental studies have clarified that the ground state is an exact singlet dimer state, but it is extremely close to a quantum critical point. This system has a built-in geometrical spin frustration. These features are directly comparable to the case of high-T_c cuprate systems. Thus, $SrCu_2(BO_3)_2$ is a unique 2D spin system which can possibly provide insights for a general understanding of how gapped (spin gap/superconducting) ground states coexist/compete with or cross over to ungapped ground states with/without magnetic order.

We show the temperature dependence of the time spectrum at zero-field (ZF) in Fig. 69. As the temperature decreases, the relaxation becomes fast. Thus, we

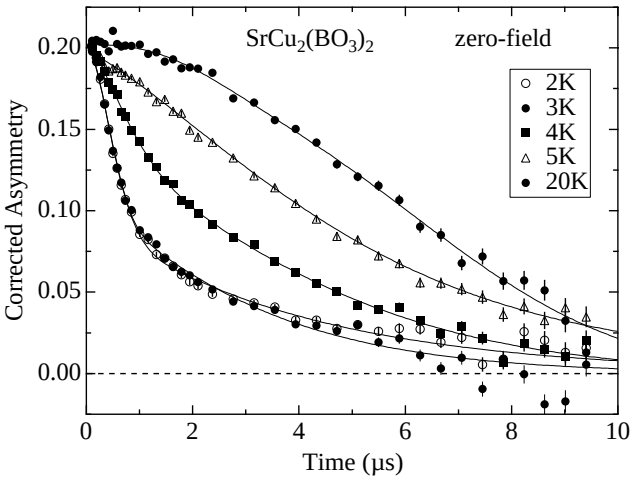

Fig. 69. Temperature dependence of the time spectrum in ZF for $SrCu_2(BO_3)_2$. An unexpected enhancement of relaxation is observed at low temperatures.

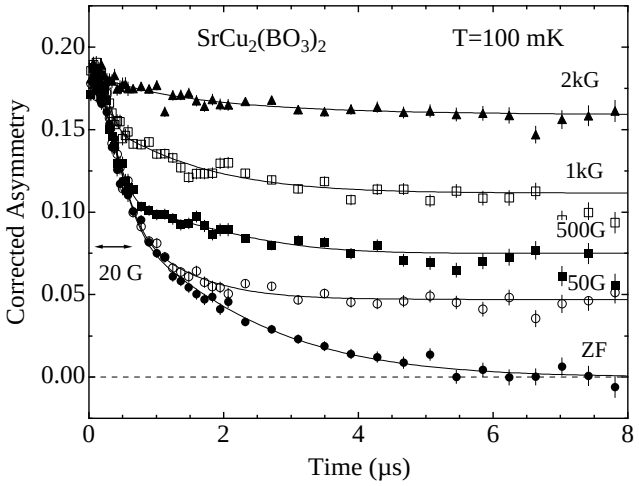

Fig. 70. LF dependence of the time spectrum in $SrCu_2(BO_3)_2$ at 100 mK. The decoupling field is ∼10 times larger than that expected from ZF measurement.

see the existence of some magnetically active spins in a nominally pure spin gap compound at low temperatures. Since the ground state is non-magnetic, muon spins should not relax at low temperatures. Since the μSR method is quite sensitive to small magnetic moments, μSR might detect intrinsic magnetic properties of samples which cannot be detected by other methods. The origin of the anomalous spin freezing, however, has not yet been clarified.

The longitudinal field (LF) dependence of the time spectrum is also quite anomalous. We show the LF dependence at 100 mK in Fig. 70. When a longitudinal field is applied, the asymmetry of the long time tail increases and does not relax. This fact suggests that the local field is static. If the local field is static and has a Gaussian distribution with width Δ, Δ is estimated to be ∼20 G from the time spectrum at early time in zero field. A local field of ∼20 G should be completely decoupled by LF∼200 G. However, even at 2 kG, the time spectrum still shows relaxation. This anomalous relaxation has been termed "undecoupleable Gaussian" relaxation, and has been observed in several systems with geometrically frustrated exchange interactions. Examples of such systems are $SrCr_8Ga_4O_{19}$, Cr-jarosite, $CePt_2Sn_2$, as well as the 1D spin system Y_2BaNiO_5 with charge doping. The details of this line shape, however, are yet to be understood.

Experiment 791
Electronic structure and dynamics of charged muonium centres in semiconductors
(K.H. Chow, B. Hitti, R.F. Kiefl, UBC/TRIUMF)

Results of experiments on muonium are generally considered to be the main source of information on *isolated* hydrogen in semiconductors. Hydrogen is an important impurity which can dramatically affect the electrical and optical properties of these technologically relevant materials. Recently, we unambiguously observed the reaction of Mu^+ with an intentional dopant in a semiconductor. This was the first microscopic study, "as-it-happens", of the formation of a hydrogen or hydrogen-like complex with an intentional dopant in a semiconductor. An important extension of these studies is the characterization of the electronic structure of the isolated precursor state. Such information is interesting for several reasons. First, it enables comparisons with the many theoretical calculations on the subject, which generally locate it at or near a distorted bond-centre position. Thus far, there has been no experimental information on the stucture of H^+ or Mu^+ in a semiconductor. Second, information on the isolated state is an integral part of understanding how the muon or hydrogen makes a transition from its precursor configuration to being part of a complex.

Structural information on a diamagnetic centre such as Mu^+ is obtained by studying the muon-induced and dipolar interactions with the host Ga and As nuclei, all of which have spin 3/2. The most powerful technique for this purpose is μLCR. Recall that a dip in the integrated polarization appears at values of $\mathbf{B}$ where resonant cross-relaxation between the muon and neighbouring nuclear spins occur due to avoided level-crossings in the combined energy levels. The positions of the resonances associated with a particular nucleus are determined by Q and θ, often giving a distinct fingerprint that identifies the neighbouring nucleus and its symmetry. Recall that Q is the strength of the quadrupole interaction and θ is the angle between the applied magnetic field and the muon-nucleus direction. A rough estimate of Q, and hence the position of the resonances, can also be obtained by studying the relaxation of the TF-μSR precession signal as a function of magnetic field. We have performed such an experiment prior to our μLCR experiments to help define a search region.

Our μLCR experiment with $\mathbf{B}||\langle 100\rangle$ in a heavily doped p-type GaAs:Zn sample at 50 K is shown in Fig. 71a. These are the only two resonances visible from 1.7 kG to 3.6 kG, the magnetic field region that we have investigated thus far. This doublet signal can be unambiguously assigned to a nearby Ga atom because the ratio of their positions is identical to the ratio of the ^{69}Ga and ^{71}Ga quadrupole moments (0.168×10^{-24} e.cm^2 and 0.106×10^{-24} e.cm^2). This is further confirmed by Fig. 71b, which shows theoretically the expected resonances. A single value of the electric field gradient was used to produce this figure. (Note that for each isotope, the signal-to-noise is too low to resolve the weaker of the pair.) The unambiguous identification of Ga as being a nearest neighbour of Mu^+ is certainly an

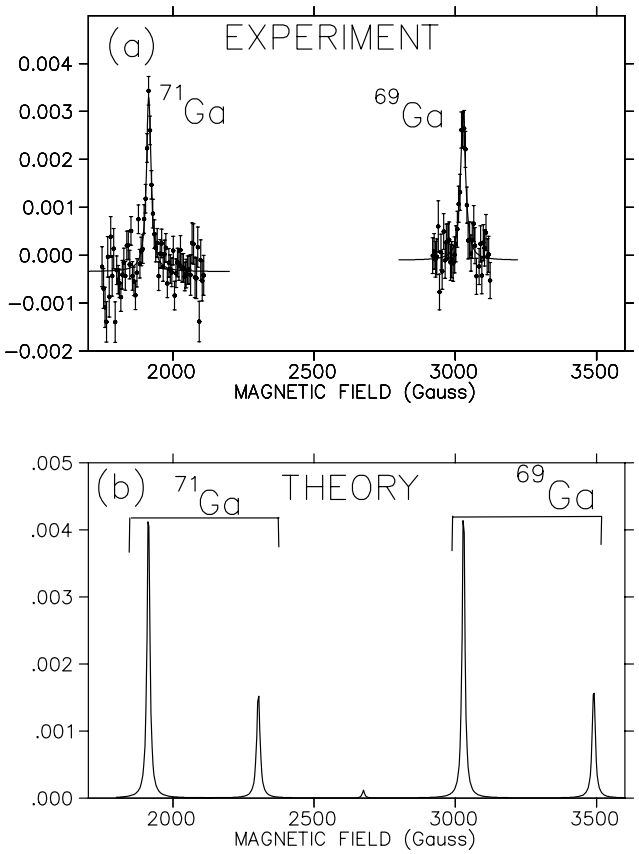

Fig. 71. (a) μLCR at 50 K in heavily doped p-type GaAs:Zn with $\mathbf{B}||\langle 100\rangle$. (b) Theoretical calculation as described in the text.

important step. However, there is nothing in Fig. 71a which tells us its symmetry. This information is obtained by performing a μLCR experiment at another orientation: we have selected $\mathbf{B}||\langle 110\rangle$. The positions and strengths of the lines in Fig. 71a change in a manner that unambiguously confirms that the muon and the Ga nucleus lie on the same $\langle 111\rangle$ axis (i.e. $\theta = 54.7°$).

Thus, all our results are consistent with Mu^+ being located near the centre of a Ga–As bond. However, since we have detected and characterized the Ga only, the picture is still incomplete. Unambiguous proof of the location will only be possible if we can also detect the ^{75}As nucleus and verify that it too has "$\langle 111\rangle$ symmetry". The corresponding resonances are expected to be located at higher magnetic fields, and experiments to locate them are currently being organized.

Experiment 804
Muonium in gallium nitride
(R.L. Lichti, Texas Tech)

The primary goal of Expt. 804 has been to investigate the muonium analogue of hydrogen defect states in GaN and other group-III nitrides. During the past year we obtained the full temperature dependence of the QLCR resonances for a partially compensated Zn-doped GaN sample and for AlN. These data represent static diamagnetic Mu^+ or Mu^- defect centres in these materials. The likely stable sites for these centres are anti-bonding locations oriented into the channels formed by the c-axis stacking order of the Wurtzite structure with Mu^+ associated with nitrogen and Mu^- with the group-III atom (Ga or Al). These sites have the bond oriented at 70° to the c-axis and are commonly noted as $AB_\perp$. Other likely sites are metastable; a second antibonding location with Mu inside the most tightly confined region of the structure and the bond along the c-axis ($AB_\parallel$) and for Mu^+ either of the two bond centred locations ($BC_\perp$ or $BC_\parallel$). QLCR resonances can identify these various sites when the muonium impurity is static. Any Ga related features will have two nearly identical sets of lines with a position ratio of 1.59 due to the two I = 3/2 Ga isotopes, while N related features will reflect a single I = 1 isotope. A single line per isotope only occurs if the bond (and electric field gradient) lies parallel to the applied field, which was along the c-axis of our highly-oriented, thick-film samples. The onset of diffusive motion for $Mu^\pm$, or a slow transition out of a given state, results in broadening of the spectral lines with the resonances disappearing for rapid dynamics in either case. When motion is rapid but highly localized, ie. involving a very few sites, QLCR spectra can still be observed.

Figure 72 shows typical QLCR data for AlN. This spectrum appears to be essentially unchanged up to roughly 850 K, above which the effects of dynamics are seen, but the QLCR is still visible at 1100 K. This single main line is associated with N and almost certainly represents a metastable Mu^+ with a Mu–N bond along the c-axis; we have therefore assigned the line centred at 42 G to the $AB_\parallel$[N] site for Mu^+ in AlN. There is a

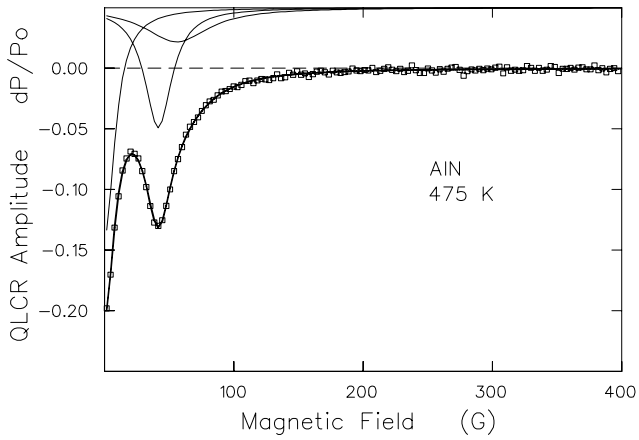

Fig. 72. Raw QLCR data for AlN at 475 K. Main spectrum is a single line centred at 42 G and is assigned to Mu^+ at an $AB_\parallel$[N] site. The broader line at higher field is also from a nitrogen neighbour but represents a second state.

smaller and broader line centred at about 70 G underlying the main resonance; this line is not yet assigned, but no partner has been located. Initial fits suggest a slightly different temperature dependence for the two observed QLCR lines in AlN, with the 70 G line broadening at a slightly lower temperature.

A fit to the QLCR spectra for GaN:Zn in one of the transition regions is shown in Fig. 73 after removal of the non-resonant zero-field feature. Three different states are identified in this spectra. The expected stable $AB_{\perp}$[Ga] site for Mu^- gives two lines per Ga isotope and is subsequently labelled Ga[70°]. The metastable $AB_{\parallel}$[Ga] site for Mu^- has a single strong line per isotope and is labelled as Ga[0°], while the metastable $AB_{\parallel}$[N] location for Mu^+ yields the line labelled N[0°]. Because these various spectra overlap significantly, fits were accomplished by a free parameter fit to the higher field ^{69}Ga lines with parameters for the ^{71}Ga partners forced to values expected from isotope ratios of natural abundances, and the quadrupole and dipole moments. Any remaining feature in the lower field region near 100 G was then fit with parameters free and assigned to an N related resonance; this was always a single dominant line. Numerous other small lines are present and may be from more distant neighbours or other possible sites; however, correlations among these weak signals and assignments have not yet been worked out.

The full temperature dependences for the QLCR linewidths and amplitudes from these fits are displayed in Fig. 74 and the resulting signal intensities along with a fit for each identified state are shown in Fig. 75. In addition to the three states seen in QLCR there is a fourth diamagnetic state which appears in zero-field relaxation measurements (ISIS data) and is tentatively associated with a mobile Mu^+ in the channel region

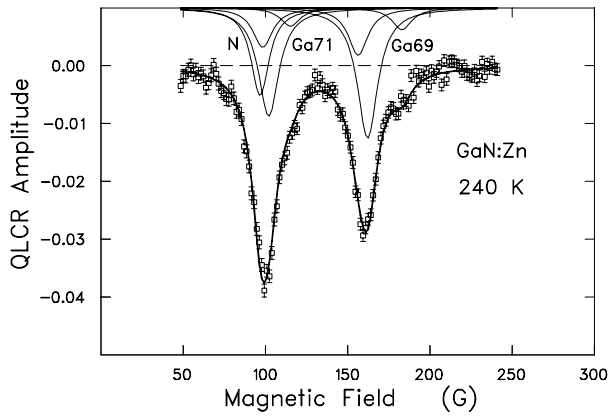

Fig. 73. Fit to QLCR spectra for the GaN:Zn sample in the region where lines from all three observed states have similar amplitudes. Ga assignments are a strong line per isotope from the stable Mu^- and weaker doublet from the metastable Mu^-; the N line is from a metastable Mu^+.

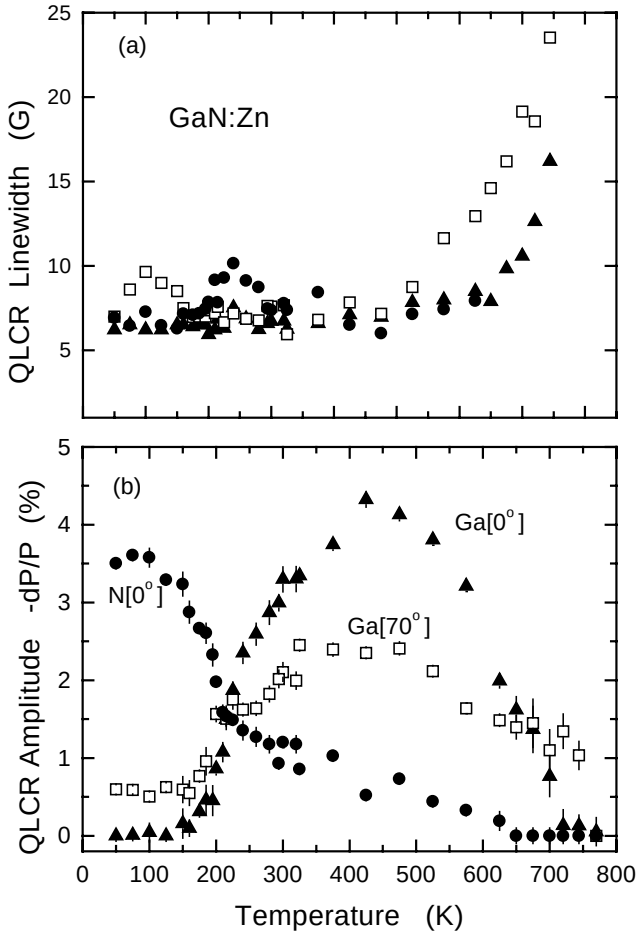

Fig. 74. The temperature dependent linewidths (a) and amplitudes (b) from fits to QLCR spectra for GaN:Zn. Three diamagnetic Mu states are identified: the stable (Ga[70°]) and metastable (Ga[0°]) Mu^- centres, and a metastable Mu^+ centre (N[0°]).

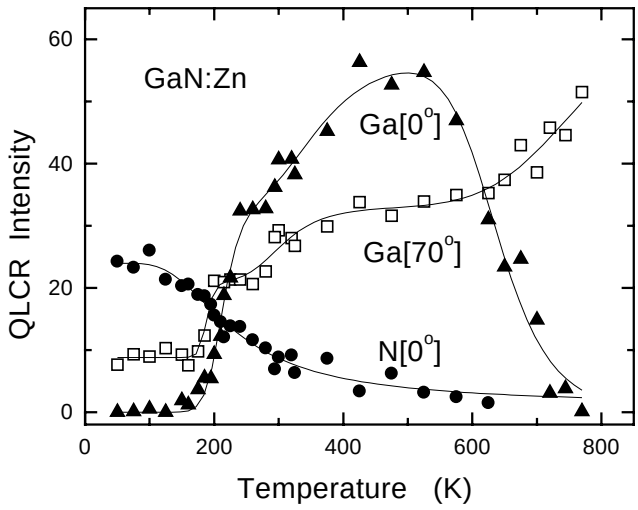

Fig. 75. Temperature dependent QLCR intensities (spectral area) for the compensated GaN:Zn sample. The general picture of the transitions and motion of stable Mu^- centres from these data is consistent with that from ZF relaxation results on more strongly n-type samples.

of the Wurtzite structure. Mu^0 states are also present, representing 30–40% of the muons at low to intermediate temperatures, having atomic-like hyperfine characteristics but with rapid dynamic relaxation based on decoupling curves (ISIS data).

The amplitudes displayed in Fig. 74b show a transition region near 200 K in which the charge state changes from positive to negative. This must presumably involve some Mu^0 centre as an intermediate state. Both the QLCR and ZF relaxation data imply multiple transitions in this region, with more than one site for the Mu^- final state. The amplitudes for the N[0°] signal seem to suggest two separate processes for the transition out of the metastable Mu^+ state; however, the intensity curve (Fig. 75) fits well to a single process. Consistency between the various data sets is poor for parameters related to the state changes near 200 K, thus a detailed model of the dynamics is not yet possible. The general picture of a switch from mostly Mu^+ states at low temperatures to predominantly Mu^- states above 200 K is the same for all of the (*n*-type) GaN samples we have studied.

The higher temperature dynamics are generally more consistent across various data sets and samples. The stable Mu^- states show diffusive motion above 500 K, which we model as hopping among $AB_\perp$[Ga] sites within the Wurtzite channels. This is indicated in the QLCR data as an increase in the linewidth but no decrease in total intensity for the Ga[70°] QLCR spectrum. Above roughly 650 K the metastable Mu^- state shows a transition into this mobile Mu^- as an increase in the Ga[0°] width accompanied by a decrease in intensity for that spectrum and a net increase in QLCR intensity for the more stable mobile state. The precise energies obtained from different data sets vary for both of these processes but are far more consistent than for the 200 K region. The overall general picture of transitions and motion of the diamagnetic $Mu^\pm$ states in GaN remains the same for all samples studied.

Experiment 814
μSR studies of unconventional superconductivity in Sr_2RuO_4
(G.M. Luke, McMaster)

Since the discovery of high temperature superconductivity in $La_{2-x}Ba_xCuO_4$ there has been an immense effort in all aspects of superconductivity. In addition to searches for higher T_c in studies of various cuprates with different structures and numbers of CuO_2 planes/unit cell, there have been great efforts to search for superconductivity in oxides without Cu. In 1994, Maeno *et al.* discovered superconductivity with $T_c = 1.5$ K in stoichiometric Sr_2RuO_4, which is isostructural to La_2CuO_4.

Many of the properties of Sr_2RuO_4 indicate that its superconducting state is of an unconventional nature. For example, the transition temperature is extremely sensitive to even non-magnetic impurities, and no Hebel-Slichter peak is seen in measurements of the NQR $1/T_1$. ^{17}O NMR measurements observed no change in the Knight shift below T_c, behaviour characteristic of *p*-wave pairing. We performed zero field muon spin relaxation (ZF-μSR) measurements under Expt. 814 and observed a spontaneous magnetic field below T_c; our results [Luke *et al.*, Nature **394**, 558 (1998)] demonstrated that the superconducting state in Sr_2RuO_4 is characterized by broken time reversal symmetry.

Since our initial ZF-μSR study we have performed measurements on an additional sample with a reduced $T_c = 1.1$ K, in order to confirm that the spontaneous magnetic field onsets at the superconducting T_c. A preliminary account of some of these data has been reported [Luke *et al.*, Physica **B289-290**, 373 (2000)] in a conference proceedings. We have fit the ZF data to the relaxation function given in equation 1 which is appropriate for a local field distribution consisting of a combination of Gaussian (to account for static nuclear dipole moments) and Lorentzian (due to the static internal field associated with the broken time reversal state) components. Equation 1 exhibits a long-time tail of 1/3 (required for any static combination of random internal fields) and reduces to the Gaussian or Lorentzian Kubo-Toyabe forms in the appropriate limits.

$$\mathcal{P}_\mu = \frac{1}{3} + \frac{2}{3}\left[1 - (\Delta t)^2 - at\right]\exp\left[-\frac{1}{2}(\Delta t)^2 - at\right]. \quad (1)$$

The Gaussian relaxation rates were held constant for each sample to a value obtained from fitting several runs simultaneously ($\Delta \approx 0.03\ \mu s^{-1}$). We plot the Lorentzian field strength (a) for samples with $T_c = 1.48,\ 1.1$ K in Fig. 76. We see that, within our resolution, the static field onsets at T_c for each sample. This provides additional evidence that the source of the field is the broken time-reversal symmetry superconducting state, rather than some magnetic spin freezing unconnected with superconductivity.

In the mixed state of a type-II superconductor, magnetic flux penetrates the sample in the form of quantized vortices. These vortices repel each other and therefore form a lattice. In most materials the resulting lattice is triangular, although the energy difference between square and triangular lattices is quite small. Square vortex lattices, which can arise from non-local effects, have been observed over narrow ranges of magnetic field in niobium and the borocarbides; the

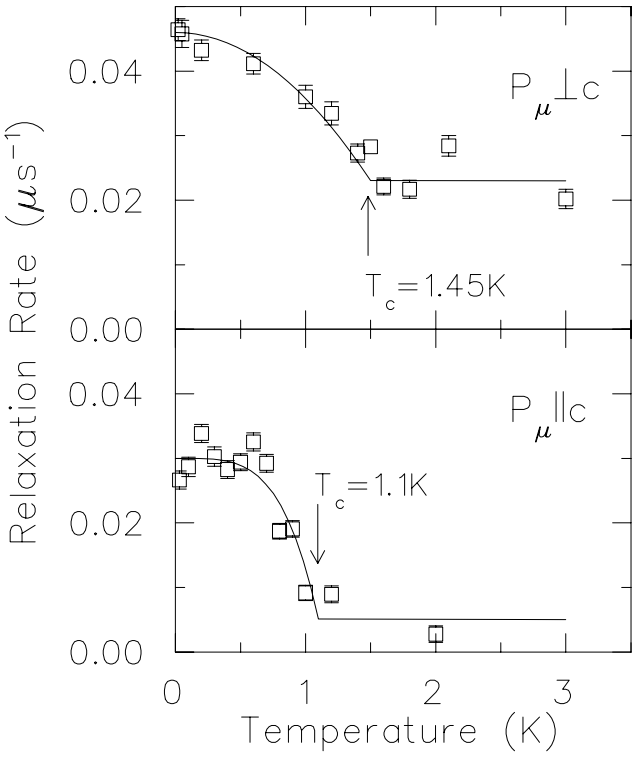

Fig. 76. Lorentzian relaxation rate measured in two samples of Sr_2RuO_4 with superconducting T_c's of 1.45 K and 1.1 K, respectively. Lines are guides to the eye.

observation of a square lattice is not by itself an indication of unconventional superconductivity. However, a prediction of a Ginzburg Landau model for the E_u state in Sr_2RuO_4 is that the Fermi surface geometry should give preferred directions for supercurrent flow within the basal plane, resulting in non-circular vortices. As a result, the vortex lattice should be square for a wide range of field and temperature. A square flux lattice was inferred from μSR measurements and then conclusively observed in neutron diffraction measurements over a wide range of temperature and field.

The presence of a vortex lattice results in a distribution of magnetic fields throughout the specimen; the shape of the field distribution depends on the lattice geometry. In a transverse field (TF-μSR) measurement, muons are implanted throughout the vortex lattice and sample the entire field distribution. A Fourier transform of the resulting precession signal directly reflects the magnetic field distribution (broadened due to the muon lifetime). We have calculated theoretical field distributions within a two-component superconducting order parameter model appropriate for Sr_2RuO_4, and incorporated these results to calculate muon polarization functions as a function of the applied field, penetration depth λ, coherence length ξ and Fermi surface anisotropy ν (where $\nu = 0$ corresponds to a cylindrical Fermi surface, and $|\nu| = 1$ corresponds to a square Fermi surface). Although this model is strictly applicable only near H_{c2}, numerical calculations carried out over a wide range of fields yield only moderate changes from the approximations used here. In fitting the spectra to this theoretical model, we have used common values of $\kappa = 2.65$ and $|\nu| = 0.335$ (μSR is insensitive to the sign of ν which orients the vortex lattice with respect to the crystalline lattice), obtained from fitting several runs simultaneously. This value of $|\nu|$ is somewhat larger than expected on the basis of H_{c2} anisotropy and neutron diffraction measurements; nonlocal corrections not included in our theoretical model may account for some of this difference. The results of our analysis are shown in Fig. 77 for our $T_c(B = 0) = 1.48$ K sample, where we plot $1/\lambda_{ab}^2$ vs. T for applied fields of 120 G (triangles) and 158 G (diamonds).

The temperature dependence of the superfluid density $n_s/m^* \propto 1/\lambda^2$ is fairly weak at low temperatures in Sr_2RuO_4, as is apparent from Fig. 77. Fitting to the temperature dependence of the superfluid density in weak coupling BCS theory gives the curves shown and provides an excellent fit to our data. Extrapolating these fits to low temperature, we obtain the zero temperature penetration depth $\lambda_{ab} = 1600$ Å for $B = 120$ G and $\lambda_{ab} = 1900$ Å for $B = 158$ G. Also shown in Fig. 77 is the low temperature linear temperature dependence of the superfluid density for the case of $YBa_2Cu_3O_{6.95}$ (which has line nodes) where we have scaled the axes to the T_c and $1/\lambda^2(T \to 0)$ values of Sr_2RuO_4. Clearly the behaviour of Sr_2RuO_4 is markedly different from that of the cuprates. While we are unable to exclude a small linear or T^2 term in $1/\lambda_{ab}^2$ at low temperatures, we can clearly exclude a large term such as exists in the cuprates. We stress that the excellence of the fit to the form of $1/\lambda_{ab}^2$

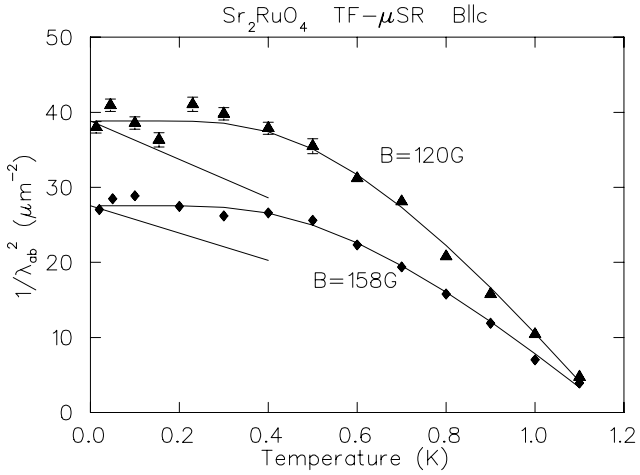

Fig. 77. Measured superfluid density ($1/\lambda^2 \propto n_s/m^*$) in Sr_2RuO_4 with the applied field $B \parallel \hat{c}$. Curves are fits to the temperature dependence of weak-coupled BCS theory, while lines follow reduced temperature dependence of $YBa_2Cu_3O_{6.97}$.

appropriate for weak coupling BCS theory does not mean that BCS is the correct theory for superconductivity in Sr_2RuO_4; rather, it indicates that the superconducting gap is fairly isotropic (and is likely characterized by weak coupling). As such, our measured results indicate that the gap in Sr_2RuO_4 is most likely nodeless, as expected for the previously identified E_u state.

Experiment 834
μSR study of transverse spin freezing in bond-frustrated magnets
(D.H. Ryan, McGill)

The random addition of antiferromagnetic (AF) exchange interactions to an otherwise ferromagnetic (FM) system leads to a loss of FM order through exchange frustration. In extreme cases, a spin glass (SG) is formed with random isotropic spin freezing and neither net magnetization nor long range order. At lower levels of frustration the system exhibits characteristics of both extremes as long-ranged FM order co-exists with SG order in the plane perpendicular to the FM order. On warming such a system from $T = 0$ K, the SG order first melts at T_{xy} followed by the loss of FM order at T_c. This picture has emerged from mean field calculations, numerical simulations and experimental measurements.

The aim of the current series of experiments is to investigate the magnetic behaviour in the region of T_{xy} in some partially frustrated alloys. Specifically, numerical simulations predict that although the freezing of transverse spin components does not represent a phase transition, it should be accompanied by significant, but non-critical, magnetic fluctuations.

Our first series of measurements confirmed that the expected signatures of transverse spin freezing could be observed using μSR (see 1999 Annual Report). However, there was a clear disagreement between the values for T_{xy} determined by μSR and those obtained earlier by applied field Mössbauer spectroscopy. The latter values were systematically lower, by as much as a factor of two in the most extreme case.

Measurements during our beam allocations in December, 1999 and May, 2000 were aimed at understanding this discrepancy. The first series focused on a–$Fe_{90-x}Ru_xZr_{10}$ for two reasons. (1) We can get cleanly into the fully frustrated state and so observe the FM→SG crossover. (2) We have been able to determine T_{xy} using zero-field Mössbauer spectroscopy in this system. The results, summarized as a phase diagram in Fig. 78, show much better agreement between the Mössbauer and μSR values for T_{xy}, indeed the Mössbauer values tend to lie slightly high in this system.

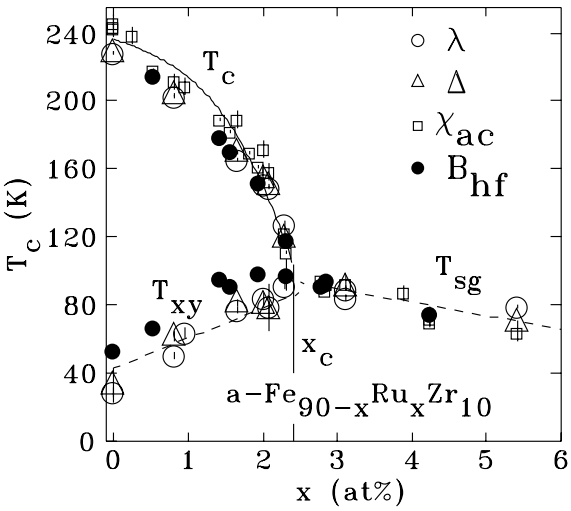

Fig. 78. Magnetic phase diagram for a–$Fe_{90-x}Ru_xZr_{10}$ showing T_c and T_{xy} deduced from μSR data. T_c's derived from χ_{ac} measurements on the same samples are also shown, as are T_c and T_{xy} values obtained using Mössbauer spectroscopy.

In May, we returned to the a–Fe_xZr_{100-x} system and concentrated around the $x = 93$ region in order to (i) confirm that the deviation from the applied field Mössbauer values for T_{xy} was a systematic effect, and (ii) determine the actual value for x_c, the composition at which the FM→SG crossover occurs. Previous estimates placed x_c around 94, while our initial μSR data from 1998 suggested that it lay below 93 (this seemingly minor issue matters because samples with $x > 93$ cannot be fabricated, and the value of $x_c = 94$ is an extrapolation). The results, summarized as a phase diagram in Fig. 79, confirmed that there is a clear systematic deviation between the applied field Mössbauer and zero-field μSR values for T_{xy}, suggesting that the ∼3 Tesla field used in the Mössbauer measurements greatly affects the value of T_{xy}. x_c was determined to lie at $x = 92.8$ in zero applied field.

Present status of Expt. 834

As we now know that the FM→SG crossover in a–Fe_xZr_{100-x} lies within the composition range that can be fabricated, we can study the full range of frustration effects in a binary rather than ternary alloy system, greatly simplifying sample quality control. We are now turning the discrepancy between the applied-field Mössbauer and zero-field μSR values for T_{xy} to our advantage. The observation offers a clean way in which to study the effects of an applied field on transverse spin freezing. Our final week of data-taking in May was devoted to following T_{xy} as a function of field in one sample. We were able to achieve a factor of four reduction in the available field of 5.5 Tesla, and confirmed that T_{xy} could indeed be observed in significant fields. This data set is currently being analyzed,

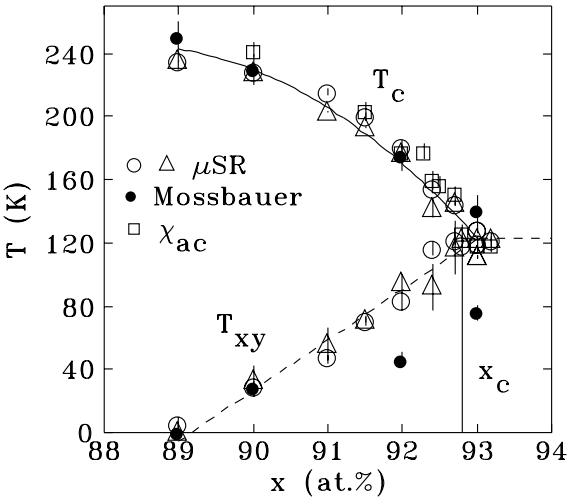

Fig. 79. Magnetic phase diagram for a–Fe_xZr_{100-x} showing T_c and T_{xy} deduced from μSR data. T_c's derived from χ_{ac} measurements on the same samples are also shown, as are T_c and T_{xy} values obtained on an independently prepared series of alloys measured using applied-field Mössbauer spectroscopy.

and we intend to follow this result with a systematic investigation across a wide range of compositions in the coming year.

Experiment 835
μSR studies on magnetic properties of layered superconductors HfNCl and ZrNCl
(T. Ito, Y.J. Uemura, Columbia)

Under Expt. 835 we have investigated a series of layered superconductors, HfNCl and ZrNCl. Organic molecules and alkali earth atoms may be intercalated between the layers in these materials, varying the interlayer spacing and doped charge respectively. Intercalated samples scale well in the universal correlation between T_c and the transverse field muon spin relaxation (TF-μSR) rate, σ, at the lowest temperature, which is observed in exotic superconductors including high-T_c cuprate superconductors.

We have measured the temperature dependence of the relaxation rate in TF-μSR at M20. The samples were aligned polycrystals mounted in a new In-sealed Kapton cell (prepared by Syd Krietzman *et al.*) to avoid decomposition by air. The spectra were analyzed using a cosine curve convoluted with Gaussian relaxation. As shown in Fig. 80, the temperature dependence of σ has a tendency to saturate at low temperatures and is quite similar to that of s-wave superconductivity, although it may be an artifact as is seen in polycrystalline high-T_c cuprate superconductors.

Correlation between T_c and $\sigma(T \to 0)$ is shown in Fig. 81. Samples co-intercalated with organic molecule THF show a simple correlation (a straight line), which

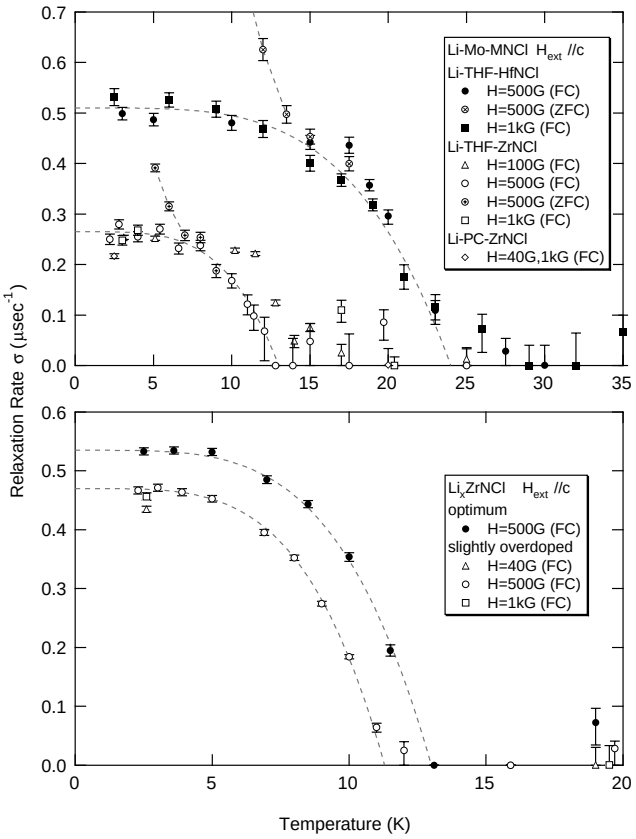

Fig. 80. TF-μSR relaxation rate vs. temperature in intercalated HfNCl and ZrNCl.

is observed in exotic superconductors such as high-T_c cuprate superconductors. All of these compounds have almost the same c-axis lattice constant (13.3 Å). On the other hand, the samples without organic molecules,

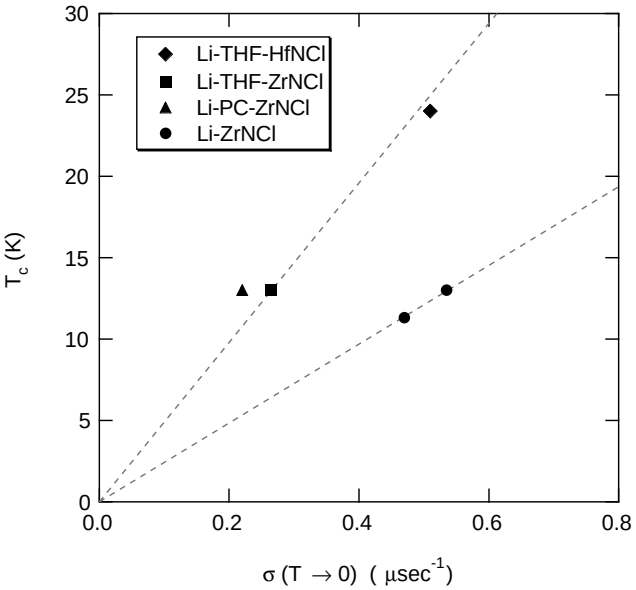

Fig. 81. The $T \to 0$ K relaxation rate vs. T_c for intercalated HfNCl and ZrNCl.

whose c-axis lattice constant is 9.4 Å, have a different slope in Fig. 81, which is closer to that expected for conventional BCS superconductors.

Further experiments will be performed using samples with (i) larger interlayer spacing and (ii) a wide range of carrier concentrations.

Experiment 842
Muonium-substituted free radicals in sub- and supercritical water
(P.W. Percival, SFU)

Experiment 842 was originally conceived to study free radicals formed in reactions of muonium with organic compounds dissolved in water at high temperatures and pressures. However, given the remarkable results of Expt. 713, reported in last year's Annual Report, the focus of this year's efforts has remained on studies of muonium reaction kinetics rather than free radical products. On a pragmatic note, the delay in free radical studies provides a better match with the timing of necessary apparatus development and funding.

The kinetics studies entail measurements of muonium decay rates in dilute aqueous solutions of the appropriate reactants, as a function of both temperature and pressure. During the past year we completed comprehensive studies of several reactions: Mu + hydroquinone, Mu + OH^-, Mu + I^-, and Mu + benzene. Preliminary results for the first three reactions were shown in the 1999 Annual Report; some data for the reaction with benzene are shown in Figs. 82 and 83. New in 2000 was a study of the reaction of Mu with alcohols (Fig. 84).

The motivation for these studies is to determine muonium rate constants under the extreme conditions found in supercritical water reactors, used for the destruction of hazardous waste, and in the cooling water cycles of pressurized water nuclear reactors. Since muonium behaves chemically as a light isotope of hydrogen, it can be used to study H atom chemistry and the properties of free radicals which incorporate H (almost all organic free radicals).

For many reactions there is a significant "kinetic isotope effect", i.e. the Mu and H rate constants are not equal. Nevertheless, a study of the temperature and pressure dependence of the Mu rate constant can provide novel data of general applicability to reactions in water under extreme conditions. Thus, our demonstration of a maximum in the rate constant as a function of temperature has obvious relevance to the efficiency of supercritical water reactors used for waste destruction.

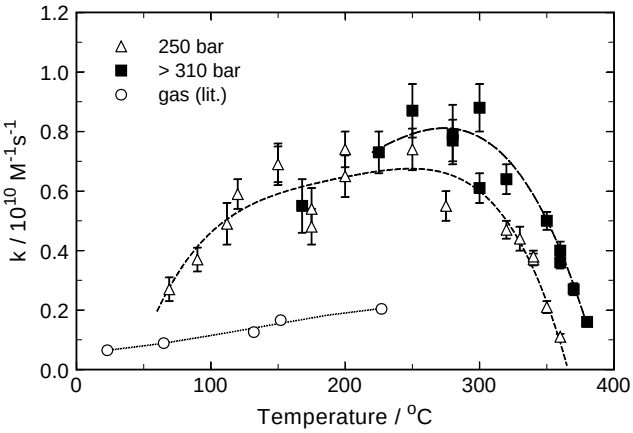

Fig. 82. Rate constants for Mu + benzene in water at two pressures, compared with literature data for gas phase measurements [Roduner, Fleming *et al.*, Ber. Bunsenges. Phys. Chem. **94**, 1224 (1990)].

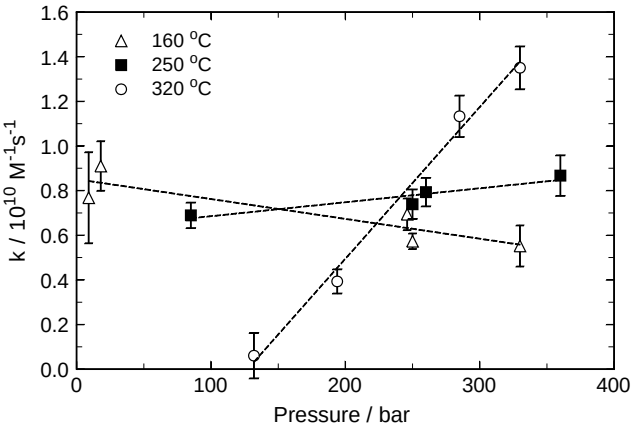

Fig. 83. Pressure dependence of rate constants for Mu + benzene in water at selected temperatures.

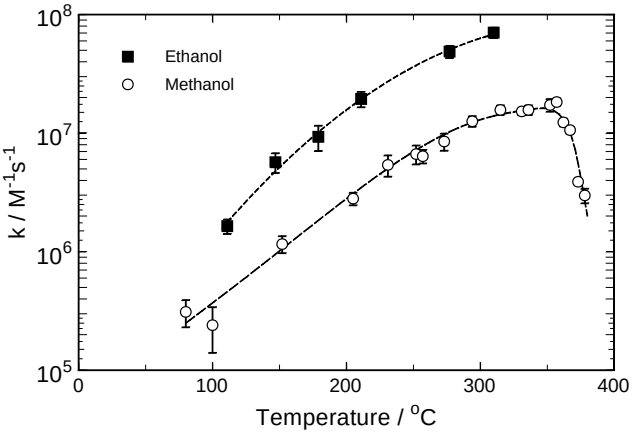

Fig. 84. Rate constants for Mu + alcohols in water at 230 bar.

Another example concerns the chemistry of radiolysis transients (hydrogen atoms, hydroxyl radicals, hydrated electrons) in the cooling water cycle of pressurized water nuclear reactors. The nuclear industry uses

a model for high temperature water radiolysis based on extrapolation of lower temperature data. The available data on the reactions of hydrogen atoms is very sparse and stops well short of the maximum temperature attained in our experiments. As a consequence, the extrapolated data for H atom kinetics shows curvature, but no maximum with temperature as found for Mu.

We have found a rate constant maximum for a wide diversity of reaction types:

addition:

$$\mathrm{Mu} + \mathrm{C_6H_6} \rightarrow \mathrm{C_6H_6Mu}$$

abstraction:

$$\mathrm{Mu} + \mathrm{CH_3OH} \rightarrow \mathrm{MuH} + \mathrm{CH_2OH}$$

muon transfer:

$$\mathrm{Mu} + \mathrm{OH^-} \rightarrow \mathrm{MuOH} + \mathrm{e^-_{aq}}$$

spin exchange:

$$\mathrm{Mu}(\uparrow) + \mathrm{Mn^{2+}}(\downarrow) \rightarrow \mathrm{Mu}(\downarrow) + \mathrm{Mn^{2+}}(\uparrow)\ .$$

This suggests that the maximum is due to some general phenomenon, such as the change in structure of the solvent as the conditions change.

A good clue to the explanation is given by the difference between the high pressure condensed phase data and the low pressure gas phase results (see Fig. 82). Such a situation is often ascribed to the "cage effect": reactants in liquids are constrained by the surrounding solvent molecules so that an encounter between reaction partners results in multiple collisions, increasing the probability of reaction over the single collision encounters that occur in gases. This effect should be important for diffusion-controlled reactions in liquid water, where hydrogen-bonded water molecules associate to form transient structures around solutes. However, the density of water falls markedly as the temperature approaches the critical point, and structural change is inevitable.

Thus the temperature dependence displayed in Fig. 82 can be qualitatively described in terms of the transition from *activation* control (where the chemical reaction is the rate-determining process) to partial *diffusion* control (chemical reaction is as fast as the inverse lifetime of reactant encounter pairs) to *collision* control. The different regimes appear to be characterized by markedly different pressure dependence (Fig. 83). In the case of a slow reaction, such as H abstraction (Fig. 84), the rate constant increases with temperature but does not reach the diffusion limit before the onset of the collision-controlled regime.

Quantitative analysis and interpretation of these data is ongoing, and, together with earlier results from Expts. 713 and 842, will comprise the Ph.D. thesis of Khashayar Ghandi, who won the 1999/2000 Westcott Fellowship for graduate research at TRIUMF.

Experiment 846
Complex order parameter symmetry in $YBa_2Cu_3O_{7-\delta}$ at low T and high magnetic field
(J.H. Brewer, TRIUMF/UBC; J.E. Sonier, SFU)

In 2000 we carried out a zero-field (ZF) μSR study of the superconducting $YBa_2Cu_3O_{6+x}$ system. The aim was to gain new insight into the role of the pseudogap (PG) phase in high-temperature superconductivity by exploiting the uniqueness of the muon as a local probe of magnetic and electronic properties. At issue is whether or not the PG is a *true* phase transition and whether or not it competes with superconductivity.

We investigated high purity $x = 0.67$ and $x = 0.95$ single crystals (with superconducting transition temperatures $T_c = 93.2(3)$ K and 67.9(1.2) K, respectively)

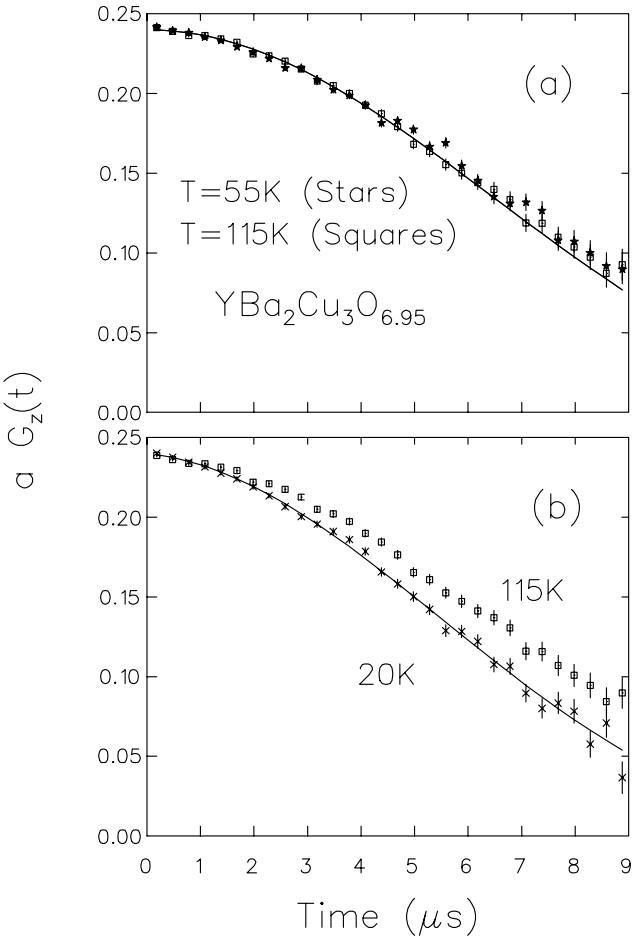

Fig. 85. The time evolution of the muon spin polarization in zero external field for $YBa_2Cu_3O_{6.95}$ crystals measured with the initial polarization $P_\mu(0)$ perpendicular to the c-axis. (a) Measurements taken above and below T_c at 115 K and 55 K, respectively. The solid curve is a fit to a Kubo-Toyabe (KT) function describing the depolarization of the muon spin by the nuclear dipoles. (b) Measurements taken above and below T_c at 115 K and 20 K, respectively. The solid curve through the 20 K data is a fit to the KT function multiplied by an exponential function $\exp(-\lambda t)$.

grown at the University of British Columbia. Our study revealed the presence of small spontaneous magnetic fields of electronic origin that appear to be related to the PG transition. Figure 85 shows the measured time evolution of the muon spin polarization in the $x = 0.95$ crystals for the case in which the initial spin polarization $P_\mu(0)$ is perpendicular to the c-axis. The relaxation observed in Fig. 85a is that due to the randomly oriented static magnetic fields of the nuclear dipoles. However, on cooling below 47 K there is a marked increase in the ZF relaxation rate (see Fig. 85b), signifying the occurrence of a small additional magnetic field at temperatures well below T_c. The additional signal relaxation was best described by an exponential function $\exp(-\lambda t)$ and was found to vanish in an applied magnetic field of 0.5 kOe. This suggests that the small magnetism originates from dilute moments of some kind which are static or fluctuating very slowly. The results of ZF measurements in the $x = 0.95$ sample for two different orientations of the initial muon spin polarization $P_\mu(0)$ are summarized in Fig. 86.

In the $x = 0.67$ sample the onset of small spontaneous magnetic fields occurred well above T_c at $\approx$170 K (see Fig. 87). This temperature is near the PG transition temperature T^* determined by other methods. Thus it appears that the small magnetic fields are intimately related to the PG phase, and that the PG coexists with superconductivity. Our findings are difficult to reconcile with current theories predicting the onset of a dense array of circulating currents at T^*.

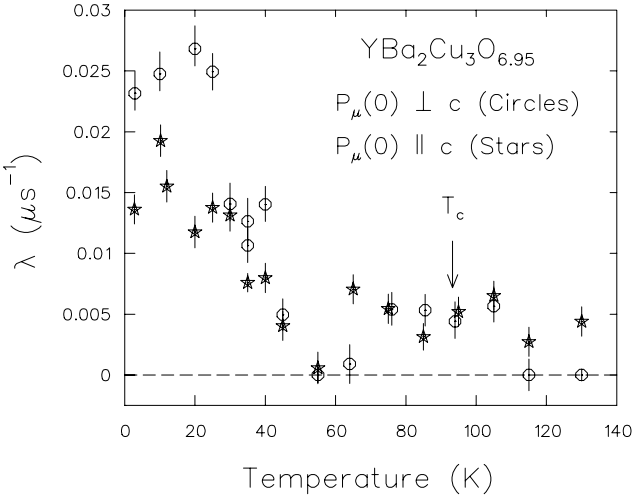

Fig. 86. The temperature dependence of the ZF exponential relaxation rate λ in $YBa_2Cu_3O_{6.95}$. Measurements were taken with the initial muon spin polarization $P_\mu(0)$ perpendicular (circles) and parallel (stars) to the c-axis of the crystals. The increase below $T \approx 47$ K signifies the onset of a small spontaneous magnetic field.

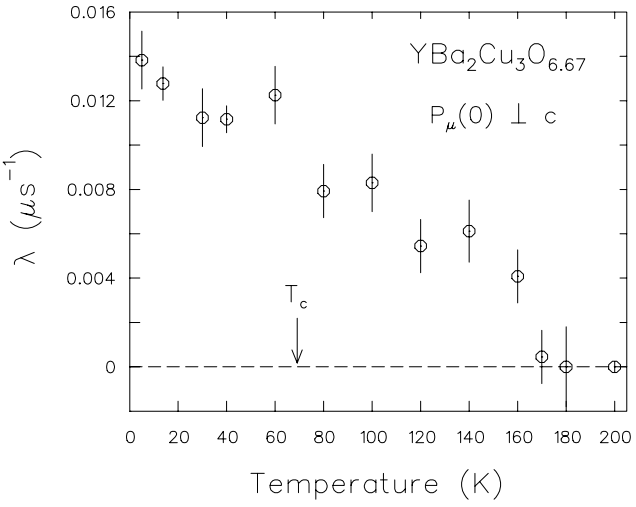

Fig. 87. The temperature dependence of the ZF exponential relaxation rate λ in $YBa_2Cu_3O_{6.67}$. Measurements were taken with the initial muon spin polarization $P_\mu(0)$ perpendicular to the c-axis of the crystals. The increase below $T \approx 170$ K signifies the onset of a small spontaneous magnetic field.

Experiment 847
Electron-doped high-T_c superconductors
(J.E. Sonier, SFU)

The identity of the pairing symmetry in the *electron-doped* high-T_c superconductors is an unsettled issue. Many of the early experiments suggested an s-wave pairing symmetry, differing from the established d-wave symmetry in *hole-doped* high-T_c superconductors. Experiment 847 was proposed to address this issue by performing *bulk* measurements of the magnetic penetration depth λ. Similar measurements in $YBa_2Cu_3O_{7-\delta}$ [Sonier *et al.*, Phys. Rev. Lett. **74**, 722 (1994); *ibid.* **79**, 2875 (1997)] contributed to the identification of the d-wave symmetry in the hole-doped materials.

In June we used the newly developed MULTI spectrometer to carry out μSR measurements on tiny crystals of $Pr_{2-x}Ce_xCuO_{4+\delta}$ grown at the University of Maryland. Because the muon counter of the MULTI spectrometer lies within the cryostat directly in front of the sample, the beam momentum could be reduced without increasing the background signal from muons stopping upstream in the cryostat window. This made it possible to measure crystals weighing as little as 3 mg. Figure 88 shows the fast Fourier transform of the muon spin precession signal in a small single crystal of $Pr_{2-x}Ce_xCuO_{4+\delta}$ at H = 200 Oe. This is the first time that the internal magnetic field distribution has been observed in this material. The ability to measure such small samples demonstrates the remarkable recent advancements in μSR spectrometer design.

Figure 89 shows the temperature dependence of the muon depolarization rate σ in $Pr_{2-x}Ce_xCuO_{4+\delta}$. It is

clear that there is a sizeable moment associated with the Pr^{3+} ion even at the lower temperatures, as evidenced by the increase of σ with decreasing temperature in the normal state. This means that crystal electric field (CEF) excitations are relevant over the temperature range of interest, since the CEF ground state of the Pr^{3+} ion is nonmagnetic. This information is important for the interpretation of experimental data obtained with other techniques. The onset of superconductivity is visible as a kink in the plot of Fig. 90, where σ is enhanced due to the broad internal field distribution associated with the formation of a vortex lattice.

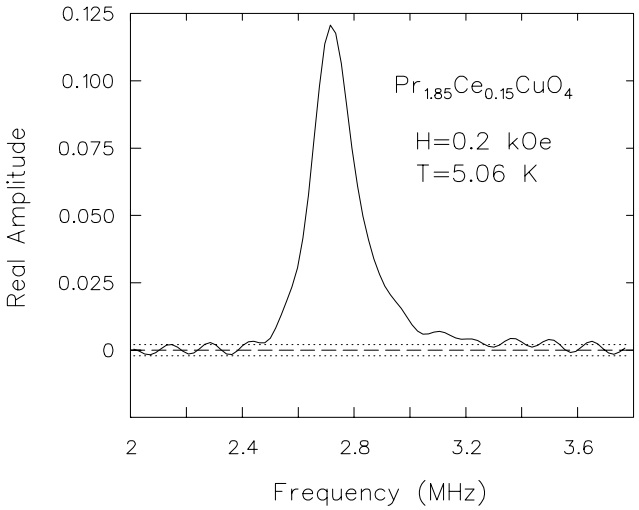

Fig. 88. The fast Fourier transform of the muon spin precession signal in $Pr_{2-x}Ce_xCuO_{4+\delta}$ after field cooling to $T = 5.06$ K in a magnetic field H = 200 Oe.

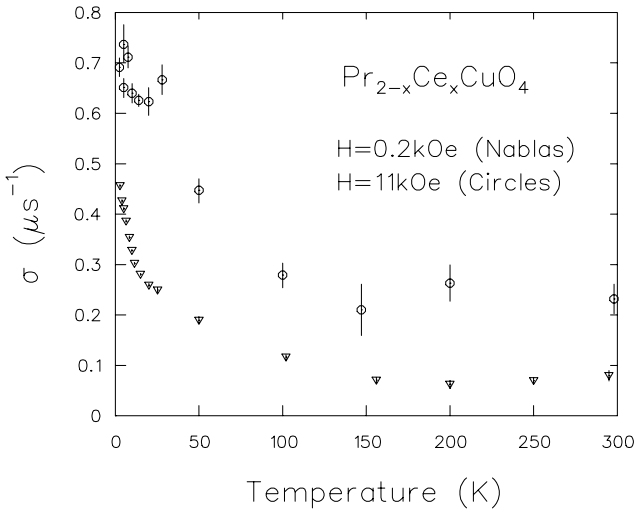

Fig. 89. Temperature dependence of the muon Gaussian depolarization rate σ in $Pr_{2-x}Ce_xCuO_{4+\delta}$ at H = 0.2 kOe and H = 11 kOe. The 0.2 kOe data were collected using the MULTI spectrometer, whereas the 11 kOe data were taken using the standard low-background insert.

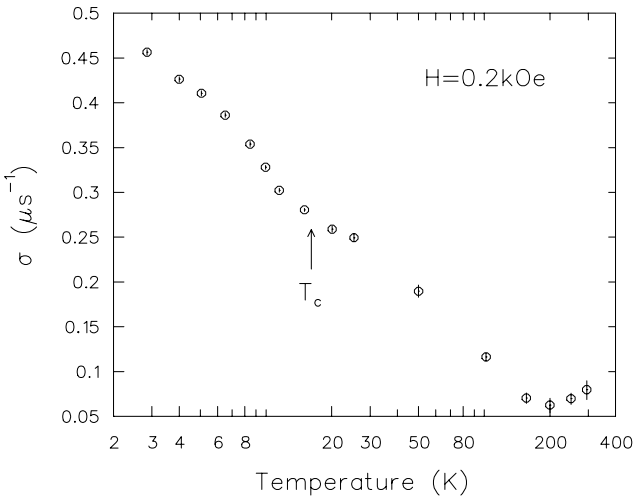

Fig. 90. Temperature dependence of the muon Gaussian depolarization rate σ.

The paramagnetism associated with the Pr^{3+} ions broadens the μSR line shape measured in the vortex state below the superconducting transition temperature T_c. In principle, this additional contribution to the linewidth can be separated from the field distribution associated with the vortex structure.

Experiment 849
Static magnetism in stage-4 $La_2CuO_{4.12}$ and $La_{1.88}Sr_{0.12}CuO_4$
(Y.J. Uemura, Columbia; K.M. Kojima, Tokyo)

The purpose of our experiment was to study superconducting samples of $La_2CuO_{4.12}$ and $La_{1.88}Sr_{0.12}CuO_4$. Single crystals were mounted in a He gas flow cryostat, which can attain temperatures down to 2 K. μSR measurements were performed for two different orientations of the crystal: with the muon beam (and muon polarization) parallel and perpendicular to the *c*-axis.

At high temperatures the spectra show a slow relaxation due to nuclear dipolar fields. Below 42 K for $La_2CuO_{4.12}$ and 20 K for $La_{1.88}Sr_{0.12}CuO_4$ the spectra exhibit a Bessel-like oscillation, characteristic of incommensurate spin-density-wave (SDW) ordering.

We found that the oscillation amplitude is significantly less than expected for the case where all incident muons reside at sites with spontaneous magnetic fields. This feature can be understood if static spin freezing occurs only in a part of the sample volume. Here we analyze our data assuming this situation, with V_M denoting the volume fraction with static spin freezing.

In order to find V_M, measurements are required for two different orientations of the crystals. The procedure and numerical values were published in Physica B [Savici *et al.*, Physica **B289-290**, 338 (2000)]. In the upper part of Fig. 91 we show the magnetic volume fraction for $La_2CuO_{4.12}$ and $La_{1.88}Sr_{0.12}CuO_4$ and we

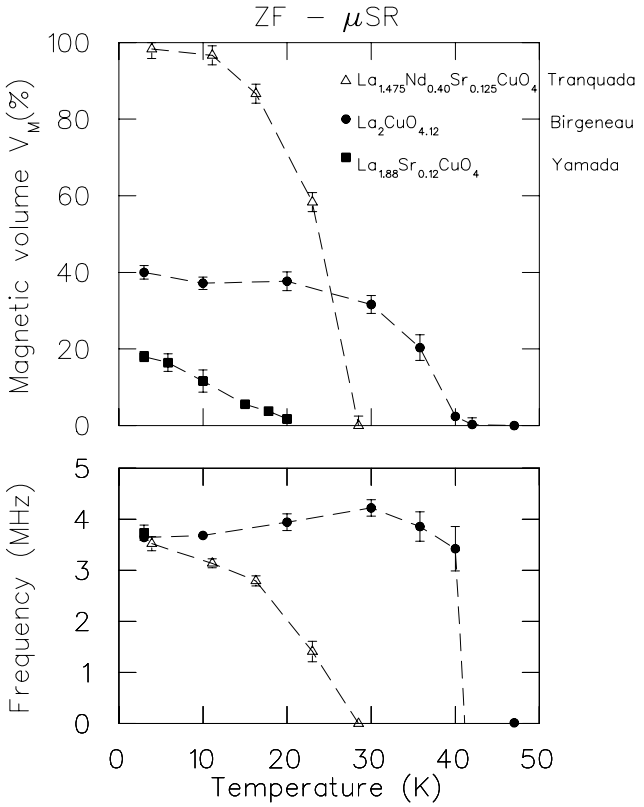

Fig. 91. Magnetic site fraction with static magnetic ordering and frequency of the precessing signal for $La_2CuO_{4.12}$, $La_{1.88}Sr_{0.12}CuO_4$ and $La_{1.475}Nd_{0.4}Sr_{0.125}CuO_4$.

compare them to $La_{1.475}Nd_{0.4}Sr_{0.125}CuO_4$ for which we have data from a previous measurement.

The lower part of Fig. 91 shows that the frequency of the oscillating signal for $La_2CuO_{4.12}$ increases very sharply below T_N and rapidly attains a constant value of 3.6 MHz. For $La_{1.88}Sr_{0.12}CuO_4$ we were able to determine this frequency only at very low temperature. This frequency is very close to that observed by μSR in $La_{1.475}Nd_{0.4}Sr_{0.125}CuO_4$ and many other "1/8" systems, indicating that the local spin structure of the frozen Cu moments is identical among these three specimens. The observed frequency corresponds to a modulated static Cu moment with a maximum amplitude of about 0.3–0.4 μ_B, as scaled from the 5 MHz μSR frequency in undoped La_2CuO_4, which has 0.5–0.6 μ_B per Cu.

Experiment 852
Magnetic phases in geometrically frustrated rare earth pyrochlores

(S. Dunsiger, R. Kiefl, UBC; J. Gardner, NRC)

In systems where magnetic ions occupy the vertices of edge or corner sharing triangular units, there is no spin configuration which simultaneously satifies all the magnetic couplings if all these interactions are *antiferromagnetic*. Stacked triangular, kagomé, fcc, and pyrochlore lattices are all examples of this *geometric* frustration. The purpose of Expt. 852 is to apply μSR to further our understanding of the effect of this frustration on the ground state and low lying magnetic excitations in the pyrochlores $A_2B_2O_7$, where magnetic ions form a network of corner sharing tetrahedra. Unlike many other systems having geometric frustration, pyrochlores are noted for their high degree of chemical order, which is important for isolating effects due to geometric frustration. Also, it is now possible to grow high quality single crystals of rare earth titanates such as $Tb_2Ti_2O_7$, $Gd_2Ti_2O_7$ and $Ho_2Ti_2O_7$.

A system of Heisenberg spins interacting via nearest-neighbour antiferromagnetic couplings on the pyrochlore lattice displays a classical ground state with macroscopic degeneracy, since the lowest energy spin configuration requires only that $\Sigma_{i=1}^{4}\mathbf{S}_i = 0$ for each tetrahedron. This feature led Villain to argue that these systems remain in a *cooperative paramagnetic* state with only short range spin-spin correlations for all $T > 0$ [Villain, Z. Physik **B33**, 31 (1979)] and this has been confirmed by Monte Carlo simulations [Reimers, Phys. Rev. **B45**, 7287 (1992)]. However, additional factors such as magnetic anisotropy, further nearest neighbour exchange and fluctuations [Bramwell *et al.*, J. Appl. Phys. **75**, 5523 (1994)] can lift the degeneracy and lead to Néel order involving complicated canted structures, as observed in $Nd_2Mo_2O_7$ [Greedan *et al.*, Phys. Rev. **B43**, 5682 (1991)] and possibly other more exotic ground states.

Oxide pyrochlores where the B site is occupied by a magnetic ion (typically a transition metal) often exhibit a type of ordering, with freezing temperatures in the range of 20–100 K. Muon spin relaxation has been important in identifying and characterizing the spin glass states in $Y_2Mo_2O_7$ and $Tb_2Mo_2O_7$ [Dunsiger *et al.*, Phys. Rev. **B54**, 9019 (1996)]. However, if magnetic ions are present on both the A and B sites it is more difficult to isolate the contributions from each species. The rare-earth (RE) titanate pyrochlores are interesting since the Ti^{4+} ion is nonmagnetic and thus there is only one magnetic species.

$Ho_2Ti_2O_7$: a spin ice

Water ice is made up of oxygen atoms which form a hexagonal lattice (Wurtzite structure). Of the 4 hydrogen atoms arranged tetrahedrally around each oxygen atom, two form strong covalent O−H bonds and are close to it to form a water molecule; the remaining two are hydrogen bonded and further removed. In a crystal of 2N bonds there are 2^{2N} possible ways of arranging the protons, not all of which satisfy these Bernal-Fowler ice rules [Pauling, *The Nature of the Chemical Bond* (Cornell Univ. Press, 1960) p.465]. Out of 2^4 =

16 ways of arranging the bonds around a single oxygen, only 6 satisfy this condition. The total number of allowed configurations is therefore of the order of $(6/16)^{\mathrm{N}}2^{2\mathrm{N}} = (3/2)^{\mathrm{N}}$. Experimentally, the associated residual entropy is found to be close to the theoretical value $S_0 = \mathrm{N}k_B \ln(3/2)$ at zero temperature. Although the H disorder can be represented as configurational entropy, there is no clear violation of the third law of thermodynamics. This is because energy barriers of the order of 1 eV would have to be surmounted to establish long range order in hydrogen ion position. As a result, relaxation through tunnelling into a lower entropy state is an extremely slow process below ice's freezing temperature and the system is therefore not in thermal equilibrium.

The hydrogen ion bonds between atoms form electric dipoles, so they can conveniently be represented by arrows placed on the bonds pointing towards the end occupied by the ion. The ice rule is then equivalent to saying that at each site there are two arrows in and two out, as shown in Fig. 92. Spin orientation thus plays a similar role to that of hydrogen position in ice and magnetic analogues of water ice, so called "spin ice", are currently of extreme interest [Ramirez *et al.*, Nature **399**, 333 (1999); Harris, Nature **399**, 311 (1999)]. Moessner [Phys. Rev. **B57**, R5587 (1998)] shows that a strongly anisotropic classical Heisenberg model on the pyrochlore lattice can be mapped onto an Ising pseudospin model with an exchange constant opposite in sign. In the case of strong anisotropy ($|\mathcal{J}/D| \ll 1$) the anisotropy term dominates, constraining the spins to lie along the $\langle 111 \rangle$ axes. The exchange term defines the direction in which they point, such that the enclosing angle between any pair may only take on values of 70.5° or 109.5°. Thus, counterintuitively, a system of spins situated on the vertices of corner sharing tetrahedra where the interactions are *ferromagnetic* may also be geometrically frustrated, provided the spins are constrained by anisotropy to point along the $\langle 111 \rangle$ axes.

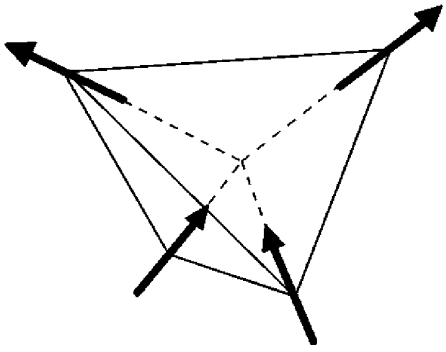

Fig. 92. Ground state configuration of spins on a single tetrahedron given ferromagnetic interactions and strong easy axis anisotropy along the dashed lines.

Experimentally, the magnetic ions in a number of pyrochlores have recently been found to be subject to significant single ion anisotropies, whose local easy axis is along the $\langle 111 \rangle$ directions and which are thus candidates for spin ice behaviour. To date, the most extensively studied spin ice material is $Ho_2Ti_2O_7$ [Harris *op. cit.*; Harris *et al.*, J. Magn. Magn. Mater. **177-181**, 757 (1998)]. The Ho^{3+} ion is Ising-like due to crystal field splittings which result in a ground state doublet with $J_z = \pm 8$ and the next excited state ~250 K higher [Siddharthan *et al.*, Phys. Rev. Lett. **83**, 854 (1999)]. This suggests that at low temperatures $Ho_2Ti_2O_7$ is well described as a quasi spin 1/2 Ising system. Neutron scattering measurements indicate that no long range order develops down to temperatures of at least 0.35 K in zero magnetic field, but instead, short range ferromagnetic correlations are observed [Harris *et al.*, J. Magn. Magn. Mater. *op. cit.*]. The idea which seems to be emerging is that there is no phase transition to a spin glass state, for example, but rather a continuous slowing down of spin fluctuations as the temperature is reduced, due to the development of energy barriers. A number of ordered phases have also been observed on application of a magnetic field, as well as history dependent behaviour. Monte Carlo simulations by Harris *et al.* [Phys. Rev. Lett. **81**, 4496 (1998)] show that the degree of degeneracy breaking depends on the direction of the applied field relative to the crystal axes and this has been confirmed by dc magnetization measurements (see Fig. 93).

Monte Carlo simulations have been able to describe the magnetic susceptibility and diffuse magnetic neutron scattering results well, but the nature of the spin

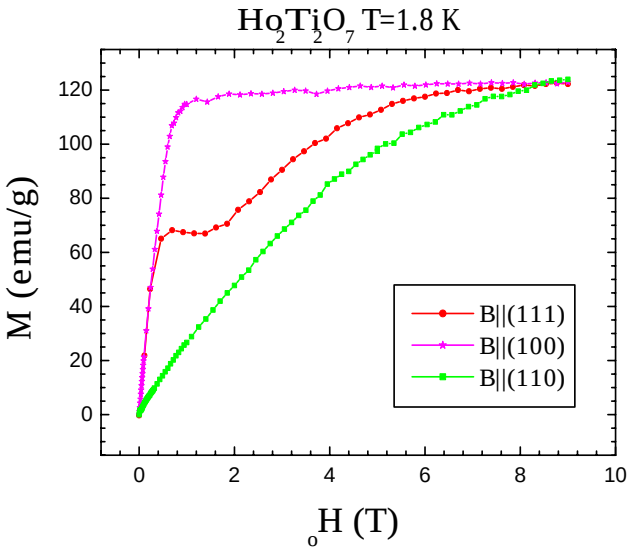

Fig. 93. DC magnetization as a function of applied magnetic field in $Ho_2Ti_2O_7$ [Cornelius, unpublished].

dynamics has only been very briefly studied in low field [Harris *et al.*, J. Magn. Magn. Mater. *op. cit.*]. In June and October we carried out a series of $1/T_1$ measurements on the $\langle 100 \rangle$ and $\langle 110 \rangle$ orientations of $Ho_2Ti_2O_7$ in the dilution refrigerator on M15. In a low longitudinal field (LF) of 0.003 T the μ^+ spin depolarized too quickly to be observed. This is attributed to rapid Ho^{3+} spin fluctuations in the paramagnetic regime.

$Ho_2Ti_2O_7$ ($H \parallel \langle 100 \rangle$)

Typical spectra at a higher field of 2 T are shown in Fig. 94. In this case a component of *all* the Ho spins lies along the applied field direction, since they point along the $\langle 111 \rangle$ directions. As shown in Fig. 95, the

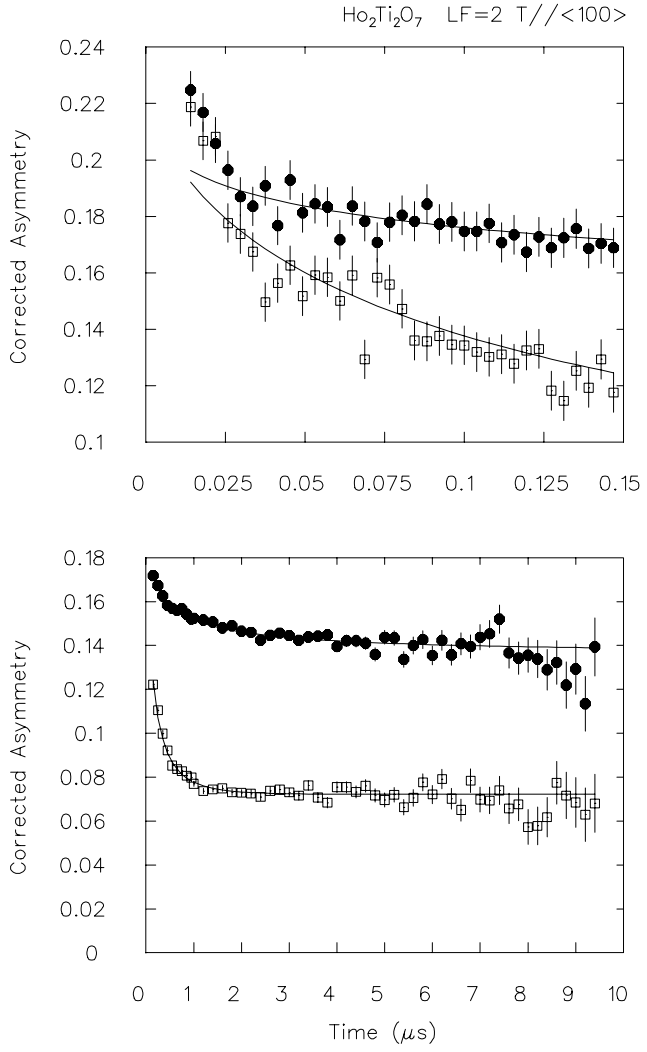

Fig. 94. Typical spectra in $Ho_2Ti_2O_7$ in a longitudinal field of 2 T applied along the $\langle 100 \rangle$ direction.

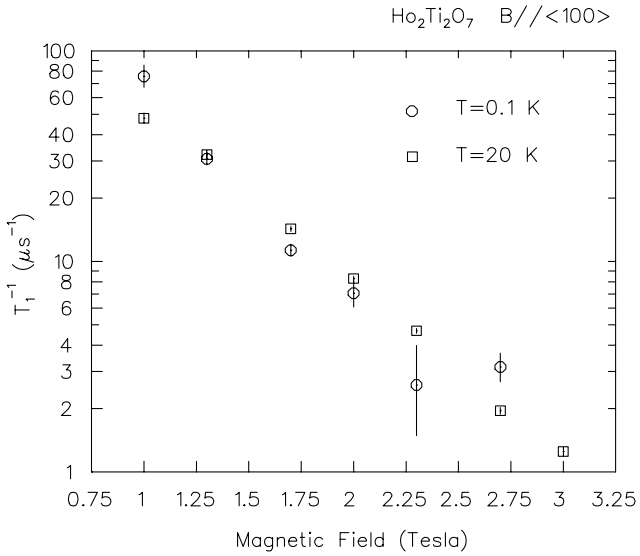

Fig. 95. Relaxation rate of muon spin polarization in $Ho_2Ti_2O_7$ as a function of applied magnetic field (along the $\langle 100 \rangle$ direction).

relaxation rate $1/T_1$ decreases with increasing field at 20 K. The decrease is likely because the spin dynamics are being altered as the electronic Zeeman splitting first becomes comparable with and then exceeds the exchange coupling $\mathcal{J}$. Extrapolating back to zero field, $1/T_1$ is in excess of 100 μs^{-1}. In low longitudinal field experiments in the "motionally narrowed" limit of rapid spin fluctuations

$$1/T_1 = \frac{2\Delta^2}{\nu},$$

where $\Delta^2/\gamma_\mu^2 = \langle B_i^2 \rangle$ is the second moment of the internal magnetic field B_i ($i = x, y, z$), ν is the mean fluctuation rate for fluctuations in B_i, and γ_μ is the muon gyromagnetic ratio. The spin fluctuation rate can thus be roughly estimated at ∼10 GHz, assuming $\Delta/\gamma_\mu = 0.70(6)$ T from studies* of the isostructural compound $Tb_2Mo_2O_7$ [Dunsiger *et al., op. cit.*], since the free Ho^{3+} and Tb^{3+} ions have comparable magnetic moments of 10.4 and 9.5 μ_B respectively. This is below the timescales accessible by neutron scattering; hence μSR is uniquely sensitive to the spin dynamics in these spin ice materials, which have not previously been studied.

The results of temperature scans in longitudinal fields of 2 and 3 T are summarized in Figs. 96 and 97. Above 5 K the data are well described by a stretched exponential function. The muon spin relaxation rate decreases with temperature as $\mu_B H/k_B T$ grows and the sample becomes increasingly magnetized. However,

* In $Tb_2Mo_2O_7$ one can measure the magnitude of H_i directly since spin freezing is observed.

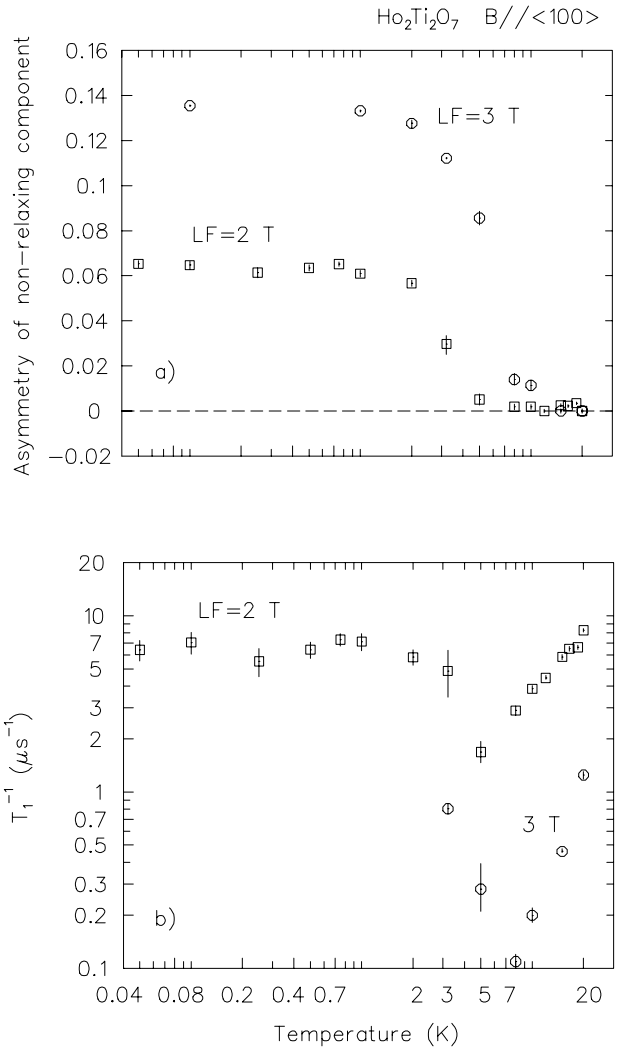

Fig. 96. a) Asymmetry of non-relaxing component and b) relaxation rate of muon spin polarization in $Ho_2Ti_2O_7$ as a function of temperature.

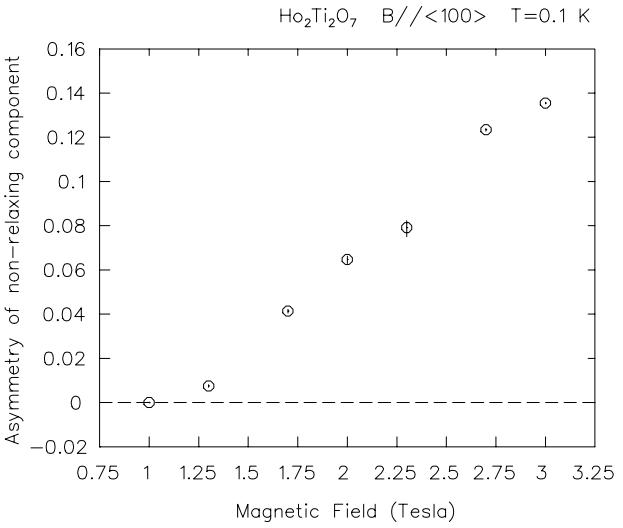

Fig. 97. Asymmetry of non-relaxing component as a function of magnetic field in $Ho_2Ti_2O_7$ at 0.1 K.

below 5 K a non-relaxing component develops at the expense of the amplitude of the relaxing component, such that almost the full amplitude of ∼0.16 is non-relaxing at 3 T. The decoupling curve shown in Fig. 97 suggests that a static component of the order of 1 T develops. The residual relaxing component is thought to be *dynamic* in nature. If the muon spin depolarization were due to a static internal field Δ of the order of 1 T, it would take place on a time scale of $\Delta^{-1} \approx 1$ ns, too fast to be observed. It is, however, difficult to understand such two component behaviour in a system of dense spins on crystallographically equivalent sites.

To better understand the non-relaxing component, a few preliminary transverse field (TF) measurements have been made very recently. The Curie-like dependence of the muon spin precession frequency above 100 K is anticipated in the paramagnetic state (see Fig. 98). However, the signal oscillating at ∼160 MHz shown in Fig. 99 is indicative of internal magnetic fields of roughly 1 T, which are static at least on the timescale of 10 ns. The size of the static internal field is consistent with the LF scans. However, the signal persists at 5 K, in contrast with the development of the non-relaxing component in the LF measurements. This may be due to hysteresis effects.

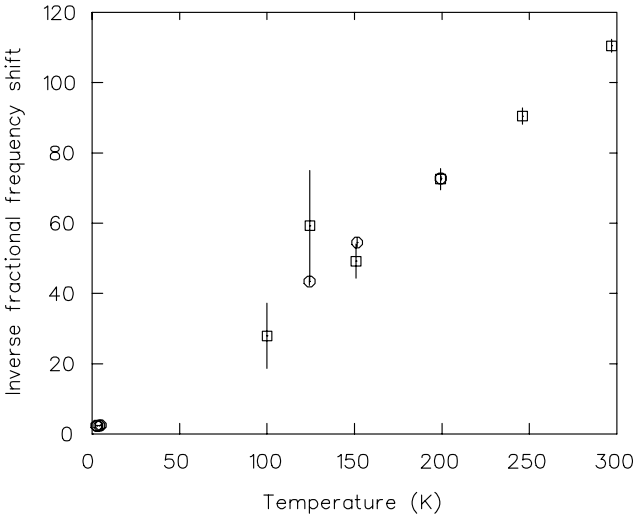

Fig. 98. Inverse paramagnetic frequency shift of the muon spin precession in $Ho_2Ti_2O_7$ in 0.099 and 2 T ($H \parallel \langle 100 \rangle$).

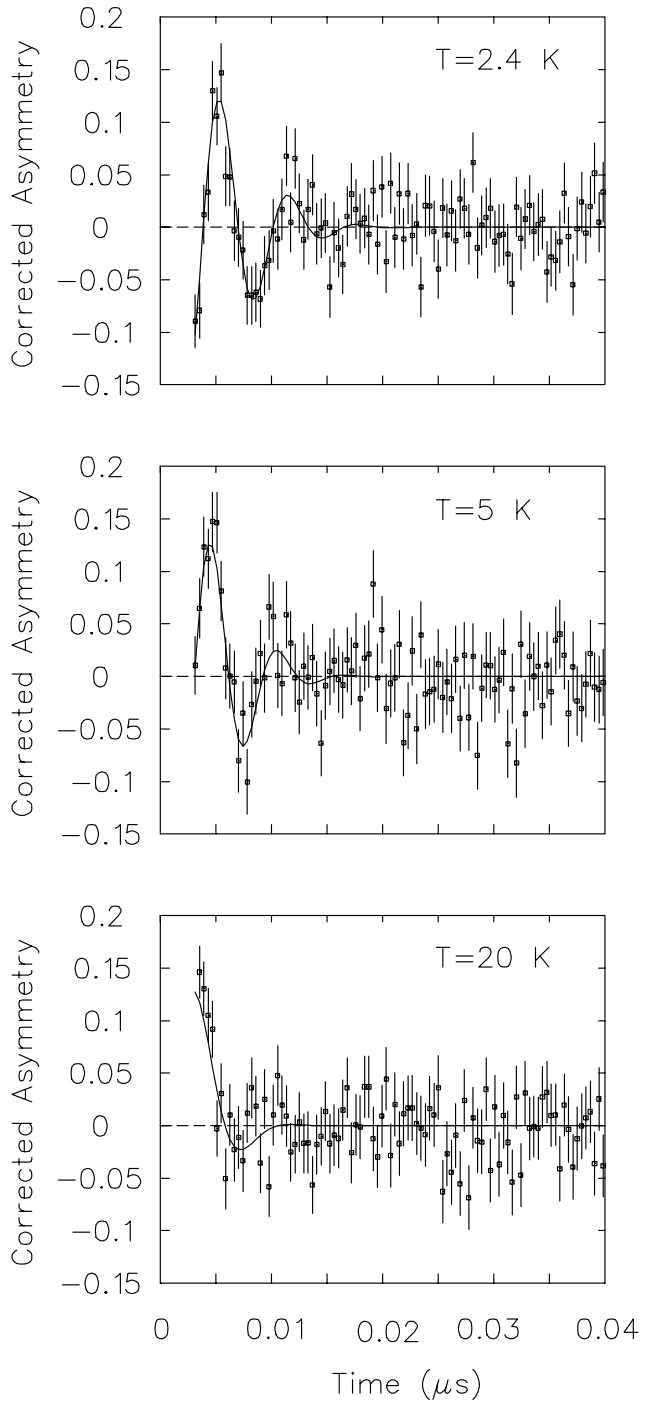

Fig. 99. Typical spectra in $Ho_2Ti_2O_7$ in a TF = 2 T ($H \parallel \langle 100 \rangle$).

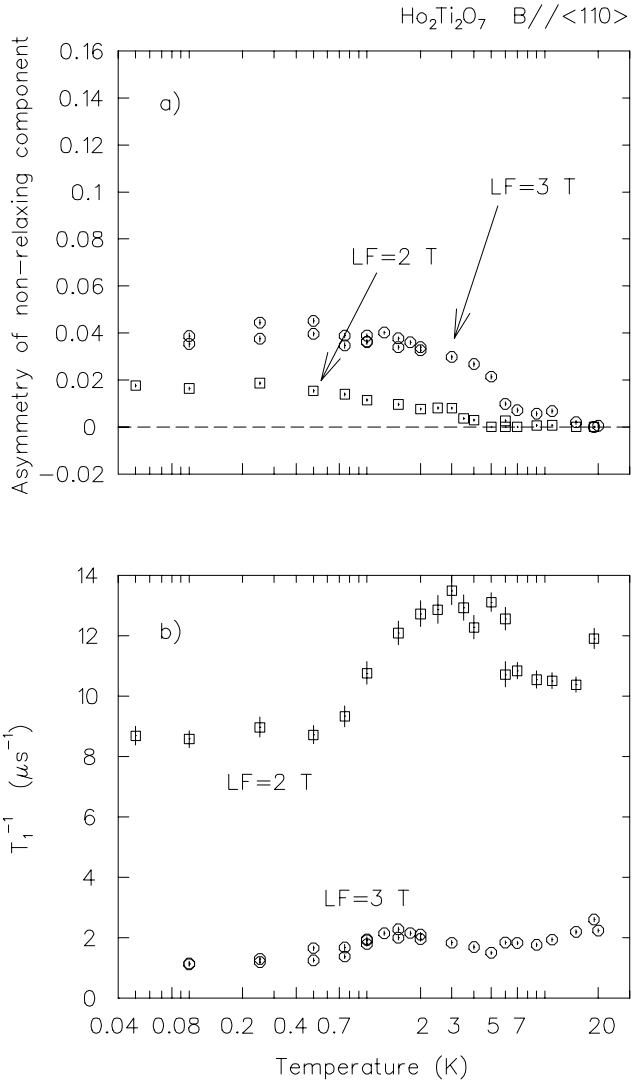

Fig. 100. a) Asymmetry of non-relaxing component and b) relaxation rate of muon spin polarization in $Ho_2Ti_2O_7$ as a function of temperature.

$Ho_2Ti_2O_7$ ($H \parallel \langle 110 \rangle$)

In this case half of the Ho spins lie perpendicular to the applied field and are thus unaffected by it. As shown in Figs. 100 and 101, the amplitude of the non-relaxing component is smaller in this orientation. The broad peak in $1/T_1$ observed at ∼1.5 K may be associated with the $\mathbf{q} = X$ ordered phase seen by inelastic neutron scattering [Harris *et al.*, Phys. Rev. Lett. *op. cit.*]. Once again, significant dynamics persist within the spin ice regime; an unexpected result.

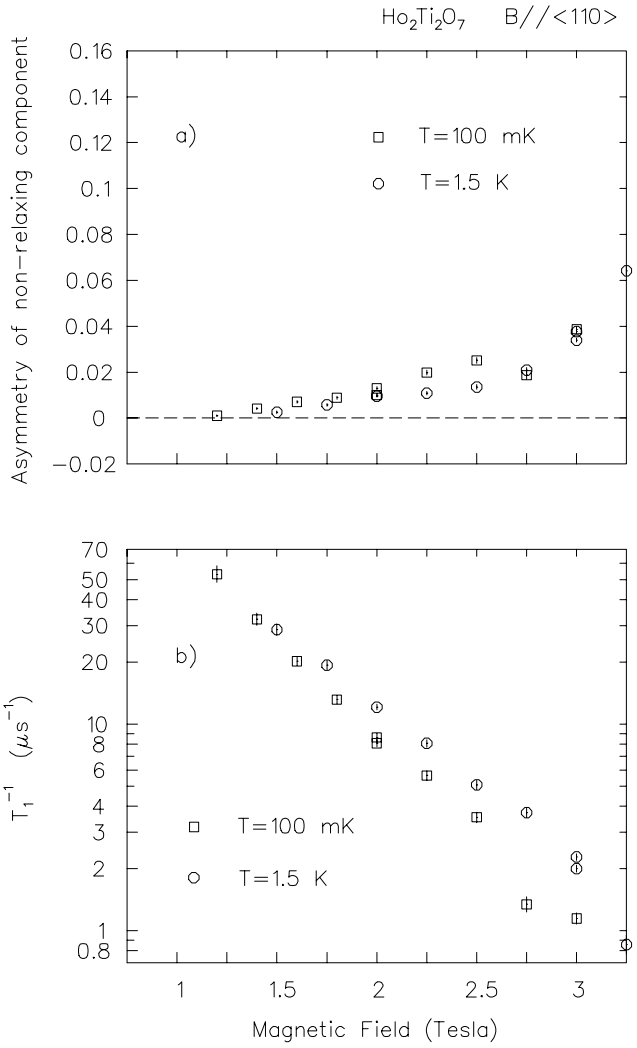

Fig. 101. a) Asymmetry of non-relaxing component and b) relaxation rate of muon spin polarization in $Ho_2Ti_2O_7$ as a function of applied magnetic field.

Experiment 860
Mass and charge transport in disordered media: orientational glasses
(J.H. Brewer, UBC; V.G. Storchak, Kurchatov Inst.)

Electron localization by orientational disorder in solid N_2-Ar mixtures

Electron transport in metals is known to be strongly affected by disorder, a dramatic example being "Anderson localization" where sufficiently strong disorder causes spatial localization of electron states near the Fermi level and thus drives the Anderson transition to an insulating state. However, the electron-electron interactions in metals dramatically modify the density of states at the Fermi level, leading to formation of the Coulomb pseudogap. To observe the effects of disorder on electron transport without the complications of electron-electron interactions, one must therefore study electron dynamics in a disordered insulating host.

A special class of solids formed by random mixtures of molecular and atomic species offers a unique opportunity for such studies. Pure molecular crystals like solid N_2 or CH_4 undergo an order-disorder phase transition from the "plastic crystal" high temperature phase (where the multipole moments associated with the molecules can rotate more or less freely) to a low temperature phase with long-range orientational order. This order is severely frustrated by the random substitution of spherical atoms or molecules (e.g. Ar in N_2, Kr in CH_4 or para-H_2 in ortho-H_2 etc.); strong enough dilution generally leads to a new type of phase called an orientational glass in which the multipole moments are "frozen" in random directions [Hochli, Knorr and Loidl, Adv. Phys. **39**, 405 (1990)]. One of the best studied orientational glass systems is the N_2-Ar mixture. Pure N_2 has two low-pressure crystalline forms, the low temperature orientationally ordered *fcc* α phase for $T < T_{\alpha\beta} = 35.6$ K and the high temperature orientationally disordered *hcp* β phase for $T > T_{\alpha\beta}$. Since N_2 and Ar are completely miscible, solid $(N_2)_{1-x}Ar_x$ is obtained by simply cooling liquid mixtures. The *hcp* sites are randomly occupied by N_2 and Ar. As the Ar concentration x is increased, $T_{\alpha\beta}$ decreases until for $x > x_c \approx 0.23$ the *hcp* lattice is stable to $T = 0$. The dynamical orientational disorder of the high-T phase eventually freezes into a static pattern of randomly oriented N_2 molecules, the orientational glass [Hamida, Genio and Sullivan, J. Low Temp. Phys. **103**, 49 (1996)]. One can gradually change the local order parameter and even switch the disorder on and off by changing the temperature and/or Ar concentration. These features make N_2-Ar mixtures very convenient systems for studying the effect of disorder on electron transport, especially since the orientational degrees of freedom are strongly coupled to lattice displacements: reorientation of a multipole moment involves changes of atomic coordinates. Because of this coupling, orientational glasses exhibit transport properties analogous to those of translational glasses like amorphous SiO_2.

Being a mixture of insulators, the N_2-Ar system has a very large energy gap (∼10 eV), so that even at high temperature the ambient density of free electronic states is exponentially low. Experimental study of electron transport in this system therefore requires that the empty conduction band be "injected" with free carriers, ideally in low enough concentrations that electron-electron interactions can be safely ignored. The ionization of molecules and/or atoms by high energy charged particles (e.g. positive muons) offers just such a source of free carriers.

Recent μ^+SR experiments [Storchak *et al.*, Phys. Lett. **A193**, 199 (1994); Phys. Rev. Lett. **72**, 3056 (1994); Phys. Rev. Lett. **75**, 2384 (1995); Phys. Rev. Lett. **76**, 2969 (1996); Phys. Rev. Lett. **78**, 2835 (1997); Appl. Mag. Reson. **13**, 15 (1997); Rev. Mod. Phys. **70**, 929 (1998); Phys. Rev. **B59**, 10559 (1999); Eshchenko, Storchak and Morris, Phys. Lett. **A264**, 226 (1999)] in liquid and solid nitrogen as well as liquid and solid neon and argon [see also 1997 TRIUMF Annual Report, Expt. 775] have shown that the spatial distribution of these ionization-track products is highly anisotropic with respect to the final position of the muon: the μ^+ generally thermalizes well "downstream" from the last ionization event where an excess electron was generated, and that electron is often mobile enough to reach the thermalized muon and form muonium. This phenomenon of delayed muonium formation (DMF) is very sensitive to the electron mobility – a free electron in the conduction band will quickly reach the μ^+, whereas an electron that undergoes localization to become a polaron will arrive much later, if at all. (Typical mobilities in insulators range from about $10^2 - 10^3$ cm^2/V.s for delocalized electrons, to about $10^{-3} - 10^{-2}$ cm^2/V.s for localized electrons.) Thus DMF forms the basis of a new technique for measurements of the electron mobility b_e in insulators and semiconductors on a microscopic scale: b_e can be estimated whenever one can measure both the characteristic time for Mu atom formation τ and the characteristic distance between the stopped muon and its last radiolysis electron R. The former is determined from the magnetic field dependence of the muonium signal amplitude and phase, using the coherence criterion for Mu formation. The latter is extracted from the dependence of the muonium formation probability on applied electric field – basically, a sufficiently high applied electric field will overcome the Coulomb attraction between the muon and electron. The characteristic distances involved are typically on the order of 10–100 nm; the characteristic times are less than 10^{-10} s for delocalized electrons and range to microseconds for localized electrons. In the simplest case of viscous motion the parameters obey $\tau = R^3\epsilon/3eb_e$, where e is the electron charge and ϵ is the dielectric constant of the medium.

The potential of the μ^+SR-DMF technique for electron mobility measurements in solids was first demonstrated for pure solid nitrogen. Excess electrons were found to be delocalized in α-N_2, which shows a long-range orientational order. We have now found evidence for strong electron localization due to orientational disorder induced by Ar impurities in the low temperature orientational glass phase of solid nitrogen-argon mixtures, which may serve as model systems for studying electron localization in the absence of electron-electron interactions, and thus shed light on electronic transport in less exotic insulators and semiconductors.

The experiments were performed on the M20 beam line at TRIUMF and on the EMU beam line of the ISIS Pulsed Muon Facility at the Rutherford Appleton Laboratory. In each experiment, mixtures of ultra high purity N_2 and Ar (less than 10^{-5} impurity content) were condensed from the gas phase into a liquid. At ISIS the sample cells were 25 mm in diameter and 5 mm thick; at TRIUMF, they were 18 mm in diameter and 4 mm thick. Solid samples were carefully grown from the liquid phase at a typical speed of about 5 mm/hr under a vertical temperature gradient of about 2 K across the cell. At both laboratories, positive muons of 28 MeV/c momentum and 100% spin polarization were stopped in the samples and μ^+SR time spectra were recorded at various temperatures and applied magnetic and electric fields. The muon decay asymmetry time spectrum $A(t)$ directly reveals the time-dependent amplitudes of the characteristic precession signals of paramagnetic (Mu) and diamagnetic (μ_D) species, both of which are present in all $(N_2)_{1-x}Ar_x$ mixtures studied.

The μ_D signal sometimes exhibits two components: one which is slowly damped due to random local fields from ^{14}N nuclear moments, and one which disappears much faster due to very delayed Mu formation. The latter is only observed in cases where the electrons form polarons which are still mobile enough to reach the μ^+ on a μs timescale. The general form of the μ^+SR asymmetry spectrum is therefore

$$\begin{aligned} A(t) &= A_{\rm Mu} e^{-\lambda_{\rm Mu} t} \cos(\omega_{\rm Mu} t + \phi_{\rm Mu}) \\ &+ A_{\rm S} e^{-\lambda_{\rm S} t} \cos(\omega_\mu t + \phi_{\rm D}) \\ &+ A_{\rm F} e^{-\lambda_{\rm F} t} \cos(\omega_\mu t + \phi_{\rm D}), \end{aligned}$$

where $A_{\rm Mu}$, $\phi_{\rm Mu}$ and $\lambda_{\rm Mu}$ are the amplitude, initial phase and relaxation rate for the muonium signal and the corresponding quantities with S and F subscripts parameterize the "slow" and "fast" decaying μ_D signals, which have a common initial phase $\phi_{\rm D}$. The sum $A_D = A_{\rm S} + A_{\rm F}$ defines the net diamagnetic asymmetry. Muonium relaxation is caused by its nuclear hyperfine interactions.

Figure 102 depicts the temperature dependences of the asymmetries (amplitudes) of the various signals in solid $(N_2)_{1-x}Ar_x$ for $x = 0$, 0.09, 0.16 and 0.25. At high temperature (above about 40 K), all the mixtures have roughly the same Mu and μ_D asymmetries as pure N_2. At low temperatures, however, adding argon causes dramatic changes. In pure N_2 below about 30 K there is a large Mu signal and a small μ_D signal, indicating efficient DMF; as Ar is added there is a progressively larger μ_D signal, indicating reduced DMF,

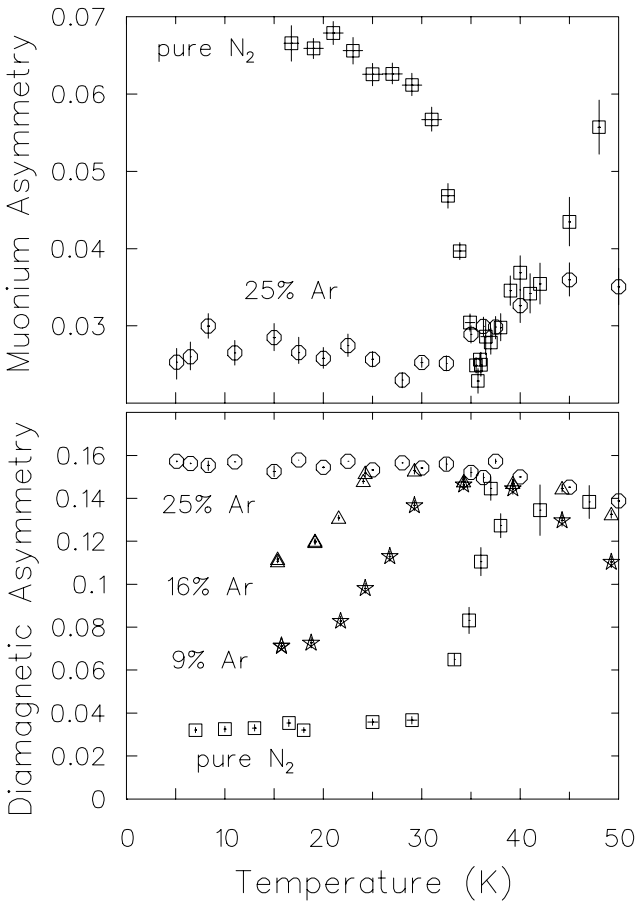

Fig. 102. Temperature dependences of muonium (top, $H \approx 5$ G) and net diamagnetic (bottom, $H \approx 100$ G) signal amplitudes in pure solid nitrogen (squares) and solid $(N_2)_{1-x}Ar_x$ (circles: $x = 0.25$; triangles: $x = 0.16$; stars: $x = 0.09$).

until at $x = 0.25$ there is only a small Mu signal. The increase in Mu amplitude is only half the corresponding decrease in μ_D amplitude because half the Mu polarization oscillates at the muonium hyperfine frequency and appears depolarized. Full asymmetry is about 0.19 in these experiments.

In solid N_2, we have shown that muonium formation proceeds via two channels: the thermal DMF process outlined above and the epithermal prompt process which takes place prior to the μ^+ thermalization and is therefore independent of temperature, electron mobility, etc. The small, temperature independent Mu amplitude in the $x = 0.25$ sample (see Fig. 102) is the same as the prompt Mu amplitude in pure solid nitrogen, suggesting a complete absence of DMF in the orientational glass.

The hypothesis that Mu formation in the $x = 0.25$ mixture is essentially all via the prompt (epithermal) channel at 20 K is further supported by the observation that $A_{\rm Mu}$ and A_D do not depend on an externally

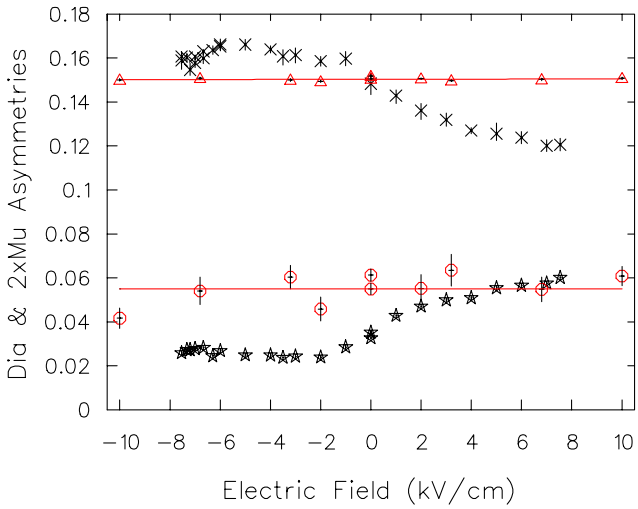

Fig. 103. Electric field dependences of $2 \times A_{\rm Mu}$ and A_D in pure solid nitrogen (crosses and stars, respectively) and in solid 75% N_2 + 25% Ar (circles and triangles, respectively) in a transverse magnetic field $H = 36$ G at $T = 20$ K. The muonium amplitudes are doubled to compensate for the 50% depolarization of Mu by hyperfine oscillations.

applied electric field for that sample, as shown in Fig. 103. Both amplitudes show significant electric field dependence in pure N_2 at 20 K, from which the characteristic muon-electron distance R is estimated to be about 50 nm; about the same value of R is found in solid Ar, which exhibits almost 100% DMF. The fact that solid N_2 and solid Ar have similar values of R is not at all surprising, since N_2 molecules and Ar atoms have about the same size and about the same ionization potential [see *Cryocrystals*, Verkin and Prikhotko, eds. (Naukova Dumka, Kiev, 1983)] and therefore about the same cross section for muon (or Mu atom) scattering. It is therefore natural to expect that R is about the same in mixtures as in the pure substances. The absence of DMF at this length scale at low temperature in the $x = 0.25$ mixture suggests that electrons are localized in this orientational glass.

One might suspect that it is the difference between lattice sites randomly occupied by N_2 molecules and Ar atoms which acts as a localizing influence, for example by simple scattering (or even trapping) of initially delocalized electrons by Ar impurities. However, Fig. 102 shows that mixtures without sufficient Ar concentrations to destroy orientational order at low temperature still exhibit efficient DMF; this process requires delocalized electrons. Scattering of these electrons by Ar impurities is unlikely to depend qualitatively on whether the 12 nearest neighbours of a typical lattice site include 1 Ar atom ($x = 0.09$), 2 Ar atoms ($x = 0.16$) or 3 Ar atoms ($x = 0.25$). Evidently the electrons are localized only by an Ar concentration of 0.25 or greater – i.e. in the glassy phase.

Experiment 876
Disordered magnetism near magnetic instabilities in *f*-electron materials
(D.R. Noakes, Virginia State)

This is an experiment to measure ZF and LF-μSR in three types of f-moment material: UPdSn, $U_{1-x}Y_xCoAl$, and $PrAu_2(Si_{1-x}Ge_x)_2$. In the first week of beam in October, powder samples of UPdSn, $PrAu_2Si_2$, $PrAu_2Ge_2$, and $PrAu_2(Si_{0.8}Ge_{0.2})_2$ were measured at M20.

Study of UPdSn extends μSR work by members of this collaboration on CeTSn materials (T = Ni, Cu, Pd, Pt) to a uranium 1:1:1 analogue. Among the 1:1:1's, the uranium moments in UPdSn seem more stable than usual, entering a long-range ordered magnetic state at a relatively high 37 K. A second transition at 25 K, however, has been interpreted as due to ordering of a component of the uranium moment left disordered in the 37 K ordering. We want to use μSR to directly probe for this disordered component within the ordered state, which so far has been deduced only indirectly.

$PrAu_2Si_2$ is a spin glass that provides a foil for URh_2Ge_2, the latter a heavy fermion system previously thought to be the only stoichiometric spin glass among the large number of known 1:2:2 materials. We want to measure the spin dynamics above $T_g \simeq 3$ K, and the development of the frozen state below this. Further, we proposed to measure μSR in $PrAu_2Ge_2$ and $PrAu_2(Si_{0.8}Ge_{0.2})_2$, to determine whether the spin glass state for $x < 0.2$ in $PrAu_2(Si_{1-x}Ge_x)_2$ can be related to the antiferromagnetic state for $x \geq 0.2$.

UPdSn

This radioactive powder was immobilized in stycast plastic. From 70 K down to 50 K in ZF, there is slow exponential relaxation, with rate increasing slightly as temperature decreases. At 45 K and 42 K, a fast-relaxing signal develops in the early bins and, at 40 K, a spontaneous oscillation frequency near 12.5 MHz is resolved. While the Néel temperature is usually placed between 35 K and 40 K (sample and probe dependent), in all neutron scattering reports [Robinson *et al.*, Phys. Rev. **B45**, 2939 (1992); J. Appl. Phys. **75**, 6589 (1994)] magnetic Bragg peaks, apparently resolution limited, are always reported up to about 43 K. The transition temperature for the neutron experiments has been interpreted as the point of maximum slope on a plot of intensity versus temperature, where the curvature switches from concave-up to concave-down (Brillouin-like). The non-Brillouin-like behaviour immediately below 43 K is reasonably interpreted as inhomogeneous freezing, not critical behaviour. Supporting this, the slow-relaxing asymmetry in our measurements starts dropping as the temperature falls below 45 K, and the oscillating signal asymmetry rises below 40 K, stabilizing at 35 K and below. The relaxation rate of the oscillating signal decreases with temperature. Between 26 K and 22 K, a two-frequency pattern is observed, with a higher frequency signal increasing in amplitude at the expense of the lower-frequency signal of higher temperatures. An example spectrum is shown in Fig. 104.

Below 22 K, only the higher-frequency signal is seen. Thus we see an ≈4 K range of inhomogeneous reordering. The temperature dependence of the observed frequencies is shown in Fig. 105.

Normally, the spontaneous oscillation frequency is proportional to the magnetic order parameter (sublattice magnetization), and so it would normally decrease as the temperature is raised toward the ordering temperature. In Fig. 105, the higher frequency

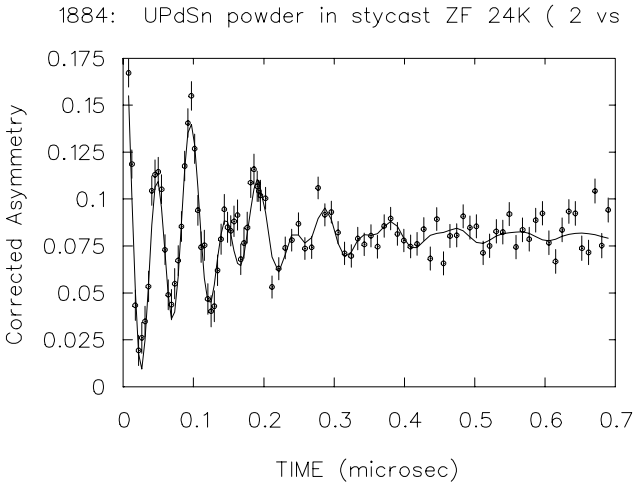

Fig. 104. ZF-μSR asymmetry spectrum of UPdSn at 24.0 K. The solid line shows a least-squares fit of a two-frequency model.

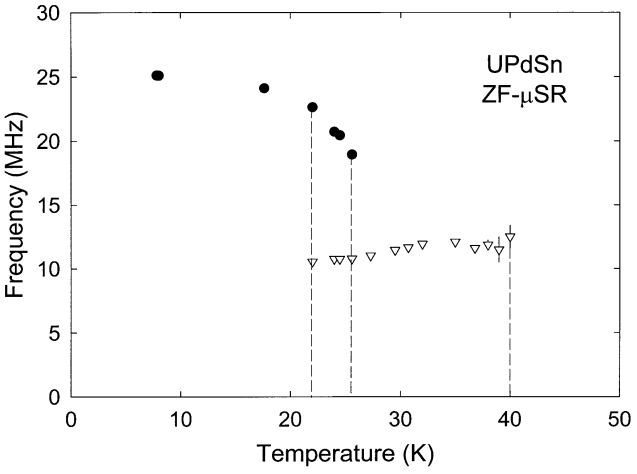

Fig. 105. Temperature dependence of the spontaneous oscillation frequencies observed in ZF-μSR of UPdSn. The dashed lines indicate 22 K, 25.6 K and 40 K.

corresponding to the lower-temperature ordered state conforms to this expectation, but it is clear that, in the higher-temperature ordered state, the frequency increases slightly with temperature. Neutron scattering results [Robinson *et al.*, J. Magn. & Magn. Mater. **128**, 143 (1993)] indicate that the ordering is complicated, with a non-collinear spin structure and a structural distortion at each transition, and that leaves scope for such μSR behaviour to occur.

In the paramagnetic state, UPdSn is hexagonal, as is CeCuSn (the other CeTSn materials we have studied are orthorhombic). It is interesting that our μSR studies of CeCuSn (Expt. 797) revealed similar behaviour in its "long-range ordered" signal [see Fig. 4 of Kalvius *et al.*, Physica **B289-290**, 252 (2000)], as shown in Fig. 106.

Less is understood about the magnetism of CeCuSn than UPdSn (no neutron scattering results have been published, for example), and there are substantial differences in their μSR behaviour. In CeCuSn, part of the sample volume enters a short-range ordered or spin-glassy state (this may be generating a higher-frequency oscillation, but the relaxation rate is so large that it is hard to be sure), associated with a heat capacity peak at 8.5 K. Then, at 7.4 K, the rest of the sample volume enters the long-range ordered state generating the frequency shown in Fig. 106, but the magnetism remains inhomogeneous to the low-temperature limit of our apparatus at the time, 2.0 K. The similarity of Fig. 106 and the lower frequency in Fig. 105 suggests that the long-range ordered fraction of CeCuSn has the same sort of spin structure as UPdSn.

$PrAu_2Ge_2$

We begin with this material because its behaviour is the most straightforward among our samples in this alloy series. In the paramagnetic state, ZF-μSR spectra showed monotonic relaxation. The 30 G TF relaxation rate is proportional to $1/T$ from the highest temperature we measured (230 K) down to at least 14 K. Extending over such a wide temperature range, and not obviously diverging at the transition temperature, this is likely to be due, at least in part, to crystalline electric field (CEF) effects [Noakes *et al.*, Phys. Rev. **B35**, 6597 (1987)] at the Pr site. Between 12.4 K and 12 K, ZF coherent oscillation sets in. Figure 107 shows the temperature dependence of the frequency, which is much more of the expected form for simple spin ordering below a second-order transition.

There is also a monotonic relaxation signal that persists below 10 K. At all temperatures, the best fits to the monotonic relaxation did not have simple exponential but power-exponential relaxation

$$G_z(t) = \exp\left[-(rt)^p\right].$$

In the paramagnetic state, the power p is roughly constant between 0.8 and 0.9. As the temperature drops below 12 K, the monotonic signal's rate rises in a manner similar to that of the frequency shown in Fig. 107, towards apparent saturation near 5 μs^{-1}, and p drops to 0.5. Temperature-dependent power less than one in the equation is generally associated with dynamic, disordered, dense magnetic moments, but there is little detailed understanding. The monotonic signal below 12 K is of approximately the same amplitude as the oscillating signal, and so is too large to be just the "1/3 tail" of the ZF spontaneous oscillation. It will require considerable careful analysis to separate the extra signal from the "1/3 tail", which must be there, decide whether the extra signal is within the same volume as the oscillating signal or represents macroscopic inhomogeneity, and decide whether it indicates substantial moment dynamics far below the ordering temperature.

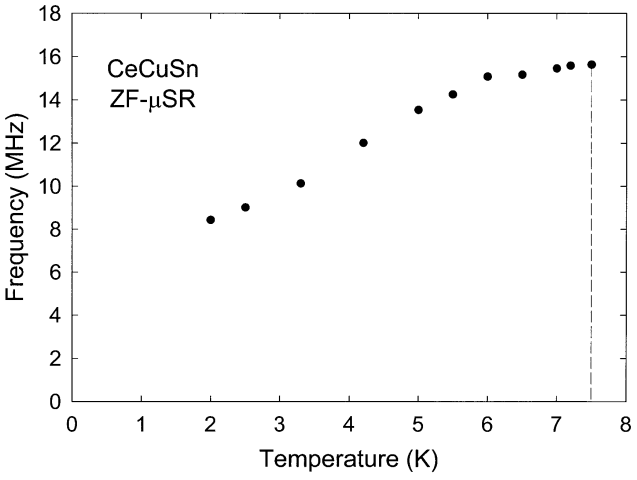

Fig. 106. Temperature dependence of the spontaneous oscillation frequency of the long-range ordered signal in ZF-μSR of CeCuSn. The dashed line indicates 7.4 K.

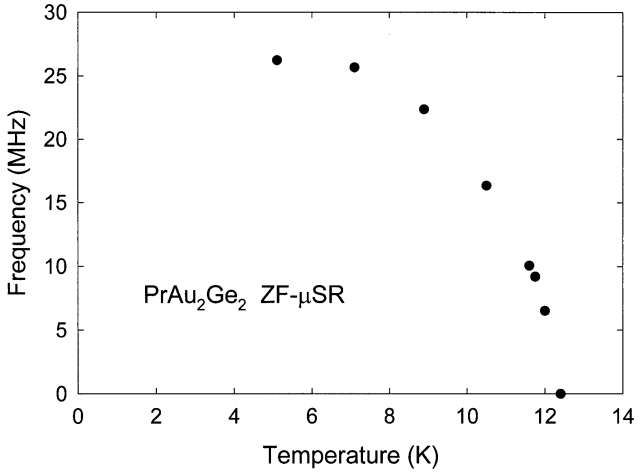

Fig. 107. Temperature dependence of the ZF-μSR spontaneous oscillation frequency in $PrAu_2Ge_2$.

With respect to the last, it may help to take LF-μSR data below 12 K to try to decouple the monotonic relaxation.

$PrAu_2Si_2$

In spite of the fact that this material is reported to spin-glass freeze at $\simeq$3 K, we saw only monotonic relaxation in ZF-μSR with the rate increasing as the temperature decreased, all the way down to 1.9 K, as low as this apparatus would take this sample. As with the previous sample, best fits to ZF data were obtained with the power exponential (see equation); in this case p dropping from 0.75 at 50 K to near 0.6 at low temperatures. As in the previous sample, the relaxation rate is proportional to $1/T$ over a wide temperature range. Rather than tending to diverge at any positive temperature, the rate below 4 K may be dropping slightly below $1/T$ dependence, which might, if we are lucky, be a very subtle indication that some spin freezing has begun. We need to measure this sample in the M15 dilution refrigerator to see if clear evidence of freezing develops well below 1.9 K.

$PrAu_2(Si_{0.8}Ge_{0.2})_2$

This sample showed monotonic relaxation at all temperatures down to near 5 K. At 5.0 K, there is a hint of a fast-relaxing signal. As the temperature drops further the fast-relaxing amplitude increases, indicating a range of inhomogeneous freezing, and at 4.0 K and below ZF spontaneous oscillation is resolved; roughly consistent with the reported Néel temperature. In this case we were able to coax the cryostat down to 1.7 K, producing the spectrum shown in Fig. 108.

We have only four spectra showing coherent oscillation, with the frequency rising from 14 MHz at 4.0 K to 24 MHz at 1.7 K. The zero-temperature limit frequency will be very similar to that of $PrAu_2Ge_2$ (Fig. 107), suggesting that the same type of ordered spin structure

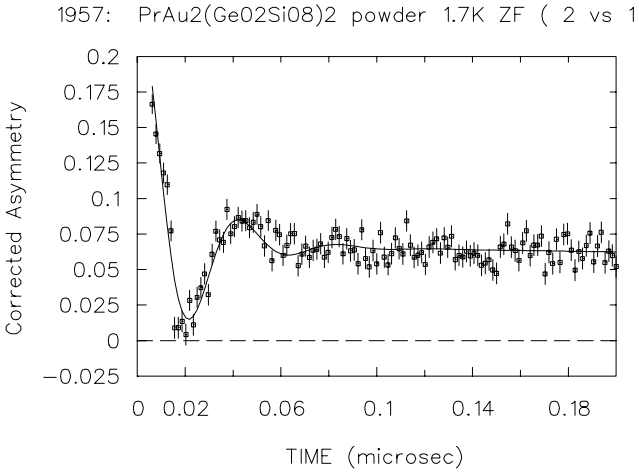

Fig. 108. ZF-μSR asymmetry spectrum of $PrAu_2(Si_{0.8}Ge_{0.2})_2$ at 1.7 K. The solid line is a least squares fit of a rapidly-relaxing oscillation.

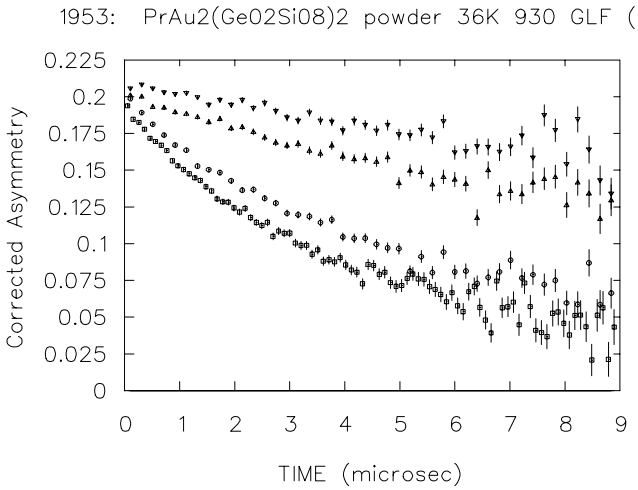

Fig. 109. μSR asymmetry spectra in $PrAu_2(Si_{0.8}Ge_{0.2})_2$ at 35 $\pm$ 1 K in ZF (squares) and longitudinal fields: 39 G (circles), 300 G (up triangles) and 930 G (down triangles).

develops, though with extra disorder induced by the non-magnetic site alloying, and also suggesting that the ordered moment at $T = 0$ is the same. The Si$\longleftrightarrow$Ge alloying reduces the transition temperature but not the ordered moment that develops, which is consistent with the introduction of frustration without reduction in the strength of the exchange coupling.

For this sample we attempted some LF decoupling and discovered, to our surprise, that not only could we decouple the ordered-state relaxation significantly with 3 kG LF, we could also decouple the paramagnetic relaxation at 35 K, as shown by Fig. 109.

Since we do not currently have a good physical model for the power-exponential form of the ZF spectrum, we have few grounds for expecting a standard model of LF decoupling to work here. Phenomenologically, the relaxation rate seems to go nearly as $1/\sqrt{B_{LF}}$, far from the standard $1/B_{LF}^2$. We should go back and check for paramagnetic LF decoupling in our end-point samples.

Experiment 882
μSR studies of unconventional superconductivity in an organic superconductor $(TMTSF)_2ClO_4$

(M.I. Larkin, Y.J. Uemura, Columbia)

Under Expt. 882 we have investigated the quasi-1 dimensional organic superconductor $(TMTSF)_2ClO_4$ using deuterated samples. Measurements of the upper-critical field H_{c2}, NMR relaxation rate and Knight shift, and sensitivity to non-magnetic impurities all suggest an unconventional (and possibly p-wave) pairing state of this and other Bechgaard Salt superconductors.

We have used zero applied field muon spin relaxation measurements (ZF-μSR) in an attempt to observe spontaneous magnetic fields below $T_c = 1.1$ K. Similar to the cases of μSR in UPt_3 and Sr_2RuO_4, such fields would indicate a superconducting state which breaks time reversal symmetry (TRS). We did not observe spontaneous fields, as shown in Fig. 110, but have an uncertainty in our measurement of ± 0.25 G, which is comparable to the $\sim$0.4 G spontaneous field seen in Sr_2RuO_4. Deuterated specimens were used in an attempt to minimize background nuclear dipole fields. The specimens, consisting of several hundred needle-like single crystals, were tiled onto a flat backing with the most conducting a-axis perpendicular to the direction of the initial muon polarization. It was not possible to align the other two crystal directions for the several hundred samples.

The material we used totalled 60 mg over $\sim$0.7 cm^2 surface area, which is near the lower limit of what may be measured in the dilution refrigerator at TRIUMF (or anywhere). Transverse field measurements (TF-μSR) indicated that the sample did enter the superconducting state, and that muons were stopping in the sample. TF-μSR may also be used to measure the superconducting penetration depth as a function of temperature. Such information is helpful in determining if gaps exist in the superconducting order parameter.

Further measurements will be performed using a larger quantity of material with aligned crystals. TF-μSR and ZF-μSR measurements will both be performed. Crystal alignment and increased sample mass would both represent substantial steps forward, and would allow us to garner much more information concerning this most interesting and exotic superconductor.

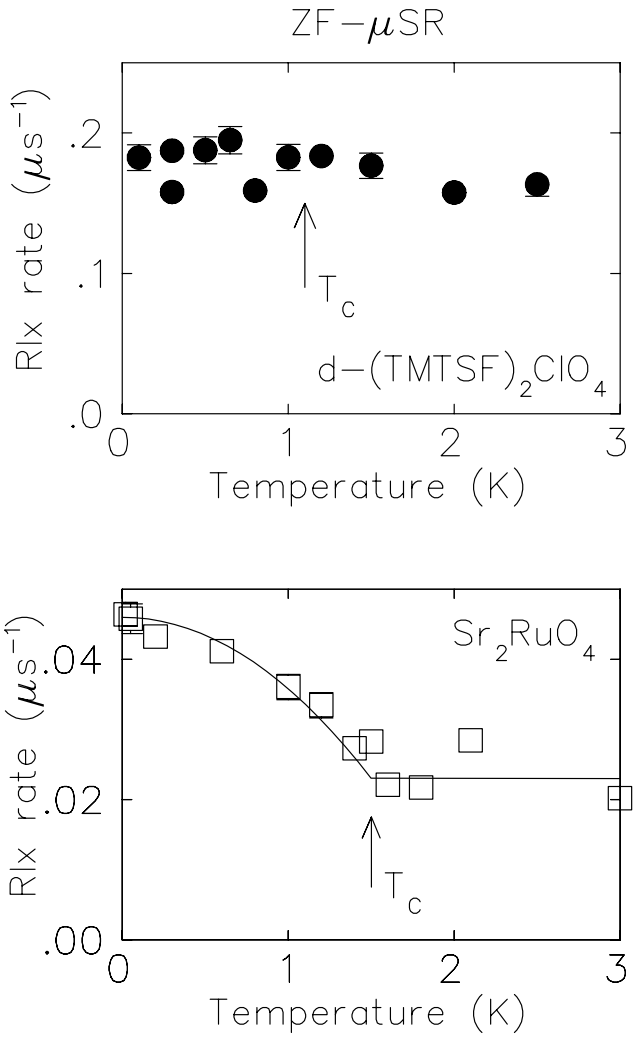

Fig. 110. ZF-μSR in deut-$(TMTSF)_2ClO_4$ and Sr_2RuO_4. No clear enhancement in relaxation is seen in deut-$(TMTSF)_2ClO_4$, in contrast to data from Sr_2RuO_4. Background nuclear dipole fields are fairly large in the TMTSF salt, however, possibly obscuring any effect.

LIFE SCIENCES

Introduction

The major news for the Life Sciences Program was the awarding of a $1,550,000 grant from the Canadian Foundation for Innovation to the PET group for the purchase of a new, high-resolution, research tomograph. It is anticipated that a companion grant application to the Provincial Government for $1,499,000 will also be successful. These grants, plus the $1,000,000 from the Canada Institutes of Health Research, will enable the PET group to install and characterize the scanner which has a resolution of 8 μl compared to the existing tomograph which has a resolution element of about 200 μl. In addition, the new tomograph will be about 3 times more sensitive than the existing camera.

As indicated in the various reports, collaboration with other groups continues to grow with projects involving the BC Cancer Agency and the University of Alberta as well as projects with Vancouver Hospital and Lions Gate Hospital. The project with Chemical Engineering at UBC appears to have exciting preliminary results which may have implications on the quantity of water needed for manufacturing paper.

The PET Target group also submitted a patent on the production of ultra high quantities of ^{18}F-fluoride from a gas target. A new water target fabricated from niobium was installed and yields are much more reliable than from the titanium one. These developments will be required in the new year as demands for more shipments of radioisotopes to Edmonton will increase.

Experiment LS0
PET facilities
(K.R. Buckley, TRIUMF)

The PET facilities comprise the TR13 13 MeV H^- cyclotron, the ECAT 953B/31 tomograph, and ancillary equipment such as counting and data acquisition systems.

TR13 cyclotron

Usage of the TR13 cyclotron rose significantly (113% by delivered beam) this year over 1999, reflecting mostly an increased demand for irradiation of lithium targets for the production of ^{7}Be (LS8). Usage of beam rose almost fourfold for LS8, while most other projects remained constant with the addition of new LS projects making use of beam time (LS32, 35, 39).

Downtime this year was significant and was caused by a number of different systems, mostly due to age related wear. A small, and as yet undetermined, leak in the ion source has resulted in four filament changes this year. The cryopump system required extensive servicing and ultimately the cold head displacer assemblies and compressor were replaced with funds budgeted for this purpose from the PET-CIHR grant. The rf amplifier tube and ion source turbo pump were replaced this year. One vacuum valve required servicing *in situ* when it developed a leak and it was discovered that extensive dismantling of the injection line would be required to remove the valve.

Intermittent problems with a power supply in the rf amplifier led to significant downtime throughout the year. This supply was built by TRIUMF and would be very expensive ($\sim$\$20k) to replace with a commercial unit. It has worked reliably until this year so it seems optimistic that the problem can be found and corrected. Downtime has been reduced since the fault was traced to this supply, but as yet the specific fault with the supply has not been found.

Ten extraction foil changes were required through the year, as well as one rebuild of the ^{18}O-O_2 gas target and four rebuilds of the CH_4 gas target. The titanium bodied water target for the production of fluoride was replaced this year when it developed a leak in a weld joint. The new target is constructed of niobium and is performing very well to date.

In addition to the above target work, an aluminum bodied water target was installed for the production of ^{13}N from natural water. This target allows us to supply the Botany group from the TR13, a capability which proved necessary during major repairs to the CP42 this fall (LS8).

One shipment of ^{18}F to Edmonton has occurred this year (LS32).

Presently there are six target locations occupied of the available eight. These consist of

- one ^{18}O-O_2 gas target
- one ^{18}O water target
- one ^{16}O water target
- one CH_4 gas target
- one experimental gas target
- one lithium metal target

The lithium target (LS8) has a reserved location and is installed and removed for each production. This target runs routinely for 15 hours at 50 μA.

ECAT tomograph

The ECAT too is showing signs of aging with new types of failures appearing.

While block detector failures continue, we have now repaired two blocks in house and are in the process of repairing more. We received information from CTI on how to access the voltage dividers in the block assembly and information on the specifications of components in use on the dividers. We are now able to repair detector

faults at this level and reseal the blocks. At present only a simple visual balance of PMT outputs is performed on the bench, but we intend to assemble the necessary components to properly calibrate the blocks prior to returning them to the scanner.

Other faults with the scanner have been traced to failed programmable logic chips in the position/energy processors on the buckets. These chips are programmed off-line and are intended to hold their programming for up to 20 years. Fortunately this circuitry is repeated for each block detector in the scanner and we were able to obtain and program new ICs with the data from an IC in a functioning channel.

An intermittent problem with 2D reconstructions in the front end of the scanner implicates a fault in the VME processor which controls data acquisition. Since this processor is obsolete, CTI is the only source of a replacement. One has been obtained and we are in the process of trying to determine whether this will solve the intermittent troubles. We are hoping this processor will also solve other intermittent troubles with data archiving to tape which have cropped up over the last couple of months.

The ^{68}Ge calibration line sources were replaced this fall with commercial sources purchased from Sanders Medical. The uniform cylinder source was replaced also, purchased from Isotope Product Laboratories.

Statistics

Table XIV. TR13 run data.

Total runs conducted	808	
Total runs lost	42	
Integrated charge delivered	923229	μA-mins
Delivered to – LS2	4506	
– LS3	264122	
– LS4	11219	
– LS8	559218	
– LS13	46456	
– LS24	23598	
– LS32	1142	
– LS35	3167	
– LS39	9155	

Table XV. ECAT scan data.

Total scans conducted	387
Total scans lost	103
Lost to – patient	31
– cyclotron	42
– chemistry	6
– scanner	24

Experiment LS2
Synthesis of radiohalogenated carbohydrates for use as imaging agents in PET and SPECT
(M.J. Adam, TRIUMF)

A number of relatively commonly-occuring genetic diseases are the result of deficiencies in lysosomal enzymes (glycosidases) responsible for the hydrolysis of glycosides. The most common such ailment is Gaucher's disease, which is caused by an inherited deficiency in glucocerebrosidase. This results in the accumulation of glucocerebrosides, mainly in the cells of the mononuclear phagocyte system. Other lysosomal diseases include Tay-Sachs disease, which is due to a deficiency in hexosaminidase A, and Hurler's syndrome, which is due to a lack of iduronidase.

Gaucher's disease can now be treated by enzyme replacement therapy, and good progress has been made in the development of other such therapies. Both diagnosis of the presence and the severity of the disease, as well as the monitoring of treatment, would benefit from new non-invasive methods of quantitating and localizing enzymes *in vivo*. Selective covalent inhibitors of these glycosidases that can be detected by positron emission tomography (PET) would be valuable in this regard. Excellent candidates for this task are 2-deoxy-2-fluoro-α-D-glycopyranosyl fluoride. These compounds have been shown to function as specific mechanism-based inactivators of "retaining" α-glycosidases via formation of a relatively stable 2-deoxy-2-fluoro-α-glycopyranosyl-enzyme intermediate. Therefore, by use of a 2-deoxy-2-[^{18}F]-fluoroglycopyranosyl fluoride it should be possible to radiolabel all functional glycosidases of that class and then localize them with PET. In an earlier approach to this problem we synthesized 2-deoxy-2-[^{18}F]-fluoro-α-D-mannopyranosyl [^{18}F]-fluoride and showed that it covalently derivatized Agrobacterium sp. α-glucosidase. We further showed that the trapped species was catalytically competent since it was capable of "turnover" with release of 2-deoxy-2-fluoro-mannose and native enzyme. Unfortunately, tests of this derivative *in vivo* revealed that hydrolysis occurred with formation of 2-deoxy-2-fluoro-mannose.

The choice of the synthesized 2-deoxy-2-fluoro-α-D-mannopyranosyl fluoride was a consequence of the relative simplicity and speed of its synthesis in radiolabelled form via electrophilic addition of [^{18}F]-fluorine gas to D-glucal. A better, more specific, analogue would appear to be synthesized 2-deoxy-2-[^{18}F]-fluoro-α-D-glucopyranosyl fluoride. However, rapid synthesis of this derivative in the desired α-anomeric form is non-trivial. Further, should spontaneous hydrolysis occur, the release of 2-deoxy-2-fluoro-glucose would become rapidly phosphorylated and trapped in the usual

manner, obliterating any imaging from labelled glycosidase. A possible solution to both problems was offered by replacement of the 6-hydroxyl group with fluorine which prohibits possible phosphorylation and offers a simpler means of radiolabelling using higher specific activity ^{18}F-fluoride. Earlier studies had demonstrated the tolerance of such enzymes for modifications of the substrate at the 6-position. Therefore, we have reported this year the synthesis and radiolabelling of 2,6-dideoxy-2,6-difluoro-α-D-glucopyranosyl fluoride (2,6FGF) 5 as a potential imaging agent for glucocerebrosidase, and the enzyme kinetic data obtained with Agrobacterium sp. α-glucosidase (Abg) and human glucocerebrosidase (GCase).

Experiment LS3
Synthesis of radiopharmaceuticals for positron emission tomography
(M.J. Adam, TRIUMF)

Daily routine production of up to 10 radiopharmaceuticals is currently performed with 3–4 radiophamaceuticals synthesized in one day. There was a total of 528 production syntheses carried out in 2000.

Out of these 10 radiopharmaceuticals, four (FDOPA, Raclopride, TBZ-OH, and MP) are used most heavily. The large increase in the number of Raclopride preparations this year is due to the "scatchard analysis" experiment that Doris Doudet is performing on monkeys. These experiments require 3–4 Raclopride preparations each day where one is at high specific activity (5–10 Ci/μmol) and the others have carrier added to give a range of specific activities of 2–35 Ci/mmol at time of injection. All preparations for these experiments are assayed by HPLC prior to injection to confirm the specific activity.

The demand for FDG for our group remains low. However, most of our FDG production is being used by Lions Gate and Vancouver Hospitals for studies in oncology and cardiology. We currently send FDG to these hospitals one day per week in amounts sufficient for imaging approximately three patients.

We have also started a pilot study into the feasibility of shipping ^{18}F-fluoride to Edmonton for tomograph calibrations as well as FDG production (see LS32). In our first shipment we produced 300 mCi for shipment and they received about 30 mCi in the lab several hours later. Nordion is handling the airline transport and Edmonton is paying all the transportation costs. More deliveries are planned.

The synthesis of ^{11}C-PMP was undertaken this year. PMP is an acetylcholinesterase inhibitor that will be used by Dr. Chong to study dementia in Parkinson's disease and diffuse Lewy body disease. Previous studies in postmortem brains have shown that choline acetyltransferase activity, but not muscarinic cholinergic receptors, was markedly reduced in PD, diffuse Lewy body disease and Alzheimer's disease and that neocortical cholinergic deficits correlate with severity of dementia in PD, diffuse Lewy body disease and Alzheimer's disease. As reduced cholinergic activity in the neocortex correlates with marked neuronal loss in the nucleus basalis of Meynert, these observations suggest that loss of cholinergic neurons in the basal forebrain may play a significant role in the pathogenesis of dementia in PD and diffuse Lewy body disease as well as in Alzheimer's disease. Recently, tracers for cholinergic neurons have become available for PET studies in human subjects. By using PET to explore cholinergic factors that contribute to the development of dementia in both PD and diffuse Lewy body disease, we will cultivate a better understanding of the pathogenetic mechanisms underlying dementia in PD and diffuse Lewy body disease. This should ultimately lead to better strategies for the pharmacological management of PD and diffuse Lewy body disease. The first human scans will start in February, 2001.

We continue to use TBAF in most of the ^{11}C methyl iodide reactions to enhance and stabilize the yields. We are fortunate to still obtain the nitro precursor of Setoperone as a gift from Jannsen Pharmaceuticals. We are also grateful to ASTRAZENECA AB for the gift of Raclopride Tartrate, used as carrier for the scatchard experiments, and Dihydroxy Raclopride as the precursor for labelling. However, for high specific activity preparations (SA = 5000–10,000 Ci/mmol) we use our own precursor since the Astra precursor contains significant amounts of carrier (maximum SA = 500–1,000 Ci/mmol). The Astra material is suitable for the carrier added runs. All other precursors are synthesized in house which requires a major time commitment from Dr. Lu.

Several new computers have been purchased and installed on the chemistry systems this year. Lookout software still needs to be implemented in some of the processes. A new QC HPLC has been purchased and installed as well as other new equipment for the lab to replace some of the 20-year-old items such as a rotary evaporator and fridge. We also anticipate a new hot cell being installed sometime early in the new year which will be located in place of the fume hood that now contains the FDG and FDOPA systems. These systems are about 15 years old now and will need to be redesigned and upgraded so that they can be housed in the new hot cell. The upgrade to the FDG system is a priority because of rapidly increasing demands for this agent by outside users such as VGH, LGH and St. Paul's Hospital. Fluoro-dopa is still heavily used by our own Movement Disorder group.

Experiment LS4
Targets for PET radioisotope production
(T.J. Ruth, TRIUMF)

New gas targets for the high yield production of ^{18}F-fluoride

There is growing demand throughout the world for a large production capacity of clinical doses of FDG. Thus there is a real need to develop a superior high yield target system.

Therefore we investigated a possible route to a higher yield target system for ^{18}F-fluoride production. Both approaches rely on gas target designs since TRIUMF has developed the technology to build gas targets capable of operating at proton beam currents greater than 100 μA.

The fluoride target will use the ^{18}O-O_2 gas target concept in an analogous manner to the F_2 double shoot system. The first irradiation would generate the ^{18}F as fluoride that sticks to the walls. But instead of performing a second irradiation, the target is washed out with water in a similar fashion to that used for ^{123}I production by MDS Nordion. Depending on the energy of bombardment, extremely high yields may be possible. For example, the saturation yields at 13 MeV are approximately 200 mCi/μA and 250 mCi/μA at 18 MeV. Thus for a 2 hour run at 100 μA one can produce 8 Ci and 10 Ci respectively, even if one has an 80% recovery from the target wash (50% saturation $\times$ 0.8 = 0.4 $\times$ saturation yield). At these rates one can imagine very long shipments. The advantages include straightforward and efficient recovery of the target material, and higher beam currents than is possible for water targets (or liquids in general). Disadvantages include having to wash and dry the target between runs and finding the best material for this process.

For the new target systems, we investigated the various steps involved in preparing ^{18}F as fluoride.

- Operation of gas target at 100 μA.
- Windows, cooling, pressure/chamber size, etc.
- Recovery of target gas.
- Efficient washing of target.
- Selection of target chamber material.
- Drying target.
- Elution of ^{18}F radioactivity.
- Recovery of ^{18}F fluoride from large volume of water.

Target materials tested thus far:

- Ni plated Al – (66.4% + 7.4%) = 73.8%, n = 4
  - H_2O Temp = 80°C
  - H_2O T60 = 50.4%
  - H_2O T20 = 38.4%
  - Each wash = 10 mL
- SS – (80.6% + 12.6%) = 93.2%
- Al – (5.6% + 1.8%) = 7.5%
- Glassy Carbon = 98.3% (single wash)

Next we spiked 30 ml of water with fluoride and passed the resulting solution through our standard QMA ion exchange resin. The ^{18}F-fluoride was quantitatively extracted onto the resin. Elution with potassium carbonate Kryptofix solution resulted in more than 90% recovery.

We performed a series of proof of principle experiments using a modified stainless steel cooling jacket to serve as a target. The irradiations were performed at 25 μA for between 15 and 30 minutes using a 5% ^{18}O-O_2 mixture. Water heated to 80°C was passed through the target and over an ion retardation column (QMA) and into a waste vessel. The column was then removed and washed with a bicarbonate solution to recover the ^{18}F-fluoride. The results of these experiments are as follows.

- Approximately 70% of theoretical yield recovered from target (n = 4). Target washes were of 100 ml volume.
- Distribution – 65% on QMA, 3% passed through column, 3% drained from target.
- Unable to measure what was retained in target (we have no way of determining whether the radioactivity was stuck on the target walls or simply not produced).
- >95% of the $^{18}F^-$ extracted by QMA was eluted with 2 $\times$ 2 ml washes of bicarbonate solution.

These results were accepted for publication in the spring.

MDS Nordion routinely operates its Xe gas target at over 100 μA. Therefore, in principle, it is possible to design a low energy gas target to operate under these conditions. In order to operate at the 50–100 μA beam current, the target cooling system must be optimized. The key aspects of the He cooling window design include flow rate, pressure, the number of ports (inlet and outlet), and the direction of the ports. Preliminary results indicate that He pressure is one of the most important parameters, as well as inlet port direction.

Experiment LS8
Radiotracers for the physical and biosciences
(T.J. Ruth, TRIUMF)

The following projects are designed to take advantage of TRIUMF's unique accelerator facilities.

The production of ^{7}Be will be done in collaboration with the Beryl group at TRIUMF as part of their effort to measure the cross section for the ^{7}Be$(p,\gamma)^8$B reaction to address anomalies in the international solar

neutrino measurements. Routine irradiations are under way (see Expt. LS0, this Annual Report).

^{13}N tracers have been used extensively at UBC for more than 10 years to study the kinetics of nitrogen incorporation by plants. The program has grown and looks forward to continued collaboration with TRIUMF in these studies.

Based on results from the nitrogen studies, the researchers in Dr. Glass' lab wish to explore the kinetics of potassium uptake in plants as a function of nitrogen concentration. In order to perform these experiments they will need access to ^{42}K.

Researchers in the Physics Department need a long-lived isotope of silver for the nuclear orientation experiments. ^{110m}Ag is the candidate of choice. Target and chemistry developments have been completed for producing ^{110m}Ag by irradiating ^{nat}Pd with low energy protons.

Details of botany program

Rice research (International Rice Research Institute (IRRI) of the Philippines)

We have demonstrated that the half-life of NH_4^+ turnover in roots of rice appears to be independent of the concentration of NH_4^+ provided to plants. This constancy, which involves the integration of influx, efflux, fluxes to vacuolar and assimilation, extends to short term perturbations of influx associated with elevating or reducing external [NH_4^+]. Despite a brief perturbation of influx and efflux, the half-life of $^{13}NH_4^+$ exchange is restored within minutes to its original value. The implications for overall control of all reactions leading to NH_4^+ accumulation within the cytosol of root cells is profound.

Nitrogen uptake in trees. A collaboration with BCRI

This project is funded by NSERC and BCRI for 3 years. The goal is to express the high-affinity NO_3^- transporter gene (AtNrt2.1), that we cloned from Arabidopsis thaliana [Zhuo *et al.* (1999)], in hybrid spruce and in poplar seedlings. Since spruce is notoriously inefficient at absorbing NO_3^- [Kronzucker *et al.* (1997)] our goal is to increase the seedling vigour of these plants for reforestation programs. We used tobacco as a model system to evaluate the methodology, and have successfully produced transgenic tobacco plants and obtained a limited number of lines that over-express the high-affinity transporter gene. We are awaiting sufficient numbers of transgenic plants to measure their $^{13}NO_3^-$ uptake rates. In order to assess the relative effects of over-expression of this gene, it has been necessary to characterize $^{13}NO_3^-$ influx in wild-type tobacco, spruce and poplar. We have completed the characterization of NO_3^- transport systems in all three species during 1999–2000. In the near future we will be evaluating $^{13}NO_3^-$ transport in transgenic plants. A preliminary report of this work was presented by Dr. Simon in Bonn in September.

NH_4^+ compartmentation in plant tissues

Dev Britto has now completed work on the compartmentation of N in plant tissues and analyses of $^{13}NH_4^+$ fluxes in leaves and roots of various crop plant and wild species. His thesis has been approved by his research committee and will be sent out to the external examiner before the end of term. Analyses reveal that excessive NH_4^+ uptake in species susceptible to NH_4^+ toxicity leads to substantial ($\sim$40%) increases in respiration that are not involved in NH_4^+ assimilation *per se*, but rather in the energy-dependent pumping out of NH_4^+ in a futile attempt to reduce cytosolic [NH_4^+].

$^{13}NH_4^+$ uptake by roots of Arabidopsis

Dr. Rawat has isolated insertional mutants, in which the gene encoding the high-affinity NH_4^+ transporter (AMT1.1) in A. thaliana is disrupted. The point of this methodology is to critically test the hypothesis that the gene in question is actually crucial for NH_4^+ transport. Since this gene was cloned in 1994, four related high-affinity genes have been identified from this species. To what extent do these other genes participate in NH_4^+ transport? By rendering the AMT1.1 inactive it is possible to evaluate the potential role of the other genes. Dr. Brent Kaiser has continued this work and fully characterized the molecular biology aspects of this mutant and has recently begun to characterize NH_4^+ transport in these mutants. Our first experiments appear to indicate little change in the rates of NH_4^+ influx, indicating that the other genes are able to compensate for the disruption of AMT1.1.

A preliminary report of this work was presented at the annual meeting of the German Soc. Plant Nutrition held in Giessen in September.

$^{13}NO_3$ influx in the fungus Aspergillus nidulans. A collaboration with St. Andrews, Scotland

The first eukaryotic NO_3^- transporter genes (crnA) were cloned from Aspergillus nidulans by Dr. Unkles and co-workers in 1991. The fungal gene served as a model system for higher plant studies, enabling the corresponding genes (highly conserved through evolution) to be isolated from roots of barley and Arabidopsis. We have cloned a second crnA homologue and also generated strains of the fungus which are mutated in each of these genes as well as a strain that is mutated in both genes. We have been able to characterize the contributions of each of the fungal gene products by means of $^{13}NO_3^-$ flux analysis. This work is in preparation for publication.

The double mutant, lacking any capacity for $^{13}NO_3^-$ transport, will be used to characterize seven

different homologues of the fungal gene that we have been able to clone from A.thaliana. The strategy will be to transform the Aspergillus double mutant with the plant genes (one at a time) and evaluate their capacity to transport $^{13}NO_3^-$.

The pathway of $^{13}NH_4^+$ assimilation in GDH mutants of tobacco. A collaboration with the University of Illinois in Carbondale

The normal pathway of NH_4^+ assimilation in crop species may be blocked by the herbicide (inhibitor) phosphinothricin. Dr. Lightfoot generated an alternate pathway of NH_4^+ assimilation in transgenic tobacco by over-expressing a bacterial enzyme glutamate dehydrogenase (GDH). His transgenic plants were immune to the herbicide by virtue of having an alternative pathway to assimilate NH_4^+. Proof was needed to demonstrate that the alternative pathway was indeed operating in this transgenic plant. Using $^{13}NH_4^+$ it was possible to show that $^{13}NH_4^+$ assimilation proceeded normally in the transgenic plants (by virtue of the alternative pathway) while non-transgenic plants incorporated virtually no NH_4^+. The accumulation of elevated NH_4^+ proves to be toxic. This work has been written up for publication.

Sabbatical visitors

The availability of ^{13}N in a context that allows for good biochemical and physiological experiments has resulted in a string of foreign and local visitors who have made use of the availability of ^{13}N. Dr. Unkles, from St. Andrews, visited from November to December. A postdoctoral fellow from Dr. Lightfoot's lab in Carbondale, IL was to have undertaken the work on the GDH transgenics but was unable to visit UBC. Together with a research associate we were able to complete the project earlier (May/June).

Production of ^{110m}Ag

A stack of two ^{nat}Pd foils was bombarded in February. The chemical processing involved dissolving the palladium target, removing excess acid through evaporation, followed by taking up the Pd in 0.01 M HCl. The Pd and Ag are separated on an alumina column with the Pd fraction eluting with the 0.01 M HCl. All indications are that the Ag fraction remains at the top of the column. Once all of the Pd has been removed, as evidenced by colour change of the column, the Ag fraction can be eluted with 0.1 M HCl. The Ag is eluted in less than 10 ml.

Aliquots of both fractions were assayed for radioactive species. The Pd fraction does not have a strong γ-ray for identification. We will have to develop a technique to determine the relative radiochemical purity, although from the colour change on the column we are certain that it is greater than 90% separation.

The silver fraction contained radioisotopes which could be identified as $^{105,\,106m,\,110m}$Ag. We performed a γ-ray spectroscopic analysis on the unseparated foil to estimate production rates. The estimated EOB yields are as follows:

- ^{105}Ag – combined foils – 26 mCi/μA at saturation;
- ^{106m}Ag – combined foils – 2.3 mCi/μA at saturation;
- ^{110m}Ag – combined foils – 0.75 mCi/μA at saturation.

At this rate it would require about 1250 μAh to achieve the required 100 μCi. However, the coproduction of ^{105,106m}Ag would be about 15 and 2.2 mCi, respectively. The exact mix would depend upon the beam current and length of bombardment.

In order to proceed we have had to modify a target so that we can irradiate with a beam of about 50 μA. At this intensity it will require about 25 hours of beam that could be spread over several days. Following irradiation, the foil would be left in place for at least 40 days to allow the decay of ^{105}Ag (50% remaining) and ^{106m}Ag (0.04 remaining). Even at this level there would be about 4.80 mCi of ^{105}Ag left. We could of course allow for a longer decay period, if needed, for the physics experiment.

Experiment LS10
Aptamer imaging agents
(H. Dougan, TRIUMF)

This work has been concerned with a DNA aptamer which has the potential to bind thrombin and image thrombi. A model thrombus in the rabbit jugular vein was used to test the radiolabelled aptamer *in vivo*. Primary goals were to measure the extent of aptamer binding, and to test if binding was specific for thrombin. Secondary goals were to relate *in vivo* results to previous *in vitro* biochemistry diffusion experiments, and to provide an *in vivo* model where the intactness of DNA could be readily evaluated. Several approaches were evaluated: (i) probe with labelled clot, (ii) imaging with labelled clot, (iii) imaging with labelled clot and heparin, (iv) imaging with applied label and clear veins, (v) fluoroscopy with applied label, double label. Without anticoagulant, the thrombus model was prone to occlude, trapping aptamer and giving the false impression of aptamer binding. On the other hand, anticoagulant would invalidate quantitative binding studies with thrombin. We turned to fluoroscopy, where bloodflow could be verified with iothalmate injections. Ovalbumin was the neutral control. The amount of aptamer binding was low, 0.1% to 1% on a single pass. We had previously shown that the lifetime of the aptamer in circulation is short, permitting

only a single passage through the thrombus. The low uptake would make it difficult to detect images, and it restricts biochemical applications of the assay. More encouraging results were obtained to a second question, whether the bound aptamer indicated thrombin, and not merely non-specific diffusion. Aptamer (ODN 1 or 2) and ovalbumin labelled the clot equally, when applied externally. A positive aspect was that after 1 hour, the ratio was 3:1 aptamer (ODN 2) to ovalbumin. This appears consistent with aptamer retention. Alternative explanations must still be ruled out. A preliminary manuscript is available.

Experiment LS29
Production and distribution of FDG for clinical studies
(T.J. Ruth, TRIUMF)

The Canadian Society of Nuclear Medicine has petitioned the regulatory authorities in Canada to strike a committee to establish the environment in which PET radiopharmaceuticals would be regulated. The committee would comprise the stakeholders who produce, use and regulate the radiopharmaceuticals labelled with positron emitting isotopes.

Experiment LS32
^{18}F-H_2O to the University of Alberta
(S. McQuarrie, Alberta)

Due to a recent success in obtaining major support from the Canadian Foundation for Innovation (CFI), the University of Alberta in collaboration with the Cross Cancer Institute is now proceeding with the design and construction of a new building that will house the cyclotron and chemistry labs necessary for the production of research radiopharmaceuticals. The proposed schedule will see the completion of a building by September, 2001 with the cyclotron installed and running before the end of 2001. We have recently obtained our first shipments of ^{18}F as fluoride from TRIUMF and we wish to have these shipments continue on a routine basis through 2001 up to the commissioning of our own machine.

The ^{18}F shipments are required in order to gain expertise in the labelling and handling of fluorinated compounds having applications in oncology. In particular, we would like first to acquire skills required to prepare and use ^{18}F-fluorodeoxyglucose (^{18}F-FDG). The value of ^{18}F-FDG in cancer diagnosis and in the assessment of treatment outcomes has been well documented. A second project will establish a synthesis of ^{18}F-fluoroestradiol. This product will be used in a research project to identify and determine treatment outcomes of breast cancer patients who show positive estrogen receptor status in their disease. As we gain expertise with fluorine chemistry we will also attempt other syntheses such as ^{18}F-misonidazole or the ^{18}F-nucleoside analogue ^{18}F-FIAZA developed at the University of Alberta. The recent acquisition of an ADAC C-PET camera will permit a limited clinical research investigation on lung cancer patients using ^{18}F-FDG and breast cancer patients with ^{18}F-FES. We have purchased a Coincidence Technologies synthesis box which will be used in the preparation of ^{18}F-FDG. We have applied for funding from the Alberta Breast Cancer Foundation, which will assist in the development of an automated synthesis unit for ^{18}F-fluoroestradiol. The development and preliminary investigations with these agents will require a routine supply of ^{18}F-fluoride.

An application has also been submitted to the Alberta Heritage Foundation for Medical Research to purchase an animal PET camera such as the microPET camera from Concord Microsystems Ltd. A variety of researchers from the Cross Cancer Institute and the University of Alberta have submitted proposals for the use of this system with ^{18}F products and some of this work will be initiated with the availability of ^{18}F-FDG and other ^{18}F products.

Experiment LS33
Evaluation and improvement of a dual head coincidence camera
(V. Sossi, TRIUMF)

The ADAC molecular coincidence dual head camera was installed at Lions Gate Hospital in North Vancouver in August/September, 1997. The attenuation correction hardware and software was implemented in September, 1999.

Studies accomplished this year

1. The effect of radioactivity, outside the field of view shielding, on image contrast was defined.
2. A patient shield has been built that reduces the scatter by 9%.
3. Experiments to determine the new NEMA NU2-2000 performance standards have been completed.
4. Monte Carlo investigation of scatter is under way as part of a Ph.D. thesis.

Experiment LS35
Development of ^{18}F labelled nitroimidazole PET imaging agents for tissue hypoxia
(M.J. Adam, TRIUMF)

Hypoxia in cells and tissues is an important component of various pathological states (e.g. ischemia and stroke). Hypoxic tumour cells are extremely important within cancer treatment because they are more likely to survive radiation and chemotherapy, leading to an increase in tumour resistance to treatment. More recent evidence suggests that hypoxia is

related to the aggressiveness of disease. Such studies employed a microelectrode, used in many centres, but were limited because of invasiveness and requirement for an accessible tumour. Derivatives of 2-nitroimidazole are used extensively as hypoxia markers. The 2-nitroimidazoles are not metabolized in oxygenated tissues, but bind to macromolecular proteins after reduction in hypoxic cells. This permits detection by a variety of techniques. For example, the products of such binding for the (pentafluoropropyl)acetamide (EF5) and (trifluoropropyl)acetamide (EF3) derivatives of 2-nitroimidazole can be detected by specific fluorescent antibodies. Earlier studies used 2-nitroimidazoles labelled with radioactive isotopes such as ^{3}H and ^{14}C, followed by autoradiographic methods. These compounds provided proof, in principle, for detection of tissue hypoxia. However, the high level of radioactivity, toxicity and price limit their application. Furthermore, this is also an invasive approach.

The preparation of hypoxia markers carrying ^{18}F allows for the use of the PET technique. The first and most investigated compound of this type is [^{18}F]fluoromisonidazole, which was developed by the Seattle group. Although widely used in research, this compound is not ideal as it shows some hypoxia-independent tissue retention. Recently, the synthesis of another fluorinated nitroimidazole, [^{18}F]fluoroetanidiazole, was reported, but it is not clear if it has the right redox and pharmacokinetics.

The synthesis of ^{18}F-EF5 has now been developed by Dolbier *et al.*, and was achieved by preparing the allyl precursor and fluorinating it with ^{18}F elemental fluorine in trifluoroacetic acid. The radiochemical yield is 17% after HPLC purification. During this year the chemistry to synthesize ^{18}F-EF5, and the subsequent purification step, was established in the TRIUMF laboratory, and several syntheses have been performed for cell and animal studies. Initially we carried out cell studies to determine the effects of hypoxic and aerobic conditions on the uptake of EF5. This experiment indicates that about 10-fold more hot EF5 is concentrated in cells under hypoxic conditions as compared to aerobic conditions, and that the addition of cold EF5 has little effect. The gamma counting results were basically the same as those obtained by using cold EF5 and flow cytometry. These cell experiments were followed by rat experiments; rats with 9L tumours were injected with ^{18}F-EF5 and imaged on our PET tomograph, followed by dissection to determine biodistribution.

An image of the brain tumour in the rat was obtained. Although the image quality is very poor, it indicates a significant uptake on the brain tumour bearing rat as compared to the image of a normal rat.

The next stage of the research is to proceed to human studies. Two proposals have been submitted for funding by research groups at the BC Cancer Research Agency. One study will focus on the use of EF5 in lung cancer, and the other on breast cancer.

Experiment LS37
^{125}Xe implantation as a source for ^{125}I brachytherapy
(J.S. Vincent, TRIUMF)

The objective was to determine whether radioxenon implanted 20–50 Å beneath common metal surfaces is stable and could provide a source of radioiodine for brachytherapy devices.

Two shifts of beam time were used to investigate the implantation of radioxenon into steel, titanium and gold using TISOL, the on-line test isotope separator. Steel foils have been analyzed to date. Implanted at 12 and 22 kV, ^{127}Xe seems to be stable within the statistics of measurement (∼10%) up to 600 hr after bombardment at room temperature. ^{125}I from ^{125}Xe decay *in situ* is quantitative within better than 10%. Measurements of electron emission from the iodine-implanted surface have been made in high vacuum using an electron multiplier with a threshold of 100 eV. There appear to be several electrons per 35 keV photon emitted from one 12 kV implanted foil. Several foils have been soaked in normal saline at room temperature and 55°C for periods up to 3 days. The saline has been dried at low temperature and the residue counted for trace ^{125}I. No statistically significant quantity of ^{125}I has been detected in the saline wash.

Experiment LS38
Dopaminergic tracers kinetic modelling with minimally invasive scanning procedures
(V. Sossi, TRIUMF)

The development of a new method for the determination of dopamine turnover has been completed. The method was fully validated on non-human primate data and is being applied to human data.

These studies complete the main scope of this research proposal regarding the study of kinetic modelling with minimally invasive scanning procedures. Cluster analysis that was initially part of this research proposal is going to be investigated as part of a new research proposal, "Modelling of the dopaminergic system in more severely affected PD patients".

Summary of the animal model results

Changes in dopamine turnover due to disease states such as Parkinson's disease may be reflected in corresponding changes in the kinetics of the positron emission tomographic tracer ^{18}F-fluorodopa. We had previously refined the conventional irreversible-tracer

graphical approach to determine both the uptake rate constant K_i and the rate constant k_{loss} that describes the slow loss of the trapped kinetic component. Because these parameters change in the opposite sense with disease, their ratios may be more powerfully discriminating than either one alone. The ratio k_{loss}/K_i is indicative of effective dopamine turnover (EDT). Its inverse K_i/k_{loss} can be interpreted as the effective distribution volume (EDV) of the specific uptake compartment referred to FD concentration in plasma. Here we present a new approach to the estimation of EDV based on reversible-tracer graphical methods. When implemented with a plasma input function, the method evaluates EDV directly. When implemented with a tissue input function, the outcome is proportional to the ratio of the distribution volumes of the specific uptake and precursor compartments. Comparison of the new and previous approaches strongly validates this alternative approach to the study of effective dopamine turnover.

Summary of the results from the human subjects data

Objectives:

There are two objectives to this study.

1. To test a new method to determine the effective dopamine distribution volume (EDV), the inverse of the effective dopamine turnover, in normal volunteers (N) and Parkinson's disease (PD) patients.
2. To compare the abilities of four data analysis methods used in the early detection of disease: plasma input uptake rate constant K_i, tissue input uptake rate constant K_{occ}, EDV, and tissue input effective distribution volume ratio (EDVR).

Method:

Twelve subjects [5 N and 7 early stage PD (UPDRS III = 16/10)] underwent a 4-hour dynamic ^{18}F-dopa (FD) PET scan. 23 blood samples were taken and selected ones analyzed for metabolites. A new method based on the reversible process analysis was used to determine the EDV and EDVR. This method had been previously developed and validated with non-human primate data and here for the first time applied to human data. Data from 90–240 min after injection were used to determine the EDV and EDVR, while data from 20–90 min were used to determine K_i and K_{occ} using the Patlak analysis. The parameter values averaged over the putamen were used to compare the N to the PD group.

Results:

The new method provided a reasonable value for the EDV and EDVR in all cases, which was not possible with a previously existing graphical method. Discriminant analysis applied to the data determined the EDV to be the best single classifier of the two groups. EDV alone correctly classified the N group at a 100% level and the PD group at 71.4%, with the misidentified PD patients having the lowest EDV value in the algorithm defined N group. A quadratic discriminant analysis using EDV and K_i combined classified both groups correctly at 100%.

Conclusion:

A new method to determine the EDV was validated with human data. The EDV was found to be the most sensitive classifier in early PD, indicating that changes in the effective dopamine turnover can be measured earlier with PET than changes in the uptake rate constant, which is related to dopamine synthesis and storage. This analysis also suggests that EDV and K_i provide some independent information on disease state.

Modelling of the dopaminergic system in more severely affected PD patients

Parkinson's disease is characterized by progressive loss of dopaminergic terminals and by a reduced neurotransmitter dopamine level in the striatum. The radiotracer ^{18}F-fluorodopa (FD) is often used to quantify the uptake rate constant of the neurotransmitter dopamine (DA) into the pre-synaptic vesicles. Traditionally the FD kinetics are described by an irreversible model approach reflecting the DA trapping in the vesicles. The plasma input or the tissue input Patlak graphical approach is applied to the tracer time activity distribution to obtain the uptake rate constants K_i or K_{occ}, respectively. We have, however, recently observed that in the case of moderately severely lesioned patients the data do not satisfy the requirements of the Patlak graphical approach, indicating that the observed process is no longer irreversible. This fact can be most likely explained by a loss of DA vesicular storage ability. The Patlak approach applied to such data introduces a significant bias into the results, thus yielding inaccurate quantification of disease progression. These observations prompted the following studies.

1. Identification of an analysis method that can correctly quantify disease progression.
2. Development of a method that can distinguish regions with different tracer behaviour. Cluster analysis is being explored for this purpose. Comparison of the location and extent of the regions with the two different tracer behaviours in repeated studies of the same subject could provide an objective tool to measure the topographical pattern of disease progression.

The results of these studies will provide a better quantitative assessment and an objective topographical pattern of disease progression.

Experiment LS39
PET (profiling) for pulp and paper
(M. Martinez, UBC)

Two everyday examples of multiphase fluids are bubbly liquids and dusty gases. The term "multiphase flow" denotes a wide variety of phenomena in which particles, drops, or bubbles are present in a flowing fluid, such as air or water. The presence of a dispersed phase often significantly affects the flow as a whole. These inter-phase effects have to be accounted for to the lowest order of approximation.

For single-phase flows of Newtonian gases and liquids, experimental, mathematical, and numerical methods have, with some exceptions, reached a state of reasonable maturity. For the broader classes of phenomena that appear in multiphase flows, this is certainly not so – the experimental measurements are notoriously difficult and usually limited to fairly dilute conditions. As for the mathematical and numerical methods encountered in multiphase flows, one often experiences problems where the existence of a solution is by no means guaranteed beforehand.

Multiphase flows are very common in industrial applications. One such example is in the pulp and paper industry where a suspension of wood pulp fibres is filtered and consolidated, at very high speeds, to form a sheet of paper. Papermaking suspensions are typically composed of a mixture of fibres with a wide distribution in both length and diameter. Each class of fibre behaves differently during the filtration process depending on the hydrodynamic force applied and its degree of mobility in the formed network. Ascertaining these effects is difficult as these suspensions are opaque and difficult to visualize at reasonable penetration depths. Clearly, there is a need to visualize the motion of the individual classes of components in a fibre suspension in order to better understand the development of the physical properties of paper.

As an initial step, we have recently conducted a gravity-settling experiment at TRIUMF to test the feasibility of using PET as a novel visualization method. In this work, a selected class of "long fibres" was radioactively labelled and allowed to settle in an untreated fibre suspension (with a distribution of fibre lengths). The suspension was agitated and allowed to settle under the action of gravity in a cylindrical jar. The radioactive fibres were moving from right to left and four different axial cross sections were observed at different times.

From this initial study it is clear that this visualization technique has the potential to help clarify the behaviour of mixtures of fibres with differing lengths during papermaking. However, further development work needs to be conducted. A collaborative project is proposed to further develop this technique. A graduate student in chemical engineering, funded by Mark Martinez, will conduct the work.

Experiment LS42
Configuration modelling and image reconstruction studies on a depth encoding research tomograph
(V. Sossi, TRIUMF)

Simulations of the interaction of 511 keV γ-rays in LSO and GSO have been accomplished using GEANT. GEANT was interfaced with DETECT, previously developed by C. Moisan, which simulates the light transport in the crystal and the crystal-photomultiplier tube (PMT) interface. The programs were modified to include two layers of different material. An algorithm that decodes the crystal position as a function of light distribution in the four PMTs has been developed.

Spatial resolution estimates as a function of γ-ray incidence angle are being obtained by simulating two detectors placed opposite to each other at varying angles.

Future plans

The following issues are going to be addressed.

1. Block testing.
2. Data reconstruction techniques.
3. Data transfer and storage schemes.

In addition to the above listed studies, patient motion correction techniques will be investigated.

THEORETICAL PROGRAM

Introduction

The Theory group at TRIUMF provides a focus for theoretical research at the laboratory and an active group of people doing high quality research in areas which are relevant, in the broadest sense, to the physics program at TRIUMF and to the interests of the subatomic physics community across Canada. The Theory group thus provides support for the TRIUMF experimental program in its many facets. Like the experimental program, the theoretical research program covers a wide range of topics in nuclear and particle physics with relevance to ISAC, to the medium energy program, and to work done by TRIUMF scientists elsewhere. Part of this research involves working directly with the experimentalists in support of particular experiments; part provides a more general background to the experimental program; and an important part deals with fundamental areas not currently directly related to the experimental program.

The Theory group has four permanent staff members: Harold W. Fearing (group leader), Byron K. Jennings, John N. Ng, and Richard M. Woloshyn, plus Erich W. Vogt (professor emeritus, UBC). This year our research associates are: J. Escher (all year), S.K. Ghosh (all year), S. Kondratyuk (since October), X. Kong (all year), A.D. Lahiff (since September), G.C. McLaughlin (until September), T.-S. Park (until September), G. Rupak (since September), and W. Schadow (all year). Long term visitors include K. Maltman (September-December) and T. Schäfer (January-August). Graduate students with the group include: M. Nobes, SFU (until August), supervised by R.M. Woloshyn; and C. Bird, U. Victoria (all year), E. Ho, UBC (all year), T. Ebertshauser, Mainz (May-July), and C. Unkmeir, Mainz (until September) supervised by H.W. Fearing.

Several others participate regularly in Theory group activities including H. Trottier (SFU faculty) and K. Kallio, M. Nobes, N. Shakespeare, K. Wong (SFU students).

The visitors to the Theory group this year include:

L. Abu-Raddad	J. Juge	K. Nollett
A. Arbuzov	K. Langanke	V. Pascalutsa
L. Canton	P. Lee	M. Ramsey-Musolf
C. Cardall	G. Li	A. Rinat
L. Chang	H. Lipkin	N. Shoresh
T. Fujita	M. Locher	R. Springer
H. Hammer	P. Matlock	I. Towner
W. Haxton	T. Mehen	D. Wilkinson
B. Holstein	A. Mekjian	L. Zamick
S. Hong	H. Murayama	

In addition to their research activities, the theorists have taken an active part in the laboratory activities including the Long Range Planning Committee, the Experiments Evaluation Committee, the NSERC 5-Year Plan Committee, computer support, and from time to time have done some teaching at member universities.

As usual the Theory group has been very active and below we briefly describe some of the specific research projects undertaken during the year by members of the group or by longer term visitors while at TRIUMF.

Nuclear Structure and Reactions, Nuclear Astrophysics

The low-energy nuclear density of states and the saddle point approximation

(S.K. Ghosh, B.K. Jennings)

The nuclear density of states plays an important role in nuclear reactions. At high energies, above a few MeV, the nuclear density of states is well described by a formula that depends on the smooth single particle density of states at the Fermi surface, the nuclear shell correction and the pairing energy. We are in the process of analyzing the low energy behaviour of the nuclear density of states using the saddle point approximation and extensions to it. We should be able to develop formulae that work better at low energies.

Nuclear structure and the solar neutrino problem

(J. Escher, B.K. Jennings; S. Karataglidis, LANL)

The $^7\mathrm{Be}(p,\gamma)^8\mathrm{B}$ reaction at solar energies (approximately 20 keV) plays an important role in the "solar neutrino puzzle" since the neutrino event rate in the existing chlorine and water Čerenkov detectors is either dominated by or almost entirely due to the high-energy neutrinos produced in the subsequent beta decay of ^{8}B. The relevant reaction rate has to be deduced by extrapolating the measured absolute (laboratory) cross sections, which diminish exponentially at low energies, from energies above 100 keV to the astrophysically relevant regime. As a result, this reaction rate is the most poorly known quantity in the entire nucleosynthetic chain that leads to ^{8}B. We are using the nuclear shell model to calculate this quantity. Our goal is to provide a better determination of this rate and thus to contribute to a clearer understanding of this rare, but crucial, solar fusion process and to more accurate estimates for the neutrino flux from our sun.

Microscopic substructure effects in potential-model descriptions of the ^{7}Be$(p,\gamma)^8$B reaction
(J. Escher, B.K. Jennings)

Cross sections of external capture reactions, such as ^{7}Be$(p,\gamma)^8$B at low energies, depend primarily on the asymptotic normalization of the bound-state wave function. The asymptotic normalization, however, is in turn connected to the short-distance behaviour of the wave function through the bound-state Lippmann-Schwinger equation. Hence microscopic substructure effects do play a role in the low-energy cross sections, and thus the astrophysical S factors, of such reactions. We investigate the relationship between potential models and the full many-body problem in order to understand how microscopic substructure effects affect the relevant transition matrix elements.

Partial dynamical symmetry in the symplectic shell model
(J. Escher; A. Leviatan, Hebrew Univ.)

In this extension of an earlier work, we present an example of a partial dynamical symmetry (PDS) in an interacting fermion system. We demonstrate the close relationship of the associated Hamiltonians with a realistic quadrupole-quadrupole interaction, thus shedding new light on this important interaction. Specifically, in the framework of the symplectic shell model of nuclei, we prove the existence of a family of fermionic Hamiltonians with partial SU(3) symmetry. We outline the construction process for the PDS eigenstates with good symmetry and give analytic expressions for the energies of these states and E2 transition strengths between them. Characteristics of both pure and mixed-symmetry PDS eigenstates are discussed and the resulting spectra and transition strengths are compared to those of real nuclei. The PDS concept is shown to be relevant to the description of prolate and oblate, as well as triaxially deformed, nuclei. Similarities and differences between the fermion case and the previously established partial SU(3) symmetry in the interacting boson model are considered.

Nuclear rotational motion and multi-$\hbar\omega$ correlations
(J. Escher)

Electron scattering observables for various deformed nuclei are calculated in the framework of the symplectic shell model, an algebraic theory, which treats the nucleus microscopically as a many-fermion system. Since the model takes the collective coherence between the major nuclear shells into full account, it correctly describes the static electromagnetic properties of nuclei without the need for effective charges. It also allows for an investigation of the influence of multi-shell correlations on nuclear charge and current densities. Such studies are important since they allow one to place quantitative limits on the contributions to the nuclear current from meson exchange. Furthermore, since electron scattering observables provide a direct probe of the nuclear current, this study is able to shed light on the dynamical character of nuclear rotational motion and thus it addresses one of the unsolved basic science problems of nuclear structure physics.

Effects of deformation on weak charge transfer transition strengths
(L. Zamick, TRIUMF/Rutgers; S.J.Q. Robinson, A. Mekjian, N. Auerbach, Rutgers)

In this work it is noted that many fundamental experiments are performed on complicated targets, e.g. ^{12}C which is highly deformed. We use sum rule techniques to show that the summed strength for the spin dipole contribution to neutrino capture is independent of deformation but the contributions to individual total angular momenta do depend on the deformation.

Nuclear structure and symmetries
(L. Zamick, TRIUMF/Rutgers)

We consider fermionic symmetries and establish the relationship between spectra of even-even and even-odd nuclei, especially those involving single and double analogue excitations. We have addressed the problem of higher shell admixtures, relativistic effects and self consistency in the nuclear shell model. We have looked at magnetic moments of excited states of nuclei in collaboration with the Rutgers and Bonn experimental groups.

Isospin and nuclear spectroscopy
(L. Zamick, TRIUMF/Rutgers)

We address the problem of what happens in nuclear spectroscopy when we set all isospin two-body matrix elements to zero. Despite the apparent severity of this approximation, we find fairly reasonable spectra with several degeneracies. We are able in part to explain these with some Regge symmetries for 6j symbols. This leads us to suggest that the energy difference of odd J states (not yet well studied experimentally) and the more familiar even J states will teach us about T=0 nucleon nucleon matrix element effects in a nucleus.

Active-sterile neutrino transformation and r-process nucleosynthesis
(G.C. McLaughlin)

The type II supernova is considered as a candidate site for the production of heavy elements. Since the supernova produces an intense neutrino flux, neutrino scattering processes will impact element formation. We

examine active-sterile neutrino conversion in this environment and find that it may help to produce the requisite neutron-to-seed ratio for synthesis of the r-process elements.

Few-Body and Medium Energy Processes

The one-pion-exchange three-nucleon force and the A_y puzzle

(W. Schadow; L. Canton, Padova)

We consider a new three-nucleon force generated by the exchange of one pion in the presence of a $2N$ correlation. The underlying irreducible diagram has been recently suggested by the authors as a possible candidate to explain the puzzle of the vector analyzing powers A_y and iT_{11} for nucleon-deuteron scattering. Herein, we have calculated the elastic neutron-deuteron differential cross section, A_y, iT_{11}, T_{20}, T_{21}, and T_{22} below break-up threshold by accurately solving the Alt-Grassberger-Sandhas equations with realistic interactions. The results indicate that this new $3NF$ diagram provides the possible additional contribution, with the correct spin-isospin structure, for the explanation of the origin of this puzzle.

Photonuclear reactions of three-nucleon systems

(W. Schadow; O. Nohadani, W. Sandhas, Bonn)

We discuss the available data for the differential and the total cross section for the photodisintegration of ^{3}He and ^{3}H and the corresponding inverse reactions below $E_\gamma = 100$ MeV by comparing with our calculations using realistic NN interactions. The theoretical results agree within the error bars with the data for the total cross sections. Excellent agreement is achieved for the angular distribution in the case of ^{3}He, whereas for ^{3}H a discrepancy between theory and experiment is found.

Why is the three-nucleon force so odd?

(W. Schadow; L. Canton, Padova)

By considering a class of diagrams which has been overlooked in the most recent literature on three-body forces, we extract a new contribution to the three-nucleon interaction which specifically acts on the triplet odd states of the two nucleon subsystem. In the static approximation, this $3N$-force contribution is fixed by the underlying $2N$ interaction, so in principle there are no free parameters to adjust. The $2N$ amplitude, however, enters in the $3NF$ diagram in a form which cannot be directly accessed or constrained by NN phase-shift analysis. We conclude that this new $3N$-force contribution provides a mechanism which implies that the presence of the third nucleon modifies the p-wave (and possibly the f-wave) components of the $2N$ subsystem in the triplet-isotriplet channels.

Isoscalar off-shell effects in threshold pion production from *pd* collisions

(W. Schadow; L. Canton, Padova)

We test the presence of pion-nucleon isoscalar off-shell effects in the $pd \to \pi^+ t$ reaction around the threshold region. We find that these effects significantly modify the production cross section and that they may provide the missing strength needed to reproduce the data at threshold.

Comparison of triton bound state properties using different separable representations of realistic potentials

(W. Schadow; W. Sandhas, J. Haidenbauer, A. Nogga, Bonn)

The quality of two different, separable expansion methods (W-matrix and Ernst-Shakin-Thaler) is investigated. We compare the triton binding energies and components of the triton wave functions obtained in this way with the results of a direct two-dimensional treatment. The Paris, Bonn A and Bonn B potentials are employed as underlying two-body interactions, their total angular momenta being incorporated up to $j \leq 2$. It is found that the most accurate results based on the Ernst-Shakin-Thaler method agree within 1.5% or better with the two-dimensional calculations, whereas the results for the W-matrix representation are less accurate.

Three-body scattering below breakup threshold: an approach without using partial waves

(W. Schadow; Ch. Elster, Ohio; W. Glöckle, Bochum)

The Faddeev equation for three-body scattering below the three-body breakup threshold is directly solved without employing a partial wave decomposition. In the simplest form it is a three-dimensional integral equation in four variables. From its solution the scattering amplitude is obtained as a function of vector Jacobi momenta. Based on Malfliet-Tjon type potentials, differential and total cross sections are calculated. The numerical stability of the algorithm is demonstrated and the properties of the scattering amplitude discussed.

Few-body states in Fermi systems and condensation phenomena

(W. Schadow; P. Schuck, Grenoble; M. Beyer, G. Röpke, A. Schnell, Rostok)

Residual interactions in many particle systems lead to strong correlations. A multitude of spectacular phenomena in many particle systems are connected to correlation effects in such systems, e.g. pairing, superconductivity, superfluidity, Bose-Einstein condensation, etc. Here we focus on few-body bound states in a many-body surrounding.

Three-nucleon portrait with pion
(W. Schadow; L. Canton, G. Pisent, Padova; T. Melde, J.P. Svenne, Manitoba)

We report on recent results obtained by the above collaboration on the collision processes involving three nucleons, where we pay particular attention to the dynamical role of the pion. After discussing the case at intermediate energies, where real pions can be produced and detected, we have considered the case at lower energies where the pions being exchanged are virtual. The study has revealed the presence of some new pion-exchange mechanisms, which leads to a new three-nucleon force of tensor structure. Recently, the effect of this tensor three-nucleon force on the spin observables for neutron-deuteron scattering at low energy has been analyzed, and will be briefly reviewed.

Spin observables for pion production from *pd* collisions
(W. Schadow; L. Canton, G. Pisent, Padova; J.P. Svenne, Manitoba)

We have calculated the proton analyzing power A_{y0} of the pion-production reaction from pd collisions for one energy close to threshold and for another in the region of the Δ-resonance. A fair reproduction of the experimental data could be obtained in both cases with a model which includes isoscalar and isovector πN rescatterings in s-waves, as well as the p-wave rescattering mechanisms mediated by the πNN and $\pi N\Delta$ vertices. For the analyzing power at threshold we found that the initial-state interaction (ISI) is also quite important.

Dressing the nucleon in a dispersion approach
(S. Kondratyuk; O. Scholten, Groningen)

We present a model for dressing the nucleon propagator and vertices. In the model the use of a K-matrix approach (unitarity) and dispersion relations (analyticity) are combined. The principal application of the model lies in pion-nucleon scattering where we find that effects of the dressing on the phase shifts can be significant. In addition to the nucleon and pion, we include other low-lying meson and baryon degrees of freedom, in particular the ρ and σ mesons and the Δ resonance. A good quantitative description of phase shifts can be achieved at the energies exceeding the scale due to the degrees of freedom explicit in the model.

Taking advantage of the known ambiguity in the choice of the interacting fields, we transform away the nucleon self-energy, which allows us to interpret effects of the dressing in terms of the πNN form factors. At large momenta squared of the off-shell nucleon, the dressed form factors decrease faster than the bare form factors. We find a large contribution of multiple meson loops.

Compton scattering in a unitary approach with causality constraints
(S. Kondratyuk; O. Scholten, Groningen)

Pion-loop corrections for Compton scattering are calculated in an approach based on the use of dispersion relations in a formalism obeying unitarity. The basic framework is developed, including an application to Compton scattering. In the approach, the effects of the non-pole contribution arising from pion dressing are expressed in terms of (half-off-shell) form factors and the nucleon self-energy. These quantities are constructed through the application of dispersion integrals to the pole contribution of loop diagrams, the same as those included in the calculation of the amplitudes through a K-matrix formalism. The resulting relativistic-covariant model combines constraints from unitarity, causality, and crossing symmetry. The prescription of minimal substitution is used to build a contact $\gamma\pi NN$ term and thereby to restore gauge invariance. We investigate the influence of the transverse part of the contact term on the γNN form factors.

We have found that the dependence of the form factors on the momentum squared of the off-shell nucleon deviates from a monopole- (or dipole-) like shape often adopted in phenomenological applications. In particular, a characteristic feature of our results is a cusp structure of the form factors in the vicinity of the pion production threshold, showing most clearly in the magnetic form factors corresponding to negative-energy states of the off-shell nucleon.

We discuss effects of the dressing on the f_{EE}^{1-} partial amplitude for Compton scattering on the proton, emphasizing the importance of the analyticity and unitarity constraints for understanding of the specific behaviour of the amplitude at the pion threshold.

Compton scattering on the nucleon at intermediate energies and polarizabilities in a microscopic model
(S. Kondratyuk; O. Scholten, Groningen)

A microscopic model is presented in which both polarizabilities of the nucleon as well as Compton scattering up to energies in the second resonance region can be calculated. To achieve a description over such a wide range of energies the model should obey the symmetries that are important in the different energy regimes. At the lowest energies, gauge invariance, CPT invariance and crossing symmetry are important for the model to obey low-energy theorems. At energies near the pion production threshold, unitarity and analyticity put strong constraints on the amplitude. Since a wide energy span needs to be described, it is most efficient to use a relativistic covariant model.

We have developed the approach called the "dressed K-matrix model". Since this model is based on a K-matrix formulation, unitarity (in the coupled channel space) and crossing symmetry are easily implemented. The kernel is formulated with dressed vertices and propagators such that certain analyticity constraints are incorporated. At the level of one-particle reducible diagrams, analyticity constraints are obeyed with small violations due to ignoring singularities of the regularization form factor, which are chosen far away from the regime of interest. On the other hand, analyticity is satisfied only approximately for one-particle irreducible diagrams. Gauge invariance is exact through the introduction of contact terms obtained by minimal substitution.

The parameters in the model Lagrangian are fixed from pion-nucleon scattering, pion photoproduction and Compton scattering. The requirement of convergence of the dressing procedure limits the allowed range of the parameters. We compare the results of the full calculation, utilizing the dressed vertices and propagators, with that in which these quantities are bare (the latter case corresponds to the conventional K-matrix approach). In general, the full calculation gives a considerable improvement in the description of the data. We also find that the dressing is important for reproducing both scalar and vector polarizabilities of the proton and neutron.

Approximations to the Bethe-Salpeter equation for pion-nucleon scattering
(A.D. Lahiff; I.R. Afnan, Flinders)

Over the past decade a number of meson-exchange models of pion-nucleon scattering have been developed. These models have all relied upon the K-matrix approximation, or approximated the 4-dimensional Bethe-Salpeter equation with a 3-dimensional quasipotential equation. Recently we have constructed a realistic model of pion-nucleon scattering based on the Bethe-Salpeter equation. In this work we compare the K-matrix approximation and several quasipotential equations to the Bethe-Salpeter equation. In particular, we consider the 3-dimensional Klein equation, which differs from other quasipotential equations in that the relative energy is integrated out, rather than being fixed by a δ-function.

A covariant model of pion photoproduction including final-state interactions
(A.D. Lahiff, S. Kondratyuk; V. Pascalutsa, Flinders)

We are constructing a microscopic model for pion photoproduction off the proton which should be applicable at photon energies up to around 1 GeV. The model is based on the 4-dimensional Bethe-Salpeter equation and fully takes into account final-state interactions. The approach should obey constraints from both unitarity and gauge invariance. We are studying the question of whether the various methods of imposing gauge invariance are applicable in the 4-dimensional unitary framework.

Quark-meson coupling model for a nucleon by using a density-dependent bag constant
(B.K. Jennings; S.W. Hong, Sungkyunkwan Univ.)

We considered the quark-meson coupling model for a nucleon. The model describes a nucleon as an MIT bag, in which quarks are coupled to the scalar and the vector mesons. A set of coupled equations for the quark and the meson fields are obtained and are solved in a self-consistent manner. We show that the mass of a dressed MIT bag interacting with σ- and ω-meson fields differs considerably from the mass of the free MIT bag. The effects of the density-dependent bag constant are investigated. We showed that including the density-dependent bag constant induces attraction and lowers the bag mass. The results of our calculations imply that the self-energy of the bag in the quark-meson coupling model is significant and needs to be considered in doing the calculations for nuclear matter or finite nuclei.

Radiative muon capture on ^{3}He
(E. Ho, H.W. Fearing)

A recent TRIUMF experiment has measured radiative muon capture in ^{3}He. The aim has been to measure the induced pseudoscalar form factor $g_P(q^2)$ over the range of four momentum transfer q^2 of the process and to test the Goldberger-Treiman relation which relates this form factor to the axial form factor g_A by the relation

$$g_P(q^2) = \frac{2m_N m_\mu g_A(0)}{m_\pi^2 - q^2}$$

where m_N, m_μ and m_π are respectively the masses of the nucleon, muon and pion.

We have used two approaches to analyze this process. One is the so-called "elementary particle method" which treats the helion, triton, muon, photon and neutrino as "elementary particles". This approach is easy but requires the *nuclear* form factors, which must be obtained from phenomenological form factors of both the helion and triton measured in other experiments or inferred using the conserved vector current hypothesis. The second method is the "impulse approximation" method. In this method the helion and triton are regarded as composed of 3 nucleons, and then a wave function for the three nucleons is derived for the nucleus. One then uses the wave function to calculate various observables. The input here comes from the *nucleon* form factors (at low momentum transfer) which

have been known quite accurately for a long time, but the approach is much more technically involved. The main new feature of our use of the impulse approximation is the evaluation of the wave functions and matrix elements in momentum space, in contrast to coordinate space which has normally been used.

Calculations for both ordinary and radiative muon capture have been performed, and a number of small improvements over existing calculations have been made. In general the results agree, to within a few per cent with previous calculations, given the same input. A variety of trinucleon wave functions (provided by W. Schadow) have been used. Both the IA RMC and OMC rates exhibit a slight model dependence (about 5%), arising from different binding energies and possibly different compositions of angular momentum eigenstates of the wave functions.

Effective Field Theories and Chiral Perturbation Theory

Contributions of the Δ resonance and the σ meson to low-energy constants of the fourth-order Lagrangian of HBChPT

(S. Kondratyuk, H.W. Fearing)

The resonance saturation hypothesis has been the principal method used to estimate values of the low-energy constants of the Lagrangian of heavy baryon chiral perturbation theory (HBChPT). Unfortunately, this approach yields rather large error bars for some of the fourth-order constants, which is mainly related to uncertainties in treating the Δ resonance contribution. In this study, a relativistic microscopic model is employed in order to extract values of fourth-order low-energy constants which are important for the description of low-energy Compton scattering. The model is based on the K-matrix formalism and obeys unitarity, crossing symmetry and gauge invariance. Also, certain analyticity constraints are incorporated through the use of dressed vertices and propagators in the K-matrix. The model yields a good quantitative description of pion photoproduction and Compton scattering at both intermediate and low energies.

The low-energy constants are estimated by comparing the predictions of the HBChPT for the nucleon polarizabilities with the values obtained from the model. The main source of errors in this procedure stems from the sensitivity of observables for photoproduction and Compton scattering to the coupling parameters in the $\Delta N\gamma$ and $\sigma\gamma\gamma$ vertices. We investigate effects of the Δ and σ couplings on the low-energy constants. While the values of the extracted low-energy constants are consistent with those obtained from the resonance saturation hypothesis, the present method yields smaller errors. This is due to the tight constraints imposed on the parameters of the model by the requirement of simultaneous description of pion photoproduction and Compton scattering in the extended energy range.

Proton-proton fusion in effective field theory

(X. Kong; F. Ravndal, Oslo)

The rate for the fusion process $p + p \rightarrow d + e^+ + \nu_e$ is calculated using non-relativistic effective field theory. Including the four-nucleon derivative interaction, results are obtained in next-to-leading order in the momentum expansion. This reproduces the effects of the effective range parameter. Coulomb interactions between the incoming protons are included non-perturbatively in a systematic way. The resulting fusion rate is independent of specific models and wave functions for the interacting nucleons. At this order in the effective Lagrangian there is an unknown counter term which limits the numerical accuracy of the calculated rate given by the squared reduced matrix element $\Lambda^2(0) = 7.37$. Assuming the counter term to have a natural magnitude, we estimate the accuracy of this result to be 6-8%. This is consistent with previous nuclear physics calculations based on effective range theory and inclusion of axial two-body weak currents. The true magnitude of the counter term can be determined from a precise measurement of the cross section for low-energy neutrino scattering on deuterons.

Neutrino deuteron scattering in effective field theory at next-to-next-to-leading order

(X. Kong; M. Butler, St. Mary's; J.-W. Chen, Maryland)

We study the four channels associated with neutrino-deuteron breakup reactions at next-to-next-to-leading order in effective field theory. We find that the total cross section is indeed converging for neutrino energies up to 20 MeV, and thus our calculations can provide constraints on theoretical uncertainties for the Sudbury Neutrino Observatory. We stress the importance of a direct experimental measurement to high precision in at least one channel, in order to fix an axial two-body counter term.

Proton-deuteron scattering in effective field theory

(X. Kong, G. Rupak)

Compared to the neutron-deuteron scattering calculation, the only difference in proton-deuteron scattering is the Coulomb effect. A formalism to treat the Coulomb effect in KSW counting has been introduced by Kong and Ravndal, and applied to proton-proton scattering and proton-proton fusion. Currently we are applying the formalism to include Coulomb effects in quartet S-wave proton-deuteron scattering.

Nucleon polarizabilities from Compton scattering on the deuteron
(G. Rupak; H.W. Griesshammer, TU München)

An analytic calculation of the differential cross section for elastic Compton scattering on the deuteron at photon energies ω in the range of 25–50 MeV is presented to next-to-next-to-leading order, i.e. to an accuracy of $\sim$3%. The calculation is model independent and performed in the low energy nuclear effective field theory without dynamical pions. The isoscalar, scalar electric and magnetic nucleon polarizabilities α_0 and β_0 enter as free parameters with a theoretical uncertainty of about 20%. Using data at $\omega_{\rm Lab} = 49$ MeV we find $\alpha_0 = 8.4 \pm 3.0(\text{exp}) \pm 1.7(\text{theor})$, $\beta_0 = 8.9 \pm 3.9(\text{exp}) \pm 1.8(\text{theor})$, each in units of 10^{-4} fm^3. With the experimental constraint for the isoscalar Baldin sum rule, $\alpha_0 = 7.2 \pm 2.1(\text{exp}) \pm 1.6(\text{theor})$, $\beta_0 = 6.9 \mp 2.1(\text{exp}) \mp 1.6(\text{theor})$. A more accurate result can be achieved by: (i) better experimental data, and (ii) a higher order theoretical calculation including contributions from a couple of so far undetermined four-nucleon-two-photon operators.

Threshold $pp \to pp\pi^0$ up to one-loop accuracy
(T.-S. Park; S.-I. Ando, South Carolina; D.-P. Min, SNU)

The $pp \to pp\pi^0$ cross section near threshold is computed up to one-loop order including the initial and final state interactions using the hybrid heavy baryon chiral perturbation theory. With the counter terms whose coefficients are fixed by the resonance-saturation assumption, we find that the one-loop contributions are quite important and bring our theoretical value of the cross section closer to the experimental data. The short-range contributions are treated by means of a cutoff, and only a mild cutoff dependence is observed when all diagrams of the given chiral order are summed. To the order treated, however, heavy baryon chiral perturbation theory converges rather slowly, calling for further studies of the process including going to higher orders.

Effective field theory for nuclei: confronting fundamental questions in astrophysics
(T.-S. Park; K. Kubodera, USC; D.-P. Min, SNU; M. Rho, Saclay)

Fundamental issues involving nuclei in the celebrated solar neutrino problem are discussed in terms of an effective field theory adapted to nuclear few-body systems, with a focus on the proton fusion process and the hep process. Our strategy in addressing these questions is to combine chiral perturbation theory – an effective field theory of QCD – with an accurate nuclear physics approach to arrive at a superior effective field theory that reveals and exploits a subtle role of the chiral-symmetry scale in short-distance effects encoded in short-range nuclear correlations. Our key argument is drawn from the close analogy of the principal weak matrix element figuring in the hep process to the suppressed matrix elements in polarized neutron-proton capture at threshold currently being measured in the laboratories.

Asymmetry in $\vec{n} + p \to d + \gamma$
(T.-S. Park; C.H. Hyun, D.-P. Min, SNU)

Heavy baryon chiral perturbation theory (HBChPT) is applied to the asymmetry A_γ in $\vec{n} + p \to d + \gamma$ at threshold, which arises due to the weak parity non-conserving interactions. Instead of appealing to Siegert's theorem, transition operators up to next-to-leading chiral order are derived and the corresponding amplitudes are evaluated with the Argonne v_{18} wave functions. In addition to the impulse contribution, both parity-conserving and parity-non-conserving two-body one-pion-exchange diagrams appear up to this order. Our prediction for the asymmetry is $A_\gamma = -0.10 h^{(1)}_{\pi NN}$, which is close to the Siegert's theorem based result, $A_\gamma \simeq -0.11 h^{(1)}_{\pi NN}$. This illustrates that HBChPT is effective in parity-non-conserving physics.

In-medium effective pion mass from heavy-baryon chiral perturbation theory
(T.-S. Park; H. Jung, Sookmyung Women's Univ.; D.-P. Min, SNU)

Using heavy-baryon chiral perturbation theory, we have calculated all the diagrams up to two-loop order which contribute to the S-wave pion self-energy in symmetric nuclear matter. Some subtleties related to the definition of pion fields are discussed. The in-medium pion mass turns out to be increased by only 6$\sim$7 per cent in normal nuclear matter density, without any off-shell ambiguity.

The KN sigma term
(T.-S. Park, A. Olin; F. Myhrer, USC)

The experimental data for the differential cross section of K^+p elastic scattering has been re-analyzed and compared to the NLO HBChPT calculation, which gives us the opportunity to extract the KN sigma term directly from the data.

Further analysis of the chiral perturbation theory meson Lagrangian to order p^6
(H.W. Fearing; T. Ebertshäuser, S. Scherer, Mainz)

Some time ago Fearing and Scherer wrote down systematically the most general Lagrangian density for mesonic ChPT of chiral order $\mathcal{O}(p^6)$, both for the normal (non-epsilon) and anomalous (epsilon) sector.

By setting up a somewhat different (and extended) approach, which is based on the use of different basic building blocks, and implementing the so-called Bianchi identities for field strength tensors, and additional trace relations, we derived a modified list containing slightly fewer independent $SU(n)$ terms than originally obtained. We also obtained explicitly its reduction to $SU(2)$ and $SU(3)$.

By rewriting (expanding) the compact structures in terms of conventional Goldstone boson and external fields, we were able to assign (at least half of) the anomalous $SU(3)$ low-energy constants to measurable physical processes and provide the respective Lagrangian densities.

Radiative pion capture by a nucleon
(H.W. Fearing; T.R. Hemmert, Jülich; R. Lewis, Regina; C. Unkmeir, Mainz)

We have calculated in heavy baryon chiral perturbation theory (HBChPT) the differential cross sections for $\pi^- p \to \gamma n$ and $\pi^+ n \to \gamma p$ up to $\mathcal{O}(p^3)$. The results at $\mathcal{O}(p)$ and $\mathcal{O}(p^2)$ have no free parameters. There are three unknown parameters at $\mathcal{O}(p^3)$, low energy constants of the HBChPT Lagrangian, which are determined by fitting to experimental data. Two acceptable fits are obtained, which can be separated by comparing with earlier dispersion relation calculations of the inverse process. Expressions for the multipoles, with emphasis on the p-wave multipoles, are obtained and evaluated at threshold. Generally the results obtained from the best of the two fits are in good agreement with the dispersion relation predictions.

Pion doubly radiative processes in heavy baryon chiral perturbation theory
(H.W. Fearing; C. Unkmeir, S. Scherer, Mainz)

We are calculating the processes $\pi + p \to n + \gamma + \gamma$ and $\gamma + p \to n + \pi + \gamma$ in heavy baryon chiral perturbation theory. Both processes contain as subdiagrams the reaction $\gamma + \pi \to \gamma + \pi$, i.e. pion Compton scattering. Thus in principle they may give some of the same information, such as pion polarizabilities, as would be obtained by a direct measurement, which is not really possible to do. The calculations are of interest also as the capture reaction has been measured at TRIUMF and the scattering reaction is under investigation at Mainz. We are calculating to $\mathcal{O}(p^3)$, that is to one loop order, in a way which allows us to check gauge invariance explicitly. The amplitude to $\mathcal{O}(p^2)$ has been obtained, most of the subsidiary processes necessary to evaluate the low energy constants have been completed, and efforts are now directed to completing the $\mathcal{O}(p^3)$ pieces.

Infrared regularization in ChPT
(C. Bird, H.W. Fearing)

When chiral perturbation theory is used to study reactions involving massive particles, the standard power counting is not valid. As a result other methods were developed, such as heavy baryon chiral perturbation theory (HBChPT). However HBChPT involves an additional series expansion of each term in the original Lagrangian and the complexity of the calculations has limited most prior work in this field to $\mathcal{O}(p^3)$.

We have been studying an alternative method, infrared regularization (IR), in which the original relativistic chiral Lagrangian is used and the loop integrals are divided into high energy and low energy components. The high energy loop integrals are absorbed into the low energy constants, while the low energy loop integrals are calculated explicitly. Using this new regularization, power counting can be recovered while maintaining the simplicity of the relativistic Lagrangian. In order to study IR and compare the results with HBChPT, we are also using IR to calculate several simple reactions at $\mathcal{O}(p^4)$ including pion photoproduction and radiative pion capture.

Hadronic Structure and QCD

Masses of heavy baryons
(N. Mathur, R.M. Woloshyn; R. Lewis, Regina)

The spectrum of baryons containing one or two heavy (b or c) quarks is calculated using improved lattice QCD in the quenched approximation. The calculations are being done in two different ways. In one approach, a relativistic action of the D234 type is used for light (up, down, strange) and charm quarks. A second calculation uses lattice NRQCD for charm and bottom quarks. One of the goals is to compare relativistic and non-relativistic treatments in the charm sector where the spectrum of charmonium, for example, has been found to be quite sensitive to higher order terms in the lattice NRQCD expansion.

***S*- and *P*-wave heavy-light mesons**
(R.M. Woloshyn; R. Lewis, Regina)

The mass spectrum of S- and P-wave mesons containing a single heavy quark was computed in the quenched approximation, using NRQCD up to third order in the inverse heavy quark mass expansion. Previous results found third order contributions which were as large in magnitude as the total second order contribution for the charmed S-wave spin splitting. We have considered variations such as anisotropic lattices, Landau link tadpole improvement, and a highly-improved light quark action, and find that the second order correction to the charmed S-wave spin splitting is about 20% of the leading order contribution,

while the third order correction is about 20%(10%) for $D^*-D(D_s^*-D_s)$. Nonleading corrections are very small for the bottom meson spectrum, and are statistically insignificant for the P-wave charmed masses.

Strange magnetic moment of the nucleon
(N. Mathur; S.-J. Dong, K.-F. Liu, Kentucky)

Recently there has been considerable interest in the strange magnetic moment of the nucleon ($G_M^s(0)$) as it can provide important information about the internal quark structure of the nucleon. There are numerous theoretical predictions over a wide range, –0.75 to $+0.30\ \mu_N$. Most of them are negative and are in the range -0.45 to -0.25. On the other hand, recent experiments of the SAMPLE collaboration on parity violating electron scattering suggest that the strange magnetic moment of the nucleon could be positive. Two of their recent results are $G_M^s(Q^2 = 0.1\,\mathrm{GeV}^2) = +0.23 \pm 0.37 \pm 0.15 \pm 0.19\,\mu_N$ and $+0.61 \pm 0.17 \pm 0.21 \pm 0.19\,\mu_N$. However, combined with data from the deuteron, the new result is closer to zero with a relatively larger error. To get the lattice QCD input on this yet unsettled problem of strange magnetic moment content of the nucleon, we extend our previous lattice calculation. We calculate the strange magnetic moment of the nucleon on a quenched $16^3 \times 24$ lattice at $\beta = 6.0$, and with Wilson fermions at $\kappa = 0.148$, 0.152 and 0.154. The strange quark contribution from the disconnected insertion is estimated stochastically by employing the Z_2 noise method. Using an unbiased subtraction along with the help of charge conjugation and hermiticity, we reduce the error by a factor of 2 with negligible overhead. Our result is $G_M^s = -0.28 \pm 0.10\ \mu_N$.

Perfect lattice action for $SO(N)$ spin model
(N. Mathur)

Non-linear sigma models are particularly interesting as they can provide important information about asymptotically free theories, like QCD. A perfect lattice action for $O(3)$ non-linear sigma model was studied sometime earlier by Hasenfratz and Niedermayer. Following their track, we investigate a perfect lattice action for the $SO(N)$ non-linear sigma model (with $N = 3$) which is asymptotically free in $1 + 1$ dimensions. We observe that along with two-point couplings, four-point couplings of the $SO(N)$ matrix spin model are equal to those of the $O(N)$ vector spin model. With a few couplings, rotational invariance is seen to be fully restored even on a small lattice. By calculating the Lüscher step scaling function, we also investigate the degree of perfection for the fixed-point action of this model.

Status report on lattice QCD and QCD sum rule determinations of the light quark masses
(K. Maltman, TRIUMF/York; R. Gupta, LANL)

At present, the light quark masses are among the least well known of the fundamental parameters of the standard model. Very recent work, from both the QCD sum rule and lattice QCD perspective, has produced significant improvement in this situation. We have performed a number of new sum rule calculations to elucidate the role of direct instanton effects, previously neglected in pseudoscalar sum rule treatments, and updated previous sum rule analyses to correspond to the latest data sets in the case of analyses based on flavour breaking in hadronic tau decay. These are combined with existing work to form an extensive review of the current situation. We find that, not only are all QCD sum rule analyses consistent within errors, and all lattice QCD analyses consistent within errors, but the two approaches are now also highly consistent. The result is a determination of m_u, m_d, and m_s with errors more than a factor of 2 smaller than those of PDG2000. We also show how the errors can be further reduced in the near future.

Vacuum condensates and finite energy sum rules
(K. Maltman, TRIUMF/York; G. Golowich, Massachussetts)

Using soft pion techniques, valid in the chiral limit, it was recently shown that the chiral limit value of the matrix element of the electroweak penguin operator, which plays an important role in determining the standard model contribution to ϵ'/ϵ, is related to dimension 6 vacuum condensates which appear in the OPE representation of the light quark isovector V-A correlator difference. The extraction of these condensate values from experimental data can, in principle, allow a significant improvement in the situation of the understanding of the value of this matrix element. Finite energy sum rule (FESR) techniques are being employed to make this extraction, the freedom in the choice of weight function being crucial to making a reliable extraction in which possible contributions from yet higher dimension operators are brought under control.

Extraction of r_s
(K. Maltman, TRIUMF/York; J. Kambor, Zurich)

The ratio, r_s, of the s and u (or d) quark condensates is a dynamical quantity in QCD which cannot be predicted beyond leading order in chiral perturbation theory (ChPT) since it involves the chiral low energy constant, H_2, which depends on the conventions employed to regularize the quark condensate in the un-

derlying theory (QCD), and hence cannot be determined experimentally. Once one determines this ratio, however, the isospin-breaking deviation of the ratio of u and d condensates from 1, which enters sum rule treatments of various isospin-breaking observables, is uniquely determined by ChPT. In some models, such as the extended NJL model, used extensively to estimate matrix elements of the operators of the effective strangeness-changing weak Hamiltonian, r_s is, in fact, significantly greater than 1. Thus, there are a number of phenomenologically important reasons for wishing to have a good determination of r_s. We have studied sum rules involving the difference of the transverse part of the flavour ud and us vector-plus-axial-vector correlator sum, with an aim to constructing FESRs which allow a theoretically optimal extraction of the product of the strange quark mass and strange condensate. Although the rather large ($\sim$20–30%) errors on the strange spectral distribution measured in hadronic tau decay above $\sim$1 GeV limit the accuracy of this extraction at present, the increase of nearly two orders of magnitude in the usable tau sample which should become available over the lifetime of an experiment like BaBar will make this a very useful method for determining r_s in the future.

Finite energy sum rule extraction of the decay constants of pseudoscalar mesons
(K. Maltman, TRIUMF/York; J. Kambor, Zurich)

The relative strengths of the couplings of hadronic states to different probes (currents or densities) can provide very useful information on spectroscopic classification. We are in the process of studying the FESR extraction of the decay constants describing the coupling of the excited strange and non-strange pseudoscalar mesons (the $\pi(1300)$, $\pi(1800)$, $K(1460)$, and $K(1830)$) to the vacuum through the relevant pseudoscalar densities. This will play a role in improving the reliability of the determination of the light quark masses from hadronic τ decay data (this is a rather technical point, and cannot be easily elaborated on in this short space), and also help to shed light on the excited η sector, whose couplings to the 8th member of the pseudoscalar density will be similarly computed, using also ChPT input, in the future.

The Standard Model and Beyond

Constraints on *T*-odd, *P*-even interactions from electric dipole moments
(G.C. McLaughlin; A. Kurylov, M.J. Ramsey-Musolf, Connecticut)

We construct the relationship between non-renormalizable, effective, time-reversal violating (TV) parity-conserving (PC) interactions of quarks and gauge bosons and various low-energy TVPC and TV parity-violating (PV) observables. Using effective field theory methods, we delineate the scenarios under which experimental limits on permanent electric dipole moments (EDMs) of the electron, neutron, and neutral atoms, as well as limits on TVPC observables, provide the most stringent bounds on new TVPC interactions. Under scenarios in which parity invariance is restored at short distances, the one-loop EDM of elementary fermions generate the most severe constraints. The limits derived from the atomic EDM of ^{199}Hg are considerably weaker. When parity symmetry remains broken at short distances, direct TVPC search limits provide the least ambiguous bounds. The direct limits follow from TVPC interactions between two quarks.

Neutrinos in extra dimensions and the anomalous magnetic moments of leptons
(G.C. McLaughlin, J.N. Ng)

The use of extra dimensional scenarios as models for neutrino mass affects many low energy observables. We consider the implications of virtual bulk neutrinos in precision experiments of the anomalous magnetic moments of the muon and the electron. We consider neutrino models in factorizable geometry of the type $M_4\times$ T as well as the sliced AdS_5 non-factorizable geometry. In both geometries we find finite contributions to g-2 after summing over the KK excitations of the bulk neutrinos. In the case of Randall-Sundrum geometry, we find that the muon experiment is approaching the precision necessary to probe these models.

The use of nuclear beta decay as a test of bulk neutrinos in extra dimensions
(G.C. McLaughlin, J.N. Ng)

Theories which include neutrinos in large extra dimensions can be constrained by nuclear beta decay experiments. We examine universality of beta decay strengths of Fermi transitions. From this we find that the extra dimensional Yukawa coupling for a higher dimensional scale of 10 TeV and two extra dimensions can be constrained to $y < 1$. Kinematic implications are also discussed. In particular, an extra dimensional scenario will produce a tritium decay endpoint spectrum with a different shape than that for just one massive state.

Higgs physics and extra dimensions
(J.N. Ng; V. Chang, Normal Univ., Taiwan)

We embed the standard model in the Randall-Sundrum model of 5 dimensional brane localized gravity. The SM gauge and chiral fermion fields are restricted on the 4D visible brane, whereas the Higgs and the right-handed neutrino are assumed to be 5D bulk fields. We calculate the effective couplings of the

lowest mass Higgs field to the SM fermions and to the gauge bosons and find that the couplings are enhanced. Furthermore, the invisible decay width of a bulk Higgs of mass 150 GeV is shown to be large.

CP violation and B physics
(J.N. Ng; Y. Zhou, Y.L. Wu, C.Q. Geng, ITP Beijing)

We present a general analysis on charmless B-meson decays $B \to \pi\pi$ and πK. It is noticed that the final state interactions and inelastic rescattering effects must be significant in order to understand the consistency of the current data. As a consequence, the isospin amplitude $a^c_{3/2}$ and the strong phase δ are found to be unexpectedly large: $a^c_{3/2} \simeq -(40 \sim 100)$, $\delta \simeq \pm(93^\circ \pm 6^\circ)$. With such a large value, it is shown that the weak phase γ is allowed to be smaller so as to be consistent with the other constraint from the standard model. While in the standard model it seems difficult to enhance $a^c_{3/2}$ by an order of magnitude. If the usual assumption on relations for strong phases is reliable, our analysis indicates that either the current measured central values of the branching ratios of decay modes $B \to \pi^0 K$ are larger than the actual values, or new physics may be necessary to provide large contributions which effectively enhance the electroweak penguins. Using current data, the branching ratio for $B \to \pi^0\pi^0$ is found to be larger by an order of magnitude compared to the one calculated based on the factorization approach. We also present the direct CP violating asymmetries in all the decay modes and find them to be close to the sensitivity of the present experiments.

Miscellaneous

Strangelets in the cosmic ray flux
(S.K. Ghosh; S. Banerjee, S. Raha, D. Syam, Calcutta)

We have shown that our proposed mechanism for strangelet propagation through the earth's atmosphere, together with a proper account of charge capture and ionization loss, would solve the problem of the requirement of unusually high penetrability of strangelets through the terrestrial atmosphere. Furthermore, this could lead to viable strategies for definitive detection of strange quark matter in the cosmic ray flux using a ground based, large area array of passive detectors.

Cosmological quark-hadron transition and massive compact halo objects
(S.K. Ghosh; A. Bhattacharyya, S. Banerjee, S. Raha, B. Sinha, Calcutta)

One of the abiding mysteries in the so-called standard cosmological model is the nature of the dark matter. It is universally accepted that there is an abundance of matter in the universe which is non-luminous due to its very weak interaction, if at all, with the other forms of matter, excepting of course the gravitational attraction. Speculations as to the nature of dark matter are numerous, often bordering on the exotic, and searches for such exotic matter is a very active field of astroparticle physics. Nevertheless, in recent years, there has been experimental evidence for at least one form of dark matter – the massive compact halo objects detected through gravitational microlensing effects proposed by Paczynski some years ago. To date, there is no clear consensus as to what these objects are. They are referred to in the literature by the acronym MACHO. In our work, we show that these objects may find a natural explanation as leftover relics from the putative first order cosmic quark-hadron phase transition that is predicted by the standard model of particle interactions to have occurred during the microsecond epoch of the early universe.

Bosonic symmetries and pionic fluctuations and correlations
(A.Z. Mekjian, TRIUMF/Rutgers)

Pionic yields, fluctuations and correlations are studied in a general framework based on a cycle class picture associated with bosonic symmetries. Various models such as the disoriented chiral condensate, the negative binomial distribution, partially coherent state emission and field emission from Lorentzian line shapes are discussed. Generalizations based on these important specific cases are developed. Connections of the cycle class picture developed from a path integral approach with other approaches based on combinants, cumulants, hierarchical models and clan variables are presented for the specific and general cases.

EXPERIMENTAL FACILITIES

Proton Irradiation Facility
(E.W. Blackmore, TRIUMF)

There were two extended runs of the proton irradiation facility (PIF) in August and December, with both the BL2C and BL1B test areas available. In addition there were several shorter runs at lower energies on BL2C which were used for calibrations and to allow the University of Alberta group to check the single event upset rate in their FPGA devices for the ATLAS calorimeter readout.

For the August run the users were from DREO in Ottawa, DERA in the UK, and MD Robotics in Brampton. In addition to proton runs at energies from 20 to 500 MeV, an attempt was made to use the BL4B CHARGEX facility to provide a monoenergetic neutron beam at 280 MeV. Calibration of the neutron beam had been carried out previously using the SASP spectrometer to measure the neutron energy spectrum via the (n, p) reaction on liquid hydrogen. The single event upset cross section of a memory device was measured in the neutron beam and compared with protons of the same energy. The uncertainty in the low energy neutron tail precluded a definitive result and further studies are planned. In addition a biological dosimetry experiment was carried out in which samples of human blood were exposed to high energy protons and to spallation neutrons produced by stopping 500 MeV protons in a steel block.

In December a high intensity irradiation set-up was commissioned on BL1B to permit small devices to be exposed to fluences up to 10^{13} protons/cm^2 in a reasonable time. There is a similar test set-up on BL2C for energies of 110 MeV and below. This capability permitted a group from DREO to measure the light output and I-V characteristics of quantum well LEDs when irradiated with protons from 50 to 500 MeV with fluences from 10^{10} to 10^{13} protons/cm^2.

A poster describing the 20–500 MeV proton irradiation facility at TRIUMF was presented at NSREC 2000 in Reno. Several potential new users of the TRIUMF facility were identified. The next meeting of this conference on nuclear and space radiation effects will be held in Vancouver in July, 2001. There is considerable interest in the space effects community in comparing the single event effect cross sections for protons with those of higher LET heavy ions. At the request of MD Robotics, a calculation using LAHET and a simple Monte Carlo routine was made to determine the LET spectrum of heavy ion recoils produced by protons of 50–500 MeV interacting with silicon. The result can then be used to determine the LET level that proton testing reaches as a function of incident proton energy.

Proton Therapy Facility
(E.W. Blackmore, TRIUMF)

A total of 6 patients with ocular melanoma were treated during 2000, bringing the total number treated at TRIUMF to 60. As mentioned in last year's Annual Report, the reduced number of patients in the last couple of years is due to fewer operating months of the cyclotron and to some changes in the selection criteria. Radioactive plaque therapy is carried out by the same group and is the treatment of choice if feasible. A recent review of plaque therapy carried out at the British Columbia Cancer Agency has indicated extremely good results for the treatment of ocular melanoma, and with low toxicity. Where the location and size of the tumour preclude plaque therapy, proton therapy is used.

There were no significant changes made to the treatment equipment during the year. One of the Exradin T1 calibration ion chambers developed a loose cap and had to be replaced.

μSR User Facility
(S. Kreitzman, TRIUMF)

The μSR facility coordinated a very productive year for its users during this millennial year. 19 groups (9 of which are Canadian university based) took a total of 77 beam weeks, 6 of which were for β-NMR. The beam delivery schedules that allowed for this (historically) increased availability of high intensity beam time were TRIUMF's successful endeavour to allow its user community to recoup the beam time lost in the previous year due to unanticipated shutdowns.

The major facility developments which highlighted the year were:

- Successful inauguration of the β-NMR facility.
- Application for a new magnet for the high timing resolution/high field spectrometer.
- Redesign of Helios spectrometer and stand.
- Integration of new technical and software staff.

The following report outlines these and related developments more fully.

β-NMR

The maiden voyage of the (user facility supported) β-NMR experiment occurred during this year. This ISAC experiment boasted a huge array of new systems ranging from broad-band rf field coils, ultra-high vacuum systems and cryostat, to laser pumped ^{8}Li nuclear polarization. Remarkably, the very first data run when everything was finally set up (with a ^{8}Li production rate of about 10^8/sec) produced a huge resonance with

signal/noise of about 50 in only 20 seconds of data-taking. It is clear from this data that β-NMR at TRIUMF can accumulate high quality data as quickly and efficiently as its more well established μSR big brother.

Spectrometers

Helios

Helios is a general purpose 6 T spectrometer used for transverse field (below 2 T) and longitudinal field (LF) studies. In this era of increasingly small samples, prompted by intense interest in high-T_c superconductors, the capability to precisely align samples and beam trajectories and counters is essential. To this end, a highly rigid and reproducible stand has been designed for the Helios magnet (see Fig. 111) so that beam, counter and sample geometries can be precisely matched without having to manually realign after an access event into the system.

OMNI′

The increased interest in studying LF relaxation in confined materials (i.e. those systems that require relatively thick walls, such as systems under pressure) has prompted us to begin a redesign of the OMNI′ spectrometer so that it will be ideally suited to this task. This redesign will again allow the rapid set up of a rigid and reproducible counter array, with integrated shielding and cryostat support mechanisms. The system is designed to easily accommodate the majority of experiments that we historically deal with on the M9B beam line so that experimental set-ups and changes proceed much more quickly and efficiently.

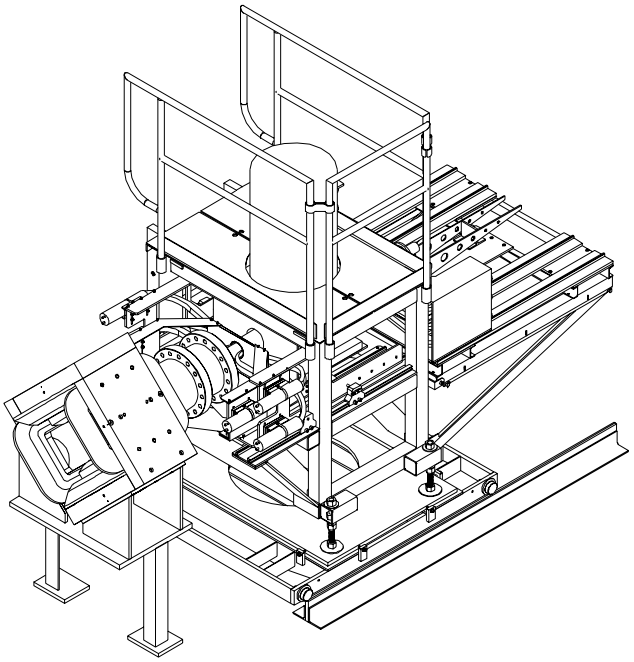

Fig. 111. The design for the new Helios stand provides a highly stable platform for superior alignment and reproducibility in the era of μSR on increasingly small samples.

It's HiTime for Belle

With the introduction of the world's only production μSR high field/high timing resolution (HTF/HTR) spectrometer over the last two years (our Belle spectrometer), not only has demand for experimental beam time on this rig burgeoned but users are also requesting experimental accuracy and precision that the Belle magnet simply cannot provide. Originally this magnet (utilized historically by Bell Labs) was loaned to us by Physikon Research to allow us to attempt building the HTF/HTR spectrometer. With technical aspects of the spectrometer (i.e. its timing resolution in high field) working well, the users have started to request magnetic field characteristics such as low drift (1 G/day) and 0.1 G homogeneity which the Belle magnet simply cannot provide. To this end a new magnet has been commissioned from American Magnetics that will exceed all the requirements that one can foreseeably require of an HTF/HTR spectrometer. This magnet's name will be HiTime and should be in service for the 2001 fall schedule.

Third generation low background inserts

Responding to user demand for effective means of carrying out clean μSR experiments on samples with sizes of the order of 1–2 mm in diameter, the facility has entered a development cycle for a new generation of low background inserts. These inserts utilize the experience gained with previous *in cryostat counter* low background systems and comprise an active collimator, muon counter, plus muon and positron vetoes; all within the cryostat in a very tight geometry. The sample is cold loadable and can be changed without system disassembly.

Software and facility documentation

Data analysis platform migration

The data analysis platform has largely been migrated to Linux based computers. All of the familiar tools, i.e. spect, fft, db, msrfit, will be available on the Linux cluster. Also, the μSR data archive has now moved to the μSR server which also provides the cpu power for the Web based portals below.

Web based data tools

Connecting to http://musr.triumf.ca/mud allows anyone to search, display and fft any data in our archive. The addition of interactive fitting is still in the works.

New look Web site

http://musr.triumf.ca will soon be officially opened as our new portal to the world.

Beam Lines

(C. Ballard, TRIUMF)

The Beam Lines group is part of the Science Division and is responsible for the installation, alignment and maintenance of the experimental facilities at TRIUMF. This year has seen the group evolve in three distinct directions. One avenue was to supply technical assistance to the existing experiments and secondary channels in the meson hall, and the other two projects were ISAC and CERN.

In ISAC, the end of 2000 saw the completion of the MEBT installation and the alignment of the DTL triplets and tanks – resulting in beam through the DTL. In parallel, the group assisted on the LEBT installation including the polarizer leading to the β-NMR platform. The next priorities were the β-NMR, 8π, DRAGON and TUDA experiments. The installation of the high voltage platform for the β-NMR experiment included the fence, interlocks and isolation transformer. The gas target was assembled for DRAGON, and the quadrupoles and bending magnets were installed in the HEBT, DRAGON and TUDA beam lines. The next major project was the assembly and alignment of DRAGON's electrostatic dipoles and installation of DRAGON's electrical, plumbing and vacuum services. The success in ISAC was, in part, achieved through the coordinated efforts of the Science Division, Cyclotron Division, and trades people with the assistance of three University of Victoria co-op students and three summer students.

In the meson hall, efforts were focused on maintenance and the preparations for the TWIST experiment in M13. The maintenance included an overhaul of the M9 separator, repairs to the M15 separator, M13 jaws, M9 beam blocker, and the TNF. The group also performed preventative maintenance on the water packages, vacuum systems and magnet interlocks. Included in the meson hall project was the ongoing technical assistance to the proton irradiation facility, proton therapy, and the experimental support in the proton hall.

The CERN Collaboration involved three technicians on two projects. The most significant of these was the beginning of the assembly of nine pulse forming network (PFN) tanks, which required the installation of a clean area with an overhead crane. This project will continue for the next five years. The other projects for CERN were the fabrication of the fast wire and fast blade scanners.

The Beam Lines group was also responsible for many of the alignment projects on site. There have been significant changes in the methods of alignment with the acquisition of the new total station which uses electronic distance measurement (EDM) and target recognition to download coordinates to a PC.

Cryogenic Targets

(C. Marshall, TRIUMF)

Ongoing experiments

Several scheduled experiments used liquid hydrogen or deuterium targets which had been built in previous years. Although only minor target improvements were undertaken, operations during 27 target-weeks of scheduled beam took up a large part of the group's efforts in 2000. Targets were in use on CHAOS (Expt. 778), parity (Expt. 761) and RMC (Expt. 864), with no extended down-times.

Design of new targets

Experiment 744: The liquid hydrogen target must operate inside the RMC detectors, allowing clean transmission of a pion beam. There must be a minimum of material along the sides of the target, where electrons of interest in the experiment exit from the interaction region. It is proposed to use a low-mass honeycomb material for the side walls. Testing of a prototype using this material has started. Entrance and exit windows will be of formed mylar.

Experiment 875: This experiment studies multiple scattering of muons in various materials, including liquid hydrogen. The liquid hydrogen target will be in the form of a cylinder with a horizontal axis, measuring 9 cm in diameter by 10 cm long, contained within a metre long evacuated scattering chamber. A conceptual design has been completed.

Computing Services

(C. Kost, TRIUMF)

Overview

Most of the approximately 800 networked devices at TRIUMF have been moved off the old FDDI token ring to the new gigabit backbone. Security concerns, hardware maintenance/upgrades, software management, and dealing with migration to a central mail system were all exacerbated by the rapid increase in the number of PC-based Linux systems. There is a strong need to minimize the number of Linux flavours and/or operating system versions in order to provide centralized software support and security. The contribution of our group to the GEANT4 collaboration continues to show benefits to all parties involved.

Modular approach to integration

Using a modular approach, our group has attempted to provide an integrated environment for the computing community. The main modules are now:

- a dual VAX-4100 VMS cluster to provide legacy support;
- public computing facilities for Linux;

- public computing facilities for Alphas running Compaq Tru64;
- a VALinux computer with DLT-8000 tape drive to provide daily site Linux/UNIX backup;
- a Linux computer with hardware RAIDed disk to provide a central mail facility;
- a Linux computer to act as the site Web server and common Linux/Tru64 software repository;
- a Linux computer to act as the site UNIX/Linux/SGI print server;
- a Windows NT computer to act as the print and file server for site PCs;
- a Windows NT computer to allow up to 15 X-sessions to run Windows applications;
- a Novell/Netware server to backup site Windows-based PCs;
- a Linux computer to provide centralized security logging.

Some of the advantages of using this modular approach were improved stability of each module, ease of management of each module, and decreased interdependency of the modules. A disadvantage was the increased hardware costs (albeit, hardware constitutes but a small fraction of the overall costs).

Hardware

Figure 112 shows the annual update for the growth in CPU power. The solid line shows the historical

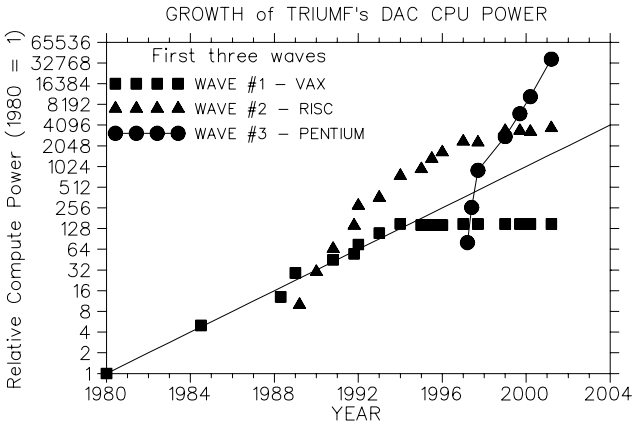

Fig. 112. Core computing growth.

doubling every two years. Technology shifts have resulted in CPU power growth considerably larger than expected. The latest data for Pentium (i.e. Linux) now include a somewhat larger group of users than in the past, accounting for a larger than expected growth for the year 2000.

The most significant hardware change this year was the switchover from FDDI to gigabit Ethernet. Figure 113 illustrates how the 23 Nortel Networks Baystack 450-24T switches were strategically located around the site. The switchover of hundreds of network connected devices, from essentially

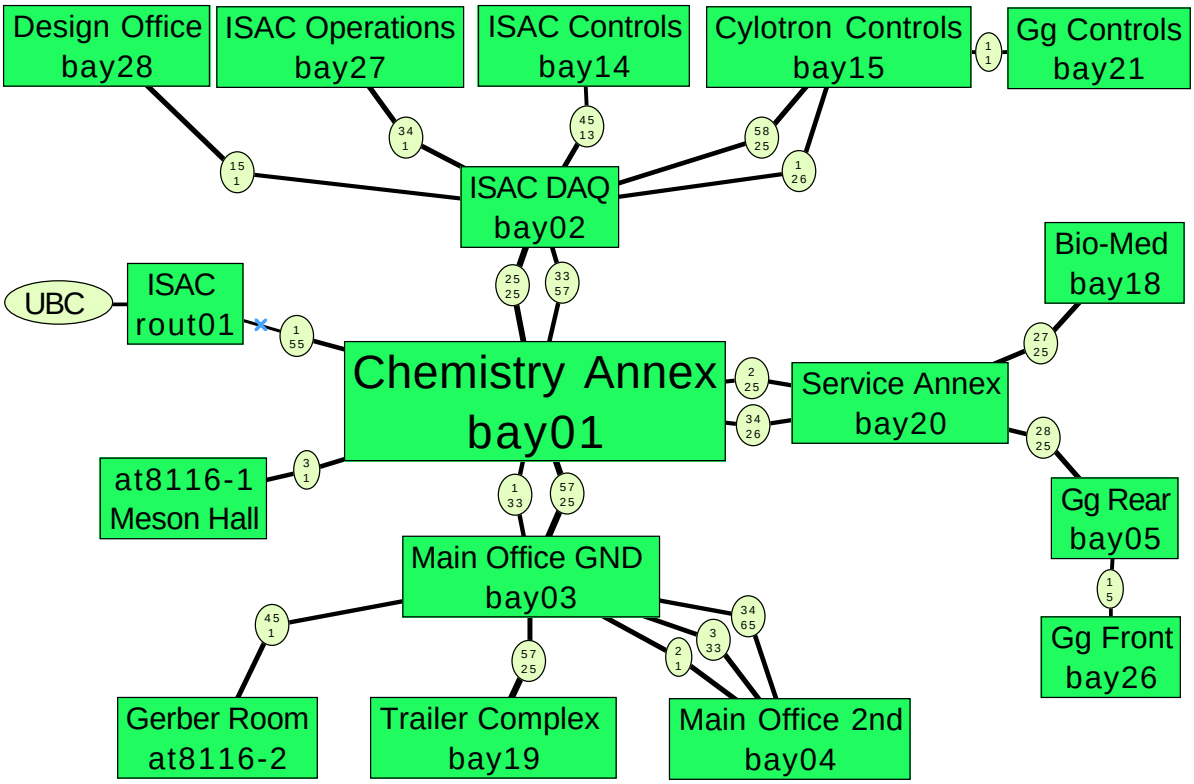

Fig. 113. Gigabit network.

10Base-T to 100Base-T connections, went very smoothly. Other significant hardware changes implemented by our group were:

- A much earlier upgrade, than was originally planned, of the RAID disks attached to our central mailer, trmail. Increases in the size of mail messages (as more of them include large attachments), as well as increased activity and diversity in the use of e-mail necessitated a tripling of the disk capacity from 18 to 54 Gbytes.
- A Dual PIII-800MHz public Linux facility was added to the existing Dual PII-450MHz, sharing both passwords and user home disk space.
- A Compaq Alpha Server DS10, running Tru64, with 768 Mb of RAM was added to allow compute intensive engineering calculations.
- Two network attached E-size inkjet printers, an HP2800CP for extremely complex graphics/drawings, and an HP500PS capable of 42 in. wide high resolution (1200×1200 dpi) colour graphics, were added to support printing poster presentations and engineering drawings.
- The Alpha based backup of UNIX systems has been replaced by a rack mountable PIII-650 VALinux machine using a single DLT-8000 tape drive and BRU software. A Web page allows users to determine when their files were last backed up.

Software developments

Web-mail and Netscape Roaming Access support were added to allow more flexibility for those accessing e-mail away from TRIUMF. Lightweight directory access protocol (LDAP) will be expanded early next year to include not only user names and e-mail addresses, but also information supplied by Human Resources on telephone and room numbers as well as placement in TRIUMF's organization chart. Users will shortly be able to upgrade their own database entries.

The two-body kinematics program Kin2Body was ported to C^{++} with an added graphical user interface (GUI). The interactive version of the beam transport program TRANSPORT, called INTRAN, was updated for Linux. The beam transport program REVMOC was updated for Tru64, Linux, VMS, and Windows9x.

GEANT4

As a member of the GEANT4 collaboration, our group continued its contribution to the Low Energy Physics, Testing and Quality Assurance, and Documentation working groups. The T & QA contribution involved various system-testing and diagnostic activities, and responsibility for the implementation of two new Web-based tools: LXR, a source code browser, and Tinderbox, an automated distributed system testing framework. These are described in more detail elsewhere in this report. TRIUMF presented a demonstration of Tinderbox at the annual GEANT4 workshop in October at Orsay, France.

Beam dynamics

A presentation on the current space charge techniques, used in the TRIUMF developed ACCSIM multi-particle tracking code, was given at KEK to collaborate on space-charge simulations. A KEK-written code was also used to study emittance growth and halo production due to non-linear space-charge resonances. Detailed comparisons made on similar runs with ACCSIM showed very close agreement between these two codes. ACCSIM was also applied to the intense-beam tracking studies of the KEK 12 GeV proton synchrotron. An intensity-doubling scheme has been proposed for this ring, which is used in the production of the KEK-to-SuperKamiokande neutrino beam.

A group member also contributed to the CERN/TRIUMF LHC collaboration in the development of an efficient and accurate treatment of image forces in space-charge simulations (reported in an EPAC 2000 paper), and the application of a fast-multipole technique, developed for ACCSIM, to study coherent beam-beam effects in the LHC. These tasks are reported in more detail in the CERN Collaboration chapter of this Annual Report.

In addition to use for KEK and CERN applications, the ACCSIM code continues to be in active use at other sites, including BNL and ORNL (for SNS accumulator ring studies), LANL (PSR studies), and Tsukuba University (Proton Therapy System).

To assist with neutrino factory studies, the synchrotron longitudinal dynamics code LONG1D was ported from DEC to IBM (AIX) use at CERN.

Physica

This popular general purpose data analysis/display program continues to evolve as bugs are fixed and new features are added:

- enhanced text match indexing in a string;
- improved binning;
- much faster input when error checking is not required;
- measures to avoid overwriting existing files;
- enhancements to the INTERP, GRAPH, and RESIZE commands.

A "bare-bones" version, written in C^{++}, is now undergoing testing on MS Windows. A few basic GUI forms and menus complement the command line interface.

Porting Physica to Alpha Linux has been problematic, but to our amazement if this FORTRAN program is compiled and linked non-shared under Tru64 Alpha

the executable runs almost flawlessly on a Linux Alpha system! Only the non-essential "call system" hook fails to work. Enhancements to Physica are expected to continue in the future, especially in light of a pending agreement to "commercialize" this software. This will not impact the free access to the executable code for all member sites of TRIUMF.

WAN

Although local network bandwidth has increased dramatically, there is still a strong pent-up demand for increased throughput to remote Internet sites. The full duplex 100 Mbit fast Ethernet link to UBC remains extremely reliable. The UBC to BCNet link and beyond are still problematic.

WWW

Our group continues to provide limited support for TRIUMF's main WWW server as well as provide consultation and coordination of the many contributors to the contents of our Web site, particularly the ISAC Internal pages and the Proton Irradiation Facility Web pages.

Linux

Linux continues to increase its dominance at TRIUMF, as it has at most of the other high energy physics laboratories worldwide. A summary trip report (http://www.triumf.ca/hepix2000/trip_report.html) of the HEPNT/HEPiX Workshop at JLAB, October 30–November 2, has been put on the Web.

Redhat Linux continues to be the recommended standard at TRIUMF. Users can now subscribe to an automated daily update procedure (most of which involves security patches) for most systems running RH5.2 through RH7.0. Monitoring to a central security machine can also be enabled. Unfortunately, manpower constraints have meant that fewer than half of the Linux machines have subscribed so far.

Thin clients

After testing diskless UNIX-based PCs as X Window terminals, it was decided to instead use disk-based PCs running Redhat Linux 7.0 as X-terminal replacements. A pilot trade-in program for four X-terminals indicated that this would be a better solution since it would provide better stability than diskless systems, and the ability for the owner to more readily use the local cpu for number crunching. The effort to replace the limited (8-bit colour) and insecure X Window terminals will be accelerated in the coming years.

Security

Security "events" are on the increase at TRIUMF. To date they have not been serious. The use of security tools (e.g. openssh) is on the increase but much more still needs to be done. Traditionally TRIUMF has maintained a very open computing environment – an asset which will be difficult to give up. Increased monitoring of incoming traffic is taking place and there are plans to put a proper firewall in place next year. As well, the drive to improve the security of all local networked computers will continue as manpower allows.

Near future

- Replace Windows NT based Windows applications running on X Windows by a much faster dual-cpu Windows 2000 server.
- Wireless portals, with safety surveillance being the first to use this technology to improve efficiency and reduce manpower requirements.

Potpourri

- The dramatic decrease in cost of disk storage (≈$10/Gbyte in 2000, which is a 1000 fold drop in just 11 years) is expected to continue at 50% every 12 months! We are seriously looking at an LTO (linear tape open) based stacker to address the resulting backup issue. Fortunately the recent site LAN upgrade to gigabit Ethernet will mitigate any network impact that would result from this large increase in backup traffic.
- Two HP9100C Digital Sender scanning units were purchased. Documents are scanned and the resulting colour PDF files can then be sent by e-mail or printed to a site printer.
- An XGA (1024×768) 1400 ANSI lumen Sony LCD projector was purchased, mainly for making PowerPoint or VHS video presentations in the auditorium.

Data Acquisition Systems

(R. Poutissou, TRIUMF)

Overview

The Data Acquisition group has continued to deploy MIDAS Linux data acquisition systems around the site. More functionality has been added to MIDAS software.

Four VAXstations were retired from active duty, two being replaced by PCs running MIDAS (parity and RMC experiments). Two more MIDAS systems were added to the detector facility. All VDACS data acquisition systems have been retired.

MIDAS software

This year the continuous development and improvement of the MIDAS software includes: a) Web-based run control flexibility such as manual trigger button, customized script button, log history button, history

plot display button, slow control page hyperlink for variable modification; b) Front-end code: implementation of "Super Event" structure for dead time and disk space reduction, BOR/EOR event handling improvement; c) Extensive Web-based MIDAS documentation, http://midas.triumf.ca/docmidas/index.html; d) New application: "webpaw" providing a Web-based interface to display experiment specific PAW data. This package is actually not part of MIDAS but has been developed in conjunction with it.

Overall, MIDAS has been quite successful not only within TRIUMF but also around the world with over a dozen laboratories using it.

NOVA

The NOVA data analysis system continues to evolve to meet the needs of new TRIUMF experiments. Version 2.2 of the system was released in 2000. Enhancements in this release include the possibility of accessing the raw data directly as Floating Point or INTEGER*4 variables (in addition to the default INTEGER*2). The display package has been updated to support log plots, as well as the ability to sum adjacent channels (making it easier to view significant features in spectra with many channels / few counts per channel). Support has been included to access the event time supplied by MIDAS, which is critical for a number of ISAC experiments. The ability to repeat a command at regular intervals has been added, allowing an updating "live time" display to be implemented. A number of minor changes were made to the system to facilitate its use in a batch environment. NOVA has been fully integrated with the latest version (1.8.2) of MIDAS. Use of NOVA beyond TRIUMF continues to increase. NOVA has now been installed at Oak Ridge, Notre Dame and KVI.

ISAC systems

The ISAC experiments (i.e. Lifetime (GPS, GP2), TRINAT, LTNO, β-NMR) have been using the MIDAS DAQ package successfully as standard data acquisition. Most of the DAQ support group interventions were for small modifications of the acquisition software or hardware upgrades. Parasitic beam tests or detector tests required attention from the DAQ staff for set-up and support. Several new PCs have been deployed for off-line analysis and required some DAQ time for package installation. As a new ISAC experimental area, the TUDA shack required the installation of a DAQ.

β-NMR at ISAC

Custom hardware has been designed, implemented and successfully integrated in the β-NMR data acquisition system. It consists of a pulse programming generator (PPG) card and frequency synthesizer control (FSC) module (both in VME and fully programmable).

The simple TD-μSR software developed in 1999 was significantly upgraded, integrating the PPG and FSC modules.

β-NMR can acquire data in two modes.

- β-NMR Type 1: I-μSR data are acquired in a dead-timeless multichannel scaler and transferred to the host computer every beam cycle. The standard MIDAS data logger is used to save the data in this experiment. Banks of data read from CAMP need to be saved along with the histogram data. A front-end program was written to read data from the CAMP server CPU and send this data into the data stream. The data is also reduced and stored in a format compatible with standard μSR archives.
- β-NMR Type 2: TD-μSR data are acquired in a dead-timeless multichannel scaler and histogrammed in the front end. Data from each beam cycle are added. The standard data archiver MDARC was upgraded. Support for extra scalers was added. The on-line database was reorganized to separate MDARC's parameters from those needed by the front end. Thus MDARC becomes independent of the particular front-end program in use. This enables MDARC to be used for the future replacement of the μSR data acquisition systems in the meson hall.

μSR systems

A project was initiated to replace the μSR data acquisition systems, currently running under VMS on VAXstations, by a MIDAS data acquisition system running under Linux on a PC. This system will share many elements developed for the β-NMR experiment at ISAC.

The present run control database (RCDB) will be replaced by the MIDAS on-line database (ODB), and a user interface is needed that has the look and feel of the existing user interface. A co-op student has written a user interface in Tcl/Tk.

The ODB arrangement for μSR was planned, and a Tcl to C interface was produced to enable the Tcl code to access the ODB.

Expt. 614 slow controls

The slow controls system for Expt. 614 (TWIST) continues to evolve towards its final form. During 2000, it was decided that much of the slow controls/monitoring would be based on a programmable digital voltmeter from Hewlett-Packard. A MIDAS driver for this device has been written, and it is currently being used to monitor temperatures and pressures in a test set-up. Real time values of slow control

variables monitored by this device are available from the MIDAS status page, and a time history of these variables is also available from a Tcl window accessible from this page.

RMC and parity

Both the RMC and the parity DAQ hardware were upgraded from VAX/VMS host CPUs to Linux PCs. The custom front end software was rewritten to function in a MIDAS environment with success.

Detector Facility

(R. Henderson, TRIUMF)

This year has been a very active one for the Detector Facility. The facility has been almost fully occupied with the Expt. 614 project. As expected, ATLAS modules are now in full production, so that group doesn't require a large amount of help from the facility. We continue to provide the services of Rich Maharaj to work full time on the ATLAS project. In addition, we continue to contribute significantly to the ISAC facility.

The Expt. 614 project is a sophisticated experiment which hopes to measure the Michel parameters to ten times the precision they are now known. TRIUMF members are playing a central role in this collaboration. Robert Henderson has designed the various detector modules and was largely responsible for the design of the complex "cradle" that will hold, align and service the nineteen modules in the experiment. Robert Openshaw has designed the complex gas system. Wayne Faszer has designed and built the high precision wire surveyor, and is now overseeing module assembly, testing and QC.

The larger mill in the scintillator shop was refitted as a 4-axis NC mill. Chris Stevens continues to work full time machining parts for Expt. 614, mostly G10 gas box and wire plane parts. With approximately 1.0 man-years of full time NC work performed so far, this mill refit has clearly saved the Expt. 614 project enormous machining costs. The curved scintillator pieces for $G\emptyset$ are also being machined on this NC mill.

Also in the scintillator shop, a variety of scintillators have been built, the biggest customer being the μSR group. Experiment 949 at BNL also requires several scintillator jobs. Two of these are small but highly complex assemblies. The first (B4) is nearing completion; the second, an active degrader, is part way through. This year fewer scintillators were required at TRIUMF and the shop committed to making a large number of scintillators for the $G\emptyset$ experiment at JLAB. This involves about 0.9 man-years of shop time over an 18 month period. After significant delays, the $G\emptyset$ group has finalized the design and these scintillators are now in production.

Robert Henderson and Dave Hutcheon designed a prototype ISAC beam monitor. A prototype of this monitor was built by Marielle Goyette in the facility. It uses 48 brass blades on a 1 mm pitch and was successfully tested in a low energy beam. Based on what we learnt from making this prototype, the design has been improved and a second prototype built. This unit will be mounted on the proper hardware for use in the ISAC beam line. Unless there are unforeseen problems, this project is essentially completed, except for passing on the construction techniques.

GEANT4

(P. Gumplinger, TRIUMF)

GEANT4 is a collection of software, arranged like a toolkit, and designed to accurately simulate the passage of particles through matter. Its capabilities include a powerful kernel, extensive physics models, the ability to visualize the detector, particle trajectories and hits, and the creation of a persistent detector description and persistent events. GEANT4 is written in C^{++} and exploits advanced software engineering techniques and object oriented technology to achieve transparency of a multitude of physics implementations. It replaces the successful and venerable GEANT3 package and is available for a variety of operating systems: flavours of UNIX, Linux, and Windows NT.

GEANT4 is also the name of a large international collaboration of scientists and software engineers whose mandate it is to perform production service, oversee the ongoing further development of the program, and provide user support. This collaboration superseded the R&D project, RD44, which produced the first public production version at the end of 1998. A Memorandum of Understanding (MoU) signed by all participating parties governs the formal collaboration. It is subject to tacit renewal every two years and sets out a collaboration structure defined by a Collaboration Board (CB), a Technical Steering Board (TSB) and several Working Groups. The MoU also specifies a key by which the collaboration's resources (money, manpower, expertise, and key roles and activities such as program librarian and documentation manager) are measured in Contribution Units (CU) and it further delineates how the boards are constituted depending on the CU count for each signatory. TRIUMF has a seat on both the Collaboration Board and the Technical Steering Board.

It is the CB's mandate to manage these resources and to monitor the agreed upon responsibilities among the affiliates. This body is also charged with the evaluation of proposals for the evolution of the MoU. The TSB, on the other hand, is the forum where technical matters like software engineering details and physics

model implementation issues are discussed and decided, and where priority is given to user requests. Its primary tasks are the supervision of the production service and the user support, and to oversee ongoing further development of the program. The TSB is chaired by the spokesperson of the collaboration, who is appointed by and reports to the CB. The spokesperson is (re-)elected every two years by a simple majority of votes. This is also the modus operandi in general for making decisions in the two boards.

Every domain of the GEANT4 software, which corresponds to a releasable component (library), is individually managed by a working group of experts. In addition, there is a working group for each of the activities: testing and quality assurance, software management and documentation management. A release coordinator, who is selected by the TSB, heads each group. This clean overall problem decomposition makes the distributed software design and development possible in a worldwide collaboration. Every group can work in parallel, thus allowing an optimal utilization of manpower and expertise. As in previous years, TRIUMF collaborators participated in the activities of the electromagnetic physics implementation, testing and quality assurance, software management, and documentation management working groups.

In particular, one of our group took responsibility for implementing WWW-based tools to improve the system testing process. System testing involves repeated cycles of testing the GEANT4 code as a whole on all supported computing platforms and in many different usage configurations. This process is crucial to maintaining the integrity of the code during development and also to certifying the code prior to public releases.

We decided to set up a dedicated WWW server at TRIUMF to support the development of the Web-tools, which are heavily based on server-side Perl scripts. Our dual-processor Linux system was configured for this purpose and made publicly accessible via http://geant4www.triumf.ca/. Following this, the implementation of LXR (a source code browser) and Tinderbox (an automated testing and reporting tool) could proceed.

The LXR browser offers a powerful source code viewing and searching facility, with point-and-click navigation of the source tree, filename search, full-text indexing, and hyperlinked cross references for identifiers such as class names, method names, and variable names. The package was modified for the GEANT4 implementation by making some improvements to the user interface and the Web page designs, but the major customization was to support different releases and reference versions of the code through a common interface. The LXR facility is now fully operational and will be useful to G4 users, developers and testers.

Tinderbox constitutes the major part of the Web-tools development work. Originating in the Mozilla open source project, it comes to us in a rather minimal and ad hoc state, although the basic machinery consisting of test-case scripts, test-result processing, a test database, and a reporting facility, is very sound and is a good base on which to build the more diversified system-test framework we need for GEANT4. This year, Tinderbox was installed and brought to a prototype stage where complete operational GEANT4 test-cycles could be performed: (1) System tests launched on various client platforms at TRIUMF and at CERN; (2) Test progress and results (job logs) sent by the clients to the "Tinderbox server" (geant4www) at TRIUMF; (3) Messages interpreted by Tinderbox and stored in a tests database; (4) Job logs scanned and hyperlinked for compilation and link errors, run-time errors, and regression test results; (5) Tables of test results, with links to logs and developer/tester messages, displayed through any Web browser.

A presentation on Tinderbox and a live demonstration were given in October at the annual GEANT4 workshop in LAL-Orsay, and plans were made for further development to bring Tinderbox into full production. The main efforts in 2001 will be (1) to create comprehensive and portable client scripts, which must duplicate the functionality of the current rather complex and fragmented collection of scripts used in system testing, and (2) to increase the capacity of the on-line displays, which must accommodate GEANT4's large number of test platforms, test cases, and code configurations.

Collaboration highlights during the past year were the June release of GEANT4.2.0 and the December release of GEANT4.3.0. The GEANT4 collaborators are: J. Chuma, P. Gumplinger, F.W. Jones, C.J. Kost, TRIUMF; L.G. Greeniaus, Alberta.

Scientific Services

(M. Comyn, TRIUMF)

The Scientific Services group encompasses the Publications Office, Library, Information Office, and Conferences. Its activities during 2000 included: producing the 1999 Annual Report, the TRIUMF preprints, and a conference proceedings; implementing a new database system for the Library; updating the display material in the front lobby; and supporting eleven past, present and future conferences and workshops.

Publications Office

The TRIUMF Annual Report Scientific Activities has been truly electronic since 1998. Electronic files

have been used throughout, from initial contributor submission, through editing, transmission via ZIP disk to the printer, and subsequent direct printing on a Xerox Docutech system. The same files are used for the WWW versions of the report which are available at http://www.triumf.ca/annrep in both Portable Document Format and PostScript file formats. Unlike the monochrome paper version, the electronic versions allow those figures which were submitted in colour to be both viewed and printed in colour. The WWW version of the 1999 report was available to readers four weeks before the printed version. During 2000, over 400 people accessed the 1999 Annual Report via the WWW. The Annual Report mailing list has been reduced and the trend is expected to continue as people become more accustomed to accessing the information over the WWW. This will result in less copies having to be printed, with subsequent cost savings.

In an attempt to aid and encourage authors to submit Annual Report contributions in the correct format, the instructions available on the WWW were condensed and simplified. The LaTeX 2_ε skeleton file was upgraded to introduce new features, and the instructions document which all authors should consult was expanded to include details of these new features, plus additional information on the correct production of Encapsulated PostScript files for the figures.

Illegal code embedded in Encapsulated PostScript files continues to be a major problem in electronic publishing. Some software packages, such as the TRIUMF graphics routines, fully conform to the Encapsulated PostScript specifications, whereas many do not. In order to alert authors to problems encountered with files they submitted the previous year, and in an attempt to prevent similar problems recurring, a post mortem of the 180 figures in the 1999 Annual Report was produced and included on the Web site to supplement that for the 170 figures in the 1998 Annual Report. This analysis and explanation of solutions is viewed as an ongoing project which will evolve as new procedures are devised and software packages become available for editing bad PostScript code. Superior TRIUMF scientific publications should result. See http://www.triumf.ca/annrep/figures.html for details. These developments were presented to the Joint Accelerator Conference Website (JACoW) committee during the European Particle Accelerator Conference (EPAC 2000), which was held in Vienna in June, and used during the processing of the contributions to the electronic proceedings.

Final work on the camera-ready manuscripts for the proceedings of the Third International Conference on Isotopes (3ICI), held in September 1999, was completed early in the year, followed by extensive efforts to assemble and check the various sections included at the beginning and end of the proceedings. Frequent liaison with the publisher, World Scientific Publishing in Singapore, was necessary before ultimate printing and distribution to the delegates late in the year.

TRIUMF preprints are now only produced electronically, and immediately posted on the WWW at http://www.triumf.ca/publications/home.html to allow rapid dissemination of the publications. This has replaced the traditional distribution of paper copies by mail, resulting in significant cost and labour savings.

Library

The Library budget was increased in 2000 to compensate for rising journal subscription costs and unfavourable exchange rates for 2001 renewals, thereby maintaining the list of journals which have been acquired since the last cutbacks in 1998. However, the journal subscription budget and electronic access alternatives are constantly under review.

The Library made a modest number of book purchases in 2000, but continues to rely on donations for most of its acquisitions.

A new Oracle database system was fully implemented during the year. It allows accurate tracking of the journal subscription acquisitions and hence aids subsequent timely requests to publishers for any missing volumes. It also identifies any volumes which have been illegally removed from the Library, prompting requests for their return during the annual spring bookbinding exercise. UBC Library catalogue records for all TRIUMF Library books acquired since 1970 were downloaded into the database. Now all books loaned from the TRIUMF Library are entered in the database and automatic e-mails are sent to borrowers who fail to return a book after a month, followed by weekly reminders. This system has proved to be extremely successful at ensuring the prompt return of books, with the added advantage that several borrowers have also returned books which have been out for extended periods. Records for books acquired before 1970 have to be entered manually whenever they are first loaned, and all new acquisitions have to be entered. Outstanding loan reports can be generated easily.

The Library operates on a self-serve basis and manages with minimal support for day-to-day operations.

Information Office

Both Information Office and Conference personnel now reside in the Information Office located adjacent to the lobby. For three quarters of the year the functions were combined during an extended leave of absence.

The Information Office coordinated tours for over 1445 people during 2000. The general public tours were

conducted by a summer student during the June to August period when tours were offered twice a day. Throughout the remainder of the year for the twice weekly general public tours, and for the many prearranged tours given to high school students and others, a small group of dedicated TRIUMF staff acted as tour guides.

During the year several new display panels were produced as part of an effort to gradually redesign the layout of the lobby and replace the existing public relations materials.

The TRIUMF Welcome Page, which is accessible directly at http://www.triumf.ca/welcome or via the TRIUMF WWW Home Page, continues to receive over 5,000 visits each year. The series of WWW pages were developed by two co-op students. They are intended to provide an overview of TRIUMF in a format understandable to the general public. The virtual tour of TRIUMF allows people to "visit" from anywhere in the world via the WWW, or to gain a good introduction before coming to TRIUMF for a real tour. The latter is particularly intended for students using TRIUMF and its science as part of school projects. The Information Office responds to any questions posed by visitors to the site. Some of the pages were updated during the year.

Various TRIUMF images found on the WWW pages are in demand for use in text books and on other Web pages. The classic shot of the interior of the cyclotron, taken by G. Roy, has featured as the picture of the week on the Web site Particle Physics Research in the UK, and was the inaugural picture of the week on the Physics Central Web site hosted by the American Physical Society.

A Sony VPL-PX20 LCD data projector was purchased for multimedia presentations in the Auditorium and other venues. The 1400 ANSI lumen device with XGA 1024×768 pixel resolution has become increasingly popular with speakers giving seminars using MS PowerPoint, Star Office, and other applications.

Support was provided to the TRIUMF Users' Group throughout the year by the TUEC Liaison Officer.

Conferences

During 2000 support was provided for the following conferences and workshops.

- Muon Source Mini-Workshop, TRIUMF, March 24–25 (40 delegates).
- Astbury Symposium, TRIUMF, April 15–16 (120 delegates).
- European Particle Accelerator Conference (EPAC 2000), Vienna, June 26–30.
- Summer Nuclear Institute at TRIUMF (SNIT 2000), TRIUMF, July 10–21 (25 delegates).
- Fourth International Symposium on Radiohalogens (4ISR), Whistler, September 9–14 (130 delegates).
- ISAC Laser Ion Source Workshop (ILISWS), TRIUMF, December 4–5 (30 delegates).
- TRIUMF Users' Group Annual General Meeting, TRIUMF, December 6–7 (60 delegates).

In addition, preparations were made for the following future conferences and workshops.

- 38th Western Regional Nuclear and Particle Physics Conference (WRNPPC'01), Chateau Lake Louise, Alberta, February 15–18, 2001.
- Particle Accelerator Conference (PAC2001), Chicago, June 18–22, 2001.
- 14th International Conference on Electromagnetic Isotope Separators and Techniques Related to Their Applications (EMIS XIV), Victoria, May 6–10, 2002.

Sudbury Neutrino Observatory
(R. Helmer, TRIUMF)

The underwater connectors used in SNO continue to operate satisfactorily in the regassed water. The rate of loss of tubes overall in the detector is about 0.6% per year; approximately half of this loss is attributable to the connector.

Simple studies carried out in a vacuum on the prototype connector fabricated last year indicated that it was subject to breakdown at a considerably higher voltage than the typical existing connectors. The improvement is mostly attributable to an increase in the distance between ground and the point where breakdown is initiated. In the connector presently in use, breakdown begins on the female side at the point where the pin enters the receptacle, then proceeds along insulator surfaces to ground on the male side. The total distance is 0.130 in. In the new design the connector was made re-entrant, eliminating the possibility of breakdown to ground on the male side and thereby forcing a longer breakdown path (0.250 in.) to ground on the female side.

This year further improvements were made by eliminating all gaps inside the connector and by increasing the distance of a possible breakdown path along insulator surfaces from the central conductor to ground on the male side at the cable entry point. The distance has been increased to 0.326 in. from 0.235 in. Six prototypes of this new design were fabricated and tests in vacuum indicated that breakdown occurs between 2900 V and 3900 V, compared with typical breakdown voltages of between 1600 and 2500 V in the connector

presently in use. The highest operating voltage in SNO is 2500 V; hence it would be expected that fewer connectors of the new design would be subject to breakdown. Some further tests in vacuum are planned to investigate whether application of a dielectric grease provides any further protection. Long term tests in degassed water will then commence as it seems unlikely that the goal of achieving a breakdown voltage of 6 kV, suggested by the SNO External Advisory Committee on Connectors, can be reached without a redesign of the entire connector.

During the year it became apparent that the effort to produce a source of ^{8}Li could benefit from some support from TRIUMF. This source is needed primarily to check on the efficiency of algorithms designed to remove non-physics events from the data stream, but it has other potential uses as well. The beta-decay of ^{8}Li is the mirror of the decay of ^{8}B, the source of neutrinos from the sun which are being detected with SNO. ^{8}Li nuclei are produced via (n, α) reactions on ^{11}B using a commercial DT neutron generator located in a pit 70 m from the SNO detector. From there the radionuclei are transported in a helium gas stream to a decay chamber located in the detector. Alphas from the breakup of the daughter nucleus, ^{8}Be, are coincident with the betas and are used to tag the decay by detection of the scintillation light produced as the alphas slow down in the helium gas. Problems had been encountered in transporting the ^{8}Li over the long distance in a narrow capillary (the lifetime of ^{8}Li is 0.84 s) and in detecting the alpha scintillation light. Drawing on expertise gained from gas jet systems used in the early days of TRIUMF, the first problem was solved by increasing the capillary diameter. This in turn led to problems in source deployment, since the capillary no longer fit on the standard SNO deployment system. Some of the equipment used for deployment was therefore redesigned and fabricated at TRIUMF. The second problem was solved by painting the inside of the decay chamber with a coating of reflective paint, and light collection was further improved by coating the paint with a wavelength shifter. The source was successfully deployed in December.

Work on the scintillation light source mentioned in last year's report was put on hold during development of the ^{8}Li source. It is anticipated that the scintillation source will be completed in the coming year. An effort to redesign the ^{8}Li source to make it more suitable for testing reconstruction algorithms and providing an energy calibration point, and possibly for providing a comparison spectrum to that measured with the ^{8}B neutrinos, is also under way at TRIUMF.

Experiment 715 Off-Line;
Precision Optical Pumping
(S. Gu, UBC; J.A. Behr, TRIUMF)

In Expt. 715's (TRINAT's) off-line lab, laser trapping and cooling technology is used to polarize atoms, and hence nuclei, of the stable isotope ^{41}K, with the intent to apply the same techniques on-line to radioactive ^{37}K, which has almost identical hyperfine structure. One goal is to measure the extent to which parity is violated in the weak interaction. Wu at Columbia in 1957 first discovered parity violation in nuclear beta decay, using a dilution refrigerator to polarize the nuclei. The trapping technologies promise a major improvement: the ability to achieve high polarization and, more importantly, to measure that polarization with atomic physics probes independent of the nuclear decays.

Our recent progress has been to achieve $\geq 90\%$ nuclear polarization of ^{41}K. We start with an ordinary MOT and turn off the trap beams for 1 ms, while turning on circularly polarized light resonant with the D_1 ($S_{1/2}$ to $P_{1/2}$) transition. Absorption of this light increases the atomic angular momentum; together with random spontaneous emission, the result is a biased random walk which "optically pumps" the atoms to the maximum angular momentum $\mathrm{F} = 2$ $\mathrm{M_F} = 2$ state. In this state, both the nucleus and the atomic angular momentum are fully polarized.

The **B** field must be weak (to avoid decoupling the atomic and nuclear angular momentum) and pointed in the direction of the optical pumping light, to avoid spoiling the quantization axis. Eventually, we will turn off the MOT's quadrupole **B** field. In this first test, we left the quadrupole field on, but attenuated the retro-reflected beams in the horizontal plane. The trapped atom cloud's equilibrium position then moved to finite **B** field in the horizontal plane, directed along the optical pumping axis. Then an additional uniform **B** field of 2 G was applied along that axis to move the atoms back to the original MOT centre.

If the light is completely circularly polarized and the atoms are completely polarized, the absorption of the D_1 light vanishes, because the $S_{1/2}$ and $P_{1/2}$ states have the same total angular momentum, so the atoms cannot absorb more angular momentum. The D_1 fluorescence was monitored with a CCD camera with a 1 nm FWHM interference filter to block the D_2 trap light. The D_1 light is tuned $\approx$ one linewidth to the red of resonance to minimize heating of the atoms.

So the polarizing and observing process was:

1) Leave trapping quadrupole **B** field on all the time.
2) Trap atoms with unbalanced trapping laser beams in a non-zero **B** field parallel to the D_1 light.
3) Turn off the trap laser beams for 1 ms.

4) At the same time, turn on D_1 laser and leave it on.
5) Turn off D_1 laser and restore the trap laser beams for 1 ms to retrap the atoms.
6) Go to 3 and repeat.

The time-averaged D_1 fluorescence is shown in Fig. 114 as a function of the polarization of the light as it is varied smoothly from circular to linear and back to circular by a liquid crystal variable retarder. The 5:1 fluorescence ratio between linear and circular polarized light, in a simple estimate where the main contaminant is F = 2 M_F = 1, implies that ≈92% nuclear polarization is achieved. The main depolarization process is believed to be the Larmor precession of the atoms in the MOT quadrupole field, which will eventually be turned off.

We implemented a similar scheme on the radioactive ^{37}K, and a test run achieved an average 70% polarization (90% in one direction and 40% in the other), as measured by the nuclear decay products (see the Expt. 715 report in the Nuclear and Atomic Physics section of this Annual Report).

Plans for the next year include: improving the polarization; fully probing the population of all magnetic sublevels (by stimulated Raman scattering followed by resonant fluorescence probing); beginning development of a circularly polarized dipole force trap [Korwin *et al.*, Phys. Rev. Lett. **83**, 1311 (1999)] which can trap the fully polarized sublevel with minimal dependence on circularly polarized light quality. Together with nuclear detector and vacuum chamber development, the goal is to begin parity violation measurements with radioactives in spring, 2002.

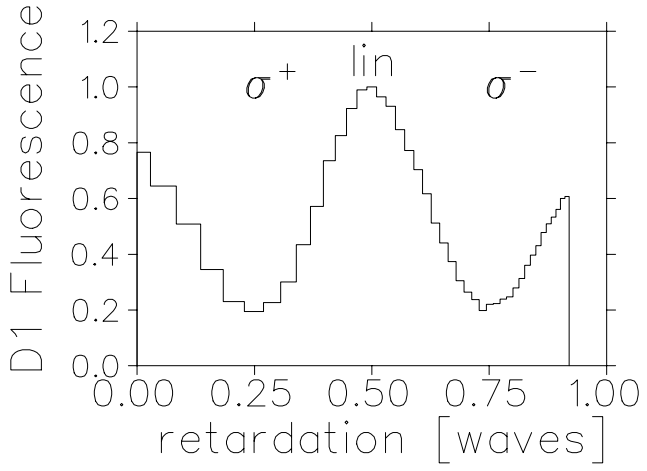

Fig. 114. D_1 fluorescence as a function of optical pumping beam polarization, showing that ^{41}K atoms are polarized. The polarization of the D_1 laser changes continuously from σ^- ($\lambda/4$ retardation) to σ^+ ($3\lambda/4$ retardation). With σ^- (σ^+) light, most of the atoms are sent to the F = 2, M_F = –2 (2) dark state, so that less fluorescence is observed. Figure 114 allows us to estimate that the polarization is ≅ 90% with σ^- (σ^+) D_1 laser light.

β-Detected Nuclear Magnetic Resonance at ISAC

(G.D. Morris, TRIUMF; R.F. Kiefl, TRIUMF/ CIAR/UBC)

We are developing a beta-detected nuclear magnetic resonance (β-NMR) facility for studying materials and phenomena of interest in condensed matter physics. The initial spectrometer, designed for experiments in high longitudinal magnetic field, is virtually complete. Development of DAQ software to enable various experiments to be performed continues as we begin the experimental program.

Introduction

Nuclear magnetic resonance is a powerful experimental technique that yields information about the electronic, chemical and magnetic environment and dynamics present in materials. In the nuclear-detected techniques of β-NMR and μSR, radioactive probes are implanted and information about the local environment is revealed through the anisotropic distribution of the outgoing decay products. Specific and often unique features of these various resonance techniques make each well suited to certain experiments. β-NMR at ISAC is being developed to take advantage of the high flux of low energy spin polarized radioisotopes, particulary for experiments on ultra-thin samples over a wide range of magnetic fields and temperatures.

The scientific motivation as well as the layout and functions of the polarizer and high field spectrometer have been described in detail previously [Kiefl *et al.*, Physica **B289-290**, 640 (2000); last year's Annual Report, p.116].

Polarization

A key milestone achieved this past year has been the polarization of ^{8}Li atoms with an in-flight optical pumping technique. The largest polarization achieved thus far has been about 40%. However, the installation of a ring laser in 2001 is expected to result in a larger and more stable nuclear polarization. Developments in the polarizer section are described in detail elsewhere in this Annual Report by C.D.P. Levy *et al.*

Beam spot imaging

In order to precisely focus and steer the radioactive ion beam spot onto small samples, we have developed a CCD camera system to image the light produced when the ion beam is stopped in a piece of scintillator at the sample position. This system allows one to make adjustments to the electrostatic optical elements which define the position and shape of the beam spot in nearly real time.

This system is based on a 16-bit monochrome CCD camera (model MX516, manufactured by Starlight Xpress, UK) incorporating a cooled, low-noise CCD sensor which allows long exposures to be made. A 50 mm f 1.4 lens provides a narrow 7° field of view on the 500 × 290 pixel CCD. Peak sensitivity of the CCD occurs at 500–550 nm, close to the emission wavelength of several types of plastic and inorganic (UHV compatible) scintillation detectors.

The camera is mounted outside the UHV chamber but views the sample face almost along the beam axis through a UHV viewport and via a first surface mirror inside the UHV chamber which provides an approximately 90° bend in the optical path. The mirror is mounted on a hinge so it may be moved into position in front of the backward counter, slightly offset from the incoming ion beam.

For each ^{8}Li ion, energy is deposited in the scintillator in three ways. The initial beam energy is the smallest contribution, and the outgoing minimum-ionizing betas contribute about 100 keV on average. Most of the light will be generated by two very short-ranged α particles produced in the decay of an excited state of ^{8}Be, contributing about 1.6 MeV. Thus, the source of light within the scintillator is well correlated with the spatial distribution of implanted ions.

Exposures of about 30 s are sufficient to record the ^{8}Li beam spot with an ion flux of $\approx 10^7$ s^{-1} incident on a 0.25 mm thick Bicron BC412 plastic scintillator.

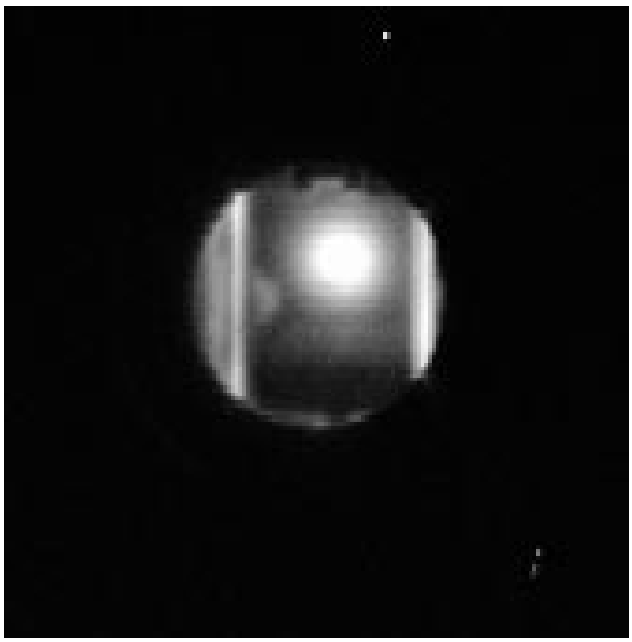

Fig. 115. An image of a slightly off-centre beam spot of ^{8}Li landing on an 8 mm wide piece of Bicron BC412 scintillator. Contrast has been adjusted to reveal the edges (bright vertical lines) of the scintillator and some of the cryostat parts; the FWHM of the spot is about 2 mm.

An example of the image of the beam spot is shown in Fig. 115. With longer exposures it is also possible to image the light produced by 100 nA beams of *stable* ions obtained from an off-line ion source.

Low energy implantation

Since the atoms in the ISAC production targets are initially thermal, they are accelerated through a potential difference of 30 kV as they are injected into the beam line which transports them to an experiment. Such a low energy allows the use of electrostatic optics in the beam line and also makes it possible to vary the implantation energy by biasing the sample to a high voltage. The design of the spectrometer takes advantage of this to enable very low implantation energies and consequently very shallow implantation depths. The entire spectrometer including the superconducting solenoid, cryostat and all the electronics are mounted on a high voltage platform so that the ion energy at the sample surface may be varied from about 1 to 90 keV. The resulting mean implantation depth ranges from about 50–3000 Å. Conventional NMR does not have sufficient sensitivity to detect a signal from the small number of atoms in such a thin layer, especially in weak magnetic fields where the low Larmor frequency would result in a very small signal in an inductive pickup coil. Experiment 897 will use this low energy and low field capability to directly probe the magnetic field just within the sample surface to make an absolute determination of the London penetration depth in superconductors in the Meissner state. Analogous μSR experiments have been performed with low energy muons (LEM) at the Paul Scherrer Institute [Jackson *et al.*, Phys. Rev. Lett. **84**, 4958 (2000)], however, the muon event rates remain at least 4 to 5 orders of magnitude lower than rates we have demonstrated at ISAC. This year, "soft landing" of ^{8}Li has been demonstrated down to 5 keV and should proceed to lower energies as tunes are developed. A long-awaited UHV-compatible replacement for the existing superconducting magnet in the high field spectrometer will be installed early in 2001. With the bakeable magnet, true UHV conditions will be reached so that low temperature experiments can be performed with kinetic energies down to about 1 keV. The electrode assembly which shapes the deceleration potential is presently being rebuilt in a more robust and more precisely aligned assembly.

RF control and DAQ

All of the electronics required to generate precise timing signals simultaneously with amplitude- and frequency-modulated rf power are now installed. A great deal of progress has been made in the software which configures and controls various types of experiments in real time.

Unlike conventional NMR, the nuclear-detected NMR techniques do not require a tuned high-Q rf coil for detecting the NMR signal. This allows the use of a broadband coil to generate the rf magnetic field and consequently one can sweep the rf frequency over a wide range – 0–40 MHz in the present design – without any need to change the coil. With appropriate modulation of the rf power, it should be possible to irradiate with several frequencies simultaneously.

Figure 116 shows the first resonance observed with the spectrometer in which ^{8}Li was stopped in a Pd foil in a magnetic field of 3 T at room temperature. During this run the beam was implanted continuously while the rf frequency was repeatedly ramped from 18.93 to 18.99 MHz in 100 Hz steps every 4 ms. Depolarization of the implanted spins occurs when the rf frequency reaches the Larmor frequency, so the resonance reflects the distribution of local magnetic field at the site of the ions. After the rf has swept over the resonance the decay asymmetry recovers as the unpolarized population of spins is gradually replaced with new, polarized ions. This mode is useful for quickly searching a range of frequencies in order to locate resonances. The width of the line in Pd was found to be about 2 kHz.

Another DAQ mode makes use of the ability to pulse the incoming beam with an electrostatic kicker and control the rf frequency and power with a pulse programmer, rf synthesizer and arbitrary function generator. In Fig. 117 the flat line was obtained with the beam polarization off, yielding a baseline which is very useful for fitting a relaxation function. The top curve shows the beta decay asymmetry in the absence of any rf power, in which the (Korringa) relaxation is known to be caused by the interaction with conduction electrons in the metal. When rf power at the Larmor frequency is applied after the beam pulse, and kept on to

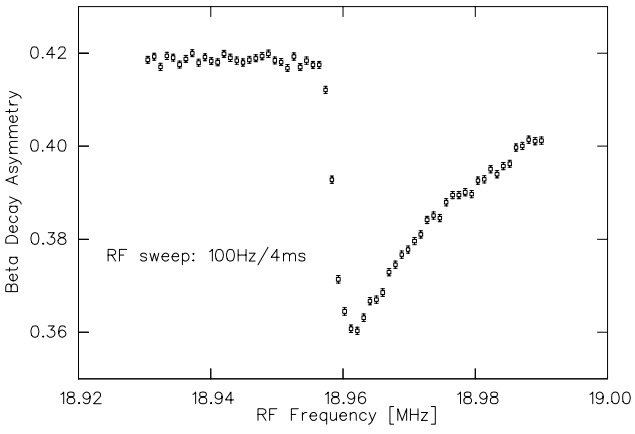

Fig. 116. First observation of resonant depolarization of ^{8}Li at ISAC. In this run the decay asymmetry was recorded while the rf frequency was rapidly swept over the resonance in a constant magnetic field of 3 T.

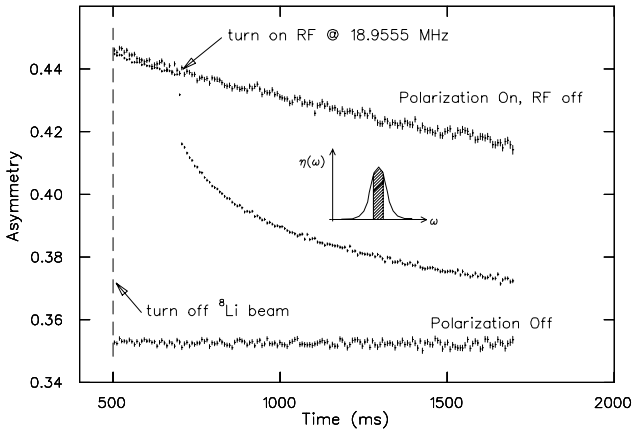

Fig. 117. Bottom curve: beta decay asymmetry without beam polarization; top: exponential spin relaxation without rf; centre: resonant depolarizaton with rf applied just after the ^{8}Li beam was switched off.

the end of the histogram, a portion of the polarization is quickly destroyed. It appears that continuous rf causes depolarization, but only of those nuclei close to the centre of the resonance line. The remaining nuclei in the wings come into resonance more slowly, probably as those ions diffuse to sites where they are subject to smaller dipolar fields.

The ability to manipulate spins with sequences of complex rf pulses is essential to many planned NMR experiments. In Fig. 118 we show a sharp step in the back-front asymmetry when a short, amplitude-modulated rf pulse is applied on resonance after the beam was shut off. The two spectra shown – with longitudinal polarization in each orientation along the z-axis – were taken by alternating the handedness of

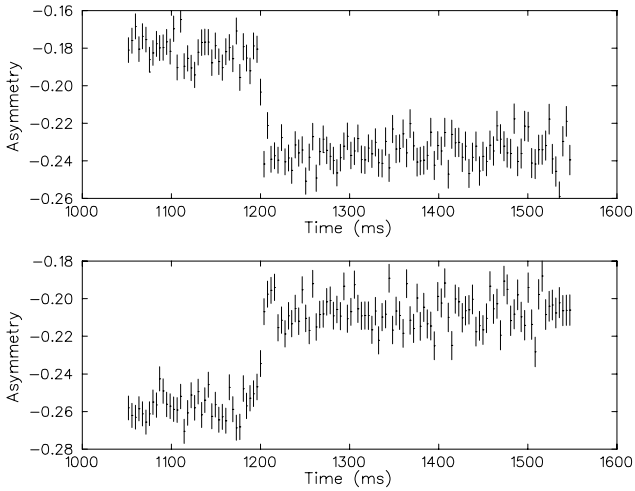

Fig. 118. Examples of time-differential spectra in which a short rf pulse was applied after the end of a pulse of beam. The step in decay asymmetry is due to precession of the spins in the rf magnetic field. Both orientations of initial polarization were acquired in the same run.

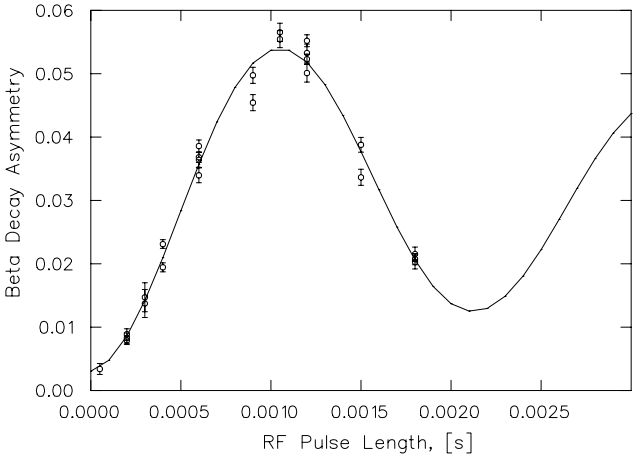

Fig. 119. Change in back-front asymmetry (the amplitude of the step in Fig. 118) as a function of rf pulse length. Asymmetry oscillates about the baseline, indicating that spins are being rotated coherently by the rf magnetic field.

the circularly polarized laser light throughout the run while routing events to the corresponding histograms. Plotting the amplitude of the resulting step in asymmetry as a function of rf pulse length (see Fig. 119), we see that the projection of the polarization along the z-axis follows a cosine dependence; spins are being flipped through 180° with a pulse of about 1 ms duration.

In summary, the first β-NMR spectrometer is virtually complete. We are currently working to optimize the polarization so that the experimental program can be carried out as efficiently as possible. Many features of the DAQ and control system are now working and more are being added. We are about to begin the first experiments on semiconductors and superconductors.

Nuclear Astrophysics with DRAGON at ISAC

(J.M. D'Auria, SFU)

Overview

The TRIUMF-ISAC facility will produce high-intensity radioactive accelerated beams of energies from 0.15 to 1.5 MeV/u and with A<31. An essential part of the experimental program with such beams is to measure the absolute rates (20%) of radiative capture reactions in which the heavy reactant is unstable and short-lived. The DRAGON facility will be used to achieve such measurements utilizing inverse kinematics, in which the beam is the heavy, radioactive nuclide, and the target is hydrogen or helium (gas). Table XVI indicates (not in order of priority) some of the reactions that are planned for study; the first reaction will be ^{21}Na$(p,\gamma)^{22}$Mg.

Table XVI. Reactions of interest (inverse kinematics/DRAGON facility).

^{13}N$(p,\gamma)^{14}$O	E805	Hot CNO cycle
^{15}O$(\alpha,\gamma)^{19}$Ne	E813	Hot CNO cycle/breakout
^{17}F$(\alpha,\gamma)^{18}$Ne		Hot CNO cycle
^{19}Ne$(p,\gamma)^{20}$Na	E813	Hot CNO cycle/breakout
^{20}Na$(p,\gamma)^{21}$Mg	E908	rp process pathway
^{21}Na$(p,\gamma)^{22}$Mg	E824	Hot NeNa cycle; ^{22}Na prod.
^{22}Mg$(p,\gamma)^{23}$Al	LOI	^{22}Na production
^{23}Mg$(p,\gamma)^{24}$Al	E810	rp process
^{23}Al$(p,\gamma)^{24}$Si	LOI	^{22}Na production
^{25}Al$(p,\gamma)^{26}$Si		^{26}Al production

The facility

Summary

The main components of the DRAGON system are a windowless, extended gas target; a two-stage electromagnetic mass separator; detectors of the heavy reaction products and detectors of the capture γ-rays. The expected radiative capture rates are of order 1 event per second for a beam intensity of 10^{10} s^{-1} or lower. The role of the DRAGON is to provide clean separation and identification of the recoiling reaction product from the relatively more intense incident beam, and to allow for the measurements of the rates of these essential reactions as a function of the energy of the incident beam.

Funding over a three year period for the building of DRAGON and its initial operation was received from NSERC (and TRIUMF) in April, 1998, while funding for the required gas target was received in 1997. In 2000, funding was received to design, build and install a BGO based gamma array around the gas target chamber. A conceptual layout of DRAGON is displayed in Fig. 120; inserted in this figure is a diagram indicating beam focusing properties at different locations. A summary of the status of the various components is provided below.

Gas target

The gas target system, including the recirculation system and the EPICS controls, was commissioned using hydrogen and helium gases, i.e. when using these gases the pressure in the inner chamber was 5 Torr, while at the upstream and downstream end chambers the pressure was of order 10^{-6} Torr. The shape of the side windows of the inner gas chamber required special design (see Fig. 121) to minimize the effects of streaming (and higher pressures) when using hydrogen gas. Approximately 4 L of X13 zeolite is used in the recirculation chamber to maintain purity of the recirculating target gas.

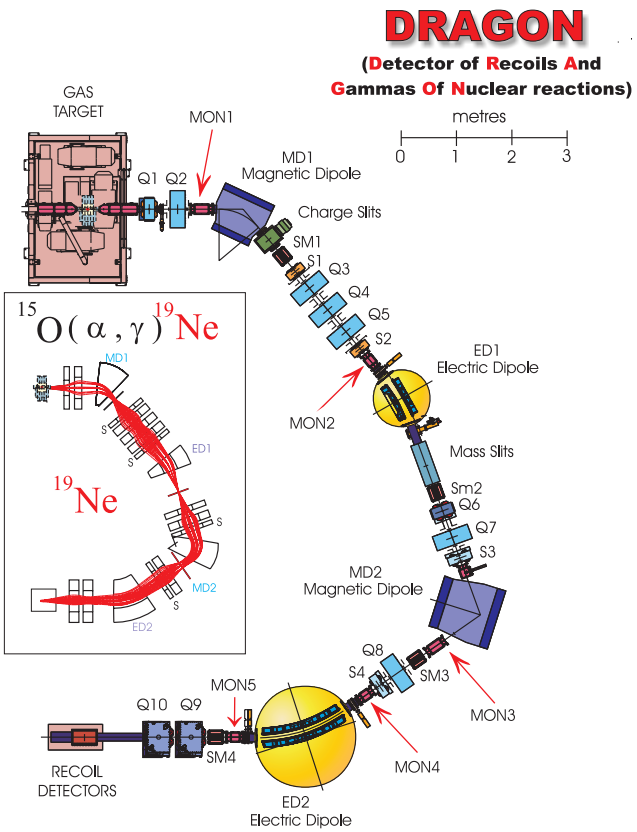

Fig. 120. Displayed is a detailed layout of DRAGON in the ISAC hall. The insert presents the calculated beam trajectory of a ^{19}Ne ion beam from the ^{15}O$(\alpha,\gamma)^{19}$Ne reaction.

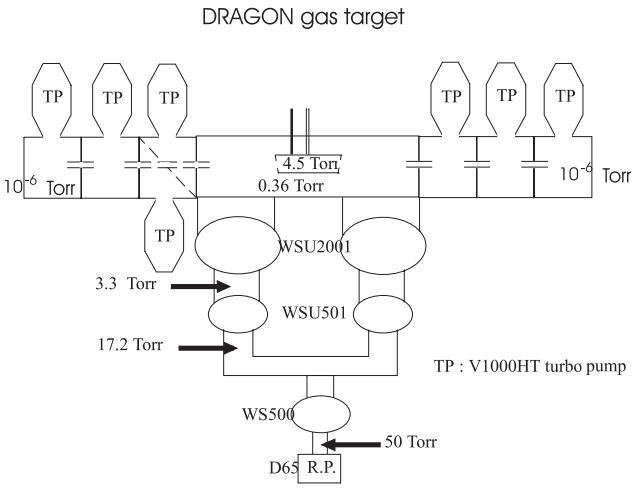

Fig. 121. Schematic representation of the DRAGON windowless gas target; measured gas (H_2, He, or air) pressures indicated.

Mass separator

The separator contains both magnetic and electrostatic dipoles in order to achieve separation of the beam and recoil product, which have essentially the same momentum. It is a two-stage device, each ending in an energy-achromatic, mass-dispersive focus. Following selection of one charge state of beam and product in the 50° magnetic dipole, an electric dipole is used to select only the product based upon its different energy. Mass dispersion of 0.47 cm/% is achieved in the first stage and 2.12 cm/% in the second stage. Each stage has 5 quadrupoles for focusing, 2 sextupoles to correct aberrations, and 2 steering magnets.

All twenty magnetic elements have been mounted on their stands in locations on the beam line. The vacuum chamber for the first dipole was installed and the second chamber is expected from the machine shop. The titanium electrodes were polished and the entire interior structure, including insulators, assembled for both sets of electrostatic dipoles.

Particle detection system

The detection system for the recoiling reaction product heavy ions consists of a thin carbon film, electron focusing, multichannel plate (MCP) detector system to provide positional and timing information, followed by a thin windowed ionization chamber (IC) with a parallel gridded avalanche counter (PGAC) as front end. This provides a second timing signal and a total energy signal. This particle detection system will provide a local time of flight for a primary mass determination. The MCP was assembled and tested successfully with an alpha source. The IC (without PGAC) was tested initially with heavy ions at Yale University, and then combined with the PGAC at the University of Notre Dame. The IC displayed resolution equivalent to an Ultra Si detector, namely 2.7% resolution with 0.9 MeV/u ^{16}O ions (4.7% at 0.2 MeV/u).

Gamma array

Funding has been received from NSERC to build a gamma detector, which will be a part of DRAGON for the first experiments in mid-2001. The detector is composed of 30 segments of BGO crystal, each segment being a hexagonal cylinder 56 mm in diameter by 76 mm long. The segments of the array will be stacked to form a closed volume around the DRAGON gas target. Capture γ-rays will be detected in coincidence with the heavy ion detected in the separator.

Prototype crystal modules were received from three suppliers and tested with radioactive sources of γ-rays. Especially important are the rate-handling capability and energy resolution of the modules. The design of the phototube base was optimized with help from TRIUMF technicians, and 31 detectors were ordered from Bicron and Scionix corporations. The Bicron detectors are more expensive and have slightly superior energy resolution. Rate-handling capability was optimized by placing a strong source of 511 keV γ-rays near each crystal and requiring minimum pulse-height shifts with varying counting rate. This test simulates the back-

ground effects expected from the small percentage of radioactive beam spilled in the target. So far about half of the detectors have been tested with radioactive sources up to 6.1 MeV γ-ray energy. NIM and CAMAC electronics were procured and tested with a version of the TRIUMF standard MIDAS data acquisition program, which runs on a PC. The electronics processes the signals from 30 independent BGO crystal channels in parallel, using fast ADCs to convert each pulse height. The maximum background rate-handling capability of each module is about 500 kcps, which translates to 15 Mcps for the whole array, if uniformly illuminated.

A mounting system, which accommodates both detectors interchangeably, has been designed and a preliminary Monte Carlo simulation of efficiency performed using GEANT. The detector layout was designed to maximize total solid angle coverage, homogenize counting rates among the detectors, and optimize z-axis sampling of a resonant γ-ray source. This last feature will facilitate monitoring of the beam energy by measuring the z-position of the resonant target gas along the beam/target intersection line. The mounting system will also allow for the positioning of a lead blanket, if deemed necessary, to reduce effects of external background. Detailed design of the mounting arrangement is under way in the TRIUMF Design Office. Present plans indicate that the entire gamma array will be installed and commissioned by the middle of April, 2001.

The work described in this section involved mainly Drs. Joel Rogers and Ahmed Hussein, and graduate student Dario Gigliotti of UNBC.

Science

^{22}Mg

In anticipation of the first study planned for DRAGON, namely the measurement of the ^{21}Na$(p,\gamma)^{22}$Mg rate, a detailed study of the levels was completed using a (p,t) reaction. The study was performed at the (now closed) University of Tokyo CNS Laboratory using the high-resolution triton spectrometer. Figure 122 displays the energies of the states that were observed; the observed precision was better than previously measured. Given the energy loss in the DRAGON gas target, it was important to know the energies with such precision. These studies have been accepted for publication in Physical Review C.

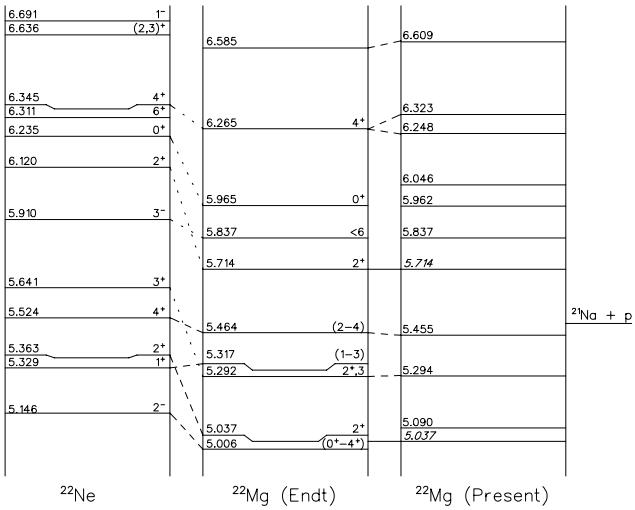

Fig. 122. Levels of ^{22}Mg as studied using a $(p,t)^{21}$Na reaction on ^{24}Mg and considered important for the $(p,\gamma)^{22}$Mg reaction.

Alpha commissioning and source preparation

The initial commissioning of the DRAGON will be performed using an alpha emitter positioned just upstream of the centre of the gas target. A small magnet and a set of slits positioned at the target centre will allow for the production of a deflectable, parallel beam of ^{4}He$^+$ ions to explore the characteristics of the optics of the magnetic elements in a systematic fashion. A ^{148}Gd source, which emits an alpha of 3.183 MeV, was produced at TRIUMF by the irradiation of a Sc foil on BL2A with 40 MeV protons under controlled conditions. A detailed radiochemical separation procedure was followed using the laboratory facilities of Simon Fraser University to separate gadolinium for the target material and other reaction products. The extracted gadolinium was then electrochemically deposited onto a Pt foil; the separation efficiency of the entire procedure was about 75%, but the final source strength was only 16 μCi due to some difficulties in the original production irradiation. The source was mounted on a standard alpha holder and sprayed with a thin layer of lacquer ($\sim$40 μg/cm^2).

Charge state distributions

When heavy ions traverse a gas, a distribution of charge states results. Depending upon the thickness of the gas, this distribution may or may not reach equilibrium conditions. This process affects the studies planned for DRAGON, as only one charge state will be measured using the spectrometer. Little information exists in the literature on this process for low energy, low Z heavy ions. Studies were performed using the windowless gas target system at the University of Naples Tandem Laboratory in Italy. Using beams of oxygen and sodium at energies relevant to the planned studies, resulting charge distributions were measured as a function of gas pressure. Figures 123 and 124 display some of the preliminary results.

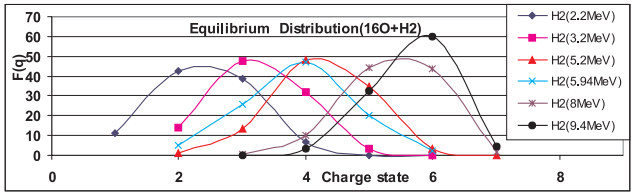

Fig. 123. Charge state distribution resulting from a ^{16}O beam in a windowless hydrogen gas target system.

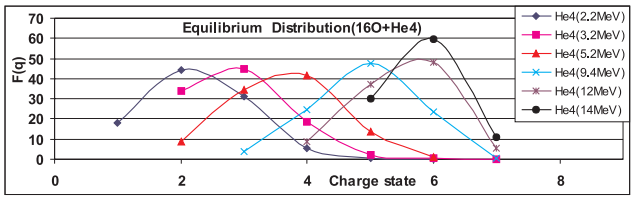

Fig. 124. Charge state distribution resulting from a ^{16}O beam in a windowless helium gas target system.

Summary

By the end of this year the DRAGON facility was approximately 80% completed. Preparations were under way to initiate commissioning of the first two sections using the ^{148}Gd alpha source positioned 50 cm upstream of the gas target centre. The emitted alphas would be detected using a Si strip detector mounted in the charge slits vacuum chamber located after the first magnetic dipole.

8π Spectrometer

(G.C. Ball, TRIUMF)

The 8π γ-ray spectrometer, designed by Canadian physicists to pursue high-spin γ-ray spectroscopy studies at TASCC, was moved to TRIUMF in March. The 8π spectrometer is a second generation instrument composed of 20 Compton-suppressed HPGe detectors, a 4π BGO γ-ray calorimeter, and a multi-element CsI(Tl) charged-particle detector array. The spectrometer is presently being modified for a vigorous program of decay studies with the non-accelerated radioactive beams available in the low energy area of ISAC-I. In these studies, the γ-rays are emitted from nuclei at rest and the Doppler broadening associated with emission from a moving source, as is typical of the experiments with accelerated beams, is no longer an issue. It is therefore possible to achieve a higher γ-ray efficiency, while retaining excellent energy resolution and peak-to-total ratio, by removing most of the inner BGO calorimeter and close-packing the 20 Compton-suppressed HPGe detectors of the 8π around the source position.

A key element of the research program with the 8π spectrometer at ISAC will be superallowed Fermi β-decay studies. A 4π array of plastic scintillators to detect positrons is also required for these studies. The <60 keV isotope-separated beams from ISAC will be implanted in aluminized mylar tape at the mutual centre of the β- and γ-arrays. Periodic movement of the tape will remove long-lived daughter activities from the vicinity of the detectors. A new LEBT has been designed to ensure a beam spot diameter of 5 mm, so that 1.27 cm wide tape will be sufficient to intercept the entire beam profile. This is achieved without the use of any slits in close proximity to the detector arrays.

The installation and commissioning of the modified 8π spectrometer is scheduled for completion by the summer of 2001. The new LEBT will be built in the fall and first experiments will begin in early 2002.

Low Temperature Nuclear Orientation

(P.P.J. Delheij, TRIUMF)

With the low temperature nuclear orientation set-up at ISAC-I, radioactive isotopes are implanted and polarized in ferromagnetic foils which are cooled to temperatures below 10 mK. As a consequence, the emitted radiation of the subsequent decay is anisotropic. This effect can be applied in studies of nuclear structure, condensed matter and fundamental symmetries.

After the first radioactive beam was delivered in the previous year, the efforts were directed towards commissioning the set-up and starting the first experiments. Two beam periods in the spring and the fall were taken. A central role in the commissioning is played by ^{79}Rb. It can be produced in abundant quantities from several production targets. Furthermore, the γ-ray decay structure provides several internal consistency checks on the measured anisotropies.

In the spring, problems with the target foil preparation led to a maximum anisotropy of 5% for the 688 keV γ-ray transition in the decay of ^{79}Rb. This is about half of the value that we obtained previously. Subsequently, problems developed with the beam diagnostics in the cryostat which reduced the efficiency of the beam delivery considerably. However, a satisfactory ^{75}Ga:^{75}Rb production ratio and intensity was still obtained (see the report on Expt. 863).

In the fall, an anisotropy of 0.110 was observed for the 688 keV γ-ray, slightly exceeding the previous large value. This proved that the problems with the target foils were solved. The beam diagnostics performed very well with a noise level of 1–2 pA on the cold Faraday cup channels in the cryostat. However, instabilities in the beam line leading to the LTNO set-up caused beam intensities to vary by a factor of 3 over timespans of a few hours. With the failure and replacement of the rf source for the NMRON scans, data with limited statistical accuracy could be acquired. Also ^{91}Rb (decaying

to the ^{91}Y isomer) was implanted with acceptable intensities (see the report on Expt. 826). In this period a power outage and a dropout of the cooling water supply plagued the refrigerator system.

The experiments with ^{79}Rb gained considerable significance with the publication of the calculation of the hyperfine fields for all elements from Rb until Xe [Cottenier and Haas, Phys. Rev. **B62**, 461 (2000)]. Excellent agreement with the experimental values is shown except for Rb and Sr. The present experimental value for Rb was obtained with an integral nuclear orientation measurement. An NMRON measurement (differential nuclear orientation) can resolve this problem. Therefore, Expt. 893 was approved by the EEC for the first hyperfine field measurement of Rb in the hosts Fe, Ni and Co.

Collaborators on the LTNO are: P.P.J. Delheij, C.A. Davis, TRIUMF; B. Turrell, J. Pond, R. Kiefl, Univ. of British Columbia; K.S. Krane, P. Schmelzenbach, J. Loats, C. Stapels, Oregon State Univ.; J. Wood, D. Kulp, Georgia Inst. of Technology; P. Mantica, W. Kumarasiri, D. Groh, Michigan State Univ.; H. Haas, Hahn Meitner Inst.; S. Cottenier, K.U. Leuven.

Experiments 870, 874, 879, 900 "TUDA" TRIUMF-UK-Detector-Array

(T. Davinson, Edinburgh)

TUDA is a general purpose scattering facility designed for use with the accelerated radioactive nuclear beams available from ISAC-I. TUDA is principally (but not exclusively) designed for the detection of charged particles using silicon strip detectors. This enables the construction of highly segmented detector systems of large solid angle [Davinson *et al.*, Nucl. Instrum. Methods **A454**, 350 (2000)]. Typical nuclear astrophysics applications are:

- elastic scattering, e.g. Expt. 879, ^{1}H(^{21}Na,^{21}Na);
- (α, p) reactions, e.g. Expt. 870, ^{4}He(^{18}Ne, p);
- studies of the 4.033 MeV state of ^{19}Ne such as:
  - Expt. 874, ^{2}H(^{18}Ne, p)^{19}Ne;
  - Expt. 900, ^{6}Li(^{15}O, d)^{19}Ne.

The TUDA apparatus can also be used for nuclear physics experiments.

TUDA's initial configuration consists of a modular vacuum chamber (length 1.5 m, diameter 0.4 m). A photograph of the chamber is shown in Fig. 125. The upstream box houses the beam collimator system. The centre box contains the target ladder, vacuum system ports and four large, uncommitted ports. The downstream box is used for the electrical, gas and coolant feedthroughs. All are connected via simple tubular sections. The modularity of the design is intended to

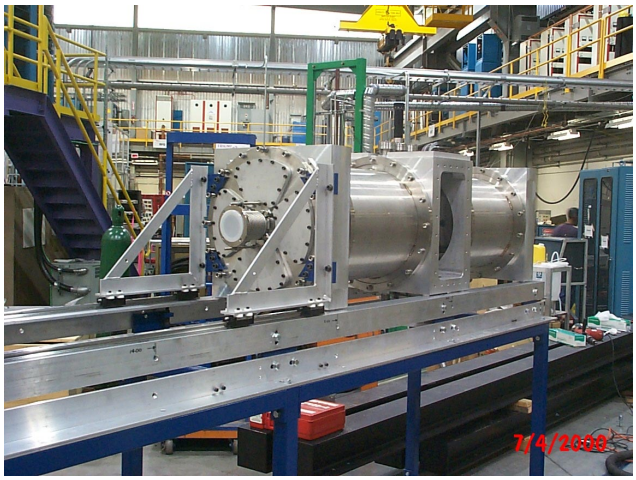

Fig. 125. Photograph of the TUDA chamber during initial assembly. The downstream flange is visible.

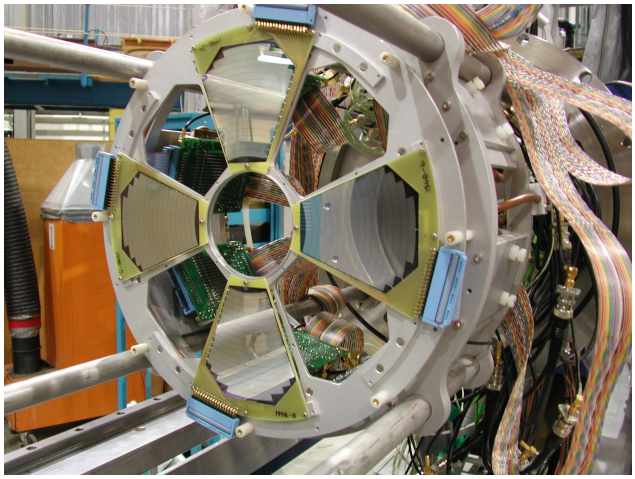

Fig. 126. Photograph of a partially installed MSL type YY1 silicon strip detector and preamplifiers within the TUDA chamber.

simplify the customization of the chamber to a wide variety of experiments. The detectors and preamplifiers are mounted on four rods arranged around the central axis of the chamber and attached to the downstream flange (Fig. 126). The entire detector assembly can be withdrawn from the chamber using a linear track system enabling convenient access to the detectors and instrumentation. The optics of the beam line have been designed to enable a minimum beam spot size of 1 mm $\times$1 mm to be produced at the target position. The TUDA vacuum chamber is designed so that it can be easily removed and the target position and beam line used by other experiments.

All of the pulse-processing instrumentation and data acquisition are housed in a purpose-built, stand-alone counting room located close to the TUDA vacuum chamber. Great care has been taken to provide clean power, high quality grounding and EMI/RFI screening from the multiple rf sources within the

ISAC-I experimental hall. The instrumentation consists of the RAL108 charge-sensitive preamplifier and the RAL109 shaping amplifier/discriminator which provide spectroscopy-level performance. Trigger logic is provided by CAMAC ECL logic modules. Detector bias is provided by a CAEN SY403 HV Mainframe (32 channels, –600 V, 0.2 mA). The data acquisition system will use a modified version of the Silena 9418/6V VME ADC (32 channel, 12-bit) and the CAEN V673 VME multihit TDC (128 channel, ∼0.8 ns LSB) which have been ordered and are expected to become available during the summer of 2001. In the interim, commissioning and early experiments will use the Silena 4418/V CAMAC ADC and LeCroy 3377 CAMAC TDC. Infrastructure (cabling, racks, etc.) to support up to 512 discrete detector elements from up to 32 silicon strip detectors has been installed.

TUDA collaborators include: T. Davinson, N. Farrington, D. Groombridge, A. Laird, P. Monroe, A. Ostrowski, C. Ruiz, F. Sarazin, K. Schmidt, A. Shotter, P. Woods (Univ. of Edinburgh); B. Fulton, B. Greenhalgh, J. Pearson, L. Watson (Univ. of York); N. Clarke (Univ. of Birmingham); J. Daly, J. Gorres, M. Wiescher (Univ. of Notre Dame); L. Buchmann, P. Walden (TRIUMF); A. Chen, J. D'Auria (Simon Fraser Univ.); S. Cherubini, P. Leleux (Univ. Louvain-la-Neuve); J. Hinnefeld (Univ. of South Bend); R. Azuma, J. King (Univ. of Toronto); E. Konobeevsky, M. Morodovskoy, V. Simonov, A. Stepanov, V. Zavarzina (INR RAS).

CYCLOTRON OPERATIONS DIVISION

INTRODUCTION

Beam delivery for the 500 MeV cyclotron was very successful during 2000. The cyclotron was available for ∼5,000 hours, or ∼93% of the scheduled time. A record total beam charge of ∼600 mAh with an availability of 93% in terms of charge delivered to BL1A was achieved. The cyclotron recovered well from the low point of 1999 that had been caused by a failure of the high-intensity beam dump cooling vessel on BL1A. During 1999 the corresponding figures were about 4,000 hours and only about 350 mAh of total beam charge. Availability in terms of beam charge delivered by BL1A was only 63%.

A key element for the improved beam delivery was the utilization of the 4th harmonic auxiliary acceleration cavity (AAC), or rf booster, for beam production. This had been installed in the cyclotron tank during the KAON project definition study. Although this cavity had been studied previously during beam development periods and beam dynamics measurements confirmed the calculated behaviour, the cavity never achieved a level of reliability suitable for routine beam production until recently. During 1999 the rf feedthrough was modified to allow reliable operation. The cavity could be powered routinely to a voltage between 120–150 kV, reducing the electromagnetic stripping in the 400–500 MeV cyclotron region by 33% and the time structure of the accelerated high-intensity beam bunches from the 4 ns structure transmitted through the cyclotron region to the 2 ns requested by the CHAOS experiment. In previous years the 2 ns feature was obtained by limiting the cyclotron phase acceptance with radial flags at significant cost to the overall intensity.

The challenge to be addressed over the next few years is to increase the total cyclotron beam intensity from the 220 μA available at present to a total of 300 μA. This will allow an additional 80 μA to ISAC. That facility was designed for 100 μA but it has been operating up to 20 μA at 500 MeV.

The major remaining limitation to achieving 300 μA is caused by beam-related electrode overheating in the centre region. The precise location of overheating has not yet been determined. Once this is done additional cooling may solve the problem. A pulsed beam with 400 μA peak current, 200 μA average, was previously accelerated to 500 MeV in 1987. This would tend to exclude space charge or beam dynamics as limiting the increase in current.

A brighter H^- ion source is also being developed. The cyclotron developments before the KAON Project Definition Study were aimed at achieving higher intensity with the use of one or two AAC cavities, higher particle accelerating voltage and rf improvements, etc. The work for H^- extraction during the KPDS era stalled this effort. Cyclotron development efforts in the direction of higher intensity must now continue with the new ISAC requirements.

With the approval of the 2000–2005 five-year plan, the need for refurbishing cyclotron systems or components to maximize the future efficiency of the machine was recognized. Special budgets were assigned to the RF, Vacuum, Ion Source, Injection Line, Diagnostics, Controls, Power Supplies, and Beam Lines groups during fiscal year 2000–01 for this effort. All of these groups took initiatives in the refurbishing direction through acquisition of much needed spares and replacements for old or obsolete components. One of the most urgent requirements, the overhaul of BL1A in the vault, was started before year-end and was actively organized for the 2001 winter shutdown. The report for the refurbishing activities will be included in the 2001 TRIUMF Annual Report.

Members of the Division were again involved in both of TRIUMF's key projects, i.e., the collaboration on the CERN LHC construction and ISAC. The Cyclotron Division is proud of the achievements for these projects during 2000. A major milestone was achieved just before year end with ISAC-I accelerating its first beam to the design total of 1.5 MeV/u. Also, routine delivery of the 500 MeV proton beam to the ISAC target for exotic ion beam operation at low energy could be increased from 10 to 20 μA.

BEAM PRODUCTION

Beam delivery for the year 2000 was quite successful with production statistics back on track after the previous year's TNF replacement. Cyclotron performance was enhanced by the use of an improved rf booster (RFB) system that was brought back into service following a successful test at the end of 1999. This allowed the delivery of 2 ns pulse width beam (as requested by Expt. 778) without the large current reductions resulting from the alternative method of using the radial flags used in the past. At the same time the RFB helped improve the cyclotron transmission and reduce the tank beam spill. Four months of shutdown left 5331 scheduled operational hours, about average, of which 4935 were achieved for an above average availability of 92.6%. These totals include 240 hours used for development and tuning and, as shown in Fig. 127, were split roughly 6:1 between high-current beam production and low-intensity, polarized operation. While high-intensity periods served a variety of users, polarized operation was for the most part shared by the parity

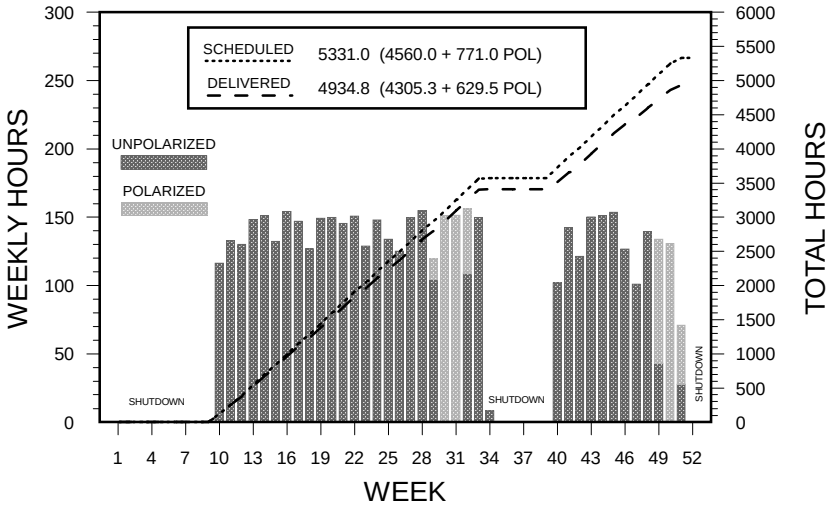

Fig. 127. Operational hours for 2000.

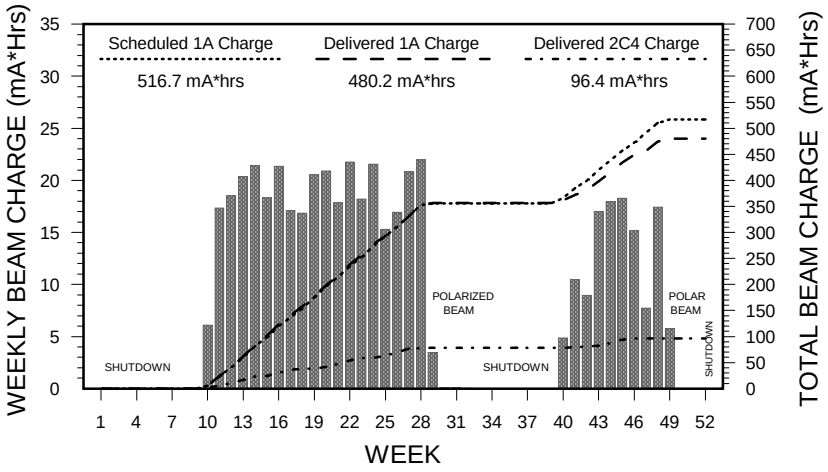

Fig. 128. Beam delivery for 2000.

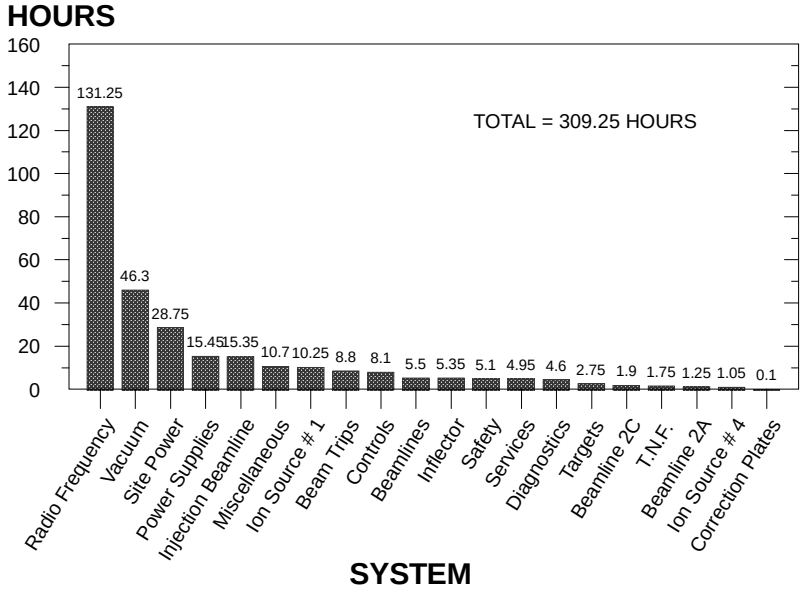

Fig. 129. Cyclotron downtime for 2000.

Table XVII. Operational record for 2000.

	Scheduled hours			Actual hours		
Cyclotron off:						
Maintenance	499.5			520.15		
Startup	100.0			94.00		
Shutdown	2762.5			2765.20		
Other	9.0			7.35		
Cyclotron downtime	0.0			309.35		
Overhead	34.0			105.15		
Totals	3405.0			3801.20		
Cyclotron on:						
Development	146.5	+	0.0 P	99.95	+	0.00 P
Cyclotron tuning	287.0	+	40.0 P	127.35	+	13.90 P
Beam to experiments	4126.5	+	731.0 P	4077.75	+	615.65 P
Totals	4560.0	+	771.0 P	4305.25	+	629.55 P
Actual/Scheduled = (4305.25 + 629.55)/(4560.0 + 771.0) = 92.6% availability						
Beam to experiments:						
1A Production	3871.5	+	0.0 P	3645.45	+	0.00 P
1A Development/tuning	0.0	+	0.0 P	27.50	+	0.00 P
1A Down/open/no user	128.0	+	634.0 P	273.50	+	528.00 P
1B Production	127.0	+	97.0 P	36.00	+	28.30 P
1B Development/tuning	0.0	+	0.0 P	3.15	+	3.70 P
1B Down/open/no user	0.0	+	0.0 P	92.35	+	55.65 P
Total 1A+1B production	3998.5	+	414.0 P	3681.45	+	341.30 P
2A2 Production	2736.0	+	575.0 P	2113.70	+	522.85 P
2A2 Development/tuning	0.0	+	0.0 P	19.05	+	1.70 P
2A2 Down/open/no user	1390.5	+	156.0 P	1945.20	+	92.80 P
2C1 Production/tests/tuning	423.0	+	155.0 P	115.95	+	17.50 P
2C4 Production/tests/tuning	3234.5	+	0.0 P	2492.00	+	0.00 P
2C5 Development/tune	8.0	+	0.0 P	3.70	+	0.00 P
4A2 Production	0.0	+	708.0 P	67.40	+	562.00 P
4A2 Development/tuning	0.0	+	0.0 P	1.40	+	17.85 P
4A2 Down/open/no user	69.0	+	0.0 P	78.35	+	12.85 P
4B Production	392.0	+	12.0 P	112.50	+	6.20 P
4B Development/tuning	12.0	+	0.0 P	12.40	+	3.20 P
4B Down/open/no user	3653.5	+	11.0 P	3805.90	+	13.55 P
Total BL4 production	392.0	+	720.0 P	179.90	+	568.20 P
1A Beam charge	516,730 μAh			480,184 μAh		
2A Beam charge	16,909 μAh			12,944 μAh		
2C4 Beam charge	133,310 μAh			96,386 μAh		

P = Polarized source on-line (although not necessarily polarized beam)

Table XVIII. Beam to experiments for 2000.

			Scheduled			Delivered		
Experiment *	Channel	Sched.#	h	h (pol)	μAh	h	h (pol)	μAh
614	M13	98	1279.0	0	161310	1101.05	0	123606
684	M9B	97	277.0	0	38780	259.90	0	36738
684	M9B	98	173.0	0	15115	108.55	0	7637
749	M20B	97	363.0	0	50820	362.35	0	52327
749	M20B	98	67.0	0	9380	60.10	0	4745
761	4A2	97,98	0	708.0	0	67.40	562.0	0
768	M15	97	127.0	0	17780	133.50	0	18649
768	M15	98	139.0	0	17850	74.20	0	9572
774	M15	97	273.0	0	33220	275.10	0	38811
774	M15	98	127.0	0	15240	127.90	0	14865
775	M20B	97	184.0	0	25760	192.10	0	27027
777	M20B	97	150.0	0	21460	147.30	0	21744
778	M13	97	2593.0	0	355350	2544.40	0	356448
778	M11	98	1279.0	0	161310	1101.05	0	123606
782	M20B	97	127.0	0	17780	99.45	0	13766
783	M15	98	268.0	0	35100	240.45	0	20361
784	M15	97	123.0	0	18230	120.55	0	17935
787/949	M11	97	127.0	0	17780	124.45	0	17612
791	M15	97	270.0	0	37800	271.30	0	38924
791	M20B	97	149.0	0	20860	147.30	0	20857
791	M20B	98	123.5	0	16620	118.45	0	11505
804	M15	97	358.0	0	50120	346.35	0	49407
804	M20B	98	64.5	0	7740	49.85	0	4204
806	2C4	97	3.0	0	0	0.10	0	0
806	4B	97	161.0	0	0	8.55	0	0
808	M20B	98	46.0	0	115	0.00	0	0
814	M15	97	150.0	0	21460	147.30	0	21744
822	M20B	97	127.0	0	17780	116.60	0	16444
833	M9B	98	148.5	0	18785	130.45	0	15764
834	M20B	97	273.0	0	38220	270.80	0	38538
835	M20B	98	127.0	0	15240	127.90	0	14865
835	M15	98	146.0	0	20440	131.95	0	18008
840	M9B	97	277.0	0	38780	273.45	0	39691
842	M9B	97	311.0	0	43540	313.90	0	45486
842	M9B	98	285.0	0	38290	206.15	0	27580
843	M15	98	127.0	0	17780	144.45	0	18077
844	M20B	97	150.0	0	21000	151.75	0	20718
846	M15	97	265.0	0	37100	269.65	0	39355
846	M20B	98	216.0	0	29080	206.15	0	27580
847	M20B	97	123.0	0	18230	120.55	0	17935
848	M20B	97	116.0	0	16240	122.35	0	18498
848	M20B	98	232.0	0	32480	241.85	0	32117
848/844	M20B	97	127.0	0	17780	128.10	0	18183
851	M15	97	277.0	0	38780	279.05	0	39549
851	M20B	98	69.0	0	9210	0.00	0	0
852	M15	97	127.0	0	17780	126.30	0	18905

Table XVIII (cont'd.)

			Scheduled			Delivered		
Experiment *	Channel	Sched.#	h	h (pol)	μAh	h	h (pol)	μAh
852	M15	98	173.0	0	15115	108.55	0	7637
856	M9B	98	193.5	0	26660	206.95	0	23371
858	M9B	97	146.0	0	20440	147.00	0	20628
860	M20B	97	150.0	0	21000	143.30	0	20294
860	M20B	98	148.5	0	18785	130.45	0	15764
864	M9A	97	397.0	0	55580	409.10	0	57846
865	M15	97	69.0	0	9660	67.50	0	9093
866	M20B	97	127.0	0	17780	131.80	0	19106
867	M20B	97	300.0	0	42000	301.20	0	42205
868	M15	97	277.0	0	29640	261.20	0	29524
868	M20B	97	127.0	0	5640	109.45	0	8806
869	M9B	97	277.0	0	38780	279.05	0	39549
869	M9B	98	127.0	0	15240	127.90	0	14865
869 TEST	M11	97	24.0	0	3360	23.95	0	3350
875	M11	97	554.0	0	77560	532.45	0	75077
876	M20B	98	150.0	0	15000	108.55	0	7637
877	M9B	97	127.0	0	17780	123.80	0	17910
877	M9B	98	150.0	0	21000	143.10	0	19322
878	M9B	98	201.5	0	26220	177.95	0	15067
880	M9B	97	550.0	0	78470	521.25	0	75207
881	M15	97	150.0	0	21000	147.15	0	20786
882	M15	97	127.0	0	17780	99.45	0	13766
883	M20B	98	58.0	0	7660	57.75	0	5189
884	M15	98	81.0	0	11340	74.30	0	10107
886	M15	98	148.5	0	18785	130.45	0	15764
887	M15	98	69.0	0	9660	68.80	0	9215
949	M11	97	146.0	0	20440	147.00	0	20628
CHARGEX	4B	97	150.0	12.0	0	99.65	6.20	0
DRAGON TEST	2C4	97	150.0	0	3000	147.20	0	676
ISAC†	2A2	97,98	2736.0	575.0	16909	2113.70	521.15	12944
ISOPROD	2C4	97,98	3081.5	0	130310	2342.90	0	95710
PIF	1B	97,98	150.0	97.0	0	36.00	28.30	0
PIF	2C1	97,98	268.0	143.0	0	94.85	7.90	0
P.THERAPY	2C1	97,98	155.0	12.0	0	20.15	7.95	0
NIF	4B	97	81.0	0	0	4.30	0	0
TEST	2C5	98	8.0	0	0	3.60	0	50
YEN	M11	97	127.0	0	17780	131.05	0	17315

* See Appendix D for experiment title and spokesman.

† Total proton beam on target for all ISAC RIB experiments and tests.

non-conservation experiment running in 4A2 and ISAC via BL2A2. As Fig. 128 shows, the total beam charge delivered to meson hall experiments along BL1A was 480 mAh or 93% of that scheduled, one of the better results for the past ten years. In addition, 96 mAh were delivered at 85 MeV to the solid target facility (STF) in beam line 2C4 for the production of radiopharmaceutical generators, and 13 mAh, twice the 1999 charge, to the west target station in BL2A2 for the production of radioactive ion beams (RIB) for experiments in ISAC. Six patients were treated for ocular melanomas during five proton therapy (PT) sessions in beam line 2C1 operated at 74 MeV. The annual downtime of 309 hours (Fig. 129) was well below average with the rf, as usual, responsible for the greatest share of this time (42%) followed by vacuum problems (15%) and power bumps (9%). The operational record and beam to experiments for the year are given in Tables XVII and XVIII.

Winter Shutdown

The year started with a fairly heavy load of shutdown activities on the main accelerator side, most of which were completed successfully. In the meson hall this included extensive BL1A work for which significant block movement was required. Jobs there included 1AT1 target MRO and the location and repair of two T1 area air leaks, one in the M13 vertical jaws and one in BL1A. There was also the repair of monitor 1AM8 whose cables had become radiation damaged. Further downstream there was the repair of the M20T2 and M9B beam blockers, 1AT2 water package MRO, M9A rf separator work, and the investigation of a T2 area air leak. In the vault section of BL1A, the radhard valve was replaced, the upper coil of 1VB1 was resecured and a new turbo pump station was added. On the BL4 side, cooling hoses were replaced on 4VQ3.

While some of the above jobs were proceeding, there was a continuing cool-down of the cyclotron until late January when the cyclotron lid was raised. Work in the cyclotron tank was rather limited and included centre region inspections (rf surfaces, correction plates, inflector), an inspection of the cryopanels, an investigation of a malfunctioning HESW spill monitor thermocouple, as well as some probe maintenance (X2C, X1 and X2A). The lid was lowered after the usual commissioning tests, but during initial low-current tuning the HE2 probe stuck. It was decided to extend the shutdown by one week to raise the lid to repair this device. The final shutdown dose was 51 mSv distributed among 73 workers with no one exceeding TRIUMF guidelines.

Beam Schedule 97

Startup was a bit hectic as experimenters hoped to get some stable beam during the tune up to high currents. After some necessary commissioning time for a new ISIS rf control system, the beam was steadily stepped up to the nominal current of 140 μA to BL1A. The TNF vacuum held steady around last year's 200 millitorr value because of an elusive leak that was too difficult to repair. Performance was unusually good for the high-intensity portion of this schedule (19.5 weeks) with a cyclotron availability of 95%. The delivered charge to BL1A was 356 mAh or just over 100% of the scheduled charge (at 140 μA). As these numbers suggest, cyclotron downtime was small; a modest 6 hours per week with about half due to the usual short-lived rf instabilities. Also, there was one extended problem with a faulty combiner capacitor and some PA damage caused by debris in the cooling system. The higher percentage for the charge is a result of converting some of the scheduled tuning time to beam time and delivering somewhat higher than scheduled currents because of efficiencies realized by running the rf booster.

Although not contributing significantly to cyclotron downtime, there were some problems with the secondary channels that affected production there. These included more trouble with the M13 and M9T2 beam blockers and with the M20B and M9A separators. The latter needed an extensive rebuild because of continuing water leaks. Monitor 1AM8 also developed a bellows air leak and had to be removed and blanked off. The 1AT2 vacuum was so marginal that it was not clear it would last until the next shutdown. Several air leaks were eventually found to be originating from the defunct M8 channel. Some increased CuALCW system losses were also noted towards the end of the operating period and determined to originate from BL1A.

In addition to the charge delivered to BL1A, BL2C4 received 78 mAh or 85% of its scheduled charge with losses primarily due to problems resulting from a poorly manufactured resin can, a large water leak (split hose) in one of the line's quadrupole magnets (2CVQ1) and from reduced currents during an Eu foil irradiation.

BL2A2 started a few weeks later and received 9.9 mAh at currents of either 1 or 10 μA, with the exception of a limited amount of 20 μA development work. This was a little less charge than scheduled because of an extended target exchange (to calcium zirconate).

Three proton therapy sessions treated the same number of patients in BL2C1. This line was also used at energies of 70 and 116 MeV and currents of a few nanoamps to irradiate objects in the proton irradiation facility (PIF). There was not much activity in

BL4B apart from some brief Chargex tests. Early in the schedule the line was used for a few follow-up irradiations of tantalum foils at 200, 350 and 500 MeV for Expt. 806, as well as for a brief neutron irradiation for NIF in conjunction with PIF at the end of the low current run.

Scheduled development shifts focused primarily on tuning higher currents through ISIS in order to achieve the higher total extracted currents required when ISAC runs full steam. The highest total extracted was about 225 μA compared to a normal production total of about 200 μA. A test installation of a higher output source at the end of the low current schedule ran into geometry problems. Some time was also allotted for OPS training when operators had time to practice machine and beam line tuning and calibrations. There was also some work done by Safety to test the recently implemented neutron monitor trip function and another test with the 2A probe programmed to cycle radially in and out of the X1 shadow. This successfully sent a few hundred nA of pulsed beam to BL2A.

After high-intensity operation ended, BL1A was used for 3 weeks as a dump for about 300 nA of 219 MeV beam stripped before parity's BL4 extraction foil in order to reduce the vertical size of the beam to that experiment. After some initial problems with the I4 microwave tube that resulted in their using a reduced high intensity ion source for a few days, parity (taking 200 nA of 222 MeV beam in BL4A2) had a fairly good run, getting 94% of their scheduled beam during the three week period. BL2A continued to run up to 1.5 μA to the end of the beam schedule including some dedicated pulsed beam delivery after parity finished. A pulser program sent five second bursts of 500 nA twice a minute to the west target station as required by the GPS experiment in ISAC. Then there was a switch to BL1B for PIF operation at 500, 350 and 200 MeV as well as the short NIF run in BL4B at 283 MeV.

Fall Shutdown

There was no overriding need to raise the lid during this one month September shutdown. The main thrust of activity was in the meson hall where work there again required a considerable amount of shielding block movement. Water leaks were located and repaired at M15Q1 and at the rotary collimator. Small and elusive vacuum leaks were found and repaired at the M11 septum. At 1AQ11 the downstream indium seal was replaced and in M8 the main and neutrals ports on the bender were blanked off to achieve the best 1AT2 vacuum in years. An air leak was repaired in the M13 beam blocker's drive piston and work continued on rebuilding the M9 rf separator. A modified 1AT1 target was prepared for installation in October with two graphite targets and a 4 mm horizontal aperture in the protect monitor as requested for Expt. 614 running in M13, and with all targets raised back 2 mm to the standard position as requested for Expt. 778 now running in M11. The disparity between optimal 1AT1 vertical positioning was confirmed by Expt. 614, but was not a serious issue this running period.

Beam Schedule 98

Cyclotron performance deteriorated in the final quarter with a number of problems reducing the availability to 86% for this period. The delivered charge to BL1A was 124 mAh or only 77% of the scheduled charge. This was primarily due to current restrictions during the first month because of inflector problems and because of a BL1A vacuum leak towards the end of the high-current portion of the schedule. Cyclotron downtime jumped to an average of 14 hours per week, half of it due to rf problems (including a phase mismatch following an IPA tube change) and most of the remainder due to the BL1A vacuum leak at 1AQ11 and some large power bumps late in the year.

Startup tuning was again interrupted with an emergency lid up, this time to repair the inflector whose positive electrode was failing to hold adequate high voltage. The lid was lowered and the main magnet turned on just as beam delivery was scheduled to begin. The reinstalled inflector required a significantly different tune to achieve standard high-current operation and, as this tuning progressed, an intermittent instability arose that hampered production for three weeks until the problem worsened and was finally traced to a bad cable or connection. Cyclotron performance improved considerably afterwards and for the remainder of the high intensity period the rf booster was again in operation.

There was some ongoing trouble with the BL1A tune including difficulties with formerly routine π^+/π^- changes. These, it seemed, were due in part to constraints of the new 1AT1 target that included a non-working target profile monitor, and 1AM8. Towards the end of the high-current run, the former (2 mm low) target ladder was installed to help clarify tuning problems. Unfortunately its profile monitor was also useless because of, it was then assumed, a faulty common signal cable between the target ladder and the electronics rack. Subsequent tuning went well, however, and the development shift went on to reduce front end and beam line 1A spills by lowering the extraction energy slightly. This gave rise to a cyclotron development shift at the end of the beam schedule that found disparities in some probe shadowing positions and recommended some measurements be taken next shutdown. Towards the end of the high-current run, a vacuum leak developed in the 1AT1 volume that was eventually tracked

down to the 1AQ11 indium seal that had been repaired in the fall shutdown. The original repair failed because the mating surfaces were not parallel and a compensating wedge-shaped seal was installed. There were also ongoing problems with the M13 and M11 beam blockers that were addressed.

In addition to the BL1A charge, there were 18 mAh delivered to the solid target facility in BL2C4 until a target failure occurred towards the end of its scheduled beam. The cause of a miniscule pinhole found in the centre of the rubidium target cassette is thought to be too high a beam density produced by too narrow an extraction foil. For various ISAC experiments, BL2A received nearly 3 mAh at currents ranging from 1 to 10 μA on calcium zirconate and SiC targets. BL2C1 was used at 74 MeV for two proton therapy sessions during which a total of 3 patients were treated. Because these took place during the high intensity schedule, the ISIS pepperpot was required to limit the injected beam during patient treatment times. There were no BL4 users but for the last couple of days of high-current operation PIF users ran BL2C1 at 70 MeV.

The last three weeks of the year had the I4 source again on-line for polarized delivery to the parity experiment that was continuing to test experimental set-up improvements. Beam was also delivered to BL2A2, taking 2 μA at 500 MeV, and PIF, running a few nanoamps at 200, 350 and 500 MeV in BL1B and 70 and 116 MeV in 2C1. When PIF finished there was a switch back to BL1A for use again as a dump for about 200 nA of vertically pre-stripped beam. The polarized source and the parity experiment ran quite well, the biggest problem being a couple of large power bumps that caused about a day of downtime. After parity finished there were two days of development and cyclotron device tests prior to shutting the various systems down prior to the Christmas holidays. The last week of the year was uneventful but a major refurbishment of the BL1 vault section and considerable tank work are included in a busy winter shutdown schedule starting in the new year.

High-Current Beam Development

TRIUMF currently operates with a maximum extracted current of 220 μA. A beam development program has begun to increase this to 300 μA, so that BL2A to ISAC can eventually operate at 100 μA without limiting the current available to other users. Additional centre region cooling and/or the installation of an improved high-brightness CUSP source will be required to achieve 300 μA.

Some beam development time has been devoted to studying high-current, low duty cycle tunes. This is the first step towards a 300 μA c.w. tune. In addition, by gradually raising the duty cycle and watching the temperature increases recorded on thermocouples located at strategic locations within the machine, we can better estimate the amount of additional cooling that will be required for running at 300 μA c.w.

TRIUMF's existing CUSP source has been optimized for 200 μA operation by making the extraction apertures small. To date, no attempt has been made to enlarge these apertures, and the current at the fast target has been limited to 470 μA.

Allowing for some decreased transmission at higher currents, it is estimated that at least 600 μA will be required to obtain 300 μA of extracted current.

During a 45 minute test at 97% duty cycle with an average extracted current of 230 μA and 58% transmission, temperature readings on the centre region thermocouples remained within allowable limits while approaching their equilibrium values. In 2001, development work will continue in order to improve the tunes and to reach higher currents. In addition, the new high-brightness CUSP source, currently being evaluated on an off-line test stand, will be installed and tested.

RADIO FREQUENCY SYSTEMS

RF Operations

The total cyclotron rf downtime for the year was 131 hours. The combination of sparking, crowbars and out of drivens caused 95 hours of this downtime. The next major downtime was an accumulation of 26 hours caused by the failure of a PA tube, an IPA driver tube, and a combiner capacitor.

The refurbishing of the rf system was delayed this year due to the loss of rf personnel. A start was made on the fabrication of the third combiner, assembly of the two preliminary combiners and the control system for the 92 MHz booster.

RF Support

The RF group was also dedicated to the following major projects in ISAC.

1. Assembly, installation, alignment and commissioning of the DTL tanks and bunchers for the successful rf and beam tests.
2. Commissioning of the 35 MHz spiral rebuncher.
3. Design, manufacture and signal level tests on the HEBT high beta buncher.
4. Prototype testing and design of the HEBT low beta buncher.
5. Prototype testing and design of the MEBT choppers.

These activities are reported in the ISAC section.

RADIO FREQUENCY CONTROLS

The 92 MHz rf booster rf control system was scheduled for replacement in 2000. The new system is a digital signal processor based system housed in a VXI mainframe. This will bring the system up to date with most of the rf control systems in the cyclotron and all of the rf control systems in ISAC. Local supervisory control of the digital signal processor is by an Intel Pentium processor communicating with the VXI mainframe via the IEEE 1394 FireWire standard. Design of the new system was completed and commerical hardware was purchased in 2000. However, due to the diversion of manpower towards ISAC, the implementation of the control system is delayed until 2001.

Incremental software upgrades were performed on both the main rf control system and the ISIS rf control system. The main rf system has developed some intermittent instability when running in the self-excited mode. Efforts are in progress to track down the source(s) of the instability. In the case of the ISIS system, software changes were made in order to provide more robust communication between the rf control system and the central control system.

CYCLOTRON PROBES AND DIAGNOSTICS

In addition to MRO activities, the major efforts throughout the year were focused on upgrading the beam line 2A extraction probe foil mechanism for high-intensity operation, and improving the ISAC target station and preseparator area diagnostics for serviceability in a highly contaminated environment. All other work was limited to essential repairs of the cyclotron probes and beam line monitors. The Diagnostics group biweekly meeting notes are available electronically via the Operations CYCINFO information service on the site computer cluster (accessible also through the TRIUMF home page on the WWW). The cyclotron shutdown activities are summarized in detail in the Diagnostics group meeting notes of March 17, 2000, and October 27, 2000.

ISAC Diagnostics

Completion of the west target station for operation and service at design beam intensities requires full remote handling capability. As part of this work the exit module service trays were modified so that they can now be removed at the hot cell without need for hands-on assistance at the containment box. Also, the commissioning profile monitor at ITW:harp5B was replaced with a properly engineered one of a smokestack design using the new style of multi-wire pc board. A new design for the diagnostics box DB0 at the preseparator was made to improve the reliability and to make the mass selection slits removable with remote handling techniques. The assembly was well under way at year end with installation scheduled during the winter shutdown.

A stripping mechanism retrieved from Brookhaven was recommissioned and techniques were developed for handling the very thin foils required for stripping of low energy ions in MEBT. The Diagnostics electronics support provided electronics modules, cabling and system integration for the diagnostics of the new ISAC installations of LEBT and MEBT.

Probes MRO

The 2A extraction probe was inspected. An rf-lossy insulating limit-switch actuator on the L-arm had overheated, resulting in intermittent operation of the L-arm limit. A new actuator made of G10 material (which is more tolerant of rf fields) was installed. The commissioning L-arm with a rotating foil cartridge of the beam line 4 style was found to suffer damage from beam heating, so a current limit of 15 μA was imposed for beam schedule 99. The design of the high-intensity L-arm similar to that on extraction 1 was completed. This L-arm utilizes a flat cartridge that holds up to 9 disposable foils and will be available in the spring of 2001.

The 2C extraction probe was cleaned, inspected and relubricated. No heat or mechanical damage was found. New foils were installed. The standard load of 2C foils lasts about 6 months.

Extraction probe EX1 was removed for routine service. All support bearings were inspected and cleaned. New drive tapes and cables were installed. No problem was found with the L-drive ball screw and a problem reported with the L motion was attributed to a fault in a stepping motor translator module in the control system. The cable-tensioning brackets were showing signs of wear, but this problem was left to a future service.

High-energy probe HE2 was removed and repaired with a minor modification, the problematic recirculating ball bearings that are prone to jamming were replaced with rollers. This change was successful but must be considered to be a temporary measure. A refurbishment project has been approved in the 5-year plan to replace one of the high-energy probes. The probe's functional requirements have been specified, but Design Office resources are required to make progress on the design.

Monitor MRO

All vault and standard beam line monitors were serviced during the shutdowns. To remedy the chronic problem of recurring leaks in aging ferrofluid feedthroughs, a refurbishment program has been

funded to replace the standard beam line monitors. Orders have been placed for the materials required and the work will be spread out over several years beginning in the summer of 2001. Smokestack monitor 1AM8F developed a leak in a bellows and was removed from service in the fall shutdown. It will be repaired and reinstalled during the winter shutdown.

Probes and Diagnostics: Developments and Upgrades

The beamspill monitors installed in BL2A have been calibrated in terms of known losses and fields nearby. This was necessary to permit operation at currents greater than 10 μA. Pairs of non-intercepting beam-position monitors had been placed at the beginning and end of the long drift through the wall of the cyclotron vault. They consist of inductive pick-up loops above, below, and to either side of the beam. They were designed by L. Rezzonico of PSI and use the same signal processing as at PSI. The linearity was checked and the units calibrated in terms of voltage output per mm displacement of beam. At the present time the voltages are displayed in the cyclotron control room, but there has been no call to upgrade the display to show actual position. This may change when higher beam currents are run.

Experiment 614 requires that the position of the proton beam not move by more than 1 or 2 mm with respect to the target 1AT1 for the length of a run that might last several days. It had been shown previously that the beam position was stable to 0.1 mm but only for a one hour period. The standard monitor had plates separated by 5 mm in both horizontal and vertical directions. The beam spot is taller than it is wide and it was possible to get sufficient signal from upper and lower plates to show that the experimental criterion was met in the vertical plane. However, it was necessary to build a new monitor with left and right plates separated by 4 mm in order to confirm long-term stability in the horizontal plane. This was installed and personnel from the experimental group monitored the readings from the four halo plates of the T1 protect monitor for several days and, with the help of Operations, calibrated that monitor. The beam position was stable to within 0.1 mm in both planes during most of that time, with brief excursions up to 1 mm. The latter may have been associated with re-optimization of the cyclotron tune.

The radioactive ion beam in ISAC is sometimes modulated in intensity in order to reduce background signals from competing decays. It is sometimes desirable to modulate the proton beam hitting the isotope production target in order to reduce the amount of undesirable isotopes created in the first place. This has been done by pulsing the beam in ISIS and this affects all other users of the cyclotron. Shortly before the fall shutdown an attempt was made to modulate the current in BL2A by moving its extraction foil into and out of the shadow cast by the extraction foil for BL1A. This would also modulate but not necessarily null the beam current in BL1A, and should not affect any beam lines at lower energy. The experiment was successful. The foil X2A was run into and out of the beam at different rates of acceleration and no evidence of vibration or jitter was seen. The rise and fall times of the BL2A current agreed with those expected from the acceleration of the foil carriage, except that the fastest transition time measured was $\geq$0.3 s. The source of this limitation on bandwidth was not determined convincingly. The experiment ended by cycling the extraction probe continuously for 3.6 hours. There was no slippage between the motor controller and an absolute position encoder. The probe mechanism was inspected carefully during the shutdown and no sign of damage was seen. We believe that cycling the radial position of X2 is one method to modulate the current in BL2A with minimal perturbation to other users.

The positions of the extraction and diagnostic probes in the cyclotron are determined first by surveying the position with respect to other cyclotron components, such as the centre post, at the time that the probe is installed and then operating the probe with the control system keeping track of the readings from shaft encoders. Drifts in encoder readings are checked occasionally by running the probe to a limit switch whose position was determined during the initial survey and by comparing the encoder reading with an absolute encoder for those probes where one has been installed. There has been growing concern that discrepancies have arisen between relative probe positions despite these procedures. A series of measurements was made in which each of several probes in turn was made to shadow, i.e. just touch, the orbit of a well-tuned beam. Such cross calibrations have been made previously. The new measurements imply that the radial position displayed by extraction probe X1 disagrees from the mean position of other probes shadowing the same orbit by as much as 1.3 inches and that this offset has increased since the time of the last check. A careful taping of the positions of the four probes that are operated through ports in the tank wall will be conducted during the forthcoming winter shutdown.

Several useful equipment items have been purchased. A digital phosphor oscilloscope with enhanced memory features has been purchased for the control room. A precision programmable pulse generator will make the calibration of diagnostic instruments in the field easier. For example, pulses matching those from a toroid or a particle detector can be generated. An

Ethernet hub installed in BL1A has allowed us to read monitor output on any X Window terminal.

VACUUM AND ENGINEERING PHYSICS

Vacuum

The cyclotron vacuum system performed well during the year. The only significant downtime was due to the failure of a seal ring in one of the B-20 cryogenerators. There were also a few brief interruptions due to unexplained pressure rises in the tank. The data available seemed to indicate a heat load from the tank, presumed to be due to rf leakage. Continued and closer observation eventually traced the problem to a leak in the cryoline vacuum jacket. The suspect area was treated with leak sealer and will be repaired during the winter, 2001 shutdown. In the course of investigating this problem, it was noticed that the consumption of liquid nitrogen in the B-20 heat exchanger increases dramatically with the time between defrosts. Economic operation will require routine defrosts in the future.

There were a few problems with the beam line 1A vacuum during the year. The pressure in both T1 and T2 rose during the spring and summer, although never to the point of disrupting beam production. The T1 area leak was traced to an indium seal that was replaced during the fall shutdown. The leak in the T2 volume was found to be in the M8 area. There was evidence of more than one leak and the decision was made to remove the slit box, blank the line at the exit of the first bender, and replace the seal in the blank flange on the zero degree port of the bend box. The M8/T2 repair was successful and the pressure is now very good there. The 1AQ11 seal is unreliable due to a component misalignment. The seal failed again in November and was replaced. By December it was failing again. The beam pipe will be realigned during the winter, 2001 shutdown to solve this problem.

Engineering Physics

The inflector, correction plates and thermocouple systems performed normally until September when an insulator in the inflector system failed. The lid was raised and all the insulators for the inflector and deflector were replaced. It was very difficult to achieve a good machine tune after this repair and it was not possible to operate at the scheduled beam current. There was some suspicion that the inflector was not positioned correctly. The major problem was eventually traced to a high voltage breakdown in the inflector negative cable system. A spare cable was connected and the situation was much improved. While full current can now be run, the inflector still seems to be more sensitive than it was. It will be removed in the winter, 2001 shutdown and the alignment checked.

ISIS AND POLISIS

The CUSP ion source and injection line continued to operate well for the past year with only minor downtime due to spurious interlock faults caused by aging equipment. As for the past few years, there were no major activities undertaken during 2000 as ISIS personnel were involved in the completion of ISAC projects. These include the high energy beam transport (HEBT) systems, the drift tube linac (DTL) optics, and the lithium beam line.

The polarized H^- ion source I4 supplied beam for the engineering runs for the parity experiment scheduled for July 19–August 8 and December 6–20. In the summer, I4 actually began operation July 23, due to a delay in installing a new 29 GHz microwave tube. The first week of the run was single user, followed by shared beam with ISAC. When sharing with ISAC, a typical beam inventory was:

- I4: 25 μA;
- Fast target: 12 μA;
- Circulating: 2 μA (17% transmission with some bunching);
- BL1 shadowing: 0.5 μA;
- ISAC: 1.3 μA;
- Parity: 0.2 μA.

Only one pumping laser was used, instead of the normal two, reducing the H^- polarization to about 70%. The other pumping laser was borrowed by ISAC for the β-NMR experiment. The argon ion photodetachment laser used to produce coherent intensity modulation of the H^- beam gradually died during the run, ending up at 5–6 W.

For the winter run, a new tube was installed in the photodetachment laser. The maximum H^- beam intensity modulation was 0.1%, about half of what was expected. Perhaps the H^- beam was off-axis. As in the summer, the beam was shared between multiple users, and required some bunching. A Pockels cell circularly polarized the light from the single pumping laser, thus increasing the H^- polarization to about 80%. The resulting increase in unwanted helicity-correlated beam parameter modulations was not important for the engineering run.

PRIMARY BEAM LINES

The year 2000 began with a cyclotron shutdown and, with it, the relocation of shielding blocks from over the 1AT2 region to outside the main cyclotron building. This was necessary to allow repairs to be made near the 1AT2 target.

The bellows unit of the M9 beam blocker was removed, repaired, and reinstalled. A vacuum leak at the connection of the first quadrupole of the M9 channel

to the 1AT2 monolith was repaired by replacing an indium seal at that point. The window of M8, a suspected source of a vacuum leak, was also blanked off.

Blocks from over the 1AT1 region were then removed to allow access to that area. Because the blocks from over 1AT2 had been removed, those from the 1AT1 area could be stacked where the others had been. In the 1AT1 area the jaws of the M11 channel were repaired, as was the "in" limit switch of the 1AT1 profile monitor.

Attention was then turned to the cyclotron vault. O-ring seals were inspected and replaced as required. In the vault section of beam line 4 a water leak was repaired by replacing a hose. In that of beam line 1, the vent valve of its combination magnet required repair. It was noted that a coil of the 19.8° dipole was not firmly constrained. With parts made in the machine shop it was possible to correct this problem.

In May, after running was resumed, the M13 beam blocker required repair. A temporary repair was made so that operation could continue until the next shutdown. At the end of the month an interlock problem at the first dipole of the M11 channel necessitated that the 1AT1 area be opened so that the problem could be corrected.

A vacuum leak at the neutrals port of the M8 channel had been suspected for some time. It had been planned to correct this problem during the September shutdown. However, the vacuum had deteriorated to an extent that other sources of leaks had to be considered. To reach this region it was again necessary to move shielding blocks from that region to outside the building. This was done in mid-August. Because other problems had arisen in the 1AT1 area, it was decided to tackle it first, thus allowing more time for the 1AT2 region to cool.

In the 1AT1 region, quadrupole 1AQ9 immediately downstream of the target had developed an interlock problem. This was traced to a faulty thermal switch and an adjustment was made to the wiring of the thermal switches. The first quadrupole of the M15 channel also had an interlock problem that was traced to a broken wire. In addition, a water connection had developed a leak. A special wrench had to be obtained before repair could be effected. Because a vacuum leak was discovered in the area, the 1AT1 target was reinstalled and pumping began. There appeared to be a recurrence of a vacuum leak at the bellows of the M11 septum. The region was sprayed with sealant and liquid epoxy but the pressure remained high. Efforts to locate the leak were suspended to allow repair of the M13 beam blocker to proceed.

As noted above, this beam blocker was temporarily repaired during the January shutdown. Its piston assembly was removed and sent to the machine shop for modification. The modified assembly was installed and its limit switches set.

Attention was now turned to the 1AT2 area. Because of the high residual radiation levels, a comprehensive radiation survey of the area was made first. Then, considerable time was spent planning how work in the area could be accomplished with a minimum risk of exposure to the persons involved in the repair.

Once adequate shielding had been arranged, all vacuum joints upstream of the M8 neutrals port were checked for leaks. None were found and it was concluded that the leak at the neutrals port had become worse. Close-in shielding around 1AT2 was replaced leaving access to the neutrals port. The M8 slit assembly was removed and the neutrals port blanked off.

Attention returned to the vacuum leak in the 1AT1 area. It was finally traced to an indium seal in the bellows at the downstream end of the 1AQ10/11 quadrupole doublet. Experience has shown that it is not unusual to make several attempts to effect a seal with these indium joints. True to form, the joint was made vacuum tight on the second attempt. This repair was deemed to be temporary; a permanent redesign of the joint support will be fabricated and installed in the January, 2001 shutdown.

In both shutdowns this year the Beam Lines group has been pressed both in manpower and time. Its duties have been well executed and group members deserve commendation for having accomplished the required work efficiently and within the time scale allotted.

2C

The production of the radioisotope ^{82}Sr in the solid target facility (STF) on 2C4 continued to be the major user of 2C beam time. This year, there was more operating time than the previous records of 121 days in 1996 and 123 days in 1997. There were 135 days of ^{82}Sr production in 2000 for a dose of 95.50 mAh and a yield of 31.87 Ci at the end of bombardment. The beam intensity was reduced to typically 40 μA because of scheduling difficulties, cyclotron intensity problems and imposed restrictions from previous target failures. This was a significant increase over 1999 production of 118 days for a dose of 70.73 mAh and a yield of 26.80 Ci. There were seven natural rubidium targets used for the 2000 production.

The STF was also used for production of a ^{148}Gd source that will be used for set-up of the DRAGON facility in ISAC. This involved irradiating a europium foil encased in aluminum foil at 28 MeV on the target, for 628 μAh in twenty shifts. Beam was extracted at 70 MeV and was restricted to a maximum intensity of 5 μA, extracted on a narrow extraction foil (0.015 in. wide) that was used to reduce the beam spills and halo

from the nominal foil (0.200 in. wide). A 0.100 in. foil was added to the 2C extraction probe during an emergency raising of the cyclotron lid in late September. This foil will be a compromise with more current than the narrow foil and less spill than the nominal foil at 70 MeV. The 0.100 in. foil was used for the only ^{127}Xe production run at 105 MeV into the cesium target on 2C5, but more tuning is required to reduced the beam spill in the 2C exit horn. The 0.100 in. foil was also used at 85 MeV for the irradiation of the rubidium target, RA20, that failed with a minor leak. The foil created a very symmetric beam spot, but increased the beam density so that the containment foil was damaged where the beam hit the target. Two short irradiations of Ta foils at 110 MeV were done on the STF. 2C1 was scheduled for 29 shifts of proton therapy and 12 shifts of proton irradiation facility (PIF).

CONTROLS

The Central Control System (CCS) continued to run reliably throughout 2000. Year 2000 (Y2K) catastrophes failed to materialize and there were no other large problems in the CCS. Cyclotron downtime due to CCS causes, as recorded by the Operations group, was listed as 8.1 hours. This is 2.6 hours more than the previous year, but the 8.1 hours represents a small fraction (2.6%) of the overall cyclotron downtime. More than 7 hours of downtime was due to hardware failures such as power supply faults.

There has been progress on general CCS goals. Replacing aging VAXes with Alpha computers has advanced, the network infrastructure has moved to a gigabit Ethernet backbone and local 10/100 Mb Ethernet switches, and the overall goal of replacing aging components has continued, albeit slowly. An additional goal of improving the reproducibility of beam tunes has also received some attention and will be of increasing importance.

CCS Facilities

There are a number of software topics to mention, including new developments and enhancements to existing items. An unusual event was the Y2K apprehension, which proved to be unfounded, and the new year came in without incident. Logged data and cyclotron messages were organized and put on CD for long-term storage. This makes retrieving old data much easier than the previous system that employed magnetic tapes. Support for the new network hardware included development of SNMP routines for gathering hub information and installation of Perl 5 for SNMP support. The beam line 2C controls and user interface continues to run reliably using Vista software. Configuration of the BL2C controls was changed by replacing the VAX with an Alphastation 600, and reorganizing and tidying up the software. With the change to the Alpha, the performance of the user interface was dramatically improved. A new data logging program, data_logger, was started. It provides for faster data retrieval than the existing program called cycscan. Development has continued on exploring a Windows NT connection to the CCS.

Numerous existing software packages were modified during 2000. Several of these packages received almost constant additions and enhancements due to their heavy use and the requests for new functionality. The five most heavily affected packages were the XT display pages (XTpages), the scans, Xstrip, the console panels, and the device (system and thumbwheel) support routines. Changes to these packages are too numerous to note here.

Software upgrades occurred on Oracle (to version 8i), and VMS (to version 7.2-1). New timers were added for beam lines 2A and 2C. Additional 2A timers will be added in the following year to support the new 2A foil cartridge. The PCI/CAMAC interface software has been modified to be autoconfiguring. Enhanced support for the pulser was added including a new XT page 5P. The histogram program now has max/min/current value markers, more colour features, and default gain setting. XRC, the X Window based remote console program, was modified to support register status and control. Improvements were made to the adjusted current calculations and the beam line 2A energy calculation. The user interface to the cables database was moved from a Web implementation to an X Window based one. The X Window program, called Xstrip, that strips out logged device data and displays it, had numerous enhancements. Xstrip has become a commonly used tool and as such will warrant further enhancements. XT pages can now dynamically call Xstrip and during the next year XRC will also be modified to call it.

There were a number of changes to the hardware configuration of the CCS. VAX computers are being phased out and Alphas are being used in their place. With the replacement of the beam line 2C VAX this year, the production cluster is now only Alphas. The proton therapy VAX was in the process of being phased out at year end and when it goes, only Alphas will need to be supported for new developments. Two VAXes are still in use for diagnostics and development, but they should be replaced during 2001. At the end of the year there were 3 DS10s, 2 Alphastation 600s, and one Alphaserver 2000 in use for production, developments and diagnostics.

The existing computers received some modifications. Such things as memory, cache, disk, and DSSI interfaces were upgraded and a CD burner was added.

The proton therapy computer and the PC server each received a DLT tape drive for doing backups. The existing FDDI based network is being phased out and a gigabit Ethernet backbone and switched 10/100 based Ethernet is being installed. We expect that by the end of 2001 all of the CCS network traffic will be running through the new system. A number of changes also occurred in the CAMAC. The last four of the old CAMAC crates that were used for trim and harmonic power supply control were replaced with two new crates. By replacing old DACs and digital controllers, fewer crates were necessary. After these changes were made, the DACs for the trim and harmonic power supplies were calibrated. UPS power was extended to more equipment and further UPS work will be done in 2001. Because even the UPS can fail, a number of the UPS units were connected to the CAMAC system so that they can be monitored. Beam line 2A and the site services received 32 channel expansions to their ADCs.

Each year there are numerous hardware failures and 2000 was no exception. The network hub that is being phased out had a power supply problem and another power supply was purchased for that system. Motor controllers had problems. The VXT X Window terminals continue to fail frequently, but in most cases they can still be repaired and put back into service. The DSSI disk systems hung up on 2 occasions for unknown reasons. There have been problems with an HP 5Si and an HP 4050 printer. One of the UPS systems had a problem. There is a large number and variety of CAMAC equipment that for the most part runs very reliably, but there were a variety of CAMAC module problems. These included such items as crate power supplies, DACs, a parallel branch coupler, a crate controller, an active extender, battery chargers, fans, etc.

A refurbishing budget was established this year. The planning had included a number of goals where the largest had been to develop and deploy a new ADC module. Unfortunately, the design has been delayed due to higher priority jobs for the group undertaking this design. An aging disk system due for refurbishing in the following year was moved ahead and the ADC project has been delayed one year.

The issue of beam reproducibility has gained a higher profile. Tools to understand beam related problems are being enhanced. The ability to switch from one tune to another more quickly will be further investigated in the next year.

Other Systems

As mentioned earlier, beam line 2C controls have been enhanced in several ways. The old VAX has been replaced by a much faster Alpha. The software directory structure was reorganized and significantly cleaned up. A change to a newer version of the Vista software has been initiated and should be completed during the next year. Support continued for the parity experiment. This was made more difficult by the departure, after almost 10 years of service at TRIUMF, of the person most familiar with the parity/ion source 4 controls. Proton therapy (PT) also received support as necessary during the year. A new PT summary panel display was developed for the Cyclotron Operations group. During the winter shutdown, replacement of the PT VAX by an Alpha was initiated. The Alpha should be operational during the spring, 2001 startup.

Miscellaneous

Security on the computer systems has been of increasing concern. A number of actions have been taken on site to enhance the situation but increased attention and resources will need to be given to security in the future.

Unfortunately, two members of the Controls group left TRIUMF during 2000. They were both very valuable contributors to TRIUMF's ongoing success and left with a combined 25 years of experience at the laboratory. Their contributions were appreciated and will be missed.

OPERATIONAL SERVICES

Remote Handling

ISAC

For another year the principal activity for Remote Handling personnel was in support of ISAC projects. Module construction continues with target modules #2 and #3, and manufacture of spare components. The south hot cell and support facility is still under development and commissioning continues on the remote controlled crane system console.

The addition of a technician-in-training for hot cell operations, dedicated to the ISAC program, will greatly ease work loads during target changeover and shutdowns. Conversely, the loss of a senior technician to the ISAC division will distribute the workload in other directions.

Cyclotron servicing

A single main shutdown was scheduled for the beginning of the year. Routine Cu-block removal, shadow shield handling and radiation surveys were performed. The major remote handling job for the shutdown was the removal and replacement of the 2C extraction probe for work by the Diagnostics group. An unplanned intervention was required in March for repair, including removal of the high energy probe #2, Cu-block removal and the installation of some shields to enable in-tank activities. Another event in September, involving the cyclotron beam inflector, again required

Cu-blockers to be removed and a small complement of shadow shields to be installed. The only effort provided for the cyclotron elevating system for the year was an alignment check and inspection service of the guide bushing at station #2.

Beam lines servicing

The ISAC radioactive ion beam lines between the preseparator magnet and both the west and east target stations were rebuilt to a revised design incorporating additional shielding. Assistance was given with the replacement of the 1VRR1 rad-hard valve in the cyclotron vault, and a vacuum leak repair at the 4BP7-SEM (Faraday cup). At the T1 area of beam line 1A a 1AQ9 thermo-interlock cable was replaced, and cooling water leaks at M15Q1 and the 1A rotary collimator were repaired. A vacuum leak in the M11 septum bellows was investigated. An indium seal downstream of the 1AQ11 magnet developed vacuum leaks twice in the last four months of the year. One occurred during a scheduled beam run and required an interim patch until a proper repair can be completed. At the T2 area the major task was the disconnection of the M8 secondary beam line vacuum volume from the main system. A blank-off plate was installed downstream of M8B1 replacing the slits box, and the blank-off at the M8B1 neutrals port was replaced. Also in the area, an indium seal was replaced in the M9Q1-T2 joint to repair a vacuum leak, an M9Q2 thermo-interlock cable was replaced, and 1AM10 and 1AM11 beam monitors were vacuum leak checked.

Hot cells and targets

Maintenance of production targets and services occupied the majority of the workload for this year. The cooling packages at 1AT1 and T2 were serviced and refilled, a pressure transducer at T1 was replaced along with a valve relay, and a mechanical flow test performed to calibrate feedback readings. The T2 cooling package had both flow and pressure transducers replaced, as well as a water conductivity cell. At T2 the air cylinder drive for the M20 secondary channel beam blocker was rebuilt using a revised design with 50% more elevating thrust. The T1 target had a "home position" microswitch replaced on the Mk1 assembly. The Mk2 target had a new protect monitor and new graphite targets installed. It was then placed in service in beam line 1A for Expt. 614 which uses these graphite targets. The Mk2 target trombone assembly was lowered to match the corresponding alignment of the Mk1 target. Work continues on the development program for vacuum brazing of new graphite targets. Assistance was given with servicing of 2C resin cans and filters, and with modification of an existing filter housing. The 1AM8 monitor was serviced in the targets storage pit for a leak check of a worn bellows. Hot cell housekeeping for the year included disposal of seven 2C spent resin cans and uranium rods used in the ferficon experiment. These items were all sampled and gamma spectra measured by TSG prior to shipment. A broken wrist-actuation tape was replaced on one hot cell master-slave manipulator. The beam line M8 slits, removed this year, were packaged for storage in the east cell. ISAC work included assistance with manufacture and construction of the new hot cell doors as well as removal and storage of the 100 μA Mo target used for a high-current experiment at the ISAC west target station.

Magnet Power Supplies

The year 2000 saw the installation of power supplies for the ISAC DTL, HEBT, DRAGON and TUDA lines. With the exception of DRAGON, where supplies from the decommissioned M8 channel were used for high power applications, the supplies are switch-mode supplies. Polarity reversal capability was also supplied for 100 A service for steering magnets.

For the existing TRIUMF facility, the majority of the work was MRO with calibration of trim and harmonic supplies as well as beam line 1A supplies occurring during the winter shutdown.

Failing Entrelec switches are being replaced, as well as cab-tire cabling related to these switches. The insulation of this wiring has become brittle and is being replaced with RW 90 cabling.

Wakefield heatsinks are being replaced with a new copper design that should provide better service.

With the added load that ISAC represents, we are having to develop expertise in switch-mode power supply technology. To this end, a training course for power supply staff is being arranged.

Electrical Engineering Services

Electrical Services is involved in both new installations for ISAC and MRO activities for existing systems. Supervision of outside contract labour for installations for ISAC and assisting with TRIUMF electrical staff as required presents a formidable challenge.

In parallel with these activities is MRO which represents a significant task because of the age of existing installations and the multiplicity of fault reports that arise and have to be addressed to keep the facility functional. Old installations that are substandard are being addressed and this is foreseen to require a significant workload. Staffing levels are a concern because of the aging and ever increasing size of the electrical system.

Electrical Systems

Activities involved new installations for ISAC and maintenance of the existing systems. The department

processed about 40 orders between large installations and minor construction tasks. These required the provision of both infrastructure and experimental support. About 200 trouble calls and numerous minor requests were attended to. Typical maintenance activities included servicing lighting systems, motors, air conditioning controls, panel boards and transformers, HV switchgear, breakers, and capacitor banks. Continuing engineering support was provided to the TRIUMF users. Design support was provided for the TWIST experiment, the refurbishing of the Batho biomedical facility, and for the site surveillance system. The site lighting upgrade is still in progress and will continue in the next fiscal year.

Services provided for new electrical installations for ISAC included DTL, HEBT, DRAGON, TUDA, LTNO, hot cells, and various other installations. Some of these installations are still in progress. The major installations for ISAC-I are foreseen to be completed in early 2001. Providing support for experiments will be an ongoing task, as will the maintenance of the new installations.

In the last few years efforts have concentrated on the new projects, with the result that the upkeep of the existing systems suffered.

Major site installations outside ISAC included the refurbishing of the Batho biomedical facility and the new maintenance support facility for ATG in the meson hall.

Power Delivery

A "bumpless" switchover was successfully completed at the beginning of September in cooperation with the Utilities Department of the University of British Columbia. This was accomplished by paralleling the two 12 MVA substation transformers for a period of time. In the future, shutdown of TRIUMF power can be limited to the time when servicing the main switchgear is required, typically every five years. Future annual maintenance of the substation equipment may be carried out without power shutdown to TRIUMF.

Power management continued as a routine activity. The monthly averaged peak power demand increased almost 13% to 6736 kVA from 5968 kVA last year (Fig. 130). Again this year May saw the largest power demand (8436 kVA). The electricity consumption jumped another 12% to 53.2 GWh from 47.4 GWh (Fig. 131). The largest consumption was reached in November (5.82 GWh). The power factor (PF), averaged over the calendar year, dropped 0.5% to 96.1% from 96.6% (Fig. 132). The power factor during operational months remained around 95.1%. This trend is expected to continue next year as more ISAC systems are brought into operation.

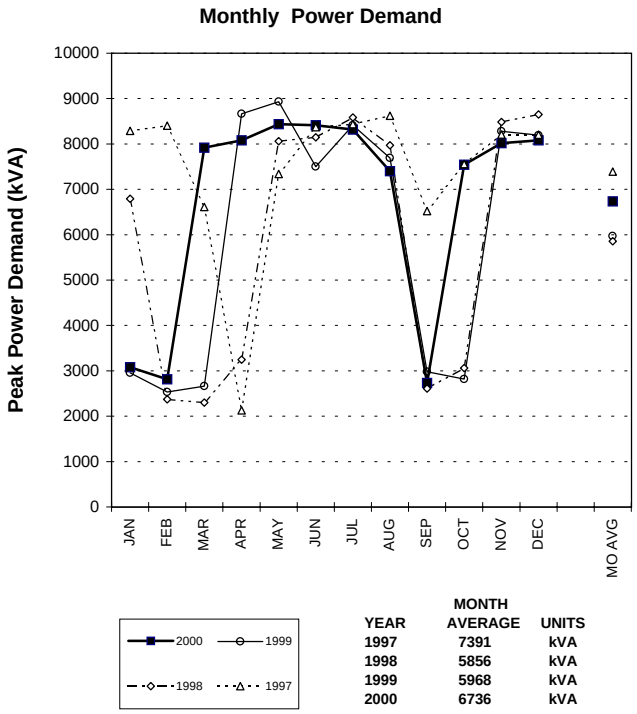

Fig. 130. Electrical system power demand – four year comparison.

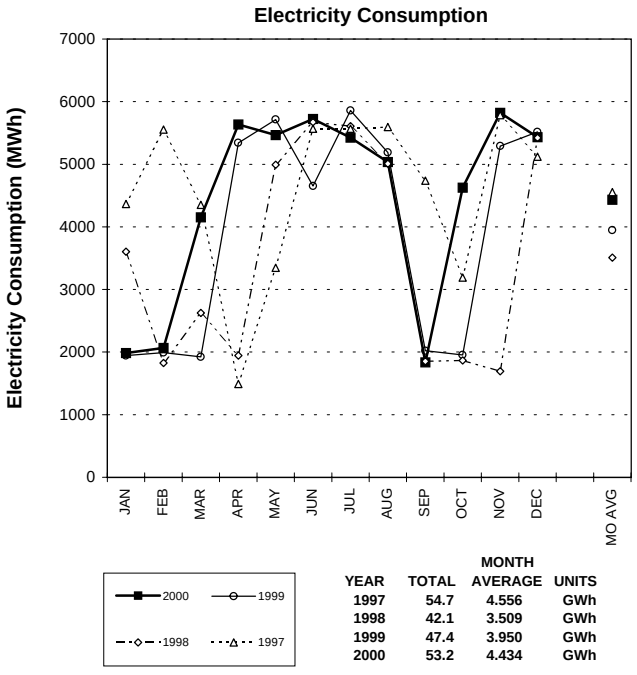

Fig. 131. Electrical system energy consumption – four year comparison.

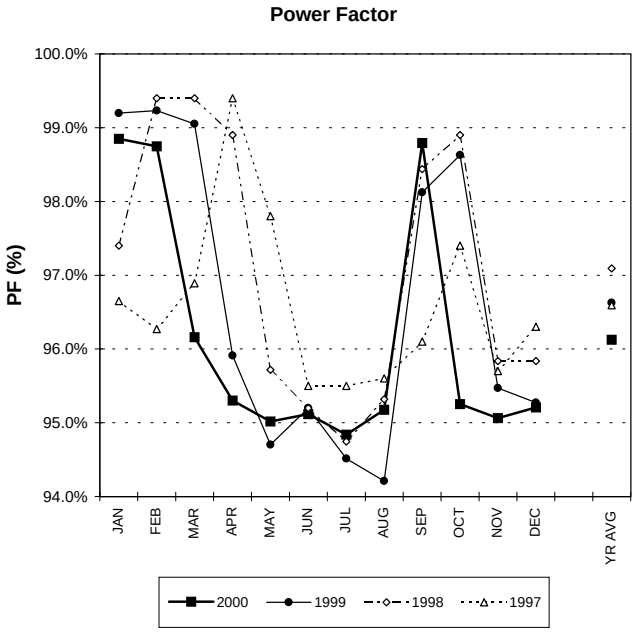

Fig. 132. Electrical system power factor – four year comparison.

Mechanical Systems

ISAC

A majority of site mechanical service engineering effort went into ISAC related projects. Notable jobs included: assembly and services for fume hoods, new compressor for chiller CH-1, new transmitter and remote for EH crane, piping services for MEBT, HEBT, DTL, DRAGON and TUDA, DRAGON hydrogen vent, air conditioning for TUDA shack, assembly of TRINAT cooling water return system, high level alarms for decontamination sump filling points, charcoal filter for target hall vacuum pump exhaust, perimeter drainage sump pump piping, and laminar flow diffusers for TRINAT. Preliminary engineering and cost estimates were provided for ISAC-II, and an estimate was given for a new target hall for a U.S. laboratory. Assistance was provided for the ISAC OPS training program. Estimates were given for a superconducting rf test facility to be located in the CRM area of the main office building.

Calculations for HEBT buncher water flow were provided and consultation provided for DTL cooling problems.

TRIUMF

Larger jobs included: medical annex HVAC overhaul and modifications to suit new occupants, reroofing, boiler burners overhaul, replacement of machine shop water pipes, new stainless gas lines in MESA, connection of TNF vacuum pump exhaust to the BL1A exhaust system, sorting out troublesome hot water circulation in the chemistry annex, and various air conditioning repairs. Annual safety inspection and testing was given for the site fire sprinklers, lifting equipment and active exhaust HEPA filters.

ISAC PROJECT

INTRODUCTION

There has been much activity and many accomplishments in ISAC this past year. The results of this effort are particularly evident in the experimental hall where free space is now at a premium. During 2000, ISAC has been gradually evolving from a construction and commissioning phase towards a fully operational facility. This has implied changes to resource allocation as well as the implementation of new procedures. Operators were trained and given the responsibility of providing radioactive beams to a fully scheduled low-energy science program. With up to 20 μA on target, ISAC has been providing record yields of selected short-lived isotopes for experiments. Yield measurements for some short-lived species indicate unanticipated enhancements as the proton current is increased. The chain of rf accelerating devices and the transport beam line required to provide beams to TUDA and DRAGON are nearing completion. The off-line ion source (OLIS) was used to commission the accelerator components as they became available. A major milestone was achieved on December 21 when a helium beam was accelerated from the OLIS up to full energy (1.5 MeV/u). Progress on the remote handling of the pre-separator slits and the storage vault for spent targets has prepared ISAC for licensing and operation with 100 μA of protons on target. A formal request has been made to the British Columbia Knowledge Development Fund for money to construct the ISAC-II buildings, and procedures have been initiated with the University of British Columbia towards obtaining the required development permits. Meanwhile, development of certain key ISAC-II technology has begun. Formal links have been established with INFN-Legnaro on the construction and testing of a medium-beta superconducting rf resonator structure, and also with ISN-Grenoble on measuring the performance of a charge state booster (1+ to n+ CSB) based on an electron-cyclotron-resonance ion source.

ISAC OPERATIONS

This year was one of transition between commissioning and operation of the ISAC-I low energy facility. Four new operators and a target hall coordinator were hired in the first quarter. Intensive training was provided in the last few weeks of April by way of more than 30 hours of formal lectures (a result of approximately 200 hours of preparation time for the lecturers). The lectures were videotaped for future use in the training of new operators. This training was introductory and should be considered as the first iteration of a training program which will be developed as a "systems approach to training" (SAT). In early May, after this initial training, the new operators were assigned to shift work and began coverage of ISAC beam production. Unfortunately, one of the new recruits left in June to accept a position closer to his home in the Okanagan. Two replacement operators were hired in October, and had received their orientation and introductory training by the end of the year. Thus, at year end, the group was composed of ten members: the head of ISAC operations, a training and documentation coordinator, seven operators including new personnel (Chris Payne, Harvey Quan, Saeideh Yeganeh, Rene Tanaja and Travis Cave), and, finally, a target hall coordinator, John McKinnon.

Less reliance was made on beam physicists during routine beam operation, although their assistance is always a welcome benefit. Their efforts have been more devoted to studying the beam reproducibility, and during commissioning of each new target they have been available to optimize the beam through the mass separator (especially the emittance) and to measure target yields.

During periods of extended maintenance, the ISAC operators have been available to assist with maintenance and other ISAC activities such as the installation of new facilities. In the target hall, much progress was made in preparing the facility for regular service. The boot change area was set up with radiation monitoring equipment and stocked with supplies of protective clothing. Special tool cabinets and work areas were set up in the hall, and the procedures for disconnecting the target services and transporting targets between the target station and the hot cell were developed.

This year, for the first time, operational performance statistics are provided for the ISAC beam production. It should be noted that as a single user facility of radioactive ion beams (RIB), there is an incentive to minimize activation when the beam is not required. This is done by stopping the RIB on a Faraday cup in the target station and, for longer periods, turning off the proton beam. For operations purposes, these appear as OFF time for each experiment. Some of this OFF time may be due to a cool down period during an acquisition cycle, or overhead for the experiment such as changing of samples or collection tapes. Therefore some care must be taken in using these statistics for analyzing the scheduled experiment beam time usage.

Table XIX gives the down time for each ISAC system and overhead for operational activities. For most systems, the down time is a sum of many different problems, e.g. for controls, related to the PLC hardware and EPICS program. The magnet power supply

time results mostly from a single event in which the mass separator power supply developed a water leak. "Beam line 2A unavailable" indicates times when the proton beam was off for a variety of reasons, including scheduled cyclotron maintenance. "ISAC idle" includes time when the proton beam may have been available but, in the absence of system failures, ISAC RIB was not delivered, e.g. when trained operators were not available or experiments were unable to take beam.

ISAC Beam Statistics for Beam Schedules 97 and 98

Table XIX. ISAC systems downtime and overhead for beam schedules 97 and 98.

ISAC system	Hours
Controls	78.20
Diagnostics	0.50
Magnet power supplies	63.60
OOPS	16.15
Safety	1.20
Services	1.65
Site power	9.40
Vacuum	2.75
OTHER	
Beam line 2A unavailable	964.50
ISAC cooldown	57.05
ISAC idle	188.05
ISAC startup	38.55
ISAC maintenance	1.00
Target/ion source conditioning	145.80
Procedures	40.40
Operator training	9.30
LEBT tuning	352.10
Target changes	92.50
Yield measurements	19.35
TOTAL	2,082.05

The history of operation of ISAC production targets is given in Table XX. Several target changes were done this year. The first ever target change scheduled during beam production, utilizing the target hall remote crane and newly commissioned hot cell facility, occurred in June. A target composed of niobium foils for the production of rubidium beams was replaced with a target of tantalum foils for the production of gallium and lithium beams. Although the planned procedures were followed, some cross contamination of residue in the target module containment box onto the exterior of the target module, most likely via the manipulator grippers, resulted in a minor spread of contamination in the target hall. The predominant species were ^{83}Rb and ^{85}Sr. The hall was cleaned up and several contamination control steps were added to the procedures. As a result, there were no incidents of contamination in the subsequent target changes. In July, the tantalum target was replaced with one of compressed calcium zirconate pellets for potassium and rubidium beams, then in October a target of silicon carbide pellets was installed for production of lithium beams. Until the second target station is commissioned, the turn around for a target change is about ten days which includes a two day cool down period, five days to effect the change and three days for conditioning of the new target.

The members of the ISAC Operations group take great pride in their contributions to the successes of the major ISAC milestones which were achieved this year and have been highlighted elsewhere in this Annual Report. RIB was available for 2,478.95 hours (1,872.85 + 155.55 + 450.55). The combined cyclotron/ISAC performance was 66.2% (2478.95/3745.00). All scheduled experiments received enough beam to satisfy their

Table XX. ISAC target history.

Target ID	In date	Out date	Charge μAh	Thickness g/cm^2	Power μAh $\times$ g/cm^2	Comments
CaO #1	25-Nov-98	15-Dec-98	70	36.00	2,520.0	Failure due to EE short
CaO #2	20-Dec-98	15-May-99	363	31.10	11,289.3	Failure due to EE short
Nb foils #1	14-Jul-99	20-Oct-99	3,242	11.10	35,986.2	Failure due to TBHT-t/c problem
Nb foils #2: R1	01-Nov-99	09-Dec-99	3,149	11.50	36,213.5	Removed for 100 μA tests
Dump only	10-Dec-99	10-Dec-99	43	0.00	0	100 μA test
Talbert	17-Dec-99	12-Jan-00	197	10.00	1,970.0	100 μA test
Nb foils #2: R2	17-Mar-00	04-Jun-00	5,913.8	11.50	68,008.7	Total: Nb foils #2 R1 + R2
Ta foils #1	10-Jun-00	19-Jul-00	3,515.83	21.25	74,711.4	Removed for $CaZrO_3$
$CaZrO_3$ #1 R1	24-Jul-00	21-Aug-00	518.7	42.27	21,925.4	9.45 g Ca/cm^2, 21.51 g Zr/cm^2
$CaZrO_3$ #1 R2	02-Oct-00	18-Nov-00	838.0	42.27	35,422.3	9.45 g Ca/cm^2, 21.51 g Zr/cm^2
SiC #1 R1	18-Nov-00		2,174.0	7.43	16,152.8	7.43 g SiC/cm^2: 5.05 g Si/cm^2, 2.38 g C/cm^2

commissioning milestones and preliminary experiment requirements. The RIB delivered to experiments is shown in Tables XXI and XXII. In the coming year, in addition to providing beam for the scheduled experiments and performing systems maintenance, the major effort will be to establish and complete the SAT training program for ISAC operators, which includes systems operation manuals.

Table XXI. Beam time available to ISAC experiments (hours).

Experiment #	Scheduled	Actual	Tune	Off
E715 (TRINAT)	912.00	606.25	14.10	55.30
β-NMR commissioning	660.00	351.90	41.75	44.80
E815 (β-NMR)	168.00	156.20	11.65	16.85
E801 (GPS1)	204.00	124.70	12.65	16.70
E823 (GPS1)	480.00	317.15	2.45	47.70
E823 (GPS2)	156.00	128.90	7.35	7.05
E826 (LTNO)	72.00	27.50	2.50	24.80
E828 (LTNO)	409.00	19.75	9.45	193.70
E863 (LTNO)	132.00	1.10	8.60	1.00
E841 (YIELD)	516.00	139.40	45.05	42.65
Mass separator development	36.00	0.00	0.00	0.00
TOTAL	3,745.00	1,872.85	155.55	450.55

Table XXII. Radioactive beams delivered to ISAC experiments (hours).

Isotope	E715 TRINAT	β-NMR Comm.	E815 β-NMR	E801 GPS1	E823 GPS1	E823 GPS2	E826 LTNO	E828 LTNO	E863 LTNO	E841 Yield	Total
^{7}Li*		17.55								1.55	19.10
^{8}Li		334.35	156.20							2.55	493.10
^{14}N*									1.10^{+}		1.10
^{26}Na										15.15	15.15
^{36}K										3.15	3.15
^{37}K	60.35				0.50					4.30	65.15
^{38}K	544.00				123.50					3.60	671.10
^{39}K*	1.90				0.85			6.60			9.35
^{64}Ga										0.40	0.40
^{74}Ga					1.15						1.15
^{75}Ga										0.90	0.90
^{76}Ga										0.45	0.45
^{74}Rb					180.65	94.75				18.95	294.35
^{75}Rb					10.50					3.90	14.40
^{79}Rb								13.15			13.15
^{80}Rb						34.15					34.15
^{85}Rb*										7.70	7.70
^{87}Rb*										0.40	0.40
^{91}Rb							27.50				27.50
^{133}Cs										0.50	0.50
^{162}Yb				124.70							124.70
Other										75.90	75.90
Total	606.25	351.90	156.20	124.70	317.15	128.90	27.50	19.75	1.10	139.40	1,872.85

* stable beam

$^{+}$ from OLIS

CONVENTIONAL FACILITIES AND INFRASTRUCTURES

The year 2000 was the last of the 4 year construction effort for ISAC! TRIUMF's endeavour to have the new ISAC beam line operational as per schedule demanded continued and focused support from the Infrastructure group. In the next fiscal year, ISAC-I will be a fully operational facility. However, construction activities will continue with the newly approved ISAC-II expansion project. Close coordination work continued with the Accelerator group, the Engineering group and the Science Division. This included attendance at regular and engineering meetings and participation in engineering design reviews and maintaining the as-built arrangement drawings. The Data Network continued to expand to accommodate the new experimental stations.

Once the β-NMR facility was completed, the focus of the installation shifted towards the services for the high-energy beam lines and the remaining infrastructure in support of the experimental program. The gas handling facility and a liquid nitrogen facility were installed late in the year. Maintenance was carried out with the help of the Plant group. A few problems surfaced in the mechanical services but they were promptly corrected. Discussion started on the functional requirements to be incorporated in the ISAC-II project and a preliminary building concept was prepared. Preliminary engineering and cost estimates were provided for ISAC-II. Assistance was provided for the ISAC operators training program.

Building Services

A significant effort was given to support the building services requirement for ISAC. Major projects included:

- A radiation shield at the DTL portion of the high-energy beam consisting of a 24 ft long $\times$ 12 ft wide $\times$ 11 ft high steel beam structure to support 18 removable composite lead on plywood panels.
- A 16 ft long $\times$ 12 ft wide $\times$ 9 ft high data acquisition cabin for the TUDA experimental facility. The cabin was built in conventional wood stud construction with vinyl coated gypsum panels on the outside and plywood on the inside. All internal surfaces were covered with a copper sheet to provide insulation from RFI noise. Dissipative tiles were installed on the floor to prevent excessive static buildup.
- An 18 ft long $\times$ 12 ft wide $\times$ 9 ft high gas storage and handling facility was installed adjacent to the east wall of the experimental hall to provide the experimental program with its gas requirements. This building is also of conventional wood stud construction with pre-finished metal siding panels on the outside and painted drywall inside. The roof deck is made of two-ply torch-on membrane. An explosion proof exhaust fan ensures the evacuation of volatile gases from this room.
- A liquid nitrogen tank was placed next to the gas handling facility.
- The sectional east hatch in the experimental hall was redesigned and replaced with a single 9 ft $\times$ 7 ft $\times$ 12 in. reinforced concrete block for ease of access to the target hall and hot cell areas.
- The access to the target hall was also redesigned to implement a radiation control zone. The new area includes washable walls, vinyl floor, sink, a worker change area and boot boxes.

Electrical Services

The installation of services in the experimental hall continued at a fast pace throughout the year. On the design front, we were very busy with finishing the β-NMR services, and continuing the design for the DTL, HEBT, DRAGON and TUDA services. Design is still in progress for the 8π station. An elaborate, electrically shielded data acquisition cabin and a single-point signal reference scheme were engineered for TUDA along with a high-isolation transformer to minimize electrical interference and disturbances to the very sensitive detector electronics.

Major tasks for the year included the installation of the dc and ac power distribution, racks for beam line power supplies, controls and diagnostics, and cable tray systems and grounding for the following systems/areas:

- β-NMR 60 kV station.
- DTL.
- Safety. Conduit runs installation for the radiation safety monitoring system in the HE experimental area. Support for the sequence and interlocks for exclusion areas and high voltage stations.
- DRAGON experimental station.
- TUDA experimental station.

The services for DRAGON, the second leg of HEBT and the gas handling facility are still in progress and will be commissioned in February, 2001.

Mechanical Services

Most of the site mechanical service engineering effort went into projects in the high-energy area of the experimental hall. Notable jobs included: assembly and services for fume hoods; new compressor for chiller CH-1; new transmitter and remote control for the experimental hall crane; piping of cooling services for MEBT,

HEBT, DTL, DRAGON and TUDA; DRAGON hydrogen vent; air conditioning for the TUDA data acquisition cabin; assembly of TRINAT cooling water return system; high level alarms for decontamination sump filling points; charcoal filter for target hall vacuum pump exhaust; breathable air supply in the target hall; perimeter drainage sump pump piping; and laminar flow diffusers for TRINAT. Estimates were given for the superconducting rf cavity assembly and test facility. Calculations for HEBT buncher water flow were provided and consultation provided for DTL cooling problems.

SAFETY AND RADIATION CONTROL

Licensing

Early in 2000 a licence amendment to operate ISAC with a proton beam current of up to 20 μA on any target up to $Z = 82$ for a limited number of shifts per month was obtained from the Canadian Nuclear Safety Commission (CNSC). Application was made in October for a new licence as required by the change from the AECB to the CNSC regime. This application also requested operation of the ion beam accelerator system and proton beam on target of up to 100 μA. A positive response is expected by April, 2001.

Access Control and Radiation Monitoring

The ion beam radiation monitoring system (IBRMS) was expanded to accommodate new experiments as they came on line. The IBRMS was also extended in anticipation of the operation of the ion beam accelerator system and the high-energy experiments. The new emphasis on quality assurance for safety critical systems meant that the TRIUMF Safety Systems group participated in the specification, documentation and acceptance testing of the high-voltage interlocks for the β-NMR experimental station. Similarly, they defined and documented the access control requirements for the DTL X-ray enclosure and the high-energy experiments.

Commissioning

The installation of all shielding as initially specified was completed during 2000. As expected, the addition of the steel shielding between the target station and the pre-separator magnet completely eliminated the problem of neutrons streaming up to the TRINAT experiment level.

Some low levels of short-lived radioactive contamination were detected in the target maintenance hall after a target exchange. Extensive tests were subsequently carried out with a dummy target module to determine the air flows into or out of the target maintenance hot cell during the target transfer. It was verified that the air flow was always directed into the hot cell under all circumstances as predicted by the design. There has been no spread of contamination on any subsequent target exchange.

REMOTE HANDLING GROUP

ISAC Target Modules

A great deal of work on the construction of new ISAC target modules was performed by Remote Handling personnel.

The module assembly area in the ISAC experimental hall was revised to better suit the installation of the HEBT beam lines. Work continued on target module #2 with further revisions to the containment box and the construction of required spare parts.

Target module #3, which has been in shielded storage in the target hall since the 100 μA beam-heated target experiment, was removed from storage. The Mo target was removed and the shielding plug and containment box assembly moved to the experimental hall module assembly area for further work.

Target Hall

During the winter shutdown, three initial remote accessible module storage silos were completed and installed in the target hall. Modules from the ITW station were transferred to both the new silos and the ITE station vacuum tank during the spring shutdown as required for installation of additional perimeter shielding at both the ITE and ITW stations.

Design was completed for a spent targets storage vault to be located in the target hall. This will allow for interim storage of irradiated targets for either eventual re-use or as short-term decay storage prior to off-site disposal.

Beam Lines Servicing

The beam line at zone #5B between ITW and the pre-separator magnet was uncovered in January and rebuilt by Remote Handling with new iron and concrete shielding around a revised beam line with a new rad-hard valve and new beam profile monitor. Existing overhead shielding blocks were cored at this time to accommodate the new, taller design of the monitor. Preparations were completed for installation of the ITE beam line section, except for the actual monitor, at the same time. Both beam line sections are now fully remote serviceable for component handling.

Hot Cell Facility

Hot cell construction for the year included an improved inert-gas capping system for the Pb glass shielding windows, and a portable shielding plug for the roof access portal. The north and south cell access doors were fabricated, fitted and filled with concrete.

Handling procedures were improved with the design and fabrication of working prototype jigs for removal and replacement of the containment box access covers as well as for handling of the target module TIS component mounting tray.

The hot cell south support area is being provided with tooling, cabinets, a fume hood and more defined area safety control barriers.

During the 2000 operational year, the Nb #2 target was replaced with the Ta #1 target in June for a short running period. This was then exchanged for the first $CaZrO_3$ target in July. This target was in turn replaced by a SiC target in November. Revised handling procedures for decontamination and control have steadily improved, reducing previously encountered levels of movable contamination to minimal values and eliminating any spread of contamination within the target hall.

Remote Crane Handling System

Improvements continued on the remote crane operating console with improved controls and displays. A PC driven video switcher and pan/tilt control now allows for general target hall viewing both at the controls console and at selected internal network PCs. Operator training has now provided us with three fully qualified remote crane operators. The requisite six remote module transports for three target exchanges this year were performed as scheduled.

ION SOURCES FOR ISAC

Electron Cyclotron Resonance (ECR) Source

The design of a radiation hard 2.45 GHz ECR source is nearing completion.

It is based on the ECR source that was tested in the ion source test stand (ISTS) and the results reported in last year's Annual Report.

The vacuum chamber of the ISTS that was used so far to test ion source prototypes must be replaced during the first quarter of 2001 by a bigger one to accommodate and test the radiation hard ECR source prior to its installation into the ISAC target module.

Off-Line Ion Source (OLIS)

It was used throughout the year to: a) commission the ISAC accelerators, b) tune the beam transport lines and accelerators prior to operation with radioactive ion beams, and c) provide the low-energy experimental facility with stable beams.

A stable beam of Mg^{1+} ions was requested in year 2000. It was newly produced by direct evaporation of a high purity magnesium plate mounted within the plasma chamber of OLIS. Plasma interaction yielded enough Mg vapour to produce a stable 200 nA Mg^{1+} beam.

Charge State Booster (CSB)

In the ISAC-II facility, the accepted mass range is extended from 30 to 150 u.

ISAC-II will utilize the existing ISAC-I RFQ for low-energy acceleration. The CSB would take the singly charged radioactive beam from the mass separator and boost the charge state to be compatible with $A/q \leq 30$ for the RFQ.

One of the few known dc methods to boost the charge state of an ion is based on the electron cyclotron resonance (ECR) source principle. Such an ECR charge breeder (CSB) has been developed at the Institut des Sciences Nucleaires (ISN) in Grenoble [Sortais *et al.*, 5th Int. Conf. on Radioactive Nuclear Beams (RNB-5), Divonne, France, April, 2000].

A research collaboration agreement between ISN Grenoble and TRIUMF was signed in September. The goal of the seven months' collaboration is to provide TRIUMF the know-how and the properties, from a realistic 1^+ beam, with the ISN charge state booster method using the ISN 14.5 GHz ECR source and $1^+/n^+$ test bench facility.

The essential points of this project are to measure: a) the efficiency of the $1^+/n^+$ process for ion species relevant to the ISAC experimental programs (such as Rb, Ga, Sr, Sn, Fe, Zn, Ar, Kr, Xe, etc.); b) the overall breeding time (of utmost importance for short-lived isotopes); and c) the proportion of unwanted species (stable contaminants) self generated by the CSB.

The TRIUMF computer controlled beam measurement system nears completion and it will be shipped to Grenoble in January, 2001. Installation and data-taking will be carried out until the end of March/April, 2001.

ISAC TARGETS

In 2000 the ISAC operating licence was upgraded to allow up to 20 μA p^+ beam current operation during four days per month for beam and target development purposes. Two target materials (Nb foils and Ta foils) have now been operated at 20 μA p^+ beam currents.

At the beginning of the 2000 ISAC run schedule, the Nb #2 foil target used in 1999 was reinstalled and continued to be used for rubidium beam production to Expts. 823 and 828/LTNO. ^{8}Li beams were also delivered to the ISAC β-NMR facility for commissioning purposes. The Nb #2 target was operated with $\leq$10 μA p^+ beam currents from April 20 to June 4. On May 26, 15 μA operation was achieved during the day shift and from June 3–4 the target was operated for 19 hours at the 20 μA proton current level. The production of ^{74}Rb was observed to increase threefold from 10 to 20 μA to a high of 6.1×10^3/s. There are indications to

suggest that the nonlinear increase is due to radiation enhanced diffusion of Rb in the Nb matrix. Including the 1999 run period, the Nb #2 target received a total of 5914 μAh of p^+ for an integral dose of 2×10^{20} protons on target. After 117 days in place, the target was still operational when retired from service.

From June 14 to July 15, a 21.3 g/cm^2 Ta foil target (Ta #1) consisting of 512 foils of 0.025 mm thickness was irradiated to produce beams of ^{162}Yb for Expt. 801, ^{75}Ga for Expt. 863 and ^{8}Li for β-NMR polarizer commissioning. The ^{162}Yb yield was of order 10^9/s under 10 μA irradiation, two orders of magnitude higher than required by the experiment. The ^{75}Ga yield at 10 μA was 2×10^5/s with <0.04% ^{75}Rb contamination. For target development, two periods of 20 μA operation were used to measure yields of Li, Na, Al and K isotopes. The measured ^{8}Li yield was 8.9×10^7/s at 10 μA, with a nonlinear rise to 5.2×10^8/s at 20 μA. Yields of ^{9}Li, ^{11}Li, ^{26}Na and ^{38m}K also displayed nonlinear increases with proton current, while the longer-lived ^{38g}K did not. As with the previous Nb foil target, the nonlinear yield increase with proton current is consistent with a radiation enhanced diffusion effect. The Ta #1 target was in place for 31 days receiving 3519 μAh of p^+ for an integral dose of 8×10^{19} protons on target. The target remains operational.

A target of pressed pellets of $CaZrO_3$ (42.3 g/cm^2) was irradiated from July 23 to August 20 and again from October 1 to November 15. The thermal properties of the target material precluded proton beam currents greater than $\sim$3 μA. However, the target was successfully operated for 73 days receiving 1357 μAh of p^+ for an integral dose of 3×10^{19} protons. The $CaZrO_3$ material proved to be superior to the CaO targets previously used for production of light K isotopes. The K isotope yields were of the same order as with CaO, but with greatly reduced target deterioration. Yields of 1×10^7/s of ^{38m}K and 5×10^6/s of ^{37}K were provided to Expt. 715/TRINAT. The Zr component of the target material also allowed delivery of ^{79}Rb and ^{91}Rb to the LTNO facility for commissioning and for Expt. 826.

A SiC pressed pellet target (7.4 g/cm^2) was irradiated from November 24 to December 20. The target was used to produce ^{8}Li beams (2×10^7/s at 10 μA) for β-NMR facility commissioning and to determine Na yields for future accelerated beam experiments. Over 26 days the target received 2155 μAh of p^+ for an integral dose of 5×10^{19} protons. The target remains in place.

ISAC POLARIZER

The first transmission of unpolarized ^{8}Li through the ISAC polarizer had been achieved in December, 1999. The first four months of this year were spent preparing the system for the first polarized beam. This entailed bringing the Na neutralizer and He re-ionizer cells into operation, and fabricating and installing deceleration electrodes, deflection plates, magnetic coils, a fluorescence monitor, laser beam polarization and transport systems, associated safety equipment and controls. The argon ion laser and Ti:sapphire laser used to collinearly pump the ^{8}Li beam were borrowed from the I4 polarized H^- ion source. The Ti:sapphire laser cavity mirrors had been customized to allow lasing at 673 nm, giving us a rudimentary polarization system.

A brief test in May produced 10–15% polarization, estimated from β-decay asymmetries. This was an encouraging result, considering that the laser parameters were far from ideal for collinear optical pumping. The standing-wave laser had a time-averaged bandwidth of approximately 2 GHz (FWHM) and lased chaotically on about 20 cavity modes with 700 mW total power. (The ideal laser should lase simultaneously on two modes separated by the 381 MHz Doppler-shifted hyperfine splitting in the ^{8}Li ground state.) The test also showed that the D_1- and D_2-transition fluorescence monitor, used for tuning the ^{8}Li beam energy into resonance with the laser, had a signal to noise ratio of about 15 at the estimated ^{8}Li current of 10^7 atoms per second. Polarized $^8Li^+$ transmission efficiency through the polarizer was 60%.

The laser was modified for the next β-NMR run, July 4–12. The laser cavity length was shortened to increase the cavity mode spacing from 220 MHz to 358 MHz ($\pm$1 MHz) and the free spectral range of the uncoated intra-cavity tuning etalon was decreased from 200 GHz to 100 GHz. (All laser cavity mode spacings were only known accurately in retrospect, following the implementation of an accurate beat measuring technique in January, 2001). This had the intended effect of reducing the number of lasing cavity modes (by a factor of 3) while leaving the total power unaffected. The highest ^{8}Li polarization observed was about 40%. In addition, polarization could be kept at 30–35% for several hours by non-specialists, using an automated stabilization system, and re-tuned by non-specialists when the polarization dropped. The stabilization system was based on a laser spectrum analyzer locked by computer to a frequency stabilized HeNe laser. The drift of the Ti:sapphire laser was monitored by computer with the spectrum analyzer, and compensating changes were made to the Na cell bias to keep the ^{8}Li beam energy in resonance with the laser. The hyperfine splitting was resolved by the fluorescence monitor, with a signal to noise ratio of about 50.

The final β-NMR run this year was $3\frac{1}{2}$ weeks in November and December. During the July run, the laser still hopped chaotically between modes. Therefore many ^{8}Li atoms, traversing the polarizer in 2 μs – much

less than the mode-hopping time – did not see the laser light, or saw only one mode. Further modifications to the laser between July and November involved increasing the mode spacing to 368 MHz, and increasing the etalon finesse by coating both surfaces with 10% reflectivity layers. This finally made it possible to produce simultaneous lasing on only 2 modes, with a total power of about 200 mW. (Note that the power per mode did not drop.) However, despite this improvement, the measured ^{8}Li polarization dropped by half compared to July, for reasons not understood. Progress on diagnosing the problem was hampered by the very low beam intensities available – approximately 10^6 atoms/s at the start of the run, dropping to 10^5 atoms/s when the polarized ion source I4 was brought into operation. In the latter case, it was not possible to obtain a useful fluorescence signal, although tuning was possible using the β-NMR asymmetry signal.

By year end, we were ready to upgrade the Ti:sapphire laser to a perfect 381 MHz spacing between just 2 cavity modes, with no drift in laser frequencies. This is achieved by placing one of the laser mirrors on a piezo-electric mount, which allows active stabilization of the cavity length using the laser spectrum analyzer as a monitor. In addition, in December a used ring dye laser arrived on site on indefinite loan from KEK, Japan. The plan is to have the ring laser set up for the next β-NMR run. A single frequency ring laser can be used as a more conventional, albeit expensive, method of polarizing ^{8}Li and it is also a precise diagnostic tool. It is also essential for polarizing ^{7}Li, which is useful for stable beam tests, and for polarizing ^{11}Li, an isotope required for a recently approved experiment.

ENGINEERING

Engineering support is initiated by the submission of a Request for Engineering Assistance (REA) form. These are assessed, assigned, and reviewed weekly. During this report period there were 35 ISAC REAs submitted. 12–15 others were carried over from the previous year as large projects, several of which will be carried over to 2001, i.e., DRAGON and target modules (TM2 and 3).

The following is a brief description of some of the major tasks that Engineering participated in during this period.

- Target modules: TM3 had been completed far enough to allow its use in a 100 μA non-RIB test in December, 1999, and then it was stored in the target hall. TM2 was built during 2000 and will be completed in the spring of 2001 as a surface ion source module. TM3 will be completed in 2001 as an ECR source (availability sometime in 2002).
- East target station: An REA was submitted and a budget approved to design and build an entrance and dump module for the east target station. This did not occur due to lack of manpower and priority, but will definitely reappear in 2001.
- Conditioning station: An REA for this job first appeared in early 1999, but work did not commence until 2000. The conditioning box and stand were manufactured and are currently awaiting assembly. The remainder of the station (i.e., beam line and diagnostics) have yet to be completed, but completion of the box would still allow for target conditioning.
- ECR source: This is another carry-over project that has been through many design iterations due to mechanical/manufacturing considerations, as well as information from development work. Release to manufacture is imminent.
- DTL: The year 2000 saw the completion of tanks 2 through 5. The tanks, stands, ridges and stems were put out for tender and manufactured by local industry. Assembly was completed at TRIUMF, and installation and alignment achieved later in the year. This also involved design and manufacture of four triplet magnets associated with tanks 2 through 5. Successful stable beam transmission was accomplished just before Christmas.
- HEBT buncher: A 35 MHz spiral buncher was designed, detailed and manufactured. This buncher was a larger version of the MEBT buncher and will be installed and commissioned in 2001.
- Remote handling issues: There were a series of engineering meetings held to discuss remote handling issues unique to ISAC (in the target hall and hot cells). This is of primary importance in order to develop procedures that allow for successful RIB production and target changes in a safe way that ensures contamination control. These meetings were a forum for exploring options for such things as hot target storage, contamination control, decontamination of components requiring maintenance, north hot cell configuration, south hot cell completion (i.e., doors and turntable), hot cell procedures and fixtures (i.e., tray removal), and priorities and schedule. Examples of some actions are as follows:
  - Hot cells: The drive for the hot cell turntable was redesigned to deal with a higher rotational resistance than expected. This will be installed in 2001. Shielding doors to both cells were designed and built during this period and will be installed in early 2001.

  - Decontamination station: There is a requirement to have a place within the target hall to work on components from the target station, vacuum system components, diagnostic equipment, etc., that have become active and contaminated. To this end it was decided to investigate ways and means of decontaminating these components. This work was undertaken by an engineering summer student who designed and began construction of a prototype test station involving pressure washing, ultrasonic cleaning, and electrocleaning. This work is still under way with tests planned in the new year (a preliminary report is available on this work).
  - Hot cell fixtures: At the beginning of this report period the south hot cell was limited to changing targets. It was soon recognized that problems with the extraction column of the target module tray or optics/diagnostics on the exit module tray probably would not be able to be repaired without removing the tray and replacing it. To this end a fixture was designed and built to do this within the hot cell. This is only a beginning and no doubt will require refinement once tested. There are many other tasks and procedures that also need to be addressed in the near future to make the cells fully operational.

- DB0: This is the diagnostic station downstream of the pre-separator magnet. It houses slits, a profile monitor and a Faraday cup. The slits become active and contaminated during operation, making maintenance of any part of the diagnostic box very difficult. Engineering provided assistance to the Probes group in redesigning the box so that the slits could be removed and stored in a pig prior to servicing. This new diagnostic box will be installed in early 2001.
- Spare components: In order to provide replacement trays for the target and exit modules, an order for spare components was put in the Machine Shop early in the year. These spares have been received and sorted. However, at the present time manpower is lacking for assembly.
- ISAC-II: An REA was submitted to provide engineering support for the superconducting prototype rf cavity currently under construction in Italy. This support so far has concentrated on a study to look at alternative cavity tuners. In-parallel engineering assistance was provided to design and build a test cryostat which has been sub-contracted to Quantum Technologies. TRIUMF will design and build a copper cavity dimensionally similar to the niobium cavity to allow for prototype testing.
- DRAGON: Engineering support for the DRAGON project continued throughout 2000, with two personnel almost full-time. A full report of the activities can be found in the Mechanical Engineering subsection of the Accelerator Technology Division section.
- Target hall tasks: Engineering, along with Operations and Remote Handling, produced a list of outstanding issues related to the target hall. These were presented and discussed at several engineering meetings. They fall under the headings of modules, target hall, ion source, and hot cell. This was done to try to identify and consolidate unfinished tasks, tasks not started, and tasks without a solution. It is hoped that this listing will provide a platform to investigate and optimize priorities, schedule and manpower for the coming year.

RF SYSTEMS

RFQ

The RFQ operated very reliably for the various stages of this year's beam commissioning tests. The only attention required was the occasional high power pulsing to reduce the buildup of dark currents.

MEBT

Bunch rotator

The triple gap split ring assembly for the bunch rotator was developed and fabricated at INR RAS, Russia. The effective voltage is 60 kV at a power level of 3 kW. The tank, originally fabricated for the prototype DTL buncher, was modified to accept the bunch rotator structure. Signal level tests confirmed the design parameters and the cavity is now ready for power tests.

Choppers

In order to meet all the demands for chopping, a system of two sets of plates at 5.9 MHz and 11.8 MHz, capable of being dc biased, was adopted. Figure 133 shows a 3D view of the dual frequency chopper.

The chopper design was completed and the fabrication started. One of the critical components of the chopper is an rf feedthrough at 7.4 kV. This was developed in-house since it was not available commercially. The feedthroughs are attached to the top plates for rf voltage, and the capacitors attached to the bottom plates are for dc bias.

Rebuncher

The 35 MHz rebuncher was commissioned this year and operated reliably for beam commissioning tests.

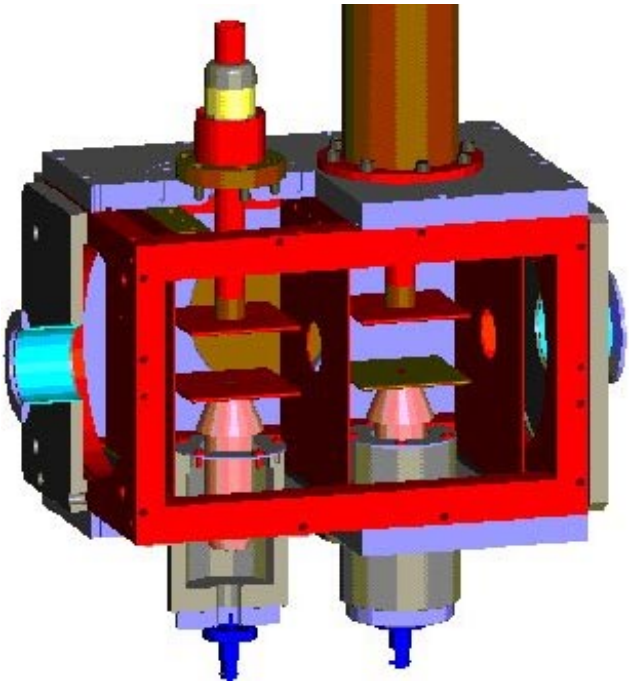

Fig. 133. 3D view of the dual frequency chopper.

DTL

The variable energy DTL is based on five independent interdigital H-type (IH) structures operating at 106 MHz. The first four tanks have been tested to full power in the test facility and are installed in the ISAC accelerating complex. Tank 5 was installed in the ISAC accelerating complex with only signal level tests performed, but has operated at half power for beam tests.

The variable energy DTL also requires three independent 106 MHz bunchers operating at low beta of 2.3%, 2.7% and 3.3% respectively. These bunchers are triple gap split ring resonators, which were developed and constructed at INR RAS, Russia and tested at TRIUMF. All three bunchers have been tested to full power in the test facility and are now installed in the ISAC accelerator complex.

Figure 134 shows the tanks and bunchers installed in the ISAC accelerator complex. All eight DTL power amplifiers have now been successfully tested into a resistive load. Five of these amplifiers have operated at half power into the five DTL tanks.

IH tanks

Following the assembly and mechanical alignment of the DTL tanks, signal level measurements were carried out. Figure 135 shows the tanks in various stages of assembly and test.

The resonant frequencies of the tanks range from 0.4% to 1.3% higher than the operating frequency. All the tanks are equipped with adjustable coarse tuners to

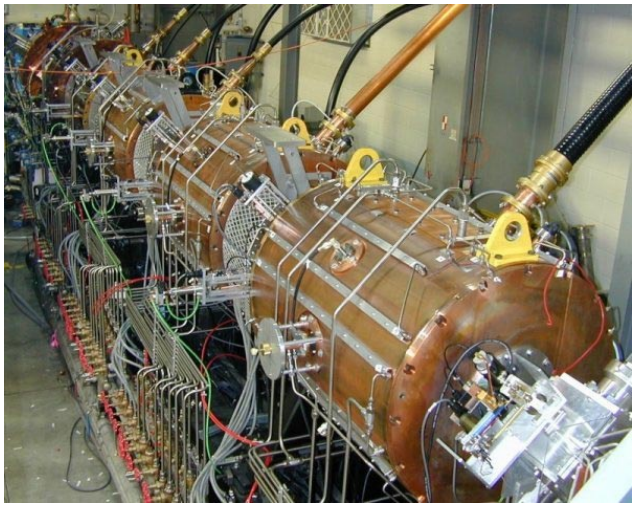

Fig. 134. DTL tanks and bunchers installed in the accelerator complex.

Fig. 135. DTL tanks in the assembly area.

bring the resonant frequencies within the tuning range of the fine tuners. The coarse tuners have a tuning range of 500 kHz, whereas the tuning range of the fine tuners is only 100 kHz. Bead pull measurements were performed on all the cavities to determine the field distribution along the drift tubes and to estimate the shunt impedance of each DTL. The field distribution agreed with the MAFIA predictions. The field distribution in tank 2 showed a slight tilt to the field along the axis, but the field variation was within ±2%. The field distribution in the remaining tanks was more typical with no evidence of a tilt. Both the shunt impedance and Q obtained from measurements are lower than values predicted from MAFIA, leading to higher power requirement from the power amplifiers. Except for the loop size, the same rf power couplers have been used in all the structures. From measured shunt impedances, the power required to attain designed peak effective voltages of 1.18 MV, 1.96 MV, 2.15 MV and 2.2 MV

for DTL tanks 2, 3, 4 and 5 respectively were calculated to be 10.0, 16.0, 19.0 and 21 kW.

When tank 2 was first powered up it became evident that we would have to add some cooling to the tank walls, even though MAFIA calculations indicated otherwise. For a quick fix, it was decided to clamp on a $\frac{1}{2}$ in. square copper cooling line with strips of indium between the cooling line and the tank wall for improved thermal conduction. This kept the outside temperature of the tank below 50 degrees for full power operation. The same solution was used for tank 3, but a further investigation was carried out with different thermal conducting compounds for a more permanent solution for tanks 4 and 5 which operate at a higher power level.

A coupon of steel material was used to simulate a section of the tank wall and a length of square copper cooling line was attached to the coupon using different materials. The coupon was heated using a normal kitchen hot plate. Thermocouples were used to keep the power somewhat constant and to measure the thermal gradient across the interface of the cooling line and the tank. The results are shown in Fig. 136 normalized to Certanium solder. Since these measurements were not done in a controlled environment there is probably a large error bar, but the evidence was strong enough to indicate that the CHEMAX compound was better than indium. The other compounds which were tested, although they showed similar thermal characteristics to CHEMAX, are pastes and very messy to deal with; whereas CHEMAX is a curing compound. With the cooling problem solved, the tanks were tested at power.

DTL tanks 2, 3 and 4 were tested to full power of 10 kW, 16 kW and 20 kW respectively in the test stand. During the power test, it became evident that the fine tuner cooling also had to be improved. The initial design had a water-cooled heat sink at the extreme end of the tuner shaft. This was replaced by a design that water-cooled the shaft all the way to the tuner plate.

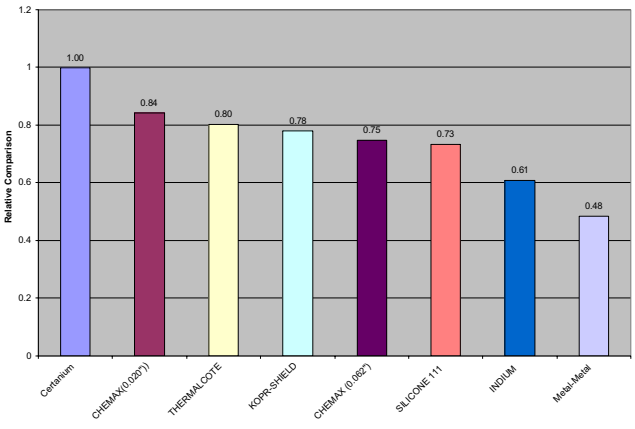

Fig. 136. Thermal conduction graph.

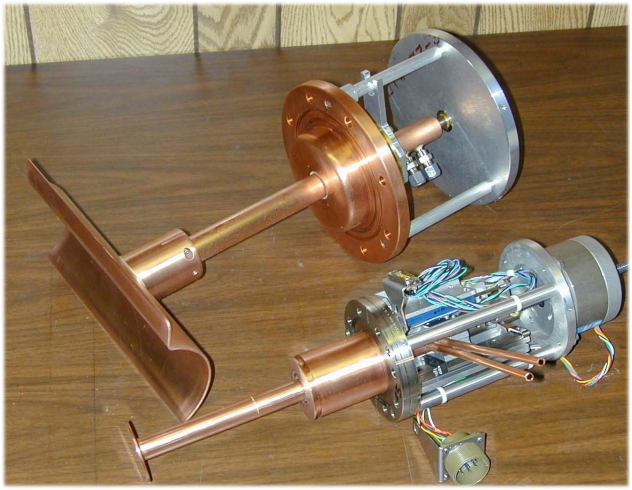

Fig. 137. DTL tank fine and coarse tuners.

The fine tuner along with the coarse tuner are shown in Fig. 137. The tanks were baked with hot water at 60°C for 6 to 8 hours to reduce the conditioning time and the time to get through multipacting. The power tests were performed inside a shielded bunker and X-ray emissions were monitored to meet the personnel safety requirements. X-rays emitted from the tanks were measured and compared with drift tube voltages estimated from input power and measured shunt impedances.

Triple gap bunchers

The rf parameters, resonant frequency, Q, shunt impedance and field distribution of the three bunchers have been determined from signal level and bead pull measurements. The bead pull measurements show that the difference between two end gaps is within ±1.8% to ±4.6% for the three bunchers. Because of the construction of the split rings, it is difficult to obtain better accuracy than this. The nominal power required for bunchers 1, 2 and 3 is 8 kW, 10.2 kW and 11.6 kW to obtain the designed peak effective voltages of 190 kV, 260 kV and 320 kV, respectively. The bunchers are equipped with fine tuners, which have a tuning range between 200 and 500 kHz. One of the bunchers is shown in Fig. 138.

The bunchers have been successfully tested to full power in the test facility. Drift tube gap voltages were measured with X-ray field emissions and compared with voltages estimated from input power and measured shunt impedances. Excellent agreement between these measurements was obtained.

HEBT

Low beta buncher

The 11.9 MHz low beta (2.2%) prototype buncher was completed and is shown in Fig. 139.

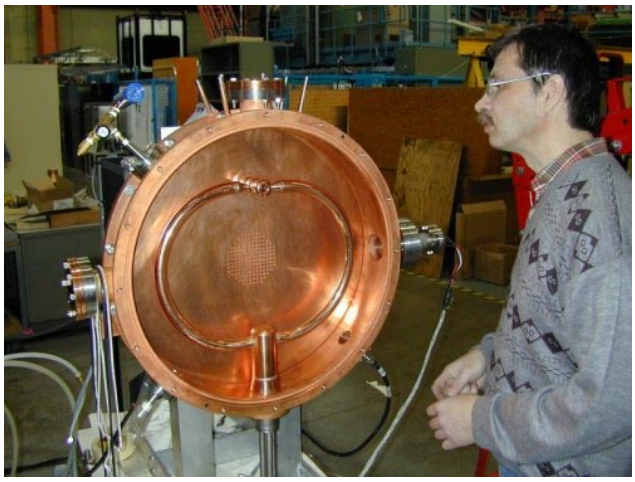

Fig. 138. One of three DTL bunchers.

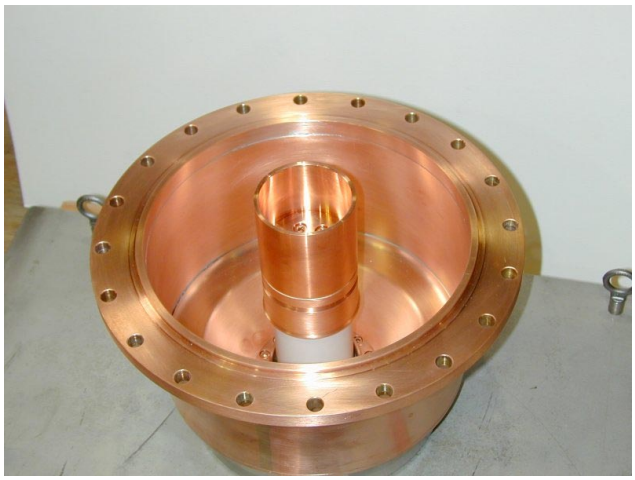

Fig. 140. Feedthrough for the 11.9 MHz buncher.

Fig. 139. The 11.9 MHz buncher prototype.

One of the critical components of the buncher is the rf feedthrough at 30 kV shown in Fig. 140. This was successfully developed and tested in-house since it was not available commercially. The design of the three-gap structure has started. The buncher requires two rf feedthroughs, two fine tuners and two resonant tank circuits driven from a single 2 kW power amplifier.

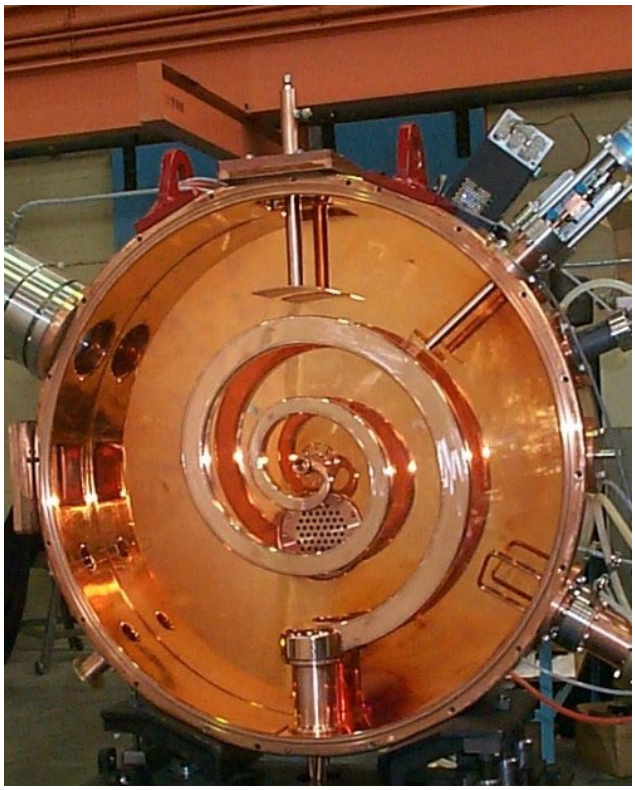

Fig. 141. The 35 MHz high beta buncher.

High beta buncher

The 35 MHz high beta (3.2%) buncher was fabricated and assembled and is shown in Fig. 141 with the tuners and coupling loop installed, ready for signal level tests.

The measured resonant frequency and Q of the buncher's two-gap cavity are within 1% and 70% of the values predicted by MAFIA 3D simulation, respectively. From the bead pull measurement the estimated power required to produce a peak effective voltage of

270 kV is 12 kW, and the field error was measured to be ±1.7%. Realigning the drift tube more precisely will further reduce the field error.

Due to a buildup of copper during the plating process, the tank edges are being re-machined and re-copper plated to provide better contact between the tank and the copper end plates. At the same time, cooling channels on the tank outer surface are being machined for the installation of water cooling lines. Following re-installation of the coarse tuner, fine tuner and coupling loop, plus precise re-alignment of the drift tube, signal level measurements will be completed before power tests can begin.

RF Controls

The RF Controls group has commissioned the entire rf structure between the MEBT and the HEBT. This includes 5 DTLs, 4 bunchers, and 1 rebuncher. The control systems for these rf structures are housed in 3 separate VXI mainframes located in the mezzanine area. Each of these structures has three separate feedback regulating loops, controlling the in-phase and the quadrature-phase control of the rf voltages, and the tuning of each rf cavity. These feedback control loops utilize digital signal processors to achieve high degrees of stability and flexibility. The stability aspect is demonstrated in achieving rf voltage regulation with amplitude error less than 0.1% and phase error less than 1°. The flexibility aspects are demonstrated in using the same design for all the rf structures, and we were able to condition and to commission all rf structures in a very short time.

ISAC ACCELERATOR COMMISSIONING

The ISAC accelerator is being commissioned in stages. The RFQ was commissioned in two stages: an initial 7 ring configuration was tested with beam in October, 1998 and the final 19 ring configuration was tested with beam in September, 1999. For historical reasons, the 19 ring test to the stripper foil box of MEBT was termed Test #1. This year Test #2 and Test #3 were completed and Test #4 was initiated. Test #2 involved beam tests with the stripping foil and the commissioning of the MEBT charge selection section, while Test #3 involved the installation and commissioning of the last section of MEBT and the first subsection of the DTL consisting of the first tank, tank 1, the first triplet, triplet 1, and the first INR buncher, buncher 1. Test #4 concerns the commissioning of the full installation of the DTL and first section of HEBT.

Test #2

In Test #2 a diagnostic station consisting of a profile monitor, a Faraday cup, a fast Faraday cup, and a transverse emittance rig were positioned downstream of the MEBT charge selection section. The test was designed primarily to observe the effects of the stripping foil on the beam and to commission the MEBT charge selection section. Beams of $^{4}He^{1+,2+}$, $^{14}N^{2+,3+,4+,5+}$, and $^{20}Ne^{4+,5+,6+}$ were used in the beam test. The profile monitor at the image point of the charge selection section was used to establish an achromatic tune through the charge selection section. The emittance rig was used to study the emittance growth of the beam through stripping and through the effects of foil aging. The data from the transverse emittance study are summarized in Table XXIII. An emittance rig located just before the RFQ is used to measure initial beam emittances. Emittance measurements for the helium beam are given in Fig. 142. The He beam is interesting in that it is not necessary to strip the beam to bend it in MEBT, so both stripped and unstripped data were taken.

Table XXIII. Normalized transverse emittance values measured before and after stripping for various beams and charge states.

Beam	E	Q	Strip	$\beta\epsilon_x$	$\beta\epsilon_y$
	(keV/u)			(mm-mrad)	(mm-mrad)
^{4}He	2	1	×	0.028π	0.027π
	153	1	×	0.048π	0.050π
	153	1	√	0.083π	0.081π
	153	2	√	0.083π	0.080π
^{14}N	2	1	×	0.031π	0.038π
	153	3	√	0.096π	0.096π
	153	4	√	0.100π	0.096π
	153	5	√	0.093π	0.096π
^{20}Ne	2	1	×	0.017π	0.016π
	153	4	√	0.052π	0.059π
	153	5	√	0.052π	0.057π
	153	6	√	0.048π	0.055π

The effect of energy straggling on the energy spread and energy of the beam were investigated both at the symmetry plane of the charge selection section where there is a dispersed focus, and at the fast Faraday cup (FFC) in the diagnostic station. Comparisons of the symmetry plane beam spot for stripped and unstripped He beams showed both an increased energy spread and energy drift due to energy straggling. The TOF of the beam to the FFC gradually increased as the stripper aged, indicative of foil thickening. The foil was observed to develop a small blackening corresponding to the irradiated spot. Mass spectra of the stripper foil box indicated oil contamination in the vacuum. It is postulated that the oil molecules crack on the foil during bombardment and progressively thicken the target. Eventually the thickened spot overheats and a rupture occurs in the foil. An illustration of the foil aging is given in Fig. 143. Here a neon beam is observed at

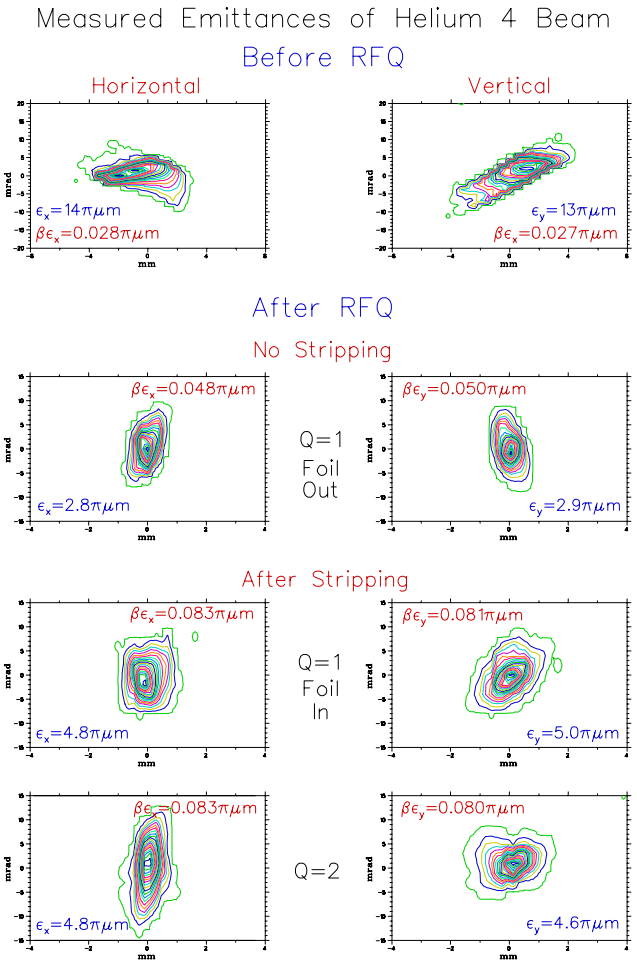

Fig. 142. Transverse emittance measurements for a He beam; both stripped and unstripped values are given, as well as the emittance before the RFQ.

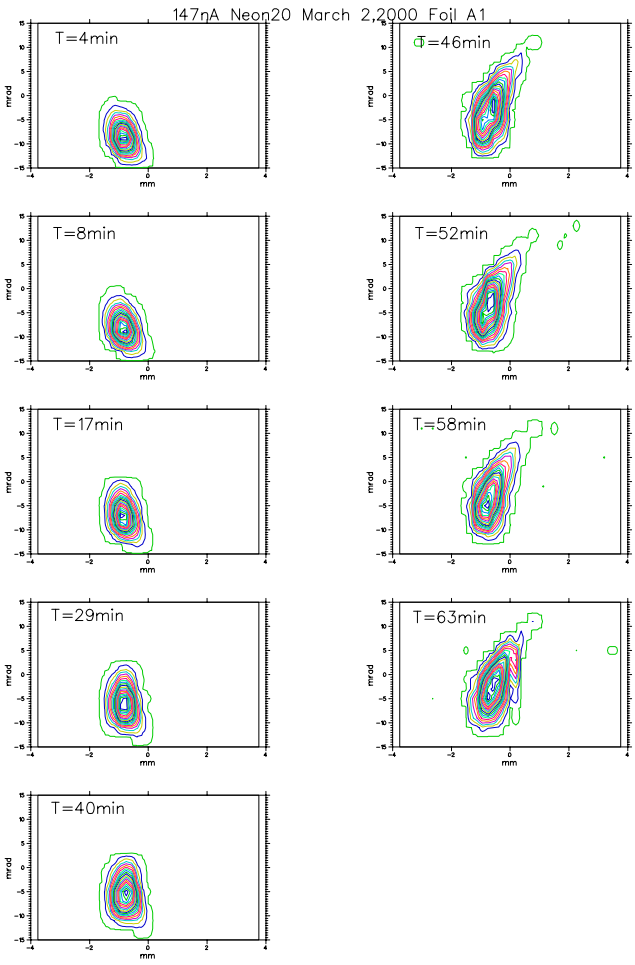

Fig. 143. Transverse emittance measurements for a Ne beam showing foil degradation over time.

the emittance rig over time in transverse phase space. Since the bend is only singly achromatic, as the foil thickens the beam slows and drifts to more positive transverse momentum and a tail develops before the foil eventually disintegrates at ∼60 minutes. Foil lifetimes shortened as beam mass increased. Foils lasted indefinitely for He beams, while with Ne beams useful foil lifetimes were in the range of 50 nAh. Although most radioactive beams will be of low intensity, the lifetime is a concern especially during stable beam operation. We plan to reduce the buildup by cleaning the section, adding a cold trap around the stripping foil and, if required, provide a beam feedback signal to a bias voltage on the stripping foil to correct for the energy loss.

Test #3

For this test the first complete subsection of the DTL consisting of the first IH tank, tank 1, plus a quadrupole triplet, triplet 1, and triple gap buncher, buncher 1, was installed. The test allows us to perform rf conditioning *in situ*, debug rf controls, establish alignment procedures, commission the injection line and triplet, determine matching conditions, and measure beam quality all well in advance of the final installation.

Beam dynamics

At full voltage the beam dynamics are typical of a 0° accelerating structure; matched beams enter each accelerating section converging in all dimensions and after acceleration the now diverging beams are refocused before the next accelerating section.

At a reduced tank voltage the particle bunch is phased negatively with respect to the synchronous phase, so that as the particles lose step with the synchronous particle and drift to more positive phases they gain the required energy. The upstream buncher is used to match the beam to the de-tuned tank. The buncher following the tank is then used to capture the diverging beam. In Fig. 144 we show the initial and final position of a grid of particles in longitudinal phase

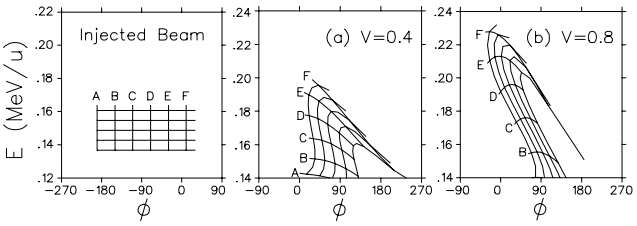

Fig. 144. Final position in $E - \phi$ space of an initial grid of particles after acceleration through tank 1 for relative voltages of 0.4 and 0.8 with respect to the full energy case.

space after simulated acceleration in tank 1 for two different relative tank voltages, $V/V_o = 0.4$ and 0.8. Distortion of phase space occurs for phases near 0°. Below this the energy gain falls off nearly linearly with phase.

Test set-up

A schematic of the test set-up is shown in Fig. 145. The medium energy beam transport (MEBT) transports the beam between the RFQ and the DTL. The MEBT consists of a matching section for the stripping foil, a charge selection section, and a final matching section before the DTL. This matching section includes a 35.4 MHz spiral buncher and four quadrupoles. Narrow diagnostic boxes upstream of both the MEBT rebuncher and DTL-tank 1 each house a profile monitor (x, y) and Faraday cup (FC).

Tank 1 consists of 9 cells covering a velocity range from 0.018 c to 0.022 c, with a maximum effective voltage of 0.5 MV, yielding a maximum final energy of 0.24 MeV/u for $A/q = 6$ and a length of 26 cm. The first split ring buncher has a design velocity of 0.023 c, a maximum effective voltage of 0.19 MV and a length of 10 cm. The diagnostic station downstream of the tank 1, triplet 1 and DTL-buncher 1 includes Faraday cups (FC) for beam transmission measurements, a slit and harp transverse emittance rig, two fast Faraday cups (FFC) for pulse width and TOF measurements, and a 90° bending magnet with a dispersion of 3 cm/%($\frac{\Delta p}{p}$) to analyze the energy and energy spread of the beam.

Beam tests

Test results reported here are for unstripped beams of $^4He^{1+}$ (300 nA) and beams of $^{14}N^{4+}$ (100 nA) stripped with a 3–5 μg carbon foil. These ions require moderate DTL voltages. In a separate test, the successful acceleration of $^{14}N^{2+}$ proves operation at high rf power ($A/q = 7$). Unfortunately the MEBT dipole's upper field strength is not sufficient to capture all the beam from the RFQ for this ion. In all cases 100% transmission through the DTL is achieved.

The transverse emittances injected into the DTL are typically 0.06 $\pi\mu$m. The longitudinal emittance is measured by varying the MEBT rebuncher while measuring beam energy spread and pulse width, and gives a

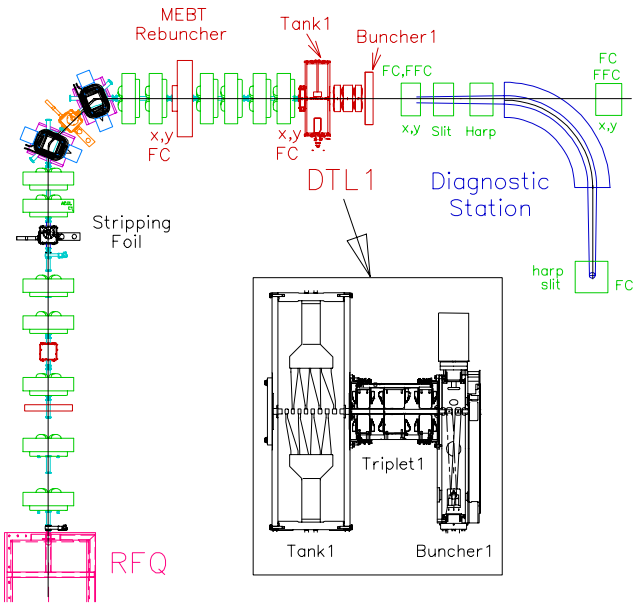

Fig. 145. Test #3 set-up.

longitudinal emittance (95% included) of 0.6 π keV/u-ns for the unstripped beam and about two to three times this for the stripped beam. Long term stability of a tune was hampered by foil aging; carbon buildup on the foils caused a gradual reduction of beam energy and thus drift in the beam phase. Typical beam intensities of 100 nA of nitrogen resulted in foil lifetimes of 1–2 hours.

Energy variation

Beam energy and pulse width measurements for various tank 1 voltage and phase values (buncher 1 off) confirm that variable energy operation works as predicted. Measured energy spectra for a relative tank voltage of 72% and at various rf phase setpoints are given in Fig. 146(a). For each setting the MEBT rebuncher voltage was optimized to produce the best longitudinal beam quality. In general there are a broad range of voltage settings available to achieve a given energy, while still maintaining acceptable longitudinal beam characteristics. For a fixed energy, a lower tank 1 voltage (more positive phase) requires a stronger MEBT rebuncher setting for best beam quality. Measured tank 1 voltage and phase values to achieve a given energy are plotted as solid contours in Fig. 146(b) and compared to simulation results (dashed lines through large open squares). Agreement is good except at the high voltage/low phase regime where some discrepancy exists that requires further investigation.

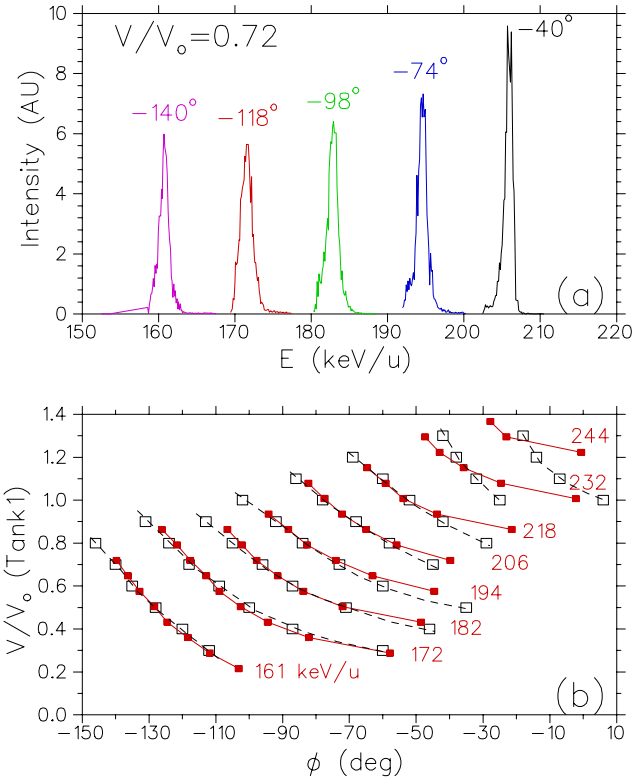

Fig. 146. In (a) the tank 1 voltage setting is fixed to $V/V_o = 0.72$ and the phase altered to produce various energy spectra for $^4He^{1+}$. In (b) a summary plot shows the resultant final energy contours as a function of tank 1 voltage and phase; the small filled squares (solid lines) correspond to measured values and the large open squares (dashed lines) correspond to simulated values.

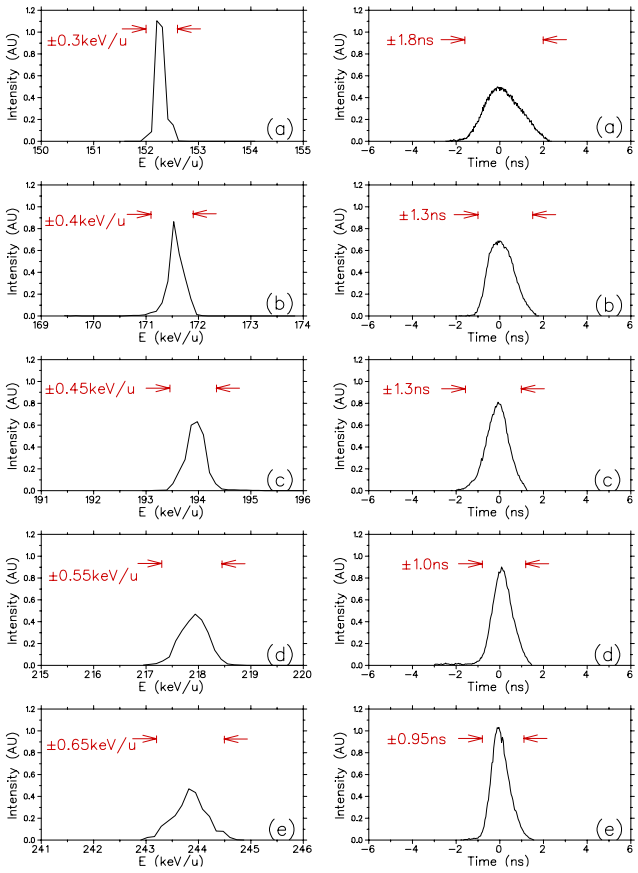

Fig. 147. Beam results giving final energy spectra and pulse width for five sample energies covering the full accelerating range of the first DTL subsection.

Longitudinal emittance

Longitudinal emittance measurements of the accelerated beam are done by varying the buncher 1 voltage and measuring the energy and time spectra at an energy spread minimum. Sample spectra are given in Fig. 147 for the $^4He^{1+}$ beam. These spectra give emittance values of 0.5–0.6 π keV/u-ns, consistent with little or no longitudinal emittance growth over the whole energy range.

Transverse emittance

Transverse emittance measurements for the $^{14}N^{4+}$ beam are summarized in Fig. 148. Shown are phase space densities and computed normalized emittances (4RMS values) before the RFQ, after RFQ acceleration and stripping, after rebunching in MEBT, after acceleration to full energy in tank 1, and finally after rebunching in buncher 1. The largest emittance increase occurs in the stripping foil, with only a small increase during acceleration. This could be improved after the planned installation of another profile diagnostic downstream of buncher 1 to further control beam size during acceleration. Emittance measurements at two lower energies, 200 keV/u and 215 keV/u, give final transverse emittances consistent with those at 230 keV/u (Table XXIV).

Table XXIV. Measured emittances of a $^{14}N^{4+}$ beam for different cases.

Description	E (keV/u)	$\beta\epsilon_x$ (mm-mrad)	$\beta\epsilon_y$ (mm-mrad)
LEBT	2	0.021π	0.021π
After stripping	153	0.059π	0.072π
After MEBT35	153	0.068π	0.074π
After tank 1	200	0.084π	0.082π
After tank 1	215	0.081π	0.078π
After tank 1	231	0.077π	0.075π
After INR1	231	0.077π	0.088π

Test #3 demonstrated the versatility of the separated function concept. New tunes were established in a short time and the measured beam quality matched predictions of beam simulations. As well, the test helped to identify potential future problems. Initial difficulties with phase-locking all rf devices due to the limited RFQ tuner range and microphonics in buncher 1 were eventually overcome. Foil thickening was

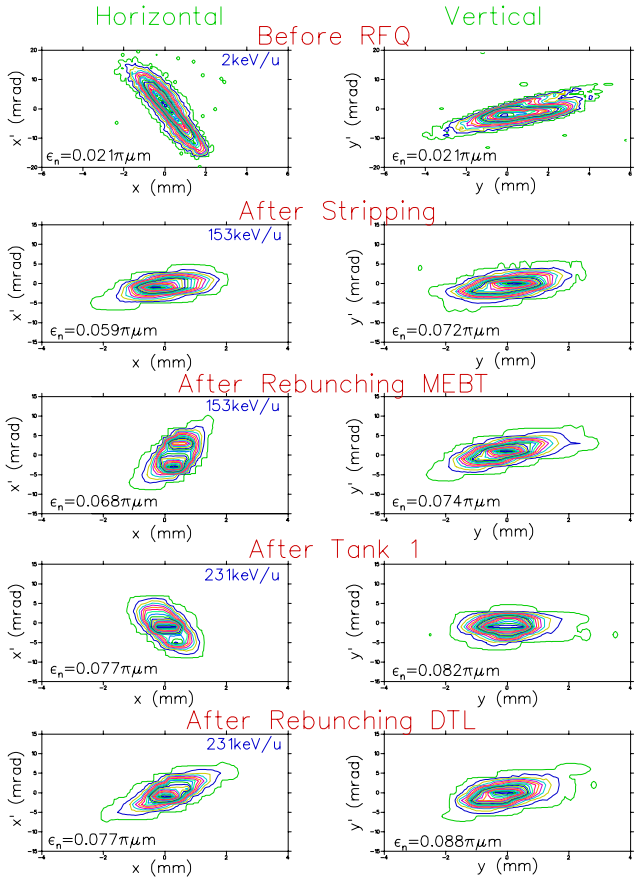

Fig. 148. Transverse emittance measurements after various stages in the beam test.

identified as being responsible for beam phase shifts in the DTL.

Test #4

The latest test (still in progress), Test #4, involves beam tests of the full DTL installation through to the first section of HEBT up to and including the HEBT beam diagnostic station. The assembly, pre-testing, installation and alignment of DTL and HEBT components was a monumental effort and resulted in the first beam being accelerated to the full ISAC design energy of 1.5 MeV/u on December 21. A first spectrum of the full energy beam from the DTL is shown in Fig. 149.

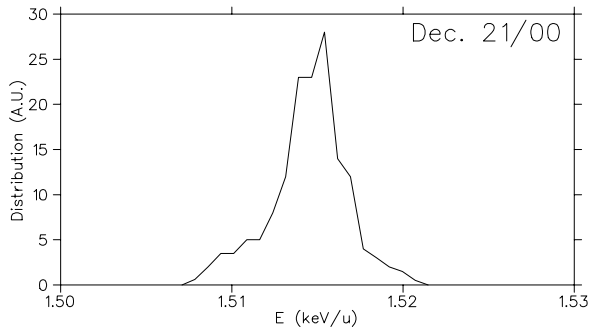

Fig. 149. First full energy beam spectra from ISAC DTL.

ISAC CONTROLS

Detailed design and implementation of additional sections for the ISAC control system again proceeded smoothly and the following major milestones were achieved.

- February: Vacuum, optics and diagnostics control for part of the MEBT beam line for Test #2.
- June: Vacuum, optics and diagnostics additions to MEBT beam line for Test #3.
- July: Upgrades to β-NMR beam line including laser control and stabilization.
- July: Vacuum system control for DRAGON gas target.
- December: Vacuum, optics and diagnostics control for DTL and HEBT into the Prague magnet.

During the year, controls for 380 new devices were added to the ISAC control system for a total of 1330 devices.

In September, Sergei Kadantsev left the group for the greener pastures of local industry. He was replaced by Evgeny Tikhomolov in December. During shutdown periods, Chris Payne from ISAC Operations was a valuable addition to the Controls group.

Hardware

Three new VME crates were added to the control system for the EPICS IOCs for DTL, HEBT, and DRAGON.

Control of the MEBT optics devices was moved from the off-line source IOC to the DTL IOC, where an additional network loop was installed with the CAN-bus controllers for the DTL and HEBT power supplies. Polarity control for the MEBT, DTL, and HEBT steering magnets was initially implemented with VME I/O modules and proved to be inefficient both from software and installation points of view. Therefore new CAN-controller adapter cards were developed, which drive the relays and contactors of the power supply load switches. For the ILE2 polarizer laser system, special CAN controllers were installed for the bi-refringent filter, etalon, spectrum analyzer bias, and cavity length stabilization.

A breakout cabinet for the diagnostics signals in the MEBT and DTL sections was installed. Due to the step-wise installation for Tests #2, #3 and #4, this panel had to be re-wired several times in the field and turned into a major labour sink. All diagnostics devices in these sections were connected and tested. Relays were installed in all rf amplifiers for remote on/off/reset control.

Three more PLC breakout cabinets were built, prewired and installed for the vacuum systems of DTL, HEBT, and the DRAGON beam line. All vacuum devices for MEBT, DTL, HEBT, the β-NMR and TUDA experiments, and the DRAGON gas target were connected and commissioned. A fourth MODICON PLC and additional Modbus segments were installed for servicing the west target station including the mass separator. This was necessary in order to decouple the target operation and the ongoing development work for the ILE1 and ILE2 beam lines.

Software

PLC ladder logic programs were written for the vacuum systems of DTL, HEBT, TUDA, the DRAGON gas target and the DRAGON beam line. The section for the β-NMR was modified to support the final beam line layout. During a two-week target change in June, the PLC ladder program for the target, mass separator and low-energy beam line sections was split and moved into two separate PLCs. This non-trivial operation was very successful and significantly simplified the commissioning of downstream systems.

ISAC standard EPICS display pages and supporting scripts were created for all subsystems. Device control panels for all new optics and diagnostics devices were created using the edd display editor. Device control panels for new vacuum devices were generated by Perl scripts. Initially, the interlock display on the vacuum device panels was generated from the interlock specification database. This led to a few confusing situations when the specification database was out of synch with the PLC program. Therefore a program was written which uses the PLC program as master for the interlock panel generation.

The EPICS display manager program was modified to allow saving and restoring of console window configurations. Also, a subtle bug was corrected which had caused annoying program crashes. These changes were fed back to the EPICS collaboration.

The parameter save/restore system was upgraded to be sensitive to the selected beam delivery modes of both the target ion source and the off-line source. In addition, a script for selective restoring of machine parameters with tolerance checking was written.

Because of the mixed experience with the available data archiving tools, a new data archiver was written. It collects data via EPICS monitors and archives to ASCII files. It supports multiple archive groups with different frequencies and conditional archiving. Maximum and minimum values of process variables since the last disk-write are archived. A matching archive retrieval program was written and embedded into a Perl/Tk GUI with GNUplot for data display. A Web-based version of the data retriever was also developed.

For the laser control on the β-NMR experiment, LabView was used to interface to several GPIB based devices. Stabilization algorithms were developed in the hybrid EPICS/LabView system. This solution proved to be rather volatile and a major effort was launched to write EPICS device support for our Ethernet-based GPIB controllers from National Instruments.

EPICS device support for interfacing to the rf control systems was upgraded from the RFQ prototype to a more general version which adapts more easily to changes in the supervised systems.

The ISAC relational device database, which is PC based and uses Paradox, saw major enhancements during this year. Initially implemented to generate specification documents, it now stores all device parameters and hardware addresses. Reports from the database with supporting Perl scripts are now used:

- to generate system level Capfast schematics for EPICS database generation,
- to check the consistency of the interlock specifications with the software implementation in the PLC ladder logic, and
- to generate VME channel documentation on the Controls Web site.

Automatic pump-down procedures for all vacuum subsystems and improved mass-selection scripts were developed.

A hacker break-in on a SUN workstation at the ISAC ion source test stand prompted the tightening of security on all control system workstations. In addition, a Linux-based firewall was set up and tested for isolating the control system from the rest of the site. It is scheduled for final installation during the spring shutdown.

More documentation, tutorial material and troubleshooting information was added to the ISAC Controls Web site.

Commissioning and Operation

As during last year, operation consisted of a mildly chaotic mix of commissioning, upgrading, and routine running. Overall, the reliability of the control system increased dramatically. This is mainly due to resolution of PLC and IOC problems during the previous year. Another contributing factor is the increasing knowledge of the Operations group.

The CAN power supply controllers showed random, but rare, erratic behaviour, which could not be reproduced in a test set-up for a long time. After detecting higher frequency incidents at the ILE2 beam line in November, a bug-fix was applied which solved the problem. The multi-monitor console PCs running Xservers under the Windows 98 operating system proved to be barely suitable for operations and

sometimes required rebooting every 8 hours. One console PC was converted to Linux on a trial basis with extremely encouraging results.

ISAC DIAGNOSTICS

Fast Faraday cups have been used to measure the longitudinal beam distribution in MEBT. One was located just before the stripping foil while the other was 3.3 m after the foil, between the charge selection slits and the drift tube linac. The narrowest FWHM measured was 0.35 ns; the rise time of the signal was 0.26 ns. At present a 2 GHz amplifier determines the bandwidth; the cups themselves are believed to be faster. The downstream cup showed clearly the increase in thickness of the stripping foil when it was bombarded by 280 nA of 0.15 MeV/u ^{20}Ne ions. The bunch centroid moved 2.5 ns after 40 minutes irradiation; this implies a reduction in energy of 24 keV, which would arise from an increase in thickness of 3 μg/cm^2. The thickening foil would increase the energy straggling and a doubling of the bunch width showed this. The transverse emittance would also increase and a reduction in beam flux on the anode was seen, consistent with beam being scattered outside the acceptance of the anode. The connector to the anode was insulated with Teflon and its low melting point limited the beam power. One needs to operate at high instantaneous currents to get reasonable signal to noise and this limitation would hinder use at the higher energies in HEBT. The design has been changed to use an SMA connector with ceramic insulation which may take between 5 and 10 W. These new cups have been installed in HEBT.

Space restrictions between tanks of the DTL meant that the ports to insert beam diagnostic instruments were only 1.25 in. longitudinally. A dc Faraday cup has been designed for this space and a slotted plate can be driven across its entrance to yield profiles of the beam in the two orthogonal directions. The EM noise is quite low, equivalent to $\sim$10 epA; however, there is also an $\sim$2 nA current of electrons from an unidentified source which may be related to the rf field and hence modulated. Capacitive pickups have been designed for this location; they have been built but not yet installed. They will be used as non-intercepting monitors of the beam phase at the commissioning currents.

Nitrogen ions were scattered from a gold foil, located at the focus of the Prague spectrometer magnet, into a silicon surface barrier detector. The detector pulses were processed to give information on beam energy and arrival time with respect to the 11.7 MHz clock referenced by the RF group. The signal processing electronics were contained in an unshielded NIM bin; the primary cables were double shielded, but the EM noise was $\pm$1.5 mV after the pre-amplifier. The ion energy was $\sim$0.23 MeV/u, i.e. 3.22 MeV, since only the first tank of the DTL was operational. The charge integrated by the pre-amplifier gave a pulse of 0.1 V with sufficient resolution for us to obtain, after correcting for kinematics, a nitrogen energy which agreed with that obtained from the known magnetic field of the spectrometer. The pre-amplifier differentiated the energy pulse to give a fast timing signal. Its amplitude was only 12 mV, and was affected by the noise. Consequently, the precision of the measurement of longitudinal distributions was only $\sim$1 ns. This was sufficient to show that the population of the weakly populated 33 MHz buckets was only 3%, and that there was no beam at this energy lying between buckets. A chopper will eventually be used to remove the sidebands. Better shielding of the electronics and a higher beam energy should improve the precision of the forthcoming measurements.

The response of most particle detectors deteriorates with prolonged exposure to beam because of changes in the surface or crystal lattice. The rate of damage caused by electrons is two or three orders of magnitude below that caused by ions. A system of tube lenses has been designed to accelerate and focus the secondary electrons produced by the passage of an ion beam through a foil onto the surface of a detector.

A ^{241}Am alpha source was used to test silicon diode detectors and a channel electron multiplier (CEM) on the bench. The CEM could be biased to repel low energy ions or electrons. It was set up first to detect alpha particles and later to detect secondary electrons created when the alpha particles hit a target. The target itself could be biased to alter the energy of the electrons accelerated into the CEM. The detection efficiency of the CEM varied across its aperture, the circumference being about half as sensitive as the centre. The response to electron energy was flatter than expected; we did not see a peak in efficiency near 1 keV as suggested by the manufacturer. The response of a microchannel plate would be more uniform over its surface, but it would share another characteristic of the CEM which is that the response is based on the secondary and tertiary electrons emitted from the surface and consequently they both respond to stray electrons and photons as well as ions. For example, the CEM counted both alpha particles and conversion electrons. Their use in beam diagnostics may therefore require electric or magnetic suppression. The response of a silicon diode detector is based on ionization throughout its bulk and the signal from a stopping ion is much greater than that from low energy electrons or photons. The background is thus much cleaner, but the signal from ions below $\sim$1 MeV is not usable.

The DRAGON team is constructing a "start" detector. This consists of a thin foil through which ions pass. A grid to accelerate secondary electrons from the back surface of the foil follows the foil. The electrons are then bent through 90° by a two grid electrostatic mirror and pass through a final grid to hit the surface of a microchannel plate (MCP). One pulse from the MCP will be used for particle identification by time of flight. Four signals from the anode behind it will provide information on the original position of the ion and these will be used to estimate its direction. A computer simulation was made of the production of the electrons and their passage was tracked through the grids to the surface of the MCP. The resolution of an image at the MCP of a point source at the foil, in space and time, was $\sigma_s \sim 2$ mm and $\sigma_t = 25$ ps. The FWHM is narrow but there are significant tails. For example, the widths at 10% of peak are 10 mm and 100 ps. This behaviour is similar to that seen at other laboratories and is caused by non-linear fields close to the grid wires.

The resolution of the MCP and anode will have to be folded with these numbers to give the resolution of the instrument, but it would appear that the timing performance should be adequate; the spatial resolution may not be. A design note has been written, DN-01-03.

A set of five independently insertable beam attenuators has been designed and drawings are being prepared for manufacture. The mechanisms insert mesh or sieve material into the beam in order to reduce the current. A sample of chemically etched sieve material with 5 μm diameter holes spaced by 50 μm has been purchased from Buckbee Mears Inc. Inspection under a microscope shows that while a few clusters of holes are occluded, the majority will transmit beam.

ISAC-II ACCELERATOR STUDIES

ISAC-II studies proceeded both on beam dynamics related issues and on hardware preparation. Beam dynamics work focused on beam simulation studies chiefly surrounding the issues of multi-charge acceleration, cavity modelling and lattice optimization. On the hardware side the prototype for the medium-β superconducting cavity was fabricated in Italy, a cryostat for cavity testing was designed locally, and efforts were made to set up a test facility at TRIUMF.

Multi-Charge Acceleration

Radioactive beam experiments in many cases are event starved. For this reason it is important that the accelerator systems are as efficient as possible. Stripping foils in accelerator systems are a necessary evil since they shorten the linac to make it economically viable, while reducing the final intensity of the beam on target by factors of 3–5. Recently the American RIA project has utilized the idea of reducing accelerator length, hence cost, by adding multiple stripping stations and maintaining beam intensity by accelerating multiple charge states. We consider here the possibility of utilizing multi-charge acceleration in the ISAC-II superconducting linac.

The linac accelerates from 0.4 MeV/u to more than 6.5 MeV/u. There will be a stripping stage at 0.4 MeV/u. It is also possible to include a second stage to (a) shorten the linac for economical reasons or (b) give flexibility to the experimenter to trade off beam energy for intensity and/or beam quality.

Figure 150 summarizes a set of possible operating modes that illustrate the benefits of multi-charge acceleration. In the model we include two stripping stages, S1 and S2, one at 0.4 MeV/u and one after the first twelve cavities or after 10 MV of effective accelerating voltage. Figure 150(a) gives the expected equilibrium charge state for stripping from each of the strippers. Stripping from S2 produces a higher charge state due to the higher incident beam velocity. Beam dynamics simulations, reported below, indicate that we can successfully accelerate particles with a relative charge difference of ∼5% in the low energy section and of ∼7% in the high energy section. These bounds give the number of possible charge states that can be simultaneously accelerated by S1 and S2. These are plotted in in Fig. 150(b). With multi-charge acceleration an experimenter could add S2 and gain a higher final energy with only minimal intensity loss. The expected final energy of the beam with two stripping foils compared to

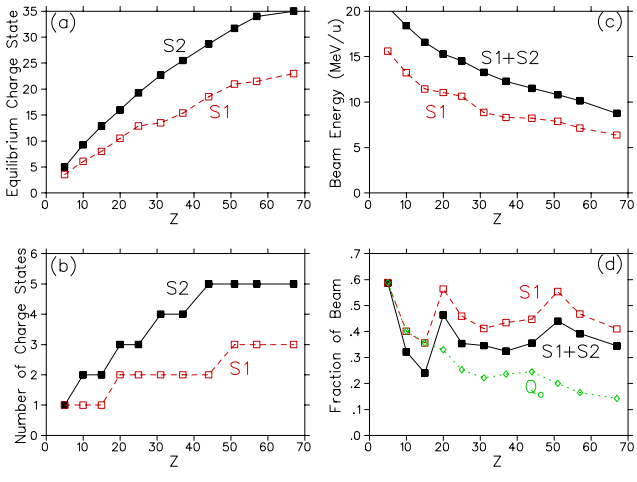

Fig. 150. Summary plots for multi-charge acceleration. Plotted in (a) are the equilibrium charge states from a carbon foil at 0.4 MeV/u and from a second foil, S2, after 10 MV of acceleration. The number of potential charge states that could be simultaneously accelerated are shown in (b). The final energies from S1 alone or S1 and S2 together are given in (c), while the acceleration efficiency for single charge acceleration (Q_o) and multi-charge acceleration with S1 and S2 are given in (d).

a single stripper, S1, is shown in Fig. 150(c). A plot of the expected acceleration efficient for the reference design case and for multi-charge acceleration with one or two stripping stages is given in Fig. 150(d). Note that even with two stripping foils the overall efficiency is improved over the single charge state case. The drawback of multi-charge acceleration is an increase in the transverse and longitudinal phase space and the increased complexity and cost of the transport and matching sections. Nevertheless, the benefits are substantial and so a beam simulation study was initiated.

Cavity modelling

Beam simulations of the superconducting linac require a definition of the field components in the cavity, so a RELAX-3D model was made of each of the three cavity types. To simplify cryostat design, all cavities have been conceptualized to have the same outer diameter. The rf frequency, beam entrance and exit tubes and inner conductor size are then selected to form a cavity geometry that will produce the design specifications. A summary of cavity specifications for the three ISAC-II superconducting cavity types are given in Table XXV.

Table XXV. Geometrical parameters of ISAC-II superconducting cavities used in the RELAX-3D modelling. Lengths in the beam direction are given for entrance and exit grounded tubes, the acceleration gaps and the inner conductor tube.

Cavity	Low	Medium	High
β (%)	4.2	7.2	10.6
f (MHz)	70.72	106.08	141.44
ID (mm)	180	180	180
Inner tube L (mm)	40	60	60
Gap L (mm)	46	40	50
Grounded tube L (mm)	24	20	10
Full bore (mm)	20	20	20

These geometric values are input into RELAX-3D to produce a static electric field distribution. The fields for all three cavity types are summarized in Fig. 151 with field values normalized to a bias of 1 V on the inner conductor. The on-axis E_z field components and the transverse field component 4 mm from the axis are given in Fig. 151(a) and (b) respectively. The asymmetry of the cavity also produces an E_y "dipole" component on-axis plotted in Fig. 151(c).

The fields are then time modulated and integrated to calculate the impact on an ion of a given velocity and phase. A summary plot of the cavity performance is shown in Fig. 152. The transit time factors for all cavities are given in Fig. 152(a). The cavities will typically be operated at a negative synchronous phase for stable longitudinal motion and this gives rise to a net transverse defocusing force and vertical steering. The

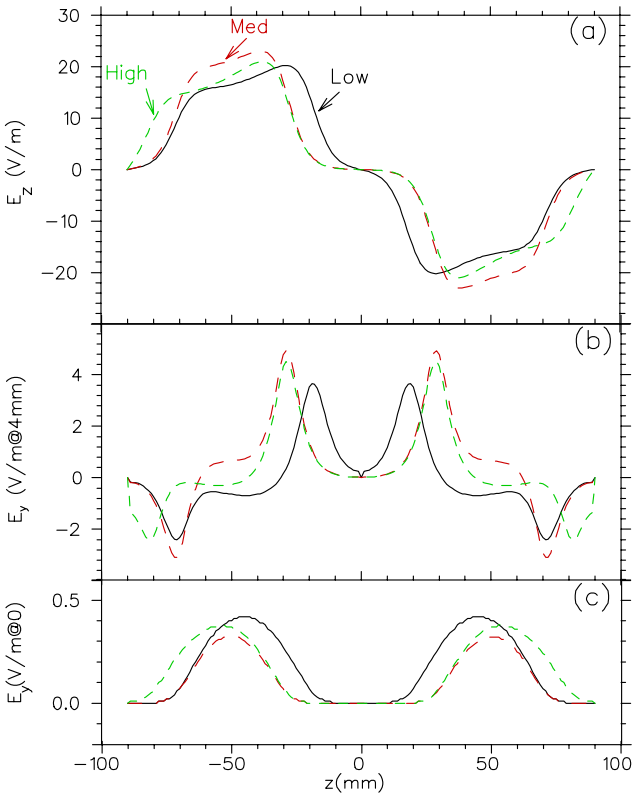

Fig. 151. The on-axis E_z field components and the transverse field component 4 mm from the axis are given in (a) and (b) respectively. The on-axis E_y component due to the cavity asymmetry is plotted in (c). All fields are normalized to a 1 V bias on the centre conductor.

defocusing focal lengths and vertical steering are plotted in Fig. 152(b) and (c) assuming a phase of $-30°$, a field gradient of 6 MV/m and an A/q of 3.

These field calculations point out the strong defocusing and steering produced in the low-β section. The latter is especially troublesome for multi-charge acceleration since the transverse phase advance per cell varies with charge so that vertical deflections on the ensemble will eventually become incoherent and lead to emittance growth. We may, as a result, alter the cavity geometry to lower the design velocity of the low-β cavity.

One-cell simulations

Initial studies of multi-charge acceleration concerned the choice of the transverse focusing lattice. The study included three kinds of transverse focusing: triplets, doublets and solenoids. The first approach was simply to consider a single non-accelerating cell made with the focusing elements separated by four accelerating cavities represented as defocusing lenses. The strength of the cavity defocusing was taken from the cavity modelling reported above. Simulations were done using the first order transport codes FLAT

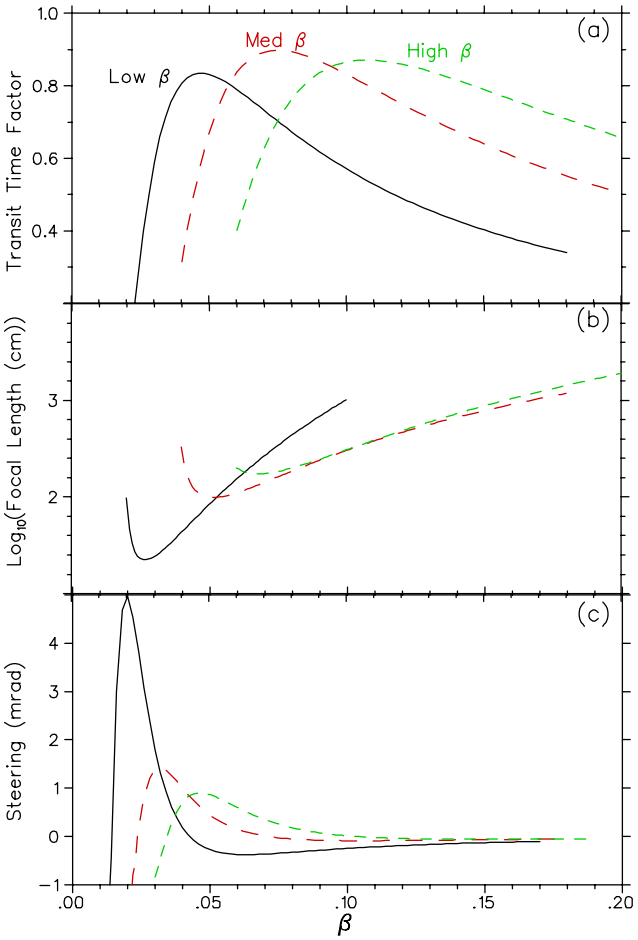

Fig. 152. (a) Gap-crossing transit time curves for the three cavities. (b) Integrated defocusing effect and (c) steering effect from a single cavity assuming 6 MV/m, $A/q = 3$, and $\phi_s = -30°$.

and TRACE3D. Lattice parameters used in the study are given in Table XXVI.

Table XXVI. Specifications for the one-cell simulations.

Parameter	Triplets	Doublets	Solenoid
A	30	30	30
q_o	5	5	5
a (cm)	1	1	1
E (MeV)	0.4/3.0/7.0	idem	idem
μ (deg)	20/40/60/80	idem	idem

Generally when two or more charges are accelerated simultaneously only one is matched to the focusing channel, the so-called *reference charge* or q_0, while all the other charges, q', will be slightly mismatched. Since the focal properties of the magnetic elements change with the charge state, each charge will undergo a different phase advance per period μ. A lattice can be characterized by envelope parameters that define the maximum beam size along the channel for a matched beam of a given emittance. For simplicity a cylindrical aperture, a, is defined and for a given emittance, ϵ, a mismatch value

$$M_{\max} = \frac{a}{\sqrt{\epsilon \beta_{\max}}}$$

can be tolerated before particles are lost, where $\beta_{\max}$ is the maximum value the β-parameter assumes along the cell. It is clear that the larger the value of $\beta_{\max}$ the lower is the mismatch factor that can be tolerated before beam loss occurs. The $\beta_{\max}$ value depends on the phase advance that is chosen for the reference charge. For each single cell calculation the phase advance for the reference particle is fixed and a matched solution for the q' charge is calculated. The two matched solutions are used to calculate a mismatch factor defined as

$$M = \sqrt{\frac{1}{2}(R + \sqrt{R^2 - 4})} - 1$$

where $R = \beta G + \gamma B - 2\alpha A$, A, B, G are the Twiss parameters for the q' ensemble and α, β, γ are the Twiss parameters for the reference particles.

Several phase advance values were studied for each lattice and for three different energy regimes corresponding to the three main sections of the linac. A phase advance near 90° was found to maximize the range of charge that can be transported within the lattice bore. Figure 153 gives the range of charge states that can be successfully transported for each lattice type as a function of energy. The range of transported charge is very narrow in the low energy section where the high cavity defocusing results in large values of $\beta_{\max}$. It should be noted that the simpified study does not differentiate between magnet bore and linac bore sizes, as would occur in a typical linac.

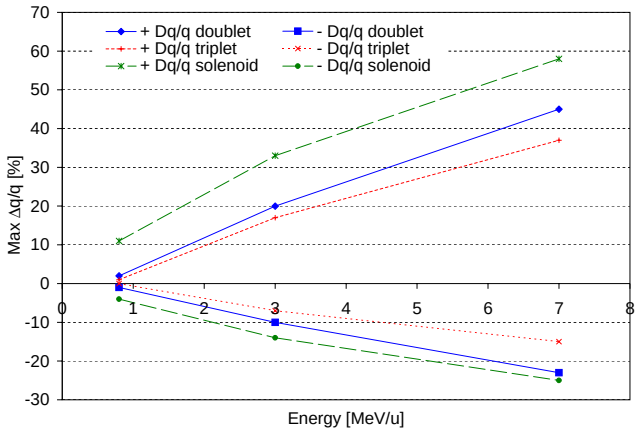

Fig. 153. Different charge transported for the three lattices and at different energies.

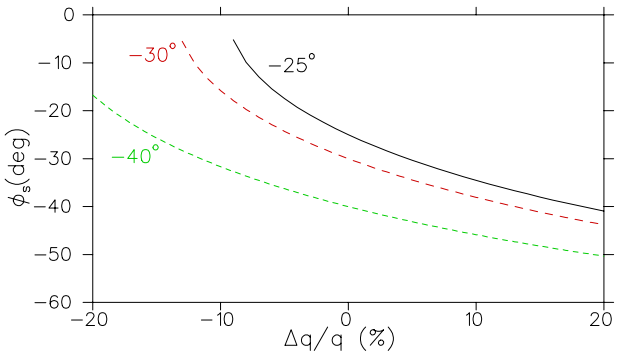

Fig. 154. The synchronous phase associated with various $\Delta Q/Q$ values for three different q_0 synchronous phases.

Longitudinal motion

In longitudinal phase space the reference particles are accelerated with a constant negative synchronous phase, ϕ_{so}, while other charges, q', oscillate around a different synchronous phase, $\phi_{s'}$. A plot of $\phi_{s'}$ values as a function of $\Delta Q/Q$ assuming ϕ_{so} values of $-25°$, $-30°$, and $-40°$ is given in Fig. 154. Longitudinal motion will be stable within a certain band of q' values, though emittance growth of the particle ensemble will result due to the different oscillation amplitudes and phase advance of the constituent charges.

Beam simulations

Each of the three lattices was studied with the multi-particle code LANA. Beams of initial emittance $\epsilon_{x,y} = 0.15\ \pi$ mm-mrad normalized and $\epsilon_z = 3\ \pi$ keV/u-ns for $A/q = 7$ were simulated using triplets, doublets or solenoids between cryostats. The longitudinal emittance is chosen to be a factor of three larger than the expected emittance to test the lattice acceptance. Each simulation was performed with 5000 particles. The linac specifications for this study are given in Table XXVII.

Table XXVII. Specifications for the linac structure.

Parameter	Low-β	Mid-β	High-β
A/q	7	7	7
β_0	4.2	7.2	10.5
E (MeV/u)	0.4 – 1.3	1.3 – 4.0	4.0 – 6.5
freq. (MHz)	70	105	140
$N_{\rm cav}$	8	20	20
$N_{\rm cryo}$	2,4[1]	5	5
E_g (MV/m)	5	6	6

Satisfactory solutions were found for each of the three cases. It is found that minimizing the intertank length is crucial for improving longitudinal acceptance and reducing the emittance growth in multi-charge mode. In the doublet case it is necessary to increase the focusing for the first eight cavities to a doublet between every two cavities. The transverse envelopes for the single charge state mode for the triplet, doublet and solenoid cases are given in Figs. 155, 156 and 157 respectively. Transverse and longitudinal emittance growth are less than 20% in all cases, with the solenoid case the superior of the three.

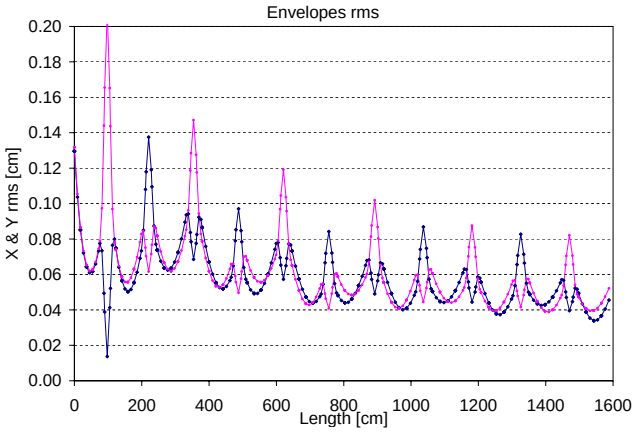

Fig. 155. Transverse envelopes for a single charge state in the linac with triplet focusing.

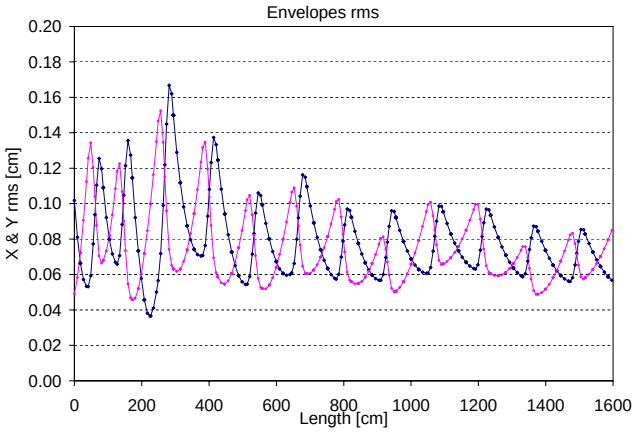

Fig. 156. Transverse envelopes for a single charge state in the linac with doublet focusing.

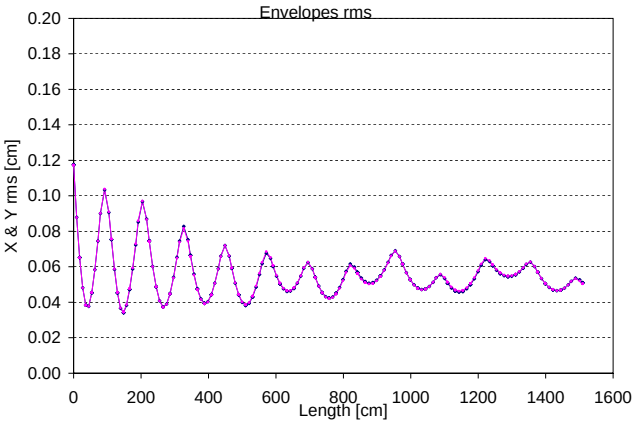

Fig. 157. Transverse envelopes for a single charge state in the linac with solenoid focusing.

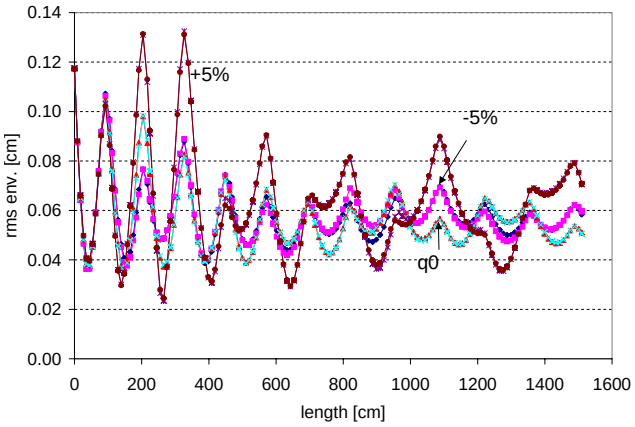

Fig. 158. Transverse envelopes for each of $\Delta q/q = -5, 0, 5\%$ and initial displacement of 500 μm in the linac with solenoid focusing.

Multi-charge simulations were done by fixing the linac parameters for the q_o case and altering the charge of the initial beam. Mis-alignment sensitivity was simulated by shifting the initial beam position by 0.5 mm in both x and y. Beam envelopes for a multi-charge run through the solenoid focused linac are given in Fig. 158. The six curves correspond to x and y envelopes for each of $\Delta q/q = -5, 0, 5\%$. In general the longitudinal dynamics proves to be more restrictive than the transverse dynamics for all cases. Figure 159(top) shows the final position in longitudinal phase space of seven charges accelerated through the solenoid case.

Ensembles of individual charge states experience relatively little growth except near the extremes of $\Delta Q/Q$ but the enfolding ellipse is 7 times larger; 20 π keV/u-ns over the single charge state value of 3 π keV/u-ns. The emittance of the transverse ensemble in the solenoid case for $\pm 5\%$ charge difference and 500 μm centroid shift is shown in Fig. 159(bottom). The enfolding ellipse increases from 0.15 π mm-mrad to 0.4 π mm-mrad over the single charge state performance. The transverse acceptance of the triplet and doublet case is less than in the solenoid case for displaced beams.

Future work will involve installing the realistic fields inside LANA to better simulate the transverse motion and to design matching and transport beam lines compatible with multi-charge acceleration.

Hardware Studies

The specification of the superconducting linac calls for three cavity types of frequency (β_o) 70.7 MHz (4.2%), 106.1 MHz (7.2%) and 141.4 MHz (10.5%) respectively. A medium-β quarter wave bulk niobium cavity has been designed and fabricated in collaboration with INFN-Legnaro. The cavity is shown in Fig. 160 along with some design parameters. Signal

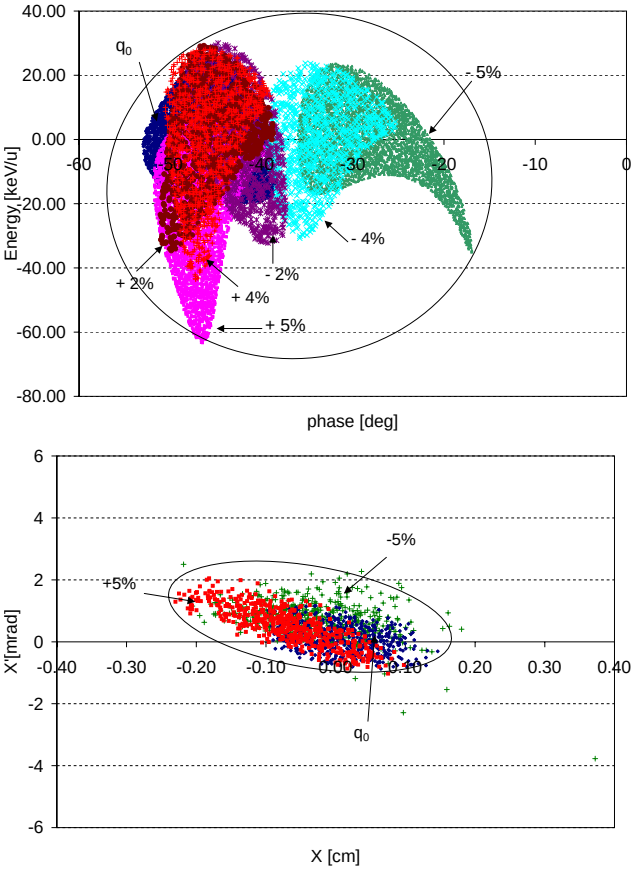

Fig. 159. Top) Final longitudinal position of seven different charge states after acceleration through the linac with solenoid focusing. The enfolding ellipse for the whole ensemble is highlighted. Bottom) Final transverse position of three different charge states with initial displacement of 500 μm after acceleration through the linac with solenoid focusing. The enfolding ellipse for the whole ensemble is highlighted.

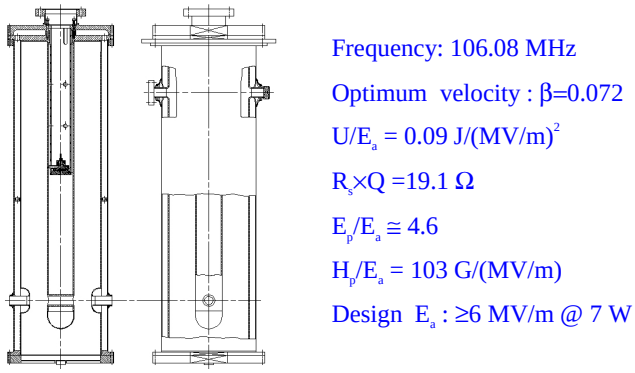

Fig. 160. The prototype 106.1 MHz medium-β cavity for the ISAC-II project at TRIUMF.

level tests were completed at Legnaro to confirm the frequency. The cavity will receive chemical polishing at CERN followed by rf tests in Legnaro with delivery to TRIUMF expected in late spring, 2001.

A superconducting rf test lab is now being planned at TRIUMF. RF testing equipment has been itemized and ordered. A single cavity test cryostat has been designed in a collaboration between TRIUMF and Quantum Technology of Whistler. The cryostat includes a large cylindrical vacuum vessel with top flange, a removable liquid nitrogen shield vessel, a top cold shield, a lower radiation baffle, a liquid helium reservoir, and a μ-metal shield. Several new ancillary devices are in the process of being prototyped for the superconducting rf development program. They include a combined coarse and fine tuner composed of a mechanical lever and a Piezo crystal and an rf coupler. A "dummy" copper model of the medium-β prototype is being manufactured at TRIUMF to aid in the development of the rf controls and ancillary equipment.

ISAC PLANNING

This year the Planning group was involved in planning, scheduling, coordinating and expediting several sub-projects for ISAC.

Various plans and PERTs were prepared and updated regularly with manpower estimates and analysis to identify critical areas and resolve any problems. ISAC priorities were evaluated and higher priority was assigned to: the consolidation of MRO and essential projects in the target area to increase beam reliability; completion of a hot cell; completion of β-NMR for the first experiment in May, and for the soft landing experiment with the high voltage cage in July.

On the accelerator side, the major milestones included: Test #2 (commission MEBT) by February; Test #3 (commission beam from DTL tank 1 including triplet and buncher) by July; and install all DTL systems and accelerate beam to 1.5 MeV/u by December. Manpower planning was done, activities were coordinated and expedited through the Design Office and Machine Shop, and the above goals were achieved on schedule.

Technical details and progress on PERTed activities are described elsewhere in this report under the respective principal group. However, following is a summary of the main projects along with the major milestones achieved.

Target Areas and Hot Cells

Extensive work was done to upgrade target areas, target hall crane interlocks and controls, hot cell (improved system for lead glass shielding windows, portable shielding plug, and access doors). Other work included: ITW5B and associated new iron and concrete shielding; DB0 redesign; ECR source; target module updates. Some contamination was experienced while changing a target, which increased the priority of designing a decontamination facility. An alternative conditioning system to expedite the process of changing ISAC targets was designed and fabrication is in progress.

MEBT

After completing Test #1 of MEBT up to DB5, installation of the MEBT was finished and Test #2 was completed on schedule in February. This test included both benders, diagnostics systems, slits, collimators, controls, the charge selection slit system (DB7), stripper foil in MEBT, and installation of a diagnostic station and emittance rig with necessary diagnostics system. The 35 MHz rebuncher was not installed for Test #2 and the MEBT chopper had to be deferred until March, 2001 due to higher priority on DTL systems.

DTL Systems

After evaluating the priorities and workload, it was decided to do Test #3 with DTL tank 1, triplet and buncher in June to gain experience and then install and test all DTL systems to accelerate the beam to 1.5 MeV/u in December. One large stand was designed, fabricated and installed in March to support all 5 DTL tanks.

Fabrication of DTL tanks 2 to 5 with stems and ridges was done in July, followed by assembly, rf tests and preparations for installation in the ISAC hall. Additional time had to be spent on installing extra cooling for tanks 2–5 after encountering problems during power tests of tank 2. Consequently only tanks 2, 3 and 4 were tested to full power in the bunker in the proton hall extension before moving to the ISAC hall with a plan to do power tests for tank 5 *in situ*. Vacuum through all DTL systems was achieved by December 15, and a helium beam from the off-line source was accelerated to 1.5 MeV/u on December 21.

HEBT

Due to increased workload, the HEBT project was divided into two parts: HEBT1 (up to upstream of benders to DRAGON and TUDA beam lines) and HEBT2 (all remaining HEBT components). Major jobs included: design, fabrication and installation of vacuum system, beam line hardware, diagnostics, and controls components for HEBT1 to commission beam through all DTL systems. HEBT1 commissioning required installation of the Prague magnet and diagnostic station with all commissioning diagnostics. Due to the heavy workload in the ISAC RF group, all rf activities had to be carefully planned, coordinated and expedited. The 11 MHz buncher, chopper and bunch rotator had to be deferred until spring, 2001 due to the higher priority on accelerating beam through DTL tank 5 to 1.5 MeV/u in December. Chalk River quads were mapped and in-

stalled and all four benders were also installed and aligned by early December.

Low Energy Experiments

These included essential modifications to GPS (lifetime), LTNO, yield station, and β-NMR. Extensive work was done on planning, coordinating and expediting activities and critical components from the Machine Shop and outside suppliers for β-NMR, laser polarization systems, spectrometer, and associated LEBT components. The first β-NMR experiment in 2000 was done in May, followed by installation of the HV cage with associated safety control systems to do a soft landing experiment in July, and then another in November with an aim to increase polarization.

High Energy Experiments

These involved DRAGON and TUDA. Installation of HEBT components up to the TUDA experimental station, with associated services, started with an aim to finish before March, 2001. A special room was designed and constructed for the TUDA detector system electronics, with all services and a special grounding system. The plan was to be ready for stable beam tests by the end of March, 2001.

DRAGON

In spite of significant efforts in the Design Office, overall progress on DRAGON was relatively slow due to a lack of resources and a higher priority on DTL and HEBT tests. All major components for legs 1–5 were installed by the end of September, and services were connected by December. ED1 and ED2 tanks were installed and electrodes assembled in September, and the tank vacuum tested in October/November. Magnetic dipoles (MD1 and MD2) were installed and the MD1 vacuum chamber was fabricated and made ready for installation. Several initial tests were done to commission the gas target with the control system. The plan is to be able to start α particle tests up to the charge slits by January, and continue these tests down the line as services are completed, with a goal of being ready for stable beam by April, 2001.

ISAC-II

PERTs were prepared that included work on specifications and design of a superconducting rf test facility and dummy cavity with an aim to install and test a Nb cavity in summer, 2001 after receiving it from Legnaro.

CONTRACT ADMINISTRATION

In the past year eight major contracts were awarded:

- Sunrise Engineering Ltd. of B.C. manufactured the DRAGON electrostatic dipole tanks, and Swiss Wire (EDM) of California manufactured the DRAGON electrostatic dipole electrodes.
- Sunrise Engineering Ltd. of B.C. manufactured DTL tanks 2, 3, 4 and 5.
- Sunrise Engineering Ltd. also made the HEBT 22.5° dipole magnet poles and assembled the magnets, with Danfysik A/S of Denmark supplying the magnet coils.
- Performance Development Ltd. of B.C. manufactured the 51 stems for DTL tanks 2, 3, 4 and 5.
- Sunrise Engineering Ltd. of B.C. manufactured the HEBT 35 MHz buncher tank.
- Sunrise Engineering Ltd. also fabricated the spent target storage tank for the ISAC target hall.

Personnel Resources

In 2000 the average monthly personnel effort for ISAC increased by approximately 4.5 people to an average of 83.75 FTE people per month (see Fig. 161). In 1999 the FTE effort per month was 79.25 people.

In 2000 the average monthly personnel effort per system was as given in Table XXVIII and shown in Fig. 162.

Table XXVIII. Personnel effort per system.

System	Monthly FTE
Project management & administration	3.44
Beam line 2A	0.75
Target station	5.43
LEBT	7.00
Accelerator	17.12
Science facilities (TRIUMF personnel)	21.02
Science facilities (non-TRIUMF personnel)	2.10
Infrastructure	9.43
Integration	16.89
ISAC-II	0.57
Total average FTE monthly personnel	83.75

Figure 163 shows the average monthly FTE personnel working on ISAC for the year 2000 based on the type of personnel. The average monthly FTE personnel effort spent on ISAC science for the year 2000 is shown in Figure 164.

The total personnel effort for ISAC since the start of the project January 1, 1996 to December 31, 2000 has been 346.62 years of work, based on a FTE workmonth of 150 hours per person.

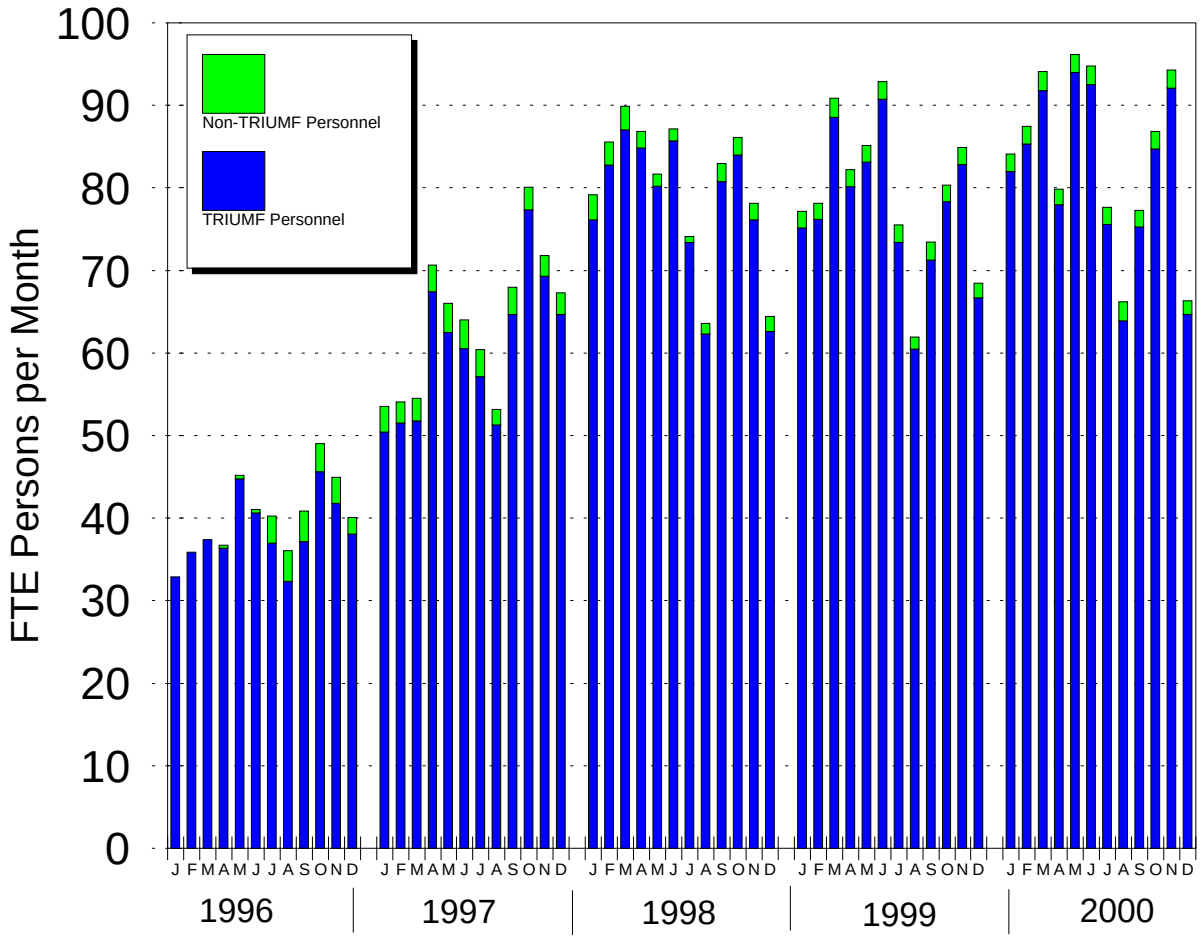

Fig. 161. ISAC monthly personnel effort, January 1, 1996 to December 31, 2000.

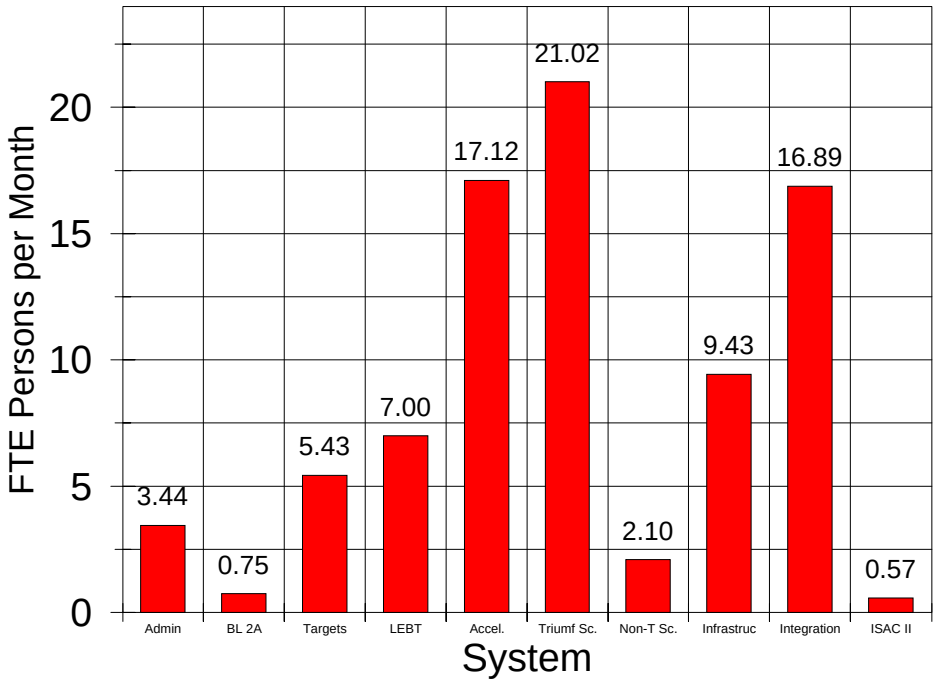

Fig. 162. ISAC average monthly personnel effort, shown by system for 2000.

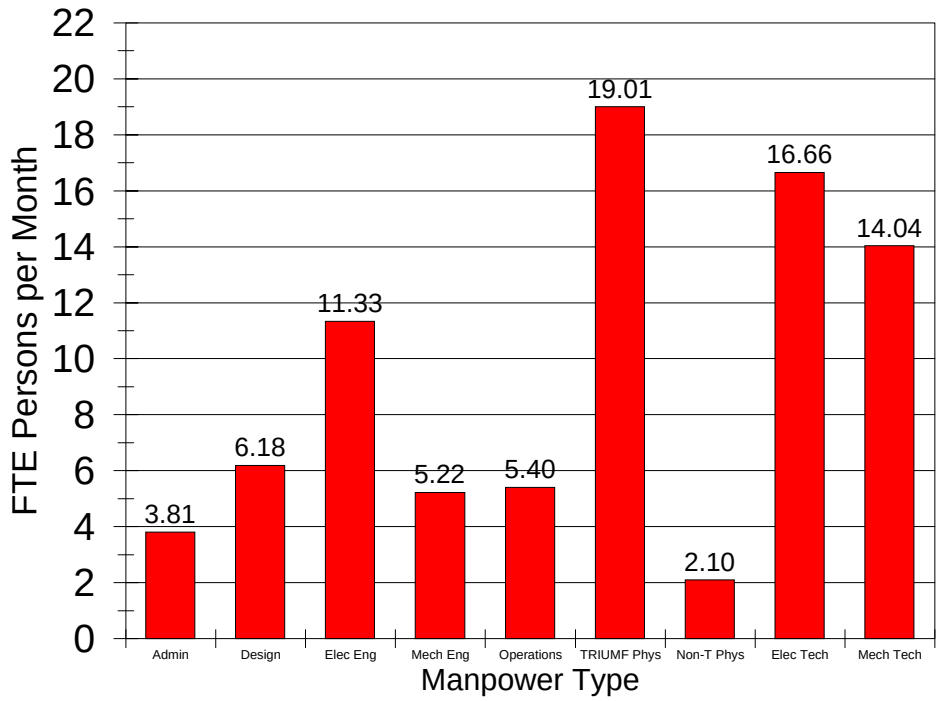

Fig. 163. ISAC average monthly personnel effort, shown by personnel type for 2000.

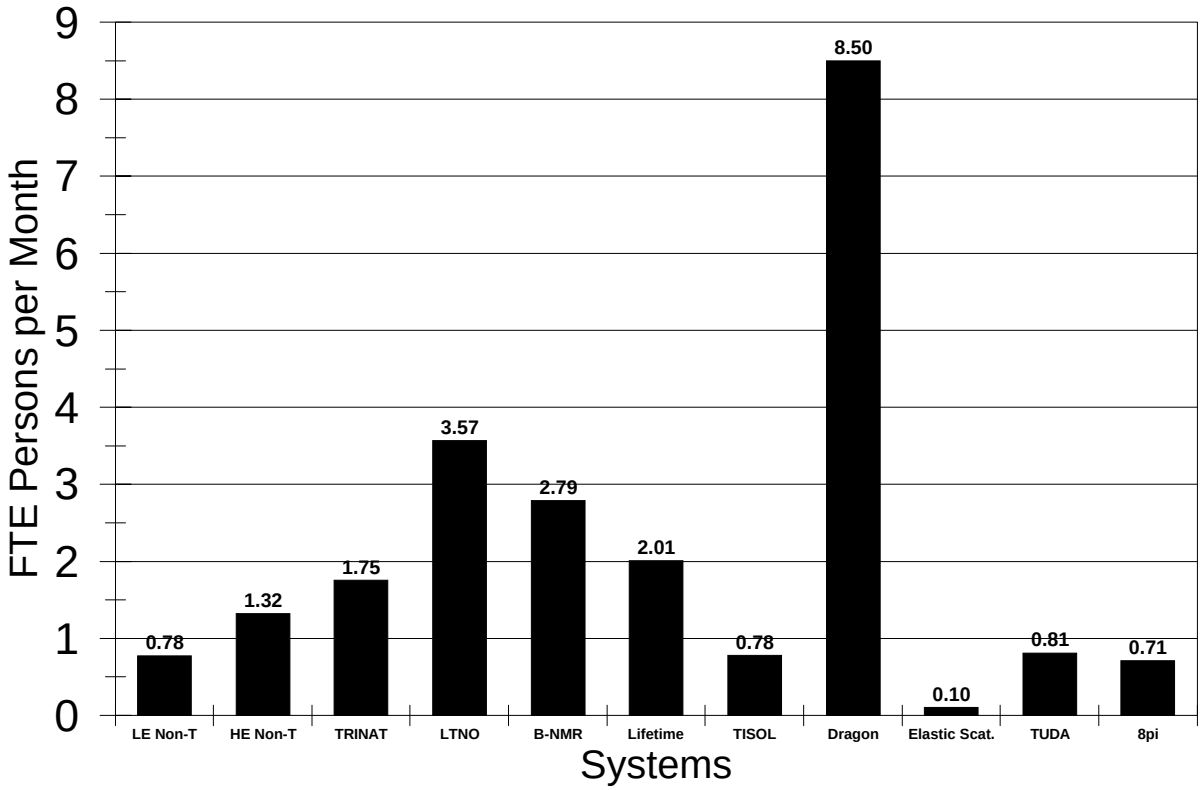

Fig. 164. ISAC average monthly personnel effort, science facilities for 2000.

ACCELERATOR TECHNOLOGY DIVISION

INTRODUCTION

As for the past few years, the ISAC project occupied most of the effort of the division during 2000. The mechanical engineering and design effort involved continuing work on the DRAGON spectrometer, drift tube linac (DTL) components, high energy beam transport (HEBT) line, further work on the ISAC target/ion source modules and target hall, and hot cell devices required for handling and servicing. The Design Office spent 71% of available hours on ISAC related work. These activities are described in more detail in the following pages and in the ISAC Project section.

There were a few non-ISAC projects which were supported, the largest being TWIST or Expt. 614 which is being mounted on the M13 secondary channel. The large solenoid magnet shield was designed and the contract let for machining of the 61 ton steel plates. This work was completed and the steel assembled around the superconducting solenoid magnet by the end of the year. There was also design work on the cradle to support the wire chamber planes and the magnet field measuring equipment for mapping the central field distribution. An even larger field mapper for the $G\emptyset$ experiment, which is to be carried out at Jefferson Laboratory, was assembled at TRIUMF and then sent to the University of Illinois where it is being commissioned. This work involved several trips to Illinois by a TRIUMF engineer.

For the CERN-LHC collaboration the assembly of large pulse forming network tanks (PFNs) began and this work, along with the ongoing saga of the twin-aperture quadrupole fabrication, is described in the CERN Collaboration section. The engineering group at the University of Victoria continued their work on the design of the large structure for mounting and rotating the HEC calorimeter modules into the ATLAS detector. Fabrication and testing of the signal feedthrough assembly also continued.

The Machine Shop coped with an ever increasing workload, also mainly on ISAC related fabrication jobs. This year, more than $1 million in work packages were sub-contracted to local fabrication shops through the Machine Shop. The Planning group provided coordinating and expediting services to ensure that important milestones were met throughout the year, and that other projects received a reasonable level of support to keep them going. A new, 5-axis, CNC milling machine was commissioned in the shop this year and several machinists took courses at BCIT on programming this machine.

ISAC also required a number of buildings and shielding structures which were designed and coordinated by the Building department. One of these structures was the electrically shielded room for housing the TUDA experiment electronics. The biomedical annex received a major renovation with offices and laboratory space for more than 20 μSR scientists created. Assistance was also given to the design and specification of the ISAC-II building.

The Electronics Services group provided support for the ISAC and CERN work and became heavily involved in producing electronics for the TWIST experiment. This work involved manufacture of the postamp modules, together with considerable cable manufacture. There was a significant increase in the demands for PC support and the new PC backup service was implemented.

The Electronics Development group continued their support of the ISAC control system design and implementation. This year there were additional requirements for the ISAC experiments including β-NMR and DRAGON. The VME data acquisition board developed for the CERN-LHC beam orbit system was successfully tested at CERN.

BEAM DYNAMICS

Three joint studies were begun with other laboratories this year, in addition to the TRIUMF-LHC collaboration. One, still involving CERN, concerned longitudinal simulations for the proposed Neutrino Factory proton accumulator and compressor rings. Another explored the feasibility of producing very short "micro-bunches" for the proposed $K_L \rightarrow \pi^0\nu\bar{\nu}$ experiment at the Brookhaven AGS. The third investigated the effectiveness of electron beam lenses for compensating space-charge effects in the Fermilab booster.

CERN Neutrino Factory Proton Driver

High-energy muons, stored in a decay ring with long straight sections, would provide a unique beam of high-energy neutrinos, enabling precise determination of several parameters of the neutrino mass matrix. CERN is studying such a Neutrino Factory to feed distant detectors at Grand Sasso, with muons produced by a 4 MW proton driver (PDAC), composed of a 2.2 GeV superconducting linac, accumulator and compressor rings. The intense proton beam could also provide a higher brilliance beam for LHC.

In support of this study, longitudinal beam dynamics simulations were begun in the spring, both for the accumulator, which collects 660 turns of H^- from the linac, and for the compressor, which rotates the bunches 90° in ≈7 turns; two variants of each machine have been studied. Enhancements were made to the LONG1D multi-turn injection algorithms to carry

out these simulations, which have so far confirmed the feasibility of using high-transition-energy lattices. The high synchrotron frequency is instrumental in smoothing the accumulated distribution in longitudinal phase space.

Bunch rotation produces a large momentum spread and short bunches with large space-charge forces. Chromatic non-linearity becomes more important for large momenta, and a higher order expansion of the "slip factor", which relates increment in orbit period to that of momentum deviation, was introduced. Further, the dispersion function is distorted by transverse space-charge forces, making the momentum compaction factor dependent on the local charge density. This effect was also modelled, but the simulations did not reveal any related problems in either the accumulator or compressor.

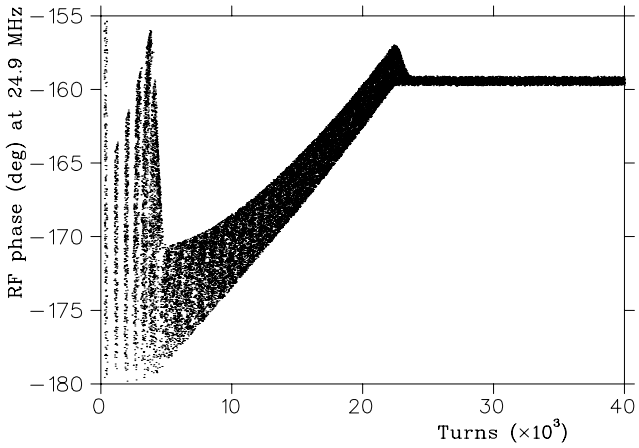

Fig. 165. Extracted proton phase angle versus turns for the first 0.1 s of a 3 s spill, showing the squeezing of the bunch to <0.1 ns.

Micro-Bunching at Brookhaven AGS

In support of a proposed measurement of the CP-violating decay $K_L \rightarrow \pi^0\nu\bar{\nu}$ at the AGS, which requires very narrow 0.15 ns proton "micro-bunches" at 40 ns intervals to allow time-of-flight (TOF) discrimination from the overwhelming background of $K_L \rightarrow \pi^0\pi^0$ decays, studies have begun as to whether the recently developed micro-bunching techniques for the slow-extracted beam can be refined sufficiently to meet this requirement.

Micro-bunching relies upon squeezing the debunched beam through the gap between empty buckets that are centred near the extraction radius. The betatron tune depends on the longitudinal momentum, and chromatic extraction is effected by a $\frac{1}{3}$-integer transverse resonance driven by sextupoles. The micro-bunches have high momenta and are preferentially extracted. The method has been tested at the AGS with a 20 kV, 93 MHz cavity yielding proton bunches 0.3 ns long with 11 ns spacing. However, the 40 ns bunch spacing for TOF implies the use of a 25 MHz rf system, and the 0.15 ns bunch length at this lower frequency is more challenging; moreover, a solution that is economical with rf voltage is required.

Two techniques may be used to further shorten the bunches: (i) a higher harmonic cavity to distort and stretch the rf buckets; and/or (ii) moving the central momentum of the buckets below the extraction threshold, so that extraction takes place from the narrow filament of particles squeezed between the flow-lines of neighbouring separatrices. A variety of single- and dual-harmonic schemes have been simulated using LONG1D; the presently preferred scheme uses fundamental and fourth-harmonic cavities each with 100 kV to produce bunches of width 0.14 MeV and length 0.17 ns (1 second spill) or 0.062 ns (3 second spill) (see Fig. 165). Thus far simulations have included neither collective effects nor the transverse dynamics leading to the betatron resonance. It is proposed to adopt or modify the SLEX code for modelling the resonance, and to include the effect of the impedance upon the longitudinal motion through a wideband resonator model.

Space-Charge Compensation with Electron Lenses at the Fermilab Booster

Electron beam lenses have been proposed to compensate space-charge in intense proton beams in the Fermilab booster. In theory, a perfectly matched electron beam can completely cancel direct intra-beam space-charge forces, but detailed tracking simulations are required to confirm the effectiveness of this compensation technique. The ACCSIM particle tracking code has been used to conduct these studies.

It was not expected that a single lens would result in substantial improvements to the booster performance as it has been shown theoretically, and later confirmed with ACCSIM simulations, that too few booster electron lenses (BELs) result in large beta-function distortions. However, good results can be achieved with as few as two BEL elements in the lattice, though for practical reasons three BELs may be required.

ACCSIM was also used to study one of the acceleration schemes proposed by the Fermilab team, in which electron lenses were used to jump across betatron resonances. This was expected to reduce emittance growth, but simulations showed that the non-adiabatic excitation of electron lenses led to beam mismatch, formation of tails, and further particle losses.

Although first results of computer simulations with ACCSIM have not demonstrated significant space-charge compensation with BELs in the existing combined-function lattice, results with F0D0 lattices are more promising. Studies are continuing.

MAGNETS

In addition to contract supervision on the fabrication of the CERN twin aperture quadrupoles described in the CERN Collaboration section, work was carried out on a number of other magnets during this year.

ISAC

Quadrupoles

Sunrise Engineering (BC), using coils from Everson Electric (USA), manufactured and delivered the DRAGON 4 in. and 6 in. quadrupoles. Assembly of the 12 drift tube linac (DTL) quadrupoles was completed; these quadrupoles fit between the ISAC DTL tanks. A trim quadrupole was designed for the ISAC HEBT line and documented in "A design for trim quadrupoles for the HEBT of ISAC" [TRI-DNA-99-5], and "Three dimensional field calculations for the ISAC HEBT trim quad" [TRI-DN-00-19]. The yokes were manufactured by Pacific Design Engineering (BC). The coils were made by Armature Electric (BC). The four magnets have been assembled.

Dipoles

Assembly of the 4 in. and 6 in. x–y steerers for ISAC and the DRAGON facility was completed. Dehnel Consulting Limited (BC) supervised the construction of four ISAC 22.5° HEBT dipoles. Sunrise Engineering machined the steel and did the assembly work. Danfysik A/S (Denmark) made the coils. A 15° switching dipole for beam line 2A has been designed and documented in "Concept Design of the 2A 15° Switching Dipole" [TRI-DN-00-18]. This dipole will allow TRIUMF to send a 500 MeV proton beam to either of the ISAC target stations. Drafting work was nearing completion at year end.

β-NMR Wien Filter

Concept design work started on a Wien filter to spin precess radioactive ions (sodium, potassium, nitrogen, lithium and fluorine) for the β-NMR experiment.

Experiment 614 – TWIST

Design of the steel return yoke for the Expt. 614 superconducting solenoid magnet was finalized in the early months of the year. Quotes were obtained for manufacture of the yoke and the contract was eventually awarded to Axton Industries. An unfortunate breakdown of the large milling machine at Axton Industries resulted in almost an additional two months to complete machining of the 61 tons of steel slabs that comprise the magnet yoke.

The yoke was pre-assembled at Axton Industries prior to shipping the pieces to TRIUMF to allow for inspection and verification of the functionality and tolerances of the assembly. After the large yoke pieces were delivered to TRIUMF and the initial preparations to the M13 experimental area were completed, the yoke was successfully assembled in the M13 area in preparation for field mapping (see Fig. 166).

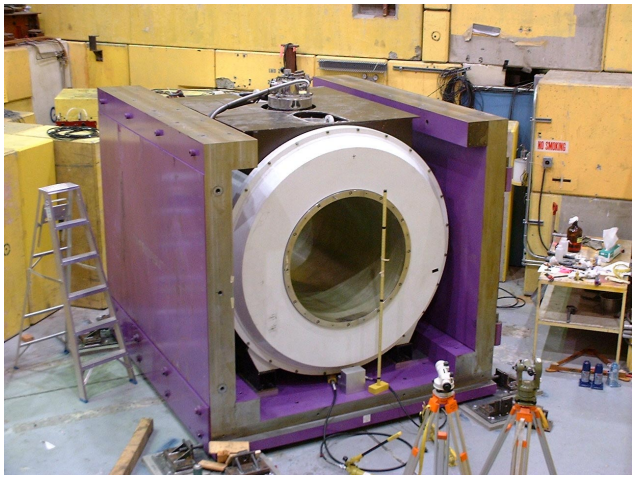

Fig. 166. Photograph of the steel return yoke being assembled around the superconducting solenoid magnet for the TWIST experiment.

Kickers

As mentioned in the 1999 Annual Report, the Kicker group designed a mass separator kicker for ISAC that generates variable pulse widths. The mass separator kicker system includes a pair of deflector plates. One plate is driven by a +10 kV FET based modulator. A –10 kV modulator drives the other plate. Each modulator has two stacks of FETs operating in push pull mode with a variable output voltage and a variable repetition rate from virtually dc to 10 Hz. The specifications for the mass separator kicker demand that a stack of FETs must be held in the "on" state for between 20 ms and 10 s. This relatively long duration required special consideration of component leakage currents and a novel drive technique. The kicker (see Fig. 167) was successfully tested, installed and commissioned. A design note, "Design of ISAC mass separator kicker" [TRI-DN-00-15] and paper, "A FET based mass separator kicker for TRIUMF ISAC project", have been written.

A charge booster unit is required for part of an upgrade to the ISAC facility at TRIUMF. ISAC is presently capable of accelerating only isotopes with atomic mass up to 30. The charge booster will allow ISAC to accelerate all the masses in the periodic table. A fast kicker system is required to study the characteristics of an existing charge booster, designed by ISN (Grenoble), to assess the suitability of using this charge booster at TRIUMF. This fast kicker will subsequently be used in the ISAC facility for TOF separation of the

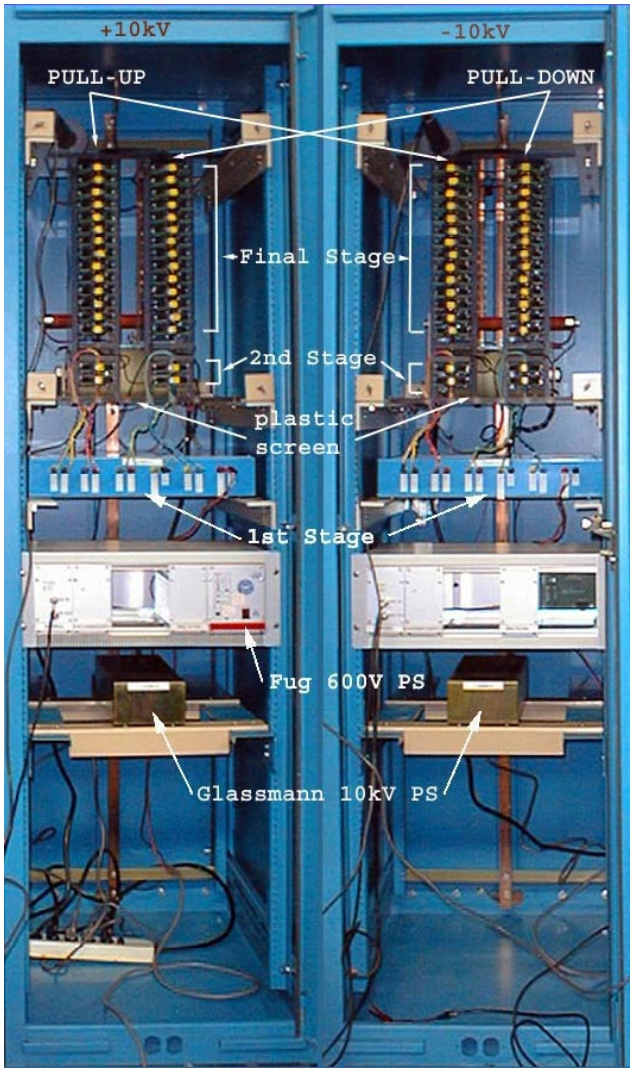

Fig. 167. Mass separator kicker.

chosen charge and to recycle higher and lower charges back to the charge booster, which will increase efficiency from 10–60%. The kicker system includes a pair of deflector plates. One plate is charged up to –4 kV by a FET based modulator, while the other plate is held at ground potential. The modulator consists of two stacks of FETs operating in push pull mode with variable output voltage, pulse width, and repetition rate from virtually dc to greater than 50 kHz. The specifications for the kicker call for rise and fall times of less than 100 ns and a minimum pulse width of 500 ns. The large dynamic range for the repetition rate and pulse width require a novel circuit design and control technique, which also results in a relatively energy efficient kicker system. The design of the kicker system was completed with the aid of PSpice. Assembly of the kicker has commenced, and the kicker will be shipped to Grenoble during January, 2001.

Magnet Measurements

73 magnets were surveyed this year and they are listed in Table XXIX.

Table XXIX. Details of surveyed magnets.

Quantity	Project	Description
1	DRAGON	5 in. x–y steering magnet from CRNL
4	ISAC	DTL triplets (12 quads)
1	TUDA	Long quad from Daresbury
6	TUDA	Short quads from Daresbury
2	DRAGON	4 in. quads
5	DRAGON	6 in. quads
1	DRAGON	Asymmetric 6 in. quad
4	ISAC	HEBT dipoles
24	ISAC	HEBT short CRNL L1 quads
2	ISAC	HEBT long CRNL L2 quads
9	ISAC	HEBT 4.5 in. double steerers
4	ISAC	HEBT $2\frac{1}{4}$ in. trim quads
2	DRAGON	6 in. x–y steerers

MECHANICAL ENGINEERING

Mechanical engineering work at TRIUMF is initiated by the submission of a Request for Engineering Assistance (REA) form which is assessed and assigned according to the size and schedule of the task. Large, complex projects may require a team approach guided by the assigned engineer. Many of the ISAC REAs fall into this category, i.e., target module 2 and 3, ISAC Remote Handling. Some requests were submitted prior to this report period, the work being extensive enough to require several years for completion, i.e., DRAGON, Expt. 614.

There were 35 ISAC REAs submitted during the year. However there were, as well, about 15 REAs carried over from the previous year of which perhaps 5 are long term projects. In non-ISAC engineering, there were 16 REAs submitted plus about 10 carried over from the previous year.

As in the past, in this report period there was continuous participation of engineering personnel in performing engineering analyses, consideration of safety related issues, design reviews and other ad hoc engineering related small jobs.

ISAC

ISAC projects again remained the major effort during the year. The emphasis, however, has shifted away from the target hall and now embraces all aspects of the project. This effort ranged from project management, i.e., DRAGON, to individual design and engineering projects which usually require involvement from design and design review, through manufacture and assembly to installation, i.e., DTL components.

Also during this report period, Engineering, along with ISAC Operations and Remote Handling, produced a list of outstanding issues related to the target hall. This was presented and discussed at engineering meetings later in the year. The list of issues falls under four main headings: modules, target hall, ion source, and hot cell. The intention of this is to consolidate and highlight all tasks that: (a) have not been completed; (b) have not commenced; and (c) are looking for a solution. This was done not only to identify and consolidate, but also to allow for planning and to assign priority, schedule and manpower in order to complete this work. High priority tasks obviously are associated with allowing for continued radioactive ion beam production, i.e., spare components for containment boxes for the target and exit modules. Other tasks have a priority related to increased radioactive ion beam current (up to 100 μA). This task list work is currently being reviewed with the object of assigning priority and establishing a schedule early in 2001, so that manpower can be allocated.

Target hall

The area immediately downstream of both target stations is the location of the 5B diagnostic station which had intentionally remained accessible during radioactive ion beam commissioning. Subsequent to that achievement, Safety requested that shielding be added to fill that volume. To achieve this, the 5B diagnostic box and stand were redesigned with a smoke stack for vertical access and the turbo molecular pump was removed. Steel and concrete shielding blocks were designed to straddle the beam line. These were installed for both the west and east target station. This will reduce the radiation level in the pre-separator magnet/DB0 area, simplifying maintenance.

Design changes were required on the hot cell roof turntable due to unexpected torque required to rotate the large turntable bearing. Conversations with the bearing manufacturer confirmed that the torque was at the high end of what was deemed acceptable for this bearing. Due to the very low duty cycle, however, it was decided that the risk was minimal relative to disabling the hot cell for six weeks while the bearing was returned to the manufacturer for inspection.

It was decided that, manpower permitting, work would commence on the east target station modules – namely the entrance and dump modules. This did not occur due to other work having priority. It is hoped that work can begin early in 2001.

Target module

The 100 μA target module used to house the Talbert high power target in December, 1999, was placed in a storage flask in the target hall subsequent to testing. This unit has now been designated as TM3 and will receive attention after a cooldown period and once TM2 is far enough along in its assembly. Although complete enough to house the 100 μA target, TM3 only required thermocouples; hence the service duct, service cap, and containment box terminations were in an incomplete state (TM3 $\sim$ 65% complete).

Meanwhile TM2, which will be built to support a surface ion source, had many problems associated with the new containment box and service duct design. In the case of the containment box, this was a result of distortion of the sheet metal components during welding and was alleviated by attaching the box to its mounting flange using screws. All flanges were re-made and holes located using a master template.

Completion of TM2 has been further delayed by the decision to provide junction blocks in the containment box so that all services can be disconnected such that not only can a target/ion source tray be removed in the hot cell, but the entire service duct can be withdrawn from the service cap (i.e., in the event of a HV breakdown).

Accelerators

RFQ work from an engineering perspective was essentially completed in 1999.

Engineering support for the RF group continued in the assembly and installation of the DTL linear accelerator tanks and associated triplet magnets, and rf buncher components and diagnostic boxes. It was found, during individual DTL tank testing, that the vacuum tank wall temperature was excessive and the RF group devised a method of fastening cooling tubes to the outer wall that alleviated the problem.

Installation of all DTL components on the support frame was a challenge due to the tight alignment requirements and restricted access. There were numerous problems associated with various components that had to be overcome. However, eventually alignment and stable beam transmission were successfully achieved.

DRAGON

This year, engineering support for DRAGON was equally divided between detailed design, fabrication and installation. While the gas target (start of the DRAGON beam line) was already installed in the fall of 1999, followed by a power supply platform (December, 1999), most of the other beam line components were installed this year.

Electrical installation started in the spring, with construction of an overhead cable tray trunk ($\approx$12 m long) from the north wall of the ISAC hall to the DRAGON power supply platform to carry the main

services for DRAGON. First the main ac feeder cables were installed, routed to the main breaker panel and transformers (at the power supply platform) for the DRAGON ac distribution. Installation of the main cooling water headers, air supply, and hydrogen exhaust duct (8 in. diameter) from the gas target to the ISAC hall roof followed in late spring.

Detailed design and fabrication of magnet supports, vacuum components and diagnostics devices were done during the summer months. Also, power supplies under and on top of the power supply platform were installed and connected to services (ac power, cooling water), as manpower was available.

Installation of magnet supports and placement of magnets and alignment began in the fall. During the same period, cable trays and dc cables were installed and connected to most devices and ac power routed along the beam line, followed by installing and connecting cooling services to the devices and installing piping for vacuum roughing and backing lines.

In preparation for the α particle test in January, 2001 (described elsewhere in this report), vacuum components were installed from the gas target to the electrostatic dipole 1 tank (DRAGON legs 1 and 2), i.e., beam pipes, BCM 1 monitor box, charge slits box, magnetic dipole 1 vacuum vessel. Components for the α test (α source holder, wobbler magnet and movable collimator, strip detector mount, etc.) are nearly complete and will be installed in January, 2001.

Fig. 168. DRAGON's ED2 electrostatic dipole during assembly.

The vacuum tanks for the ED1 and ED2 electrostatic dipoles were fabricated and vacuum tested. After thorough cleaning of inside surfaces, they were installed in the beam line and aligned. Assembly of ED1 and ED2 dipoles was done during the summer and fall period (see Fig. 168). Since electrostatic dipoles are expected to be tested up to 230 kV, assembly was a labourious task. All parts were cleaned and polished to a mirror finish and assembly was done in a dust-free temporary cleanroom. Both dipole assemblies were pre-aligned to close tolerances. The ED1 dipole assembly was installed in the vacuum vessel in early December.

Finally, engineering support was provided for various projects including 1A vault quad lifting beam and counter weights, BL2A switching magnet stand and vacuum box, and various support frames for the DRAGON beam line.

Engineering – Other

***G∅* experiment**

The magnetic field mapper gantry for the superconducting magnet system (SMS) destined ultimately for the *G∅* experiment at Jefferson Laboratory was delivered to NPL at the University of Illinois (UIUC) in the summer (see Fig. 169). The gantry system will be used

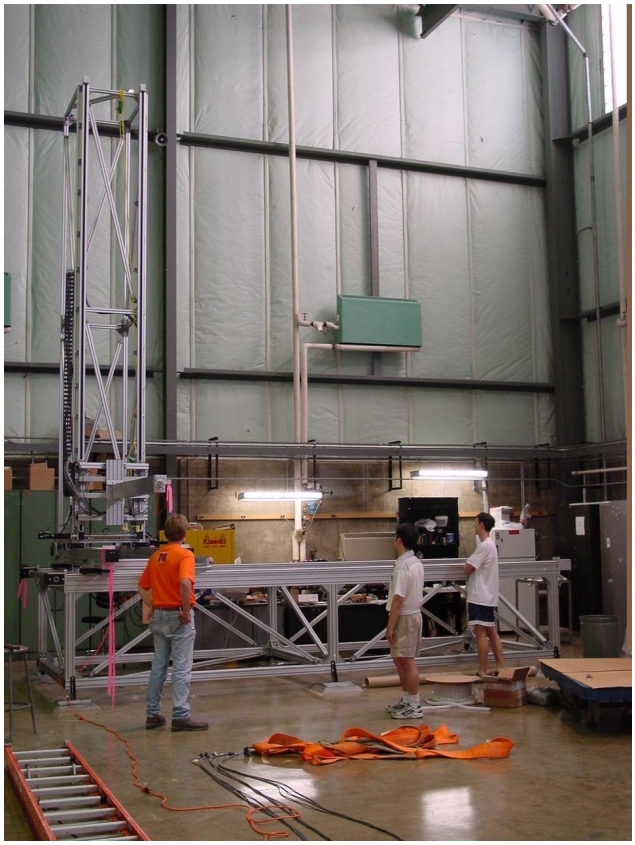

Fig. 169. Photograph of the *G∅* magnetic field mapper under test at the University of Illinois.

for magnetic field verification of the giant magnet in its actual operating state. After two further trips later in the year by TRIUMF engineers, the gantry system was fully operational and tested in the following areas:

- motion control and dynamic properties,
- position calibration and reproducibility,
- electronics safety interlocks,
- laser target tracking, and
- system control software.

The system has been used extensively by UIUC physicists for interim measurements and development work. Two more trips are needed in the spring of 2001 to finish software development and preparation, and to do the actual SMS magnetic field verification measurements.

M9 solenoid

Ongoing engineering support was provided throughout the year for operation and maintenance of the M9B superconducting solenoid and helium refrigerator.

ATLAS – University of Victoria

The physics activities of the ATLAS group are described in the Science Division section. Here, the engineering support tasks undertaken by the TRIUMF team at Victoria are described.

Hadronic endcap (HEC)

The two main tasks of the group this year have been the design of the assembly equipment for the four HEC wheels at CERN in collaboration initially with CRPP and now with Alberta, and the design and construction of the shipping container for the HEC modules produced at TRIUMF. In addition, the group has provided mechanical engineering support for the HEC group at CERN by providing the services of a chief engineer. This aspect heavily involved the group in planning for ATLAS construction at CERN.

Each of the four HEC wheels is assembled on a table. This table must be raised well off the ground so that the module, once built, can be taken from the assembly table, rotated, and presented to the cryostat. This equipment is being designed at Victoria in collaboration with Alberta. Figure 170 shows the layout of this equipment at CERN.

The design and manufacture of this equipment will be completed during 2001. Testing with dummy loads will commence early in 2002.

The shipping of series modules from TRIUMF to CERN entails shipping 157 tonnes of modules. A cost effective and safe method is required. The plan is to

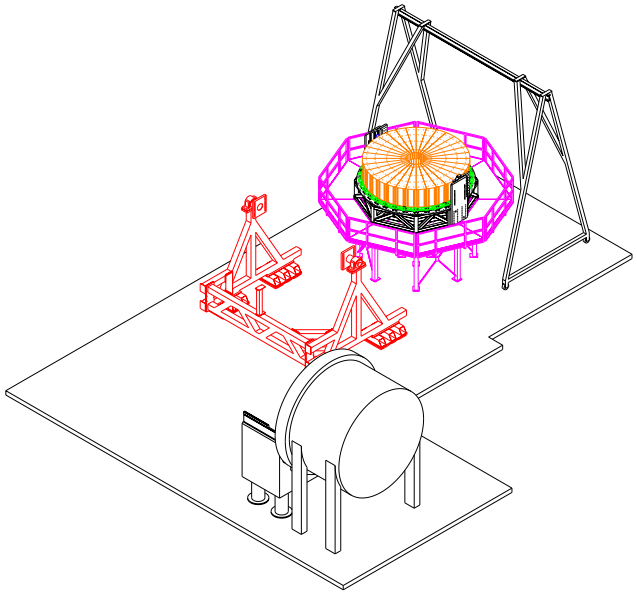

Fig. 170. Early concept of the layout of the proposed HEC wheel assembly equipment in B180 at CERN. All the equipment, except the cryostat and acceptance cradle, shown at the lower right hand corner of the figure, is a Canadian responsibility.

ship by a container outfitted with a frame for the modules that has a spring-damped system. The design, construction, and testing of this container system was finished this year. The container will be used to ship 10 payloads each of about 20 tonnes. Early analysis of the best route showed that the overland route to the east coast of North America and then on to CERN was the cheapest and fastest route. However, this route puts the modules in too much danger of experiencing high g forces, so it is only used for the return journey of our empty container. The chosen route is via the Panama Canal, Antwerp, Rhine barge to Basle, then by Swiss autoroute to CERN. This route has now been travelled twice without tripping the g monitors.

Signal feedthrough project

The signal feedthrough project moved into the production stage in the summer. Procurement of all materials, except the pin carriers, has proceeded without problems. Difficulties, apparently due to variations between batches of rolled steel used for the pin carriers, has caused considerable difficulties with their production in industry. The Victoria group, in collaboration with the ATLAS group at BNL, has been actively pursuing an understanding of and solution to this problem. Some delay in the project completion date is anticipated due to these problems, and it can only be estimated accurately once full production has restarted; it is likely to be in the 3 to 6 month range.

It was always anticipated, once the design of the feedthrough and production methods was complete,

that the design team would move on to the design of a warm flange heater plate. This heater plate provides heating for the flange to prevent condensation on the feedthrough. The design and testing of this component was successfully completed this year. Radiation testing of critical components in the heater plate was undertaken at Dubna, in collaboration with the ATLAS Montreal group.

PLANNING

This year the Planning group was involved in planning, scheduling, coordinating and expediting several sub-projects for ISAC; planning and coordinating activities for two scheduled shutdowns (December 22, 1999 – March 8, and August 22 – October 5); and planning some of the CERN collaboration projects (resonant charging power supplies (RCPS) and pulse forming networks (PFN)).

ISAC

Various plans and PERTs were prepared and updated regularly with manpower estimates and analysis to identify critical areas and resolve any problems. ISAC priorities were evaluated and higher priority was assigned to: the consolidation of MRO and essential projects in the target area to increase beam reliability; completion of a hot cell; completion of β-NMR for the first experiment in May, and for the soft landing experiment with the high voltage cage in July.

On the accelerator side, major milestones included: Test #2 (commission MEBT) by February; Test #3 (commission beam from DTL tank 1 including triplet and buncher) by July; and install all DTL systems and accelerate beam to 1.5 MeV/u by December. Manpower planning was done, activities were coordinated and expedited, and the above goals were achieved on schedule.

Technical details and progress on PERTed activities are described elsewhere in this report under the respective principal group. However, following is a summary of the main projects along with the major milestones achieved.

Target areas and hot cells

Extensive work was done to upgrade target areas, target hall crane interlocks and controls, hot cell (improved system for lead glass shielding windows, portable shielding plug, and access doors). Some contamination was experienced while changing a target, which increased the priority of designing a decontamination facility. An alternative conditioning system to expedite the process of changing ISAC targets was designed and fabrication is in progress.

Drift tube linac (DTL) systems

After evaluating the priorities and workload, it was decided to do Test #3 with DTL tank 1, triplet and buncher in June to gain experience and then install and test all DTL systems to accelerate the beam to 1.5 MeV/u in December. One large stand was designed, fabricated and installed in March to support all 5 DTL tanks.

Fabrication of DTL tanks 2 to 5 with stems and ridges was done in July, followed by assembly, rf tests and preparations for installation in the ISAC hall. Vacuum through all DTL systems was achieved by December 15, and a helium beam from the off-line source was accelerated to 1.5 MeV/u on December 21.

HEBT

Due to increased workload, the HEBT project was divided into two parts: HEBT1 (up to upstream of benders to DRAGON and TUDA beam lines); and HEBT2 (all remaining HEBT components). Major jobs included: design, fabrication and installation of vacuum system, beam line hardware, diagnostics, and controls components for HEBT1 to commission beam through all DTL systems. Due to the heavy workload in the ISAC RF group, all rf activities had to be carefully planned, coordinated and expedited. The 11 MHz buncher, chopper and bunch rotator had to be deferred until spring 2001.

Low energy experiments

These included essential modifications to GPS (lifetime), LTNO, yield station, and β-NMR. Extensive work was done on planning, coordinating and expediting activities and critical components from the Machine Shop and outside suppliers for β-NMR, laser polarization systems, spectrometer, and associated LEBT components. The first β-NMR experiment was done in May, followed by installation of the HV cage with associated safety control systems to do a soft landing experiment in July.

High energy experiments

These involved DRAGON and TUDA. Installation of HEBT components up to the TUDA experimental station, with associated services, started with an aim to finish before March, 2001. A special room was designed and constructed for the TUDA detector system electronics, with all services and a special grounding system.

In spite of significant efforts in the Design Office, overall progress on DRAGON was relatively slow due to a lack of technical resources and a higher priority on DTL and HEBT tests. All major components for legs 1–5 were installed by the end of September, and services were connected by December. ED1

and ED2 tanks were installed and electrodes assembled in September, and the tank vacuum tested in October/November. Magnetic dipoles (MD1 and MD2) were installed and the MD1 vacuum chamber was fabricated and made ready for installation.

ISAC-II

PERTs were prepared that included work on specifications and design of a superconducting rf test facility and dummy cavity with an aim to install and test a Nb cavity in summer, 2001 after receiving it from Legnaro.

CERN

The Planning group was involved in planning and scheduling the activities for five 66 kV resonant charging power supplies (RCPS), and nine pulse forming networks (PFN). The assembly and testing area for RCPS and PFN production was designed and constructed with crane and associated services. Several contracts for PFN tanks and other components were awarded to local machine shops.

Shutdown Activities

There were two major shutdowns during the year: the winter shutdown (December 22, 1999 – March 8), and the fall shutdown (August 22 – October 5). Major cyclotron jobs completed in the winter shutdown included: shim plate clearance, 2C work, EX2A, EX1 MRO, ISIS, and rf MRO. Meson hall jobs included: 1AT1 target MRO, 1AM8 cabling, T2 water package MRO, M13 jaws vacuum leak repair, M15 separator vacuum leak, M20 beam blocker repair, M9A rf separator, T1 profile monitor, and BL1A exhaust modifications.

The main purpose of the fall shutdown was to blank off M8B1 to repair a vacuum leak in this area. Cyclotron jobs in the fall shutdown included: jack #2 MRO, duct cleaning in computer and control room, tiles in control room, water systems MRO, and measurements for vault services upgrade (to prepare for January, 2001 shutdown). The lid was raised on September 28 to fix inflector problems encountered during the usual start up.

TWIST (Expt. 614)

The Planning group got actively involved in this project in the second half of 2000. PERTs were prepared with an emphasis on design, fabrication and installation of magnet yoke, detectors, detector cradle, transport cart, field mapper, and other associated components.

DESIGN OFFICE

The ISAC project received 12,325 hours of Design Office time, which is 71% of available hours. The office has been kept very busy preparing conceptual and detailed designs for many different aspects of the project. Specifically, and in order of magnitude, they are: (a) DRAGON electrostatic dipoles, charge selection diagnostics, mass slits, beam position diagnostics, beam line components for vacuum systems, and other mechanical support; (b) HEBT1 and 2, beam line components, support stand systems and diagnostics sufficient to transport beam to DRAGON and TUDA; (c) ITW5B and mass separator DB0 redesign; (d) ECR target design, test box, conditioning system, and target module updates; (e) rf cavities for ME chopper, DTL and HE rebuncher; (f) beam line 2A extraction probe modifications and switchyard magnet design; and (g) TUDA experimental beam line components.

The CERN contribution still received a significant 10% of Design Office time, with most effort concentrated on the pulse forming network and HV switches.

The most significant TRIUMF project undertaken was the Expt. 614 superconducting solenoid for the TWIST experiment. At 9.3%, this included design of the magnet yoke, detector cradle, transport cart, and field mapping device(s).

The demand for photographic and visual art services continues to increase in support of seminars, conferences, and publications, such as the work displayed in the 1999/2000 Annual Financial and Administrative Report and the foyer of the administration building.

MACHINE SHOP

The TRIUMF Machine Shop, with 22 technicians, produced approximately $140,000 worth of fabricated and machined components for various on-site groups each month. Our shop charge out rate is $60/hour. The distribution by TRIUMF divisions and other groups is shown in Table XXX. In addition, 285 separate work packages worth more than $1,030,000 were subcontracted through the Machine Shop to local industrial companies.

Table XXX. Machine Shop utilization.

ISAC	40.6%
Science	21.4%
ISAC Operations	18.3%
Cyclotron	7.1%
NSERC	4.2%
ISAC Development	2.4%
Affiliated Institutions	1.6%
Cyclotron Refurbishing	1.6%
Nordion	1.1%
CERN	1.0%
Accelerator	0.3%
Administration	0.1%

The Machine Shop continued to be fully loaded throughout the year with overtime needed to meet priorities. ISAC continued to be the major user of our services. Early in the year we commissioned a new 5-axis CNC machining centre which has greatly enhanced our machining capabilities.

BUILDING PROGRAM

The year 2000 demanded continued support from the Building department in TRIUMF's endeavour to have the new ISAC beam lines operational within the projected time frame. To this extent we designed and contracted construction for several ISAC projects:

- A radiation shield at the DTL portion of the high energy beam line consisting of a 24 ft long × 12 ft deep × 11 ft high steel column and beam structure with 18 removable composite lead on plywood panels.
- For the TUDA experiment a 16 ft × 12 ft × 9 ft high monitoring cabin was built in conventional wood construction with vinyl coated gypsum panels on the outside and sheet copper clad plywood walls and ceiling inside, together with an electrically conducting floor of vinyl tiles on plywood and sheet copper.
- An 18 ft × 12 ft × 9 ft high facility had to be built outside the east wall of the ISAC experimental hall to store and dispense the various required gases. An explosion proof exhaust fan evacuates volatile gases from this room.
- Adjacent to the gas handling facility a 15 ft × 15 ft × 18 in. thick reinforced concrete slab was cast to accommodate a liquid nitrogen tank.
- A new one piece 9 ft × 7 ft × 12 in. reinforced concrete hatch cover was cast for easier access to the target hall and hot cells.

An extensive renovation of the upper two floors of the biomedical annex was carried out to provide office and laboratory space for the μSR group. This work was started in December, 1999, and was completed in April, allowing the experimental groups to move in. Seven offices were created on the top floor with sufficient space for 20 work stations, and three offices and a laboratory on the second floor. The annex roof was replaced in the fall.

The space requirements for the Applied Technology group dictated the construction of a 34 ft × 7 ft extension to the existing mezzanine floor along the east wall of the meson hall in the accelerator building. This structure is a cantilevered steel frame with metal deck and concrete topping and an enclosure with exhaust for a sandblaster.

Maintenance and repair of buildings on the TRIUMF site has become a more prominent issue as most facilities are now 30 years old. Approximately $25,000 was spent during the year on routine upkeep, such as painting and minor repairs. A new roof on the accelerator building is now our next priority.

ELECTRONICS SERVICES

Overview

It was another busy year for the Electronics Services group. Major upgrades to site communications infrastructure were performed, along with continued support for CERN and ISAC. In the last quarter we got involved with TWIST (Expt. 614) and now have the equivalent of 5 full-time staff members working on this project. Our other main efforts are in PC support, as well as equipment repairs and calibrations. We continue to assist many groups and numerous experimenters on a daily basis.

Technical Support

Technical Support continued its versatile support to over a dozen different experiments and groups during the year. Major jobs included the design and construction of fibre optic link modules for the BOPPIS experiment at BNL, the packaging and wiring of a very complicated rf control box for β-NMR, and PCB layout for MEBT motor drivers, as well as construction of some voltage to frequency modules for sale to Jefferson Laboratory. In June, Technical Support shifted 80% of its efforts to the TWIST experiment. This included layout, packaging and coordinating, and manufacture of the production version of three hundred 16-channel postamp modules.

Experimental and Target Support

Year 2000's involvement was primarily with CERN and ISAC. CERN work involved manufacturing and assembling the control system for the kicker magnets. Assembly continued for the 60 kV PFN system, which included design and assembly of the kicker PCB. ISAC work involved wiring of the kicker assemblies for the integration separators. Support was also started for the TWIST experiment and involved cabling, plus design of the electronics rack system.

Electronics Shop

Highlights of the year were the great demand for cables and intelligent flow-switch control units. The variety of cables produced included delay cables, communication cables, control cables, patch cables, BNC cables, jumper cables, Varian gauge cables, Lemo cables, ribbon cables, VHF cables, extension cables and many others, custom made, along with a variety of modules for ISAC, TRINAT, Controls group, DRAGON, HERMES, and other set-ups. A group of electronics panels

and boards was assembled for CERN. Our in-house designed IFS8 flow-switch controllers were needed for every stage of the expanding ISAC beam lines. There are now 80 of these units on site and this has saved TRIUMF over $300,000 in the last 10 years on this item alone. Late in the year a massive job for the TWIST experiment was started. This job entails the construction of 4000 miniature coax cables and will continue until April, 2001.

Electronics Repair Shop

As usual, the Electronics Repair Shop has been very busy this year – especially with the demand to refurbish numerous pieces of electronic equipment recovered from Chalk River for use in the experimental program here. In total, 281 pieces of electronic equipment were given checkout to confirm functionality, repaired, and/or recalibrated. This included: 19 terminals, 71 monitors (46 colour units and 25 monochrome), 13 SCSI devices, 74 power supplies (which included 27 NIM devices, 11 CAMAC devices, 19 high voltage units, and 17 generic types), 54 nucleonics modules (of which 25 were NIM and 29 were CAMAC), 14 test equipment devices, and 36 miscellaneous electronic devices.

High Level Software Support

For CERN, a system was developed to measure special capacitors for the kicker work. ISAC had a number of motor systems installed for MEBT, HEBT and designed for DRAGON. For ISAC-II, the charge booster measurement was worked on. Site support went to the PIF motor control system, BL2A extraction probe software upgrades, as well as solving problems with the M15 and M9 separators. LTNO received software support, as well as assistance in replacing the computer controlled rf source. For TWIST, the magnet measurement system as well as the wire chamber measurement system were worked on.

PC Support – Hardware

This year brought a significant increase in end user support. The number of consultations and evaluations increased by 150% to about 875 incidents. PC hardware repairs increased by 11% to 300 occurrences. New PC configurations and old PC rebuilds increased 37% to 55 units. Major tasks performed in 2000 included: migrating the Windows virus protection software from Norton AntiVirus to McAfee Virus Scan, defining a new network interface card as a TRIUMF standard, and implementing recommendations for Notebooks. A method was created to efficiently distribute and control Windows software at TRIUMF. User support was enhanced by keeping the PC Web site up to date. It is estimated that there are over 400 PCs in use on the site.

PC Support – Systems

During 2000, the TRIUMF PC backup service design and testing was completed, although problems with throughput across the site held up implementation. The problem was corrected, deployment continued and a tape autoloader purchased to increase capacity. A Web site was created with service information and policies available, as well as an application form for user sign-up. Posted backup schedules and results are forthcoming. The NetWare 3.x servers are being backed up regularly, and several dozen users are on the schedule so far. The service has been in production for several months.

A network server upgrade has been in the planning and testing stages for several months. The Design Office and trailer Gg seven-year-old NetWare 3.x servers are being upgraded and consolidated into one NetWare 5.1 server. The server hardware and software has been purchased, deployment scenarios have been planned and migration and configuration tests are being performed. This major upgrade is analogous to a user upgrading from DOS to Windows 2000. This server will service a majority of the Accelerator Technology division, with a few extra groups from other divisions.

Communications Support

Communications Support had the busiest year in 10 years due to massive network cable upgrading. Most of the work involved new 100 Base-T cables. The main office building had 150 cables installed, biomed got 60, trailers Gg and Rr had 90, and trailer X got 22. In addition there were about 35 other cables installed around the site. Other improvements included fibre optics installation to trailer Gg, biomed, as well as repairs in ISAC. Communications also assisted in the cable installation for the ISAC PA system. Ongoing maintenance included a speedy recovery from the January 10 lightning strike that required replacement of multiple transceivers all over the site that had failed. Documentation is now routinely updated and posted on the TRIUMF Web page for easy reference.

ELECTRONICS DEVELOPMENT

This year again, the majority of the group's effort went into support of the ISAC control system design and installation, and the CERN collaboration. Between February and June, one BCIT co-op student was supervised.

ISAC Support

A Gauss-meter module was designed for readout of Hall probes on the HEBT dipole magnets and the

DRAGON beam line quadrupoles. It is based on the ADPS 2861 DSP chip and can be read via CAN-bus and RS232. A prototype module was built and tested in the lab. The major source of error was found to be the temperature sensitivity of the sensor offset voltage. This was corrected by the module software. Testing will be conducted in February, 2001, to establish resolution and stability of the measurements under actual operating conditions.

On the high voltage power supply for the DRAGON electrostatic dipoles, testing of the Cockroft-Walton 300 kV stack continued. Connector breakdown difficulties plagued the project during the first part of the year. Using a modified automotive spark plug solved the problem. Both a positive and a negative stack were tested successfully at their nominal operating voltage of 200 kV for 30 days. Further design was undertaken to modify the Glassman driver supplies for conditioning of the dipoles.

The group assisted in design and fabrication of the ISAC low energy chopper. Several PCBs were designed, assembled and tested: FET driver cards, fibre optic drivers and receivers, and controllers.

Design and construction commenced on a chopper for the charge state booster. This design is a modified version of the ISAC low energy chopper. Four PCBs were designed, assembled, and tested: FET driver, pulse generator/first stage driver, power supply filter, and an interlock module.

Several specialized CAN-bus controller modules were designed and built. A module with bipolar DAC was designed and used for the etalon position controller and the birefringent filter of the laser system for the β-NMR experiment. Also for β-NMR, a fibre optics board was developed for control of three Bertan high voltage supplies which are located on the experiment's platform. This board allows the CAN-bus to cross a galvanic isolation.

Also for the β-NMR laser system, a piezo positioner was developed for controlling cavity depth on the laser.

CERN

A project to develop a data acquisition board (DAB) for the LHC beam orbit system is described in the CERN Collaboration section. This project occupied three members of the Electronics Development group throughout the year.

Miscellaneous

Experiment 497 – parity

An ADC/averaging module was designed and built. This VME module digitizes and sums signals from the TRIC chambers. It was successfully tested during beam runs in July and December.

M9 vacuum system

After several failures of the PLC processor memory and PLC programmer, it was decided to replace the obsolete Modicon 884 processor. It was replaced with a remote I/O adapter and the system was integrated into the beam line 2A Modicon Quantum PLC system. This solution retains full use of all existing I/O modules. The needed re-write of the ladder logic software was made, conforming to the ISAC standard. Changes were completed and tested during the fall shutdown. EPICS screens for a graphical user interface have been prototyped.

For the ISAC β-NMR experiment, two VME modules were developed at fairly short notice. They interface to a commercial rf synthesizer and allow fast steerage of the β-NMR rf program.

CERN COLLABORATION

INTRODUCTION

Funding for a second accelerator contribution to the Large Hadron Collider (LHC) at CERN was provided in the Five-Year Plan (2000–2005) which was announced at the end of February. These funds will allow TRIUMF to complete the two large commitments that were already under consideration: the series production of 52 twin aperture quadrupole magnets, and the components for the LHC injection system.

This year saw the completion of the last tasks that were included in the PS Conversion project, with the wrapping up of two beam dynamics projects associated with the PS Booster and the delivery of the final two 250 kW power supplies. Two beam dynamics tasks related to the LHC continue. A CERN yellow report, "The PS Complex as Proton Pre-injector for the LHC – Design and Implementation Report", was released in April, describing this project and the TRIUMF involvement.

A new instrumentation task, started in 1999, involves the design and fabrication of electronics for the readout of the LHC beam position monitors. Prototypes of this VME based data acquisition board (DAB) were successfully tested in the SPS beam during the summer. Some changes related to moving the digital portion of the readout system out of the LHC tunnel are now being considered and a new version of this board will be tested in 2001 prior to the series production.

In 1999, ALSTOM Canada (Tracy, Quebec) was awarded the contract for the production of the first 17 of the twin aperture quadrupole magnets, with the awarding of the remaining 35 magnets contingent on the new Five-Year Plan funding, and on the successful completion of the first series magnet. ALSTOM had previously built a prototype magnet which did not meet the magnetic field requirements due to poor assembly tolerances, which were to some extent inherent in the design. New tooling for the redesigned laminations and the stacking tables was required. This year ALSTOM produced the necessary tooling and produced laminations to the required accuracy. The stacking of one type of lamination to the required straightness tolerance proved very difficult, but was eventually solved. The production of coils was plagued with a number of problems, but eventually sufficient coils for the first series magnet were produced. However, the final assembly of the first magnet was delayed at the end of the year by union problems at the factory and delivery is now expected in February, 2001.

TRIUMF is also designing and building 6 resonant charging power supplies (RCPS), 9 pulse forming networks (PFN), and 20 thyratron switch tanks for the LHC injection kickers. During this year the RCPS were completed, although final testing was delayed due to a capacitor failure in the dummy load. The clean room with crane coverage for assembling the PFN tanks was completed in the proton hall extension, and contracts for fabrication of components for the PFNs were awarded. The 5.2 metre long tanks are being fabricated by Brandt Industries (Saskatchewan), with the remaining parts being manufactured by local machine shops. Capacitors were obtained from ZEZ Silko (Czech Republic), and resistors from HVR Advanced Power Components (USA). By the end of the year the first 28 cell PFN was assembled to the point where low voltage testing could begin.

BEAM DYNAMICS

This year has seen the successful completion of the two beam dynamics tasks associated with the LHC injector chain, both involving the PS Booster. The first explored ways of improving the longitudinal dynamics at high beam intensity, including the addition of second-harmonic rf. The second involved development of our simulation code ACCSIM – now adopted at several major labs – for studies of injection and collimation.

Of the ongoing tasks, beam stability studies have taken a new direction by providing support for simulations of the beam-beam interaction near the LHC collision points, enabling space-charge effects to be more accurately modelled. The collimation insertions and their beam optics had their final details settled this year, and efforts on that task have now shifted to studies of the sensitivity of the "resonance-free lattice" to magnetic field errors.

Second Harmonic in the PS Booster

Bunches which are hollow in longitudinal phase-space have the advantage of lower peak charge density and space-charge forces. Acceleration of hollow bunches in the PS Booster became almost routine in 1999. One component of that success was the use of high-harmonic rf "clearing sweeps" to homogenize the coasting beam prior to the deposition of empty buckets – a procedure that was developed empirically, but whose mechanism was not understood. Another component was the availability of longitudinal tomography for visualization of the hollow phase-space.

In late 1999, an experimental study revealed that the voids in the linac beam, dubbed "bubbles", and the holes introduced by the empty bucket deposition survive in the PSB much longer than anticipated (see Fig. 171). It was recognized that these "cold-spots"

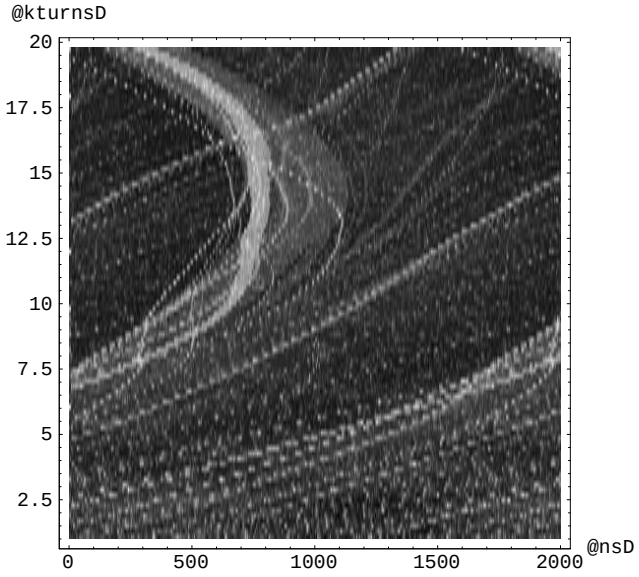

Fig. 171. Waterfall plot of coasting beam density around the PS Booster observed with 4×10^{12} protons over 20,000 turns, showing the survival and drift of voids or "bubbles".

could be stabilized by space-charge forces. Experimental evidence indicates that hole longevity increases with beam current; and by imposing an $h = 1$ modulation it was shown that holes are steered by momentum differences.

These observations initiated a comprehensive set of LONG1D computer simulations of periodic arrays of holes, single stationary holes and two-hole collisions. This culminated in an understanding of: (i) the method of "clearing sweeps"; (ii) the role of momentum steering as an agent for collisions; and (iii) the non-coalescing of holes. A simple Hamiltonian criterion for self-consistency and stationarity of holes was derived in terms of the competition between space-charge and momentum spread.

It became clear that the longevity of the holes could not be explained in terms of the usual Keil-Schnell criteria for perturbations on coasting beams. The mystery was solved in August, by suggesting a radical departure from the usual treatment of the Vlasov equation. Based on the observation that this equation is "obsessed by derivatives", the steady-state distribution is neglected in comparison with the highly localized perturbation, and this leads to an equation for soliton-like holes propagating over a background distribution, provided the particle density is high enough.

Tomography is the technique whereby several projections of an object are combined to infer its internal structure. A particle beam confined in a potential well rotates in phase-space, and over time presents many different projections. Hence one may infer the longitudinal distribution of a bunched beam by recording the bunch shape turn-by-turn. Space-charge forces do not require any knowledge of the phase-space distribution (which is initially unknown) but can be derived purely from the measured profiles. This realization led this year to our developing a longitudinal space-charge option for the tomographic software originated at the CERN PS, and to showcasing the technique using mixed dual/single harmonic operation of the PSB.

Injection and Collimation in the PSB

This task, which came to the end of its term on March 31, involved the development and support of the ACCSIM multi-particle tracking and simulation code, used to study the behaviour of intense proton beams in synchrotrons. In the closing months a further milestone was passed in the treatment of space-charge effects, with the introduction of image forces to account for the effects of the charge and current induced in conducting vacuum chambers. These forces depend on the beam position, the charge distribution, and the chamber shape and dimensions, which may vary around the ring. In practice, they are often omitted in space-charge simulations because the FFT-based field solvers usually used do not admit the necessary boundary conditions. At energies above 1 GeV, however, their contribution becomes significant.

In ACCSIM, which uses a fast-multipole field solver, a new method was developed for accurately deriving the image-force contributions for arbitrary beam distributions and vacuum chamber geometries, with only a modest computing time requirement. Once the "direct" (free space) field has been computed, there is a second processing stage where a discrete fast Poisson solver, using harmonic functions and a minimization technique, is applied to a set of boundary points representing the vacuum chamber surface. The result is a parameterized solution for the image field and consequently a rapid evaluation of the image force for each macro-particle.

With suitable sets of points to represent the boundary surfaces, tracking tests were carried out for various "textbook" cases of centred and offset beams in circular, elliptical and rectangular chambers, where the space-charge tune shifts contain a known image-force term. Tunes measured from ACCSIM tracking data were found to be in good agreement with these predictions. A paper and poster on this work were presented at EPAC'2000.

Beam Stability

Following last year's feasibility study, a new project was begun this year in support of studies of the "beam-beam" effects caused by electrical forces between the counter-rotating bunches of protons in the LHC interaction regions, where the two beams approach and

cross each other. The problem here is how to compute the beam-beam forces efficiently in the large-scale multi-particle simulations which are used to identify potentially unstable coherent oscillation modes.

Our main activity was to introduce the hybrid-fast-multipole (HFM) techniques, previously developed for ACCSIM space-charge computations in the PSB, into a beam-beam simulation code ss_HOLR in use at CERN. The relevant ACCSIM routines were modified and made into a self-contained package which accepts two arbitrary macro-particle distributions and returns the electric field components at each macro-particle location. The ss_HOLR code was formerly limited to a non-self-consistent "soft-Gaussian" model which did not give a complete description of the beam-beam interaction and tended to overestimate the lower of the two fundamental coherent-mode frequencies for head-on collisions. With the new fast-multipole field solver, this problem was cleared up and the spectrum of coherent motion exhibited all the expected characteristics.

Initial tests with parasitic (long-range) "collisions" have also obtained reasonable results, but the computation times need to be reduced somewhat, either through further code optimizations or by migration to faster (e.g., 1.5 GHz) computing platforms, in order to get the desired turnaround times for a full-scale study of beam-beam coherent effects. This work will continue in 2001, and pending further validation the HFM beam-beam field solver package will be made available from the ACCSIM Web page on the TRIUMF WWW server.

Beam Optics and Collimation

LHC collimation

During the past year, with the LHC engineering in its final stages, the collimation insertion layouts remained essentially unchanged. Nevertheless, some lattice work (mostly rematching) had to be carried out as a consequence of revisions to the database terminology and input formats during the year. Via careful optical matching, the collimation quality for beam 2 was made equal to that previously reported for beam 1. Beam 2 requires a slightly different collimator set-up, since the final hardware does not allow some of the collimators to be placed at exactly the optimum locations, while the optics of the two LHC beams are linked via common focusing fields. Some database errors of a technical nature also had to be corrected.

Resonance-free LHC optics

Using "resonance-free" linear optics for the LHC ring means that the strengths of the two families of main quadrupoles are set to achieve a special betatron phase advance in the arc cells. This has been demonstrated to cancel many non-linear resonances, since their driving terms are proportional to "systematic-per-arc" higher-order multipole errors. Systematic-per-arc errors dominate if the dipoles in each arc are manufactured on a single production line, but different arcs on different lines (the scenario foreseen).

Our task has been to look at the effect of field gradient errors. While easily correctable and therefore not very important for the nominal LHC optics, these can destroy the beneficial effects of the resonance-free optics, since they change the betatron phases. For the most important higher-order errors (normal and skew sextupole b_3 and a_3, and normal and skew octupole b_4 and a_4, the task is to find the tolerable level of normal gradient error b_2. With the quite complicated multipole error table (up to 11th order), this by itself also provides a good proof that the improvements – higher dynamic aperture (MAD8 and DIMAD codes) and lower driving terms (SODD code) – are indeed caused by resonance cancellations.

The study of gradient error effects has been completed for the case of the normal sextupole b_3, while the studies of a_3 and b_4 are under way. The a_3 task is also linked to the proposal to convert three normal sextupole correctors in each arc to skew correctors, and to improve the nominal optics.

CONTROLS AND INSTRUMENTATION

Fast Blade Scanner

Measurement of the transverse beam emittance is an important diagnostic for obtaining high performance beams destined for the LHC. The fast blade scanner (FBS) built at TRIUMF and shipped to CERN in May, 1999, is to be used for destructive diagnosis of the betatron amplitude distribution in ring 1 of the PS Booster. TRIUMF involvement is essentially completed.

In December, 1999, CERN prepared a laser/photodiode system for recalibration and to gain more experience with the scanner prior to installation in the spring. CERN activities with the wire scanners delayed beam tests of the FBS until September through November. In these tests, the blade scanner was compared against the "Beam Scope" and profiles in an external measurement line. Beam energies of 1.0 and 1.4 GeV, and intensities from 3 to 13 injected turns were used with FBS speeds ranging from 500 to 1500 rpm. To facilitate the comparison, measurements were made in the vertical plane to avoid the effects of dispersion and of the longitudinal beam control. Although there is a rather satisfactory agreement of the average emittances between all three methods, as shown in Fig. 172, the repeatability and calibration of the FBS still needs some improvement. The FBS was dismounted from the machine later in the year and placed on the concrete

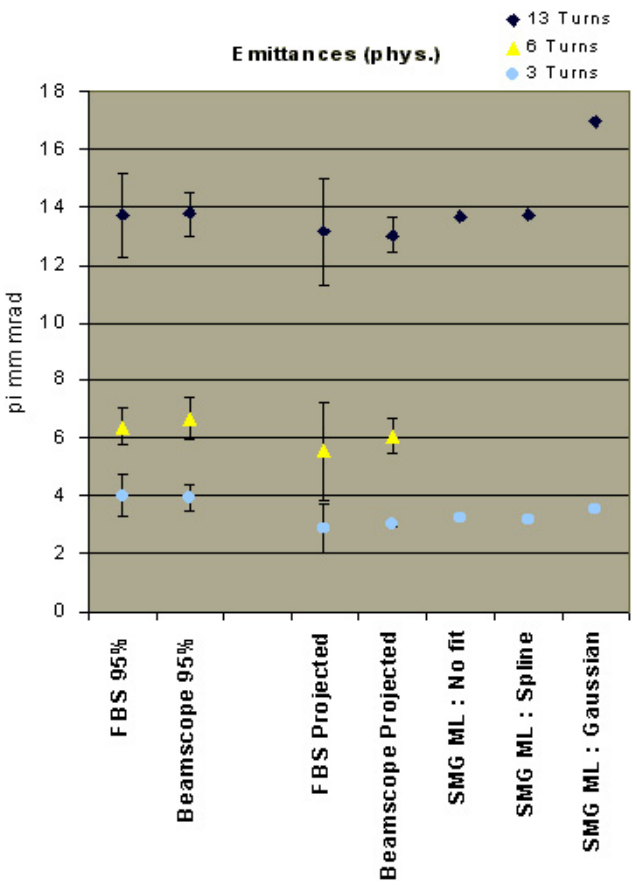

Fig. 172. Average emittances between all three methods.

pedestal next to its normal place, set under vacuum and connected to its normal cables, so that calibrations can be made under real operating conditions.

Fast Wire Scanner

Fast wire scanners (FWS) provide an almost non-destructive measurement of horizontal or vertical beam profiles. In 1998, CERN requested TRIUMF to build 4 horizontal, 4 vertical and 1 spare wire scanners. This work was essentially completed in 1999. The scanners were assembled and tested to 20 m/s at TRIUMF and, together with the stand and the calibration device, they were shipped to CERN in December, 1999. The scanners were calibrated in February, and two sets of X and Y wire scanners were installed in the PSB (see Fig. 173), one in ring 1 and the other in ring 3, in line with the beam PS. The other two sets will be installed during the winter/spring shutdown of year 2001. Integration with the control system was much delayed due to the need for new motor control processors to replace parts no longer commercially available, and the need to develop new software to accept them. Completion of this work is anticipated in the summer of 2001.

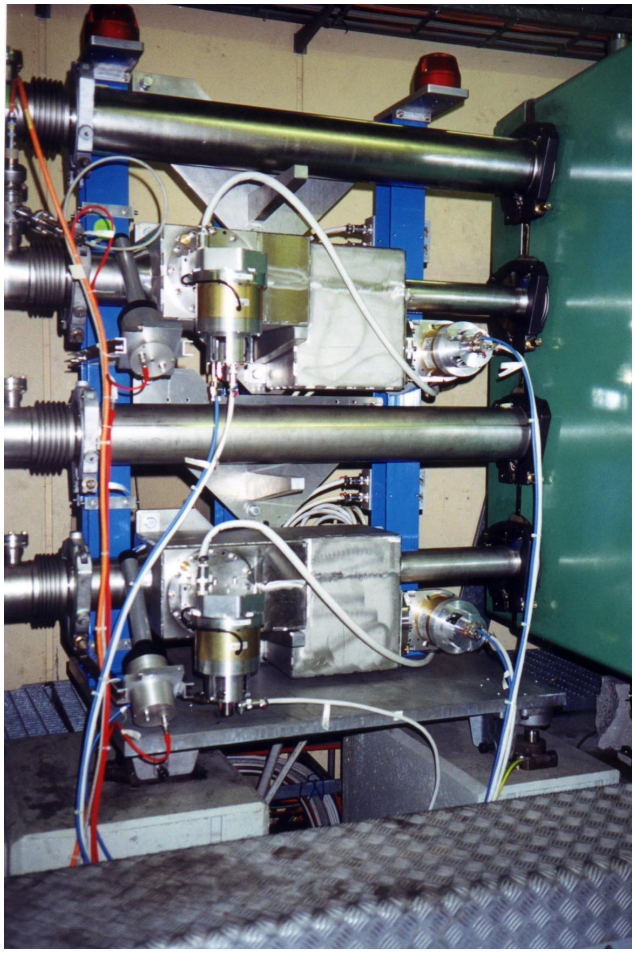

Fig. 173. Two sets of X and Y wire scanners installed in the PSB.

LHC Orbit System Components

The electronics intended to read out the LHC beam position monitors (BPM) comprise a calibrator, 70 MHz low-pass filter, wide-band (time) normalizer (WBTN), and 40 MHz digitization of the signals and some data treatment. TRIUMF was asked to build a prototype VME data acquisition board (DAB), write application software, and find suitable commercial matched-pairs of filters; leading to a production run of about 1200 boards and 2500 filters to be managed by TRIUMF. Partial specifications were received in August, 1999, and prototypes of three DABs and several filters were delivered to CERN during the year for testing.

The DAB VME module groups all the necessary digital functions associated with a BPM: 2-plane position measurement, intensity measurement, and test and calibration control. On-board logic provides the interface to the VME bus and control of data transfers from the WBTN to the SRAM local memory. A phase-locked loop (PLL) synchronizes all internal timing using signals provided by an external timing control

module. Simulations of the VME hardware began in October, 1999, followed by parts/vendor selections. A detailed design document was sent for CERN approval in January, and PC board manufacturing and component assembly followed. After successful local testing, the three DABs were delivered to CERN in June for evaluation: two were used for beam tests and the third for irradiation tests.

After adjustments to the PLL, laboratory tests with various timing sources and the CERN normalizer (WBTN) demonstrated that the board worked as specified in calibration and capture modes. Following this, the board captured LHC-beam position data in the SPS ring. Figure 174 shows the average position and standard deviation of all 84 bunches in an LHC batch during 80 turns. It can be seen that the orbit appears to vary along the batch, but this might be an artifact of the normalizer. Figure 175 shows the turn-by-turn position of a single bunch which commences an instability at around 1000 turns.

The third DAB module was tested during operation in a radiation field of approximately 100 Gy/year.

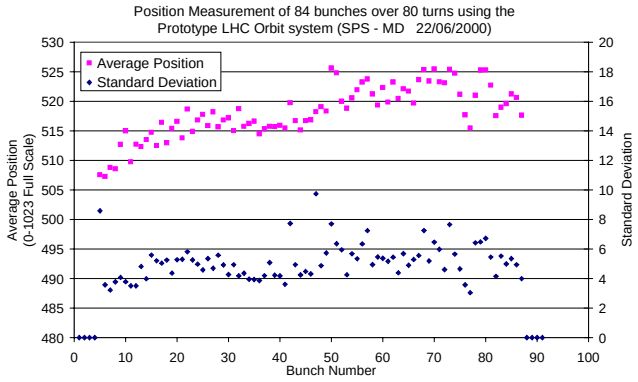

Fig. 174. Average position and standard deviation of all bunches in one LHC batch for 80 consecutive turns compiled from DAB acquisition data.

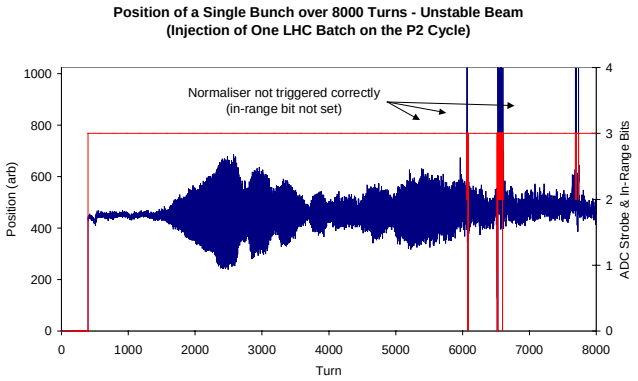

Fig. 175. DAB acquisition of a single bunch. Acquisition begins 200 turns before injection. An instability is seen to occur around 1000 turns after injection. Beam losses lead to incorrect triggering of the normalizer as indicated by the status bits (red trace) which the DAB receives.

Although components survived, results showed significant single event error rates in the SRAM. To eliminate the need to qualify all the components in the VME acquisition system for radiation tolerance, it was decided, in November, to move the system out of the radiation field entirely. This requires the redesign of both the WBTN and the DAB. The digital portion of the WBTN will reside on a 2U daughter card that plugs into the DAB module. The analogue portion will remain in the LHC tunnel. The WBTN analogue signal will be transmitted through 3 km of fibre optic cable to the DAB module. Specifications will be finalised in 2001.

To aid in DAB testing and software design, a VME software development package has been loaned by CERN since November, 1999. With CERN input on software specification and procedures in March, driver/equipment module development progressed smoothly from design through testing of the driver and diagnostic software on the prototype boards, to firmware and software completion in preparation for beam tests in the SPS in July.

Sample low pass filters were received from Lorch (2 pairs) and K&L Microwave (1 pair), tested in January, and shipped to CERN in February. The CERN evaluation revealed that input reflection and mechanical tolerance were a problem for both manufacturers. In general, the K&L filters had better electrical characteristics. Measurements were passed to the manufacturers and improved prototypes were requested. Lorch corrected the component values in their design and, in September, sent two more filter pairs which are in much better compliance with the specifications. Lorch was chosen as the supplier and it is anticipated that a pre-production run of 150 pairs will be ordered in January, 2001.

POWER SUPPLIES

Booster Transfer Line Power Supplies

The year saw completion of the two power converters rated at 250 kW output power. These units had associated modules which permitted reversal as well as energy recovery during ramping down of the magnets. The supplies were based on the design of batch 1 supplied earlier by Inverpower Controls, and were a further development of the six 100 kW supplies provided last year by I.E. Power in Toronto.

The project proceeded relatively smoothly with some difficulties experienced with the temperature of some of the magnetic components. These were resolved and final factory testing was witnessed by CERN prior to shipment.

All major equipment has now been shipped with provision of a few spare parts being under way. This

effectively brings to an end the magnet power portion of the CERN collaboration for the PS division, with a total of 44 magnet supplies delivered.

MAGNET DEVELOPMENT

TRIUMF has agreed to provide CERN with fifty-two twin aperture resistive quadrupole magnets for the LHC cleaning insertions. The prototype magnet was delivered in 1998. As a result of measurements on the prototype, CERN asked that TRIUMF improve the magnetic properties of the magnets by a factor of 5 to 10.

In 1999, TRIUMF awarded three contracts related to these magnets to ALSTOM Canada (Tracy, Quebec). The first contract was for new punching dies needed because the lamination shapes changed. The second contract is to supply stacking tables, and the third contract is to manufacture the first 17 quadrupoles. TRIUMF expects to increase the order to 52 quadrupoles once ALSTOM delivers a satisfactory magnet.

After die corrections in February and press corrections in March, ALSTOM supplied acceptable laminations. In April, ALSTOM punched enough laminations to make two magnets. In August, the die was found to be out of tolerance. ALSTOM made several changes to the press set-up and modified the die, and at year-end the laminations were again acceptable.

By March, ALSTOM had manufactured the stacking tables. During installation they found that the factory floor was not strong enough for the precision alignment required. Portions of the floor were torn up and heavy concrete foundations were poured. After installing the stacking tables, ALSTOM began learning how to stack and weld straight stacks. Stacking and welding type 1 stacks is considerably easier than type 2 stacks, probably because these stacks have some symmetry. After considerable trial and error, ALSTOM learnt how to make acceptable type 2 stacks.

ALSTOM had manufactured prototype coils without difficulty, but the production coils were plagued by problems. The problems that they encountered included bad fibreglass tape, bad sealing brazes, water inside the coil cooling channel turning to steam during impregnation, bond breaker contamination on the fibreglass tape, and vacuum system failures. The subcontractor winding the bare coils had difficulty keeping the coils in tolerance. ALSTOM will try to recover the copper from some reject coils by burning off the epoxy.

The year-end status at ALSTOM was not good. They are well behind schedule on delivering the first series magnet. The first half-magnet is ready to weld, but labour union problems have temporarily stopped the work.

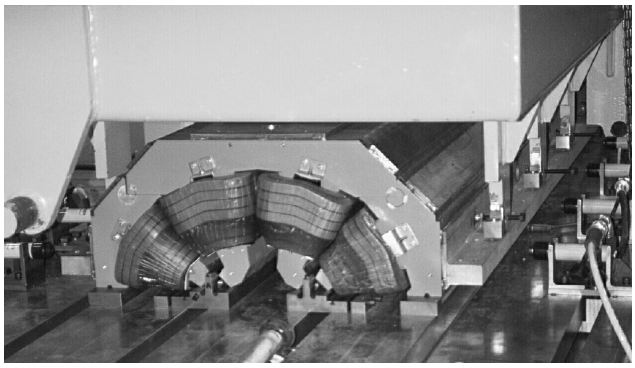

Fig. 176. The first MQW half-magnet ready to weld.

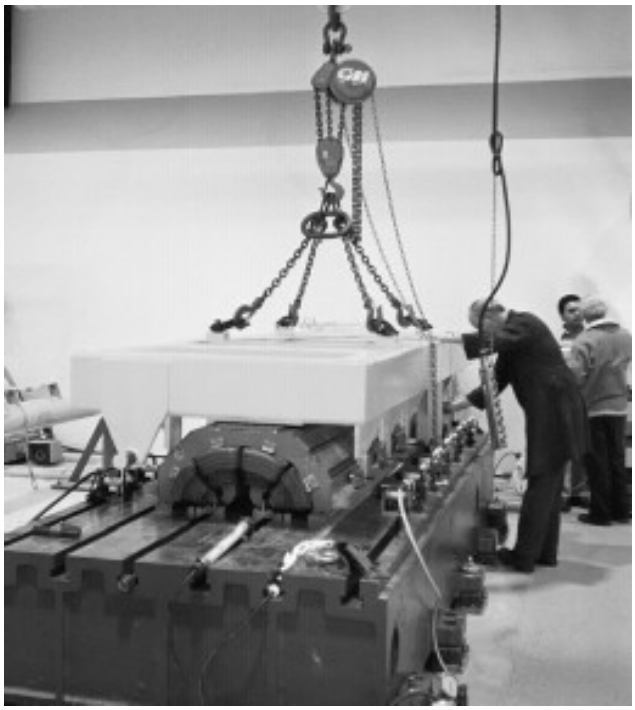

Fig. 177. Assembling the first MQW half-magnet.

When work restarts, ALSTOM has enough stacks and coils to make the first magnet. They have enough copper and steel to make the next three or four magnets. CERN has the magnet measurement bench ready to measure the first magnet when it arrives, hopefully sometime in February, 2001. The MQW half-magnet is shown in Figs. 176 and 177.

KICKER MAGNETS

In collaboration with CERN, TRIUMF is designing, building and testing 6 resonant charging power supplies (RCPS), 9 pulse forming networks (PFN), and 20 thyratron switch tanks which will operate at 66 kV. A CERN LHC injection kicker system will consist of one RCPS, two 5 Ω PFNs, four thyratron switch tanks and two kicker magnets. Four such systems plus

spares are required. The prototype RCPS that was designed and built at TRIUMF and shipped to CERN in June, 1998 was extensively tested for over 1 million cycles during 1998 and 1999, in conjunction with the prototype 60 kV, 25 cell PFN which was designed by CERN/TRIUMF and built at CERN. Some design weaknesses were discovered and improvements were incorporated in the design of the final versions of the RCPS and the PFN.

Lab space

Lab space was organized to prepare for testing of 5 RCPSs, and assembly and testing of PFNs and thyratron switch tanks. One section of the kicker lab was enclosed and reorganized for high voltage testing of RCPSs and PFNs. Adjacent to the high voltage test area, the RF group clean lab was removed and a 5 ton bridge crane was installed by Kaverit Crane. The bridge crane structure now houses a clean room which is being used to assemble the PFNs, and in the future to assemble thyratron switch tanks.

RCPS

An RCPS has two parallel outputs, to charge two 5 Ω PFNs to 66 kV. The RCPS has a 2.6 mF storage capacitor bank charged to 3 kV. A thyristor is used to switch the energy on the capacitor bank onto the primary of a 1:23 step-up transformer of low leakage inductance. The output of the secondary is transferred to two 5 Ω PFNs through two coaxial cables, two diode stacks and two 70 Ω resistors. The RCPS is designed so that the PFNs can be charged up to 66 kV in less than 1 ms at a repetition rate of 0.2 Hz.

The TRIUMF Kicker group has now completed series production of 5 RCPSs, which incorporate several improvements over the prototype RCPS. The two dummy loads that were used for prototype PFN testing were returned to TRIUMF. The dummy loads were dismantled, cleaned and reassembled with new ceramic insulators, new charging resistors and new discharge resistors. While turning up the voltage on RCPS #4, one of the dummy load capacitors from NCL failed to an open circuit at only 51 kV. This capacitor had experienced more than 1 million shots at 60 kV at CERN. Four new 1.1 μF, 66 kV capacitors were ordered from ZEZ Silko (Czech Republic), and are due to be delivered at the start of February, 2001. Testing of the RCPS will proceed as soon as the dummy load capacitors are installed.

PFN

Each 5 Ω PFN is comprised of two parallel 10 Ω lumped element delay lines consisting of 4.3 m long precision wound coils, high voltage and high current capacitors, and damping resistors. There is a thyratron switch tank at each end of the 5 Ω PFN. In order to increase the duration of flat-top field from 6.8 μs to 7.8 μs, it was necessary to increase the number of cells of the PFN from 25 to 28.

The complete set of PFN drawings was ready for review by the end of January. An engineering design committee reviewed the manufacturing procedures for the PFN tanks and lifting devices. Major contracts have been awarded as follows:

- ZEZ Silko for 650 pieces of 66 kV capacitors. Based on their experience, ZEZ Silko was able to supply 560 type 1 capacitors in 12 batches. The nominal capacitance value is 19 nF with a variation of approximately ±0.6% per batch. All the capacitors passed their factory tests and have been delivered to TRIUMF.
- HVR Advanced Power Components for 620 pieces of tubular damping resistors and 180 resistor disks for the end cells. All of these resistors have been received. All resistor values and their temperatures were measured and stored in an Excel file.
- Permali for 18 pieces of 5 m long fibreglass tubes for coil formers.
- Talvan Machine Shop (BC) for machining fibreglass tubes and winding 18 precision coils with copper tubing. Talvan also machined the PFN assembly stands and soldered more than 500 resistor connectors. All of the stands and resistor connectors and 4 of the coils were received by year-end.
- Sunrise Engineering (BC) for 9 sets of 28 cell capacitor tables and coaxial capacitor housings – one set has been received.
- Sicom (BC) for the CNC machining of internal PFN parts. 90% of these parts have been received.
- Brandt Industries (Saskatchewan) for the 9 PFN tanks and 2 sets of lifting beams. 3 tanks and 1 set of lifting beams have been received.
- Axton (BC) for the omega shields. These are expected in January, 2001.

The first 28 cell PFN (Fig. 178) has progressed as follows:

- One left hand and one right hand coil have been filled with NCL epoxy. The capacitor tables were aligned and installed on the tall assembly stands above the PFN tank.
- Selected capacitors were installed in the housings to give the correct capacitance grading and precision for the pair of 10 Ω PFN lines.
- The main switch (MS) and dump switch (DS) end-housings, resistors and capacitors were installed.

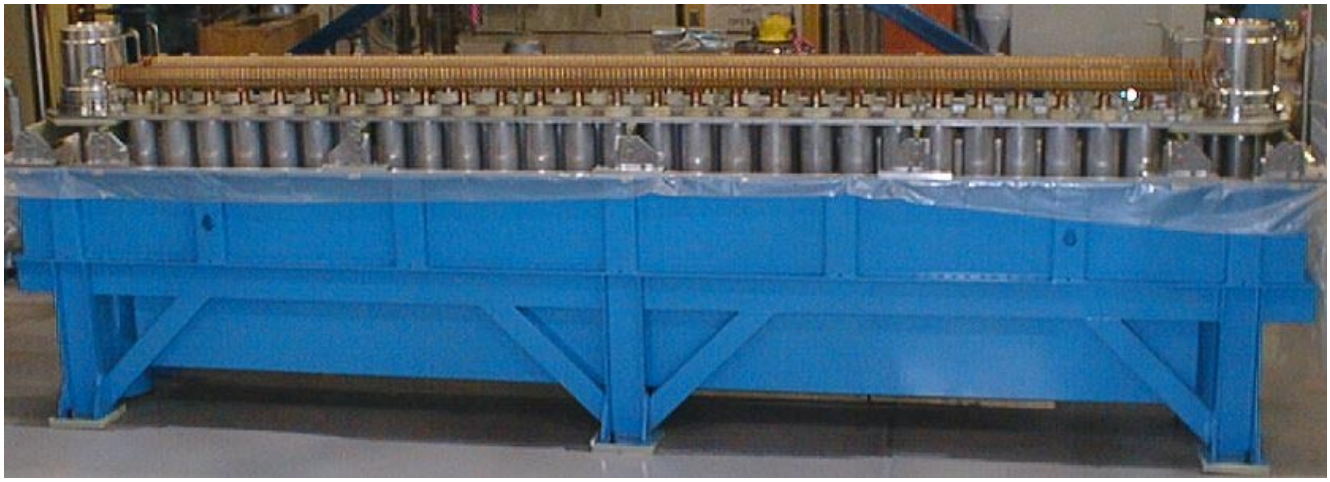

Fig. 178. The first 28 cell PFN.

- The RH and LH coils were installed.
- A test switch from CERN permits testing the PFN at low voltages. The PFN was tested at low voltage without damping resistors and without the omega shield present.

Thyratron switch tanks

The thyratron switch tanks will mount on the ends of the PFN tanks. The main switch (MS) thyratron will be connected to a 5 Ω transmission line kicker magnet, via 10 parallel 50 Ω coaxial cables, and the kicker magnet output is connected to a 5 Ω resistive terminator. The dump switch (DS) thyratron will also be connected to a 5 Ω resistive terminator.

The TRIUMF Kicker group designed a prototype HV grid/heater/reservoir bias circuit for the thyratrons. The electrical design was more or less fixed by CERN, although modern components needed to be specified. Two complete circuit boards, each consisting of four prototype transformers, were shipped to CERN in early September. CERN has requested that the bias supply circuit board be reduced in size to increase the clearance from the (floating) Faraday box to ground planes, and has agreed to allow the use of physically smaller capacitors, in place of four mechanically large Bosch capacitors.

The drawings for the thyratron switch tanks have been received from CERN. The final mechanical design of the 20 thyratron switch systems has been started.

TECHNOLOGY TRANSFER DIVISION

INTRODUCTION

Technology Transfer is the TRIUMF division responsible for the commercial interactions for the laboratory. It is composed of a small group dedicated to ongoing technology transfer, plus the Applied Technology group that is responsible for the operations of the on-site commercial cyclotrons on behalf of MDS Nordion.

TECHNOLOGY TRANSFER

The mandate of the Division is the pursuit of all financially and technically viable opportunities for commercializing the technologies evolving from research at TRIUMF, in any appropriate manner that will enhance the Canadian economy.

The current Contribution Agreement between the National Research Council (NRC) and TRIUMF includes the requirements for TRIUMF to enhance its impact on the economies of western Canada. Specifically, there is an emphasis on providing benefits to small and medium-sized businesses in the western provinces, both through the TRIUMF purchasing practices, and through the transfer of technical knowledge and skills.

TRIUMF's strength lies in the unique aspects of the facilities, combined with the scientific excellence of the staff and the research conducted here. The Division has established a network of contacts with many commercialization offices and facilities throughout North America and the world, and constantly utilizes those contacts in its own activities. The division is also responsible for patent protection at TRIUMF, but it must be noted that although it can be important in identifying a novel technology, at this level of scientific discovery, merely patenting cannot be relied on as a long-term shield from competitive alternatives.

New technology such as that emanating from TRIUMF is, by definition, a high-risk venture. Although projects may appear to have promising potential, from experience it can be predicted that not all of them will actually fulfill expectations. The Division always takes a conservative approach in projecting current opportunities into future commercial activities.

APPLIED TECHNOLOGY GROUP

500 MeV Isotope Production Facility

During this year, the 500 MeV irradiation facility received 287.6 mAh. Four targets were irradiated and delivered to produce ^{82}Sr/^{82}Rb for MDS Nordion.

CP42 Facility

The total beam delivery for 2000 was 665 mAh. The weekly beam delivery graph is shown in Fig. 179, the quarterly time evolution of the beam delivery is shown in Fig. 180. The downtime and maintenance statistics are analyzed in Fig. 181 and compared with the TR30.

In September, the lower main magnet coil of the CP42 failed and had to be replaced. The repair, which required the whole cyclotron to be dismantled, caused a downtime of approximately two months.

Work is proceeding on the upgrade to the CP42 control system and the power supplies.

TR30 Facility

The total beam delivery for 2000 was 2905 mAh. The weekly beam delivery graph is shown in Fig. 182, the quarterly time evolution of the beam delivery is displayed in Fig. 180. Maintenance and downtime statistics are presented in Fig. 181 and compared to the CP42. 80% of the downtime was due to rf problems and conditioning as well as failures of the north and south solid target stations (1281 hours total).

ATG Development Projects

During 2000, ATG made extensive improvements to the design of the solid target units including further development of the dynamic braking system and the pneumatic transfer system.

The insertion of a dedicated tuning loop into the TR30 rf amplifier led to an increased stability of the system and helped reduce conditioning time. As part of the TR30 Reliability Upgrade Project, an additional quadrupole magnet was installed on the 1B beam line to reduce beam spills on the target station and to permit higher beam currents for radioisotope production.

RADIOISOTOPE PROCESSING (MDS NORDION)

During the year 2000, MDS Nordion shipped large quantities of short-lived medical isotopes produced using the TR30 and CP42 cyclotrons. The main radioisotopes produced and shipped were iodine-123 used in thyroid imaging and research, palladium-103 used in prostate brachytherapy and thallium-201 used in cardiac imaging.

The TRIUMF 500 MeV cyclotron was used to produce large-scale batches of strontium-82 whose daughter product, rubidium-82, is used in PET studies for imaging the heart blood flow. As well, work continued on the development of new isotopes and applications in cooperation with TRIUMF.

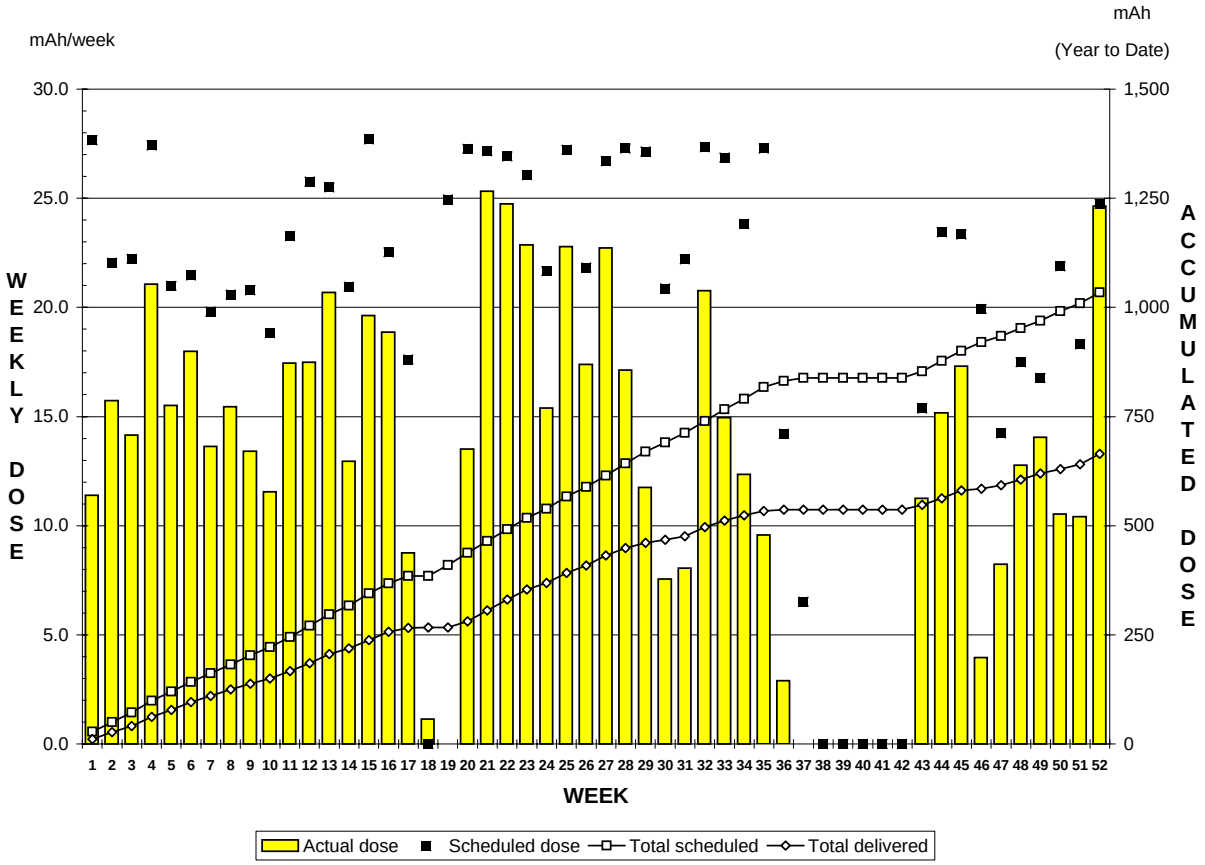

Fig. 179. Weekly beam delivery for the CP42.

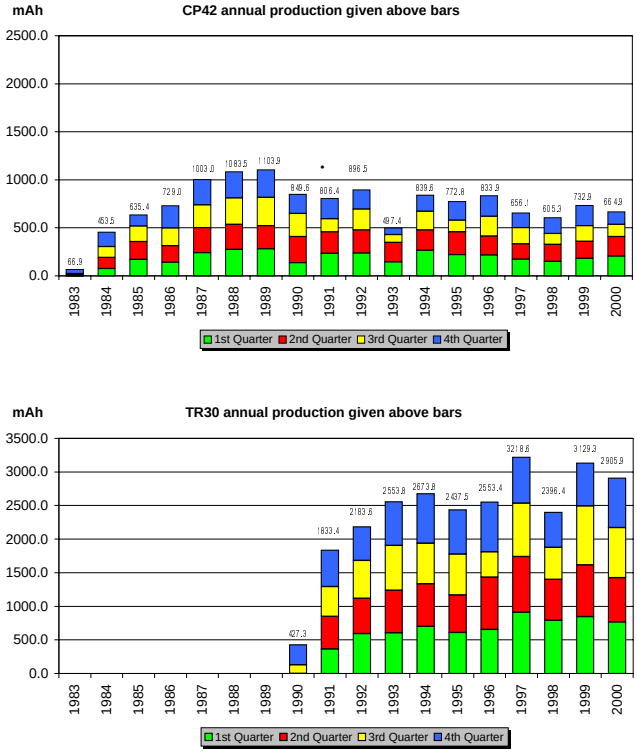

Fig. 180. Annual time evolution of the beam delivery for the CP42 (top) and the TR30 (bottom).

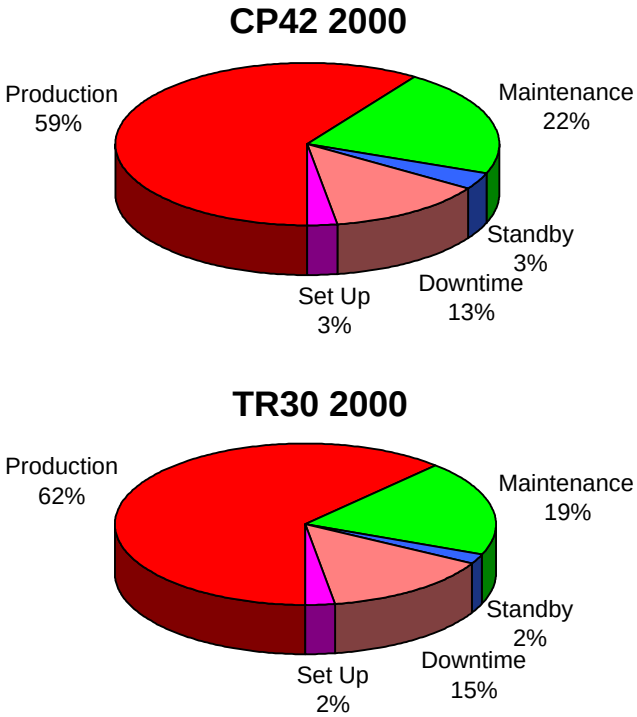

Fig. 181. Breakdown of downtime and maintenance for the CP42 (top) and the TR30 (bottom) during operational hours.

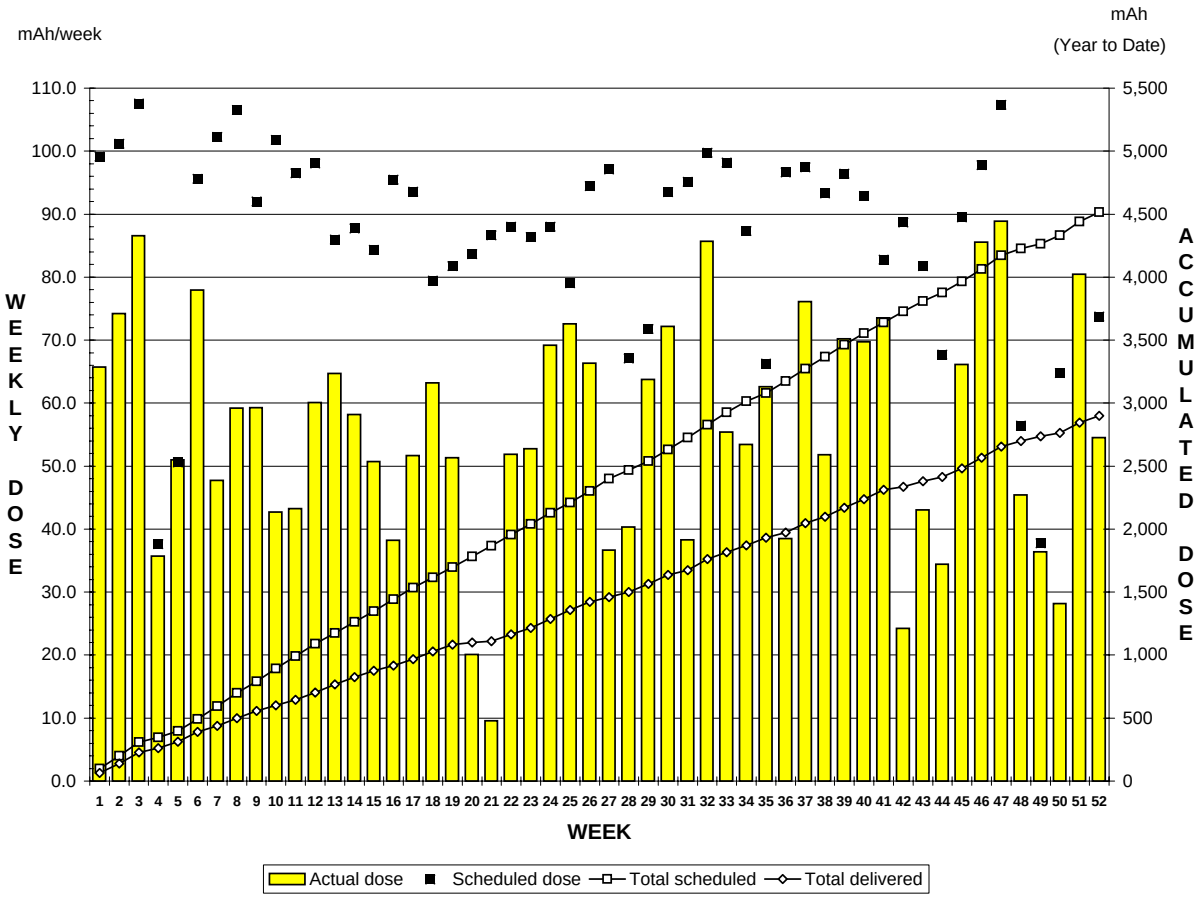

Fig. 182. Weekly beam delivery for the TR30.

ADMINISTRATION DIVISION

INTRODUCTION

The Administration Division is made up of Human Resources and Administration, Accounting and Materials Control, Administrative Computing, and Safety. The manager of each group reports to the Director. A summary of Division activities in included in this report.

HUMAN RESOURCES AND ADMINISTRATION

Another year of Performance Planning and Review was completed, whereby all employee performance was evaluated and measured site wide. A number of Personnel Policies and Procedures, applicable to all employee groups, were approved by the TRIUMF Board of Management for implementation.

The insurance program was renewed with no increase in premium from the previous year and third party liability coverage remains at $50 M. All buildings operated by TRIUMF are owned by the University of British Columbia and insurance coverage for these buildings and contents is provided by the Canadian Universities Reciprocal Insurance Exchange (CURIE).

Carleton University became a full member of the Joint Venture. The Joint Venture Agreement was modified to reflect the inclusion of Carleton, and each member university now has two voting members on the Board of Management. Two additional voting members are appointed by the Board from the private sector. The associate members each retain one non-voting member on the Board.

A review of the system for keeping track of both short term and long term visitors was initiated and the revised system will be implemented during 2001. All visitors will be recorded in a database which will keep track of data such as their home institution, length of stay, contact person at TRIUMF, radiation badge, and keys issued.

Site security is being reviewed, and it is expected that motion detectors with cameras will be installed by the end of 2001. An ID card system for access behind the security fence is also being considered.

Negotiations with UBC for the construction of the ISAC-II building began, and approval was received from the UBC Board of Governors to proceed with this project. Construction of the building is expected to commence in the spring of 2001.

OPERATIONAL SAFETY

AECB/CNSC Licensing

In May the Canadian Nuclear Safety Act came into force. This act retired the Atomic Energy Control Board (AECB) and created a new agency called the Canadian Nuclear Safety Commission (CNSC). The Commission put into effect a new set of regulations that had been under discussion for a number of years. The new regulations codify many of the practices that the AECB had instituted over the years and also brought the dose limits in line with the recommendations of the International Commission on Radiological Protection (ICRP 60).

As a consequence, the operating licences granted by the AECB will no longer be valid and TRIUMF has had to apply to the CNSC for new licences. Licence applications were prepared for both the TRIUMF facility and ISAC, and were submitted by late October. These submissions included completely revised Safety Reports for both facilities. The ISAC licence submission included an upgrade to bombard the ISAC production targets with proton beam currents of up to 100 μA and also to operate the ion beam accelerator system. No formal reply to these requests had been received from the CNSC by the end of the year.

Training

Because of the increasing demand for training in all areas of safety as well as operational procedures, TRIUMF hired a training coordinator within the Safety Department. The first task was to bring the Radiation Safety Training in line with the CNSC guidelines. These require a systematic approach to training (SAT) that proceeds from an analysis of the training needs and the setting of training objectives, to a program design stage. Finally, it requires that there be an evaluation to see whether the objectives have been met. The process was well under way by the end of the year and the new Radiation Safety training program should be ready for implementation in the spring of 2001.

Occupational Health and Safety also organized a number of training sessions this year. Table XXXI lists the training modules and the number of people who successfully completed the training.

Table XXXI. Occupational Health and Safety training.

Module	No. Trained
Asbestos Awareness and Abatement	5
Fire Extinguisher Use	25
Level I First Aid	10
Level II First Aid	3
Powder Actuated Tools Certification	16
Lock-Out Procedures	10

Occupational Health and Safety

New fire wardens were appointed in preparation for the Vancouver Fire Department (VFD) inspections which now include two scheduled fire drills per year. TRIUMF scored high in fire safety awareness during the most recent fire drill witnessed by the VFD. The Workers' Compensation Board of B.C. made two unannounced visits to the TRIUMF site this year. They issued a total of five orders, all of which have been satisfied. Mike Adam retired as chair of the TRIUMF Accident Prevention Committee (TAPC) after many years of service. The TAPC now has a number of new faces and an additional member at large to help maintain a quorum at the monthly meetings.

Interlocks and Monitoring

ISAC continued to occupy much of the time of the Safety Systems group. In addition, the effort to upgrade the reliability of systems that protect against the prompt radiation hazard continued. These systems were scrutinized by CNSC staff and by an expert panel assembled by the CNSC. In response to their findings the neutron monitoring system, which is entirely independent from the beam loss monitoring system, was upgraded so as to shut off the 500 MeV cyclotron whenever levels greater than 1 mSv h^{-1} are detected outside the shielding. With the implementation of this function the beam shut-off systems can now achieve the required reliability.

Much progress was achieved in improving the quality assurance and change control for the design, construction and maintenance of the TRIUMF safety systems.

Personnel Dosimetry

The collective dose for TRIUMF personnel for the year 2000 was 338 mSv as measured by the direct reading dosimeter service. This dose is approximately 10% higher than the previous year and likely reflects the influence of the start of operation of the ISAC facility with significant proton beam currents. Table XXXII shows the breakdown of the collective dose by various work groups.

Table XXXII. Collective dose for TRIUMF personnel by group.

Group	Dose (mSv)	Fraction of Total (%)	Median (mSv)
Applied Technology	115.0	34.5	7.0
Life Sciences	33.5	10.0	0.8
Remote Handling	24.4	7.3	1.8
500 MeV Operations	17.7	5.3	1.0
Safety Group	17.5	5.2	0.5
Vacuum Group	15.1	4.5	1.7
Plant Group	13.8	4.1	0.3
ISAC Operations	11.8	3.5	1.0
Tech Support	11.7	3.5	1.6
Beam Lines/Probes	11.5	3.4	0.7
Outside Contractors	10.7	3.2	0.2
RF Group	5.1	1.5	0.1
ISIS	4.3	1.3	0.2
Others	42.6	12.8	-.-
Total	333.7	100.0	0.3

ADMINISTRATION COMPUTING

Data Processing

The year 2000 started, of course, with the "Y2K event". As at most computing facilities, this ended up being a non-event, since no significant (and very few insignificant) problems arose as a result of dates changing year from 1999 to 2000. The smoothness of the transition was a result of the hardware and software review that had been completed in 1998. It is important to note that many software changes were made during that review; had this not been done, many significant problems would have occurred.

New development in data processing was concentrated in two areas: human resources and Web serving. The review and redesign of the HR database and applications, started in 1999, was delayed in order to accommodate an HR requirement to change employee vacation calculations from employee anniversary years to calendar years. The overall HR review and redesign will continue in 2001.

The administration Web server was also enhanced significantly during the year. The largest amount of new document "content" was provided by the HR department. New Web server capabilities were implemented towards the end of the year, including a site search tool and the ability for users to log in to the server to obtain customized personal information as well as internal-only documents. The site document repository was greatly enlarged, to become a centralized electronic source for forms from many TRIUMF departments.

Word Processing

Word processing systems saw only incremental changes in 2000. Towards the end of the year, a small number of users moved to the Windows 2000 platform. It is expected that most word processing system users will be migrated to that platform in 2001.

Telephones

Year 2000 was an extremely uneventful one for the site telephone system. This was most welcome after 1999, which included a number of severe and lengthy outages. This change in system reliability appears to confirm the assumption made in 1999 that most problems in prior years were caused by improper line voltage, and not by hardware, software, or maintenance problems.

The central switch continued to operate at or near full capacity for the entire year. Towards the end of the year, orders were placed to enlarge the switch, and to update it to a current software release level, with the installation date being early in 2001.

CONFERENCES, WORKSHOPS AND MEETINGS

MUON SOURCE MINI-WORKSHOP

On March 24–25, TRIUMF was host to a workshop with about 40 invited participants, organized jointly by TRIUMF (D. Bryman) and KEK (Y. Kuno), to discuss various aspects of future intense sources of muons. Its principal motivation was to investigate the creation of ultra-high intensity (10^{11} – 10^{12} s^{-1}) cooled muon beams for lepton flavour violation (LFV) experiments such as $\mu \rightarrow e\gamma$ and $\mu \rightarrow e$ conversion, as well as other applications.

About a dozen presentations outlined various aspects of the techniques and technologies that will be required to collect copious muons from pion decay, cool, and eventually accelerate them. One focus of these discussions was a scheme called PRISM (phase rotation intense slow muons) which uses the rf structure in a fixed field alternating gradient (FFAG) synchrotron to cool a muon beam injected with a large momentum acceptance to a narrow ∼1 MeV energy spread. Among the topics discussed were pion production and proton drivers, targetry, muon capture solenoids, injection and dispersion matching, as well as aspects of the rf systems involved. Several design and prototype studies ongoing at KEK were described.

To complement these sessions, a number of presentations were made and discussions were held relating to the physics possibilities. There were talks on the LFV experiments as well as on the prospects to exploit these facilities for μSR studies.

An important goal of the workshop was met in identifying several key issues for research and development and in exploring the possibilities for collaboration, particularly between TRIUMF and KEK.

ASTBURY SYMPOSIUM

A reception and a symposium to mark the occasion of TRIUMF Director Alan Astbury's 65th birthday were held on April 15 and 16. The Vancouver Maritime Museum was the venue for a reception, attended by 150 friends and colleagues, while the scientific symposium at TRIUMF attracted 120 physicists who listened to speakers covering the many achievements of Dr. Astbury, most notably the discovery of the massive Z and W particles, and also the promising avenues for future advancements of the science he loves.

The speakers included two Nobel prize laureates, R. Taylor (SLAC) and C. Rubbia (CERN), former colleagues J. Deutsch (Louvain la Neuve) and W. Scott (RAL), University of Victoria faculty colleagues R. Keeler, M. Lefebvre and R. Sobie, and TRIUMF scientists R. Kiefl and J.-M. Poutissou. Dr. W.J. Macdonald (University of Alberta) gave the TRIUMF Board of Management greetings and read some of the numerous telegrams received on this occasion.

The most gracious Vancouver weather set the tone for a joyful celebration of a most productive career.

SUMMER NUCLEAR INSTITUTE AT TRIUMF

The 2000 Summer Nuclear Institute at TRIUMF was held July 10–21. The general theme of the Institute was Experimental Techniques at ISAC and the specific topics were chosen following a poll of the growing number of graduate students associated with this facility. The lecturers and their subjects are given below:

- G. Savard, Argonne National Lab, *Gross Properties of Nuclei and their Determination*
- L. Buchmann, TRIUMF, *Low Energy Nuclear Scattering*
- A. Shotter, University of Edinburgh, *Nuclear Astrophysics Studies with Radioactive Ion Beams*
- J. Wood, Georgia Tech., *Gamma-Ray Spectroscopy and Nuclear Structure*
- K. Krane, Oregon State University, *Angular Distributions and Correlations*
- R. Baartman, TRIUMF, *The Mechanics of Particle Beam Transport*

As in previous years, the general format involved three lectures each morning with an informal problem solving and discussion session in the afternoon. There were 19 registrants including 6 undergraduate students working at ISAC. The Institute was organized by J.-M. Poutissou, K.P. Jackson and G.C. Ball.

FOURTH INTERNATIONAL SYMPOSIUM ON RADIOHALOGENS (4ISR)

The Fourth International Symposium on Radiohalogens (4ISR) was held September 9–13 at Whistler.

Radiohalogens are unique among the radioactive elements of interest to diagnostic and therapeutic nuclear medicine because of their broad range of chemical, biological and nuclear properties. The radiochemistry of ^{18}F has been tamed so that radiofluorination of metabolic substrates is almost routine, and ^{18}F-labelled products are readily available for on-site "molecular" positron emission tomography (PET). The radioiodines in mainstream medical use include ^{125}I and ^{131}I, the traditional workhorses of biochemistry and radiotherapy, respectively. ^{123}I is commonly used for single photon emission tomography (SPET) imaging, while ^{124}I is the most recent addition to the list of PET radionuclides. Speakers at this symposium focused primarily on these five radionuclides,

but also addressed radiobromines (^{74m,75,76,77}Br) and the most esoteric radiohalogen, astatine (^{211}At). Radionuclide production, radio-organic chemistry, medical applications, and commercialization of these radionuclides were discussed.

An ad hoc committee from within the radiopharmaceutical and radiochemical communities again organized the fourth in a series of radiohalogen symposia. As in earlier meetings, this year's committee, which comprised Drs. M. Adam (University of British Columbia), S. Wilbur (University of Washington, Seattle), H. Coenen (Forschungszentrum Jülich) and B. Abeysekera (Nordion International Inc.), created a program that was more of a workshop than a symposium. Invited speakers presented papers to a specialist audience. The small number of papers and the absence of a poster session ensured extensive dialogue and animated discussion throughout the meeting. The program included reviews on radiohalogen production, chemistry and special applications of the radiohalogens including ^{18}F, radioiodines, radiobromines, and ^{211}At. Approximately 130 scientists from North America, Europe and Asia participated.

S.M. Qaim (Forschungszentrum Jülich) opened the proceedings with a review of radiohalogen production. Production of radiohalogens such as ^{123}I, ^{124}I, ^{120g}I, ^{18}F, ^{76}Br, ^{77}Br were discussed in this session.

M. Kilbourn (University of Michigan) reviewed developments in radiofluorination chemistry from the early electrophilic reactions to the predominantly nucleophilic reactions now in use.

B. Mazière (CAE, Paris) reviewed the radiobromines and dismissed all, including ^{77,82}Br but with the exception of ^{74m,75,76}Br ($t_{\frac{1}{2}}$ = 0.7, 1.6 and 16.2 h, respectively), as useful for imaging. These positron emitters have been incorporated into nucleosides, nucleotides, monoclonal antibodies and receptor ligands, especially for study of the dopaminergic system.

Evidence of a role for boron intermediates in radiohalogen chemistry was presented by G. Kabalka (University of Tennessee Medical Center). Advantages of these compounds include low toxicity and applicability to compounds that have a broad range of functional groups.

H. Kung (University of Pennsylvania) reported the synthesis of ^{123}I-labelled CNS receptors, with emphasis on destannylation radioiodination of aryl- and vinyl-tributylstannyl precursors, for dopamine receptor imaging.

The generation and biological effectiveness of Auger electrons associated with ^{123,125}I decay were explained by A. Kassis (Harvard Medical School). Situating these atoms directly on, or inserting them into, the nucleic acid chain (e.g., via IUdR) will produce an average of one DNA double-strand break per decay event (21 Auger electrons per decay), resulting in an 8-fold increase in radiotoxicity compared to ^{131}I.

Y. Arano (Chiba University, Japan) presented the only paper on radioiodination of monoclonal antibodies and peptides. This work concentrated on the development of hydrolyzable linkers between the protein and the labelled (^{99m}Tc or ^{125}I) synthons.

R. Counsell (University of Michigan) evaluated a number of iodophenyl-phospholipid ethers as potential tumour imaging agents based on the rationale that tumours exhibit elevated phospholipids. Studies of human tumours in SCID mice that have validated structure-activity models form the basis for phase I studies.

S. Wilbur and D. Hamlin (University of Washington, Seattle) described the applications of ^{211}At in open source radiotherapy. Dr Wilbur reviewed At chemistry and production (there are no stable or long-lived nuclides; ^{209,210,211}At have $t_{\frac{1}{2}}$ values of 5.4, 8.3 and 7.2 h, respectively), and concentrated on ^{211}At which, through a branched decay chain, is essentially a 100% α-emitter.

Of the application themes presented, nucleoside-based radiopharmaceuticals spanned the full range of radiohalogens. L. Wiebe (University of Alberta) provided an introduction to molecular biology and gene therapy, and a review of critical elements of nucleoside and nucleotide biochemistry.

B. Abeysekera (Nordion International Inc.) and J. Lu (University of British Columbia) closed the symposium with presentations on the impact of radionuclide production (nuclear reactions, production chemistry), delivery, and end-user applications on the commercial producers.

One of the symposium highlights was the barbecue banquet on top of Whistler Mountain in the Roundhouse building, thanks in part to the generous financial support from the US DOE, MDS Nordion, Mallinckrodt, Nycomed Amersham, and the BC Information Science and Technology Agency.

ISAC LASER ION SOURCE WORKSHOP

The ISAC Laser Ion Source Workshop was held at TRIUMF from December 4–5. The main themes were:

- To explore the possibility of installation of a resonant laser ion source at ISAC.
- Determine the best technique for producing the laser light.
- Define the infrastructure required.
- Determine the resources required for the operation of such an ion source, and emphasize the new and exciting developments that are imminent in this fast growing field.

Over 30 participants from Europe, Asia and America attended the two day workshop. The meeting started with a presentation of the ISAC facility, followed by the physics to define the need for special isotopes.

One of the main problems of ion sources for on-line mass separators is to obtain a pure ion beam. The usual ion sources used on-line are the thermo-ionic or gas-discharge plasma types. The ionization process in those ion sources is not selective. Hence, the separated ion beams are contaminated by isobars. The process of resonance laser ionization of atoms is non-thermal by nature. The atoms are ionized only when the laser radiation frequency matches the element's atomic transitions. Since each element has its own energy level structure, the laser ionization process can be very selective. Furthermore, the photo-ionization of atoms is very efficient and can lead to very high yields.

Dr. Klaus Wendt gave a very nice description of his system used for trace analysis, developed at the Johannes Gutenberg-Universität, Mainz. The separation he was able to accomplish with his laser system is new, competitive with the AMS technique.

A description of the laser system developed at the Russian Academy of Sciences, Troitsk by Dr. Viatcheslav Mishin showed the usefulness of the on-line laser ionization. It is currently used at several on-line facilities: ISOLDE-CERN, Petersburg Nuclear Institute, etc. This system used powerful copper-vapour lasers that are suitable for producing the laser radiation needed for the ISAC program.

After the workshop a collaboration between TRIUMF and Troitsk was initiated.

TRIUMF USERS' GROUP ANNUAL GENERAL MEETING

The TRIUMF Users' Group Annual General Meeting was held December 6–7, sandwiched between the Materials Science and Subatomic EEC meetings. See http://www.triumf.ca/tug/agm2000 and below for details of the sessions and talks.

J.H. Brewer, the TRIUMF Users' Executive Committee chair for 2000, reported on TUEC business conducted during the year.

TUEC met with each of the candidates for the next TRIUMF Director and conveyed evaluations to the Search Committee, which subsequently considered all input and presented its recommendations to the Board of Management, which then selected Prof. Alan Shotter as the new Director.

Following a mandatory membership renewal during 2000, the TRIUMF Users' Group (TUG) had 235 reconfirmed members from 11 countries. A Web-based survey of User interests and priorities conducted in conjunction with the mandatory membership renewal can be viewed in Appendix C and at http://www.triumf.ca/tug/new/tugstats.php .

TUEC selected two members to represent the Users on the TRIUMF Operating Committee: J. Vincent (TRIUMF) and E. Mathie (U. Regina) with alternates G.M. Marshall (TRIUMF) and G.M. Luke (McMaster U.), respectively. G.M. Marshall replaced J. Vincent in mid-2000 with S Yen (TRIUMF) becoming the alternate.

As a result of the annual ballot, G.M. Luke (McMaster U.) was elected as chair-elect for 2001. G.D. Morris (TRIUMF) and W.D. Ramsay (U. Manitoba) were elected as members for 2001/2002.

TUEC Membership for 2000

J.H. Brewer	UBC	*Chair*
N. Rodning	U. Alberta	*Chair-elect*
J.M. D'Auria	SFU	*Past-chair*
G.M. Marshall	TRIUMF	1999/2000
B. Turrell	UBC	1999/2000
R. Helmer	TRIUMF	2000/2001
A.K. Opper	Ohio U.	2000/2001
M. Comyn	TRIUMF	*Liaison Officer*

Program of the 2000 Annual General Meeting

Wednesday, December 6

Director's Report	A. Astbury
Accelerator Technology/ CERN Collaboration	E. Blackmore
Cyclotron Division	G. Dutto
Science Division	J.-M. Poutissou
KOPIO and TRIUMF	R. Poutissou
Materials Science at ISAC	R. Kiefl
NSERC SAP 5-Year Plan	M. Vetterli

"What Comes After ISAC-II?"

Neutrino Schemes	A. Konaka
Open Discussion	
Buffet Dinner at TRIUMF	

Evening Session

NSERC SAP GSC Business	R. Keeler
TUEC Business	J. Brewer

Thursday, December 7

"What to do with ISAC-II?"

ISAC-I Progress, ISAC-II Plans	P. Schmor
Nuclear Structure with TIGRESS	C. Svensson
Studies of Nuclei at the Limits of Stability Using Recoil Separators	J. Batchelder
The HERACLES Array at ISAC-II	Y. Larochelle
Nucleosynthesis in Supernovae — What Can We Learn with ISAC-II?	B. Fulton
Open Discussion	

ORGANIZATION

Board of Management

The Board of Management of TRIUMF manages the business of the facility and has equal representation from each of the four founding universities and Carleton University which has, in 2000, become a full member. At the end of 2000 the Board comprised:

University of Alberta	Dr. W.J. McDonald	
	Dr. A. Noujaim	
University of British Columbia	Dr. I. Samarasekera	
	Dr. B. Turrell	
Carleton University	Dr. F. Hamdullahpur	
	Dr. P.J.S. Watson	
Simon Fraser University	Dr. W.S. Davidson	
	Dr. C.H.W. Jones	Chairman
University of Victoria	Dr. V. Paetkau	
	Dr. M. Taylor	

Towards the end of 1987, Board membership was expanded in anticipation of a broadening of the TRIUMF joint venture to include a more national representation of Canadian universities long associated with the TRIUMF experimental program. The University of Manitoba and Université de Montréal became associate members, and the University of Toronto joined as an observer. At the end of 1988, University of Toronto status changed from that of observer to associate member. In March, 1989 the University of Regina became an associate member. In December, 1998 Carleton University and Queen's University became associate members. In March, 2000 Carleton University's status changed from that of associate member to full member. Associate membership at year-end:

Associate members:	Dr. W.T.H. van Oers	University of Manitoba	
	M G. Michaud	Université de Montréal	
	Dr. A.B. McDonald	Queen's University	
	Dr. K. Denford	University of Regina	
	Dr. P. Sinervo	University of Toronto	
Non-voting members:	Ms. J. Verrett	National Research Council	
	Dr. P. Sinervo	ACOT/University of Toronto	
	Dr. A. Astbury	Director, TRIUMF	
	Dr. J.-M. Poutissou	Associate Director, TRIUMF	
	Mr. J. Hanlon	TRIUMF	Recording Secretary

The following changes occurred in Board membership in 2000: Drs. P. Kitching (University of Alberta), R.G. Korteling (Simon Fraser University), and Ms. G. Gabel (University of Victoria) completed their terms. Dr. I. Samarasekera replaced Drs. D. Dolphin and L. Skarsgard as University of British Columbia member. Dr. W.T.H. van Oers replaced Dr. J. Keselman as University of Manitoba member. The Board met 5 times during the year.

Administration

Under the directorship of Dr. A. Astbury, TRIUMF personnel were grouped into divisions, with division heads as follows:

Division Head, Science Division	J.-M. Poutissou
Division Head, Accelerator Technology Division	E.W. Blackmore
Division Head, Cyclotron Operations Division	G. Dutto
Division Head, Technology Transfer Division	P.L. Gardner
Division Head, ISAC	P.W. Schmor
Division Head, Administration Division	A. Astbury

Operating Committee

The TRIUMF Operating Committee is responsible for the operation of the facility. It reports to the Board of Management through its chairman, the Director, Dr. A. Astbury. The Operating Committee consists of one voting member from each of the five universities, two voting members representing the interests of the Users, and one representing TRIUMF staff. The Associate Director is a non-voting member. Members of the committee (alternate members in parentheses) at the end of 2000 were:

Dr. A. Astbury	Chairman	Director	
Dr. J.-M. Poutissou	*(ex officio)*	Associate Director	
Dr. N. Rodning		University of Alberta	(Dr. L.G. Greeniaus)
Dr. G. Oakham		Carleton University	(Dr. D. Karlen)
Dr. P. Percival		Simon Fraser University	(Dr. K.P. Jackson)
Dr. R. Keeler		University of Victoria	(Dr. M. Roney)
Dr. C. Hearty		University of British Columbia	(Dr. M.D. Hasinoff)
Dr. E. Mathie		Users	(Dr. G. Luke)
Dr. G. Marshall		Users	(Dr. S. Yen)
Mr. K. Reiniger		TRIUMF	(Mr. R. Baartman)
Mr. J. Hanlon	Recording Secretary	TRIUMF	
Ms. J. Verrett	*(ex officio)*	National Research Council	

Changes in 2000: Dr. G. Luke replaced Dr. J. Waddington as alternate for Dr. E. Mathie. Dr. G. Marshall replaced Dr. J. Vincent as one of the Users members, with Dr. S. Yen as alternate. Mr. K. Reiniger replaced Dr. T.J. Ruth as TRIUMF member, with Mr. R. Baartman as alternate. The Operating Committee met 11 times in 2000.

NRC Advisory Committee on TRIUMF

Dr. P. Sinervo	Chairman	University of Toronto
Dr. D. Santry	Secretary	National Research Council
Dr. A.J. Berlinsky		McMaster University
Dr. R. Boyd		Ohio State University
Dr. A. Fenster		J.P. Robarts Research Institute
Dr. J. Guigné		Guigné International Ltd.
Dr. P.-G. Hansen		Michigan State University
Dr. G. Kalmus		Rutherford Appleton Lab
Prof. V. Soergel		Werner-Heisenberg-Institut
Dr. R. Taylor		SLAC
Dr. P. Vincett		FairCopy Services Inc.
Dr. R. Carnegie	*(ex officio)*	Carleton University
Dr. C.H.W. Jones	*(ex officio)*	Simon Fraser University
Dr. R. Keeler	*(ex officio)*	University of Victoria

Changes in 2000: Dr. R. Keeler replaced Dr. P. Kalyniak.

Agency Committee on TRIUMF

Dr. A.J. Carty	Chairman	President, National Research Council
Dr. T. Brzustowski		President, Natural Sciences and Engineering Research Council
Ms. M. Tobin		Director General, Innovation Policy Branch, Industry Canada
Mr. M. Moffat		Director, Knowledge Infrastructure, Industry Canada
Mr. N. Lloyd		Director General, Research Grants & Scholarships, NSERC
Ms. J. Verrett	Secretary	National Research Council

Changes in 2000: Mr. K. Lynch and Ms. O. Lennie retired from the committee; Ms. M. Tobin, Mr. M. Moffat and Mr. N. Lloyd joined the committee.

TRIUMF Safety Management Committee

Dr. A. Astbury		Director, TRIUMF
Dr. J.-M. Poutissou		Associate Director/Head, Science Division
Dr. E.W. Blackmore		Head, Accelerator Technology Division
Dr. G. Dutto		Head, Cyclotron Operations Division
Mr. P.L. Gardner		Head, Technology Transfer Division
Dr. P.W. Schmor		Head, ISAC Division
Mr. M. Stenning		Head, Operations Group
Dr. M. Adam		TAPC Chairman
Mr. G. Wood		Industrial Safety Officer/TAPC
Mr. L. Moritz		Head, Environmental Health & Safety
Mr. J. Hanlon		Manager, Human Resources & Administrative Services
Dr. S. Zeisler		Head, Applied Technology Group
Mrs. K. Gildert	Recording Secretary	

Experiments Evaluation Committee

Subatomic Committee:

Dr. I.S. Towner	Chairman	Queen's University
Dr. J.-M. Poutissou	Associate Director/*(ex officio)*	TRIUMF
Dr. H. Fearing	Secretary	TRIUMF
Dr. J.M. D'Auria		TUEC Past Chairman/SFU
Dr. W.C. Haxton		University of Washington
Dr. K. Langanke		Aarhus University
Dr. H.O. Meyer		Indiana University
Dr. A. Richter		Technische Universität Darmstadt
Dr. M.C.T. Wiescher		University of Notre Dame

Materials Science Committee:

Dr. I.K. Affleck	Chairman	University of British Columbia
Dr. J.-M. Poutissou	Associate Director/*(ex officio)*	TRIUMF
Dr. P.W. Percival	Secretary/*(ex officio)*	SFU/TRIUMF
Dr. J.H. Brewer		TUEC Chairman/UBC
Dr. S.F.J. Cox		Rutherford Appleton Laboratory
Dr. B. Gaulin		McMaster University
Dr. S. Roorda		Université de Montréal
Dr. G.A. Sawatzky		University of Groningen
Dr. R.E. Wasylishen		University of Alberta

In July, 1994 the Experiments Evaluation Committee was formally split into two committees representing subatomic physics and μSR physics. In 2000 the μSR Committee changed its name to the Materials Science Committee. Changes in membership during the year: on the Subatomic Committee, Dr. I.S. Towner replaced Dr. K. Langanke as chairman and Dr. J.M. D'Auria replaced Dr. L. Buchmann as TUEC past chairman. On the Materials Science Committee, Dr. I.K. Affleck replaced Dr. M. Thewalt as chairman, Dr. J.H. Brewer joined as TUEC chairman, Dr. D.K. Bohme completed his term; the committee welcomed Drs. S.F.J. Cox and G.A. Sawatzky.

Life Sciences Project Evaluation Committee

Dr. T. Lewellen	Chairman	University of Washington
Dr. J.-M. Poutissou	Associate Director	TRIUMF
Dr. L.P. Robertson	Secretary	University of Victoria
Dr. R. Finn		Memorial Sloan-Kettering Cancer Center
Dr. D.C. Price		University of California, San Francisco
Dr. R.L. Wahl		University of Michigan
Dr. A. Fenster		J.P. Robarts Research Institute
Dr. J.E. van Lier		Université de Sherbrooke

Changes in 2000: Drs. D.A. Axen and J. Fowler completed their terms. The committee welcomed Drs. A. Fenster and J.E. van Lier.

Appendix A

PUBLICATIONS

This appendix lists publications describing work performed at TRIUMF and also work conducted elsewhere by TRIUMF personnel and TRIUMF users.

Journal Publications

Particle, Nuclear and Atomic Physics

D.E. Appelbe, R.A.E. Austin, G.C. Ball, J.A. Cameron, B. Dejerroud, T.E. Drake, S. Flibotte, C.D. O'Leary, A. Melarangi, C.E. Svensson, J.C. Waddington and D. Ward, *Gamma-ray spectroscopy of $^{57}Mn_{32}$ and $^{58}Mn_{33}$*, Eur. Phys. J. **A8**, 153 (2000).

S. Adler, M.S. Atiya, I.H. Chiang, J.S. Frank, J.S. Haggerty, T.F. Kycia, K.K. Li, L.S. Littenberg, A. Sambamurti, A. Stevens, R.C. Strand, D.S. Akerib, M. Ardibilli, M. Convery, M. Ito, D.R. Marlow, R.A. McPherson, P.D. Meyers, M.A. Selen, F.C. Shoemaker, A.J.S. Smith, E.W. Blackmore, D.A. Bryman, L. Felawka, P. Kitching, A. Konaka, V. Kujala, Y. Kuno, J.A. Macdonald, T. Nakano, T. Numao, P. Padley, J.-M. Poutissou, R. Poutissou, J. Roy and R. Soluk, *Further search for the decay $K^+ \to \pi^+\nu\overline{\nu}$*, Phys. Rev. Lett. **84**, 3768 (2000) [BNL-67142, KEK-99-171, PRINCETON-HEP-2000-1, TRI-PP-00-04, hep-ex/0002015].

S. Adler *et al.* (BNL E787 collaboration), *Measurement of structure dependent $K^+ \to \mu^+\nu_\mu\gamma$ decay*, Phys. Rev. Lett. **85**, 2256 (2000) [BNL-67217, PRINCETON-HEP-2000-2, TRI-PP-00-05, KEK-PREPRINT-99-183, hep-ex/0003019].

S. Adler *et al.* (BNL E787 collaboration), *Measurement of direct photon emission in $K^+ \to \pi^+\pi^0\gamma$ decay*, Phys. Rev. Lett. **85**, 4856 (2000) [TRI-PP-00-21, KEK-PREPRINT-2000-16, hep-ex/0007021].

G. Feldman, G.V. O'Rielly, B.L. Berman, W.J. Briscoe, R. Igarashi, N.R. Kolb, R.E. Pywell, D.M. Skopik, J.R. Calarco, N.M. Karlsson, J.C. Sanabria and W. Schadow, *Charge symmetry in the $A = 3$ system*, Bull. Am. Phys. Soc. **45**, 36 (2000).

F. Bonutti *et al.* (CHAOS collaboration), *The $\pi\pi$ interaction in nuclear matter from a study of the $\pi^+A \to \pi^+\pi^\pm A'$ reactions*, Nucl. Phys. **A677**, 213 (2000) [nucl-ex/0007017].

J.B. Lange, A. Ambardar, F. Duncan, A. Feltham, G. Hofman, R.R. Johnson, G. Jones, M.E. Sevior, D. Vetterli, J.T. Brack, D. Ottewell, K. Raywood, G.R. Smith and M. Pavan, *Determination of the $\pi^\pm p \to \pi^\pm\pi^+n$ cross section near threshold*, Phys. Rev. **C61**, 025201 (2000).

D.V. Dementev, M.P. Grigorev, A.P. Ivashkin, M.M. Khabibullin, A.N. Khotyantsev, Yu.G. Kudenko, O.V. Mineev, M. Aoki, J. Imazato, Y. Kuno, T. Baker, M. Blecher, P. Depommier, M. Hasinoff, Y. Igarashi, T. Ikeda, J.A. Macdonald, C.R. Mindas, C. Rangacharyulu, S. Shimizu and T. Yokoi, *CsI(Tl) photon detector with PIN photodiode readout for a $K_{\mu 3}$ T-violation experiment*, Nucl. Instrum. Methods **A440**, 151 (2000).

S.L. Stephenson, J.D. Bowman, F. Corvi, B.E. Crawford, P.P.J. Delheij, C.M. Frankle, M. Iinuma, J.N. Knudson, L.Y. Lowie, A. Masaike, Y. Masuda, Y. Matsuda, G.E. Mitchell, S.I. Penttila, H. Postma, N.R. Roberson, S.J. Seestrom, E.I. Sharapov, H.M. Shimizu, Y.-F. Yen, V.W. Yuan and L. Zanini, *Parity violation in neutron resonances in ^{115}In*, Phys. Rev. **C61**, 045501 (2000).

G.E. Mitchell, J.D. Bowman, B.E. Crawford, P.P.J. Delheij, C.M. Frankle, M. Iinuma, J.N. Knudson, L.Y. Lowie, A. Masaike, Y. Matsuda, S.I. Penttila, H. Postma, N.R. Roberson, S.J. Seestrom, E.I. Sharapov, S.L. Stephenson, Y.-F. Yen and V.W. Yuan, *New search for parity violation in nonresonant neutron scattering on thorium*, Phys. Rev. **C61**, 045503 (2000).

E.I. Sharapov, J.D. Bowman, B.E. Crawford, P.P.J. Delheij, C.M. Frankle, M. Iinuma, J.N. Knudson, L.Y. Lowie, J.E. Lynch, A. Masaike, Y. Matsuda, G.E. Mitchell, S.I. Penttila, H. Postma, N.R. Roberson, S.J. Seestrom, S.L. Staphenson, Y.-F. Yen and V.W. Yuan, *Parity violation in ^{232}Th neutron resonances above 250 eV*, Phys. Rev. **C61**, 025501 (2000).

B. Djerroud, B. Schaly, S. Flibotte, G.C. Ball, S. Courtin, M. Cromaz, D.S. Haslip, T. Lampman, A.O. Macchiavelli, J.M. Nieminen, C.E. Svensson, J.C. Waddington, D. Ward and J. Wilson, *Fission barriers, coupled-channel and shell effects at the Coulomb barrier in the A$\sim$190 mass region*, Phys. Rev. **C61**, 024607 (2000).

Y. Larochelle, L. Gingras, G.C. Ball, L. Beaulieu, P. Gagne, E. Hagberg, Z.Y. He, D. Horn, R. Laforest, R. Roy and C. St-Pierre, *Isospin of intermediate mass fragments produced in peripheral, midperipheral and central collisions from the $^{58}Ni + ^{12}C$, ^{24}Mg reactions at 34.5A MeV*, Phys. Rev. **C62**, 051602(R) (2000).

C.E. Svensson, A.O. Macchiavelli, A. Juodagalvis, A. Poves, I. Ragnarsson, A. Aberg, D.E. Appelbe, R.A.E. Austin, C. Baktash, G.C. Ball, M.P. Carpenter, E. Caurier, R.M. Clark, M. Cromaz, M.A. Deleplanque, R.M. Diamond, P. Fallon, M. Furlotti, A. Galindo-Uribarri, R.V.F. Janssens, G.J. Lane, I.Y. Lee, M. Lipoglavsek, F. Nowacki, S.D. Paul, D.C. Radford, D.G. Sarantites, D. Seweryniak, F.S. Stephens, V. Tomov, K. Vetter, D. Ward and C.H. Yu, *Superdeformation in the $N = Z$ nucleus ^{36}Ar: experimental, deformed mean field and spherical shell model descriptions*, Phys. Rev. Lett. **85**, 2693 (2000).

Zhi-Yong He, L. Gingras, Y. Larochelle, D. Ouerdane, L. Beaulieu, P. Gagne, Xing Qian, R. Roy, C. St-Pierre, G.C. Ball and D. Horn, *Fragment emission time from well defined sources in $^{58}Ni + ^{197}Au$ at 34.5 MeV/nucleon*, Phys. Rev. **C63**, 011601(R) (2000).

M.C. Fujiwara *et al.* (TRIUMF Muonic Hydrogen collaboration), *Resonant formation of dμt molecules in deuterium: an atomic beam measurement of muon catalyzed dt fusion*, Phys. Rev. Lett. **85**, 1642 (2000) [TRI-PP-00-24, nucl-ex/0008002].

Y.-H. Shin *et al.* (KEK PS E246 collaboration), *A kinematically complete measurement of $K^+ \to \pi^+\pi^0\pi^0$ decays*, Eur. Phys. J. **C12**, 627 (2000).

S. Shimizu *et al.* (KEK E246 collaboration), *Test of exotic scalar and tensor couplings in $K^+ \to \pi^0 e^+ \nu$ decay*, Phys. Lett. **B495**, 33 (2000) [EXP KEK-246].

K. Yamamoto *et al.* (E885 collaboration), *Search for double-Λ hypernuclei and the H-dibaryon in the (K^-, K^+) reaction on ^{12}C*, Phys. Lett. **B478**, 401 (2000).

P. Khaustov *et al.* (AGS E885 collaboration), *Evidence of Ξ hypernuclear production in the $^{12}C(K^-, K^+)^{12}_{\Xi}Be$ reaction*, Phys. Rev. **C61**, 054603 (2000) [nucl-ex/9912007].

P. Khaustov *et al.* (AGS E885 collaboration), *Search for double-Λ hypernuclei formation via $(\Xi^-, ^{12}C)_{atom} \to ^{12}_{\Lambda\Lambda}B + n$*, Phys. Rev. **C61**, 027601 (2000).

A. Airapetian *et al.* (HERMES collaboration), *Measurement of the spin asymmetry in the photoproduction of pairs of high-p_T hadrons at HERMES*, Phys. Rev. Lett. **84**, 2584 (2000) [DESY-99-071, hep-ex/9907020].

A. Airapetian *et al.* (HERMES collaboration), *Observation of a single spin azimuthal asymmetry in semi inclusive pion electro production*, Phys. Rev. Lett. **B84**, 4047 (2000) [DESY-99-149, hep-ex/9910062].

K. Ackerstaff *et al.* (HERMES collaboration), *Nuclear effects on $R = \sigma_L/\sigma_T$ in deep inelastic scattering*, Phys. Lett. **B475**, 386 (2000) [DESY-99-150, hep-ex/9910071].

K. Ackerstaff *et al.* (HERMES collaboration), *Measurement of angular distributions and $R = \sigma_L/\sigma_T$ in diffractive electroproduction of ρ^0 mesons*, Eur. Phys. J. **C18**, 303 (2000) [DESY-99-199, hep-ex/0002016].

A. Airapetian *et al.* (HERMES collaboration), *Exclusive leptoproduction of ρ^0 mesons from hydrogen at intermediate virtual photon energies*, Eur. Phys. J. **C17**, 389 (2000) [DESY-00-058, hep-ex/0004023].

A. Airapetian *et al.* (HERMES collaboration), *The Q^2 dependence of the generalized Gerasimov-Drell-Hearn integral for the proton*, Phys. Lett. **B494**, 1 (2000) [DESY-00-096, hep-ex/0008037].

G. Abbiendi *et al.* (OPAL collaboration), *A study of parton fragmentation in hadronic Z^0 decays using $\Lambda\bar{\Lambda}$ correlations*, Phys. Lett. **C13**, 185 (2000) [CERN-EP-98-114].

G. Abbiendi *et al.* (OPAL collaboration), *Search for acoplanar lepton pair events in e^+e^- collisions at $\sqrt{s}$ = 161 GeV, 172 GeV and 183 GeV*, Eur. Phys. J. **C12**, 551 (2000) [CERN-EP-98-122].

G. Abbiendi *et al.* (OPAL collaboration), *Measurement of the B^+ and B^0 lifetimes and search for CP(T) violation using reconstructed secondary vertices*, Eur. Phys. J. **C12**, 609 (2000) [CERN-EP-98-195].

G. Abbiendi *et al.* (OPAL collaboration), *Search for R-parity violating decays of scalar fermions at LEP*, Eur. Phys. J. **C12**, 1 (2000) [CERN-EP-99-043, hep-ex/9904015].

G. Abbiendi *et al.* (OPAL collaboration), *Total hadronic cross section of photon-photon interactions at LEP*, Eur. Phys. J. **C14**, 199 (2000) [CERN-EP-99-076, hep-ex/9906039].

G. Abbiendi *et al.* (OPAL collaboration), *Measurement of inclusive semileptonic branching fractions of B hadrons in Z^0 decays*, Eur. Phys. J. **C13**, 225 (2000) [CERN-EP-99-078, hep-ex/9906041].

G. Abbiendi *et al.* (OPAL collaboration), *A study of spin alignment of $\rho(770)^{\pm}$ and $\omega(782)$ mesons in hadronic Z^0 decays*, Eur. Phys. J. **C16**, 61 (2000) [CERN-EP-99-082, hep-ex/9906043].

G. Abbiendi *et al.* (OPAL collaboration), *Measurement of the production rate of charm quark pairs from gluons in hadronic Z^0 decays*, Eur. Phys. J. **C13**, 1 (2000) [CERN-EP-99-089, hep-ex/9908001].

G. Abbiendi *et al.* (OPAL collaboration), *Search for pair produced leptoquarks in e^+e^- interactions at $\sqrt{s} \approx 189$ GeV*, Eur. Phys. J. **C13**, 15 (2000) [CERN-EP-99-091, hep-ex/9908007].

G. Abbiendi *et al.* (OPAL collaboration), *A study of three prong τ decays with charged kaons*, Eur. Phys. J. **C13**, 197 (2000) [CERN-EP-99-095, hep-ex/9908013].

G. Abbiendi *et al.* (OPAL collaboration), *Search for neutral Higgs bosons in e^+e^- collisions at $\sqrt{s} \approx 189$ GeV*, Eur. Phys. J. **C12**, 567 (2000) [CERN-EP-99-096, hep-ex/9908002].

G. Abbiendi *et al.* (OPAL collaboration), *Tests of the standard model and constraints on new physics from measurements of fermion pair production at 189 GeV at LEP*, Eur. Phys. J. **C13**, 553 (2000) [CERN-EP-99-097, hep-ex/9908008].

G. Abbiendi *et al.* (OPAL collaboration), *Search for anomalous production of acoplanar di-lepton events in e^+e^- collision at $\sqrt{s}$ = 183 GeV and 189 GeV*, Eur. Phys. J. **C14**, 51 (2000) [CERN-EP-99-122, hep-ex/9909052].

G. Abbiendi *et al.* (OPAL collaboration), *Search for chargino and neutralino production at $\sqrt{s}$ = 189 GeV at*

LEP, Eur. Phys. J. **C14**, 187 (2000), erratum, *ibid.* **C16**, 707 (2000) [CERN-EP-99-123, hep-ex/9909051].

G. Abbiendi *et al.* (OPAL collaboration), *Precision luminosity for Z^0 line shape measurements with a silicon tungsten calorimeter*, Eur. Phys. J. **C14**, 373 (2000) [CERN-EP-99-136, hep-ex/9910066].

G. Abbiendi *et al.* (OPAL collaboration), *Tau decays with neutral kaons*, Eur. Phys. J. **C13**, 213 (2000) [CERN-EP-99-154, hep-ex/9911029].

G. Abbiendi *et al.* (OPAL collaboration), *Inclusive production of $D^{*\pm}$ mesons in photon-photon collisions at $\sqrt{s_{ee}}$ = 183 GeV and 189 GeV and a first measurement of $F_{2,c}^{\gamma}$*, Eur. Phys. J. **C16**, 579 (2000) [CERN-EP-99-157, hep-ex/9911030].

G. Abbiendi *et al.* (OPAL collaboration), *Leading particle production in light flavor jets*, Eur. Phys. J. **C16**, 407 (2000) [CERN-EP-99-164, hep-ex/0001054].

G. Abbiendi *et al.* (OPAL collaboration), *Search for unstable heavy and excited leptons at LEP-2*, Eur. Phys. J. **C14**, 73 (2000) [CERN-EP-99-169, hep-ex/0001056].

G. Abbiendi *et al.* (OPAL collaboration), *Measurements of R_B and A_{FB}^b, and A_{FB}^c in e^+e^- collisions at 130–189 GeV*, Eur. Phys. J. **C16**, 41 (2000) [CERN-EP-99-170, hep-ex/0002024].

G. Abbiendi *et al.* (JADE and OPAL collaborations), *QCD analyses and determinations of α_s in e^+e^- annihilation at energies between 35 GeV and 189 GeV*, Eur. Phys. J. **C17**, 19 (2000) [CERN-EP-99-175, hep-ex/0001055].

G. Abbiendi *et al.* (OPAL collaboration), *QCD studies with e^+e^- annihilation data at 172–189 GeV*, Eur. Phys. J. **C16**, 185 (2000) [CERN-EP-99-178, hep-ex/0002012].

G. Abbiendi *et al.* (OPAL collaboration), *Search for new physics in rare B decays*, Phys. Lett. **B476**, 233 (2000) [CERN-EP-99-179].

G. Abbiendi *et al.* (OPAL collaboration), *Transverse and longitudinal Bose Einstein correlations in hadronic Z^0 decays*, Eur. Phys. J. **C16**, 423 (2000) [CERN-EP-2000-004, hep-ex/0002062].

G. Abbiendi *et al.* (OPAL collaboration), *Z boson pair production in e^+e^- collisions at $\sqrt{s}$ = 183 GeV and 189 GeV*, Phys. Lett. **B476**, 256 (2000) [CERN-EP-2000-017, hep-ex/0003016].

G. Abbiendi *et al.* (OPAL collaboration), *Measurement of $|V_{cb}|$ using $\bar{B}^0 \to D^{*+}\ell^-\bar{\nu}$ decays*, Phys. Lett. **B482**, 15 (2000) [CERN-EP-2000-032, OPAL-PR-305].

G. Abbiendi *et al.* (OPAL collaboration), *Photonic events with missing energy in e^+e^- collisions at $\sqrt{s}$ = 189 GeV*, Eur. Phys. J. **C18**, 253 (2000) [CERN-EP-2000-050, hep-ex/0005002].

G. Abbiendi *et al.* (OPAL collaboration), *A measurement of the τ mass and the first CPT test with τ leptons*, Phys. Lett. **B492**, 23 (2000), [CERN-EP-2000-056, hep-ex/0005009].

G. Abbiendi *et al.* (OPAL collaboration), *First measurement of the inclusive branching ratio of b hadrons to ϕ mesons in Z^0 decays*, Phys. Lett. **B492**, 13 (2000) [CERN-EP-2000-065, hep-ex/0007015].

G. Abbiendi *et al.* (OPAL collaboration), *Search for trilinear neutral gauge boson couplings in $Z\gamma$ production at $\sqrt{s}$ = 189 GeV at LEP*, Eur. Phys. J. **C17**, 553 (2000) [CERN-EP-2000-067, hep-ex/0007016].

G. Abbiendi *et al.* (OPAL collaboration), *Multiplicities of π^0, η, K^0 and of charged particles in quark and gluon jets*, Eur. Phys. J. **C17**, 373 (2000) [CERN-EP-2000-070, hep-ex/0007017].

G. Abbiendi *et al.* (OPAL collaboration), *Measurement of the low-x behavior of the photon structure function F_2^{γ}*, Eur. Phys. J. **C18**, 15 (2000) [CERN-EP-2000-082, hep-ex/0007018].

G. Abbiendi *et al.* (OPAL collaboration), *Measurement of the B^0 lifetime and oscillation frequency using $\bar{B}^0 \to D^{*+}\ell^-\bar{\nu}$ decays*, Phys. Lett. **B493**, 266 (2000) [CERN-EP-2000-090, CERN-EP-2000-90, hep-ex/0010013].

G. Abbiendi *et al.* (OPAL collaboration), *A measurement of the rate of charm production in W decays*, Phys. Lett. **B490**, 71 (2000) [CERN-EP-2000-100, hep-ex/0009020].

G. Abbiendi *et al.* (OPAL collaboration), *W^+W^- production cross section and W branching fractions in e^+e^- collisions at 189 GeV*, Phys. Lett. **B493**, 249 (2000) [CERN-EP-2000-101, hep-ex/0009019].

Instrumentation/Accelerator Physics/Computing Sciences

R. Tafirout and G. Azuelos, *EXOTIC: a heavy fermion and excited fermion Monte Carlo generator for e^+e^- physics*, Erratum-ibid. **133**, 136 (2000).

G. Cojocaru, *Experiments with a microwave plasma as a cathode for cold or hot reflex discharge ion source*, Rev. Sci. Inst. **71**, 966 (2000).

J. Boger *et al.* (SNO collaboration), *The Sudbury Neutrino Observatory*, Meth. Phys. Res. **A449**, 172 (2000) [SNO-STR-99-025].

R. Helmer, *The Sudbury Neutrino Observatory*, IEEE Trans. Nucl. Sci. **47**, 2087 (2000).

M. Benedikt (ed.), A. Blas, J. Borburgh, R. Cappi, M. Chanel, V. Chohan, G. Daems, A. Fowler, R. Garoby, J. Gonzalez, D. Grier, J. Gruber, S. Hancock, C.E. Hill, A. Jansson, E. Jensen, A. Krusche, P. Maesen, K.D. Metzmacher, R. Losito, J. Olsfors, M. Paoluzzi, J. Pedersen, U. Raich, J.P. Riunaud, J.P. Royer, M. Sassowsky, K. Schindl, H. Schonauer, L. Sermeus, M. Thivent, H. Ullrich, W. Van Cauter, F. Volker, M. Vretenar, M. Barnes, E. Blackmore, F. Cifarelli, G. Clark, S. Koscielniak, F. Mammarella, A. Mitra, R. Poirier, K. Reiniger and T. Ries, *The PS complex*

as proton pre-injector for the LHC: design and implementation report [CERN report: CERN-2000-003].

D. Kaltchev, *Effect of b_3 on nominal and resonance-free lattices with gradient errors*, SLAP Beam Phys. Note **48** (2000).

E. Borsato, R. Caracciolo, C. Fanin, F. Galeazzi, M. Morandin, S. Santi, C. Voci, F. Bronzini, A. Buccheri, F. Ferroni, K. Fratini, S. Morganti, P.M. Patel, A. Pelosi, G. Piredda, R. Fernholz, R. Henderson and M. Kelsey, *The automated stringing system for the BaBar drift chamber*, Nucl. Instrum. Methods **A451**, 414 (2000).

J. Doornbos, *Possibilities for a 15 GeV/c – 25 GeV/c RF-separated charged kaon beam*, Nucl. Instrum. Methods **A455**, 253 (2000).

J. Doornbos and F. Iazzi, *A two-stage separated 1-GeV/c antideuteron beam*, Nucl. Instrum. Methods **A452**, 1 (2000).

J. Doornbos, M. Aoki, E.W. Blackmore, C.J. Kost, J.A. Macdonald, T. Nakano, P. Pile, I.H. Chang, K.K. Li and F. Meot, *Optics design and performance of LESB3, a two-stage separated 800 MeV/c kaon beam line*, Nucl. Instrum. Methods **A444**, 546 (2000).

S. Hu, J.V. Cresswell, D.A. Bryman and H.L. Kwok, *Light absorption in a resistive gate GaAs charge coupled device*, J. Vac. Sci. Tech. **A18**, 2 (2000).

Chemistry and Solid-State Physics

H.A. Blackstead, J.D. Dow, D.R. Harshman, M.J. DeMarco, M.K. Wu, D.Y. Chen, F.Z. Chien, D.B. Pulling, W.J. Kossler, A.J. Greer, C.E. Stronach, E. Koster and B. Hitti, *Magnetism and superconductivity in $Sr_2\,YRu_{1-u}\,Cu_u\,O_6$ and $Ba_2\,GdRu_{1-u}\,Cu_u\,O_6$*, Eur. Phys. J. **B15**, 649 (2000).

S.R. Dunsiger *et al.*, *Low temperature spin dynamics of the geometrically frustrated antiferromagnetic garnet $Gd_3\,Ga_5\,O_{12}$*, Phys. Rev. Lett. **85**, 3504 (2000).

V.G. Storchak, D.G. Eshchenko, J.H. Brewer, G.D. Morris, S.P. Cottrell and S.F.J. Cox, *Electron localization in a disordered insulating host*, Phys. Rev. Lett. **85**, 166 (2000).

J.E. Sonier, J.H. Brewer and R.F. Kiefl, *μSR studies of the vortex state in type-II superconductors*, Rev. Mod. Phys. **72**, 769 (2000).

J.E. Sonier, R.H. Heffner, D.E. MacLaughlin, G.J. Nieuwenhuys, O. Bernal, R. Movshovich, P.G. Pagliuso, J. Cooley, J.L. Smith and J.D. Thompson, *μ^+ Knight shift measurements in $U_{0.965}\,Th_{0.035}\,Be_{13}$ single crystals*, Phys. Rev. Lett. **85**, 2821 (2000).

P.W. Percival, K. Ghandi, J.-C. Brodovitch, B. Addison-Jones and I. McKenzie, *Detection of muoniated organic free radicals in supercritical water*, Phys. Chem. Chem. Phys. **2**, 4717 (2000).

Y.J. Uemura, *Superfluid density, condensation, and phase separation in high-T_c and other exotic superconductors*, Physica C **341-348**, 2117 (2000).

K.H. Chow, R.F. Kiefl, B. Hitti, T.L. Estle and R.L. Lichti, *Novel behavior of bond-centered muonium in heavily doped n-type silicon: Curie-like spin susceptibility and charge screening*, Phys. Rev. Lett. **84**, 2251 (2000).

M.I. Larkin, Y. Fudamoto, I.M. Gat, A. Kinkhabwala, K.M. Kojima, G.M. Luke, J. Merrin, B. Nachumi, Y.J. Uemura, M. Azuma, T. Saito and M. Takano, *Crossover from dilute to majority spin freezing in two leg ladder system $Sr(Cu,Zn)_2\,O_3$*, Phys. Rev. Lett. **85**, 1982 (2000).

R.I. Miller, R.F. Kiefl, J.H. Brewer, J. Chakhalian, S. Dunsiger, G.D. Morris, J.E. Sonier and W.A. MacFarlane, *Low temperature limit of the vortex core radius and the Kramer-Pesch effect in $NbSe_2$*, Phys. Rev. Lett. **85**, 1540 (2000).

J.J. Pan, D.J. Arseneau, M. Senba, D.G. Fleming, U. Himmer and Y. Suzuki, *Measurements of Mu + NO termolecular kinetics up to 520 bar: isotope effects and the Troe theory*, Phys. Chem. Chem. Phys. **2**, 621 (2000).

U. Himmer and E. Roduner, *Addition reaction of X to O_2 (X = Mu, H, D): isotope effects in intra- and intermolecular energy transfer*, Phys. Chem. Chem. Phys. **2**, 339 (2000).

D.H. Ryan, J.M. Cadogan and J. van Lierop, *Transverse spin freezing in $a-Fe_xZr_{100-x}$ studied using μSR*, J. Appl. Phys. **87**, 6525 (2000).

D.H. Ryan, J.M. Cadogan and J. van Lierop, *μSR study of transverse spin freezing in $a-Fe_xZr_{100-x}$*, Phys. Rev. **B61**, 6816 (2000).

D.H. Ryan, J.M. Cadogan and J. van Lierop, *Transverse spin freezing in Ruthenium-doped $a-Fe_{90}Zr_{10}$*, Phys. Rev. **B62**, 8638 (2000).

Life Sciences

D.J. Doudet, J.E. Holden, S. Jivan, E. McGeer and J. Wyatt, *In vivo PET studies of the dopamine D2 receptors in rhesus monkeys with long-term MPTP-induced Parkinsonism*, Synapse **38**, 105 (2000).

X. Min, M.Y. Siddiqi, R.D. Guy, A.D.M. Glass and H.J. Kronzucker, *A comparative kinetic analysis of nitrate and ammonium influx in two early-successional tree species of temperate and boreal forest ecosystems*, Plant Cell and Environ. **23**, 321 (2000).

H.J. Kronzucker, A.D.M. Glass, M.Y. Siddiqi and G.J.D. Kirk, *Comparative kinetic analysis of ammonium and nitrate acquisition by tropical lowland rice: implications for rice cultivation and yield potential*, New Phytologist **145(3)**, 471 (2000).

J.J. Vidmar, D. Zhuo, M.Y. Siddiqi and A.D.M. Glass, *Isolation and characterization of HvNRT2.3 and HvNRT2.4,*

cDNAs encoding high-affinity nitrate transporters from roots of Hordeum Vulgare, Plant Physiol. **122**, 783 (2000).

J.J. Vidmar, D. Zhuo, M.Y. Siddiqi, J.K. Schjoerring, B. Touraine and A.D.M. Glass, *Regulation of HvNRT2 expression and high-affinity nitrate influx in roots of Hordeum Vulgare by ammonium and amino acids*, Plant Physiol. **123**, 307 (2000).

E.T.C. Ngan, T.J. Ruth and P.F. Liddle, *Decrease 5-HT2a receptor densities in neuroleptic naïve schizophrenic patients: A PET study using [18F]setoperone*, Am. J. Psychiatry **157**, 1016 (2000).

R. de la Fuente-Fernandez, A. Kishore, T.J. Ruth, D.B. Calne and A.J. Stoessl, *Nigrostriatal dopamine system and motor lateralization*, Behavioural Brain Res. **112**, 63 (2000).

R. de la Fuente-Fernandez, P.K. Pal, F.J.G. Vingerhoets, A. Kishore, M. Schulzer, E.K. Mak, T.J. Ruth, B.J. Snow, A.J. Stoessl and D.B. Calne, *Evidence for impaired presynaptic dopamine function in Parkinsonian patients with motor fluctuations*, J. Neural Trans. **107**, 49 (2000).

C.S. Lee, A. Samii, V. Sossi, T.J. Ruth, M. Schulzer, P.K. Pal, D.B. Calne and A.J. Stoessl, *In vivo PET evidence for compensatory changes in presynaptic dopaminergic nerve terminals in Parkinson's disease*, Ann. Neurol. **47**, 493 (2000).

V. Sossi, J.E. Holden, A.J. Stoessl, G.L.-Y. Chan and T.J. Ruth, *Analysis of four dopaminergic tracer kinetics using two different tissue input function methods*, J. Cereb. Blood Flow Metab. **20**, 653 (2000).

K.R. Buckley, J. Huser, S. Jivan, K.S. Chun and T.J. Ruth, *^{11}C-methane production in small volume, high pressure gas targets*, Radiochim. Acta **88**, 201 (2000).

H. Dougan, D.M. Lyster, C.V. Vo, A.R. Stafford, J.I. Weitz and J.B. Hobbs, *Extending the lifetime of anticoagulant oligodeoxynucleotide aptamers in blood*, Nucl. Med. Biology **27**, 289 (2000).

S. Zeisler, *Medical applications of accelerators at TRIUMF*, Trans. Am. Nucl. Soc. **82**, 20 (2000).

M.J. Adam, S. Jivan, J.M. Huser and J. Lu, *^{11}C-methylations using ^{11}C-methyl iodide and tetrabutylammonium fluoride*, Radiochim. Acta **88**, 207 (2000).

Theoretical Program

P.F. Bedaque, H.W. Hammer and U. van Kolck, *Effective theory of the triton*, Nucl. Phys. **A676**, 357 (2000) [DOE-ER-40561-57, TRI-PP-99-24, KRL MAP-248, NT UW-99-30, nucl-th/9906032].

H.W. Fearing and S. Scherer, *Field transformations and simple models illustrating the impossibility of measuring off-shell effects*, Phys. Rev. **C62**, 034004 (2000) [TRI-PP-99-30, MKPH-T-99-21, nucl-th/9909076].

T. Schäfer, *Patterns of symmetry breaking in QCD at high baryon density*, Nucl. Phys. **B575**, 269 (2000) [TRI-PP-99-31, hep-ph/9909574].

C.H. Hyun, D.P. Min and T.-S. Park, *A higher order calculation of np scattering in cutoff effective field theory*, Phys. Lett. **B473**, 6 (2000) [TRI-PP-99-33, SNUTP-99-045, nucl-th/9908073].

L. Canton and W. Schadow, *Isoscalar off-shell effects in threshold pion production from pd collision*, Phys. Rev. **C61**, 064009 (2000) [DFPD-99-TH-51, TRI-PP-99-34, nucl-th/9911058].

H.W. Fearing, *The off-shell nucleon-nucleon amplitude: why it is unmeasurable in nucleon-nucleon bremsstrahlung*, Few-Body Syst. Suppl. **12**, 263 (2000) [TRI-PP-99-36].

R.M. Woloshyn, *Hyperfine effects in charmed baryons*, Phys. Lett. **B476**, 309 (2000) [TRI-PP-00-03].

S. Furihata, *Statistical analysis of light fragment production from medium-energy proton induced reactions*, Nucl. Instrum. Methods **B171**, 251 (2000) [TRI-PP-00-07, nucl-th/0003036].

R. Lewis and R.M. Woloshyn, *S and P wave heavy light mesons in lattice NRQCD*, Phys. Rev. **D62**, 114507 (2000) [TRI-PP-00-08, hep-lat/0003011].

L. Canton and W. Schadow, *Why is the three nucleon force so odd?*, Phys. Rev. **C62**, 044005 (2000) [TRI-PP-00-09, nucl-th/0004046].

M.A. Nobes and R.M. Woloshyn, *Decays of the B_c meson in a relativistic quark-meson model*, J. Phys. **G26**, 1079 (2000) [TRI-PP-00-20, hep-ph/0005056].

H.W. Fearing, T.R. Hemmert, R. Lewis and C. Unkmeir, *Radiative pion capture by a nucleon*, Phys. Rev. **C62**, 054006 (2000) [TRI-PP-00-23, MKPH-T-00-03, FZJ-IKP-TH-2000-03, hep-ph/0005213].

D.H. Wilkinson, *Limits to second-class nucleonic and mesonic currents*, Eur. Phys. J. **A7**, 307 (2000) [TRI-PP-00-68].

D.H. Wilkinson, *Limits to second-class nucleonic currents*, Nucl. Instrum. Methods **A455**, 656 (2000) [TRI-PP-00-72].

S. Banerjee, S.K. Ghosh and S. Raha, *The Chandrasekhar limit for quark stars*, J. Phys. **G26**, Ll (2000).

S. Banerjee, S.K. Ghosh, A. Mazumdar, S. Raha and D. Syam, *Strange quark matter in cosmic ray flux and exotic events*, Astrophys. and Space Sci. **274**, 655 (2000).

S. Banerjee, S.K. Ghosh, S. Raha and D. Syam, *Can cosmic strangelets reach the earth?*, Phys. Rev. Lett. **85**, 1384 (2000).

W. Schadow, Ch. Elster and W. Glöckle, *Three-body scattering below breakup threshold: an approach without using partial waves*, Few-Body Syst. **28**, 15 (2000) [nucl-th/9903020].

W. Schadow, W. Sandhas, J. Haidenbauer and A. Nogga, *Comparison of triton bound state properties using different separable representations of realistic potentials*, Few-Body Syst. **28**, 241 (2000).

P. Schuck, M. Beyer, G. Röpke, W. Schadow and A. Schnell, *Few-body states in Fermi-systems and condensation phenomena*, Few-Body Syst. Suppl. **12**, 50 (2000).

K.F. Liu, S.J. Dong, T. Draper, J. Sloan, W. Wilcox and R.M. Woloshyn, *Reply to Isgur's comments on valence QCD*, Phys. Rev. **D61**, 118502 (2000) [SLAC-PUB-8334, UK-99-21, hep-lat/9912049].

S. Kondratyuk and O. Scholten, *Dressing the nucleon in a dispersion approach*, Phys. Rev. **C62**, 025203 (2000).

S. Kondratyuk and O. Scholten, *Compton scattering in a unitary approach with causality constraints*, Nucl. Phys. **A677**, 396 (2000).

R.M. Davidson, N. Mathur and N.C. Mukhopadhyay, *The role of the $D_{13}(1520)$ resonance in eta electroproduction*, Phys. Rev. **C62**, 058201 (2000).

N. Mathur, S.J. Dong, K.F. Liu, L. Mankiewicz and N.C. Mukhopadhyay, *Quark orbital angular momentum from lattice QCD*, Phys. Rev. **D62**, 114504 (2000).

N. Mathur, S.-J. Dong, K.-F. Liu and N.C. Mukhopadhyay, *Proton spin content from lattice QCD*, Nucl. Phys. Proc. Suppl. **83**, 247 (2000).

X. Kong and F. Ravndal, *Coulomb effects in low energy proton-proton scattering*, Nucl. Phys. **A665**, 137 (2000) [nucl-th/9903523].

X. Kong and F. Ravndal, *Relativistic corrections to the pionium lifetime*, Phys. Rev. **D61**, 077506 (2000) [hep-ph/9905539].

J. Escher and A. Leviatan, *Partial dynamical symmetry in a fermion system*, Phys. Rev. Lett. **84**, 1866 (2000).

G.C. McLaughlin and J.N. Ng, *Neutrinos in extra dimensions and the anomalous magnetic moments of leptons*, Phys. Lett. **B493**, 88 (2000) [hep-ph/0008209].

S.J.Q. Robinson, L. Zamick, A. Mekjian and N. Auerbach, *Effects of deformation on weak charge transfer transition strengths*, Phys. Rev. **C62**, 017302 (2000).

B.K. Jennings and S. Das Gupta, *Canonical partition function in nuclear physics*, Phys. Rev. **C62**, 014901 (2000).

S.K. Ghosh and B. Jennings, *ρ nucleus bound state in Walecka model*, Phys. Rev. **C61**, 67604 (2000).

B.K. Jennings, *Low-energy behavior of the $^7Be(p,\gamma)^8B$ reaction*, Phys. Rev. **C62**, 027602 (2000) [nucl-th/9910005].

T.-S. Park, K. Kubodera, D.P. Min and M. Rho, *Effective field theory approach to $\vec{n}+\vec{p}\to d+\gamma$ at threshold*, Phys. Lett. **B472**, 232 (2000) [KIAS-P99035, nucl-th/9906005].

R. Rapp, T. Schäfer, E.V. Shuryak and M. Velkovsky, *High density QCD and instantons*, Ann. Phys. **280**, 35 (2000).

S. Karataglidis, P.J. Dortmans, K. Amos and C. Bennhold, *Alternative evaluations of halos in nuclei*, Phys. Rev. **C61**, 024319 (2000) [nucl-th/9811045].

C.V. Chang and J.N. Ng, *Bulk Higgs boson decays in brane localized gravity*, Phys. Lett. **B488**, 390 (2000) [hep-ph/0006164].

Han-Xin He, F.C. Khanna and Y. Takahashi, *Transverse Ward-Takahashi identity for the fermion boson vertex in gauge theories*, Phys. Lett. **B480**, 222 (2000).

A.M. Rakhimov, Y.T. Yakhshev and F.C. Khanna, *Meson-nucleon vertex form-factors at finite temperature*, Phys. Rev. **C61**, 024907 (2000) [nucl-th/9908061].

A. Rakhimov, U. Yakshiev and F.C. Khanna, *Meson-nucleon form factors at finite temperature*, Phys. Rev. **C61**, 024907 (2000).

F.C. Khanna and E. Truhlik, *Weak axial exchange currents of the Bethe-Salpeter equation*, Nucl. Phys. **A673**, 455 (2000) [nucl/th-9911022].

A.E. Santana, A. Matos Neto, J.D.M. Vianna and F.C. Khanna, *Symmetry groups, density matrix equations and covariant Wigner functions*, Physica **A280**, 405 (2000).

S.P. Kim, A.E. Santana and F.C. Khanna, *Generalised invariants and quantum evolution of open fermionic system*, Phys. Lett. **A272**, 46 (2000) [ALBERTA-THY-18-99, hep-th/9910189].

B.K. Patra, C.P. Singh and F.C. Khanna, *Isentropic quark hadron phase boundary and strangeness enhancement*, Int. J. Mod. Phys. **A15**, 3563 (2000).

Journal Publications In Press or Submitted

Particle, Nuclear and Atomic Physics

S. Adler *et al.*, *E949: An experiment to measure the branching ratio $B(K^+\to\pi^+\nu\overline{\nu})$ at Brookhaven National Laboratory* [TRI-PP-00-06].

A. Astbury, *Is there a link between cancer and cosmic rays?* [TRI-PP-00-33].

A.R. Berdoz, J. Birchall, J.B. Bland, J.D. Bowman, J.R. Campbell, G.H. Coombes, C.A. Davis, P.W. Green, A.A. Hamian, Y. Kuznetsov, L. Lee, C.D.P. Levy, R.E. Mischke, S.A. Page, W.D. Ramsay, S.D. Reitzner, T. Ries, G. Roy, A.M. Sekulovich, J. Soukup, T. Stocki, V. Sum, N.A. Titov, W.T.H. van Oers, R.J. Woo and A.N. Zelenski, *A monitor of beam polarization profiles for the TRIUMF parity experiment* (submitted to Nucl. Instrum. Methods A) [TRI-PP-00-34, physics/0011007].

S. Adler *et al.* (BNL E787 collaboration), *Search for the decay $K^+\to\pi^+\pi^0\nu\bar{\nu}$* (submitted to Phys. Rev. D) [BNL-67631, KEK-PREPRINT-2000-68, PRINCETON-HEP-2000-5, TRI-PP-00-54].

D. Hutcheon, R. Abegg, E.G. Auld, R.M. Churchman, C.A. Davis, R.M. Finlay, P.W. Green, L.G. Greeniaus, R. Henderson, K.H. Hicks, D.V. Jordan, W. Kellner, E. Korkmaz, A.K. Opper, G.V. O'Rielly, T.P. Porcelli, S.D. Reitzner, G. Sheffer, P.L. Walden and S. Yen, *Apparatus for a measurement of charge symmetry* (Nucl. Instrum. Methods A, in press) [TRI-PP-00-55].

S. Page and W.T.H. van Oers, *Parity violation in proton-proton scattering* (submitted to Nucl. Phys. News Int.) [TRI-PP-00-65].

N. Bateman, K. Abe, G. Ball, L. Buchmann, J. D'Auria, Y. Fuchi, C. Iliadis, H. Ishiyama, K.P. Jackson, S. Karataglidis, S. Kato, S. Kubono, K. Kumagai, M. Kurokawa, X. Liu, P. Strasser and M.H. Tanaka, *Measurement of the $^{24}Mg(p,t)^{22}Mg$ reaction and implications for the $^{21}Na(p,\chi)^{22}Mg$ stellar reaction rate* (Phys. Rev. C, in press).

G.C. Ball, S. Bishop, J.A. Behr, G.C. Boisvert, P. Bricault, J. Cerny, J.M. D'Auria, M. Dombsky, J.C. Hardy, V. Iacob, J.R. Leslie, T. Lindner, J.A. Macdonald, H.-B. Mak, D.M. Moltz, J. Powell, G. Savard and I.S. Towner, *Precise half-life measurement for the superallowed $0^+ \rightarrow 0^+$ β emitter ^{74}Rb: first results from the new radioactive beam facility (ISAC) at TRIUMF* (Phys. Rev. Lett., in press).

C.E. Svensson, A.O. Macchiavelli, A. Juodagalvis, A. Poves, I. Ragnarsson, S. Aberg, D.E. Appelbe, R.A.E. Austin, G.C. Ball, M.P. Carpenter, E. Caurier, R.M. Clark, M. Cromaz, M.A. Deleplanque, R.M. Diamond, P. Fallon, R.V.F. Janssens, G.J. Lane, I.Y. Lee, F. Nowacki, D.G. Sarantites, F.S. Stephens, K. Vetter and D. Ward, *Lifetimes of highly-collective rotational states in ^{36}Ar* (submitted to Phys. Rev. C).

G.M. Huber, G.J. Lolos, Z. Papandreou, J. Hovdebo, S.I.H. Naqvi, D.F. Ottewell, P.L. Walden, G. Jones and X. Aslanoglou, *Study of two step mechanisms in pion absorption on ^6Li, ^{12}C via deuteron emission* [nucl-ex/0009010].

B. Khurelbaatar, V.S. Kiselev, R.Kh. Kutuev, Zh. Musulmanbekov, V.A. Nikitin, P.V. Nomokonov, A.V. Pavlyuk, I.A. Rufanov, R.Ya. Zulkarneev, A.D. Avezov, A.A. Gafarov, Yu.N. Koblik, V.V. Myalkovsky, D.A. Mirkarimov, A.V. Morozov, V.A. Pirogov, G.A. Radyuk, B.S. Yuldashev, D. Hutcheon, S. Yen, V. Chaloupka, W.M. Dougherty, G. Liang, H.J. Lubatti, W.G. Weitkamp and T.C. Zhao, *Measurement of the analyzing power of the reactions C(p,pp)X and C(p,pd)X at 500 MeV* (submitted to Nucl. Phys. A) [JINR-E1-99-37].

A. Lagoyannis, F. Auger, A. Musumarra, N. Alamanos, E.C. Pollacco, A. Pakou, Y. Blumenfeld, F. Braga, M. La Commara, A. Drouart, G. Fioni, A. Gillibert, E. Khan, V. Lapoux, W. Mittig, S. Ottini-Hustache, D. Pierroutsakou, M. Romoli, P. Roussel-Chomaz, M. Sandoli, D. Santonocito, J.A. Scarpaci, J.L. Sida, T. Suomijarvi, S. Karataglidis and K. Amos, *Probing the ^6He halo structure with elastic and inelastic proton scattering* (submitted to Phys. Lett. B) [nucl-ex/0004001].

K.A. Aniol *et al.* (HAPPEX collaboration), *New measurement of parity violation in elastic electron-proton scattering and implications for strange form-factors* (submitted to Phys. Rev. Lett.) [WM-00-107, nucl-ex/0006002].

A. Airapetian *et al.* (HERMES collaboration), *Hadron formation in deep inelastic positron scattering in a nuclear environment* (submitted to Phys. Lett. B) [hep-ex/0012049].

A. Airapetian *et al.* (HERMES collaboration), *Measurement of longitudinal spin transfer to Λ hyperons in deep inelastic lepton scattering* (submitted to Phys. Lett. B.) [DESY-99-151, hep-ex/9911017].

A. Airapetian *et al.* (HERMES collaboration), *Hadron formation in deep inelastic positron scattering in a nuclear environment* [DESY-00-191, hep-ex/0012049].

G. Abbiendi *et al.* (OPAL collaboration), *Bose-Einstein correlations in $K^{\pm}K^{\pm}$ pairs from Z^0 decays into two hadronic jets* (submitted to Eur. Phys. J.) [CERN-EP-99-163, hep-ex/0001045].

G. Abbiendi *et al.* (OPAL collaboration), *Searches for prompt light gravitino signatures in e^+e^- collisions at $\sqrt{s}$ = 189 GeV* (submitted to Phys. Lett. B) [CERN-EP-2000-078, hep-ex/0007014].

G. Abbiendi *et al.* (OPAL collaboration), *A study of one prong τ decays with a charged kaon* (submitted to Eur. Phys. J. C) [CERN-EP-2000-091, OPAL-PR-315, hep-ex/0009017].

G. Abbiendi *et al.* (OPAL collaboration), *Two Higgs doublet model and model independent interpretation of neutral Higgs boson searches* (submitted to Eur. Phys. J. C) [CERN-EP-2000-092, hep-ex/0007040].

G. Abbiendi *et al.* (OPAL collaboration), *Measurement of W boson polarizations and CP violating triple gauge couplings from W^+W^- production at LEP* (submitted to Eur. Phys. J. C) [CERN-EP-2000-113, hep-ex/0009021].

G. Abbiendi *et al.* (OPAL collaboration), *Measurement of triple gauge boson couplings from W^+W^- production at LEP energies up to 189 GeV* (submitted to Eur. Phys. J. C) [CERN-EP-2000-114, hep-ex/0009022].

G. Abbiendi *et al.* (OPAL collaboration), *Production rates of $b\bar{b}$ quark pairs from gluons and $b\bar{b}b\bar{b}$ events in hadronic Z^0 decays* (submitted to Eur. Phys. J. C) [CERN-EP-2000-123, hep-ex/0010029].

G. Abbiendi *et al.* (OPAL collaboration), *Investigation of the decay of orbitally-excited B mesons and first measurement of the branching ratio $BR(B_J^* \rightarrow B^*\pi(X))$* (submitted to Eur. Phys. J. C) [CERN-EP-2000-125, hep-ex/0010031].

G. Abbiendi *et al.* (OPAL collaboration), *Charged multiplicities in Z decays into U, D and S quarks* (submitted to Eur. Phys. J. C) [CERN-EP-2000-128, hep-ex/0011022].

G. Abbiendi *et al.* (OPAL collaboration), *A study of B_s meson oscillation using D_s^- lepton correlations* (submitted to Eur. Phys. J. C) [CERN-EP-2000-136, OPAL-PR-327, hep-ex/0011052].

G. Abbiendi *et al.* (OPAL collaboration), *Precise determination of the Z resonance parameters at LEP: 'Zedometry'* (submitted to Eur. Phys. J. C) [CERN-EP-2000-148, OPAL-PR-328, hep-ex/0012018].

G. Abbiendi *et al.* (OPAL collaboration), *Search for the standard model Higgs boson in e^+e^- collisions at $\sqrt{s} \approx$ 192–209 GeV* (Phys. Lett. B, in press) [CERN-EP-2000-156, hep-ex/0101014].

Chemistry and Solid-State Physics

R. Kadono, W. Higemoto, A. Koda, K. Ohishi, T. Yokoo, J. Akimitsu, M. Hedo, Y. Inada, Y. Ōnuki, E. Yamamoto and Y. Haga, *Possible nodal vortex state in $CeRu_2$* (Phys. Rev. B, in press).

J.E. Sonier, J.H. Brewer, R.F. Kiefl, R.I. Miller, G.D. Morris, C.E. Stronach, J.S. Gardner, S.R. Dunsiger, D.A. Bonn, W.N. Hardy and R. Liang, *Anomalous weak magnetism in superconducting $YBa_2Cu_3O_{6+x}$* (submitted to Science).

J.E. Sonier, J.H. Brewer, R.F. Kiefl, D.A. Bonn, J. Chakhalian, S.R. Dunsiger, W.N. Hardy, R. Liang, W.A. MacFarlane, R.I. Miller, D.R. Noakes, T.M. Riseman and C.E. Stronach, *Melting and dimensionality of the vortex lattice in $YBa_2Cu_3O_{6.60}$* (Phys. Rev. B, Rapid Comm., in press).

J.M. Cadogan and D.H. Ryan, *Muon spin relaxation (μSR) studies of amorphous magnetic materials: application to $a-Fe_xZr_{90-x}$ and $a-Fe_{90-x}Ru_xZr_{10}$* (submitted to Austr. J. Phys.).

D.H. Ryan, J. van Lierop, M.E. Pumarol, M. Roseman and J.M. Cadogan, *A zero-field examination of transverse spin freezing in $a-Fe_xZr_{90-x}$* (submitted to J. Appl. Phys.).

E.S. Bates, R.L. Lichti, S.F.J. Cox and C. Schwab, *Low temperature diamagnetic muonium states in n-type gallium arsenide* (submitted to Physica B).

Life Sciences

V. Sossi, J.E. Holden and D.J. Doudet, *A reversible tracer approach to the study of effective dopamine turnover* (J. Cereb. Blood Flow and Metab., in press).

P.K. Pal, Z.K. Wszolek, A. Kishore, V. Sossi, R.J. Uitti, T. Dobko, D.B. Calne and A.J. Stoessl, *Positron emission tomography in pallido-ponto-nigral degeneration (PPND) family (frontotemporal dementia with Parkinsonism linked to chromosome 17 and point mutation in tau gene)*, (PARD, in press).

D.M. Martinez, A. Lindstrom, R. Thiruvengadaswamy, R.J. Kerekes, K. Buckley, S. Jivan, T.J. Ruth and J.A. Olson, *The flocculation tendency of papermaking suspensions as determined by sedimentation.*

T.J. Ruth, K.R. Buckley, K.S. Chun, E.T. Hurtado, S. Jivan and S. Zeisler, *A proof of principle for targetry to produce ultra high quantities of 18F-flouride: a work in progress* (Appl. Radiat. Isotopes, in press).

A.W. Wong, M.J. Adam and S. Withers, *Synthesis of 2,6-dioxy-2-fluoro-6-[18F]-fluoro-α-D-glucopyroanosyl fluoride (2,6FGF) as a potential imaging probe for glucocerebrosidase* (submitted to J. Lab. Compd. Radiopharm.).

C.J. Lane, E.T.C. Ngan, L. Yatham, T.J. Ruth and P.F. Liddle, *Immediate effects of risperidone on cerebral activity in healthy subjects: A comparison with first episode schizophrenic subjects* (submitted to Arch. Psych.).

E.T.C. Ngan, C.J. Lane, T.J. Ruth and P.F, Liddle, *Immediate and delayed effects of risperidone on cerebral metabolism in neuroleptic naïve schizophrenia: correlations with symptom change* (submitted to Arch. Psych.).

L.N. Yatham, P.F. Liddle, I.S. Shiah, G. Scarrow, R.W. Lam, M.J. Adam, A.P. Zis and T.J. Ruth, *Brain 5HT2 receptor density in patients with major depression: A PET study* (Arch. Gen. Psych., in press).

A.D.M. Glass *et al.*, *Nitrogen transport in plants, with emphasis on the regulation of fluxes to match demand* (Z. Planzenernhr. Bod., in press).

D.T. Britto and H.J. Kronzucker, *Can unidirectional influx be measured in higher plants? A mathematical approach using parameters from efflux analysis* (New Phytologist, in press).

D. Britto, A.D.M. Glass, H.J. Kronzucker and M.Y. Siddiqi, *Cytosolic concentrations and transmembrane fluxes of NH_4^+/NH_3: an analysis of a recent proposal* (Plant Physiol., in press).

D.J. Doudet and T.J. Ruth, *Imaging the brain in Parkinson's disease* (submitted to BCMA).

D.J. Doudet, G.L.Y. Chan, S. Jivan, C. English, J.E. Holden and T.J Ruth, *Simplified quantitative analysis of the density and affinity of the dopamine D1 and D2 receptors: PET studies with [11C]Raclopride and [11C]Sch23390* (submitted to J. Cereb. Blood Flow and Anal.).

J.E. Holden, V. Sossi, G. Chan, D.J. Doudet, A.J. Stoessl and T.J. Ruth, *Effect of population k2 values in graphical estimation of DV ratios of reversible ligands* (submitted to J. Cereb. Blood Flow and Anal.).

R. de la Fuente-Fernandez, Jian-Qiang Lu, V. Sossi, S. Jivan, M. Schulzer, J.E. Holden, C.S. Lee, T.J. Ruth, D.B. Calne and A.J. Stoessl, *Biochemical variations in the synaptic level of dopamine precede motor fluctuations in Parkinson's disease: PET evidence for increased dopamine turnover* (Ann. Neurol., in press).

A. Kishore, G.L.-Y. Chan, T. Dobko, M. Schulzer, V. Sossi,

R. de la Fuente-Fernandez, E. Mak, T.J. Ruth, D.B. Calne and A.J. Stoessl, *Dopamine D1 and D2 receptors and motor complications in idiopathic Parkinsonism: a PET study* (submitted to Brain).

G. Matte, M.J. Adam and D. Lyster, *Biological evaluation of radioiodinated 2-fluoro-2-iodo-mannose (FIM) and comparison with 18F-FDG and 18F-difluoro-deoxy glucose (DFDG)* (Nucl. Med. Biol., in press).

Theoretical Program

V.E. Shapiro, *Comment on nonadiabatic dynamics of atoms in nonuniform magnetic fields* (submitted to Phys. Lett. A) [TRI-PP-99-06].

B.D. Jones, *A follow-up to "Mesonic decay constants in lattice NRQCD"* (submitted to Phys. Rev.) [TRI-PP-99-23].

V.E. Shapiro, *Proposals for new improved methods for magnetic trapping and measurements of neutral atoms* (submitted to Phys. Rev. Lett.) [TRI-PP-99-37, TRI-PP-00-64].

S. Ando, T.-S. Park and D.P. Min, *Threshold* $pp \to pp\pi^0$ *up to one loop accuracy* (submitted to Phys. Lett. B) [SNUTP-99-052, TRI-PP-00-01, USC-NT-00-1, nucl-th/0003004].

G.C. McLaughlin and J.N. Ng, *The use of nuclear beta decay as a test of bulk neutrinos in extra dimensions* (Phys. Rev. D, in press) [TRI-PP-00-11, nucl/th-0003023].

W. Schadow, O. Nohadani and W. Sandhas, *Photonuclear reactions of three nucleon systems* (Phys. Rev. C, in press) [TRI-PP-00-29, nucl-th/0006069].

L. Canton and W. Schadow, *The one pion exchange three nucleon force and the* A_y *puzzle* (submitted to Phys. Rev. Lett.) [TRI-PP-00-32, nucl-th/0006070].

J. Escher and B.K. Jennings, *Role of spectroscopic factors in the potential model description of the* $^7Be(p,\gamma)^8B$ *reaction* (submitted to Phys. Rev. C).

J. Escher and B.K. Jennings, *Microscopic substructure effects in potential model descriptions of the* $^7Be(p,\gamma)^8B$ *reaction* (submitted to Phys. Rev. C) [TRI-PP-00-49, nucl-th/0007069].

J. Escher and A. Leviaton, *Partial dynamical symmetry in the symplectic shell model* (submitted to Phys. Rev. C) [TRI-PP-00-57].

H.W. Griesshammer and G. Rupak, *Nucleon polarizabilities from Compton scattering on the deuteron* [NT-UW-00-022, TRI-PP-00-62, TUM-T39-00-18, nucl-th/0012096].

D.H. Wilkinson, *Second-class currents and* Δs *in* $\nu(\bar{\nu})p$ *elastic scattering* (submitted to Nucl. Instrum. Methods) [TRI-PP-00-67].

A. Kurylov, G.C. McLaughlin and M.J. Ramsey-Musolf, *Constraints on T-odd, P-even interactions from electric dipole moments, revisited* [hep-ph/0011185].

A.Z. Mekjian, *Bosonic symmetries and pionic fluctuations and correlations.*

S.W. Hong and B.K. Jennings, *Quark-meson coupling model for a nucleon* (submitted to Nucl. Phys. A) [nucl-th/0009089].

M. Butler, J.-W. Chen and X. Kong, *Neutrino deuteron scattering in effective field theory at next-to-next-to-leading order* (Phys. Rev. C, in press) [nucl-th/0008032].

Y.F. Zhou, Y.L. Wu, J.N. Ng and C.Q. Geng, *The interplay of weak and strong phases and direct CP violation in charmless B meson decays* (Phys. Rev. D, in press) [hep-ph/0006225].

C. Pinheiro and F.C. Khanna, *Quantum gravity in (D=5)-dimensions* [CBPF-NF-043-00, hep-th/0006124].

C. Pinheiro, F.C. Khanna and R. Riche, *Godel type solution with rotation, expansion and closed timelike curves* [CBPF-NF-044-00, hep-th/0006125].

C. Pinheiro and F.C. Khanna, *Black hole entropy in (D=2+1)-dimensions from extended Chern-Simons term in a gravitational background* [CBPF-NF-045-00, hep-th/0006126].

C. Pinheiro and F.C. Khanna, *Some comments on Vlasov-Liouville equation and its relation with gravitational field* [CBPF-NF-047-00, hep-th/0006127].

C. Pinheiro, C.G. Pinheiro and F.C. Khanna, *Nonabelian magnetic monopoles in a background of gravitation with fermions* [CBPF-NF-048-00, hep-th/0006128].

C. Pinheiro and F.C. Khanna, *Nonparallel electric and magnetic fields in a gravitational background, stationary gravitational waves and gravitons* [hep-th/0006129].

C. Pinheiro and F.C. Khanna, *Black hole entropy in 1+1 dimensions from a quasi-Chern Simons term in a gravitational background* [hep-th/0006131].

S.A. Diniz, C. Pinheiro and F.C. Khanna, *Analysis of Maxwell equations in a gravitational field* [hep-th/0006133].

C. Pinheiro and F.C. Khanna, *Some comments on Wheeler-de Witt equation for gravitational collapse and the problem of time* [CBPF-NF-049-00, hep-th/0006142].

C. Pinheiro and F.C. Khanna, *New solutions for evolution of the scale factor with a variable cosmological term* [CBPF-NF-046-00, hep-th/0006174].

E. Truhlik, J. Smejkal and F.C. Khanna, *Electromagnetic isoscalar* $\rho\pi\gamma$ *exchange current and the anomalous action* [nucl-th/0010080].

S.P. Kim and F.C Khanna, *Non-Gaussian effects on domain growth* (submitted to Phys. Rev. Lett.) [hep-ph/0011115].

A. Rakhimov and F.C. Khanna, *Finite temperature amplitudes and reaction rates in thermofield dynamics* (submitted to Phys. Rev. C) [nucl-th/0011039].

W. Zhao and F.C. Khanna, *Screening length, dispersion relations and quark potential in thermofield dynamics* (submitted to Phys. Rev. D) [hep-ph/0011182].

M. de Montigny, F.C. Khanna and A.E. Santana, *Lie algebras and the doubling in thermo field dynamics* (Can. Appl. Math. Quarterly, in press).

S.J.Q. Robinson, L. Zamick, A. Mekjian and N. Auerbach, *Further comments on the effects of deformation on isovector electromagnetic and weak transition strengths* [nucl-th/0001021].

X. Kong and F. Ravndal, *Proton-proton fusion rate in effective field theory* (submitted to Phys. Rev. C) [nucl-th/0004038].

S. Banerjee, A. Bhattacharyya, S.K. Ghosh, S. Raha and B. Sinha, *The cosmological quark hadron transition and massive compact halo objects* [astro-ph/0002007].

Conference Publications

Particle, Nuclear and Atomic Physics

A. Astbury, B.A. Campbell, F.C. Khanna, J.L. Pinfold, M.G. Vincter, eds., Proc. **Lake Louise Winter Institute: Electroweak Physics, Lake Louise, February 14–20, 1999** (World Scientific, Singapore, 2000).

N.L. Rodning, P. Amaudruz, W. Andersson, M. Comyn, Yu. Davydov, P. Depommier, J. Doornbos, W. Faszer, C.A. Gagliardi, D.R. Gill, P. Green, P. Gumplinger, J.C. Hardy, M. Hasinoff, R. Helmer, R. Henderson, A. Khruchinsky, P. Kitching, D.D. Koetke, E. Korkmaz, Yu. Lachin, D. Maas, J.A. Macdonald, R. Manweiler, T. Mathie, J.R. Musser, P. Nord, A. Olin, D. Ottewell, R. Openshaw, L. Piilonen, T. Porcelli, J.-M. Poutissou, R. Poutissou, M.A. Quraan, J. Schaapman, V. Selivanov, G. Sheffer, B. Shin, F. Sobratee, J. Soukup, T.D.S. Stanislaus, G. Stinson, R. Tacik, V. Torokhov, R.E. Tribble, M.A. Vasilev, H.C. Walter and D. Wright, *Experiment E614 at TRIUMF: a close look at muon decay, ibid.* 510.

M. Maggiora *et al.* (DISTO collaboration), *Spin observables in hyperon production*, Proc. **15$^{\mathbf{th}}$ Int. Conf. on Particles and Nuclei (PANIC'99), Uppsala, June 10–16, 1999**, G. Faldt, B. Hoistad, S. Kullander, eds. (Nucl. Phys. **A663**, 2000) p.477.

P. Khaustov, D.E. Alburger, P.D. Barnes, B. Bassalleck, A.R. Berdoz, A. Biglan, T. Bürger, D.S. Carman, R.E. Chrien, C.A. Davis, H. Fischer, G.B. Franklin, J. Franz, L. Gan, A. Ichikawa, T. Iijima, K. Imai, Y. Kondo, P. Koran, M. Landry, L. Lee, J. Lowe, R. Magahiz, M. May, R. McCrady, C.A. Meyer, F. Merrill, T. Motoba, S.A. Page, K. Paschke, P.H. Pile, B. Quinn, W.D. Ramsay, A. Rusek, R. Sawafta, H. Schmitt, R.A. Schumacher, R.W. Stotzer, R. Sutter, F. Takeutchi, W.T.H. van Oers, K. Yamamoto, Y. Yamamoto, M. Yosoi and V.J. Zeps, *Production of doubly-strange systems in the (K^-, K^+) reaction in E885 at BNL, ibid.* 485.

A.K. Opper, E.G. Auld, R.M. Churchman, C.A. Davis, R.W. Finlay, P.W. Green, L.G. Greeniaus, D.A. Hutcheon, D.V. Jordan, E. Korkmaz, J.A. Niskanen, G.V. O'Rielly, T. Porcelli, S.D. Reitzner, P.L. Walden and S. Yen, *Charge symmetry breaking in the reaction $np \to d\pi^0$, ibid.* 505.

W. Kuhn *et al.* (DISTO collaboration), *Production of η' and K^- mesons in pp reactions at 2.85 GeV, ibid.* 569.

M. Quraan, P. Amaudruz, W. Andersson, M. Comyn, Yu. Davydov, P. Depommier, J. Doornbos, W. Faszer, C.A. Gagliardi, D.R. Gill, P. Green, P. Gumplinger, J.C. Hardy, M. Hasinoff, R. Helmer, R. Henderson, A. Khruchinsky, P. Kitching, D.D. Koetke, E. Korkmaz, Yu. Lachin, D. Maas, J.A. Macdonald, R. Manweiler, T. Mathie, J.R. Musser, P. Nord, A. Olin, D. Ottewell, R. Openshaw, L. Piilonen, T. Porcelli, J.-M. Poutissou, R. Poutissou, N.L. Rodning, J. Schaapman, V. Selivanov, G. Sheffer, Y. Shin, F. Sobratee, J. Soukup, T.D.S. Stanislaus, G. Stinson, R. Tacik, V. Torokhov, R.E. Tribble, M.A. Vasilev, H.K. Walter and D. Wright, *A precision measurement of muon decay, ibid.* 903.

M. Abe *et al.* (KEK-E246 collaboration), *Test of time reversal invariance in the decay $K^+ \to \pi^0 \mu^+ \nu$, ibid.* 919.

F.T. Avignone, B.D. Anderson, T.C. Awes, S. Berridge, E. Bilpuch, C. Britton, W. Bryan, W.M. Bugg, R.L. Burman, J. Busenitz, H.K. Carter, L. Chatterjee, V. Cianciolo, A.K. Cochran, H.O. Cohn, M.V. Danilov, L. De Braeckeleer, P. Degtyarenko, Yu.V. Efremenko, M.A. Elaasar, A.R. Fazely, S. Frank, T.A. Gabriel, C.R. Gould, V. Gudkov, R. Gunasingha, T. Handler, E.L. Hart, R.L. Imlay, U. Jagadish, Yu.A. Kamyshkov, E. Khosrovi, D.D. Koetke, C. Lane, R.W. Manweiler, W.J. Metcalf, A. Mezzacappa, L.W. Mo, V.Z. Nosik, T.A. Nunamaker, S. Nussinov, A. Piepke, F. Plasil, J. Reidy, C. Rosenfeld, D. Smith, I. Stancu, T.D.S. Stanislaus, R. Steinberg, R. Svoboda, R. Tashakkori, W. Tornow, G. VanDalen, J. Walker, J.W. Watson, A. Wintenberg, J. Wolf, D.H. Wright, O.Ya. Zeldovich and W.M. Zhang, *ORLaND: A proposed neutrino facility at the Oak Ridge National Laboratory*, Proc. **2$^{\mathbf{nd}}$ Int. Conf. on Nonaccelerator New Physics (NANP'99), Dubna, June 28–July 3, 1999**, V.A. Bednyakov, V.B. Brudanin, S.G. Kovalenko, eds. (Phys. Atom. Nucl. **63**, 1007, 2000; Yad. Fiz. **63**, 1082, 2000).

M.G. Vincter, *The spin asymmetry in the photoproduction of pairs of high transverse momentum hadrons at HERMES*, Proc. **Circum-Pan-Pacific RIKEN Symp. on High Energy Spin Physics, Wako, Japan, November 4–6, 1999** (RIKEN Rev. **28**, 2000) p.70.

D. Bryman, *Prospects for measuring $K_L^0 \to \pi^0 \nu\overline{\nu}$*, Proc. **3$^{\mathbf{rd}}$ Workshop on Physics and Detectors for DAΦNE (DAPHNE 99), Frascati, Italy, November 16–19, 1999**, S. Bianco *et al.*, eds. (Frascati Physics Series **XVI**, Frascati, 1999) p.189 [TRI-PP-99-43].

A. Olin, *Kaon nucleon scattering and reactions at low energies, ibid.* 627 [TRI-PP-00-02].

M. Kobel *et al.* (Two-Fermion Working Group), *Two-Fermion production in electron-positron collisions*, Proc. **LEP2 Monte Carlo Workshop: Report of the Working Groups on Precision Calculations for LEP2 Physics, Geneva, 1999**, S. Jadach, G. Passarino, R. Pittau, eds. (CERN, Geneva, 2000) p.269 [CERN-2000-09-D].

N. Grion *et al.* (CHAOS collaboration), *Interacting pion pairs in nuclear matter*, Proc. **28$^{\mathbf{th}}$ Int. Workshop on Gross Properties of Nuclei and Nuclear Excitation: Hadrons in Dense Matter (Hirschegg 2000), Hirschegg, Austria, January 16–22, 2000**, M. Buballa *et al.*, eds. (Darmstadt, GSI, 2000) p.63.

M. Hartig *et al.* (HERMES collaboration), *Diffractive vector meson production at HERMES*, Proc. **Int. Conf. on Quark Nuclear Physics (QNP 2000), Adelaide, Australia, February 21–25, 2000**, C. Boros, K. Tsushima and A.W. Thomas, eds. (Nucl. Phys. **A680**, 2000) p.264.

W.T.H. van Oers, *Constraints on a parity even/time reversal odd interaction*, Proc. **3$^{\mathbf{rd}}$ Int. Symp. on Symmetries in Subatomic Physics, Adelaide, March 13–17, 2000**, X.H. Guo, A.W. Thomas, A.G. Williams, eds. (AIP Conf. Proc. **539**, 2000) p.66 [TRI-PP-00-18, hep-ph/0005097].

A.K. Opper, *Charge symmetry violation in* $np \to d\pi^0$*, ibid.* 238.

S.A. Page, A.R. Berdoz, J. Birchall, J.B. Bland, J.D. Bowman, J.R. Campbell, C.A. Davis, A.A. Green, P.W. Green, A.A. Hamian, D.C. Healey, R. Helmer, Y. Kuznetsov, L. Lee, C.D.P. Levy, R.E. Mischke, W.D. Ramsay, S.D. Reitzner, G. Roy, P.W. Schmor, A.M. Sekulovich, J. Soukup, G.M. Stinson, T. Stocki, V. Sum, N.A. Titov, W.T.H. van Oers, R.J. Woo and A.N. Zelenski, *Parity violation in* $p-p$ *scattering: the TRIUMF experiment, ibid.*, 298.

T. Numao, *Rare kaon decays, ibid.* 333 [TRI-PP-00-26, hep-ex/0010039].

P.A. Żołnierczuk *et al.* (RMC collaboration), *The* $(\pi^-, \gamma\gamma)$ *program at TRIUMF*, Proc. **6$^{\mathbf{th}}$ Int. Workshop on Production, Properties and Interaction of Mesons (Meson 2000), Cracow, Poland, May 19–23, 2000** (Acta Phys. Polonica **B31**, 2000) p.2349.

P. Salabura *et al.* (DISTO collaboration), *Meson and hyperon production results from the DISTO spectrometer at Saturne, ibid.* 2419 [EXP SATURNE-213].

N. Grion *et al.* (CHAOS collaboration), *Scalar meson pairs in nuclei: experimental results, ibid.* 2645.

M.G. Vincter, *Spin structure functions and the spin structure of the nucleon*, Proc. **7$^{\mathbf{th}}$ Conf. on Intersections Between Particle and Nuclear Physics (CIPANP 2000), Quebec City, May 22–28, 2000**, Z. Parsa, W.J. Marciano, eds. (AIP, New York, 2000) **CP 549** p.62.

D. Bryman, *Three generations of quarks and leptons: Who ordered that?, ibid.* 150 [TRI-PP-00-50].

M.D. Hasinoff, D.S. Armstrong, J. Clark, T.P. Gorringe, M. Kovash, S. Tripathi, D.H. Wright and P.A. Żołnierczuk, *Rare pion double radiative capture reactions in hydrogen and deuterium, ibid.* 403 [TRI-PP-00-53].

J.H.D. Clark, D.S. Armstrong, T.P. Gorringe, M.D. Hasinoff, P.M. King, T.J. Stocki, S. Tripathi, D.H. Wright and P.A. Żołnierczuk, *Ortho-para transition in muonic molecular hydrogen, ibid.* 407.

B. Seitz [HERMES collaboration], *Q2-dependence of the generalized GDH integral for the proton, ibid.* 651.

C.A. Miller, *Single-spin/azimuthal asymmetries in semi-inclusive and exclusive DIS, ibid.* 712.

M.D. Hasinoff, *A test of time reversal invariance in stopped* K^+ *decay, ibid.* 969 [TRI-PP-00-52].

J.H.D. Clark, D.S. Armstrong, P.M. King, T.P. Gorringe, P.A. Żołnierczuk, S. Tripathi, M.D. Hasinoff, T. Stocki and D.H. Wright, *Ortho-para transition in muonic molecular hydrogen*, Proc. **Fall Meeting of the Division of Nuclear Physics of the APS, Williamsburg, VA, October 4–7, 2000** (Bull. Am. Phys. Soc. **45**, 2000) paper DE.002.

S. Tripathi, *On the first measurement of the* $\gamma\gamma n$ *capture mode of pionic hydrogen and pion Compton scattering at TRIUMF, ibid.*

R. Tacik, *Pion nucleus double scattering reactions, ibid.*

Instrumentation/Accelerator Physics/Computing Sciences

W.R. Rawnsley, R.E. Laxdal, L. Root and G.H. Mackenzie, *Bunch shape measurements using fast Faraday cups and an oscilloscope operated by LABVIEW over Ethernet*, Proc. **9$^{\mathbf{th}}$ Beam Instrumentation Workshop (BIW 2000), Cambridge, MA, May 8–11, 2000**, K. Jacobs, R.C. Sibley Melville, eds. (AIP Conf. Proc. 546, 2000) p.547.

A. Boudsko, O.R. Jones, H. Schmickler, M. Wendt and F. Willeke, *Chromaticity measurements at HERA-p using the head-tail technique with chirp excitation*, Proc. **4$^{\mathbf{th}}$ European Workshop on Diagnostics and Instrumentation for Particle Accelerators (DIPAC'99), Chester, UK, May 16–18, 1999**, B.G. Martlew, R.J. Smith, eds. (Daresbury Laboratory, Warrington, UK, 2000) p.99.

C. Boccard, T. Bogey, J. Brazier, J. de Vries, S. Jackson, O.R. Jones, J.P. Papis, W. Rawnsley, K. Rybaltchenko and H. Schmickler, *Performance of the new SPS beam position orbit system (MOPOS), ibid.* 122.

Y. Mori, K. Ikegami, A. Takagi, A.N. Zelenski, G. Dutto, S. Kadantsev, C.D.P. Levy, G.W. Wight, J. Alessi and M. Okamura, *Optically pumped polarized* H^- *ion source for RHIC spin project*, Proc. **8$^{\mathbf{th}}$ Int. Conf. on Ion Sources (ICIS'99), Kyoto, September 6–10, 1999**, J. Ishkawa, ed. (AIP, New York, Rev. Sci. Instrum. **71**, 2000) p.1237.

D. Kaltchev, *Two-stage betatron and momentum collimation studies with applications to LHC*, Proc. **Beam Halo**

and Scraping, 7th ICFA Mini-Workshop on High Intensity Hadron Beams, Lake Como, WI, September 13–15, 1999, N.V. Mokhov, W. Chou, eds. (FERMILAB-Conf-00/185, 2000) p.101 [TRI-PP-99-39].

S. Koscielniak *Observations in betatron collimation and tune splitting, ibid.* 131 [TRI-PP-99-47].

A. Gorelov, J.A. Behr, D. Melconian, M. Trinczek, P. Dubé, O. Häusser, U. Giesen, K.P. Jackson, T. Swanson, J.M. D'Auria, M. Dombsky, G. Ball, L. Buchmann, B. Jennings, J. Dilling, J. Schmid, D. Ashery, J. Deutsch, W.P. Alford, D. Asgeirsson, W. Wong and B. Lee, *β^+-ν correlation experiments on laser trapped ^{38m}K, ^{37}K*, Proc. **1st Euroconf. on Atomic Physics at Accelerators: Laser Spectroscopy and Applications (APAC99), Mainz, Germany, September 19–24, 1999** (Hyp. Int. **127**, 2000) p.373.

A.N. Zelenski, V. Klenov, S.A. Kokhanovski, V. Zoubets, G. Dutto, C.D.P. Levy, G.W. Wight, J. Alessi and Y. Mori, *Optically-pumped polarized H^- ion sources for RHIC and HERA colliders, ibid.* 475.

G.S. Clark, O. Hans, G. de Rijk and M. Racine, *A twin aperture resistive quadrupole for the LHC*, Proc. **16th Int. Conf. on Magnet Technology (MT16), Pointe Vedra Beach, FL, September 26–October 2, 1999** (IEEE Trans. Appl. Superconductivity **10**, 2000) p.147.

L. Moritz, *Using the Moyer model at energies below 1 GeV*, Proc. **9th Int. Conf. on Radiation Shielding, ICSR-9, Tsukuba, Japan, October 17–22, 1999** (J. Nucl. Sci. & Tech., Japan Atomic Energy Soc., 2000) supp. 1.

M. Comyn, *LaTeX 2ε prepared documents*, Proc. **First Joint Accelerator Conference Website (JACoW) Workshop on Electronic Publication of Proceedings of Particle Accelerator Conferences, Brookhaven National Laboratory, Upton, NY, December 1–4, 1999**, http://accelconf.web.cern.ch/accelconf/workshop99/proceedings/comyn_latex_prep_docs.pdf.

M. Comyn, *Building the table of contents and the author index, ibid.* http://accelconf.web.cern.ch/accelconf/workshop99/proceedings/comyn_toc_ai.pdf.

R.L. Poirier, P. Bricault, G. Dutto, K. Fong, R. Laxdal. A.K. Mitra, L. Root, P. Schmor, G. Stanford, B. Uzat, Y.V. Bylinsky and A. Facco, *ISAC RF structures and commissioning*, Proc. **7th European Particle Accelerator Conf. (EPAC 2000), Vienna, June 26–30, 2000**, J.-L. Laclare *et al.*, eds. (EPS-IGA, Geneva, 2000), p. 321 [TRI-PP-00-36].

S. Dewan, R. Holmes, K. Reiniger and F. Voelker, *High power switch-mode power converters for the 1.4 GeV PS-booster beam transfer lines at CERN, ibid.* 333 [TRI-PP-00-37].

M. Benedikt, A. Blas, J. Borburgh, R. Cappi, M. Chanel, V. Chohan, G. Cyvoct, R. Garoby, D. Grier, J. Gruber, S. Hancock, C.E. Hill, E. Jensen, A. Krusche, M. Lindroos, E. Métral, G. Métral, K.D. Metzmacher, J. Olsfors, J. Pedersen, U. Raich, J.P. Riunaud, J.P. Royer, M. Sassowsky, K. Schindl, H. Schönauer, M. Thivent, H. Ullrich, F. Völker, M. Vretenar, M. Barnes, E. Blackmore, F. Cifarelli, G. Clark, F. Jones, S. Koscielniak, F. Mammarella, A. Mitra, R. Poirier, K. Reiniger and T. Ries, *The PS complex produces the nominal LHC beam, ibid.* 527 [TRI-PP-00-38, CERN-PS-2000-039-OP].

S. Koscielniak, *A precise description of longitudinal motion with synchrotron radiation modelled by "fat photons", ibid.* 637 [TRI-PP-00-39].

R. Cappi, B. Autin, M. Chanel, J. Gareyte, R. Garoby, M. Giovannozzi, H. Haseroth, M. Martini, E. Métral, D. Möhl, K. Schindl, H. Schönauer, I. Hoffmann, C.R. Prior, G.H. Rees and S. Koscielniak, *Design of a 2.2 GeV accumulator and compressor for a neutrino factory, ibid.* 921 [TRI-PP-00-40].

F.W. Jones and H.O. Schönauer, *A method for incorporating image forces in multiparticle tracking with space charge, ibid.* 1381 [TRI-PP-00-41].

A. Blas, S. Hancock, M. Lindroos and S. Koscielniak, *Hollow bunch distributions at high intensity in the PS booster, ibid.* 1528 [TRI-PP-00-42, CERN-PS-2000-040-OP].

F. Schmidt, A. Verdier, L. Jin and D. Kalchev, *Correction of the systematic b_3 error with the resonance-free lattice in the LHC, ibid.* 1561 [TRI-PP-00-43, CERN-LHC-PROJECT-REPORT-401].

S. Hancock, M. Lindroos and S. Koscielniak, *Longitudinal phase space tomography with space charge, ibid.* 1726 [TRI-PP-00-44, CERN-PS-2000-021-RF].

K. Koba, Y. Mori and R. Poirier, *Ultra high gradient rf cavity for the phase rotation, ibid.* 1969 [TRI-PP-00-45].

A.K. Mitra and R.L. Poirier, *High power test of the 35 MHz spiral re-buncher cavity for the TRIUMF ISAC Facility, ibid.* 1978 [TRI-PP-00-46].

M.J. Barnes, G.D. Wait and L. Ducimetière, *Inductance calculations and measurements for the CERN LHC injection pulse forming network, ibid.* 2355 [TRI-PP-00-47].

M.J. Barnes and G.D. Wait, *A FET based mass separator kicker for TRIUMF ISAC project, ibid.* 2376 [TRI-PP-00-48].

P. Gardner and V.J. Verma, *Commercializing research: the leadership challenges for the 21st century, ibid.* 2603 [TRI-PP-00-35].

P. Bricault, G. Dutto, R. Laxdal, A. Mitra, D. Pearce, R. Poirier, P. Schmor, G. Stanford, Y. Bylinsky, A. Feschinko, L. Kravchuk, A. Kvasha, A. Menshov and A. Yasyuchenko, *Status report on the construction of the ISAC drift tube linac*, Proc. **20th Int. Linac Conf. (Linac 2000), Monterey, August 21–25, 2000**, A. Chao, ed. (eConf C000821, 2000) [physics/0008210, SLAC-R-561] p.208.

P. Bricault, *A charge state breeder based on a low frequency RFQ for the ISAC accelerator complex, ibid.* 211.

R.E. Laxdal, P. Bricault, G. Dutto, K. Fong, G.H. Mackenzie, R. Poirier, W. Rawnsley, R. Ruegg and G. Stinson, *First beam test with the ISAC separated function DTL, ibid.* 244.

R.E. Laxdal, R. Baartman, P. Bricault, M. Dombsky, G. Dutto, K. Fong, A. Mitra, R. Poirier, P. Schmor, G. Stanford and A. Facco, *ISAC at TRIUMF: recent achievements and future goals, ibid.* 247.

A.K. Mitra, R.L. Poirier and R.E. Laxdal, *Design of 11.8 MHz buncher for ISAC at TRIUMF, ibid.* 941 [physics/0008213].

R.L. Poirier, R. Baartman, P. Bricault, K. Fong, S. Koscielniak, R. Laxdal, A.K. Mitra, L. Root, G. Stanford and D. Pearce, *CW performance of the TRIUMF 8 meter long RFQ for exotic ions, ibid.* 1023 [TRI-PP-00-71].

S. Hancock, S. Koscielniak and M. Lindroos, *Longitudinal phase space tomography with space charge*, Proc. **6th Int. Computational Accelerator Physics Conf. (ICAP 2000), Darmstadt, September 11–14, 2000**, T. Weiland, ed. (Phys. Rev. ST Accel. & Beams **3**, 2000) p.124202 [TRI-PP-00-69, CERN-PS-2000-068-OP].

Chemistry and Solid-State Physics

J.E. Sonier, R.H. Heffner, D.E. MacLaughlin, J.L. Smith, J. Cooley and G.J. Nieuwenhuys, *Anomalous Knight shift in the superconducting state of UBe_{13}*, Proc. **8th Int. Conf. on Muon Spin Rotation, Relaxation and Resonance (μSR 99), Les Diaberlets, Switzerland, August 30–September 3, 1999** (Physica B **289-290**, 2000) p.20.

M.I. Larkin, Y. Fudamoto, I.M. Gat, A. Kinkhabwala, K.M. Kojima, G.M. Luke, J. Merrin, B. Nachumi, Y.J. Uemura, M. Azuma, T. Saito and M. Takano, *Exponential field distribution in $Sr(Cu_{1-x}Zn_x)_2O_3$, ibid.* 153.

G.M. Kalvius, D.R. Noakes, G. Grosse, W. Schäfer, W. Kockelmann, S. Fredo, I. Halevy and J. Gal, *Magnets frustrated by competing exchange ($TbFe_6Al_6$ and $ErFe_6Al_6$), ibid.* 225.

D.R. Noakes and G.M. Kalvius, *Spin-slip structure induced by the crystalline electric field in the incommensurate magnetic ordering of CePtSn, ibid.* 248.

G.M. Kalvius, A. Kratzer, H. Nakotte, D.R. Noakes, C.E. Stronach and R. Wäppling, *μSR magnetic response of CeCuSn, ibid.* 252.

G.M. Kalvius, A. Kratzer, G. Grosse, D.R. Noakes, R. Wäppling, H. v. Löhneysen, T. Takabatake and Y. Echizen, *The onset of magnetism in $CeNi_{1-x}T_xSn$ (T = Cu, Pt), ibid.* 256.

D.R. Noakes, R. Wäppling, G.M. Kalvius, Y. Andersson, A. Broddefalk, M.F. White and C.E. Stronach, *μSR magnetic response of stoichiometric and non-stoichiometric PrP, ibid.* 303.

A.T. Savici, Y. Fudamoto, I.M. Gat, M.I. Larkin, Y.J. Uemura, G.M. Luke, K.M. Kojima, Y.S. Lee, M.A. Kastner and R.J. Birgenau, *Static magnetism in superconducting stage – 4 La_2CuO_{4+y} (y=0.12), ibid.* 338.

D.R. Harshman, W.J. Kossler, A.J. Greer, C.E. Stronach, E. Koster, B. Hitti, M.K. Wu, D.Y. Chen, F.Z. Chien, H.A. Blackstead and J.D. Dow, *Location of the superconducting hole condensate in $Sr_2YRu_{1-u}Cu_uO_6$ by μ^+SR, ibid.* 360

G.M. Luke, Y. Fudamoto, K.M. Kojima, M.I. Larkin, J. Merrin, B. Nachumi, Y.J. Uemura, J.E. Sonier, T.M. Riseman, Y. Maeno, Z.Q. Mao, Y. Mori and D.F. Agterberg, *Unconventional superconductivity in Sr_2RuO_4, ibid.* 373.

K. Ohishi, K. Kakuta, J. Akimitsu, W. Higemoto, R. Kadono, R.I. Miller, A. Price, R.F. Kiefl, J.E. Sonier, M. Nohara, H. Suzuki and H. Takagi, *Anomalous field dependence of the vortex-core radius and magnetic penetration depth in YNi_2B_2C probed by μSR, ibid.* 377.

Y.J. Uemura, Y. Fudamoto, I.M. Gat, M.I. Larkin, G.M. Luke, J. Merrin, K. Itoh, S. Yamanaka, R.H. Heffner and D.E. MacLaughlin, *μSR studies of intercalated HfNCl superconductors, ibid.* 389.

G.D. Morris and J.H. Brewer, *Spatial distribution of muonium-forming electrons in solid argon, ibid.* 414.

J.H. Brewer, G.D. Morris, D.J. Arseneau, D.G. Eshchenko, V.G. Storchak and J. Bermejo, *Delayed muonium formation in quartz, ibid.*, 425.

J.D. Brewer, J.H. Brewer, G.D. Morris, D.G. Eshchenko and V.G. Storchak, *Electric-field-induced muonium formation in sapphire, ibid.* 428.

K. Ghandi, J.C. Brodovitch, B. Addison-Jones, J. Schüth and P.W Percival, *Hyperfine coupling constants of muonium in sub- and supercritical water, ibid.* 476.

D.J. Arseneau, M. Senba, J.J. Pan and D.G. Fleming, *The rate constant for $Mu + O_2$ addition in competition with rapid spin exchange, ibid.* 503.

R.L. Lichti, S.F.J. Cox, M.R. Dawdy, T.L. Head, B. Hitti, R.J. Molnar, C. Schwab and R.P. Vaudo, *Sites and motion of Mu^- defect centers in n-type gallium nitride, ibid.* 542.

M.R. Dawdy, R.L. Lichti, S.F.J. Cox, T.L. Head and C. Schwab, *Muonium transitions in n-type gallium nitride, ibid.* 546.

B. Hitti, S.R. Kreitzman, R. Lichti, T. Head, T.L. Estle, D. Wynne and E.E. Haller, *Muon dynamics in GaAs lpe lightly doped material: initial RFμSR study, ibid.* 554.

D.G. Fleming, M. Shelley, D.J. Arseneau, M. Senba, J.J. Pan, E. Roduner and S.R. Kreitzman, *Hfcs of the C_6H_6Mu radical in NaY zeolites, ibid.* 603.

R.F. Kiefl, G.D. Morris, P. Amaudruz, R. Baartman, J. Behr, J.H. Brewer, J. Chakhalian, S. Daviel, J. Doornbos, S. Dunsiger, S.R. Kreitzman, T. Kuo, C.D.P. Levy, R.

Miller, M. Olivo, R. Poutissou, G.W. Wight and A. Zelenski, *Complementarity of low-energy spin polarized radioactive nuclei and muons, ibid.* 640.

J. Schüth, P.W. Percival, B. Addison-Jones, J.C. Brodovitch and K. Ghandi, *Zero frequency resonance: another way to measure muon-electron hyperfine constants, ibid.* 681.

D.J. Arseneau, A. Daviel, S.R. Kreitzman and B. Hitti, *The B980: a time-to-digital converter microcoded for μSR, ibid.* 706.

Life Sciences

N. Stevenson, ed. Proc. **Third Int. Conf. on Isotopes (3ICI), Vancouver, September 6–10, 1999** (World Scientific, Singapore, 2000).

J.-M. Poutissou, *Portrait of ISAC the new radioactive beam facility at TRIUMF, ibid.* 3 [TRI-PP-99-53].

L.E. Moritz, *Radiation safety considerations for ISAC, the accelerated radioactive ion beam facility at TRIUMF, ibid.* 256 [TRI-PP-99-54].

M.J. Adam, S. Jivan, J.M. Huser and J. Lu, *C-methylations using tetrabutylammonium fluoride as the base, ibid.* 313 [TRI-PP-99-55].

A. Wong, W.Z. Gelbart, N.R. Stevenson and R. Wong, *Radioisotope production with horizontally-oriented solid targets, ibid.* 387 [TRI-PP-99-56].

R. Wong, W. Gelbart, N.R. Stevenson and A. Wong, *Investigation of thermal-mechanical properties of solid targets for radioisotope production, ibid.* 390 [TRI-PP-99-57].

K.R. Buckley, J.M. Huser, J. Lu, M.J. Adam and T.J. Ruth, *Optimisation of the single pass gas phase synthesis of ^{11}C-methyl bromide from ^{11}C-methane, ibid.* 427 [TRI-PP-99-58].

R. Ruegg, B.F. Milton, D. Dale, D. Bishop, B. Roberts, P.W. Schmor, J. Sredniawski, S. Melnychuk, J. Rathke and E. Kamykowski, *Contraband detection based on $^{13}C(p,\gamma)^{14}N$, ibid.* 447 [TRI-PP-99-59].

M.J. Adam, A. Wong and S.G. Withers, *Synthesis of 6-deoxy-6-[18F]fluoro-2-deoxy-2-fluoro-α-D-glucosyl fluoride as a potential imaging probe for glucocerebrosidase*, Proc. **47th Annual Meeting of the Society of Nuclear Medicine, St. Louis, MO., June 3–7, 2000** (J. Nucl. Med. **41**, 2000) p.124.

M.J. Adam, S. Jivan and J. Lu., *11C-methylations using 11C-methyl iodide and tetrabutylammonium fluoride, ibid.* 244.

Theoretical Program

T.-S. Park, K. Kubodera, D.P. Min and M. Rho, *On making predictions with effective field theories in nuclear physics*, Proc. **INT Workshop on Nuclear Physics with Effective Field Theory, Seattle, WA, February 25–26, 1999**, P.F. Bedaque *et al.*, eds. (World Scientific, Singapore, 2000) p.225 [TRI-PP-99-05, KIAS-P99024, nucl-th/9904053].

H.W. Hammer, *Effective theory for neutron deuteron scattering and the triton, ibid.*, 281 [TRI-PP-99-04, nucl-th/9905036].

R. Lewis and R.M. Woloshyn, *P-wave heavy light mesons using NRQCD and D234*, Proc. **17th Int. Symp. on Lattice Field Theory (Lattice 99), Pisa, Italy, June 29–July 3, 1999** (Nucl. Phys. B Proc. Suppl. **83**, 2000) p.316 [TRI-PP-99-29, hep-lat/9909106].

S.W. Hong and B.K. Jennings, *Quark-meson coupling model for a nucleon by using a density-dependent bag constant*, Proc. **Int. Workshop on the Frontiers in Nuclear Physics, Seoul, February 18–19, 2000**, H. Bhang, M. Fujiwara, B.T. Kim, eds. (Sungkyunkwan Univ. Press, 2000) p.179.

G.C. McLaughlin, *Active sterile neutrino transformation and r-process nucleosynthesis*, Proc. **7th Conf. on Intersections Between Particle and Nuclear Physics (CIPANP 2000), Quebec City, May 22–28, 2000**, Z. Parsa, W.J. Marciano, eds. (AIP **CP 549**, 2000) p.800 [hep-ph/0008211].

Conference Presentations

Particle, Nuclear and Atomic Physics

M. Fujiwara, *Using thin film targets for muonic atoms and muon catalyzed fusion studies*, Proc. **KEK Int. Workshop on High Intensity Muon Sources (HIMUS 99), Tsukuba, December 1–4, 1999**, Y. Kuno, T. Yokoi, eds. (World Scientific, Singapore, in press) [TRI-PP-00-51].

G.C. Ball *et al.* (E823 collaboration), *Tests of the standard model from nuclear beta-decay studies at ISAC*, Proc. **Lake Louise Winter Institute: From Particles to the Universe, Lake Louise, February 20–26, 2000** (World Scientific, Singapore, in press).

G.C. Ball, *The physics program at the ISAC radioactive beam facility at TRIUMF: first results and future plans*, Proc. **ISOLDE Physics Workshop, CERN, March 10–12, 2000**.

G.C. Ball, *Tests of the standard model from superallowed Fermi β-decay studies at ISAC*, Proc. **ACS 219th National Meeting, San Francisco, March 26–30, 2000**.

J. D'Auria, *Astrophysics with a DRAGON at ISAC*, Proc. **5th Int. Conf. on Radioactive Nuclear Beams (RNB5), Divonne, France, April 3–8, 2000** (Nucl. Phys. A, in press) [TRI-PP-00-10].

P. Bricault *et al.*, *TRIUMF-ISAC target station and mass separator commissioning, ibid.* [TRI-PP-00-12].

C.D.P. Levy, R. Baartman, K. Jayamanna, R. Kiefl, T. Kuo, M. Olivo, G.W. Wight, D. Yuan and A.N. Zelenski, *A polarized beams facility at ISAC, ibid.* [TRI-PP-00-13].

P.W. Schmor, *Target handling at high intensity RNB facilities, ibid.* [TRI-PP-00-14].

M. Dombsky *et al.*, *Online isotope separation at ISAC with a 10 μA proton driver beam, ibid.* [TRI-PP-00-15].

R.E. Laxdal, *RNB post-accelerator for ISAC at TRIUMF – present and future, ibid.* [TRI-PP-00-16].

J. D'Auria *et al.*, *Development of detection systems for low-energy heavy ions at DRAGON, ibid.* [TRI-PP-00-17].

M.C. Fujiwara *et al.* (Muonic Hydrogen collaboration), *Time-of-flight spectroscopy of muonic hydrogen atoms and molecules*, Proc. **Hydrogen Atom II – Precise Physics with Simple Atomic Systems, Castiglione della Pescaia, Tuscany, June 1–3, 2000** (Springer, Berlin, in press) [TRI-PP-00-60].

G.C. Ball, *Tests of the standard model from superallowed Fermi β-decay studies at ISAC*, Proc. **CAP Congress, University of York, Toronto, June 4–7, 2000**.

R. Austin, D. Appelbe, G.C. Ball, M. Belleguic, R.M. Clark, J. Duprat, P. Fallon, S. Flibotte, T. Lampman, B. Schaly, C.E. Svensson, J.C. Waddington and D. Ward, *Deformation effects in incomplete fusion reactions, ibid.*

P.P.J. Delheij, *Low temperature nuclear orientation at TRIUMF-ISAC, ibid.*

E.L. Mathie, *Experimental tests of chiral perturbation theory, ibid.*

M. Vetterli, *Overview of spin physics*, Proc. **Int. EuroConference in Quantum Chromodynamics: 15 Years of the QCD (QCD 00), Montpellier, France, July 6–13, 2000** (Nucl. Phys. B, in press).

R. Tacik, *The CNI experiment at TRIUMF*, Proc. **3rd Workshop on Chiral Dynamics – Chiral Dynamics 2000: Theory and Experiment, Newport News, VA, July 17–22, 2000** (in press).

B. Aubert *et al.* (BABAR collaboration), *Measurement of inclusive production of charmonium states in B meson decays*, Proc. **30th Int. Conf. on High-Energy Physics (ICHEP 2000), Osaka, July 27–August 2, 2000** (World Scientific, Singapore, in press) [SLAC-PUB-8526, BABAR-CONF-00-04, hep-ex/0008049].

B. Aubert *et al.* (BABAR collaboration), *Exclusive B decays to charmonium final states, ibid.* [SLAC-PUB-8527, BABAR-CONF-00-05, hep-ex/0008050].

B. Aubert *et al.* (BABAR collaboration), *Measurement of the branching fractions for $B^0 \to D^{*-}\pi^+$ and $B^0 \to D^{*-}\rho^+$, ibid.* [SLAC-PUB-8528, BABAR-CONF-00-06, hep-ex/0008051].

B. Aubert *et al.* (BABAR collaboration), *A measurement of the charged and neutral B meson lifetimes using fully reconstructed decays, ibid.* [SLAC-PUB-8529, BABAR-CONF-00-07, hep-ex/0008060].

B. Aubert *et al.* (BABAR collaboration), *A measurement of the $B^0\bar{B}^0$ oscillation frequency and determination of flavor tagging efficiency using semileptonic and hadronic B^0 decays, ibid.* [SLAC-PUB-8530, BABAR-CONF-00-08, hep-ex/0008052].

B. Aubert *et al.* (BABAR collaboration), *Measurement of the B^0 meson properties using partially reconstructed $B^0 \to D^{*-}\pi^+$ and $B^0 \to D^{*-}\ell^+\nu_\ell$, ibid.* [SLAC-PUB-8531, BABAR-CONF-00-09, hep-ex/0008053].

B. Aubert *et al.* (BABAR collaboration), *Measurement of the time dependence of $B^0\bar{B}^0$ oscillations using inclusive dilepton events, ibid.* [SLAC-PUB-8532, BABAR-CONF-00-10, hep-ex/0008054].

B. Aubert *et al.* (BABAR collaboration), *A measurement of the branching fraction of the exclusive decay $B^0 \to K^{*0}\gamma$, ibid.* [SLAC-PUB-8534, BABAR-CONF-00-12, hep-ex/0008055].

B. Aubert *et al.* (BABAR collaboration), *Study of inclusive $D_s^{(*)\pm}$ production in B decays and measurement of $B^0 \to D^{*-}D_s^{(*)+}$ decays using a partial reconstruction technique, ibid.* [SLAC-PUB-8535, BABAR-CONF-00-13, hep-ex/0008056].

B. Aubert *et al.* (BABAR collaboration), *Measurement of branching fractions for two-body charmless B decays to charged pions and kaons at BABAR, ibid.* [SLAC-PUB-8536, BABAR-CONF-00-14, hep-ex/0008057].

B. Aubert *et al.* (BABAR collaboration), *Measurement of charmless three-body and quasi-two-body B decays, ibid.* [SLAC-PUB-8537, BABAR-CONF-00-15, hep-ex/0008058].

B. Aubert *et al.* (BABAR collaboration), *Search for $B^+ \to K^+\ell^+\ell^-$ and $B^0 \to K^{*0}\ell^+\ell^-$, ibid.* [SLAC-PUB-8538, BABAR-CONF-00-16, hep-ex/0008059].

B. Aubert *et al.* (BABAR collaboration), *The first year of the BABAR experiment at PEP-II, ibid.* [SLAC-PUB-8539, BABAR-CONF-00-17, hep-ex/0012042].

B. Aubert *et al.* (BABAR collaboration), *A study of time dependent CP violating asymmetries in $B^0 \to J/\psi K_s^0$ and $B^0 \to \psi(2S)K_s^0$ decays, ibid.* [SLAC-PUB-8540, BABAR-CONF-00-01, hep-ex/0008048].

A. Piechaczek, E.F. Zganjar, G.C. Ball, B. Bricault, J.A. Macdonald, J. D'Auria, H.-B. Mak, J.R. Leslie, I.S. Towner, M. Lipoglavsek, G. Savard, V. Iacob, J.C. Hardy, J. Wood, D. Kulp, D.M. Moltz and J. Cerny, *Experimental determination of the isospin mixing correction in the ^{74}Rb superallowed β-decay via conversion electron spectroscopy*, Proc. **Nuclear Structure (NS2000), East Lansing, August 15–19, 2000** (Nucl. Phys. A, in press).

E.L. Mathie, *Overview of TRIUMF pion nucleon experiments*, Proc. **8th Int. Oberjoch Meeting on Broken Symmetries and Meson Nuclear Physics, Oberjoch, Germany, September 4–9, 2000**.

H. Denz, *Pion proton cross sections in the Coulomb nuclear interference region, ibid.*

E. Fragiacomo, *Scalar pion pairs in nuclear matter, ibid.*

R. Tacik, *Evidence for a three nucleon reaction mechanism in pion nucleus DCX, ibid.*

J. Wendland, *Spin asymmetries*, Proc. **Hadron Structure 2000 (HS2000), Stara Lesna, Slovak Republic, October 2–8, 2000**.

W.T.H. van Oers, *Constraints of a parity-conserving/time-reversal-non-conserving interaction*, Proc. **14th Int. Spin Physics Symp. (SPIN 2000), Osaka, October 16–21, 2000** (AIP, New York, in press) [TRI-PP-00-66].

G.C. Ball *et al.* (E823 collaboration), *Tests of the standard model from superallowed Fermi β-decay studies at ISAC*, Proc. **16th Int. Conf. on the Application of Accelerators in Research and Industry (CAARI 2000), Denton, TX, November 1–4, 2000** (AIP Conf. Proc., in press).

G.C. Ball, *Tests of the standard model from superallowed Fermi β-decay studies at ISAC*, **Pacifichem 2000, Honolulu, December 14–19, 2000**.

Instrumentation/Accelerator Physics/Computing Sciences

H. Schonauer, B. Autin, R. Cappi, M. Chanel, G. Franchetti, J. Gareyte, R. Garoby, H. Haseroth, M. Martini, E. Metral, D. Mohl, K. Schindl, W. Pirkl, G.H. Rees, C. Prior, I. Hofmann, S. Koscielniak, K. Bongardt and Yu. Senichev, *Proton drivers for neutrino factories: the CERN approach*, Proc. **Int. Workshop, Muon Storage Ring for a Neutrino Factory (NuFACT'00), Monterey, May 22–26, 2000**, S. Chattopadhyay, ed. (Elsevier, Amsterdam, in press) [CERN-PS-2000-065-PP, CERN-NUFACT-NOTE-46].

R. Helmer, *Status of the Sudbury Neutrino Observatory*, Proc. **6th Int. Workshop on Tau Lepton Physics (TAU 2000), Victoria, B.C., September 18–21, 2000** (Nucl. Phys. B, Proc. Supp., in press).

E. Fosshag, M. Hecht, K.R. Buckley, D.W. Becker, K. Jayamanna, J.M. D'Auria, J.S. Vincent and T.J. Ruth, *A target system for the production of ^{15}O beams for ISAC*, Proc. **Int. Nuclear Target Development Society, Belgium, October, 2000** (Nucl. Instrum. Methods, in press).

G.D. Morris, *Applications of β-NMR in materials science*, Proc. **RIA Applications Workshop, Los Alamos, October 29–30, 2000**.

P. Bricault, *Status report on the ISAC radioactive beam facility*, Proc. **16th Int. Conf. on the Application of Accelerators in Research and Industry (CAARI 2000), Denton, TX, November 1–4, 2000** (AIP Conf. Proc., in press).

Life Sciences

V. Sossi, P. Cohen, B. Pointon, R.R. Johnson and T.J. Ruth, *Dual head coincidence cameras: challenges imposed by count rate limitations and open geometry*, Proc. **Canadian Society of Nuclear Medicine, Mont Tremblant, Que., April, 2000**.

P. Cohen, V. Sossi, R.R. Johnson, T. Ruth, D. Lyster and D. Mankoff, *Coincidence PET scanning with the first Canadian coincidence dual SPECT/PET system, ibid.*

C.S. Lee, R. de la Fuente-Fernandez, V. Sossi, T.J. Ruth, M. Schulzer, J.E. Holden, D.B. Calne and A.J. Stoessl, *In-vivo PET studies in normal human subjects show that ratios of DAT to VMAT2 in the striatum decrease with a rostrocaudal gradient and also with aging: implications for the pathogenesis of Parkinson's disease*, Proc. **American Academy of Neurology, San Diego, May, 2000**.

M.J. Adam, A. Wong and S.G. Withers, *Synthesis of 6-deoxy-6-[18F]fluoro-2-deoxy-2-fluoro-α-D-glucosyl fluoride as a potential imaging probe for glucocerebrosidase*, **4th Int. Symp. Radiohalogens, Whistler, B.C., September 9–13, 2000**.for AR01

M.J. Adam, H. Adomat, K. Skov and C. Koch, *18F-EF5, a new PET agent with potential for hypoxia imaging, ibid.*

M.J. Adam, *Radiohalogenated carbohydrates as potential imaging agents for PET and SPECT, ibid.*

H. Dougan, J.I. Weitz, J.B. Hobbs, D.M. Lyster, P. Klement, K.D. Gillespie, A.R. Stafford, C.V. Vo and R. MacDonald, *Radiohalogenated DNA aptamers, ibid.*

V. Sossi, B. Pointon, C. Boudoux, P. Cohen, K. Hudkins, S. Jivan, K. Nitzek, J. deRosario, C. Stevens and T.J. Ruth, *NEMA NU 2-2000 performance measurements on an ADAC MCD camera*, Proc. **IEEE Nuclear Science Symp. and Medical Imaging Conf., Lyon, France, October 15–20, 2000** (IEEE Trans. Med. Imaging, in press).

B. Pointon and V. Sossi, *Monte Carlo investigation of scatter in dual head coincidence imaging, ibid.*

T.J. Ruth, *The production of ultra high quantities of ^{18}F-fluoride: a work in progress*, Proc. **16th Int. Conf. on the Application of Accelerators in Research and Industry (CAARI 2000), Denton, TX, November 1–4, 2000** (AIP Conf. Proc., in press).

M.J. Adam, A.W. Wong and S. Withers, *18F-labelled 2-deoxy-2-fluoro-α-D-glucosyl fluoride derivatives as potential imaging probes for glucocerebrosidase*, **Pacifichem 2000, Honolulu, December 14–19, 2000**.

J.S. Vincent, A. Zyuzin, J. D'Auria, T. Ruth, D. Ottewell and D. Harshman, *Feasibility of ^{125}Xe implantation for brachytherapy, ibid.*

Theoretical Program

T. Schäfer, *Color superconductivity*, Proc. **10th Int. Conf. on Recent Progress in Many-Body Theories (MBX), Seattle, WA, September 10–15, 1999**, R.F. Bishop *et al.*, eds. (World Scientific, Singapore, in press) [TRI-PP-99-38, nucl-th/9911017].

S. Kondratyuk and O. Scholten, *Nucleon dressing from dispersion relations*, Proc. **Int. Conf. on Quark Nuclear Physics (QNP 2000), Adelaide, Australia, February 21–25, 2000** (Nucl. Phys., in press).

T.-S. Park, K. Kubodera, D.P. Min and M. Rho, *Effective field theory for nuclei: confronting fundamental questions in astrophysics*, Proc. **XVIth Int. Conf. on Few-Body Problems in Physics, Taipei, March 6–10, 2000** (Nucl. Phys. A, in press) [TRI-PP-00-25, nucl-th/0005069].

W.T.H. van Oers, *Symmetries and symmetry breaking, ibid.* [TRI-PP-00-27, hep-ph/0006058].

L. Canton, G. Pisent, W. Schadow and J.P. Svenne, *Spin observables for pion production from pd collisions, ibid.* [TRI-PP-00-28, nucl-th/0006027].

H.W. Fearing, Th.R. Hemmert, R. Lewis and C. Unkmeir, *Charged radiative pion capture on the nucleon in heavy baryon chiral perturbation theory, ibid.* [TRI-PP-00-30, hep-ph/0007090].

S. Scherer and H.W. Fearing, *A simple model illustrating the impossibility of measuring off-shell effects, ibid.* [MKPH-T-00-11, TRI-PP-00-31, nucl-th/0006076].

E. Truhlik and F.C. Khanna, *Lepton $U_l 1$ symmetry and interaction of neutrinos with deuterons at high-energies, ibid.* [nucl-th/0007037].

F.C. Khanna and A.E. Santana, *Topics in thermal field theory*, Proc. **2nd Int. School on Field Theory and Gravitation, Vitoria, Brazil, April 25–28, 2000**, C. Pinheiro, A.J. Helayal Neto and G.O. Pires, eds. (Springer Verlag, in press).

J. Escher, *Partial dynamical symmetry in a fermionic many-body system*, Proc. **Bologna 2000: Structure of the Nucleus at the Dawn of the Century, Bologna, May 29–June 3, 2000** (Supp. Czech J. Phys., in press) [TRI-PP-00-56, nucl-th/0008069].

R.M. Woloshyn, *Charmed baryons from lattice QCD*, Proc. **4th Int. Conf. on Hyperons, Charm and Beauty Hadrons, Valencia, Spain, June 27–30, 2000** (Nucl. Phys. Proc. Suppl., in press) [TRI-PP-00-58, hep-ph/0009332].

R. Lewis and R.M. Woloshyn, *The charmed and bottom meson spectrum from lattice NRQCD, ibid.* [hep-ph/0010013].

H.W. Fearing, T.R. Hemmert, R. Lewis and C. Unkmeir, *Radiative pion capture in ChPT*, Proc. **3rd Workshop on Chiral Dynamics – Chiral Dynamics 2000: Theory and Experiment, Newport News, VA, July 17–22, 2000** (in press).

J. Escher, *Partial dynamical symmetry in an interacting fermion system*, Proc. **Int. Conf. Symmetries and Spin (PRAHA-SPIN-2000), Prague, July 17–22, 2000** (Czech. J. Phys., in press) [TRI-PP-00-59].

R. Gupta and K. Maltman, *Status report on lattice QCD and QCD sum rule determinations of the light quark masses*, Proc. **Meeting of the Division of Particles and Fields of the American Physical Society (DPF 2000), Columbus, August 9–12, 2000** (World Scientific IJMP, in press).

N. Mathur *et al.* (Kentucky Field Theory collaboration), *Strange magnetic moment of the nucleon from lattice QCD*, Proc. **18th Int. Symp. on Lattice Field Theory (Lattice 2000), Bangalore, India, August 17–22, 2000** (Nucl. Phys. Proc. Suppl., in press) [TRI-PP-00-61, hep-lat/0011015].

R. Lewis and R.M. Woloshyn, *Heavy light meson spectrum with and without NRQCD, ibid.* [hep-lat/0010001].

L. Canton, *Three-nucleon portrait with pion*, Proc. **8th Convegno su Problemi di Fisica Nucleare Teorica, Cortona, Italy, October 18–21, 2000** (World Scientific, Singapore, in press) [TRI-PP-00-63].

Technology Transfer

P.L. Gardner, *Technology transfer: internal and international perspectives*, Proc. **Society of Research Adminstrators, Portland, OR, March, 2000**.

Books

I.J. Bingham, A.D.M. Glass, H.J. Kronzucker, D. Robinson and C.M. Scrimgeour, *Isotope techniques*, in Root Methods: a Handbook, A.L. Smith *et al.*, eds. (Springer-Verlag, New York, 2000) p.365.

M.K. Craddock, *Cyclotrons*, in McGraw-Hill Encyclopedia of Science and Technology, 9th Edition (McGraw-Hill, New York, in press).

J.W. Negele and E. Vogt, eds., Advances in Nuclear Physics (Kluwer Academic/Plenum, New York, 2000).

S. Karataglidis, *Nucleon-nucleus scattering: a microscopic nonrelativistic approach, ibid.* p.276.

J.E. Holden, V. Sossi, G. Chan, D.J. Doudet, A.J. Stoessl and T.J. Ruth, *Effect of population k2 values in graphical estimation of DV ratios of reversible ligands*, in Molecular and Pharmacological Brain Imaging, A. Gjedde, S.B. Hansen, G. Moos Knudsen, eds. (Academic Press, 2000) p.127.

V. Sossi, J.E. Holden, G. Chan, M. Krzywinski, A.J. Stoessl and T.J. Ruth, *Measuring the BP of four dopaminergic tracers utilizing a tissue input function, ibid.* 131.

V. Sossi, J.E. Holden, G. Chan, M. Krzywinski, A.J. Stoessl and T.J. Ruth, *Measuring the BP of four dopaminergic tracers utilizing a tissue input function*, in Quantification of Brain Function Using PET (Academic Press, 2000).

Theses

C.U. Jackson, *Muon spin rotation (μSR) study of the anomalous f-electron compound Ce_7Ni_3* (M.Sc., Physics, Virginia State University).

D.G. Melconian, *A positron detector for precision beta decay experiments from a magneto-optic trap* (M.Sc., Physics, Simon Fraser University).

F. Sobratee, *M11 at TRIUMF, another surface muon source* (M.Sc., Physics, University of Alberta).

A. Wong and R. Wong, *Design and improvement of the solid target station and radioisotope production system* (M.Sc., Mechanical Engineering, University of British Columbia).

B. Addison-Jones, *Muon spin resonance studies of fullerenyl radicals and associated organic radicals* (Ph.D., Chemistry, Simon Fraser University).

P.C. Bergbusch, *Measurement of the decay $K^+ \to \pi^+\nu\bar{\nu}$* (Ph.D., Physics and Astronomy, University of British Columbia).

J.C. Chow, *The β-delayed 3-body breakup of ^{17}Ne and its relation to astrophysics* (Ph.D., Physics, University of Toronto).

S.R. Dunsiger, *Spin relaxation in geometrically frustrated pyrochlores*, (Ph.D., Physics, University of British Columbia).

Y. Fudamoto, *Anomalous magnetic phase transitions in the quasi-one-dimensional systems NaV_2O_5 and Cu_3WO_6 detected by muon spin relaxation* (Ph.D., Physics, Columbia University).

M. Landry, *Microstrip gas detectors and a search for Xi-hypernuclei* (Ph.D., Physics, University of Manitoba).

M.I. Larkin, *Evolution of the ground state in two leg spin ladder system $SrCu_2O_3$ upon (Cu,Zn) substitution* (Ph.D., Physics, Columbia University).

A. Toyoda, *Studies of muon-catalyzed fusion in ortho-para controlled solid D_2* (Ph.D., Physics, University of Tokyo).

Appendix B

SEMINARS*

The following seminars were presented at TRIUMF this year.

06/01 *A New Proposal for a Precision Measurement of the Muon Lifetime*, David Hertzog, U. Illinois at U-C.
07/01 *New Results on the Muon Anomalous Magnetic Moment*, David Hertzog, U. Illinois at Urbana-Champaign.
10/01 *Early Data from BELLE*, Daniel Marlow, Princeton U.
11/01 *Ground-Based Gamma Ray Astronomy with STACEE*, Ken Ragan, McGill U.
12/01 *New Results from E787*, Paul Bergbusch, UBC.
18/01 *Effective Field Theory for Two Nucleons*, Thomas Mehen, Caltech.
20/01 *Electron Neutrino Studies with ^{100}Mo by Double-Beta Decays and Solar ν Induced Inverse-Beta Decays*, Hiro Ejiri, U. Washington.
25/01 *New CLEO Results on Rare and Radiative B Decays*, Vladimir Savinov, SLAC.
01/02 *Few-Body Nuclear Physics in the Big Bang*, Ken Nollett, U. Chicago.
03/02 *Neutrino Flavour Mixing: Theory and Phenomenology*, Christian Cardall, SUNY at Stonybrook.
11/02 *KEK-Tanashi Short Lived Nuclear Beam Facility*, Ichiro Katayama, KEK Tanashi.
15/02 *Photoproduction of Pseudoscalar Mesons from Nuclei*, Laith Abu-Raddad, Florida State U.
16/02 *Solar Neutrinos and Neutral Current Detection at SNO*, Steve Elliot, U. Washington.
17/02 *Isotope Shift Measurements in Neutron Deficient Francium Atoms*, Matt Pearson, SUNY at Stonybrook.
18/02 *Effective Field Theory for Two-Nucleon Systems*, Gautam Rupak, U. Washington.
21/02 *Characterization and Control of Ultracold Collisions*, Steve Gensemer, U. Connecticut.
29/02 *Measurements of $|V_{cs}|$ in W Decays with the OPAL Detector*, Alain Bellerive, U. Chicago.
02/03 *Low-Energy Manifestations of Supersymmetry*, Hitoshi Murayama, U. California, Berkeley.
03/03 *Neutrino Currents in Supernova Core*, Gang Li, Indiana U.
16/03 *Experimental Studies of the Coulomb Dissociation of the Radioactive Beam Boron-8*, Brad Davids, MSU/NSCL.
17/03 *New Particles and Physics at the Energy Frontier*, Rick Van Kooten, Indiana U.
23/03 *PRISM*, Noboru Sasao, U. Kyoto.
30/03 *Measurements of Muon Catalyzed Fusion in Solid HD*, Tracy Porcelli, UNBC.
07/04 *Neutrino Factories: A New Tool for Physics*, Steve Geer, Fermilab.
13/04 *Pion Physics*, Gerhard Wagner, U. Tübingen.
02/05 *Mini Review on OZI Violation and the Role of Strangeness in Proton-Antiproton Annihilation at Rest*, Milan Locher, PSI and U. Zürich.
04/05 *(Mostly) Nuclear Astrophysics and (a Little) Weak Interactions Using Radioactive Beams at TAMU*, Bob Tribble, Texas A&M U.
11/05 *Still Flat After All These Years*, Douglas Scott, UBC.
15/05 *Ultra-Sensitive Detection by Laser Spectroscopy*, H.A. Schuessler, Texas A&M U.
19/05 *Circular Rydberg States and Quantum Entanglement Experiments*, Sihong Gu, Max-Planck-Institut für Quantenoptik, U. München.
23/05 *Director Search Public Lecture*, Pekka Sinervo, U. Toronto.
29/05 *The Proton Drivers for the CERN Neutrino Factory Study*, Horst Schoenauer, CERN.
01/06 *Recent Progress in AMS at IsoTrace*, Ted Litherland, U. Toronto.
19/06 *Director Search Public Lecture, TRIUMF: Nuclear Astrophysics and Beyond*, Alan Shotter, U. Edinburgh.
21/06 *Director Search Public Lecture, Three Generations of Quarks and Leptons: Who Ordered That?*, Douglas Bryman, UBC.
28/06 *Bose Einstein Condensation and Ultracold Molecules*, Roahn Wynar, U. Texas at Austin.
10/07 *Stochastic Cooling: History & Recent Results*, Fritz Caspers, CERN.
12/07 *RIA: The Next Generation Radioactive Beams Project in the USA*, Guy Savard, ANL.
13/07 *The KARMEN Time Anomaly: Search for a Neutral Particle of Mass 33.9 MeV in Pion Decay*, Jason Koglin, U. Virginia.
20/07 *Large Extra Dimensions and Neutrinos*, Gail McLaughlin, TRIUMF.
27/07 *Search for Neutralino Dark Matter and the PICASSO project*, Viktor Zacekv, U. Montréal.
28/07 *Measurement of the Parity-Violating Asymmetry in the Scattering of Polarized Electrons from Protons*, Gary Rutledge, College of William & Mary.
04/08 *Charge Symmetry Breaking in $np \to \pi^0$ and QCD*, Ubirajara van Kolck, Caltech/U. Arizona.
10/08 *Selected Weak Interactions in Hadrons and Nuclei with Effective Field Theory*, Roxanne Springer, Duke U.
15/08 *Effective Field Theory at Finite Density: Dilute Fermi Systems*, Hans Hammer, Ohio State U.
17/08 *The CDF Silicon Tracker for the Tevatron Run II*, Igor Volobouev, LBNL.

11/09 *Study of the Light Meson Spectroscopy at BNL E852*, Jingliang Hu, Jefferson Lab.
14/09 *LIGO and Prospects for Detection of Gravitational Waves*, Barry Barish, Caltech.
15/09 *The Mystery of Ultrahigh Energy Cosmic Rays: Exotic and Not-So-Exotic Hypotheses and the Pierre Auger Observatory*, John Swain, Northeastern U.
21/09 *Measurement of the Pion Light-Cone Wave Function*, Danny Ashery, Tel-Aviv U.
06/10 *The Parton Model and the Mossbauer Effect – From Crystals with Synchrotron Radiation to Heavy Quarks*, Harry Lipkin, Weizmann Inst.
12/10 *Clustering in Nuclei: Nuclear Chains, Nuclear Molecules, and Other Exotic States of Nuclear Matter*, Brian Fulton, York U.
16/10 *Problems in Treatment of Fields with Spin 3/2 and Higher*, Vladimir Pascalutsa, U. Flinders.
24/10 *Nuclear Astrophysics at the Ruhr-Universität Bochum: Direct Measurements of Important Nuclear Reaction Cross Sections*, Frank Strieder, U. Bochum.
26/10 *A Covariant Model of Pion-Nucleon Scattering*, Andrew Lahiff, TRIUMF.
03/11 *ISOLDE: Present Status and Future Plans*, Mats Lindroos, CERN.
06/11 *Energy Measurement in the Forward Region of the ATLAS Detector at LHC*, Peter Loch, U. Arizona.
08/11 *Latest Developments at the RIB Cyclotron Facility in Louvain La Neuve*, Marc Loiselet, U. Catholique de Louvain.
09/11 *40 Years of Nuclear Parity Violation*, Barry Holstein, U. Massachusetts.
24/11 *A Physics Program Based on a New Asymmetrical $e-p$ Collider in the Energy Regime $1.4 < \sqrt{s} < 2.5$ GeV*, Rinaldo Baldini, INFN-LNF.
29/11 *Development, Operation, and Applications of the National Accelerator Centre Cyclotrons*, Lowry Conradie, NAC Laboratory, Cape Town.
30/11 *A 2nd Generation Long Baseline Neutrino Experiment – Neutrino Program at JHF*, Akira Konaka, TRIUMF.
14/12 *QCD Results from LEP*, Hasko Stenzal, Max-Planck-Institut, München.

The following lunchtime seminars were presented at TRIUMF this year.

09/06 *Neutrino Experiment at JHF*, Akira Konaka, TRIUMF.
07/09 *Beta-NMR at ISAC*, Gerald Morris, TRIUMF/UBC.
06/11 *Report on the IEEE Nuclear Science Symposium and Medical Imaging Conference – Detector Developments and Data Acquisition*, Joel Rogers and Renée Poutissou, TRIUMF.

---

* All matters concerning TRIUMF seminars should be referred via e-mail to seminar@triumf.ca

The latest listing of TRIUMF seminars can be seen at http://www.triumf.ca/seminars/

Appendix C

USERS GROUPS

TRIUMF USERS' GROUP

From the TRIUMF Users' Group Charter:

The TRIUMF Users' Group is an organization of scientists and engineers with special interest in the use of the TRIUMF facility. Its purpose is:

(a) to provide a formal means for exchange of information relating to the development and use of the facility;

(b) to advise members of the entire TRIUMF organization of projects and facilities available;

(c) to provide an entity responsive to the representations of its members for offering advice and counsel to the TRIUMF management on operating policy and facilities.

Membership of the TRIUMF Users' Group (TUG) is open to all scientists and engineers interested in the TRIUMF program.

At the end of 2000, following a mandatory membership renewal in which members were asked to provide more detailed information about their interests and affiliations, TUG had 235 newly reconfirmed members from 11 countries.

TRIUMF Users' Executive Committee (TUEC)

The TRIUMF Users' Executive Committee (TUEC) is a committee of elected members whose role is to represent the interests of TUG to the TRIUMF administration.

Among other things, TUEC maintains the TUG Web site at http://www.triumf.ca/tug/ where detailed information is available about its membership, that of related committees, and various TUG activities.

TUEC Membership for 2000

J.H. Brewer	UBC	*Chair*
N. Rodning	U. Alberta	*Chair-elect*
J.M. D'Auria	SFU	*Past-chair*
G.M. Marshall	TRIUMF	1999/2000
B. Turrell	UBC	1999/2000
R. Helmer	TRIUMF	2000/2001
A.K. Opper	Ohio U.	2000/2001
M. Comyn	TRIUMF	*Liaison Officer*

G.M. Luke (McMaster U.) was elected as chair-elect for 2001. G.D. Morris (TRIUMF) and W.D. Ramsay (U. Manitoba) were elected as members for 2001/2002.

In addition, TUEC selected two members to represent the Users on the TRIUMF Operating Committee: J. Vincent (TRIUMF) and E. Mathie (U. Regina) with alternates G.M. Marshall (TRIUMF) and G.M. Luke (McMaster U.), respectively. G.M. Marshall replaced J. Vincent in mid-2000 with S. Yen (TRIUMF) becoming the alternate.

User Survey

Results of the Web-based survey of User interests and priorities conducted in conjunction with the mandatory 2000 membership renewal can be viewed at http://www.triumf.ca/tug/new/tugstats.php . The results at year end were:

Number with non-blank *topics*: 223
Number with non-blank *facil*: 178
Number with non-zero *OffSite* research: 145
Average *OffSite* = 70.8%
Total *OffSite* FTE = 102.6

Research Topics

Topic	# listed in *topics*	# with non-zero %	Average non-zero %	Total FTE
Sym	63	69	35.5	24.5
HEP	50	51	56.7	28.9
IEP	60	62	43.8	27.2
LENP	72	76	39.1	29.7
NAP	60	64	46.2	29.6
Acc	34	35	43.6	15.3
CMP	50	52	57.4	29.8
Chem	34	37	45.8	16.9
Life	24	25	50.8	12.7
Appl	37	37	59.2	21.9
Eng	20	21	29.3	6.2
OthTop	23	23	49.9	11.5

where

Sym	=	fundamental symmetries
HEP	=	high energy (> 10 GeV) particle physics
IEP	=	int. energy (< 10 GeV) particle physics
LENP	=	low energy nuclear physics
NAP	=	nuclear astrophysics
Acc	=	accelerator physics
CMP	=	condensed matter physics
Chem	=	atomic physics and chemistry
Life	=	life sciences
Appl	=	applied program
Eng	=	engineering
OthTop	=	other topic

TRIUMF Facilities

Facility	# listed in *facil*	# with non-zero %	Average non-zero %	Total FTE
CHAOS	12	12	68.8	8.3
TWIST	21	23	58.7	13.5
pPol	11	11	43.9	4.8
pSpect	8	8	46.3	3.7
pThpy	14	14	63.9	9.0
Isot	13	13	78.8	10.3
LEISAC	32	33	51.2	16.9
HEISAC	30	32	55.0	17.6
TRINAT	11	12	46.9	5.6
muSR	38	40	75.3	30.1
bNMR	14	16	29.4	4.7
LTNO	12	12	86.7	10.4
Det	30	32	40.8	13.1
AccTech	16	16	30.9	5.0
Comp	46	47	58.7	27.6
OthFac	31	33	66.2	21.9

where

CHAOS	=	CHAOS pion spectrometer
TWIST	=	TRIUMF Weak Int. Symmetry Test
pPol	=	polarized proton beams
pSpect	=	proton spectrometers (MRS, SASP)
pThpy	=	proton therapy (BL1B)
Isot	=	isotope production (medical & other)
LEISAC	=	Low Energy ISAC spectrom. + TISOL
HEISAC	=	High E ISAC (*e.g.* DRAGON, TUDA)
TRINAT	=	TRIUMF Neutral Atom Trap
muSR	=	μSR User Facility
bNMR	=	β-NMR facility
LTNO	=	Low Temp. Nuclear Orientation
Det	=	detector construction (incl. scint.)
AccTech	=	accelerator technology
Comp	=	TRIUMF computing facilities (DAC)
OthFac	=	other facilities at TRIUMF

μSR USERS GROUP

Full details regarding the μSR Users Group and μSR facilities can be obtained via the WWW at http://musr.triumf.ca/users/.

Appendix D

EXPERIMENT PROPOSALS

The following lists experiment proposals received up to the end of 2000 (missing numbers cover proposals that have been withdrawn or replaced by later versions, rejected, or combined with another proposal). Experiments 1–699 are omitted from this listing (except for those reporting results in this Annual Report). Please refer to the 1999 Annual Report or see http://www.triumf.ca/annrep/experiments.html for a full listing of these earlier experiments. Page numbers are given for those experiments which are included in this Annual Report. Page

497. Measurement of the flavour-conserving hadronic weak interaction [completed data-taking], J. Birchall, J. Bland, J.R. Campbell, A.A. Green, L. Lee, S.A. Page, W.D. Ramsay, S.D. Reitzner, A.M. Sekulovich, V. Sum, W.T.H. van Oers, R.J. Woo *(U. Manitoba)*, C.A. Davis, D.C. Healey, R. Helmer, W. Kellner, R. Laxdal, C.D.P. Levy, P.W. Schmor *(TRIUMF)*, P.W. Green, G. Roy, J. Soukup, T. Stocki, G.M. Stinson *(U. Alberta)*, J.D. Bowman, R.E. Mischke *(Los Alamos Nat. Lab)*, Y. Kuznetsov, N.A. Titov, S. Zadorozhny, A.N. Zelenski *(INR Moscow)*, A.A. Hamian *(U. Washington)*, A.R. Berdoz *(Carnegie Mellon U.)* 5

614. Precise measurement of the ρ, σ and $(P_\mu\xi)$ parameters in muon decay [active], M. Comyn, D.R. Gill, P. Gumplinger, R. Helmer, R. Henderson, J.A. Macdonald, A. Olin, J.-M. Poutissou, R. Poutissou, H.-C. Walter D. Wright *(TRIUMF)*, P. Depommier *(U. Montréal)*, P. Green, P. Kitching, M. Quraan, R. MacDonald, N. Rodning, F. Sobratee, G.M. Stinson *(U. Alberta)*, M. Hasinoff *(UBC)*, E.L. Mathie, R. Tacik *(U. Regina)*, W. Shin *(U. Saskatchewan)*, E. Korkmaz, T. Porcelli *(UNBC)* Y. Davydov *(JINR, Moscow)*, C. Gagliardi, J. Hardy, J. Musser, R. Tribble, M. Vasiliev *(Texas A&M U.)*, D. Koetke, R. Manweiler, P. Nord, S. Stanislaus *(Valparaiso U.)*, Y. Davydov , A. Khruchinsky, V. Selivanov, V. Torokhov *(KIAE, Moscow)* 10

684. μSR spin relaxation studies of small molecules in the gas phase [active], D. Arseneau, J. Pan, *(TRIUMF)*, D. Fleming *(UBC)*, M. Senba *(Dalhousie U.)*, T. Claxton *(U. Leicester)*, S.F.J. Cox *(Rutherford Appleton Lab.)*, U. Himmer, E. Roduner *(U. Stuttgart)* 59

700. Measuring cross sections of long-lived radionuclides produced by 200-500 MeV protons in elements found in meteorites and lunar rocks [active], J. Vincent *(TRIUMF)*, J.M. Sisterson *(Harvard U.)*, K. Kim *(San Jose State U.)*, A.J.T. Jull *(U. Arizona)*, M.W. Caffee *(Lawrence Livermore National Lab)*, R.C. Reedy *(Los Alamos Nat. Lab)*

702. Measurement of kaon-nucleon elastic scattering at 16 MeV [active], G.A. Beer, P. Knowles, G.R. Mason, A. Olin, L.P. Robertson *(U. Victoria)*, P. Amaudruz, D.R. Gill, G. Smith, S. Yen *(TRIUMF)*, L. Lee *(U. Manitoba)*, G. Tagliente *(UBC)*

703. Study of the decay $\pi^+ \to e^+\nu$ phase I – lifetime measurement of the pion [active], D.A. Bryman, T. Numao, A. Olin *(TRIUMF)*

704. Charge symmetry breaking in $np \to d\pi^0$ close to threshold [active], R. Abegg*, P.W. Green, D.A. Hutcheon *(TRIUMF–U. Alberta)*, L.G. Greeniaus *(U. Alberta–TRIUMF)*, R.W. Finlay, A.K. Opper, S.D. Reitzner *(Ohio U.)*, E. Korkmaz, T.A. Porcelli *(UNBC)*, J.A. Niskanen *(U. Helsinki)*, P. Walden *(TRIUMF–UBC)*, S. Yen *(TRIUMF)*, C.A. Davis *(TRIUMF–U. Manitoba)*, D.V. Jordan *(Ohio U.–U. Alberta)*, E. Auld *(UBC)* 35

705. Development of modular gas microstrip chambers as in-target tracking devices for an experiment to detect $\Lambda\Lambda$ hypernuclei at the BNL AGS (BNL885) [completed data-taking], C.A. Davis *(TRIUMF–U. Manitoba)*, B. Bassalleck, R. Stotzer *(U. New Mexico)*, A.R. Berdoz, A. Biglan, D.S. Carman, G.B. Franklin, P. Khaustov, P. Koran, R. Magahiz, R. McCrady, C.A. Meyer, K. Paschke, B. Quinn, R.A. Schumacher, *(Carnegie-Mellon U.)*, J. Birchall, L. Gan, M.R. Landry, L. Lee, S.A. Page, W.D. Ramsay, W.T.H. van Oers *(U. Manitoba)*, T. Bürger, H. Fischer, J. Franz, H. Schmitt *(U. Freiburg)*, D.E. Alburger, R.E. Chrien, M. May, P.H. Pile, A. Rusek, R. Sawafta, R. Sutter *(Brookhaven National Lab)*, A. Ichikawa, K. Imai, Y. Kondo, K. Yamamoto, M. Yosoi *(Kyoto U.)*, F. Takeutchi *(Kyoto Sangyo U.)*, V.J. Zeps *(U. Kentucky)*, P.D. Barnes, F. Merrill *(Los Alamos Nat. Lab)*, V.J. Zeps *(U. Kentucky)*, T. Iijima *(KEK)*, J. Lowe *(U. Birmingham)*

706. μSR studies of spin fluctuations in $CePt_2Sn_2$ and other Kondo spin systems [active], A. Keren, K. Kojima, G.M. Luke, Y.J. Uemura, W.D. Wu *(Columbia U.)*, K. Andres, G.M. Kalvius *(Tech. U. Munich)*, H. Fujii, G. Nakamoto, T. Takabatake, H. Tanaka *(Hiroshima U.)*, M. Ishikawa *(ISSP, U. Tokyo)*, B. Andraka *(U. Florida)*, D.L. Cox *(Ohio State U.)*

707. μSR measurements on two-dimensional site-diluted antiferromagnets [active], K. Kojima *(Columbia U.–U. Tokyo)*, A. Keren, G.M. Luke, Y.J. Uemura, W.D. Wu *(Columbia U.)*, H. Ikeda *(KEK–KENS)*, R.J. Birgeneau *(MIT)*, K. Nagamine *(U. Tokyo)*

708. The spin relaxation and chemical reactivity of muonium-substituted organic radicals in the gas phase [active], D.G. Fleming, J.J. Pan, M. Shelley *(UBC)*, D.J. Arseneau *(TRIUMF–UBC)*, M. Senba *(TRIUMF)*, J.C. Brodovitch, P.W. Percival *(SFU)*, H. Dilger, E. Roduner *(U. Zürich)*, S.F.J. Cox *(Rutherford Appleton Lab)*

709. ^{90,92,94,96}Zr$(n,p)^{90,92,94,96}$Y reaction at 200 MeV [active], A.G. Ling, P.L. Walden *(TRIUMF)*, J. Rapaport *(Ohio U.)*, D.A. Cooper, D.L. Prout, E.R. Sugarbaker *(Ohio State U.)*, M. Halbert *(Oak Ridge National Lab)*, D. Mercer *(U. Colorado)*, J. Campbell *(U. Manitoba–TRIUMF)*, M. Hartig *(U. Muenster)*

710. Dynamics of muonium in Ge and GaAs [completed data-taking], R.L. Lichti *(Texas Tech. U.)*, S.F.J. Cox *(Rutherford Appleton Lab)*, R.F. Kiefl *(UBC)*, K.H. Chow *(Lehigh U.)*, T.L. Estle *(Rice U.)*, B. Hitti *(TRIUMF)*, E.A. Davis *(Leicester U.)*, C.R. Schwab *(CNRS, Strasbourg)*

712. μSR study of superconducting spin glasses [active], V. McMullen, D.R. Noakes , C.E. Stronach *(Virginia State U.)*, E.J. Ansaldo *(U. Saskatchewan)*, J.H. Brewer *(UBC)*, G. Cao, J.E. Crow *(NHMFL)*, S. McCall *(Florida State U.–NHMFL)*

713. Muonium chemistry in supercritical water [active], B. Addison-Jones, J.-C. Brodovitch, K. Ghandi, I. McKenzie, P. Percival *(SFU)*, J. Schüth *(U. Bonn)*

714. Atomic PNC in francium: preparations [active], J.A. Behr, L. Buchmann, M. Dombsky, P. Jackson, C.D.P. Levy *(TRIUMF)*, J.M. D'Auria, P. Dubé, A. Gorelov, D. Melconian, T. Swanson, M. Trinczek *(SFU)*, O. Häusser *(SFU–TRIUMF)*, U. Giesen *(U. Alberta)*, I. Kelson, A.I. Yavin *(Tel Aviv U.)*, J. Deutsch *(U. Catholique de Louvain)*, J. Dilling *(SFU–Heidelberg)*

715. Weak interaction symmetries in β^+ decay of optically trapped ^{37,38m}K [active], J.M. D'Auria, A. Gorelov, D. Melconian, T. Stocki, M. Trinczek *(SFU)*, G. Ball, J.A. Behr, P. Bricault, M. Dombsky, K.P. Jackson, B.K. Jennings *(TRIUMF)*, U. Giesen *(U. Notre Dame)*, W.P. Alford *(U. Western Ontario)*, J. Deutsch *(U. Catholique de Louvain)*, D.A. Ashery *(Tel Aviv U.)*, G. Savard *(Argonne National Lab/U. Chicago)*, S. Gu *(UBC)* 39

716. Complete beta-delayed particle emission study of ^{31}Ar [deferred], J. Cerny, D.M. Moltz, T. Ognibene, M.W. Rowe, R.J. Tighe *(Lawrence Berkeley Lab)*, L. Buchmann *(TRIUMF)*, J. D'Auria *(SFU)*, M. Dombsky *(SFU–U. Alberta)*, G. Roy *(U. Alberta)*

717. Muon hyperfine transition rates in light nuclei [completed], J.H. Brewer, E. Gete, M.C. Fujiwara, J. Lange, D.F. Measday, B.A. Moftah, M.A. Saliba, T. Stocki *(UBC)*, T.P. Gorringe *(U. Kentucky)*

718. Superconductivity and magnetism in quaternary boron carbides [active], A. Keren, G.M. Luke, Y.J. Uemura, W.D. Wu *(Columbia U.)*, K. Kojima *(Columbia U.–U. Tokyo)*, S. Uchida *(U. Tokyo)*

719. ^{4}He(π^+,π^-pp) invariant mass measurement with CHAOS [completed data-taking], P. Amaudruz, L. Felawka, D. Ottewell, G. Smith *(TRIUMF)*, E.T. Mathie, R. Tacik, D.M. Yeomans *(U. Regina)*, H. Clement, J. Gräter, R. Meier, G.J. Wagner *(U. Tübingen)*, J. Clark, M. Sevior *(U. Melbourne)*, A. Ambardar, G.J. Hofman, M. Kermani, G. Tagliente *(UBC)*, F. Bonutti, P. Camerini, N. Grion, R. Rui *(U. di Trieste)*, J. Brack, R. Ristinen *(U. Colorado)*, E. Gibson *(California State U., Sacramento)*, M. Schepkin *(ITEP Moscow)*

720. Muonium's nucleophilicity [active], G.B. Porter, D.C. Walker *(UBC)*, J.M. Stadlbauer* *(Hood Coll.)*, K. Venkateswaran *(Hindustan Lever Ltd.)*, M.V. Barnabas *(Proctor & Gamble Ltd.)*

721. The delta nucleon reaction in CHAOS [completed data-taking], F. Farzanpay, P. Hong, E.L. Mathie, N. Mobed *(U. Regina)*, R. Tacik *(TRIUMF–U. Regina)*, P.A. Amaudruz, L. Felawka, R. Meier, D. Ottewell, G.R. Smith *(TRIUMF)*, N. Grion *(INFN, Trieste)*, P. Camerini, R. Rui *(U. di Trieste)*, E. Gibson *(California State U., Sacramento)*, G. Hofman, G. Jones, M. Kermani *(UBC)*, M.E. Sevior *(U. Melbourne)*, J.T. Brack, R.A. Ristinen *(U. Colorado)*

722. Pion initial state interactions in the ^{12}C(π^+,ppp) reaction [completed data-taking], T. Mathie, R. Tacik *(U. Regina)*, P.A. Amaudruz, L. Felawka, D. Ottewell, K. Raywood, G.R. Smith *(TRIUMF)* M. Kermani, S. McFarland *(UBC)*, F. Bonutti, P. Camerini, R. Rui *(U. di Trieste)*, N. Grion *(INFN, Trieste)*, E.F. Gibson *(California State U., Sacramento)*, M. Sevior *(U. Melbourne)*, J. Brack, G. Hofman *(U. Colorado)*, R. Meier *(U. Tübingen)*

723. Study of pion-nucleus double-scattering reactions [completed data-taking], R. Tacik *(TRIUMF–U. Regina)*, T. Mathie *(U. Regina)*, P. Amaudruz, L. Felawka, D. Ottewell, K. Raywood, G. Smith *(TRIUMF)*, M. Kermani, S. McFarland *(UBC)*, F. Bonutti, P. Camerini, R. Rui *(U. di Trieste)*, N. Grion *(INFN, Trieste)*, J. Brack, G. Hofman *(U. Colorado)*, R. Meier *(U. Tübingen)*, M. Sevior *(U. Melbourne)*, E. Gibson *(California State U. Sacramento)*

724. μSR measurements on spin ladder systems [active], A. Keren, G.M. Luke, Y.J. Uemura, W.D. Wu *(Columbia U.)*, K. Kojima *(Columbia U.–U. Tokyo)*, M. Takano *(Kyoto U.)*, K. Nagamine *(U. Tokyo)*

725. Pion double charge exchange reactions on ^{3,4}He in the energy range 50–100 MeV [completed], P. Amaudruz, L. Felawka, R. Meier, D. Ottewell, G. Smith *(TRIUMF)*, T. Mathie, R. Tacik, M. Yeomans *(U. Regina)*, J. Graeter, G. Wagner *(U. Tübingen)*, J. Clark, M. Sevior *(U. Melbourne)*, G. Hofman, M. Kermani, P. Tagliente *(UBC)*, F. Bonutti, P. Camerini, N. Grion, R. Rui *(U. di Trieste)*, J. Brack, R. Ristinen *(U. Colorado)*, E. Gibson *(California State U., Sacramento)*, O. Patarakin *(Kurchatov Inst.)*, E. Friedman *(Hebrew U. Jerusalem)*

726. Beta-delayed proton and γ-decay of ^{65}Se, ^{69}Kr and ^{73}Sr [active], D. Anthony, J. D'Auria, M. Trinczek *(SFU)*, R.E. Azuma, J.D. King *(U. Toronto)*, L. Buchmann, K.P. Jackson, J. Vincent *(TRIUMF)*, M. Dombsky *(SFU–U. Alberta)*, U. Giesen *(TRIUMF–U. Alberta)*, J. Görres, H. Schatz, M. Wiescher *(U. Notre Dame)*, C. Iliadis *(TRIUMF–U. Toronto)*, G. Roy *(U. Alberta)*

728. Search for population and de-excitation of low-spin superdeformed states in Po-Hg region via β^+ and α decays [active], Y.A. Akovali, M. Brinkman *(Oak Ridge National Lab)*, J.M. D'Auria *(TRIUMF–SFU)*, J.A. Becker, E.A. Henry *(Lawrence Livermore National Lab)*, M. Dombsky *(SFU)*, P.F. Mantica *(UNISOR)*, W. Nazarewicz *(Joint Inst. for Heavy Ion)*, J. Rikovska, N.J. Stone *(Oxford U.)*, M.A. Stoyer *(Lawrence Berkeley National Lab)*, R.A. Wyss *(MSI, Sweden)*

729. Gamow-Teller and spin-dipole strengths from ^{17,18}O(n,p) [active], D.P. Beatty, H.T. Fortune, P.P. Hui, R.B. Ivie, Z.Q. Mao, M.G. McKinzie, D.A. Smith *(U. Pennsylvania)*, W.P. Alford *(U. Western Ontario)*, K.P. Jackson, A.G. Ling, C.A. Miller, P. Walden, S. Yen *(TRIUMF)*

730. The solar neutrino problem and a new measurement of ^{7}Be$(p,\gamma)^8$B [deferred], R.E. Azuma, J.D. King *(U. Toronto)*, P. Bricault, L. Buchmann, T. Ruth, H. Schneider, J. Vincent, S. Zeisler *(TRIUMF)*, J. D'Auria, R. Korteling *(SFU)*, M. Dombsky *(SFU–U. Alberta)*, U. Giesen *(TRIUMF–U. Alberta)*, C. Iliadis *(TRIUMF–U. Toronto)*, G. Roy *(U. Alberta)*, M. Wiescher *(U. Notre Dame)*

731. Investigation of spin-polarized muonium in metallic semiconductors [active], K.H. Chow, S. Dunsiger, R.F. Kiefl, W.A. MacFarlane, J. Sonier *(UBC)*, S.F.J. Cox *(Rutherford Appleton Lab)*, E.A. Davis, A. Singh *(Leicester U.)*, T.L. Estle, B. Hitti *(Rice U.)*, R.L. Lichti *(Texas Tech. U.)*, P. Mendels *(Orsay U.)*, C. Schwab *(CRN, Strasbourg)*

732. Quantum impurities in one dimensional spin 1/2 chains [active], I. Affleck, J.H. Brewer, K. Chow, S. Dunsiger, S. Eggert, R.F. Kiefl, A. MacFarlane, J. Sonier *(UBC)*, A. Keren, Y.J. Uemura *(Columbia U.)*

733. Probing high T_c superconductor with "paramagnetic" (μ^-O) system [active], H. Kojima, I. Tanaka, E. Torikai *(Yamanashi U.)*, K. Nishiyama *(U. Tokyo)*, K. Nagamine *(U. Tokyo–RIKEN)*, I. Watanabe *(RIKEN)*, T.P. Das *(State U. New York)*, S. Maekawa *(Nagoya U.)*

734. Radiative muon capture on nickel isotopes [completed], D.S. Armstrong, P. McKenzie *(Coll. of William & Mary)*, G. Azuelos, P. Depommier *(U. de Montréal)*, P. Bergbusch, P. Gumplinger, M. Hasinoff, E. Saettler *(UBC)*, B. Doyle, T.P. Gorringe, R. Sedlar *(U. Kentucky)*, M. Blecher, C. Sigler *(Virginia Polytechnic Inst.)*, J.A. MacDonald, J.-M. Poutissou, R. Poutissou, D. Wright *(TRIUMF)*

735. Studies of single layer cuprate superconductors [active], G.M. Luke, B. Nachumi, Y.J. Uemura *(Columbia U.)*, K. Kojima *(Columbia U.–U. Tokyo)*, S. Uchida *(U. Tokyo)*, R.H. Heffner, L.P. Le *(Los Alamos Nat. Lab)*, R. MacLaughlin *(U. California, Riverside)*, M.B. Maple *(U. California, San Diego)*

736. Tests of electro-weak theory using ^{14}O beam [deferred], M. Bahtacharya, A. Garcia, R. Rutchi, M. Wayne *(U. Notre Dame)*, L. Buchmann *(TRIUMF)*, C. Iliadis *(TRIUMF–U. Toronto)*, B. Fujikawa *(Lawrence Berkeley Lab.)*, S.J. Freedman, J. Mortara *(U. California, Berkeley)*

737. Magnetic and superconducting behaviour in selected oxide materials [active], R.H. Heffner, L.P. Le *(Los Alamos Nat. Lab)*, D.E. Maclaughlin *(U. California, Riverside)*, G. Luke, B. Nachuma, Y.J. Uemura *(Columbia U.)*, K. Kojima *(Columbia U.–U. Tokyo)*

740. Irradiation of silicon tracker components [active], R. Lipton, L. Spiegel *(Fermilab)*, K.F. O'Shaughnessy *(U. California, Santa Cruz)*, B. Barnett, J. Cameratta, J. Skarha *(Johns Hopkins U.)*, N. Brunner, M. Frautschi, M. Gold, Y. Ling, J. Matthews, S. Seidel *(U. New Mexico)*, D. Bortoletto, A. Garfinkel, A. Hardman, K. Hoffman, T. Keaffaber, N.M. Shaw *(Purdue U.)*

741. Beta-delayed proton decay of ^{17}Ne to α-emitting states in ^{16}O [active], R.E. Azuma, J. Chow, J.D. King, A.C. Morton *(U. Toronto)*, L. Buchmann, M. Dombsky *(TRIUMF)*, U. Giesen *(U. Notre Dame)*, T. Davinson, A.C. Shotter *(U. Edinburgh)*, R.N. Boyd *(Ohio State U.)*, C. Iliadis *(U. North Carolina)*, J. Powell *(U. California, Berkeley)*, 43

742. Scattering of muonic hydrogen isotopes [active], V.M. Bystritsky, V.A. Stolupin *(JINR)*, R. Jacot-Guillarmod, P.E. Knowles, F. Mulhauser *(U. Fribourg)*, G.M. Marshall *(TRIUMF)*, M. Filipowicz, J. Wozniak *(Fac. Phys., Nucl. Tech., Krakow)*, A. Adamczak *(Inst. Nucl. Physics, Krakow)*, A.R. Kunselman *(U. Wyoming)*, V.E.

Markushin, C. Petitjean *(PSI)*, T.M. Huber *(Gustavus Adolphus Coll.)*, G.A. Beer, M. Maier, A. Olin, T.A. Porcelli *(U. Victoria)*, P. Kammel *(U. California, Berkeley)*, M.C. Fujiwara *(UBC)*, J. Zmeskal *(IMEP Vienna)*, S.K. Kim *(Jeonbuk National U.)*

743. Gamow-Teller strength in ^{64,66,68}Zn and ^{63,65}Cu(n,p) [active], W.P. Alford *(U. Western Ontario)*, D. Beatty, H.T. Fortune, P.P. Hui, R.B. Ivie, Z. Mao, M.G. McKinzie, D.A. Smith *(U. Pennsylvania)*, S. Yen *(TRIUMF)*

744. Hadronic weak and electromagnetic form factors via $\pi^- p \to e^+ e^- n$ [active], D. Armstrong *(Coll. of William & Mary)*, P. Gumplinger, M.D. Hasinoff, D.H. Wright *(UBC)*, M. Blecher *(Virginia Polytech. Inst. & State U.)*, E. Christy, B.C. Doyle, T.P. Gorringe, M.A. Kovash *(U. Kentucky)*, J.A. Macdonald *(TRIUMF)*

745. μ^-SR measurements on one-dimensional spin systems [active], K. Kojima *(Columbia U.–U. Tokyo)*, K. Nagamine, K. Nishiyama, S. Uchida *(U. Tokyo)*, G.M. Luke, B. Nachumi, Y.J. Uemura *(Columbia U.)*, I. Affleck, S. Dunsiger, S. Eggert, R.F. Kiefl *(UBC)*

746. Muonium dynamics in Si, Ge and GaAs studied by RF-μSR and μW-μSR [active], S.R. Kreitzman *(TRIUMF)*, T.L. Estle, B. Hitti *(Rice U.)*, R. Lichti *(Texas Tech.)*, K. Chow *(UBC)*, S.F.J. Cox *(Rutherford Appleton Lab)*, E.A. Davis *(Leicester U.)*, C. Schwab *(CRN Strasbourg)*

747. μSR study of re-entrant spin glasses a-FeMn, AuFe, and $Fe_{70}Al_{30}$ [active], I.A. Campbell *(U. Paris Sud Orsay)*, S. Dunsiger, R.F. Kiefl *(UBC)*, M.J.P. Gingras *(TRIUMF)*, M. Hennion, I. Mirebeau *(Saclay, LLB)*, K. Kojima, G.M. Luke, B. Nachumi, Y.J. Uemura, W.D. Wu *(Columbia U.)*

749. Muonium-substituted free radicals [active], B. Addison-Jones, J.C. Brodovitch, K. Ghandi, I. McKenzie, P.W. Percival *(SFU)*, J. Schüth *(U. Bonn)* 59

750. Liquid chemistry μSR [active], G.B. Porter, D.C. Walker *(UBC)*, J.M. Stadlbauer* *(Hood Coll.)*, K. Venkateswaran *(Lever Hindustan Ltd.)*, M.V. Barnabas *Procter & Gamble Ltd.)*

751. Tests in preparation for μSR measurements of off-axis internal magnetic fields in anisotropic superconductors [active], E. Csomortani, W.J. Kossler, X. Wan *(Coll. of William & Mary)*, D.R. Harshman *(Physikon Research Inc.)*, A. Greer *(Gonzaga U.)*, E. Koster, D.L. Williams *(UBC)*, C.E. Stronach *(Virginia State U.)*

752. Muonium centres in Si and GaAs [active], K.H. Chow *(Oxford U.)*, S.F.J. Cox *(Rutherford Appleton Lab)*, E.A. Davis *(Leicester U.)*, S. Dunsiger, R.F. Kiefl, W.A. MacFarlane *(UBC)*, T.L. Estle *(Rice U.)*, B. Hitti *(TRIUMF)*, R.L. Lichti *(Texas Tech.)*, C. Schwab *(CRN Strasbourg)*

753. Studies of magnetic correlations in planar oxides [active], K. Kojima *(Columbia U.–U. Tokyo)*, M. Larkin, G.M. Luke, J. Merrin, B. Nachumi, Y.J. Uemura *(Columbia U.)*, B.J. Sternlieb *(Brookhaven Nat. Lab)*, S. Uchida *(U. Tokyo)*

754. A search for the muonium substituted hydroxyl radical [deferred], T.A. Claxton, G. Marston *(Leicester U.)*, S.F.J. Cox *(Rutherford Appleton Lab)*, D. Arseneau, D. Fleming, M. Senba, P. Wassell *(UBC)*, J.-C. Brodovitch, P.W. Percival *(SFU)*

755. Muonium formation in Zn-spinels [deferred], G.M. Kalvius, A. Kratzer, W. Potzel *(Tech. U. Munich)*, R. Wäppling *(U. Uppsala)*, D.R. Noakes *(Virginia State U.)*, S.R. Kreitzman *(TRIUMF)*, A. Martin *(U. Jena)*, M.K. Krause *(U. Leipzig)*

756. Mu+NO spin relaxation: electron exchange or paramagnetism? [deferred], D.G. Fleming, J.J. Pan, M. Senba, M. Shelley *(UBC)*, D.J. Arseneau *(TRIUMF)*, E. Roduner *(U. Zürich)*

757. Study of muon dynamics in ferroelectric materials and proton ionic conductors – comparison with proton dynamics [active], W.K. Dawson, K. Nishiyama, S. Ohira, K. Shimomura *(U. Tokyo)*, K. Nagamine *(U. Tokyo–RIKEN)*, S. Ikeda *(KEK)*, S. Shin *(U. Tokyo –ISSP)*, N. Sata *(Tohoku U.)*

758. Electronic structure of muonium and muonium-lithium complexes in graphite and related compounds [active], J. Brewer, J. Chakhalian, S. Dunsiger, R.F. Kiefl, W.A. MacFarlane, R. Miller, J. Sonier *(UBC)*, J. Dahn *(Dalhousie U.)*, J. Fischer *(U. Pennsylvania)*, B. Hitti, S.R. Kreitzman *(TRIUMF)*

759. Study of the isotropic hyperfine coupling constant of muonium at high temperature and under uniaxial pressure [active], W.K. Dawson, K. Nishiyama, S. Ohira, K. Shimomura *(U. Tokyo)*, K. Nagamine *(U. Tokyo–RIKEN)*, T.P. Das *(U. New York, Albany)*

761. Parity violation in $p-p$ scattering at 450 MeV [active], J. Birchall, E. Gamroth, D.A. Horning, L. Lee, S.A. Page, W.D. Ramsay, A.W. Rauf, G. Rutledge, W.T.H. van Oers *(U. Manitoba)*, C.A. Davis, J. Doornbos, R. Helmer, R. Laxdal, C.D.P. Levy *(TRIUMF)*, P.W. Green, G. Roy, G.M. Stinson *(U. Alberta)*, N.A. Titov, S. Zadorozhny, A.N. Zelenski *(INR, Moscow)*, J.D. Bowman, R.E. Mischke, W.S. Wilburn *(Los Alamos Nat. Lab)*, N.T. Okumusoglu *(Karadeniz Tech. U.)*, E. Korkmaz, *(UNBC)*, A.A. Hamian *(U. Washington)* 14

762. Gamow-Teller and spin-flip dipole strengths near A=90 [active], W.P. Alford *(U. Western Ontario)*, D.P. Beatty, H.T. Fortune, P.P. Hui, R.B. Ivie, D. Koltenuk, J. Yu *(U. Pennsylvania)*, A. Ling, S. Yen *(TRIUMF)*, S. El-Kateb *(King Fahd U.)*

763. Muon cooling and acceleration in an undulating crystal channel [deferred], S.A. Bogacz, D.B. Cline, D.A. Sanders *(UCLA)*, L.M. Cremaldi, B. Denardo, Q. Jie, D.J. Summers *(U. Mississippi–Oxford)*, G.M. Marshall *(TRIUMF)*

764. Calibration of a segmented neutron detector [active], E. Korkmaz, G. O'Rielly *(UNBC)*, D.A. Hutcheon *(TRIUMF)*, A.K. Opper *(U. Alberta)*, G. Feldman, N.R. Kolb *(U. Saskatchewan)*

766. The ortho-para transition rate in muonic molecular hydrogen [completed data-taking], D.S. Armstrong, J.H.D. Clark, P. King *(Coll. of William & Mary)*, T.P. Gorringe, S. Tripathi, P.A. Żołnierczuk *(U. Kentucky)*, M.D. Hasinoff, T. Stocki *(UBC)*, D.H. Wright *(TRIUMF)*

767. Direct measurement of sticking in muon catalyzed $d-t$ fusion [active], J.M. Bailey *(Chester Technology, UK)*, G.A. Beer, M. Maier, G.R. Mason, T.A. Porcelli *(U. Victoria)*, K.M. Crowe, P. Kammel *(U. California, Berkeley–LBL)*, M.C. Fujiwara, E. Gete, T.J. Stocki *(UBC)*, T.M. Huber *(Gustavus Adolphus Coll.)*, S.K. Kim *(Jeonbuk National U.)*, A.R. Kunselman *(U. Wyoming)*, G.M. Marshall, A. Olin *(TRIUMF)*, C.J. Martoff *(Temple U.)*, V.S. Melezhik *(JINR, Dubna)*, F. Mulhauser *(U. Fribourg)*, C. Petitjean *(PSI)*, J. Zmeskal *(IMEP Vienna)*

768. Generalized Fulde-Ferrell-Larkin-Ovchinnikov state in heavy fermion and intermediate valence systems [active], J. Akimitsu, K. Oishi, H. Takagiwa, T. Yokoo *(Aoyama Gakuin U.)*, W. Higemoto, R. Kadono, A. Koda *(KEK-IMSS)*, M. Nohara *(U. Tokyo)*, M. Hedo *(Ryukyu U.)*, Y. Onuki *(Osaka U.)* 60

769. Effects of uniaxial stress on muonium in semiconductors [active], K.H. Chow *(Oxford)*, B. Hitti *(TRIUMF)*, R.F. Kiefl *(UBC)*, T.L. Estle *(Rice U.)*, R. Lichti *(Texas Tech. U.)*

770. μSR studies of organic conductors: (BEDT-TTF)$_2$–X and (TMTTF)$_2$Br [active], K. Kojima, M. Larkin, G.M. Luke, J. Merrin, B. Nachumi, Y.J. Uemura *(Columbia U.)*, P.M. Chaikin *(Princeton U.)*, G. Saito *(Kyoto U.)*

771. μSR studies of geometrically frustrated S = 1/2 spin systems [active], K. Kojima, M. Larkin, G.M. Luke, J. Merrin, B. Nachumi, Y.J. Uemura *(Columbia U.)*, M.J.P. Gingras *(TRIUMF)*, S. Dunsiger, R.F. Kiefl *(UBC)*, D.C. Johnston, S. Kondo *(Iowa State U.)*, S. Uchida *(U. Tokyo)*, R.J. Cava *(AT&T Bell Labs)*

772. Search for the $\Delta-\Delta$ dibaryon [active], R. Abegg*, C.A. Miller, P. Walden, S. Yen *(TRIUMF)*, R. Bent *(Indiana U.)*, T.Y. Chen, F. Wang, C.H. Ye *(Nanjing U.)*, W. Falk *(U. Manitoba)*, D. Frekers, M. Hartig *(U. Muenster)*, T. Goldman *(Los Alamos Nat. Lab)*, M. Heyrat, C.W. Wong *(UCLA)*, G. Jones *(UBC)*, E. Korkmaz, G. O'Rielly *(UNBC)*, C. Rangacharyulu *(U. Saskatchewan)*, I. Strakovsky *(Virginia Tech. Inst.)*, Z.X. Sun, J.C. Xu *(Inst. Atomic Energy, China)*, T. Walton *(Cariboo U. Coll.)*

773. Muon-electron interaction in n-type silicon [active], D. Arseneau, B. Hitti, S.R. Kreitzman *(TRIUMF)*, J.H. Brewer, R.F. Kiefl, G. Morris *(UBC)*, K. Chow *(Oxford U.)*, S.F.J. Cox *(Rutherford Appleton Lab)*, D.G. Eshchenko *(INR, Moscow)*, T.L. Estle *(Rice U.)*, R. Lichti *(Texas Tech. U.)*, V.G. Storchak, *(Kurchatov Inst.)*

774. Muonium dynamics in GaAs studied by rf and μ-wave μSR [active], B. Hitti, S.R. Kreitzman *(TRIUMF)*, T.L. Estle *(Rice U.)*, R. Lichti *(Texas Tech. U.)* 61

775. Electron transport in insulators, semiconductors and magnetic materials [active], J.H. Brewer, A. Izadi, D.M.C. Liu, K.M. Nichol, S. Sivanandam, A.T. Warkentin *(UBC)*, G.D. Morris *(TRIUMF)*, V.G. Storchak *(Kurchatov Inst.)*, D.G. Eshchenko *(INR, Moscow)*, J.D. Brewer *(SFU)*

776. Rare earth materials with disordered spin structures [completed data-taking], J.H. Brewer *(UBC)*, K. Fukamichi *(Tohoku U.)*, G.M. Kalvius *(Tech. U. Munich)*, D.R. Noakes, C.E. Stronach, M.F. White, Jr. *(Virginia State U.)*, R. Wäppling *(Uppsala U.)* 62

777. Vortex state of s-wave superconductors investigated by muon spin rotation [active], J.C. Chakhalian, K. Chow, R. Miller, A.N. Price *(UBC)*, J.H. Brewer, R.F. Kiefl *(UBC/TRIUMF)*, G.M. Luke *(McMaster U.)*, J.E. Sonier *(SFU)* 62

778. $\pi^{\pm}p$ differential cross sections in the Coulomb-nuclear interference region [active], P. Amaudruz, G. Hofman, D. Ottewell, M. Pavan, K. Raywood *(TRIUMF)*, P. Camerini, E. Fragiacomo, N. Grion, S. Piano, R. Rui *(U. di Trieste)*, K. Babcock, E. Mathie, R. Tacik, M. Yeomans *(U. Regina)*, J. Breitschopf, H. Denz, R. Meier, F. von Wrochem, G. Wagner *(U. Tübingen)*, G. Moloney, M. Sevior *(U. Melbourne)*, J. Brack, J. Patterson, R. Ristinen *(U. Colorado)*, E. Gibson *(California State U., Sacramento)*, O. Patarakin *(Kurchatov Inst.)*, G. Smith *(Jefferson Lab)* 46

779. Accelerator mass spectrometry experiments at ISAC [active], S. Calvert, A. Glass, R.R. Johnson, T. Petersen *(UBC)*, Z. Gelbart, D. Ottewell *(TRIUMF)*, R. Schubank *(unaffiliated)*, C.S. Wong *(Inst. of Ocean Sciences)*, J. Clague *(Geological Survey Canada)*, M. Paul *(Hebrew U. Jerusalem)*

780. Deeply bound pionic states through ^{208}Pb(p,^{3}He)^{206}Pb$\bigotimes\pi^-$ [completed], D. Frekers, W. Garske, K. Grewer, M. Hartig, H. Wörtche *(U. Muenster)*, H. Machner *(KFA, Jülich)*, D. Hutcheon, P. Walden, S. Yen *(TRIUMF)*, A. Opper *(U. Ohio)*

781. Investigations of the $\pi\pi$ invariant mass distributions of nuclear ($\pi^+,\pi^-\pi^+$) reactions with the CHAOS detector [completed data-taking], J. Clark, G. Moloney, M.E. Sevior *(U. Melbourne)*, G. Hofman *(UBC–U. Colorado)*, M. Kermani, S. McFarland, K. Raywood *(UBC)*, P. Amaudruz, L. Felawka, D.F. Ottewell, G.R. Smith *(TRIUMF)*, R. Meier *(TRIUMF–U. Tübingen)*, F. Bonutti, P. Camerini, E. Fragiacomo, R. Rui *(INFN, Trieste–U. Trieste)*, N. Grion *(INFN, Trieste)*, E.L. Mathie, R. Tacik, *(U. Regina)*, J. Brack *(TRIUMF–U. Colorado)*, R.A. Ristinen *(U. Colorado)*, E. Gibson *(California State U., Sacramento)*, J. Graeter, G. Wagner *(U. Tübingen)*, V. Mayorov, O. Patarakin, V. Tikhonov *(Kurchatov Inst.)*

782. Non-fermi-liquid behaviour and other novel phenomena in heavy-fermion alloys [active], D.E. MacLaughlin *(U. California, Riverside)*, R.H. Heffner *(Los Alamos Nat. Lab)*, Y.J. Uemura *(Columbia U.)*, G.J. Nieuwenhuys *(U. Leiden)*, M.B. Maple *(U. California, San Diego)*, O.O. Bernal *(Cal. State U., Los Angeles)*, G.M. Luke *(McMaster U.)*, J.E. Sonier *(SFU)*, B. Andraka *(U. Florida)* 64

783. Paramagnetic frequency shifts in unconventional superconductors [active], R.H. Heffner, J.L. Smith *(Los Alamos Nat. Lab)*, D.E. MacLaughlin *(U. California, Riverside)*, G.J. Nieuwenhuys *(U. Leiden)*, O.O. Bernal *(Cal. State U., Los Angeles)*, J.E. Sonier *(SFU)* 66

784. μSR studies of spin singlet states in oxides [active], A. Fukaya, I. Gat, M. Larkin, A. Savici, Y.J. Uemura *(Columbia U.)*, T. Ito *(Columbia U./ETL)*, H. Kageyama, K. Ueda, Y. Ueda *(U. Tokyo)*, P.P. Kyriakou, G.M. Luke, M.T. Rovers *(McMaster U.)* 67

785. Pion double charge exchange on ^{3}He with CHAOS [completed data-taking], R. Tacik *(TRIUMF–U. Regina)*, E.L. Mathie, M. Yeomans *(U. Regina)*, H. Clement, J. Graeter, R. Meier, J. Petzold, G.J. Wagner *(U. Tübingen)*, E. Friedman *(Hebrew U. Jerusalem)*, N. Grion *(INFN Trieste)*, P. Camerini, E. Fragiacomo, R. Rui *(U. Trieste)*, L. Felawka, D. Ottewell, K. Raywood, G.R. Smith *(TRIUMF)*, G. Hofman, B. Jamieson, G. Tagliente *(UBC)*, J. Clark, G. Molony, M.E. Sevior *(U. Melbourne)*, E. Gibson *(California State U. Sacramento)*, H. Staudenmeyer *(U. Karlsruhe)*, S. Filippov, Y. Gavrilov, T. Karavicheva *(Moscow Meson Factory)*

786. Low energy structures in the β-delayed particle decays of ^{9}C, ^{12}N and ^{17}Ne [active], N. Bateman *(TRIUMF–SFU–U. Toronto)*, L. Buchmann, K.P. Jackson, T. Shoppa *(TRIUMF)*, J. Chow, J.D. King, C. Mortin *(U. Toronto)*, T. Davison, A. Ostrowski, A. Shotter *(U. Edinburgh)*, J. D'Auria *(SFU)*, E. Gete, D. Measday *(UBC)*, U. Giesen *(U. Alberta)*

788. Nuclear and atomic physics with the CPT spectrometer [active], B. Barber, K.S. Sharma *(U. Manitoba)*, X. Feng *(U. Manitoba–McGill U.)*, F. Buchinger, J. Crawford, S. Gulick, J. Lee, B. Moore *(McGill U.)*, E. Hagberg, J. Hardy, V. Koslowsky, G. Savard *(Chalk River Nuclear Lab)*

789. μSR studies of magnetic fluctuations in hydronium jarosites, model Kagomé antiferromagnets [active], A. Harrison, A.S. Wills *(U. Edinburgh)*, Y. Fudamoto, K. Kojima, M. Larkin, G.M. Luke, J. Merrin, B. Nachumi, Y.J. Uemura *(Columbia U.)*, T. Mason *(U. Toronto)*

790. μSR studies of stripe order in $La_{1.6-x}Sr_xNd_{0.4}CuO_4$ modified cuprate superconductors [active], Y. Fudamoto, K. Kojima, M. Larkin, G.M. Luke, J. Merrin, B. Nachumi, Y.J. Uemura *(Columbia U.)*, M. Crawford *(Du Pont)*, A. Moodenbaugh *(Brookhaven National Lab)*, S. Uchida *(U. Tokyo)*

791. Electronic structure and dynamics of charged muonium and muonium-dopant centers in semiconductors [active], K.H. Chow *(Oxford U.)*, R.F. Kiefl *(UBC)*, B. Hitti *(TRIUMF)*, T.L. Estle *(Rice U.)*, R. Lichti *(Texas Tech. U.)*, S.F.J. Cox *(Rutherford Appleton Lab)*, C. Schwab *(CRN, Strasbourg)* 68

792. Muonium in III-V semiconductors: identification of states and transitions [active], K.H. Chow *Oxford U.)*, S.F.J. Cox *(Rutherford Appleton Lab)*, B. Hitti *(TRIUMF)*, T.L. Estle *(Rice U.)*, R.L. Lichti *(Texas Tech. U.)*, C. Schwab *(CRN, Strasboug)*

793. Production of an intense ^{15}O beam for ISAC [completed], J. D'Auria, R. Lange *(SFU)*, M. Dombsky, T. Ruth, J. Vincent *(TRIUMF)*, K. Carter *(Oak Ridge National Lab)*, B. Zhuikov *(INR, Moscow)*

794. μ^+SR study on the magnetic properties of $LaCoO_3$ and $La_{1-x}Sr_xCoO_3$ [active], V.V. Krishnamurthy, I. Watanabe *(RIKEN)*, K. Asai, N. Yamada *(U. Electro-communications)*, K. Nagamine *(U. Tokyo–RIKEN)*

795. μSR study on non fermi liquid behaviour [active], Y. Miyako, Y. Yamamoto *(Osaka U.)*, S. Murayama *(Muroran Inst. Tech.)*, K. Nagamine *(U. Tokyo)*, K. Nishiyama *(U. Tokyo–RIKEN)*

796. μSR studies in ionic crystals doped with either colour centres or impurity [deferred], Y. Miyake, K. Nagamine, K. Nishiyama, K. Shimomura *(U. Tokyo)*, A. Matsusita *(RIKEN)*

797. Magnetic correlations in the ternary equiatomic Ce compounds CeTSn [completed], G. Grosse, G.M. Kalvius A. Kratzer *(Tech. U. Munich)*, R. Wäppling *(U. Uppsala)*, T. Takabatake *(Hiroshima U.)*, D.R. Noakes, C.R. Stronach *(Virginia State U.)*, Y. Echizen *(Hiroshima U.)*, H. Nakotte *(New Mexico State U.)*, H.v. Löhneysen *(U. Karlsruhe)*

798. μSR studies on the competition of RKKY exchange and Kondo effect in CeT_2X_2 compounds (T=transition metal, X=Si,Ge) [active], H.-H. Klauss, W. Kopmann, F.J. Litterst, W. Wagener, H. Walf *(Tech. U. Braunschweig)*, E. Baggio Saitovitch, M.B. Fontes *(CBPF Rio de Janeiro)*, A. Krimmel, A. Loidl *(U. Augsburg)*

799. Hyperfine structure and site determination of (μ^-O) system in LaSuCuO high T_c superconductors [active], H. Kojima, I. Tanaka, E. Torikai *(Yamanashi U.)*, K. Nishiyama *(U. Tokyo–RIKEN)*, K. Nagamine, K. Shimomura *(U. Tokyo)*, I. Watanabe *(RIKEN)*, T.P. Das *(State U. New York)*

801. Studies of multi-phonon states via β-decay [active], C.J. Barton, M.A. Caprio, R.F. Casten, N.V. Zamfir *(Yale U.)*, D.S. Brenner *(Clark U.)*, R.L. Gill *(Brookhaven National Lab)*, G.C. Ball, K.P. Jackson *(TRIUMF)* 47

802. Superdeformation and smooth band termination on and near the $N = Z$ line: Part 1 ^{60}Zn [active], J.A. Cameron, S. Flibotte, D.S. Haslip, J. Nieminen, C. Svensson, J.C. Waddington, J.N. Wilson *(McMaster U.)*, G. Ball *(TRIUMF)*, A. Galindo-Uribarri, D.C. Radford *(Oak Ridge National Lab)*, D. Ward *(Lawrence Berkeley National Lab)*

803. Experimental studies of interaction and properties of neutron-rich nuclei at ISAC [active], A.S. Iljinov, A.V. Klyachko, E.S. Konobeevsky, M.V. Morodovskoy, M.A. Prohvatilov, A.I. Reshetin, Yu.V. Ryabov, K.A. Shileev, V.A. Simonov, V.M. Skorkin, S.V. Zuyev *(INR, Moscow)*

804. Muonium in gallium nitride [active], R.L. Lichti, S.K.L. Sjue *(Texas Tech. U.)*, K.H. Chow, B. Hitti *(TRIUMF)*, S.F.J. Cox *(Rutherford Appleton Lab)*, C. Schwab *(CRN Strasbourg)*, E.A. Davis *(Leicester U.)* 69

805. A study of the ^{13}N$(p,\gamma)^{14}$O reaction with a ^{13}N beam [active], R.E. Azuma, J. Chow, J.D. King, A.C. Morton *(U. Toronto)*, N. Bateman *(TRIUMF–Toronto)*, L. Buchmann, K.P. Jackson, T. Shoppa *(TRIUMF)*, J.M. D'Auria *(SFU)*, U. Giesen *(SFU–TRIUMF)*, G. Roy *(U. Alberta)*, W. Galster *(U. Catholique de Louvain)*, A.C. Shotter *(U. Edinburgh)*, R.N. Boyd *(Ohio State U.)*, U. Greife, C. Rolfs, F. Strieder, H.-P. Trautvetter *(Ruhr U. Bochum)*

806. Excitation of high-spin isomeric states and compound nucleus formation by intermediate energy protons and stopped pions [active], A.S. Iljinov, V.M. Kokhanyuk, B.L. Zhuikov *(INR, Moscow)*, I. Liu, J. Vincent, A.Z. Zyuzin *(TRIUMF)*

808. Spin glass order in magnets frustrated by competing ferro- and antiferromagnetic exchange [active], G.M. Kalvius, A. Kratzer, E. Schreier *(Techn. U. Munich)*, R. Wäppling *(U. Uppsala)*, D.R. Noakes *(Virginia State U.)*, J. Gal *(Beer Sheva U.)*, W. Schäfer *(Bonn U.)*

809. Quantum diffusion of muonium in crystals with orientational degrees of freedom [active], D. Arseneau, B. Hitti, S.R. Kreitzman *(TRIUMF)*, J.H. Brewer, A. Izadi, G.D. Morris *(UBC)*, D.G. Eshchenko *(INR, Moscow)*, V.G. Storchak *(Kurchatov Inst.)*, J.D. Brewer *(SFU)*

810. First direct study of the ^{23}Mg$(p,\gamma)^{24}$Al reaction with a recoil mass separator (DRAGON) [active], N.P.T. Bateman, J.M. D'Auria, D. Hunter, R. Korteling *(SFU)*, R.N. Boyd *(Ohio State U.)*, L. Buchmann, R. Helmer, D. Hutcheon, K.P. Jackson, A. Olin, J. Rogers *(TRIUMF)*, U. Giesen, G. Roy *(U. Alberta)*, L. Gialanella, U. Greife, C. Rolfs, F. Strieder, H.-P. Trautvetter *(Ruhr U. Bochum)*, A. Hussein *(UNBC)*, M. Junker *(INFN Gran Sasso)*, J.D. King *(U. Toronto)*, P.D. Parker *(Yale U.)*, A. Shotter *(U. Edinburgh)*, M. Wiescher *(U. Notre Dame)*

811. A direct study of the ^{19}Ne$(p,\gamma)^{20}$Na reaction with a recoil mass separator (DRAGON) [active], N.P.T. Bateman, J.M. D'Auria, D. Hunter, R. Korteling *(SFU)*, R.N. Boyd *(Ohio State U.)*, L. Buchmann, R. Helmer, D. Hutcheon, K.P. Jackson, A. Olin, J. Rogers *(TRIUMF)*, U. Giesen, G. Roy *(U. Alberta)*, L. Gialanella, U. Greife, C. Rolfs, F. Strieder, H.-P. Trautvetter *(Ruhr U. Bochum)*, A. Hussein *(UNBC)*, M. Junker *(INFN Gran Sasso)*, J.D. King *(U. Toronto)*, P.D. Parker *(Yale U.)*, A. Shotter *(U. Edinburgh)*, M. Wiescher *(U. Notre Dame)*

812. Proposed study of the ^{8}Li$(\alpha,n)^{11}$B reaction [active], R.N. Boyd, A. Murphy, L. Sahin, E. Smith, M. Zahar *(Ohio State U.)*, L. Buchmann, P. Walden *(TRIUMF)*, J.M. D'Auria *(SFU)*, J.D. King *(U. Toronto)*, M. Nishimura, S. Nishimura, I. Tanihata *(RIKEN)* 48

813. A study of the ^{15}O$(\alpha,\gamma)^{19}$Ne reaction at the astrophysically important energy [active], N.P.T. Bateman, J.M. D'Auria, D. Hunter, R. Korteling *(SFU)*, R.N. Boyd *(Ohio State U.)*, L. Buchmann, R. Helmer, D. Hutcheon, K.P. Jackson, A. Olin, J. Rogers *(TRIUMF)*, U. Giesen, G. Roy *(U. Alberta)*, U. Greife, C. Rolfs, F. Strieder, H.-P. Trautvetter *(Ruhr U. Bochum)*, A. Hussein *(UNBC)*, J.D. King *(U. Toronto)*, P.D. Parker *(Yale U.)*, A. Shotter *(U. Edinburgh)*, M. Wiescher *(U. Notre Dame)*

814. μSR studies of unconventional superconductivity in Sr_2RuO_4 [active], Y. Fudamoto, K.M. Kojima, M. Larkin, G.M. Luke, J. Merrin, B. Nachumi, Y.J. Uemura *(Columbia U.)*, Y. Maeno *(Kyoto U.)*, R.J. Cava *(Princeton U.)* 71

815. β-NMR investigation of magnetic multilayers and giant magnetoresistance [active], J.C. Chakhalian, S. Dunsiger, W.A. MacFarlane, R. Miller, J. Pond, J. Sonier, B. Turrell *(UBC)*, R.F. Kiefl *(UBC–TRIUMF)*, B.D. Gaulin *(McMaster U.)*, M. Gingras *(U. Waterloo)*, R. Heffner *(Los Alamos Nat. Lab)*, B. Heinrich *(SFU)*, B. Ittermann *(U. Marburg)*

816. Semiconductor quantum wells investigated by β-NMR [active], J.H. Brewer, J.C. Chakhalian, S. Dunsiger, R. Miller, T. Tiedje *(UBC)*, M. Gingras *(U. Waterloo)*, B. Ittermann *(U. Marburg)*, B. Hitti, P. Levy, S.R. Kreitzman, A. Zelenski *(TRIUMF)*, R.F. Kiefl *(TRIUMF–UBC)*

817. β-NMR investigation of type II superconductors [active], D. Bonn, J.H. Brewer, J.C. Chakhalian, S. Dunsiger, W. Hardy, R. Liang, R.F. Kiefl, W.A. MacFarlane, R. Miller, J. Sonier *(UBC)*, M. Gingras *(U. Waterloo)*, R. Heffner *(Los Alamos Nat. Lab)*, B. Itterman *(U. Marburg)*, B. Hitti, P. Levy, S.R. Kreitzman, A. Zelenski *(TRIUMF)*, G.M. Luke *(Columbia U.)*, J.W. Brill *(U. Kentucky)*

818. μ^+SR study of magnetic ordering in the one-dimensional spin-1/2 antiferromagnet copper benzoate [active], J.C. Chakhalian, S. Dunsiger, R.F. Kiefl, W.A. MacFarlane, R. Miller, J. Sonier *(UBC)*, C. Broholm, D.C. Dender, P. Hammar, D. Reich *(Johns-Hopkins U.)*, G. Luke, T. Uemura *(Columbia U.)*

819. μ^+SR studies of the antiferromagnetic instability and metastable state in colossal magnetoresistance system $(Nd_{1-y}Sm_y)_{1/2}Sr_{1/2}MnO_3$ ($y = 0.875$) [active], W. Higemoto, I. Watanabe *(RIKEN)*, K. Nishiyama *(KEK)*, K. Nagamine *(RIKEN–KEK)*, A. Asamitsu, H. Kuwahara, Y. Tokura *(JRCAT, U. Tokyo)*

821. Shape coexistence and shape mixing in neutron-deficient platinum isotopes: on-line nuclear orientation studies of the decays of ^{182}Au and ^{186}Au [active], K.S. Krane *(Oregon State U.)*, J.L. Wood *(Georgia Inst. Tech.)*, J. D'Auria *(SFU)*

822. Effect of disorder on quantum spin liquid state [active], J. Akimitsu, K. Ishii, K. Oishi, T. Yokoo *(Aoyama Gakuin U.)*, R. Kadono, K. Nagamine *(RIKEN)*, K. Nishiyama *(KEK)*

823. Pure fermi decay in medium mass nuclei [active], G.C. Ball, R. Beaton, P. Bricault, P. Klages, J.A. Macdonald, E. Vandervoort *(TRIUMF)*, J. Cerny, D.M. Moltz, J. Powell *(Lawrence Berkeley Lab)*, G. Savard *(Argonne National Lab)*, J.C. Hardy, V. Iacob *(Texas A&M U.)*, S. Bishop, J. D'Auria *(SFU)*, J.R. Leslie, H.-B. Mak, I.S. Towner *(Queen's U.)*, J.L. Wood *(Georgia Inst. Tech.)*, E.F. Zganjar, A. Piechaczek *(Louisiana State U.)* 49

824. Measurement of the astrophysical rate of the $^{21}Na(p,\gamma)^{22}Mg$ reaction [active], N.P.T. Bateman, J.M. D'Auria, U. Giesen, D. Hunter, R. Korteling *(SFU)*, R.N. Boyd *(Ohio State U.)*, L. Buchmann, R. Helmer, D. Hutcheon, K.P. Jackson, A. Olin, J. Rogers *(TRIUMF)*, U. Giesen *(SFU-TRIUMF)*, G. Roy *(U. Alberta)*, U. Greife, C. Rolfs, F. Strieder, H.-P. Trautvetter *(Ruhr U. Bochum)*, A. Hussein *(UNBC)*, J.D. King *(U. Toronto)*, P.D. Parker *(Yale U.)*, A. Shotter *(U. Edinburgh)*, M. Wiescher *(U. Notre Dame)*, S. Kubono *(U. Tokyo)*, T. Motobayashi *(Rikkyo U.)*

825. Equilibrium defects and order in intermetallic compounds studied using isomeric probes [active], G.S. Collins *(Washington State U.)*

826. Studies of ultrathin magnetic films with implanted isotopes [active], R. Kiefl, J. Pond, B.G. Turrell *(UBC)*, C.A. Davis, P.P.J. Delheij *(TRIUMF)*, K.S. Krane. J. Loats, P. Schmelzenbach, C. Stapels *(Oregon State U.)*, D. Groh, W. Kumarasiri,P. Mantica *(Michigan State U.)*, D. Kulp, J.L. Wood, *(Georgia Inst. Tech.)* 51

827. Parity violation in ^{182}W [active], J. D'Auria *(TRIUMF–SFU)*, C.A. Davis P.P.J. Delheij *(TRIUMF)*, R. Kiefl, A. Kotlicki, J. Pond, B. Turrell *(UBC)*, K.S. Krane *(Oregon State U.)*

828. Nuclear moments in the mass-100 region [active], K.S. Krane, J. Loats, P. Schmelzenbach, C. Stapels *(Oregon State U.)*, D. Kulp, J.L. Wood *(Georgia Inst. Tech.)*, C.A. Davis, P.P.J. Delheij *(TRIUMF)*, D. Groh, W. Kumarasiri, P. Mantica *(Michigan State U.)*, R. Kiefl, J. Pond, B.G. Turrell *(UBC)*

829. Muonium as a hydrogen isotope: reactions in solution [active], D.P. Chong, G.B. Porter, D.C. Walker *(UBC)*, K. Venkateswaran *(Hindustan Lever Ltd.)*, H.A. Gillis *(St. Francis Xavier U.)*

830. The hot entropy bubble and the decay of ^{9}Li [active], N. Bateman *(TRIUMF–SFU–Toronto)*, L. Buchmann, K.P. Jackson, S. Karataglidis, T. Shoppa, E. Vogt *(TRIUMF)*, J. Chow, J.D. King, C. Mortin *(U. Toronto)*, T. Davison, A. Ostrowski, A. Shotter *(U. Edinburgh)*, J. D'Auria, U. Giesen *(SFU)*, E. Gete, D. Measday *(UBC)*

831. Magnetic properties of $REBa_2Cu_3O_x$ [active], D. Andreica, F.N. Gygax, M. Pinkpank, A. Schenck *(ETH Zürich)*, B. Hitti *(TRIUMF)*, A. Amato *(PSI)*, J.H. Brewer *(UBC–TRIUMF)*

832. Study of the non-magnetic-magnetic transition in the $Yb(Cu_{1-x}Ni_x)_2Si_2$ system [active], D. Andreica, F. Gygax, M. Pinkpank, A. Schenck *(ETH Zürich–PSI)*, A. Amato *(PSI)*, B. Hitti *(TRIUMF)*

833. μSR studies of doped MnSi and $V_{2-y}O_3$: non-fermi-liquid behaviour, spin fluctuations and itinerant magnetism [active], Y. Fudamoto, K. Kojima, M. Larkin, G.M. Luke, B. Nachumi, O. Tchernyshyov, Y.J. Uemura *(Columbia U.)*, R.H. Heffner, J. Sorrao *(Los Alamos Nat. Lab)*, D.E. MacLaughlin *(U. California, Riverside)*, M. Isobe, K. Ueda, Y. Ueda *(U. Tokyo)*, Z. Fisk *(Florida State U.)*, J.H. Brewer *(Columbia U.–UBC)*

834. μSR study of transverse spin freezing in bond-frustrated magnets [active], M. Pumarol, M. Roseman, D.H. Ryan, J. van Lierop *(McGill U.)*, J.M. Cadogan *(U. New South Wales)* 73

835. μSR studies of intercalated HfN and Bi2212 superconductors [active], R. Breslow, I.M. Gat, K. Groves, M.I. Larkin, A. Savici, Y.J. Uemura *(Columbia U.)*, P. Kyriakou, G.M. Luke, M. Rovers *(McMaster U.)*, K.M. Kojima *(U. Tokyo)*, R.H. Heffner *(Los Alamos Nat. Lab)*, D.E. MacLaughlin *(U. California, Riverside)*, S. Yamanaka *(Hiroshima U.)*, T. Ito *(Columbia U.–ETL)* 74

836. Elasticks [active], R.E. Azuma, J.D. King *(U. Toronto)*, G. Ball, L. Buchmann, K.P. Jackson, B. Jennings, S. Karataglidis, E. Vogt *(TRIUMF)*, N. Bateman *(TRIUMF–SFU–U. Toronto)*, T. Davison, A. Ostrowski, A. Shotter *(U. Edinburgh)*, J. D'Auria *(SFU)*, W. Galster *(U. Catholique de Louvain)*, G. Roy *(U. Alberta)*

837. Pion-induced errors in memory chips [active], J.T. Brack, G. Hofman, J. Patterson R.J. Peterson, R.A. Ristinen *(U. Colorado)*, J.F. Ziegler *(IBM)*, M.E. Nelson *(US Naval Academy)*, G. Smith *(TRIUMF)*

838. Measurement of the $\pi^- p \to \gamma\gamma n$ capture mode of pionic hydrogen [active], T. Gorringe, M. Kovash, S. Tripathi, P. Żołnierczuk *(U. Kentucky)*, D. Armstrong, J. Clark *(Coll. of William & Mary)*, M. Hasinoff *(UBC)*, D. Healey, D. Wright *(TRIUMF)* 52

839. Thermal test of prototype high power ISAC target [active], D. Drake, D. Liska, W.L. Talbert, M. Wilson *(Amparo Corp.)*, P. Bricault, M. Dombsky, P. Schmor *(TRIUMF)*, E. Dalder, C. Landram, K. Sale, D. Slaughter *(Lawrence Livermore National Lab)*, J. Nolen, G. Savard *(Argonne National Lab)*, G. Alton *(Oak Ridge National Lab)*

840. Muon transfer from excited states of muonic hydrogen with x-ray measurement [active], S. Sakamoto, K. Shimomura *(KEK)*, K. Nagamine *(KEK–RIKEN)*, K. Ishida, N. Kawamura, Y. Matsuda, T. Matsuzaki, S.N. Nakamura, P. Strasser *(RIKEN)*

841. ISAC beam and target development [active], P. Bricault, M. Dombsky *(TRIUMF)*

842. Muonium-substituted free radicals in sub- and supercritical water [active], B. Addison-Jones, J.-C. Brodovitch, K. Ghandi, I. McKenzie, P.W. Percival *(SFU)*, J. Schüth *(U. Bonn)* 75

843. Quadrupole ordering in dense Kondo system studied by μLCR [active], J. Akimitsu, K. Kakuta, K. Ohishi *(Aoyama Gakuin U.)*, W. Higemoto, R. Kadono *(KEK–IMSS)*, T. Yokoo *(CREST)*

844. Quantum impurities in one dimensional spin 1/2 chains [active], I. Affleck, J. Brewer, J. Chakhalian, S. Dunsiger, R.F. Kiefl, R. Miller, A. Price *(UBC)*, S. Eggert *(Chalmers U.)*, B. Hitti *(TRIUMF)*, A.A. Keren *(Israel Inst. Tech.)*, W.A. MacFarlane *(U. Paris-Sud)*, G. Morris *(UBC–TRIUMF)*, Y.J. Uemura *(Columbia U.)*, M. Verdaguer *(CNRS)*, I. Yamada *(Chiba U.)*

845. μSR studies of vortex phases in (Ba,K)BiO_3 [active], G.M. Luke, M.A. Lumsden *(McMaster U.)*, Y. Fudamoto, M.I. Larkin, Y.J. Uemura *(Columbia U.)*, K.M. Kojima *(U. Tokyo)*, M. Gingras *(U. Waterloo)*, I. Joumard, T. Klein, J. Marcus *(U. Grenoble)*

846. Complex order parameter symmetry in $YB_2Cu_3O_{7-\delta}$ at low T and high magnetic field [active], D.A. Bonn, J.H. Brewer, W.N. Hardy, R.F. Kiefl, R.-X. Liang, R.I. Miller *(UBC)*, S.R. Dunsiger, R.H. Heffner *(Los Alamos Nat. Lab)*, G.D. Morris *(TRIUMF)*, J.S. Gardner *(Chalk River Nuclear Labs)*, J.E. Sonier *(SFU)*, C.E. Stronach *(Virginia State U.)* 76

847. Electron-doped high-T_c superconductors [active], R.H. Heffner *(Los Alamos Nat. Lab)*, P. Kyriakou, G.M. Luke, M. Rovers *(McMaster U.)*, P. Fournier *(U. de Sherbrooke)*, J.E. Sonier *(SFU)*, C.E. Stronach *(Virginia State U.)* 77

848. μSR investigation of the vortex state of $YBa_2Cu_3O_{6+x}$ [active], D. Bonn, J.C. Chakhalian, S. Dunsiger, W.N. Hardy, R.X. Liang, R. Miller, A. Price *(UBC)*, J.H. Brewer, R.F. Kiefl *(UBC–TRIUMF)*, J. Sonier *(Los Alamos Nat. Lab)*

849. Spin structure and magnetic volume fraction of La214 systems: revisiting "1/8", "stripes", "spin glass", and "swiss cheese" [active], K.M. Kojima *(U. Tokyo)*, Y. Fudamoto, I.M. Gat, M.I. Larkin, A.T. Savici, Y.J. Uemura *(Columbia U.)*, G.M. Luke *(McMaster U.)*, M.A. Kastner, Y.S. Lee *(MIT)*, R.J. Birgeneau *(U. Toronto)*, K. Yamada *(Kyoto U.)* 78

850. Effects of dilute (Cu,Zn) substitution in spin gap systems $SrCu_2O_3$ and $CuGeO_3$ [active], Y. Fudamoto, I. Gat, M.I. Larkin, Y.J. Uemura *(Columbia U.)*, K.M. Kojima, K. Manabe, K. Uchinokura *(U. Tokyo)*, G.M. Luke *(McMaster U.)*, M. Azuma, M. Takano *(Kyoto U.)*

851. μSR in ruthenate and cuprate high-T compounds [active], D.R. Harshman *(Physikon Research Inc.)*, H.A. Blackstead *(U. Notre Dame)*, D.Y. Chen, M.K. Wu *(Nat. Tsing Hua U.)*, F.Z. Chien *(Tamkang U.)*, J.D. Dow *(Arizona State U.)*, A.J. Greer *(Gonzaga U.)*, B. Hitti *(TRIUMF)*, W.J. Kossler *(Coll. of William & Mary)*, E. Koster *(UBC)*, C.E. Stronach *(Virginia State U.)*

852. Magnetic phases in geometrically frustrated rare earth pyrochlores [active], R. Kiefl *(UBC–TRIUMF)*, B.D. Gaulin, G. Luke *(McMaster U.)*, M.J.P. Gingras *(U. Waterloo)*, J.M. Roper *(Los Alamos Nat. Lab)*, J. Chakhalian, K. Chow, S. Dunsiger, R. Miller, G. Morris *(UBC)*, P. Mendels *(U. Paris-Sud)* J.S. Gardner *(NRC)* 79

856. μSR study on CuO [active], W. Higemoto, K. Nishiyama, K. Shimomura *(KEK)*, M. Suzuki, S. Tanaka, N. Tsutsumi, X.G. Zheng *(Saga U.)*

857. Investigation of the magnetic properties of the cerium compound probed by negative muon [active], W. Higemoto, K. Nagamine, K. Nishiyama, K. Shimomura *(KEK)*, V.V. Krishnamurthy *(RIKEN)*

858. Repolarization of muonic atom in semiconductors by laser optical pumping in solids [active], W. Higemoto, R. Kadono, K. Nagamine, K. Nishiyama K. Shimomura *(KEK)*

859. A search for non-Markovian μ^+ diffusion in solids: μ^+ spectral spin hopping in high transverse field [active], G. Alexandrowicz, A. Grayevsky, N. Kaplan, T. Tashma *(Racah Inst. Physics)*, A. Schenck *(ETH Zürich)*

860. Mass and charge transport in disordered media: orientational glasses [active], J.H. Brewer, A. Izadi, D.M.C. Liu, K.M. Nichol, S. Sivanandam, A.T. Warkentin *(UBC)*, G.D. Morris *(TRIUMF)*, V.G. Storchak *(Kurchatov Inst.)*, D.G. Eshchenko *(INR, Moscow)*, J.D. Brewer *(SFU)* 84

862. Polarization observables in the $\vec{p}(\pi^{\pm},\pi^{+},\pi^{\pm})$ reactions: a test of chiral perturbation theory [active], P. Amaudruz, D. Ottewell, K. Raywood, G. Smith, R. Tacik *(TRIUMF)*, K. Babcock, R. Lewis, E. Mathie, N. Mobed, H. Xu, M. Yeomans *(U. Regina)*, P. Camerini, E. Fragiacomo, N. Grion, R. Rui *(U. di Trieste)*, H. Clement, H. Denz, R. Meier, G. Wagner *(U. Tübingen)*, J. Clark, G. Maloney, M. Sevior *(U. Melbourne)*, J. Brack, G. Hofman, J. Patterson, R. Ristinen *(U. Colorado)*, E. Gibson *(California State U. Sacramento)*

863. Magnetic dipole moments measurements of ^{75,77,79}Ga using low temperature nuclear orientation and β-NMR [active], A. Davies, D. Groh, P.F. Mantica *(Michigan State U.)*, C.A. Davis, P.P.J. Delheij *(TRIUMF)*, K.S. Krane, J. Loats, P. Schmelzenbach, C. Staples, *(Oregon State U.)*, B. Turrell *(UBC)*, D. Kulp, J.L. Wood *(Georgia Inst. Tech.)*, W.F. Rogers *(Westmont College)* 53

864. Measurement of the two-photon capture mode of the pionic deuterium atom [active], S. Arole, T. Gorringe, C. Nenkov, S. Tripathi, P. Żołnierczuk *(U. Kentucky)*, D. Armstrong, J. Clark *(Coll. of William & Mary)*, M. Hasinoff *(UBC)*, D. Wright *(TRIUMF)* 52

865. Electronic structure and diffusion kinetics of muonium in group III nitrides [active], W. Higemoto, R. Kadono, K. Nishiyama, K. Shimomura *(KEK–IMSS)*, M. Mizuta *(NEC Corp.)*, M. Saito *(NEC Inf. Syst. Ltd.)*

866. $S = 0$ doping to the $1d$ spin chain: comparison between the $S = 1/2$ and $S = 1$ chains [active], I. Eisaki, K.M. Kojima, T. Masuda, S. Uchida, K. Uchinokura *(U. Tokyo)*, Y. Fudamoto, I. Gat, M.I. Larkin, Y.J. Uemura *(Columbia U.)*, G.M. Luke *(McMaster U.)*

867. μSR studies of magnetic properties of strontium/calcium ruthenates [active], Y. Fudamoto, I. Gat, M. Larkin, A. Savici, Y.J. Uemura *(Columbia U.)*, G.M. Luke *(McMaster U.)*, K. Kojima *(U. Tokyo)*, S. Ikeda, Y. Maeno *(Kyoto U.)*

868. Magnetic correlations in impurity doped one dimensional spin systems [active], D. Baabe, H.-H. Klauss, W. Kopmann, F.J. Litterst, D. Mienert *(Tech. U. Braunschweig)*, U. Ammerahl, B. Büchner *(U. Köln)*, C. Geibel *(MPI Dresden)*

869. Measurement of the ^{1}H$(\pi^-,\pi^0)n$ differential cross section at 100–140 MeV/c and forward angles [active], S. Arole, T. Gorringe, M. Kovash, S. Tripathi, P. Żołnierczuk *(U. Kentucky)*, M. Hasinoff *(UBC)*, D. Armstrong *(Coll. of William & Mary)*, M. Pavan *(TRIUMF)* 53

870. Breakout from the hot CNO cycle via the ^{18}Ne$(\alpha,p)^{21}$Na reaction [active], T. Davinson, A. Ostrowski, F. Sarazin, A. Shotter, P. Woods *(U. Edinburgh)*, L. Buchmann, J. D'Auria *(TRIUMF)*, J. Daly, J. Görres, M. Wiescher *(U. Notre Dame)*, P. Leleux *(U. Catholique de Louvain)*

871. Meson and quark effects in nuclear β-decay of ^{20}Na [active], M. Fukuda, K. Matsuta, M. Mihara, K. Minamisono, T. Minamisono, T. Sumikama *(Osaka U.)*, J. Behr, P. Bricault, M. Dombsky, K.P. Jackson, P. Levy *(TRIUMF)*, R. Kiefl *(UBC–TRIUMF)*, K. Koshigiri *(Osaka Kyoiku U.)*, M. Morita *(Josai Int. U.)*

872. Weak interaction studies with trapped radioactive ions [active], J. Dilling, D. Melconian *(SFU)*, G. Savard *(Argonne National Lab/U. Chicago)*, G.C. Ball, J.A. Behr, P. Bricault, K.P. Jackson *(TRIUMF)*, F. Buchinger, J.E. Crawford, J.K.P. Lee, R.B. Moore *(McGill U.)*, K.S. Sharma *(U. Manitoba)*

874. Study of ^{19}Ne α-decay properties related to the hot-CNO breakout reaction $^{15}O(\alpha,\gamma)^{19}Ne$ [active], T. Davinson, D. Groombridge, A.M. Laird, A.N. Ostrowski, F. Sarazin, K. Schmidt, A.C. Shotter, P.J. Woods *(U. Edinburgh)*, L. Buchmann *(TRIUMF)*, S. Cherubini, P. Leleux *(U. Catholique de Louvain)*, J. Hinnefeld *(U. South Bend)*

875. Muon scattering in low Z materials for muon cooling studies [active], T.R. Edgecock, M. Ellis, J. Lidbury, W. Murray, P.R. Norton, K.J. Peach *(Rutherford Appleton Lab)*, K. Ishida, Y. Matsuda, K. Nagamine *(RIKEN)*, P. Bell, S. Bull, A. May, T. McMahon, J.A. Wilson *(U. Birmingham)*, A. Jamdagni, K. Long, E. McKigney, P. Savage *(Imp. Coll., London)*, W. Allison *(U. Oxford)*, S. Benveniste, D. Cline, Y. Fukui, K. Lee, Y. Pischalnikov *(UCLA)*, R. Fernow *(Brookhaven National Lab)*, P. Gruber, C. Johnson, A. Lombardi *(CERN)*, S.N. Nakamura *(U. Tohoku)*, G. Marshall *(TRIUMF)* 54

876. Disordered magnetism near magnetic instabilities in f-electron materials [active], B. Kessler, D.R. Noakes, C.E. Stronach *(Virginia State U.)*, G.M. Kalvius, E. Schreier *(Tech. U. Munich)*, A. Loidl *(Augsburg U.)*, H. Nakotte *(New Mexico State U.)*, R. Wäppling *(Uppsala U.)* 87

877. μSR studies of strongly correlated electron systems under a high pressure [active], W. Higemoto, R. Kadono, A. Koda, K. Nishiyama *(KEK–MSL)*, K. Satoh *(Saitama U.)*, Y. Kitaoka, K. Ishida *(Osaka U.)*, K. Nagamine *(RIKEN–KEK–MSL)*

878. μ^+SR studies on magnetism of layered compounds $Cu_2(OH)_3X$(X=Cl,Br,I) [active], G. Maruta, K. Nishiyama *(KEK-MSL)*, S. Takeda *(Gunma U.)*

879. Proton-^{21}Na elastic scattering at astrophysical energies [active], L. Buchmann *(TRIUMF)*, T. Davinson, A. Ostrowski, F. Sarazin, A. Shotter, P. Woods *(U. Edinburgh)*, R.E. Azuma, J.D. King *(U. Toronto)*, A. Chen *(TRIUMF–SFU)*, J. Daly, J. Görres, M. Wiescher *(U. Notre Dame)*, J. D'Auria *(SFU)*, E.S. Konobeevsky, M.V. Mordovskoy, V.A. Simonov, A.V. Stepanov, V.P. Zavarzina *(INR, Moscow)*

880. Ortho-para effect of muon catalyzed fusion in solid deuterium [completed data-taking], K. Ishida *(RIKEN–KEK)*, K. Nagamine *(KEK–RIKEN)*, A. Toyoda *(U. Tokyo–RIKEN–KEK)*, K. Shimomura *(KEK)*, S.N. Nakamura *(RIKEN–Tohoku U.)*, Y. Matsuda *(RIKEN)* 57

881. Magnetism of Ce-based heavy fermion superconductor [active], W. Higemoto, R. Kadono, A. Koda *(KEK-IMSS)*, K. Ishida, Y. Kitaoka *(Osaka U.)*, C. Geibel, F. Steglich *(Max-Planck Inst.)*

882. μSR studies of unconventional superconductivity in an organic superconductor $(TMTSF)_2ClO_4$ [active], I.M. Gat, M.I. Larkin, A. Savici, Y.J. Uemura *(Columbia U.)*, T. Ito *(Columbia U.–ETL)*, P. Kyriakou, G.M. Luke, M. Rovers *(McMaster U.)*, K.M. Kojima *(U. Tokyo)*, P.M. Chaikin, I.J. Lee *(Princeton U.)*, M.J. Naughton *(Boston Coll.)* 89

883. Muonium-substituted methyl and associated free radicals [active], J.-C. Brodovitch, K. Ghandi, I. McKenzie, P.W. Percival *(SFU)*, B. Addison-Jones *(Capilano Coll.)*

884. μSR studies on magnetic ground state of $S = 1/2$ kagomé spin system $Cu_3V_2O_7(OH)-2{\cdot}2H_2O$ [active], I.M. Gat, T. Ito, M.I. Larkin, A. Savici, Y.J. Uemura *(Columbia U.)*, A. Keren *(Technion-Israel Inst. of Tech.)*, G.M. Luke *(McMaster U.)*, Z. Hiroi, K.M. Kojima *(U. Tokyo)*

885. High-TF line-shape measurement of impurity-doped high-T_c cuprates [active], K.M. Kojima, Y. Kojima, Y. Maeda, T. Okamura, S. Uchida *(U. Tokyo)*, I. Gat, T. Itoh, A. Kinkhabwala, M.I. Larkin, Y.J. Uemura *(Columbia U.)*, G.M. Luke *(McMaster U.)*, S.R. Dunsiger, R.F. Kiefl, R. Miller *(UBC)*, J.E. Sonier *(Los Alamos Nat. Lab)*

886. Study of field dependent T_1 relaxation and coexistence of order parameters in the (anti)ferromagnetic ruthenate-cuprate superconductors $RuSr_2(Gd,Eu,Y)Cu_2O_8$ [active], C. Bernhard *(Max Planck Inst.)*. C. Niedermayer, V. Oehmichen *(U. Konstanz)*, E.J. Ansaldo *(U. Saskatoon)*, J.L. Tallon *(NZIIRD)*

887. Search for broken time reversal symmetry in high temperature superconductors [active], P. Kyriakou, G.M. Luke, M. Rovers *(McMaster U.)*, R.H. Heffner *(Los Alamos Nat. Lab)*, M.I. Larkin, Y.J. Uemura *(Columbia U.)*, J. Sonier *(SFU)*, K.M. Kojima *(U. Tokyo)*

888. Test of delayed-muonium model for hydrocarbon liquids [active], D.C. Walker *(UBC)*, K. Venkateswaran *(Hindustan Lever Ltd.)*, H.A. Gillis *(St. Francis Xavier U.)*, G.B. Porter *(UBC)*

889. Study of field induced gap in Cu benzoate [active], Y. Ajiro, T. Asano, Y. Inagaki *(Kyushu U.)*, H. Nojiri *(Tohoku U.)*, W. Higemoto, R. Kadono, A. Koda *(KEK-IMSS)*

890. Anisotropic Kondo effect in $Ce_{0.8}La_{0.2}Al_3$? [active], D.E. MacLaughlin *(U. California, Riverside)*, O.O. Bernal *(Cal. State U., Los Angeles)*, R.H. Heffner *(Los Alamos Nat. Lab)*, G.M. Luke *(McMaster U.)*, G.J. Nieuwenhuys *(U. Leiden)*, J.E. Sonier *(SFU)*, B. Andraka *(U. Florida)*

891. Superconductivity and magnetism in $Ce_nT_mIn_{3n+2m}$ [active], R.H. Heffner, J. Sarrao, B. Simovic *(Los Alamos Nat. Lab)*, J.E. Sonier *(SFU)*, D.E. MacLaughlin *(U. California, Riverside)*, G.J. Nieuwenhuys *(U. Leiden)*

892. Resonance ionization spectroscopy of stable and radioactive nuclides at TISOL [deferred] F. Buchinger, J.E. Crawford, S. Gulick, J.K.P. Lee *(McGill U.)*, K. Sharma *(U. Manitoba)*, J. Pinard *(Lab. Aimé Cotton, Orsay)*

893. Hyperfine field of Rb in the ferromagnets Fe, Ni, Co [active], C.A. Davis, P.P.J. Delheij *(TRIUMF)*, S. Cottenier *(K.U. Leuven)*, H. Haas *(Hahn Meitner Inst.)*, K.S. Krane *(Oregon State U.)*, B. Turrell *(UBC)*, J. Wood *(Georgia Inst. Tech.)*

894. Muonium kinetics and free radical formation in solutions of fullerenes [active], B. Addison-Jones *(Capilano Coll.)*, J.-C. Brodovitch, K. Ghandi, I. McKenzie, P.W. Percival *(SFU)*

895. The vortex structure and magnetism of electron-doped cuprate superconductors [active], K.M. Kojima, S. Uchida *(U. Tokyo)*, W. Higemoto, R. Kadono, A. Koda *(KEK)*, M. Azuma, M. Fujita, M. Takano, K. Yamada *(Kyoto U.)*, K. Ishida, Y. Kawasaki, Y. Kitaoka *(Osaka U)*, M.I. Larkin, Y.J. Uemura *(Columbia U.)*

896. Investigation of spin liquid behaviour in chromium and manganese spinels [active], H. Dabkowska, J. Greedan, P.P. Kyriakou, G.M. Luke, M.T. Rovers *(McMaster U.)*, I.M. Gat, M.I. Larkin, A.T. Savici, Y.J. Uemura *(Columbia U.)*, K.M. Kojima *(U. Tokyo)*

897. Absolute magnetic penetration depth in the Meissner state of superconductors measured with low frequency beta-NMR [active], D. Bonn, J.H. Brewer, K.H. Chow, W. Hardy, R. Liang, R. Miller, G. Morris *(UBC)*, S. Dunsiger, B. Heffner *(Los Alamos Nat. Lab)*, R.F. Kiefl *(UBC–TRIUMF)*, S. Kreitzman, P. Levy *(TRIUMF)*, G. Luke *(McMaster U.)*, J. Sonier *(SFU)*, C. Stronach *(Virginia State U.)*

898. MULTI development with applications in superconductors and semiconductors [active], P. Amadruz, D. Arseneau, S. Chan, K.H. Chow, B. Hitti, G. Morris, R. Poutissou *(TRIUMF)*, J. Chakhalian, S. Dunsiger, R.F. Kiefl, R. Miller *(UBC)*

900. A determination of the α+^{15}O radiative capture rate by a measurement of the ^{15}O(^{6}Li,d)^{19}Ne reaction [active], B.R. Fulton, B. Greenhalgh, J. Pearson, D.L. Watson *(U. York)*, N.M. Clarke *(U. Birmingham)*, T. Davinson, N. Farrington, P. Monroe, C. Ruiz, F. Sarazin, K. Schmidt, A.C. Shotter, P.J. Woods *(U. Edinburgh)*, L. Buchmann, P. Walden *(TRIUMF)*, J. D'Auria *(SFU)*

902. Muon capture on ^{45}Sc, ^{51}V, ^{55}Mn and ^{59}Co [active], D.F. Measday *(UBC)*, T.P. Gorringe *(U. Kentucky)*

903. Spectroscopic study of ^{11}Be with polarized ^{11}Li beam [active], Y. Hirayama, H. Izumi, M. Kawabata, K. Matsuta, K. Minamisono, T. Minamisono, S. Shimizu, T. Shimoda *(Osaka U.)*, H. Ishiyama, S.C. Jeong, H. Miyatake *(IPNS, KEK)*, K.P. Jackson, C.D.P. Levy *(TRIUMF)*

907. Improving $S_{E1}(300)$: the $\beta - \alpha$ branching ratio of ^{16}N [deferred] R.E. Azuma, J.D. King *(U. Toronto)*, L. Buchmann *(TRIUMF)*

909. Isospin symmetry breaking in superallowed Fermi beta decays [active], C.E. Svensson *(Guelph U.)*, R.A.E. Austin, J.A. Cameron, J.C. Waddington *(McMaster U.)*, G.C. Ball, P. Bricault, N. Kintz, J.A. Macdonald *(TRIUMF)*, J.C. Hardy, V. Iacob *(TAMU)*, J.R. Leslie *(Queen's U.)*, D.M. Moltz *(Lawrence Berkeley National Lab)*, G. Savard *(Argonne National Lab/U. Chicago)*

910. Study of the ground state proton emitter ^{73}Rb and implications for the astrophysical rp-process [active], A. Piechaczek, E.F. Zganjar *(Louisiana State U.)*, G.C. Ball *(TRIUMF)*, J.C. Batchelder *(Oak Ridge Assoc. U.)*, D. Kulp, B.D. MacDonald, J.L. Wood *(Georgia Inst. Tech.)*

*deceased

Appendix E

LIFE SCIENCES PROJECT PROPOSALS

The following lists life sciences project proposals received up to the end of 2000 (missing numbers cover proposals that have been withdrawn or replaced by later versions, rejected, or combined with another proposal). Page numbers are given for those experiments which are included in this Annual Report. Page

LS0. PET facilities [active], K.R. Buckley, E.T. Hurtado, E. Piccioni *(TRIUMF)*, C. English, S. Jivan, M. McNamara, C. Williams *(UBC–TRIUMF)* 91

LS1. Attenuation maps for quantitative SPECT [completed], A. Celler *(UBC–VH&HSC)*, S. McFarland *(UBC)*, S. Barney, M. Limber *(SFU)*

LS2. Synthesis of ^{18}F-glycosides as potential imaging agents for the study of glycosidase activity in the brain [active], M.J. Adam *(TRIUMF)*, D. Lyster *(VH&HSC)*, G. Matte *(Halifax H.)* 92

LS3. Synthesis of radiopharmaceuticals for positron emission tomography [active], M.J. Adam, K.R. Buckley, E.T. Hurtado, J. Huser, S. Jivan, J.-M. Lu, T.J. Ruth *(TRIUMF)* 93

LS4. TR13 targets for PET radioisotope production [active], K. Buckley, T. Hurtado, T.J. Ruth, S.K. Zeisler *(TRIUMF)* 94

LS5. Production and on-line separation of ^{124}I from enriched tellurium [inactive], W.Z. Gelbart, E.T. Hurtado, T.J. Ruth, N.R. Stevenson, S.K. Zeisler *(TRIUMF)*, R.R. Johnson *(UBC)*

LS6. Bone calcium resorption studies in pre- and peri-menopausal women using accelerator mass spectrometry [completed], R.R. Johnson, A. Priestman, J.C. Prior *(UBC)*, A. Altman, W.Z. Gelbart, V. Sossi *(TRIUMF)*, D. Berkovits, S. Ghelberg, M. Paul *(Racah Inst., Hebrew U. Jerusalem)*, L.M. Shulman *(Chaim Sheba Med. Centre)*, R. Chechik *(Weizmann Inst.)*, E. Venzel *(SFU)*

LS7. PET 3D data quantification and integration into a research clinical environment [completed], K.S. Morrison, T.J. Ruth, V. Sossi, M.W. Stazyk *(UBC–TRIUMF)*, K.R. Buckley *(TRIUMF)*, J.S. Barney *(VH&HSC)*, D. Sirota, B.J. Snow *(UBC)*

LS8. Radiotracers for the physical and biosciences [active], L. Buchmann, T.J. Ruth, S.K. Zeisler *(TRIUMF)*, A.D.M. Glass, R.R. Johnson, M. Lowe, C.E.R. Orvig *(UBC)*, T.F. Budinger *(Lawrence Berkeley National Lab)* 94

LS10. Biological evaluation of radiohalogenated DNA aptamers [completed], H. Dougan *(TRIUMF)*, J.B. Hobbs, D.M. Lyster *(UBC)*, J.I. Weitz *(McMaster U.)* 96

LS11. Development of single photon imaging agents [inactive], D. Lyster *(UBC–VH&HSC)*, L. Alcorn, M. Hampong, T. Lutz, C. Vo *(UBC)*

LS12. A simulation platform for the design of position encoding multicrystal detectors [completed], A. Altman, C. Moisan, J.G. Rogers *(TRIUMF)*, E. Hoskinson, G. Tsang *(UBC)*

LS13. Utility of 2-[F-18]-fluoro-2-deoxy-d-glucose SPECT imaging in the evaluation of patients with solitary pulmonary nodules [completed], A. Celler, D. Lyster, D. Worsley *(UBC)*, M. Adam *(TRIUMF)*

LS14. Production of ^{127}Xe from cesium with 90–110 MeV protons [inactive], D. Pearce, J. Vincent *(TRIUMF)*

LS15. Investigation of frame realignment on the reproducibility of ^{18}F-6-fluorodopa positron emission tomography [inactive], K.S. Morrison, T.J. Ruth *(UBC–TRIUMF)*, B.J. Snow *(UBC)*

LS17. Table-top radiocarbon facility [inactive], W. Gelbart, R.B. Schubank *(TRIUMF)*, E. Venczel *(UBC–SFU)*, S. Calvert, R.R. Johnson, J. Nagel, T. Peterson, V. Sossi *(UBC)*, D.E. Nelson *(SFU)*, J. Prior, K. Schoenholzer, R. Sutton, V. Walker *(UBC–VH&HSC)*, R. Middleton *(U. Pennsylvania)*, M. Paul *(Hebrew U. Jerusalem)*, J. Clague, L. Jackson, J. Lutenauer, D. Templeman-Kluit *(Geological Survey of Canada)*, R.N. McNeely, J.-S. Vincent *(GSC Ottawa)*, V. Barrie *(Pacific Geoscience Center)*, D. Prior, K.R. Robertson, G. Vilks *(Bedford Inst. Oceanography)*, R. Brown, S. Wang *(Elemental Research Inc.)*, J. Vogel *(Lawrence Livermore National Lab)*, A.E. Litherland *(U. Toronto)*, S. Dias, S. Sood *(Ontario Hydro)*, H.R. Andrews, R.M. Brown, R.J. Cornett *(AECL)*, D.B. Carlisle *(Environment Canada)*, J. Carron, A. Kabir, R.C.J. Wilkinson *(Canadian Centre for Inland Waters)*, R. Gephart, P. Molton, D. Robertson *(Batelle Pacific Northwest Labs)*

LS18. Cooperative development of ^{82}Sr-Rb generators for human use in Canada [completed], J. Vincent *(TRIUMF)*, R. Beanlands *(U. Ottawa Heart Inst.)*, B. Bowen *(McMaster U.)*, W. Dickie *(Nordion Int.)*

LS19. An ^{15}O-water generator: a feasibility study [inactive], K.R. Buckley, T.J. Ruth *(TRIUMF)*

LS20. Prototype heat-pipe water target for ^{18}F-production [inactive], K.R. Buckley, E.T. Hurtado, T.J. Ruth *(TRIUMF)*, J.W. Lenz *(private consultant)*

LS21. Aluminum kinetics in plants [inactive], A. Glass, R.R. Johnson, L. Oliveira *(UBC)*, K. Buckley, Z. Gelbart *(TRIUMF)*, D. Berkovitz, M. Paul *(Hebrew U. Jerusalem)*, E. Venczel *(SFU)*

LS22. Virtual national biomedical tracer facility [inactive], T.J. Ruth, J.S. Vincent *(TRIUMF)*, E.J. Peterson, D. Phillips *(Los Alamos National Lab)*

LS24. Scanning for early detection and staging of breast cancer: a comparative study using FDG PET and MIBI SPECT [deferred], P.F. Cohen, P. Klimo *(Lions Gate H.–UBC)*, M. Cackette *(EBCO Industries Ltd.)*, J. Whiffen *(JALORN)*, V. Sossi *(TRIUMF–UBC)*, J. Porter *(Nordion Int.)*, R.R. Johnson *(UBC)*

LS25. 3D PET in human neuroreceptor studies: quantification and reconstruction [completed], K.S. Morrison, T. Oakes, T.J. Ruth, V. Sossi *(UBC–TRIUMF)*, K.R. Buckley *(TRIUMF)*, M. Krzywinski, M. Schulzer, J. Stoessl *(UBC)*

LS26. A gaseous planar positron source for routine 3D PET normalization [completed], T. Oakes, T.J. Ruth, V. Sossi *(UBC–TRIUMF)*, K. Buckley, S. Jivan, R. MacDonald *(TRIUMF)*

LS27. The feasibility and efficacy of using 2-(F-18)-fluoro-2-deoxy-D-glucose (18-FDG) to evaluate children with musculoskeletal neoplasm [deferred], R. Anderson, J. Davis, D. Lyster, H.R. Nadel, T.J. Ruth, M. Stilwell, D. Worsley *(UBC)*

LS28. Evaluation of potentially viable myocardium with dobutamine myocardial SPECT imaging [completed], H. Abbey, A.-Y. Fung, L. Hook, D.M. Lyster, D.F. Worsley *(VH&HSC)*, M. Adam, S. Jivan *(TRIUMF)*

LS29. Production and distribution of FDG for clinical studies [active], D. Lyster, D. Worsley *(VH&HSC)*, P. Cohen *(Lions Gate H.)*, H. Nadel *(Children's H.)*, M.J. Adam, S. Jivan, T.J. Ruth, V. Sossi *(TRIUMF)* 97

LS31. Auger electron emitters for therapy-physics and chemistry [inactive], D. Pearce, T.J. Ruth, J. Vincent, A. Zyuzin *(TRIUMF)*, V. Kokhanyuk, V. Kravchuk, B.L. Zhuikov *(INR Moscow)*

LS32. $^{18}F\text{-}H_2{}^{18}O$ supply to the University of Alberta [active], S.A. McQuarrie, J.R. Mercer *(U. Alberta)*, A.J.B. McEwan *(CCI)*, R.R. Johnson *(UBC–EBCO)*, T.J. Ruth *(UBC–TRIUMF)* 97

LS33. Evaluation and improvement of a dual head coincidence camera [active], K.S. Morrison, T.J. Ruth, V. Sossi *(UBC–TRIUMF)*, M. Krzywinski *(UBC)*, P. Cohen *(Lions Gate H.)*, P. Klimo *(Lions Gate H.–UBC)*, T.K. Lewellen, D.A. Mankoff *(U. Washington)* 97

LS34. Production of ^{103}Pd [inactive], R.R. Johnson, R. Pavan *(UBC)*, M. Cackette, K.L. Erdman *(EBCO Industries Ltd.)*, Z. Gelbart *(TRIUMF)*

LS35. Development of F-18 labelled nitroimidazole PET imaging agents for tissue hypoxia [active], M.J. Adam *(TRIUMF)*, K. Skov *(BCCRC–UBC)*, S. Evans, C. Koch, A. Kachera *(U. Pennsylvania)*, I. Baird, B. James *(UBC)* 97

LS37. Feasibility of ^{125}Xe implantation as a ^{125}I brachytherapy source [active], D. Ottewell, T. Ruth, J. Vincent, A. Zyuzin *(TRIUMF)* 98

LS38. Dopaminergic tracers kinetic modeling with minimally invasive scanning procedures [completed], G. Chan, M. Krzywinski, T.J. Ruth, V. Sossi *(UBC–TRIUMF)*, J. Holden *(U. Wisconsin)*, D. Doudet, J. Stoessl *(UBC)* 98

LS39. Positron emission profiling (PEP) for pulp and paper fluid dynamic studies [active], M. Martinez, J. Olson *(UBC)*, M.J. Adam, K. Buckley, S. Jivan, T.J. Ruth, V. Sossi *(TRIUMF)* 100

LS40. F-18 FDG cardiac PET scans using a coincidence PET/SPECT camera to assess myocardial viability in patients with fixed abnormalities and low ejection fractions on gated sestamibi stress tests [deferred], P.F. Cohen, J. Imrie, K. Woo *(Lions Gate H.)*, D. Worsley *(Vancouver General H.)*, V. Sossi *(TRIUMF–UBC)*, T. Ruth *(UBC–TRIUMF)*, R.R. Johnson *(UBC)*

LS41. Impact of the ADAC coincidence PET camera in the management of selected cancer patients [deferred], P.F. Cohen, J. Imrie, K. Woo *(Lions Gate H.)*, J. Powe *(Vancouver General H.)*, V. Sossi *(TRIUMF–UBC)*, T. Ruth *(UBC–TRIUMF)*, R.R. Johnson *(UBC)*

LS42. Configuration modeling and image reconstruction studies on a depth encoding research tomograph [active], T. Ruth, V. Sossi *(UBC–TRIUMF)*, V. Astakhov *(UBC)*, K. Buckley *(TRIUMF)*, S. Houle *(Centre Addiction & Mental Health, Toronto)*, C. Moisan *(U. Laval)* 100